Proceedings of the
Helmholtz International School
"HEAVY QUARK PHYSICS" HQP08

August 11-21, 2008
Dubna, Russia

Impressum

Proceedings of the Helmholtz International School
"HEAVY QUARK PHYSICS" (HQP08)
August 11-21, 2008, Dubna, Russia

Conference homepage
http://theor.jinr.ru/~hq2008/index.htm

Slides at
http://theor.jinr.ru/~hq2008/index.htm

Online proceedings at
http://www-library.desy.de/preparch/desy/proc/proc09-07.pdf

The cover photograph is taken by Daniel Zablocki.

Organizing Committee

Co-organizers:
A. Ali (DESY)
M. A. Ivanov (BLTP, JINR)

Local organizers:
Yu. M. Bystritskiy (Scientific Secretary, BLTP, JINR)
V. K. Novikova (JINR)
J. Schmelzer (Rostock Uni. & BLTP, JINR)
V. I. Zhuravlev (BLTP, JINR)

Supported by:

Helmholtz-Gesellschaft
Deutsches Elektronen-Synchrotron DESY
Bogoliubov Laboratory of Theoretical Physics, JINR, Dubna
Gesellschaft für Schwerionenforschung GSI, Darmstadt

Preface

The Helmholtz International Summer School "HEAVY QUARK PHYSICS" was held at the Bogoli-ubov Laboratory of Theoretical Physics of the Joint Institute of Nuclear Physics JINR, Dubna, Moscow region, in the period August 11 – 21. 2008. This school is a continuation of a series of workshops on heavy quark physics held in Dubna (1993, 1996, 2000), Bad Honnef (1994), Rostock (1997) and the Helmholtz-JINR School held in Dubna in 2005.

Heavy quark physics is one of the frontiers of research in high energy physics. In the past, the experi-mental collaborations ARGUS and CLEO at the e^+e^- storage rings at DESY and Cornell respectively, the four collaborations, ALEPH, DELPHI, L3 and OPAL at LEP, and the SLD experiment at SLAC, spearheaded this field of research. However, in the recent past, the experiments BABAR and BELLE at the asymmetric B-factories at SLAC and KEK, respectively, and the two experiments CDF and D0, operating at the $p\bar{p}$ collider Tevatron at Fermilab, have moved to the forefront of heavy quark physics, providing a wealth of data. The highlights of the B-factory experiments are, among other topics, precise measurements of the matrix elements V_{cb} and V_{ub} of the quark mixing matrix, V_{CKM}, CP asymmetries, determining the three inner angles of the CKM-unitarity triangle, weak-interaction induced mass differ-ence ΔM_{B_d} involving the neutral meson complex $B_d^0 - \overline{B_d^0}$, and rare B-meson decays involving flavour changing neutral currents, such as $B \to X_{s,d}\,(\gamma, \ell^+\ell^-)$. Likewise, the two $p\bar{p}$ experiments, CDF and D0, have provided seminal results on the physics of the B_s^0 meson (and its antiparticle), highlighted by the measurement of the $B_s^0 - \overline{B_s^0}$ mass difference ΔM_{B_s}, and on Λ_b and other higher mass b-baryons. More recently, these experiments have also provided first experimental results on the measurements of the phase of the $B_s^0 - \overline{B_s^0}$ system, ϕ_{B_s}, defined as $\phi_{B_s} = -2\beta_s = \arg(-V_{ts}V_{tb}^*/V_{cs}V_{cb}^*)$. Currently the measuremens are off by 2.2σ from the Standard Model value $\phi_{B_s} \simeq -2°$. These and other re-lated studies will be set forth in the experiments (ATLAS, CMS, and, in particular, LHCb) at the Large Hadron Collider, which has just started its operations. If the current trends in the $b \to s$ quark transitions are confirmed by the subsequent experiments, it would imply evidence of physics beyond the standard model in the quark sector, crowning the weak interaction studies carried out over the last 50 years.

The main thrust of theoretical studies in heavy quark physics is on achieving theoretical precision com-mensurate with those in experiment (or better). This requires development of reliable calculational tools with firm theoretical underpinnings. For this purpose, effective field theories, obtained by integrating out the heavy degrees of freedom, provide the framework to study the physics of the hadrons containing the b- and c-quarks. They enable us to carry out perturbative QCD improvements in the various tran-sition amplitudes and prescribe the hadronic matrix elements to be calculated using a non-perturbative approach. The four most-popular approaches to handle the non-perturbative parts are: Lattice QCD, heavy quark effective theory (HQET), soft collinear effective theory (SCET) and the QCD sum rules. These approaches were discussed at great length at the school, both in terms of their structure and appli-cations to the weak decays of the heavy hadrons. Another topic taken up at this school was the physics involving the top quark. In particular, the role of the top quark in the context of the electroweak radiative corrections, and the QCD radiative corrections to the top quark decays, were discussed in detail. Apart from these, a number of topics related to the properties of charmonia, heavy (b- and c-) baryons, double heavy baryons and heavy tetraquarks were covered by several speakers.

The school on Heavy Quark Physics was well-attended, judged from more than 65 participants and lecturers, listed in these proceedings. They include a large number of students and young researchers who presented their work in contributed talks. Quite a few of these contributions, though not all, are

included in the proceedings. However, the slides of all the talks are available at the web address:
`http://theor.jinr.ru/~hq2008/index.htm`.
The online proceedings are available at:
`http://www-library.desy.de/preparch/desy/proc/proc09-07.pdf`.

Co-editors:
Ahmed Ali and Mikhail Ivanov

Contents

Three Lectures on
Meson Mixing and CKM phenomenology

Ulrich Nierste

Institut für Theoretische Teilchenphysik
Universität Karlsruhe
Karlsruhe Institute of Technology,
D-76128 Karlsruhe, Germany

I give an introduction to the theory of meson-antimeson mixing, aiming at students who plan to work at a flavour physics experiment or intend to do associated theoretical studies. I derive the formulae for the time evolution of a neutral meson system and show how the mass and width differences among the neutral meson eigenstates and the CP phase in mixing are calculated in the Standard Model. Special emphasis is laid on CP violation, which is covered in detail for K–$\overline{K}$ mixing, B_d–$\overline{B}_d$ mixing and B_s–$\overline{B}_s$ mixing. I explain the constraints on the apex $(\overline{\rho}, \overline{\eta})$ of the unitarity triangle implied by ϵ_K, ΔM_{B_d}, $\Delta M_{B_d}/\Delta M_{B_s}$ and various mixing-induced CP asymmetries such as $a_{\mathrm{CP}}(\overline{B}_d \to J/\psi K_{\mathrm{short}})(t)$. The impact of a future measurement of CP violation in flavour-specific B_d decays is also shown.

1   First lecture: A big-brush picture

1.1   Mesons, quarks and box diagrams

The neutral K, D, B_d and B_s mesons are the only hadrons which mix with their antiparticles. These meson states are flavour eigenstates and the corresponding antimesons $\overline{K}$, $\overline{D}$, $\overline{B}_d$ and $\overline{B}_s$ have opposite flavour quantum numbers:

$$
\begin{aligned}
K &\sim \overline{s}d, & D &\sim c\overline{u}, & B_d &\sim \overline{b}d, & B_s &\sim \overline{b}s, \\
\overline{K} &\sim s\overline{d}, & \overline{D} &\sim \overline{c}u, & \overline{B}_d &\sim b\overline{d}, & \overline{B}_s &\sim b\overline{s},
\end{aligned}
\tag{1}
$$

Here for example "$B_s \sim \overline{b}s$" means that the B_s meson has the same flavour quantum numbers as the quark pair $(\overline{b}, s)$, i.e. the beauty and strangeness quantum numbers are $B = 1$ and $S = -1$, respectively. The meson states in Eq. (1) are also eigenstates of the strong and electromagnetic interactions. As long as we neglect the weak interaction, they are also mass eigenstates, with the same mass for meson and antimeson. In the Standard Model (SM) all interaction vertices conserve flavour, except for the couplings of W bosons to fermions.[1] The piece of the SM Lagrangian which describes the W couplings to quarks reads

$$
\mathcal{L}_W = \frac{g_w}{\sqrt{2}} \sum_{j,k=1,2,3} \left[V_{jk}\, \overline{u}_{jL}\, \gamma^\mu d_{kL}\, W_\mu^+ + V_{jk}^*\, \overline{d}_{kL}\, \gamma^\mu u_{jL}\, W_\mu^- \right].
\tag{2}
$$

---

[1]Strictly speaking, this statement assumes that the so-called unitary gauge for the weak gauge bosons is adopted. The unphysical charged pseudo-Goldstone bosons, which appear in other gauges, also have flavour-changing vertices. Changing the gauge shuffles terms between the pseudo-Goldstone bosons and the longitudinal components of the gauge bosons.
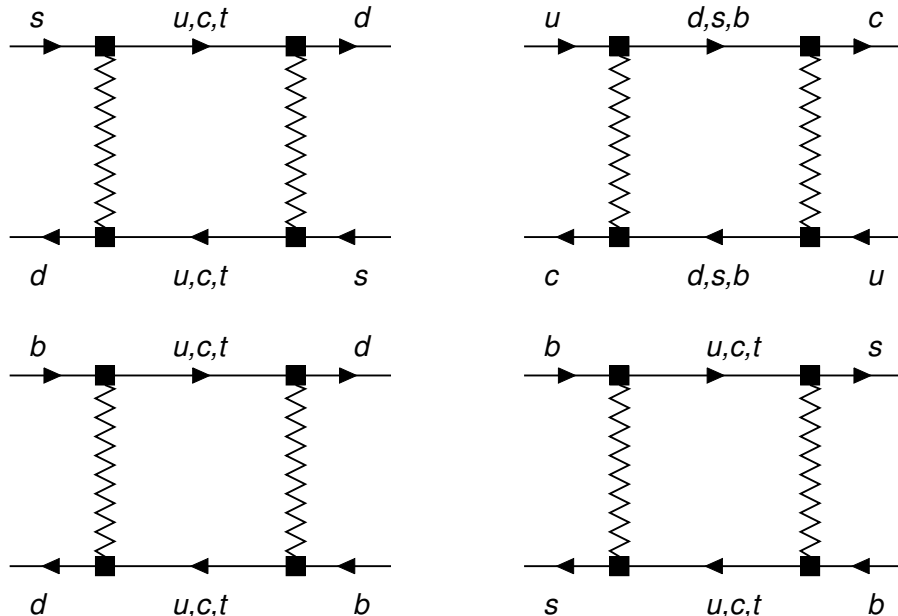
Figure 1: Box diagrams for $K-\overline{K}$, $D-\overline{D}$, $B_d-\overline{B}_d$ and $B_s-\overline{B}_s$ mixing. The zigzag lines represent W bosons. For each process there is also a second box diagram, obtained by a 90° rotation.

Here g_w is the weak coupling constant and V is the 3×3 unitary *Cabibbo-Kobayashi-Maskawa (CKM) matrix*:

$$V \quad = \quad \begin{pmatrix} V_{ud} & V_{us} & V_{ub} \\ V_{cd} & V_{cs} & V_{cb} \\ V_{td} & V_{ts} & V_{tb} \end{pmatrix}. \tag{3}$$

In Eq. (2) I have further used the notations $(d_1, d_2, d_3) = (d, s, b)$ and $(u_1, u_2, u_3) = (u, c, t)$. The W boson only couples to the left-handed components of the quark fields as indicated by the subscript "L" in Eq. (2). At fourth order in the weak coupling we can change the flavour quantum numbers by two units and obtain transitions between mesons and antimesons. The corresponding Feynman diagrams are shown in Fig. 1. These $|\Delta F| = 2$ diagrams, where F denotes the appropriate flavour quantum number $F = S$, C or B, represent the lowest non-vanishing contribution to the transition matrix element Σ_{12} defined by

$$-i(2\pi)^4 \delta^{(4)}(p_M - p_{\overline{M}})\Sigma_{12} \quad = \quad \frac{\langle M(\vec{p}_M)|S|\overline{M}(\vec{p}_{\overline{M}})\rangle}{2M_M} \tag{4}$$

with the S-matrix S and the generic notation $M = K, D, B_d$ or B_s. (The notation Σ_{12} refers to the quantum-mechanical two-state system with $|1\rangle = |M\rangle$ and $|2\rangle = |\overline{M}\rangle$.) I comply with the standard relativistic normalisation of the meson states, $\langle M(\vec{p}')|M(\vec{p})\rangle = 2E\,(2\pi)^3\delta^{(3)}(\vec{p}' - \vec{p})$.

The meson mass $M_M = \sqrt{E^2 - \vec{p}^2}$ in the denominator in Eq. (4) is introduced for later convenience. In terms of the Hamiltonian (density) $H_{\text{int}}^{SM}(x) = -\mathcal{L}_{\text{int}}^{SM}(x)$, which encodes all interactions of the SM, the S-matrix is given by the usual time-ordered exponential

$$S = \mathbf{T} e^{-i \int d^4 x H_{\text{int}}^{\text{SM}}(x)}. \tag{5}$$

In order to link Eqs. (4) and (5) to the diagrams of Fig. 1 we must consider the contribution from $\mathcal{L}_W$ in Eq. (2) to $-H_{\text{int}}^{SM}$ and expand the time-ordered exponential in Eq. (5) to order g_w^4. The determination of this term amounts to the calculation of the two contributing box diagrams with the usual Feynman rules of the weak interaction. To this point we have only used standard text-book quantum field theory, noting an important omission: No effect of the strong interaction has been taken into account by now. Most importantly, we do not know yet how to take care of quark confinement, which forces the external quarks in the diagrams of Fig. 1 to form mesons. As an important feature, Quantum Chromodynamics (QCD) behaves very differently at short and long distances: At short distances (probed by large energies) the QCD coupling constant g_s is small and we can apply perturbation theory [1], just as we did with the weak interaction. That is, effects of short-distance QCD can be included by adding gluons to the diagrams in Fig. 1. At large distances, corresponding to low energies, QCD is non-perturbative and one must resort to different methods, such as lattice gauge theory or QCD sum rules. Long-distance QCD is also referred to as *hadronic physics*, because its degrees of freedom are hadrons rather than quarks and gluons. In many cases the associated theoretical uncertainties are the main obstacle in the relation between measured quantities and the fundamental parameters of nature encoded in the Lagrangian $\mathcal{L}$. Theorists pursue a two-fold strategy to deal with hadronic uncertainties: On one hand they try to refine non-perturbative methods such as lattice gauge theory. On the other hand they try to identify quantities in which hadronic uncertainties are small or even absent or look for ways to eliminate hadronic uncertainties through clever combinations of different observables. We will encounter both strategies in our discussion of meson-antimeson mixing. Weak processes of hadrons involve several largely-separated energy scales.[2] For example, in $B - \overline{B}$ mixing we encounter $m_t > M_W \gg m_b \gg \Lambda_{\text{QCD}}$, where $\Lambda_{\text{QCD}} \sim 0.4\,\text{GeV}$ is the fundamental scale of the strong interaction governing e.g. the size of binding energies. In order to correctly calculate Σ_{12} we must separate the different scales from each other and apply different computational methods to large and small energy scales. However, without detailed understanding of the strong interaction we can roughly assess the relative importance of the contributions from the different internal quark flavours in Fig. 1: In the case of $B_d - \overline{B}_d$ mixing and $B_s - \overline{B}_s$ mixing one finds that the box diagram with internal top quarks vastly dominates over the diagrams with light quarks, because the result of the diagram grows with the internal quark mass. For $K - \overline{K}$ mixing and $D - \overline{D}$ mixing no such estimate is possible, because the contribution with the heaviest quark is suppressed by small CKM elements.

Owing to $\Sigma_{12} \neq 0$, M and $\overline{M}$ mix and are no more mass eigenstates. The latter are obtained by diagonalising the 2×2 matrix Σ_{ij}, where

$$-i(2\pi)^4 \delta^{(4)}(p_i' - p_j) \Sigma_{ij} = \frac{\langle i, \vec{p}_i' | S^{\text{SM}} | j, \vec{p}_j \rangle}{2M_M} \tag{6}$$

with $|1, \vec{p}_1\rangle = |M(\vec{p}_1)\rangle$ and $|2, \vec{p}_2\rangle = |\overline{M}(\vec{p}_2)\rangle$ generalises Eq. (4). We list two important aspects of meson-antimeson mixing:

---

[2] I use natural (or Planck) units with $\hbar = c = 1$, so that masses and momenta have units of GeV.

i) The two mass eigenstates are linear combinations of M and $\overline{M}$. The degeneracy is lifted and we can denote the two mass eigenstates by M_H and M_L, where "H" and "L" stand for "heavy" and "light", respectively. M_H and M_L not only differ in their masses, but also in their lifetimes.

ii) If we produce a meson M at some time $t = 0$, the corresponding state will evolve into a superposition of M and $\overline{M}$ at later times $t > 0$. One observes meson-antimeson oscillations.

We will calculate the differences among the masses and decay widths in the second and third lectures. Studies of neutral Kaons mainly exploit property i), while the mixings of the other three neutral meson systems are investigated through property ii). The reason for the Kaon's special role here is the vast lifetime difference between K_H and K_L. The former state, usually denoted as K_{long}, lives roughly 500 times longer than $K_L = K_{\text{short}}$, so that one can easily produce a K_{long} beam. For D, B_d and B_s mesons the width differences are much smaller than the average decay width of the two eigenstates and this method is not feasible. The identification of the meson (discriminating between M and $\overline{M}$) needed to track the meson-antimeson oscillations is called *flavour tagging*. To observe the oscillations the mesons must move sufficiently fast in the detector. Modern B factories, which produce $(B_d, \overline{B}_d)$ pairs via the $\Upsilon(4S)$ resonance, have therefore asymmetric beam energies, so that the centre-of-mass frame (coinciding with the rest frame of the $\Upsilon(4S)$) moves with respect to the laboratory frame. At hadron colliders studies of meson-antimeson oscillations profit from the large boost of the produced mesons. Tevatron and LHC are especially powerful for B_s physics, because the B_s–$\overline{B}_s$ oscillations are very rapid.

1.2 A bit of history

Meson-antimeson mixings belong to the class of *flavour-changing neutral current (FCNC)* processes, which involve different flavours with the same electric charge. Since in the SM such processes are forbidden at tree-level, they are sensitive to new heavy particles appearing as virtual particles in loop diagrams. Historically, the first new particle predicted from the consideration of FCNCs was the charm quark, which was needed to eliminate large tree-level FCNC couplings in conflict with experiment [2]. Subsequently, the rough size of the charm quark mass m_c was predicted from the size of the mass difference $\Delta M_K = M_H - M_L$ in the neutral Kaon system [3]. A great success story of flavour physics has been the exploration of the discrete symmetries charge conjugation (C), parity (P) and time reversal (T). Charged Kaon decays had revealed in 1956 that P and C are not conserved by the weak interaction, while physicists kept their faith in a good CP symmetry. If CP were conserved, we could assign CP quantum numbers to K_{long} and K_{short}. The latter meson was observed to decay into a two-pion state, and each pion is CP-odd and contributes a factor of -1 to the total CP quantum number (which is multiplicative). A further contribution to the CP quantum number of a two-particle state stems from the angular momentum: States with orbital angular momentum quantum number l involve the spherical harmonic $Y_m^l(\vec{n})$, where $\vec{n} = \vec{p}/|\vec{p}|$ and $\vec{p}$ is the relative momentum of the two particles considered. Since $Y_m^l(\vec{n}) = (-1)^l Y_m^l(-\vec{n})$, states with odd l have P and CP quantum numbers -1, while those with even l are even under P and CP. Since the decaying Kaon has no spin and the total angular momentum is conserved in any decay process, the two pions in the final state have have $l = 0$ in the Kaon rest frame. (In general the spin wave function also matters, but pions have spin zero.) In total we find that the two-pion state is

CP-even. Now K_{long} was only seen to decay into three pions, so that this meson was believed to be CP-odd. In fact, its long lifetime stems from the kinematical suppression of the decay into the CP-odd three–pion state. To understand that a three-pion state is always CP-odd, first note that we get a contribution of $(-1)^3 = -1$ from the intrinsic CP quantum numbers of the three pions. Next pick any two of the pions and call there relative orbital angular momentum quantum number l_1. Likewise we denote the quantum number for the relative orbital angular momentum between this pair and the third pion by l_2. One of the selection rules for the addition of angular momenta implies that the total quantum number l satisfies $l \geq |l_1 - l_2|$. Since $l = 0$, this means that $l_1 = l_2$ and the "orbital" contribution to the CP quantum number is $(-1)^{l_1+l_2} = (-1)^{2l_1} = 1$. Thus the three-pion state is CP-odd, irrespective of the value of l_1.

In 1964 the decay $K_{\text{long}} \rightarrow \pi\pi$ was observed, establishing CP violation [4]. The two-generation Standard Model, whose construction was completed later in that decade [5], could not accommodate this phenomenon: We will see below that CP-violating interactions of quarks necessarily involve complex couplings. While the V_{jk}'s in Eq. (2) are a priori complex, one can render them real in the two-generation SM by transforming the quark fields as

$$d_j \rightarrow e^{i\phi_j^d} d_j, \qquad\qquad u_k \rightarrow e^{i\phi_k^u} u_k. \qquad (7)$$

with appropriate phases ϕ_j^d and ϕ_k^u. The net effects of these rephasings are the replacements of the V_{jk}'s by

$$V_{jk} e^{i(\phi_j^d - \phi_k^u)}. \qquad (8)$$

These expressions involves three independent phases and we may choose e.g. $\phi_1^d - \phi_1^u$, $\phi_1^d - \phi_2^u$ and $\phi_2^d - \phi_1^u$ in such a way that the three complex phases of a unitarity 2×2 matrix are eliminated, arriving at the real Cabibbo matrix. In 1973 Kobayashi and Maskawa have pointed out that a physical CP-violating phase persists in the quark mixing matrix, if there are at least three generations [6]: A unitary 3×3 matrix has 6 complex phases while we have only 5 phase differences $\phi_j^d - \phi_k^u$ at our disposal. The finding of Kobayashi and Maskawa was largely ignored at that time and only appreciated after the third fermion generation was experimentally established. In 1987 the ARGUS experiment at DESY observed B_d–$\overline{B}_d$ mixing, at an unexpectedly large rate [7]. This finding was the first hint at a truly heavy top quark, which enters the lower left box diagram of Fig. 1.

1.3 CP violation

The last stroke of the brush is devoted to CP violation. Defining

$$CP | M(\vec{p_M}) \rangle = -| \overline{M}(-\vec{p_M}) \rangle, \qquad\qquad CP | \overline{M}(\vec{p_M}) \rangle = -| M(-\vec{p_M}) \rangle \qquad (9)$$

we first look at decays $M \rightarrow f_{\text{CP}}$ and $\overline{M} \rightarrow f_{\text{CP}}$, where f_{CP} is a CP eigenstate:

$$CP | f_{\text{CP}} \rangle = \eta_{\text{CP}} | f_{\text{CP}} \rangle \qquad (10)$$

with $\eta_{\text{CP}} = \pm 1$. The CP operator appearing in Eqs. (9) and (10) is unitary, i.e. $(CP)^{-1} = (CP)^\dagger$. To get an idea of the importance of meson-antimeson mixing for the study of CP violation we first assume that M and $\overline{M}$ do not mix. We could still measure the decay rates of the CP-conjugate processes $M \rightarrow f_{\text{CP}}$ and $\overline{M} \rightarrow f_{\text{CP}}$. If we find them different we establish *direct CP*

violation (often called *CP violation in decay*). However, it is very difficult to relate a direct *CP* asymmetry to a fundamental *CP* phase in $\mathcal{L}$: A non-zero direct *CP* asymmetry also requires final state interaction related to the rescattering process $M \to f'_{\text{CP}} \to f_{\text{CP}}$. Rescattering leads to *CP*-conserving complex phases in the decay amplitude. In the absence of such phases the amplitudes of $M \to f_{\text{CP}}$ and $\overline{M} \to f_{\text{CP}}$ would simply be related by complex conjugation since all phases would switch sign under *CP*. But then the two decay amplitudes would have the same magnitude leading to identical decay rates. For $M = D, B_d, B_s$ this hadronic rescattering process is mainly inelastic and intractable with present theoretical methods.

But thanks to meson-antimeson mixing we can study meson states which are superpositions of $|M\rangle$ and $|\overline{M}\rangle$. The mass eigenstates $|M_H\rangle$ and $|M_L\rangle$ are linear combinations of $|M\rangle$ and $|\overline{M}\rangle$:

$$
\begin{array}{rcl}
|M_L\rangle &=& p|M\rangle + q|\overline{M}\rangle\,, \\
|M_H\rangle &=& p|M\rangle - q|\overline{M}\rangle\,,
\end{array}
\tag{11}
$$

with $|p|^2 + |q|^2 = 1$. We can calculate p and q from the box diagrams in Fig. 1 and will do so in the following sections. A commonly used shorthand notation for decay amplitudes is

$$
A_f = A(M \to f) = \langle f|S|M\rangle, \qquad \overline{A}_f = A(\overline{M} \to f) = \langle f|S|\overline{M}\rangle.
\tag{12}
$$

A key quantity to study *CP* violation is the combination

$$
\lambda_f \;=\; \frac{q}{p}\frac{\overline{A}_f}{A_f}.
\tag{13}
$$

λ_f encodes the essential feature of the interference of the $M \to f$ and $\overline{M} \to f$ decays, the relative phase between q/p (from meson-antimeson mixing) and $\overline{A}_f/A_f$ (stemming from the studied decay). In a first application, I discuss the decays of neutral Kaons into two charged or neutral pions. A neutral K or $\overline{K}$ meson state is a superposition of $K_H = K_{\text{long}}$ and $K_L = K_{\text{short}}$. At short times the decays of the K_{short} component of our Kaon beam will vastly dominate over the K_{long} decays and one can access the decay rates $\Gamma(K_{\text{short}} \to \pi\pi)$ for $\pi\pi = \pi^+\pi^-, \pi^0\pi^0$. At large times, say, after 10 times the K_{short} lifetime, our beam is practically a pure K_{long} beam and we can study the *CP*-violating $\Gamma(K_{\text{long}} \to \pi\pi)$ decays. It is advantageous to switch to the eigenbasis of strong isospin I:

$$
\begin{array}{rcl}
|\pi^0\pi^0\rangle &=& \sqrt{\dfrac{1}{3}}\,|\,(\pi\pi)_{I=0}\rangle - \sqrt{\dfrac{2}{3}}\,|\,(\pi\pi)_{I=2}\rangle\,, \\[2ex]
|\pi^+\pi^-\rangle &=& \sqrt{\dfrac{2}{3}}\,|\,(\pi\pi)_{I=0}\rangle + \sqrt{\dfrac{1}{3}}\,|\,(\pi\pi)_{I=2}\rangle\,,
\end{array}
$$

The strong interaction respects strong-isospin symmetry to an accuracy of typically 2%, so that we can neglect any rescattering between the $I = 0$ and $I = 2$ states. Consequently, no *direct CP* violation contributes to the famous *CP*-violating quantity

$$
\epsilon_K \equiv \frac{\langle(\pi\pi)_{I=0}|K_{\text{long}}\rangle}{\langle(\pi\pi)_{I=0}|K_{\text{short}}\rangle}.
\tag{14}
$$

Abbreviating $A_0 \equiv A_{(\pi\pi)_{I=0}}$, $\overline{A}_0 \equiv \overline{A}_{(\pi\pi)_{I=0}}$ and (see Eq. (13)) $\lambda_0 \equiv \lambda_{(\pi\pi)_{I=0}}$ we insert Eq. (11) into Eq. (14) and readily find

$$
\epsilon_K = \frac{1-\lambda_0}{1+\lambda_0}\,.
\tag{15}
$$

The experimental value [8]

$$\epsilon_K^{\mathrm{exp}} = e^{i\,\phi_\epsilon}\,(2.23 \pm 0.01) \times 10^{-3} \qquad \text{with} \quad \phi_\epsilon \;=\; (0.967 \pm 0.001)\,\frac{\pi}{4}\,. \qquad (16)$$

therefore allows us to determine λ_0, which in our example is apparently close to 1. In our case with $|A_0| = |\overline{A}_0|$ (absence of direct CP violation) we have $|\lambda_0| = |q/p|$. With Eq. (15) we find

$$\epsilon_K \simeq \frac{1}{2}\,[1 - \lambda_0] \;\simeq\; \frac{1}{2}\left(1 - \left|\frac{q}{p}\right| - i\,\mathrm{Im}\,\lambda_0\right) \qquad (17)$$

up to corrections of order ϵ_K^2. Remarkably, from the real and imaginary part of ϵ_K we infer two CP-violating quantities:

  i) the deviation of $|q/p|$ from 1 and

  ii) the deviation of $\mathrm{Im}\,\lambda_0$ from 0.

The first quantity is independent of the studied final state f and codifies *CP violation in mixing*. The second quantity, $\mathrm{Im}\,\lambda_f$, measures CP violation in the interference of mixing and decay or, in short, *mixing-induced CP violation* in the decay $M \to f$.

   In the case of D, B_d or B_s mixing studies one tags the flavour at some time $t = 0$. The corresponding meson states are called $|M(t)\rangle$ and $|\overline{M}(t)\rangle$ and satisfy $|M(t = 0)\rangle = |M\rangle$ and $|\overline{M}(t = 0)\rangle = |\overline{M}\rangle$. For $t > 0$ these time-dependent states are calculable superpositions of $|M\rangle$ and $|\overline{M}\rangle$ and by observing the time-dependence of $M(t) \to f$ we can infer λ_f. The presently most prominent application of this method is the precise determination of $\mathrm{Im}\,\lambda_f$ in the decay $B_d \to J/\psi K_{\mathrm{short}}$ by the B factories BaBar and BELLE. Needless to say that we will discuss this important topic in detail below.

   While C, P, and T are violated in nature, the combination CPT is a good symmetry. This *CPT theorem* holds in any local Poincaré-invariant quantum field theory [9]. It implies that particles and antiparticles have the same masses and total decay widths. When applied to our mixing problem characterised by Σ in Eq. (6) the CPT theorem enforces $\Sigma_{11} = \Sigma_{22}$. However, while the CPT theorem implies $\Gamma_{\mathrm{tot}}(M) = \Gamma_{\mathrm{tot}}(\overline{M})$, one still has different time-integrated total decay rates for tagged mesons, $\int_0^\infty dt\,\Gamma_{\mathrm{tot}}(M(t)) \neq \int_0^\infty dt\,\Gamma_{\mathrm{tot}}(\overline{M}(t))$. This quantity is sensitive to the "arrow of time" and the difference $\Gamma_{\mathrm{tot}}(M(t)) - \Gamma_{\mathrm{tot}}(\overline{M}(t))$ measures CP violation rather than CPT violation. Throughout my lectures I assume CPT invariance and therefore identify CP symmetry with T symmetry. Still, experiments have tested the CPT theorem by probing $\Sigma_{11} = \Sigma_{22}$ in $K - \overline{K}$ mixing. We may speculate that Poincaré invariance and CPT symmetry are violated by the unknown dynamics of quantum gravity. If we are lucky the size of CPT violation scales linearly in the inverse Planck Mass M_{Planck}. Interestingly, today's accuracy of the CPT test $\Sigma_{11} = \Sigma_{22}$ is roughly M_K/M_{Planck}.

2 Second lecture: Time evolution

2.1 Time-dependent meson states

In the Schrödinger picture, the time evolution of a quantum-mechanical state $|\psi\rangle = |\psi, t = 0\rangle$ is given by $|\psi, t\rangle = \mathcal{U}(t, 0)|\psi\rangle$, with the unitary time-evolution operator $\mathcal{U}(t, 0)$. Consider first the case of a weakly-decaying charged meson (i.e. K^+, D^+ or B^+), which cannot mix with other
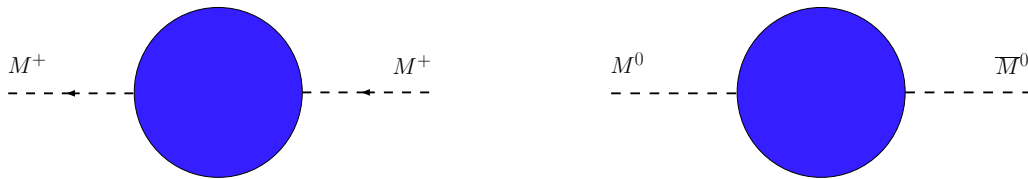
Figure 2: Left: generic self energy Σ of a charged meson. Right: $M^0 - \overline{M}^0$ mixing amplitude Σ_{12}.

states. The corresponding state at $t = 0$, $|M^+\rangle$, will evolve into a superposition of all states allowed by energy-momentum conservation. This class of states consists of the original meson state $|M^+\rangle$ and all final states $|f\rangle$ into which M^+ can decay. Defining

$$|M^+(t)\rangle \;=\; |M^+\rangle\langle M^+|\mathcal{U}(t,0)|M^+\rangle \tag{18}$$

we can write

$$\mathcal{U}(t,0)|M^+\rangle \;=\; |M^+(t)\rangle + \sum_f |f\rangle\langle f|\mathcal{U}(t,0)|M^+\rangle.$$

In order to find $|M^+(t)\rangle$ we take a shortcut, by employing the exponential decay law to deduce

$$|M^+(t)\rangle \;=\; e^{-iM_M t}e^{-\Gamma t/2}|M^+\rangle \tag{19}$$

in the meson rest frame. The first term is the familiar time evolution factor of a stable state with energy $E = M_M$. The second factor involving the total width Γ is understood by considering the probability to find an undecayed meson at time t:

$$\left|\langle M^+|M^+(t)\rangle\right|^2 \;=\; e^{-\Gamma t}$$

Whenever I work in the Schrödinger picture I normalise the states as $\langle M^+|M^+\rangle = 1$. Since $M_M - i\Gamma/2$ is independent of t, we can compute it using the familiar covariant formulation of quantum field theory. The optical theorem tells us that M_M and $-\Gamma/2$ are given by the real and imaginary parts of the self-energy Σ (depicted in the left diagram of Fig. 2), where

$$-i(2\pi)^4\delta^{(4)}(\vec{p}' - \vec{p})\Sigma \;=\; \frac{\langle M^+(\vec{p}')|S|M^+(\vec{p})\rangle}{2M_M} \tag{20}$$

(To be precise, the diagram in Fig. 2 corresponds to $2M_M\Sigma$, so that $\Sigma = M_M - i\Gamma/2$ has mass dimension 1.) From Eq. (19) we find

$$i\frac{d}{dt}|M^+(t)\rangle \;=\; \left(M_M - i\frac{\Gamma}{2}\right)|M^+(t)\rangle. \tag{21}$$

This equation can be generalised to a two-state system describing neutral meson mixing:

$$i\frac{d}{dt}\begin{pmatrix} |M(t)\rangle \\ |\overline{M}(t)\rangle \end{pmatrix} \;=\; \Sigma\begin{pmatrix} |M(t)\rangle \\ |\overline{M}(t)\rangle \end{pmatrix} \tag{22}$$

8

where now Σ is the 2×2 matrix defined in Eq. (6). Recall that any matrix can be written as the sum of a hermitian and an antihermitian matrix. We write

$$\Sigma = M - i\frac{\Gamma}{2} \tag{23}$$

with the *mass matrix* $M = M^\dagger$ and the *decay matrix* $\Gamma = \Gamma^\dagger$. Then

$$M_{12} = \frac{\Sigma_{12} + \Sigma_{21}^*}{2}, \qquad\qquad \frac{\Gamma_{12}}{2} = i\frac{\Sigma_{12} - \Sigma_{21}^*}{2}. \tag{24}$$

The expressions on the RHS of Eq. (24) are called *dispersive* and *absorptive* parts of Σ_{12}, respectively. The right diagram in Fig. 2 generically represents all contributions to Σ_{12}. To compute Σ_{12} we can certainly use perturbation theory for the weak interaction (which to lowest order amounts to the calculation of the box diagram in Fig. 1), but we must take into account the non-perturbative nature of the strong binding forces. The diagonal elements M_{11} and M_{22} are the masses of M and $\overline{M}$ and are generated from the quark mass terms in $\mathcal{L}$ and from the binding energy of the strong interaction. However, the off-diagonal elements $M_{12} = M_{21}^*$ and all elements of Γ stem from the weak interaction and are therefore tiny in comparison with M_{11} and M_{22}. The only reason why we can experimentally access M_{12} roots in the *CPT* theorem: *CPT* symmetry enforces

$$M_{11} = M_{22}, \qquad\qquad \Gamma_{11} = \Gamma_{22}, \tag{25}$$

so that the eigenvalues of Σ are exactly degenerate for $\Sigma_{12} = \Sigma_{21} = 0$. Even the smallest Σ_{12} can lift the degeneracy and can lead to large meson-antimeson mixing.

With our shortcut we have avoided to prove that Eq. (21) holds with time-independent M and Γ. In fact, Eq. (21) and the inferred exponential decay law in Eq. (19) are not valid exactly, but receive tiny (and phenomenologically irrelevant) corrections [10]. The same statement is true for Eqs. (22) and (23), a proper derivation of Eq. (22) using time-dependent perturbation theory for the weak interaction employs the so-called *Wigner-Weisskopf approximation* [11]. Corrections to this approximation have been addressed in Ref. [13] and are below the 10^{-10} level.

We now proceed with the solution of our Schrödinger equation in Eq. (22). Eq. (11) means that the eigenvectors of Σ in Eq. (6) are $(p, q)^T$ and $(p, -q)^T$. That is, Σ is diagonalised as

$$Q^{-1}\Sigma Q = \begin{pmatrix} M_L - i\Gamma_L/2 & 0 \\ 0 & M_H - i\Gamma_H/2 \end{pmatrix} \tag{26}$$

with

$$Q = \begin{pmatrix} p & p \\ q & -q \end{pmatrix} \qquad \text{and} \qquad Q^{-1} = \frac{1}{2pq}\begin{pmatrix} q & p \\ q & -p \end{pmatrix}. \tag{27}$$

The ansatz in Eq. (27) works because $\Sigma_{11} = \Sigma_{22}$. The mass eigenstates $|M_{L,H}(t)\rangle$ obey an exponential decay law as $|M^+(t)\rangle$ in Eq. (19) with (M_M, Γ) replaced by $(M_{L,H}, \Gamma_{L,H})$. Transforming back to the flavour basis gives

$$\begin{pmatrix} |M(t)\rangle \\ |\overline{M}(t)\rangle \end{pmatrix} = Q \begin{pmatrix} e^{-iM_L t - \Gamma_L t/2} & 0 \\ 0 & e^{-iM_H t - \Gamma_H t/2} \end{pmatrix} Q^{-1} \begin{pmatrix} |M\rangle \\ |\overline{M}\rangle \end{pmatrix} \tag{28}$$

I adopt the following definitions for the average mass and width and the mass and width differences of the mass eigenstates:

$$
\begin{aligned}
m &= \frac{M_H + M_L}{2} = M_{11} = M_{22}\,, & \Gamma &= \frac{\Gamma_L + \Gamma_H}{2} = \Gamma_{11} = \Gamma_{22}\,, \\
\Delta M &= M_H - M_L\,, & \Delta\Gamma &= \Gamma_L - \Gamma_H\,.
\end{aligned}
\tag{29}
$$

Note that ΔM is positive by definition while $\Delta\Gamma$ can have either sign. Experimentally the sign of $\Delta\Gamma$ is only known for Kaons and my sign convention in Eq. (29) corresponds to $\Delta\Gamma_K > 0$. The Standard-Model prediction for $\Delta\Gamma_{B_d}$ and $\Delta\Gamma_{B_s}$ is also positive, while no reliable prediction is possible for the sign of $\Delta\Gamma_D$. The matrix appearing in Eq. (28) can be compactly written as

$$
Q \left(
\begin{array}{cc}
e^{-iM_L t - \Gamma_L t/2} & 0 \\
0 & e^{-iM_H t - \Gamma_H t/2}
\end{array}
\right) Q^{-1} =
\left(
\begin{array}{cc}
g_+(t) & \frac{q}{p} g_-(t) \\
\frac{p}{q} g_-(t) & g_+(t)
\end{array}
\right)
\tag{30}
$$

with

$$
\begin{aligned}
g_+(t) &= e^{-imt}\, e^{-\Gamma t/2} \left[\cosh\frac{\Delta\Gamma\, t}{4} \cos\frac{\Delta M\, t}{2} - i \sinh\frac{\Delta\Gamma\, t}{4} \sin\frac{\Delta M\, t}{2} \right], \\
g_-(t) &= e^{-imt}\, e^{-\Gamma t/2} \left[-\sinh\frac{\Delta\Gamma\, t}{4} \cos\frac{\Delta M\, t}{2} + i \cosh\frac{\Delta\Gamma\, t}{4} \sin\frac{\Delta M\, t}{2} \right].
\end{aligned}
\tag{31}
$$

Inserting Eq. (30) into Eq. (28) gives us a transparent picture of the meson-antimeson oscillations:

$$
\begin{aligned}
|M(t)\rangle &= g_+(t)\,|M\rangle + \frac{q}{p}\, g_-(t)\,|\overline{M}\rangle\,, \\
|\overline{M}(t)\rangle &= \frac{p}{q}\, g_-(t)\,|M\rangle + g_+(t)\,|\overline{M}\rangle\,,
\end{aligned}
\tag{32}
$$

We verify $g_+(0) = 1$ and $g_-(0) = 0$ and find that $g_\pm(t)$ has no zeros for $t > 0$ if $\Delta\Gamma \neq 0$. Hence an initially produced M will never turn into a pure $\overline{M}$ or back into a pure M. We will frequently encounter the combinations

$$
\begin{aligned}
|g_\pm(t)|^2 &= \frac{e^{-\Gamma t}}{2} \left[\cosh\frac{\Delta\Gamma\, t}{2} \pm \cos\left(\Delta M\, t\right) \right], \\
g_+^*(t)\, g_-(t) &= \frac{e^{-\Gamma t}}{2} \left[-\sinh\frac{\Delta\Gamma\, t}{2} + i \sin\left(\Delta M\, t\right) \right].
\end{aligned}
\tag{33}
$$

2.2 ΔM, $\Delta\Gamma$ and CP violation in mixing

We still need to solve our eigenvalue problem. The secular equation for the two eigenvalues $\sigma_{L,H} = M_{L,H} - i\Gamma_{L,H}/2$ of Σ is $(\Sigma_{11} - \sigma_{L,H})^2 - \Sigma_{12}\Sigma_{21} = 0$. The two solutions of this equation therefore satisfy

$$
(\sigma_H - \sigma_L)^2 = 4\,\Sigma_{12}\Sigma_{21}
$$

or

$$
(\Delta M + i\frac{\Delta\Gamma}{2})^2 = 4 \left(M_{12} - i\frac{\Gamma_{12}}{2} \right) \left(M_{12}^* - i\frac{\Gamma_{12}^*}{2} \right).
\tag{34}
$$

Taking real and imaginary part of this equation leads us to

$$(\Delta M)^2 - \frac{1}{4}(\Delta\Gamma)^2 \quad = \quad 4\,|M_{12}|^2 - |\Gamma_{12}|^2\,, \tag{35}$$

$$\Delta M\,\Delta\Gamma \quad = \quad -4\,\mathrm{Re}\,(M_{12}\Gamma_{12}^*)\,, \tag{36}$$

Further Eq. (26) implies $[Q^{-1}\Sigma Q]_{12} = [Q^{-1}\Sigma Q]_{21} = 0$, which determines

$$\frac{q}{p} \quad = \quad -\frac{\Delta M + i\,\Delta\Gamma/2}{2M_{12} - i\,\Gamma_{12}} = -\frac{2M_{12}^* - i\,\Gamma_{12}^*}{\Delta M + i\,\Delta\Gamma/2}\,. \tag{37}$$

(There is also a second solution with the opposite sign, which, however, is eliminated by imposing $\Delta M > 0$.) For the simplification of Eqs. (35–37) it is useful to identify the physical quantities of the mixing problem in Eqs. (22) and (23). In quantum mechanics we can always multiply either $|M\rangle$ or $|\overline{M}\rangle$ by an arbitrary phase factor without changing the physics. This will change the phases of M_{12}, Γ_{12} and q/p, none of which can therefore have any physical meaning. The three physical quantities of meson-antimeson mixing are

$$|M_{12}|, \qquad\quad |\Gamma_{12}|, \qquad \text{and} \quad \phi = \arg\left(-\frac{M_{12}}{\Gamma_{12}}\right). \tag{38}$$

Eq. (36) then reads

$$\Delta M\,\Delta\Gamma \quad = \quad 4\,|M_{12}||\Gamma_{12}|\cos\phi. \tag{39}$$

We can easily solve Eqs. (35) and (39) to express ΔM and $\Delta\Gamma$, which we want to measure by studying meson time evolutions, in terms of the theoretical quantities $|M_{12}|$, $|\Gamma_{12}|$ and ϕ. We recognise that the phase ϕ is responsible for CP violation in mixing introduced after Eq. (17): By multiplying the two expression for q/p in Eq. (37) with each other we find

$$\left(\frac{q}{p}\right)^2 \quad = \quad \frac{2M_{12}^* - i\,\Gamma_{12}^*}{2M_{12} - i\,\Gamma_{12}} \quad = \quad \frac{M_{12}^*}{M_{12}}\,\frac{1 + i\left|\dfrac{\Gamma_{12}}{2M_{12}}\right|e^{i\phi}}{1 + i\left|\dfrac{\Gamma_{12}}{2M_{12}}\right|e^{-i\phi}}. \tag{40}$$

We immediately verify from this expression that $\phi \neq 0, \pi$ indeed implies $|q/p| \neq 1$, which defines CP violation in mixing.

Interestingly, CP violation in mixing is small (if quantified in terms of $|q/p| - 1$) for the K, B_d and B_s systems. For $D-\overline{D}$ mixing this is most likely also the case, but the experimental data are not accurate enough at present. In the case of $K-\overline{K}$ mixing we have established this phenomenon in Eq. (17) from the measured value of $\mathrm{Re}\,\epsilon_K$ in Eq. (16). In the $B-\overline{B}$ systems the line of arguments is as follows: Experimentally we know $\Delta M \gg \Delta\Gamma$ and theoretically $|\Gamma_{12}| \ll \Delta M$ is firmly established from a SM calculation, since the possible impact of new physics on $|\Gamma_{12}|$ is small. Then Eqs. (35) and (39) imply $\Delta M \approx 2|M_{12}|$ and therefore $|\Gamma_{12}| \ll |M_{12}|$, so that the second term in the numerator and denominator of Eq. (40) is small, irrespective of the value of ϕ. Thus $|q/p| \simeq 1$ for B_d and B_s mesons. It is useful to define the quantity a through

$$\left|\frac{q}{p}\right|^2 \quad = \quad 1 - a. \tag{41}$$

For the K, B_d and B_s systems we know that a is small. By expanding $(q/p)^2$ in Eq. (40) in terms of ϕ or Γ_{12}/M_{12} we find

$$
\begin{aligned}
a &= \frac{4|\Gamma_{12}|\,|M_{12}|}{4|M_{12}|^2 + |\Gamma_{12}|^2}\,\phi + \mathcal{O}(\phi^2), && \text{for } K-\overline{K}\text{ mixing} && (42) \\
a &= \operatorname{Im}\frac{\Gamma_{12}}{M_{12}} + \mathcal{O}\left(\left(\operatorname{Im}\frac{\Gamma_{12}}{M_{12}}\right)^2\right) = \left|\frac{\Gamma_{12}}{M_{12}}\right|\sin\phi\,, && \text{for } B-\overline{B}\text{ mixing.} && (43)
\end{aligned}
$$

With this result it is straightforward to solve Eqs. (35) and (39) for ΔM and $\Delta\Gamma$. Incidentally, in both cases we have

$$
\begin{aligned}
\Delta M &\simeq 2\,|M_{12}|, && (44) \\
\Delta\Gamma &\simeq 2\,|\Gamma_{12}|\cos\phi. && (45)
\end{aligned}
$$

which holds up to corrections of order ϕ^2 for Kaons and of order $|\Gamma_{12}/M_{12}|^2$ for B mesons. Of course, in the former case one can also replace $\cos\phi$ by 1. Importantly, in B physics one deduces from Eq. (37) that

$$
\frac{q}{p} = -\frac{M_{12}^*}{|M_{12}|}\,[1 + \mathcal{O}(a)]. \qquad (46)
$$

That is, the phase of $-q/p$ is essentially given by the phase of the $B_d-\overline{B}_d$ or $B_s-\overline{B}_s$ box diagram in Fig. 1. Since $B-\overline{B}$ mixing is dominated by the box diagram with internal tops we readily infer

$$
\frac{q}{p} = -\frac{V_{tb}^* V_{tq}}{V_{tb} V_{tq}^*} = -\exp[i\arg(V_{tb}^* V_{tq})^2] \qquad \text{for } B_q-\overline{B}_q\text{ mixing with } q = d, s \quad (47)
$$

up to tiny corrections of order a.

2.3 Time-dependent decay rates

Flavour factories are e^+e^- colliders whose CMS energy matches the mass of an excited quarkonium state which predominantly decays into $(M, \overline{M})$ pairs. Running on the $\psi(3770)$, $\Upsilon(4S)$ or $\Upsilon(5S)$ resonances, one copiously produces $(D, \overline{D})$, $(B_d, \overline{B}_d)$ or $(B_s, \overline{B}_s)$ mesons. The $(M, \overline{M})$ pairs are in an entangled quantum-mechanical state until the decay of one of the mesons is observed. If the decay mode $M \to f$ is allowed while $\overline{M} \to f$ is forbidden one calls $M \to f$ a *flavour-specific* mode or a *tagging mode*. The most prominent examples are the semileptonic decays $M \to X\ell^+\nu_\ell$. For the discovery of $B_s-\overline{B}_s$ mixing the flavour-specific mode $B_s \to D_s^-\pi^+$ has played an important role [14]. A flavour-specific decay tags the decaying meson as either M or $\overline{M}$. The Einstein-Podolsky-Rosen effect then ensures that the other meson is an $\overline{M}$ or M, respectively. The time of the flavour tagging "starts the clock", i.e. defines $t = 0$ in Eqs. (31) and (32). This method is called *opposite-side tagging*. In hadron colliders pairs of different hadrons can be produced, e.g. a B_s can be produced together with a B^- or Λ_b plus several lighter hadrons. Still, at the quark level $(\overline{b}, b)$ pairs are produced, so that the flavour tagging works as well. As an additional possibility, hadron colliders permit *same-side tagging*, where the flavour is determined at the time of the hadronisation process: When, say, a b-quark hadronises into a $\overline{B}$ meson several pions and Kaons are produced as well. The charges of these light mesons

are correlated with the charge of the light valence quark, which in the case of the $\overline{B}$ meson is an anti-d quark.

The time-dependent decay rate of a meson tagged at $t = 0$ as M is defined as

$$\Gamma(M(t) \to f) = \frac{1}{N_M} \frac{d\,N(M(t) \to f)}{d\,t}\,, \tag{48}$$

where $d\,N(M(t) \to f)$ denotes the number of decays into the final state f occurring within the time interval between t and $t + d\,t$. N_M is the total number of M's produced at time $t = 0$. An analogous definition holds for $\Gamma(\overline{M}(t) \to f)$. One has

$$\Gamma(M(t) \to f) = \mathcal{N}_f \left| \langle f | S | M(t) \rangle \right|^2, \qquad \Gamma(\overline{M}(t) \to f) = \mathcal{N}_f \left| \langle f | S | \overline{M}(t) \rangle \right|^2 \tag{49}$$

with the time-independent normalisation factor $\mathcal{N}_f$ comprising the result of the phase-space integration. It is straightforward to calculate $\Gamma(M(t) \to f)$ and $\Gamma(\overline{M}(t) \to f)$ in terms of A_f and $\overline{A}_f$ defined in Eq. (12), we just need to insert $|M(t)\rangle$ and $|\overline{M}(t)\rangle$ from Eq. (32) into Eq. (49). Trading $\overline{A}_f$ for λ_f (see Eq. (13)) and a (see Eq. (41)) and making use of Eq. (33) we find the desired formulae:

$$\Gamma(M(t) \to f) = \mathcal{N}_f |A_f|^2 e^{-\Gamma t} \left\{ \frac{1 + |\lambda_f|^2}{2} \cosh \frac{\Delta\Gamma\, t}{2} + \frac{1 - |\lambda_f|^2}{2} \cos(\Delta M\, t) \right.$$
$$\left. - \mathrm{Re}\,\lambda_f\, \sinh \frac{\Delta\Gamma\, t}{2} - \mathrm{Im}\,\lambda_f\, \sin(\Delta M\, t) \right\}, \tag{50}$$

$$\Gamma(\overline{M}(t) \to f) = \mathcal{N}_f |A_f|^2 \frac{1}{1 - a} e^{-\Gamma t} \left\{ \frac{1 + |\lambda_f|^2}{2} \cosh \frac{\Delta\Gamma\, t}{2} - \frac{1 - |\lambda_f|^2}{2} \cos(\Delta M\, t) \right.$$
$$\left. - \mathrm{Re}\,\lambda_f\, \sinh \frac{\Delta\Gamma\, t}{2} + \mathrm{Im}\,\lambda_f\, \sin(\Delta M\, t) \right\}. \tag{51}$$

Often we want to compare these decay modes with the corresponding decays into the final state which is CP-conjugate with respect to f. For states f with two or more particles we define

$$|\overline{f}\rangle = CP\,|f\rangle\,, \tag{52}$$

while for the initial one-particle states we have defined CP in Eq. (9). For example, for $f = D_s^- \pi^+$ the CP-conjugate state is $\overline{f} = D_s^+ \pi^-$. Whenever we discuss CP (or any other discrete transformation) in decay processes, we apply the transformation in the rest frame of the decaying meson. The transformation in Eq. (52) is understood to reverse the signs of three-momenta as in Eq. (9). For two-body final states, which are our prime focus, we can rotate this mirror-reflected state by $180°$, so that the three-momenta of the rotated CP-transformed state coincide with those of the original state. This procedure is usually implicitly understood when people discuss decays into CP eigenstates composed of two distinct particles, such as $K \to \pi^+ \pi^-$. For a CP eigenstate f_{CP} Eqs. (10) and (52) imply $|\overline{f}_{\mathrm{CP}}\rangle = \eta_{f_{CP}} |f_{\mathrm{CP}}\rangle$.

In the $M(t) \to \overline{f}$ decay rates it is advantageous to keep $\overline{A}_{\overline{f}}$ while trading $A_{\overline{f}}$ for $\lambda_{\overline{f}}$:

$$
\begin{aligned}
\Gamma(M(t) \to \overline{f}) \;=\; & \mathcal{N}_f \left| \overline{A}_{\overline{f}} \right|^2 e^{-\Gamma t} (1-a) \left\{ \frac{1 + |\lambda_{\overline{f}}|^{-2}}{2} \cosh \frac{\Delta \Gamma \, t}{2} - \frac{1 - |\lambda_{\overline{f}}|^{-2}}{2} \cos(\Delta M \, t) \right. \\
& \left. - \mathrm{Re}\, \frac{1}{\lambda_{\overline{f}}} \sinh \frac{\Delta \Gamma \, t}{2} + \mathrm{Im}\, \frac{1}{\lambda_{\overline{f}}} \sin(\Delta M \, t) \right\} ,
\end{aligned} \tag{53}
$$

$$
\begin{aligned}
\Gamma(\overline{M}(t) \to \overline{f}) \;=\; & \mathcal{N}_f \left| \overline{A}_{\overline{f}} \right|^2 e^{-\Gamma t} \left\{ \frac{1 + |\lambda_{\overline{f}}|^{-2}}{2} \cosh \frac{\Delta \Gamma \, t}{2} + \frac{1 - |\lambda_{\overline{f}}|^{-2}}{2} \cos(\Delta M \, t) \right. \\
& \left. - \mathrm{Re}\, \frac{1}{\lambda_{\overline{f}}} \sinh \frac{\Delta \Gamma \, t}{2} - \mathrm{Im}\, \frac{1}{\lambda_{\overline{f}}} \sin(\Delta M \, t) \right\} .
\end{aligned} \tag{54}
$$

Eqs. (50–51) and Eqs. (53–54) are our master formulae to calculate any time-dependent decay rate of interest. We discuss two important applications here. The first one is the time dependence of a flavour-specific decay, which satisfies $\overline{A}_f = A_{\overline{f}} = \lambda_f = 1/\lambda_{\overline{f}} = 0$. In addition we consider a decay mode with $|\overline{A}_{\overline{f}}| = |A_f|$, that is without direct CP violation. Semileptonic decays satisfy both conditions. Our master formulae become very simple for this case. Defining the *mixing asymmetry*,

$$
\mathcal{A}_0(t) = \frac{\Gamma(M(t) \to f) - \Gamma(M(t) \to \overline{f})}{\Gamma(M(t) \to f) + \Gamma(M(t) \to \overline{f})} , \tag{55}
$$

one finds to order a:

$$
\mathcal{A}_0(t) = \frac{\cos(\Delta M \, t)}{\cosh(\Delta \Gamma \, t/2)} + \frac{a}{2} \left[1 - \frac{\cos^2(\Delta M \, t)}{\cosh^2(\Delta \Gamma \, t/2)} \right] . \tag{56}
$$

Note that $\mathcal{A}_0(t)$ is not a *CP* asymmetry. Instead $\Gamma(M(t) \to f) \propto |\langle M | M(t) \rangle|^2$ is proportional to the probability that an "unmixed" M decays to f at time t, while $\Gamma(M(t) \to \overline{f}) \propto |\langle \overline{M} | M(t) \rangle|^2$ is the corresponding probability for the process $M \to \overline{M} \to f$. The asymmetry $\mathcal{A}_0(t)$ is often employed to measure ΔM. In the ARGUS discovery of $B_d - \overline{B}_d$ mixing [7] no time-dependence was observed. Instead so-called like-sign dilepton events were observed in semileptonic $(B_d, \overline{B}_d)$ decays, meaning that one of the two mesons must have mixed. By counting these events and comparing the number with the number of opposite-sign dilepton events one can infer the quantity $x = \Delta M / \Gamma$. The corresponding formula can be found by integrating our master formulae over t.

The *CP asymmetry in flavour-specific decays* (often called *semileptonic CP asymmetry*) reads

$$
a_{\mathrm{fs}} \;\equiv\; \frac{\Gamma(\overline{M}(t) \to f) - \Gamma(M(t) \to \overline{f})}{\Gamma(\overline{M}(t) \to f) + \Gamma(M(t) \to \overline{f})} \;=\; \frac{1 - (1-a)^2}{1 + (1-a)^2} \;=\; a + \mathcal{O}(a^2). \tag{57}
$$

Define the untagged decay rate

$$
\Gamma[f, t] \;=\; \Gamma(\overline{M}(t) \to f) + \Gamma(M(t) \to f) \tag{58}
$$

to find:

$$
a_{\mathrm{fs,unt}}(t) \;=\; \frac{\Gamma[f, t] - \Gamma[\overline{f}, t]}{\Gamma[f, t] + \Gamma[\overline{f}, t]} \;=\; \frac{a_{\mathrm{fs}}}{2} - \frac{a_{\mathrm{fs}}}{2} \frac{\cos(\Delta M \, t)}{\cosh(\Delta \Gamma t/2)}. \tag{59}
$$

Hence no tagging is needed to measure $a_{\rm fs}$! We observe that we can determine the three physical quantities characterising meson-antimeson mixing, $|M_{12}|$, $|\Gamma_{12}|$ and a, by measuring ΔM, $\Delta\Gamma$ and $a_{\rm fs}$. At present all three quantities are only measured for $K-\overline{K}$ mixing! Also the semileptonic CP asymmetry of B mesons can be measured without observing any time dependence. In the spirit of ARGUS we can compare the number of positively-charged like-sign dilepton pairs with the number of negatively-charged ones. Such measurements are performed at the B factories and the Tevatron, but no non-zero semileptonic CP asymmetry has been established by now.

Amusingly, the oscillations drop out from the tagged quantity in Eq. (57), while they persist in Eq. (59). In most applications one can neglect the tiny a in Eqs. (50–51) and Eqs. (53–54). Then we realise that in the untagged rates, obtained by adding Eqs. (50) and (51) or Eqs. (53) and (54), the terms involving $\cos(\Delta M t)$ and $\sin(\Delta M t)$ vanish.

The second application of our master formulae are decays into CP eigenstates, $M \to f_{\rm CP}$. The time-dependent CP asymmetry is

$$a_{f_{\rm CP}}(t) = \frac{\Gamma(\overline{M}(t) \to f_{\rm CP}) - \Gamma(M(t) \to f_{\rm CP})}{\Gamma(\overline{M}(t) \to f_{\rm CP}) + \Gamma(M(t) \to f_{\rm CP})} \,. \tag{60}$$

Using Eq. (50) and Eq. (51) one finds

$$a_{f_{\rm CP}}(t) = -\frac{A_{CP}^{\rm dir} \cos(\Delta M t) + A_{CP}^{\rm mix} \sin(\Delta M t)}{\cosh(\Delta\Gamma t/2) + A_{\Delta\Gamma} \sinh(\Delta\Gamma t/2)} + \mathcal{O}(a) \,, \tag{61}$$

with (for $f = f_{\rm CP}$)

$$A_{CP}^{\rm dir} = \frac{1 - |\lambda_f|^2}{1 + |\lambda_f|^2} \,, \qquad A_{CP}^{\rm mix} = -\frac{2\,{\rm Im}\,\lambda_f}{1 + |\lambda_f|^2} \,, \qquad A_{\Delta\Gamma} = -\frac{2\,{\rm Re}\,\lambda_f}{1 + |\lambda_f|^2}. \tag{62}$$

Note that $|A_{CP}^{\rm dir}|^2 + |A_{CP}^{\rm mix}|^2 + |A_{\Delta\Gamma}|^2 = 1$. Experimentally one can track the time-dependence of $a_f(t)$ and read off the coefficients of $\cos(\Delta M t)$ and $\sin(\Delta M t)$, so that one can determine $|\lambda_f|$ and ${\rm Im}\,\lambda_f$. When studying decay amplitudes we can treat the weak interaction perturbatively by drawing quark-level Feynman diagrams involving the exchange of W-bosons. While we cannot fully compute those diagrams, because we cannot estimate how the quarks are "dressed" by the strong interaction, we can still assess the CP-violating phases by identifying the CKM elements in the diagrams. Decays in which all contributing Feynman diagrams carry the same CP-violating phase are called *golden modes*. These modes satisfy $|A_f| = |\overline{A}_{\overline{f}}|$, so that there is no direct CP violation. In a golden $M \to f_{\rm CP}$ decay this means $|\lambda_{f_{\rm CP}}| = 1$ and in Eqs. (61) and (62) we have $A_{CP}^{\rm dir} = 0$ and

$$A_{CP}^{\rm mix} = {\rm Im}\,\lambda_{f_{\rm CP}}. \tag{63}$$

Moreover the phase of $\overline{A}_{f_{\rm CP}}/A_{f_{\rm CP}}$ is trivially read off from the phase of the CKM elements. In B physics, where we also know the phase of q/p from Eq. (47), we can therefore directly relate the measured ${\rm Im}\,\lambda_{f_{\rm CP}}$ to phases of CKM elements, if $M \to f_{\rm CP}$ is golden.

3 Third lecture: Linking quarks to mesons

3.1 The Cabibbo-Kobayashi-Maskawa matrix

We have encountered the CKM matrix V in Eq. (3). A unitary 3×3 matrix can be parameterised by three angles and six complex phases. With the rephasings in Eqs. (7) and (8) we can eliminate

five phases from V leaving us with one physical CP-violating phase. In the parameterisation favoured by the Particle Data Book one has

$$
V = \begin{pmatrix}
c_{12}c_{13} & s_{12}c_{13} & s_{13}e^{-i\delta_{13}} \\
-s_{12}c_{23} - c_{12}s_{23}s_{13}e^{i\delta_{13}} & c_{12}c_{23} - s_{12}s_{23}s_{13}e^{i\delta_{13}} & s_{23}c_{13} \\
s_{12}s_{23} - c_{12}c_{23}s_{13}e^{i\delta_{13}} & -c_{12}s_{23} - s_{12}c_{23}s_{13}e^{i\delta_{13}} & c_{23}c_{13}
\end{pmatrix}, \tag{64}
$$

where $c_{ij} = \cos\theta_{ij}$ and $s_{ij} = \sin\theta_{ij}$. The real angles θ_{ij} may be chosen so that $0 \leq \theta_{ij} \leq \pi/2$, and the phase δ_{13} so that $-\pi < \delta_{13} \leq \pi$. For the discussion of CKM metrology it is useful to introduce the Wolfenstein parameterisation [15]

$$
V = \begin{pmatrix}
1 - \frac{1}{2}\lambda^2 & \lambda & A\lambda^3(\rho - i\eta) \\
-\lambda & 1 - \frac{1}{2}\lambda^2 & A\lambda^2 \\
A\lambda^3(1 - \rho - i\eta) & -A\lambda^2 & 1
\end{pmatrix} + O(\lambda^4), \tag{65}
$$

which is an expansion in terms of the small parameter $\lambda = 0.22$. The remaining three parameters A, ρ and η are a bit smaller than 1. The Wolfenstein parameterisation nicely reveals the hierarchical structure of the CKM matrix, with diagonal elements of order 1 and smallest elements in the upper right and lower left corners. We can now understand why the prediction of m_c from ΔM_K in 1974 was successful: Any contribution involving the top quark (at that time unknown and unimagined by the authors of Ref. [3]) to the upper left diagram in Fig. 1 is highly suppressed by small CKM elements, since $|V_{td}V_{ts}| \simeq \lambda^5$, while $|V_{cd}V_{cs}| \simeq |V_{ud}V_{us}| \simeq \sin\theta_c \simeq \lambda$. Further the upper left 2×2 submatrix, the Cabibbo matrix, is almost unitary and involves only a single parameter, the Cabibbo angle θ_c with $V_{ud} \simeq V_{cs} \simeq \cos\theta_c$ and $V_{us} \simeq -V_{cd} \simeq \lambda$. Therefore the two new elements V_{cd} and V_{cs} predicted in Ref. [2] were completely fixed in terms of the known θ_c. In the Wolfenstein approximation only V_{ub} and V_{td} have a complex phase and CP violation is characterised by $\eta \neq 0$.

Any unitary 3×3 matrix satisfies

$$
V_{1j}^* V_{1k} + V_{2j}^* V_{2k} + V_{3j}^* V_{3k} = \delta_{jk} \tag{66}
$$

$$
\text{and} \qquad V_{j1}^* V_{k1} + V_{j2}^* V_{k2} + V_{j3}^* V_{k3} = \delta_{jk}. \tag{67}
$$

If we choose $j \neq k$ the three terms add to zero. We can depict the relations in Eqs. (66) and (67) as triangles in the complex plane, e.g. for Eq. (66) the three corners are located at 0, $V_{1j}^* V_{1k}$ and $-V_{2j}^* V_{2k}$. The three sides can be associated with the three terms summing to zero. The area of all six triangles is the same and given by $J/2$, where J is the *Jarlskog invariant* [16]

$$
J \equiv \text{Im}\left[V_{td}^* V_{tb} V_{ub}^* V_{ud}\right] = c_{12}c_{23}c_{13}^2 s_{12}s_{23}s_{13}\sin\delta_{13} \simeq A^2\lambda^6\eta. \tag{68}
$$

Here the third expression refers to the exact parameterisation of Eq. (64) and the last result uses the Wolfenstein approximation. Four of the six *unitarity triangles* are squashed, the three sides are similar only for the choice $(j,k) = (3,1)$. Moreover, within the Wolfenstein approximation the shapes of the triangles corresponding to Eqs. (66) and (67) are equal for $(j,k) = (3,1)$. Applying the phase transformations of Eqs. (7) and (8) rotates the unitarity triangles in the complex plane, but leaves their shape fixed. Seeking a definition of a rephasing-invariant unitarity triangle with a physical meaning we divide Eq. (66) (for $(j,k) = (3,1)$) by $V_{23}^* V_{21} = V_{cb}^* V_{cd}$ to arrive at

$$
\frac{V_{ub}^* V_{ud}}{V_{cb}^* V_{cd}} + \frac{V_{tb}^* V_{td}}{V_{cb}^* V_{cd}} + 1 = 0 \tag{69}
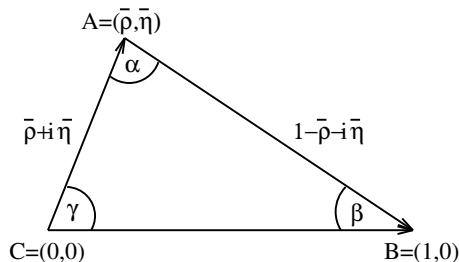$$

Figure 3: The (standard) unitarity triangle.

When people speak of "the" unitarity triangle they refer to the rescaled triangle defined by Eq. (69). Since its baseline coincides with the interval $[0, 1]$ of the real axis, the unitarity triangle is completely determined by the location of its apex $(\overline{\rho}, \overline{\eta})$, where

$$\overline{\rho} + i\overline{\eta} \equiv -\frac{V_{ub}^* V_{ud}}{V_{cb}^* V_{cd}}. \tag{70}$$

Inserting Eq. (65) into Eq. (70) one realises that $(\overline{\rho}, \overline{\eta}) = (\rho, \eta)$ within the Wolfenstein approximation, which here is good to an accuracy of 3%. The unitarity triangle is depicted in Fig. 3. The two non-trivial sides of the triangle are

$$R_u \equiv \sqrt{\overline{\rho}^2 + \overline{\eta}^2}, \qquad R_t \equiv \sqrt{(1 - \overline{\rho})^2 + \overline{\eta}^2}. \tag{71}$$

CP-violating quantities are associated with the triangle's three angles

$$\alpha = \arg\left[-\frac{V_{td}V_{tb}^*}{V_{ud}V_{ub}^*}\right], \qquad \beta = \arg\left[-\frac{V_{cd}V_{cb}^*}{V_{td}V_{tb}^*}\right], \qquad \gamma = \arg\left[-\frac{V_{ud}V_{ub}^*}{V_{cd}V_{cb}^*}\right]. \tag{72}$$

The angle γ coincides with δ_{13} of Eq. (64) at the sub-permille level. With Eqs. (70–72) one obtains

$$\overline{\rho} + i\overline{\eta} = R_u e^{i\gamma}, \qquad 1 - \overline{\rho} - i\overline{\eta} = R_t e^{-i\beta}. \tag{73}$$

The unitarity relation of Eq. (69) now simply reads

$$R_u e^{i\gamma} + R_t e^{-i\beta} = 1 \tag{74}$$

Taking real and imaginary parts of Eq. (74) reproduces formulae which you know from high-school geometry, allowing us to express any two of the four quantities R_u, R_t, γ, β in terms of the remaining two ones. By multiplying Eq. (74) with either $\exp(-i\gamma)$ or $\exp(i\beta)$ one finds analogous relations involving $\alpha = \pi - \beta - \gamma$.

Sometimes one needs to refine the Wolfenstein approximation to higher orders in λ. It is prudent to define [17]

$$\lambda \equiv s_{12}, \qquad A\lambda^2 \equiv s_{23} \tag{75}$$

to all orders in λ and to expand all CKM elements in terms of λ, A, $\overline{\rho}$ and $\overline{\eta}$ to the desired order in λ. Then, for example:

$$V_{ub} \quad = \quad A\lambda^3(\overline{\rho} - i\overline{\eta})\left(1 + \frac{\lambda^2}{2} + \mathcal{O}(\lambda^4)\right). \tag{76}$$

The phase

$$\beta_s = \arg\left[-\frac{V_{ts}V_{tb}^*}{V_{cs}V_{cb}^*}\right] = \lambda^2\overline{\eta} + O(\lambda^4) \tag{77}$$

plays an important role in $B_s - \overline{B}_s$ mixing; β_s is small, of order 0.02 (equal to 1 degree). In the phase convention of Eq. (64) the phase of $V_{cs}V_{cb}^*$ is $\mathcal{O}(\lambda^6)$ and

$$\arg(-V_{ts}) = \beta_s(1 + O(\lambda^2)). \tag{78}$$

Organising the phases in powers of λ, we find all CKM elements real to order λ^2 except for V_{ub}, V_{td} and V_{ts}. Going to higher orders one encounters $\arg(-V_{cd}) \simeq A^2\overline{\eta}\lambda^4$ and $\arg(V_{cs}) \simeq -A^2\overline{\eta}\lambda^6$.

3.2 Effective Hamiltonians

We now address the strong interaction, which is the main obstacle on our way from quark diagrams to mesonic amplitudes like M_{12} and $A(M \to f)$. In Sect. 1.1 we have seen that weak processes of mesons are multi-scale processes. For instance, $B - \overline{B}$ mixing involves three largely separated scales, since $m_t \sim M_W \gg m_b \gg \Lambda_{\text{QCD}}$. These scales must be disentangled to separate the short-distance QCD, which is described by the exchange of quarks and gluons, from the long-distance hadronic physics, whose characteristic property is the confinement of quarks into hadrons. The key tool to separate the physics associated with the scale m_{heavy} from the dynamics associated with $m_{\text{light}} \ll m_{\text{heavy}}$ is the construction of an *effective field theory*. The corresponding *effective Hamiltonian* H^{eff} is designed to reproduce the S-matrix elements of the Standard Model up to corrections of order $(m_{\text{light}}/m_{\text{heavy}})^n$ where n is a positive integer:

$$\langle f|\mathbf{T}e^{-i\int d^4x H_{\text{int}}^{\text{SM}}(x)}|i\rangle \quad = \quad \langle f|\mathbf{T}e^{-i\int d^4x H^{\text{eff}}(x)}|i\rangle\left[1 + \mathcal{O}\left(\frac{m_{\text{light}}}{m_{\text{heavy}}}\right)^n\right] \tag{79}$$

I exemplify the method with an effective Hamiltonian which reproduces the amplitude for $B - \overline{B}$ mixing up to corrections of order m_b^2/M_W^2. That is, we employ Eq. (79) for the case $i = \overline{B}$ and $f = B$ (where $B = B_d$ or B_s), $m_{\text{light}} = m_b$ and $m_{\text{heavy}} = M_W \sim m_t$. The corresponding effective Hamiltonian reads

$$H^{\text{eff}} \quad = \quad H^{\text{QCD(f=5)}} + H^{\text{QED(f=5)}} + H^{|\Delta B|=2}. \tag{80}$$

Here the first two terms are the usual QCD and QED interaction Hamiltonians with 5 "active flavours", meaning that they do not involve the top quark. The last term describes the weak interaction. Adapted to the process under study, $H^{|\Delta B|=2}$ only encodes the physics related to $B - \overline{B}$ mixing, but does not describe other weak processes such as meson decays. It is called $H^{|\Delta B|=2}$, because it describes physical processes in which the bottom quantum number B changes by two units. $H^{|\Delta B|=2}$ does not contain W-boson, Z-boson or top-quark fields, instead the $\Delta B = 2$ transition of the box diagram in Fig. 1 is mediated by an effective four-quark coupling:

$$Q \quad = \quad \overline{q}_L\gamma_\nu b_L\,\overline{q}_L\gamma^\nu b_L \qquad \text{with } q = d \text{ or } s. \tag{81}$$
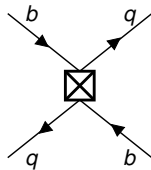
Figure 4: The four-quark operator Q for $B_q - \overline{B}_q$ mixing with $q = d$ or s.

For historical reasons Q is called a *four-quark operator*, but it is nothing but a point-like coupling of four quark fields as shown in Fig. 4. We have

$$H^{|\Delta B|=2} = \frac{G_F^2}{4\pi^2} \left(V_{tb} V_{tq}^*\right)^2 C^{|\Delta B|=2}(m_t, M_W, \mu)\, Q(\mu) + h.c. \tag{82}$$

where the lengthy expression multiplying Q is just the effective coupling constant multiplying the four-quark interaction of Fig. 4. This coupling constant is split into several factors, the first of which contains the Fermi constant G_F. The second factor summarises the CKM elements of the box diagram and the third factor $C^{|\Delta B|=2}(m_t, M_W, \mu)$ is the *Wilson coefficient*, which contains the information on the heavy mass scales M_W and m_t. Finally μ is the renormalisation scale, familiar from QCD. Just as any other coupling also Q must be renormalised. The renormalised operator Q depends on μ through the renormalisation constant $Z_Q(\mu)$ via $Q = Z_Q Q^{\text{bare}}$ and (in a mass-independent scheme like $\overline{\text{MS}}$) the latter dependence is only implicit through $g(\mu)$, where g is the QCD coupling constant.[3] With the decomposition in Eq. (82) $C^{|\Delta B|=2}$ has dimension two and is real.

$C^{|\Delta B|=2}$ is calculated from the defining property of H^{eff} in Eq. (79): We compute the $\Delta B = 2$ process both in the Standard Model and with the interactions of H^{eff} and adjust $C^{|\Delta B|=2}$ such that the two results are the same, up to corrections of order m_b^2/M_W^2. Obviously we cannot do this with mesons as external states i and f. But a crucial property of H^{eff} is the independence of the Wilson coefficient on the external states. We can compute it for an arbitrary momentum configuration for the external quarks as long as the external momenta are of the order of m_{light}. That is, we do not need to know the complicated momentum configuration of quarks bound in a meson state. Further all QCD effects in $C^{|\Delta B|=2}$ are purely perturbative:

$$C^{|\Delta B|=2} = C^{|\Delta B|=2,(0)} + \frac{\alpha_s(\mu)}{4\pi} C^{|\Delta B|=2,(1)} + \dots \tag{83}$$

We can understand why and how this works if we expand the result of the box diagram of Fig. 1 in terms of the momenta of the external quarks, which are at most of order m_b. The leading term consists of the result of a loop integral with external momenta set to zero and the spinors of the external quark states. Now the "effective theory side" of Eq. (79) involves the tree-level

---

[3]The analogy with the renormalisation of the QCD coupling constant is more obvious if one reads the product $C Z_Q Q^{\text{bare}}$ in a different way: By assigning Z_Q to C rather than Q one may view C as a renormalised coupling constant. The notion of a "renormalised" operator instead of a "renormalised Wilson coefficient" has historical reasons.

diagram corresponding to

$$\langle f|\mathbf{T}e^{-i\int d^4 x H^{\mathrm{eff}}(x)}|i\rangle^{(0)} \quad \simeq \quad -i\int d^4 x \langle f|H^{\mathrm{eff}}(x)|i\rangle^{(0)} \;=\; -i\int d^4 x \langle f|H^{|\Delta B|=2}(x)|i\rangle^{(0)}$$

$$= \quad -i(2\pi)^4 \delta^{(4)}(p_f - p_i)\, \frac{G_F^2}{4\pi^2}\, (V_{tb}V_{tq}^*)^2\, C^{|\Delta B|=2,(0)}\, \langle f|Q|i\rangle^{(0)}$$

where $|i\rangle = |p_b, s_b; p_{\overline{q}}, s_{\overline{q}}\rangle$ and $|f\rangle = |p_q, s_q; p_{\overline{b}}, s_{\overline{b}}\rangle$ are the external states characterised by the momenta and spins of the quarks. The superscript "(0)" indicates the lowest order of QCD everywhere. Since $\langle f|Q|i\rangle$ reproduces the spinor structure ("Dirac algebra") of the box diagram, the coefficient $C^{|\Delta B|=2,(0)}$ inferred from this *matching calculation* is solely determined in terms of the loop integral and therefore only depends on M_W and m_t. The matching calculation becomes less trivial when we go to the *next-to-leading order (NLO)* of QCD. Now H^{QCD} enters the matching calculation and we must dress both the box diagram and the effective diagram in Fig. 4 with gluons in all possible ways. Denoting the SM amplitude by

$$\mathcal{M} \quad = \quad \mathcal{M}^{(0)} + \frac{\alpha_s}{4\pi}\mathcal{M}^{(1)} + \dots, \tag{84}$$

our NLO matching calculation amounts to the determination of $C^{|\Delta B|=2,(1)}$ from

$$-\mathcal{M}^{(0)} - \frac{\alpha_s}{4\pi}\mathcal{M}^{(1)} \quad = \quad \frac{G_F^2}{4\pi^2}\, (V_{tb}V_{tq}^*)^2 \left[C^{|\Delta B|=2,(0)} + \frac{\alpha_s}{4\pi}C^{|\Delta B|=2,(1)} \right]$$

$$\cdot \left[\langle Q\rangle^{(0)} + \frac{\alpha_s}{4\pi}\langle Q\rangle^{(1)} \right] \left[1 + \mathcal{O}\left(\frac{m_b^2}{M_W^2}\right) \right] \;+\; \mathcal{O}\left(\alpha_s^2\right) \tag{85}$$

On the RHS the external states are suppressed for simplicity of notation. The QCD corrections to the box diagram in $\mathcal{M}^{(1)}$ not only depend on the light scales, i.e. external momenta and light quark masses, they also suffer from infrared (IR) divergences. These divergences signal the breakdown of QCD perturbation theory at low energies. However, the gluonic corrections to Fig. 4, which are comprised in $\langle Q\rangle^{(1)}$, exactly reproduce the infrared structure of the SM diagrams: They involve the same IR divergences and have the same dependence on the light mass scales. Collecting the $\mathcal{O}(\alpha_s)$ terms from Eq. (85),

$$-\mathcal{M}^{(1)} \quad = \quad \frac{G_F^2}{4\pi^2}\, (V_{tb}V_{tq}^*)^2 \left[C^{|\Delta B|=2,(0)}\langle Q\rangle^{(1)} + C^{|\Delta B|=2,(1)}\langle Q\rangle^{(0)} \right], \tag{86}$$

one finds identical IR structures on the LHS and in the first term in the square brackets, while $C^{|\Delta B|=2,(1)}$ only contains heavy masses and no IR divergences. In conclusion, the IR structure of the SM amplitude properly factorises with an "infrared-safe" $C^{|\Delta B|=2}$. This success can be understood by separately discussing the regions of small and large loop momentum passing through a gluon line in the diagrams of $\mathcal{M}^{(1)}$. The infrared-sensitive diagrams are identified as those in which the gluon connects two external quark lines. (The other diagrams are infrared-finite and one can set the light mass parameters to zero.) If the loop momentum traversing the gluon line is small, we can neglect it in the heavy top and W propagators. Therefore the loop integration factorises into two one-loop integrations and the second loop integral involving the heavy particles simply reproduces the one-loop result contained in $C^{|\Delta B|=2,(0)}$. The gluon-loop integration —still over soft momenta only— is equal to the one in the corresponding diagram in $\langle Q\rangle^{(1)}$, where the gluon connects the same quark lines. Therefore the region of integration

with a soft gluon factorises with the leading-order coefficient $C^{|\Delta B|=2,(0)}$ in Eq. (85). The region of the momentum integration with a hard gluon momentum does not factorise in this way and contributes to $C^{|\Delta B|=2,(1)}$. However, the region of large gluon loop momentum is not infrared-sensitive and we can neglect the light momenta and masses. Therefore $C^{|\Delta B|=2,(1)}$ does not depend on the light mass scales. Conversely, $\langle Q \rangle$ contains only small scales of order m_{light} and encodes the full infrared structure of $\mathcal{M}$. Therefore our quark-level calculation is meaningful for $C^{|\Delta B|=2}$, but not for $\langle Q \rangle$. In order to make a theoretical prediction for the $B - \overline{B}$ mixing amplitude, we must compute $\langle B|Q|\overline{B} \rangle$ with nonperturbative methods. The factorisation of $\mathcal{M}$ into short-distance coefficients and long-distance operator matrix elements is also called *operator product expansion.*

Here I only derive the result for the leading-order (LO) Wilson coefficient $C^{|\Delta B|=2,(0)}$. In a first step let us decompose $\mathcal{M}^{(0)}$ as

$$\mathcal{M}^{(0)} = \sum_{j,k=u,c,t} V_{jb}^* V_{jq} \, V_{kb}^* V_{kq} \, \mathcal{M}_{jk}^{(0)} \langle Q \rangle^{(0)}, \qquad q = d \text{ or } s, \qquad (87)$$

where $\mathcal{M}_{jk}^{(0)} \langle Q \rangle^{(0)}$ is the result of the box diagram containing internal quark flavours (j, k) with the CKM elements factored out. We then write

$$\mathcal{M}_{jk}^{(0)} = -\frac{G_F^2}{4\pi^2} M_W^2 \, \widetilde{S}(x_j, x_k) \qquad (88)$$

with $x_j = m_j^2/M_W^2$. The function $\widetilde{S}(x_j, x_k)$ is symmetric, $\widetilde{S}(x_j, x_k) = \widetilde{S}(x_k, x_j)$. In the next step we use CKM unitarity to eliminate $V_{ub}^* V_{uq} = -V_{tb}^* V_{tq} - V_{cb}^* V_{cq}$ from Eq. (87):

$$-\mathcal{M}^{(0)} = \frac{G_F^2}{4\pi^2} M_W^2 \left[(V_{tb}^* V_{tq})^2 S(x_t) + 2 V_{tb}^* V_{tq} V_{cb}^* V_{cq} S(x_c, x_t) + (V_{cb}^* V_{cq})^2 S(x_c) \right] \langle Q \rangle^{(0)}. \qquad (89)$$

S and $\widetilde{S}$ are related as

$$\begin{aligned} S(x_j, x_k) &= \widetilde{S}(x_j, x_k) - \widetilde{S}(x_j, 0) - \widetilde{S}(0, x_k) + \widetilde{S}(0,0), \qquad \text{for } j, k = c, t, \\ S(x) &\equiv S(x, x), \end{aligned} \qquad (90)$$

where I have set the up-quark mass to zero. In Eq. (89) the last two terms are tiny, because $x_c \sim 10^{-4}$ and

$$S(x_c) = \mathcal{O}(x_c), \qquad S(x_c, x_t) = \mathcal{O}(x_c \ln x_c). \qquad (91)$$

This consequence of CKM unitarity is called the *Glashow-Iliopoulos-Maiani (GIM)* suppression, related to the vanishing of FCNCs in the limit of equal internal quark masses (here m_c and $m_u = 0$). No GIM suppression occurs in top loops, because $x_t \sim 4$. The dominant contribution to Eq. (87) involves

$$S(x_t) = x_t \left[\frac{1}{4} + \frac{9}{4} \frac{1}{1 - x_t} - \frac{3}{2} \frac{1}{(1 - x_t)^2} \right] - \frac{3}{2} \left[\frac{x_t}{1 - x_t} \right]^3 \ln x_t \approx 2.3. \qquad (92)$$

The tiny charm contribution does not contribute to $C^{|\Delta B|=2,(0)}$ at all; to accommodate for it we must refine our operator product expansion to include higher powers of $(m_{\text{light}}/m_{\text{heavy}})$ in Eq. (79). We can read off $C^{|\Delta B|=2,(0)}$ from Eqs. (85) and (89):

$$C^{|\Delta B|=2,(0)}(m_t, M_W, \mu) = M_W^2 \, S(x_t). \qquad (93)$$

The functions $S(x)$ and $S(x_c, x_t)$ are called *Inami-Lim* functions [28].

The factorisation in Eqs. (79) and (85) also solves another problem: No largely separated scales appear in $C^{|\Delta B|=2}(m_t, M_W, \mu)$ provided that we take $\mu = \mathcal{O}(M_W, m_t)$, so that no large logarithms can spoil the convergence of the perturbative series. While no explicit μ-dependence is present in our LO result in Eq. (93), there is an implicit μ-dependence through $m_t(\mu)$, which is a running quark mass (typically defined in the $\overline{\text{MS}}$ scheme). $C^{|\Delta B|=2,(1)}$ also contains an explicit $\ln(\mu/M_W)$ term. Two sources contribute to this term: First, there is already a $\ln(\mu/M_W)$ term in $\mathcal{M}^{(1)}$, familiar to us from matrix elements with $\overline{\text{MS}}$-renormalised UV divergences. Second, $\mathcal{M}^{(1)}$ contains the large logarithm $\ln(m_b/M_W)$ which is split between matrix elements and Wilson coefficients as

$$\ln \frac{m_b}{M_W} \quad = \quad \ln \frac{m_b}{\mu} + \ln \frac{\mu}{M_W}. \tag{94}$$

This feature is transparent from Eq. (86).

The scale $\mu_{tW} = \mathcal{O}(M_W, m_t)$ at which we invoke Eq. (85) to find $C^{|\Delta B|=2}$ is called the *matching scale* and $C^{|\Delta B|=2}(m_t, M_W, \mu_{tW})$ has a good perturbative behaviour. Similarly, no large logarithms occur in $\langle Q(\mu_b)\rangle$, if we choose a scale $\mu_b \sim m_b$ in the matrix element. Since the μ-dependence in $H^{|\Delta B|=2}$ is spurious, we can take any value of μ we want, but this value must be the same in $C(\mu)$ and $\langle Q(\mu)\rangle$. That forces us to either relate $C(\mu_{tW})$ to $C(\mu_b)$ or to express $\langle Q(\mu_b)\rangle$ in terms of $\langle Q(\mu_{tW})\rangle$ in such a way that large logarithms

$$\alpha_s^n \ln^n \frac{\mu_{tW}}{\mu_b} \tag{95}$$

are summed to all orders $n = 0, 1, 2 \ldots$ in perturbation theory. This can be achieved by solving the *renormalisation group (RG) equation* for either $C(\mu)$ or $\langle Q(\mu)\rangle$. All steps of this procedure are analogous to the calculation of the running quark mass, which can be found in any textbook on QCD. RG-improvement promotes our LO result to a *leading-log (LL)* quantity:

$$C^{|\Delta B|=2,(0)}(m_t, M_W, \mu_b) \quad = \quad u^{(0)}(\mu_b, \mu_{tW}) C^{|\Delta B|=2,(0)}(m_t, M_W, \mu_{tW}) \tag{96}$$

$$\langle Q(\mu_{tW})\rangle \quad = \quad u^{(0)}(\mu_b, \mu_{tW}) \langle Q(\mu_b)\rangle \tag{97}$$

$$u^{(0)}(\mu_b, \mu_{tW}) \quad = \quad \left(\frac{\alpha_s(\mu_{tW})}{\alpha_s(\mu_b)}\right)^{\frac{\gamma_+^{(0)}}{2\beta_0^{(5)}}} \qquad \text{with } \gamma_+^{(0)} = 4. \tag{98}$$

The evolution factor $u^{(0)}(\mu_b, \mu_{tW})$ depends on the *anomalous dimension* of Q, which equals $(\alpha_s/(4\pi))\gamma_+^{(0)}$ to LL accuracy. $\beta_0^{(f)} = 11 - 2f/3$ is the first term of the QCD β function. One usually writes

$$C^{|\Delta B|=2}(m_t, M_W, \mu_b) \quad = \quad \eta_B b_B(\mu_b) C^{|\Delta B|=2,(0)}(m_t, M_W, \mu_{tW}) \tag{99}$$

where all dependence on μ_b is absorbed into $b_B(\mu_b)$ and all heavy scales reside in η_B. This factorisation is possible to all orders in α_s. It is trivially verified in the LL approximation of Eq. (98), where simply $u^{(0)}(\mu_b, \mu_{tW}) = \eta_B b_B(\mu_b)$. In Eq. (99) m_t is understood as $m_t(m_t)$ (and not as $m_t(\mu_{tW})$). In this way η_B is independent of μ_{tW} to the calculated order; the residual μ_{tW} dependence is already tiny in the NLL result. η_B mildly depends on $x_t = m_t^2/M_W^2$ and in practice one can treat it as a constant number [18]:

$$\eta_B = 0.55, \qquad b_B(\mu_b = m_b = 4.2\,\text{GeV}) = 1.5. \tag{100}$$

The dependences of b_B on μ_b and the chosen renormalisation scheme cancel in the product $b_B(\mu_b)\langle Q(\mu_b)\rangle$. The quoted number is for the $\overline{\text{MS}}$–NDR scheme, where "NDR" refers to the treatment of the Dirac matrix γ_5. Details on this topic can be found in [19]. We see that the impact of short-distance QCD corrections is moderate, since $\eta_B\, b_B(\mu_b) = 0.84$. The NLL calculation of Ref. [18] has found only small two-loop corrections and the remaining uncertainty affects η_B only in the third digit behind the decimal point. RG-improved perturbation theory works superbly! Combining Eqs. (82), (93) and (99) we obtain our final expression for the $|\Delta B| = 2$ hamiltonian:

$$H^{|\Delta B|=2} \;=\; \frac{G_F^2}{4\pi^2}\,M_W^2\,(V_{tb}V_{tq}^*)^2\,\eta_B\,S(x_t)b_B(\mu_b)Q(\mu_b) \;+\; h.c. \tag{101}$$

Finally we cannot escape from quark confinement! Our hadronic matrix element is conventionally parameterised as

$$\langle B_q|Q(\mu_b)|\overline{B}_q\rangle \;\;=\;\; \frac{2}{3}M_{B_q}^2\,f_{B_q}^2\,\frac{\widehat{B}_{B_q}}{b_B(\mu_b)} \tag{102}$$

with the B_q meson decay constant f_{B_q} and the *bag factor* $\widehat{B}_{B_q}$. The parameterisation in Eq. (102) is chosen in such a way that $\widehat{B}_{B_q}/b_B(\mu_b)$ is close to one. It will be especially useful once precise experimental data on $f_{B_d}\sim f_{B^+}$ from leptonic B^+ decays will be available. With the help of our effective field theory we have beaten the problem of long-distance QCD in $B-\overline{B}$ mixing down to the calculation of a single number. Lattice gauge theory computations cover the ranges [29]

$$f_{B_d}\sqrt{\widehat{B}_{B_d}} \;\;=\;\; (225\pm 35)\,\text{MeV}, \qquad\qquad f_{B_s}\sqrt{\widehat{B}_{B_s}} \;\;=\;\; (270\pm 45)\,\text{MeV}. \tag{103}$$

The quoted hadronic uncertainties are the main problem in the extraction of $|V_{tb}V_{tq}|$ from the measured ΔM_{B_q}. $\widehat{B}_{B_d}$ could differ from $\widehat{B}_{B_s}$, but no computation has established any significant difference by now.

Putting Eqs. (101) and (102) together we find the desired element of the $B-\overline{B}$ mass matrix:

$$\begin{aligned} M_{12} &\;=\; \frac{\langle B_q|H^{|\Delta B|=2}|\overline{B}_q\rangle}{2M_{B_q}} \\[2mm] &\;=\; \frac{G_F^2}{12\pi^2}\,\eta_B\,M_{B_q}\,\widehat{B}_{B_q}f_{B_q}^2\,M_W^2\,S\!\left(\frac{m_t^2}{M_W^2}\right)\left(V_{tb}V_{tq}^*\right)^2. \end{aligned} \tag{104}$$

We remark that there is no contribution of $H^{|\Delta B|=2}$ to Γ_{12}, because $\langle B_q|H^{|\Delta B|=2}|\overline{B}_q\rangle$ has no absorptive part. By inspecting Eq. (24) we can verify that the dispersive or absorptive part of some amplitude can be calculated by replacing the loop integrals by their real or imaginary parts, respectively, while keeping all complex CKM elements. But only diagrams with light internal quarks involve loop integrals with a non-zero imaginary part. Hence we must extend our effective-Hamiltonian formalism to include the effects of light internal quarks in the box diagrams, if we want to predict $\Delta\Gamma_{B_q}$. Contracting the heavy W-boson lines in the diagrams of Fig. 1 to a point does not correspond to a contribution from $H^{|\Delta B|=2}$ in the effective theory. Instead this is a second-order effect involving some effective $|\Delta B| = 1$-Hamiltonian $H^{|\Delta B|=1}$, which we must add to H^{eff} in Eq. (80). The relevant piece from the RHS of Eq. (79) is

$$-\frac{1}{2}\int d^4x\,d^4y\,\langle B|\mathbf{T}H^{|\Delta B|=1}(x)H^{|\Delta B|=1}(y)|\overline{B}\rangle. \tag{105}$$
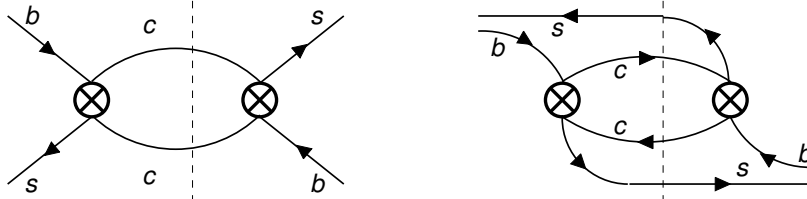
Figure 5: Second-order contribution of $H^{|\Delta B|=1}$ to $B_s - \overline{B}_s$ mixing. The diagrams constitute the dominant contribution to $\Delta\Gamma_{B_s}$.

The LO contribution to this bilocal matrix element is depicted in Fig. 5 for the case of $B_s - \overline{B}_s$ mixing. The contribution from Eq. (105) to $B - \overline{B}$ mixing is much smaller than the one from $H^{|\Delta B|=2}$, which is enhanced due to the heavy top mass entering Eq. (92). Therefore we can neglect the bilocal contribution in M_{12} and only need to consider it for Γ_{12}. From this observation we also conclude that $|\Gamma_{12}| \ll |M_{12}|$ leading to $|\Delta\Gamma| \ll \Delta M$, which we already exploited in Eqs. (43–47).

3.3 SM predictions of ΔM, $\Delta\Gamma$ and a_{fs}

In Sec. 3.2 we have collected all ingredients of the SM calculation of $\Delta M = 2|M_{12}|$ for the B_d and B_s systems. Looking at Eq. (65) we realise that $|V_{tb}|$ is well-known and $|V_{ts}|$ is essentially fixed by the well-measured $|V_{cb}|$. From Eqs. (104) and (103) we find the SM prediction

$$\Delta M_{B_s} = (12.5 \pm 4.3)\,\text{meV} = (19.0 \pm 6.6)\,\text{ps}^{-1}. \tag{106}$$

The first unit is milli-electronvolt, a unit which we do not encounter often in high-energy physics. By dividing with $\hbar$ one finds the second expression in terms of inverse picoseconds, which is more useful since ΔM is measured from the oscillation frequency in Eq. (55). Eq. (106) is in good agreement with the Tevatron measurement of [14, 20]

$$\Delta M_{B_s}^{\text{exp}} = \left(17.77 \pm 0.10_{(\text{stat})} \pm 0.07_{(\text{syst})}\right)\,\text{ps}^{-1}. \tag{107}$$

The corresponding quantity for $B_d - \overline{B}_d$ mixing is well-measured by several experiments with [8]

$$\Delta M_{B_d}^{\text{exp}} = (333.7 \pm 3.3)\,\mu\text{eV} = (0.507 \pm 0.005)\,\text{ps}^{-1}. \tag{108}$$

We can use ΔM_{B_d} to determine $|V_{td}|$. From Eq. (104) we infer

$$\Delta M_{B_d} = (0.52 \pm 0.02)\,\text{ps}^{-1} \left(\frac{|V_{td}|}{0.0082}\right)^2 \left(\frac{f_{B_d}\sqrt{\widehat{B}_{B_d}}}{225\,\text{MeV}}\right)^2. \tag{109}$$

The 16% error of the lattice value in Eq. (103) dominates the uncertainty on the extracted $|V_{td}|$. The all-order Wolfenstein parameterisation defined by Eqs. (70) and (75) implies

$$|V_{td}| = A\lambda^3 R_t + \mathcal{O}(\lambda^5). \tag{110}$$

Since $A\lambda^2 \simeq |V_{cb}|$ is well-known, ΔM_{B_d} essentially determines R_t, i.e. one side of the unitarity triangle. Even better, we can use the ratio $\Delta M_{B_d}/\Delta M_{B_s}$ for the same purpose: If one forms the ratio of the hadronic quantities in Eq. (103), many uncertainties drop out:

$$\xi = \frac{f_{B_s}\sqrt{\widehat{B}_{B_s}}}{f_{B_d}\sqrt{\widehat{B}_{B_d}}} = 1.20 \pm 0.06. \tag{111}$$

In the limit of exact flavour-SU(3) symmetry (corresponding to $m_u = m_d = m_s$) one has $\xi = 1$ which reduces the calculational task to compute the deviation of ξ from 1. The somewhat large error in Eq. (111) reflects the ongoing discussion on potentially large chiral logarithms [21] which may increase ξ significantly. This problem occurs, because lattice simulations use values for the pion mass which are larger than the physical value. The extrapolation to $m_\pi \simeq 140\,\mathrm{MeV}$ with the help of chiral perturbation theory introduces this source of error. Sum-rule calculations of ξ (or rather f_{B_s}/f_{B_d}) which automatically include these logarithms, however, give values at the lower end of the range in Eq. (111) [22]. Further all short-distance QCD drops out from the ratio $\Delta M_{B_d}/\Delta M_{B_s}$, so that one simply has

$$\left|\frac{V_{td}}{V_{ts}}\right| = \sqrt{\frac{\Delta M_{B_d}}{\Delta M_{B_s}}}\sqrt{\frac{M_{B_s}}{M_{B_d}}}\,\xi. \tag{112}$$

The Wolfenstein expansion leads to

$$\left|\frac{V_{td}}{V_{ts}}\right| = R_t\lambda\left[1 + \lambda^2\left(\frac{1}{2} - \overline{\rho}\right) + \mathcal{O}(\lambda^4)\right]. \tag{113}$$

Combining Eqs. (112) and (113) (and using $M_{B_s}/M_{B_d} = 1.017$) we easily derive a home-use formula for R_t:

$$R_t = 0.887\,\frac{\Delta M_{B_d}}{0.507\,\mathrm{ps}^{-1}}\,\frac{17.77\,\mathrm{ps}^{-1}}{\Delta M_{B_s}}\,\frac{\xi}{1.2}\,\frac{\lambda}{0.2246}\,[1 + 0.05\,\overline{\rho}] \tag{114}$$

Neither $\overline{\rho} \approx 0.2$ nor the 1% error on $\lambda \simeq 0.2246$ have an impact on the error of R_t. Using the numerical input from Eqs. (107–108) and Eq. (111) we find

$$R_t = 0.90 \pm 0.04 \tag{115}$$

and the uncertainty is essentially solely from ξ in Eq. (111).

Next we discuss $\Delta\Gamma$ and the quantity a_{fs} in Eq. (57), which governs CP violation in mixing. In order to find these quantities we need to calculate Γ_{12}. This involves the diagrams of Fig. 5 and brings in a new feature, power corrections of order $\Lambda_{\mathrm{QCD}}/m_b$ [23]. NLL QCD corrections to Γ_{12} in the B system have been calculated in Ref. [24, 25, 26]. In the SM the CP phase ϕ of Eq. (38) is so small that one can set $\cos\phi$ to 1 in Eq. (45). If we normalise $\Delta\Gamma$ to ΔM we can eliminate the bulk of the hadronic uncertainties. Updated values, obtained by using an improved operator basis, are [27]

$$\Delta\Gamma_{B_s} = \left(\frac{\Delta\Gamma_{B_s}}{\Delta M_{B_s}}\right)^{\mathrm{th}}\Delta M_{B_s}^{\mathrm{exp}} = 0.088 \pm 0.017\,\mathrm{ps}^{-1}, \tag{116}$$

$$\Delta\Gamma_{B_d} = \left(\frac{\Delta\Gamma_{B_d}}{\Delta M_{B_d}}\right)^{\mathrm{th}}\Delta M_{B_d}^{\mathrm{exp}} = \left(26.7^{+5.8}_{-6.5}\right)\cdot 10^{-4}\,\mathrm{ps}^{-1}. \tag{117}$$
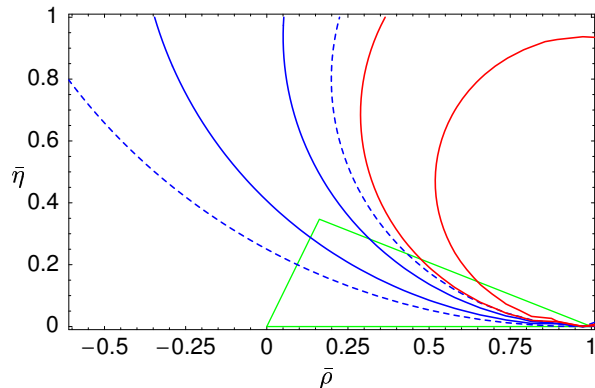
Figure 6: Impact of $a_{\rm fs}^d$ on the $(\overline{\rho}, \overline{\eta})$ plane: The solid blue curves limit the allowed range (defined by the error in Eq. (120)) for a hypothetical measurement of $a_{\rm fs}^{d\,\exp} = -5 \cdot 10^{-4}$. The solid red curves are for $a_{\rm fs}^{d\,\exp} = -10^{-3}$ instead. For further information see Ref. [25], from which the figure is taken.

The width difference in the B_s system amounts to $12.7 \pm 2.4\%$ of the average width $\Gamma_{B_s} \simeq \Gamma_{B_d}$ [27] and is in the reach of present experiments. Needless to say that there are no useful data on $\Delta\Gamma_{B_d}$. The predictions for the CP asymmetries in flavour-specific decays of Eq. (57) are calculated from Eq. (43) and read [25, 26, 27]

$$a_{\rm fs}^s = (2.06 \pm 0.57) \cdot 10^{-5} \tag{118}$$

$$a_{\rm fs}^d = \left(-4.8^{+1.0}_{-1.2}\right) \cdot 10^{-4}. \tag{119}$$

Also the current data for these CP asymmetries are not useful for CKM metrology. A future measurement of $a_{\rm fs}^{d\,\exp}$ will add an interesting new constraint to the $(\overline{\rho}, \overline{\eta})$ plane [25]:

$$(\overline{\eta} - R_{\rm fs})^2 + (1 - \overline{\rho})^2 = R_{\rm fs}^2 \qquad \text{with} \qquad R_{\rm fs} = -\frac{a_{\rm fs}^{d\,\exp}}{\left(10.1^{+1.8}_{-1.7}\right) \cdot 10^{-4}}. \tag{120}$$

The theory prediction of Refs. [25, 26] enters the denominator of $R_{\rm fs}$, the quoted value is consistent with Eq. (119) and stems from the update in Ref. [27]. Eq. (120) defines a circle with radius $R_{\rm fs}$ centred around $(\overline{\rho}, \overline{\eta}) = (1, R_{\rm fs})$. Therefore the circle touches the $\overline{\rho}$ axis at the point $(1, 0)$, see Fig. 6.

We have seen that the three quantities related to $B_s - \overline{B}_s$ mixing discussed in Eqs. (106), (116) and (118) have little dependence on $\overline{\rho}$ and $\overline{\eta}$. Only ΔM_{B_s} has an impact on CKM metrology, through Eq. (114). The small sensitivity to $\overline{\rho}$ and $\overline{\eta}$ becomes a virtue in searches for new physics, where $B_s - \overline{B}_s$ mixing plays an important role.

Next we discuss $K - \overline{K}$ mixing: The calculation of M_{12} now forces us to compute box diagrams of Fig. 1 with all possible quark flavours u, c, t, because the top contribution involving $S(x_t)$ is suppressed by the small CKM factor $(V_{ts}^* V_{td})^2 \simeq A^4 \lambda^{10} (1 - \overline{\rho} + i\overline{\eta})^2$. The charm and up contributions, however, are proportional to only two powers of λ. Therefore we cannot neglect these contributions despite of the smallness of $S(x_c)$ and $S(x_c, x_t)$ (discussed around Eq. (91)).

Their calculation proceeds in two major steps: First, the top quark and W-boson are integrated out. In the resulting effective theory the $\Delta S = 2$ transitions receive second-order contributions from a $|\Delta S| = 1$-Hamiltonian $H^{|\Delta S|=1}$. We have already seen this in our discussion of $\Delta B = 2$ transitions, the corresponding expression for $K - \overline{K}$ mixing is obtained by replacing $H^{|\Delta B|=1}$ with $H^{|\Delta S|=1}$ in Eq. (105) (and is described by the analogous diagrams of Fig. 5). In addition to this bilocal contribution, the term with $S(x_c, x_t)$ also involves a $|\Delta S| = 2$-Hamiltonian $H^{|\Delta S|=2}$ which mediates $K - \overline{K}$ mixing via a local four-quark operator, just as in the case of $B - \overline{B}$ mixing. The $|\Delta S| = 1$ and $|\Delta S| = 2$ Wilson coefficients of this effective field theory are evolved down to the scale $\mu_{bc} = \mathcal{O}(m_c)$ at which the second step of the calculation is performed: Now the bottom and charm quarks are integrated out and the effective field theory set up in the first step is matched to another effective field theory. The new theory treats m_b and m_c as heavy scales, so that all box diagrams involving at least one charm quark are effectively contracted to a point. All information on m_c (and m_b which plays a minor role) resides in the Wilson coefficient of the local $\Delta S = 2$ operator

$$Q = \overline{d}_L \gamma_\nu s_L \, \overline{d}_L \gamma^\nu s_L. \tag{121}$$

The effective $|\Delta S| = 2$ Hamiltonian can therefore be written in a similar way as the $|\Delta B| = 2$ Hamiltonian of Eq. (101):

$$H^{|\Delta S|=2} = \frac{G_F^2}{4\pi^2} M_W^2 \left[(V_{ts} V_{td}^*)^2 \, \eta_{tt} \, S(x_t) + 2 V_{ts} V_{td}^* V_{cs} V_{cd}^* \, \eta_{ct} \, S(x_c, x_t) \right.$$
$$\left. + (V_{cs} V_{cd}^*)^2 \, \eta_{cc} \, x_c \right] \, b_K(\mu_K) Q(\mu_K) \, + \, h.c. \tag{122}$$

The NLL results for the short-distance QCD factors read

$$\eta_{tt} = 0.57, \qquad \eta_{ct} = 0.47 \pm 0.05, \qquad \eta_{cc} = (1.44 \pm 0.35) \left(\frac{1.3 \, \text{GeV}}{m_c} \right)^{1.1}. \tag{123}$$

The QCD coefficients in Eq. (123) were calculated to LL accuracy in Ref. [30]. The NLL calculation of η_{tt} [18] is analogous to that of η_B, with one new feature: When crossing the threshold μ_{bc} one must change the number of active flavours in the QCD β function and the NLL anomalous dimension γ_+ from $f = 5$ to $f = 3$. The NLL results for η_{ct} [31] and η_{cc} [32] have a sizable uncertainty, because they are sensitive to the low scale of $\mu_{bc} \sim m_c$ where α_s is large. η_{cc} also exhibits a sizable dependence on $\alpha_s(M_Z)$ and on $m_c = m_c(m_c)$, so that the central values quoted in the literature vary over some range. The expression in Eq. (123) approximates the dependence on m_c and corresponds to $\alpha_s(M_Z) = 0.119 \pm 0.002$. The scale μ_K must be chosen below m_c and is typically taken around $1 \, \text{GeV}$, where perturbation theory is still applicable. One finds $b_K(\mu_K = 1 \, \text{GeV}) = 1.24 \pm 0.02$ and the error stems from the uncertainty in α_s.

In the discussion of $|\Delta S| = 2$ transitions we must also address corrections of order $m_{\text{light}}^2 / m_{\text{heavy}}^2$ which correspond to subleading terms in the operator product expansion of Eq. (79). While these corrections are of order $\Lambda_{\text{QCD}}^2 / m_t^2$ for the first term in $H^{|\Delta S|=2}$, they are of order $\Lambda_{\text{QCD}}^2 / m_c^2$ in the case of the charm contributions involving $S(x_c, x_t) = \mathcal{O}(x_c \ln x_c)$ and $S(x_c) \simeq x_c$ in Eq. (122). The largest of these power corrections involves two $|\Delta S| = 1$ operators and corresponds to the box diagram in Fig. 1 with two internal up-quarks. To understand the power counting, recall that the charm contribution in $H^{|\Delta S|=2}$ is proportional to $M_W^2 x_c = m_c^2$, while

the box with up-quarks involves no power of m_c, so that its size is characterised by the hadronic energy scale $\Lambda_{\rm QCD}$. Including this bilocal contribution we write:

$$M_{12} = \frac{1}{2m_K} \langle K|H^{|\Delta S|=2}|\overline{K}\rangle - \text{Disp} \, \frac{i}{4m_K} \int d^4x \, \langle K|H^{|\Delta S|=1}(x) \, H^{|\Delta S|=1}(0)|\overline{K}\rangle \,. \qquad (124)$$

Here "Disp" denotes the dispersive part of the matrix element, which is introduced in Eq. (24) and is discussed after Eq. (104). The enhancement of the second term stems from the so-called $\Delta I = 0$ *rule* which describes the non-perturbative enhancement of the decay $K_{\rm short} \to (\pi\pi)_{I=0}$. The two terms in Eq. (124) are usually referred to as *short-distance* and *long-distance* contributions. The long-distance contribution has defied any reliable calculation from first principles so far. In this humbling situation we can only compare the experimental value of ΔM_K to the short-distance contribution

$$\Delta M_K^{\rm SD} = \frac{|\langle K|H^{|\Delta S|=2}|\overline{K}\rangle|}{m_K} \,. \qquad (125)$$

In order to compute $\Delta M_K^{\rm SD}$ we need the hadronic matrix element

$$\langle K|Q(\mu_K)|\overline{K}\rangle = \frac{2}{3} M_K^2 \, f_K^2 \, \frac{\widehat{B}_K}{b_K(\mu_K)}. \qquad (126)$$

Contrary to the situation in the B system, the Kaon decay constant $f_K = 160\,\text{MeV}$ is well-measured. We remark here that we know $\widehat{B}_K$ in a particular limit of QCD: If the number of colours N_c is taken to infinity, $\langle K|Q(\mu_K)|\overline{K}\rangle$ can be expressed in terms of the current matrix element $\langle 0|\overline{d}_L\gamma_\nu s_L|\overline{K}\rangle$ which defines f_K. For $N_c = \infty$ one finds $\widehat{B}_K/b_K(\mu_K) = 3/4$; including certain calculable ("factorisable") $1/N_c$ corrections changes this to $\widehat{B}_K/b_K(\mu_K) = 1$. A recent lattice calculation finds [33]

$$\widehat{B}_K = 0.72 \pm 0.04. \qquad (127)$$

The experimental value of the $K_{\rm long}$–$K_{\rm short}$ mass difference is [8]

$$\Delta M_K^{\rm exp} = (3.483 \pm 0.006)\,\mu\text{eV} = (5.292 \pm 0.009) \cdot 10^{-3}\,\text{ps}^{-1}. \qquad (128)$$

Inserting Eqs. (122) and (126) into Eq. (125) gives

$$\frac{\Delta M_K^{\rm SD}}{\Delta M_K^{\rm exp}} = (0.98 \pm 0.22)\widehat{B}_K. \qquad (129)$$

$\Delta M_K^{\rm SD}$ is dominated by the term proportional to $(V_{cs}V_{cd}^*)^2$ and the error in Eq. (129) essentially stems from η_{cc} in Eq. (123). This uncertainty will shrink when η_{cc} is calculated to NNLL accuracy. With Eq. (127) we find that $H^{|\Delta S|=2}$ contributes $(70 \pm 25)\%$ to the measured ΔM_K.

The off-diagonal element of the decay matrix is given by

$$\Gamma_{12} = \text{Abs} \, \frac{i}{2m_K} \int d^4x \, \langle K|H^{|\Delta S|=1}(x) \, H^{|\Delta S|=1}(0)|\overline{K}\rangle \qquad (130)$$

$$= \frac{1}{2m_K} \sum_f (2\pi)^4 \delta^4(p_K - p_f)\langle K|H^{|\Delta S|=1}|f\rangle \, \langle f|H^{|\Delta S|=1}|\overline{K}\rangle \simeq \frac{1}{2m_K} A_0^* \overline{A}_0 \,. \quad (131)$$

Here "Abs" denotes the absorptive part of the matrix element. Γ_{12} is an inclusive quantity built out of all final states f into which both K and $\overline{K}$ can decay. A special feature of the neutral Kaon system is the saturation of Γ_{12} by a single decay mode, which is $K \to (\pi\pi)_{I=0}$. The notation A_0 and $\overline{A}_0$ for the corresponding decay amplitudes has been introduced after Eq. (14). Γ_{12} is a non-perturbative quantity and its computation on the lattice involves the difficult task to understand and master the $\Delta I = 0$ rule. The relation between Γ_{12} and $\Delta\Gamma_K$ has been derived in Eq. (45). Experimentally we have [8]

$$\Delta\Gamma_K^{\text{exp}} = (7.335 \pm 0.004)\,\mu\text{eV} = (11.144 \pm 0.006) \cdot 10^{-3}\,\text{ps}^{-1}. \tag{132}$$

With Eqs. (128) and (132) we have precise experimental information on $|M_{12}| \simeq \Delta M_K/2$ and $|\Gamma_{12}| \simeq \Delta\Gamma_K/2$. To fully characterise $K - \overline{K}$ mixing we also need to know the phase ϕ defined in Eq. (38). As in the case of $B - \overline{B}$ mixing we study a CP asymmetry in a flavour-specific decay mode. With Eqs. (11) and (41) one easily finds

$$
\begin{aligned}
A_L &\equiv \frac{\Gamma(K_{\text{long}} \to \ell^+ \nu\, \pi^-) - \Gamma(K_{\text{long}} \to \ell^- \bar{\nu}\, \pi^+)}{\Gamma(K_{\text{long}} \to \ell^+ \nu\, \pi^-) + \Gamma(K_{\text{long}} \to \ell^- \bar{\nu}\, \pi^+)} \\
&= \frac{1 - |q/p|^2}{1 + |q/p|^2} \simeq \frac{a}{2}.
\end{aligned}
\tag{133}
$$

At this point it is worthwhile to look back at the quantity ϵ_K which we have encountered in the first lecture in Eq. (14). From Eq. (17) we have learned that $\text{Re}\,\epsilon_K$ measures CP violation in mixing quantified by $1 - |q/p|$, just as A_L in Eq. (133). While $\text{Im}\,\epsilon_K$ is related to a different physical phenomenon, namely mixing-induced CP violation, it provides the very same information on the fundamental parameters of $K - \overline{K}$ mixing: Since $K \to (\pi\pi)_{I=0}$ dominates Γ_{12}, the CP-violating phase of $\overline{A}_0/A_0$ equals $\arg\Gamma_{12}$, see Eq. (131). With this observation and the help of Eq. (42) we can express ϵ_K in Eq. (17) entirely in terms of ΔM_K, $\Delta\Gamma_K$ and ϕ. Interestingly, the phase ϕ_ϵ of ϵ_K (see Eq. (14)) is simply given by

$$\phi_\epsilon = \arctan\frac{\Delta M_K}{\Delta\Gamma_K/2}. \tag{134}$$

More details of this calculation can be found in Chapter 1.6 of Ref. [34]. Nature chose $\Delta M_K \approx \Delta\Gamma_K/2$ by accident, so that ϕ_ϵ in Eq. (14) is close to $45°$. The bottom line is that ϕ_ϵ carries no information on CP violation and that $|\epsilon_K|$ and A_L involve the same fundamental CP-violating quantity, which is ϕ. To extract ϕ from A_L in Eq. (133) or from ϵ_K in Eq. (17) we use Eq. (42), with $2|M_{12}|/|\Gamma_{12}| \simeq \Delta M_K/(\Delta\Gamma_K/2)$ traded for $\tan\phi_\epsilon$:

$$
\begin{aligned}
A_L &= \frac{1}{2}\sin(2\phi_\epsilon)\phi + \mathcal{O}(\phi^2) \\
\epsilon_K &\simeq \frac{1}{2}\sin(\phi_\epsilon)e^{i\phi_\epsilon}\phi + \mathcal{O}(\phi^2)
\end{aligned}
\tag{135}
$$

Using the experimental value

$$A_L^{\text{exp}} = (3.32 \pm 0.06) \times 10^{-3}$$

gives

$$\phi = (6.77 \pm 0.12) \times 10^{-3}. \tag{136}$$

This number is in reasonable agreement with $\phi = (6.48 \pm 0.03) \times 10^{-3}$ found from ϵ_K with Eq. (135). Next we relate ϕ to a constraint on $(\overline{\rho}, \overline{\eta})$: Specifying to the standard phase convention for the CKM matrix (with $V_{us} V_{ud}^*$ real and positive) we start from Eq. (38) to write

$$\phi = \arg\left(-\frac{M_{12}}{\Gamma_{12}}\right) \simeq \frac{\operatorname{Im} M_{12}}{|M_{12}|} - \arg(-\Gamma_{12}) = 2\left[\frac{\operatorname{Im} M_{12}}{\Delta M_K^{\mathrm{exp}}} + \xi_K\right] \qquad (137)$$

where

$$2\xi_K \equiv -\arg(-\Gamma_{12}) \simeq -\arg\left(-\frac{\overline{A}_0}{A_0}\right). \qquad (138)$$

In Eq. (137) I have used that the phases of M_{12} and $-\Gamma_{12}$ are separately small in the adopted phase convention and further traded $|M_{12}|$ for the experimental $\Delta M_K / 2$. In Eq. (138) the saturation of Γ_{12} by $A_0^* \overline{A}_0$ in Eq. (131) has been used. Thus $-\xi_K$ is just the CP-odd phase in the decay $\overline{K} \to (\pi\pi)_{I=0}$. A recent analysis has estimated $\xi_K \approx -1.7 \cdot 10^{-4}$ [35], so that ξ_K contributes roughly -6% to the measured value of ϕ. The dominant term proportional to $\operatorname{Im} M_{12} = \operatorname{Im} \langle K | H^{|\Delta S|=2} | \overline{K} \rangle$ involves the CKM factors

$$\begin{aligned} \operatorname{Im}(V_{ts} V_{td}^*)^2 &\simeq 2(A\lambda^2)^4 \lambda^2 \overline{\eta}(1-\overline{\rho}) \\ \operatorname{Im}(2 V_{ts} V_{td}^* V_{cs} V_{cd}^*) &\simeq -\operatorname{Im}(V_{cs} V_{cd}^*)^2 \simeq 2(A\lambda^2)^2 \lambda^2 \overline{\eta}, \end{aligned} \qquad (139)$$

where the lowest-order Wolfenstein expansion has been used. Inspecting the dependences of the CKM factors on $\overline{\rho}$ and $\overline{\eta}$ we see that the experimental constraint from ϕ defines a hyperbola in the $(\overline{\rho}, \overline{\eta})$ plane. Combining Eq. (139) with Eqs. (122) and (137), inserting the QCD factors from Eq. (123) and the matrix element from Eq. (126) and finally using $\phi = (6.48 \pm 0.03) \times 10^{-3}$ from ϵ_K this hyperbola reads

$$\overline{\eta} = \frac{1}{\widehat{B}_K} \frac{0.34 \pm 0.03}{1.3 \pm 0.1 - \overline{\rho}}. \qquad (140)$$

The uncertainties in $\widehat{B}_K$ from Eq. (127) and from η_{cc} and η_{ct} in Eq. (123) (reflected by 1.3 ± 0.1) inflict errors of similar size on the $\overline{\eta}$ extracted from Eq. (140). The numerator 0.34 ± 0.03 is calculated with $|V_{cb}| = A\lambda^2 = 0.0412 \pm 0.0011$. The 10% uncertainty of this number stems solely from the error in $|V_{cb}|$, which enters $\overline{\eta}$ in Eq. (140) with the fourth power.

The neutral Kaon system is the only neutral meson system for which all three quantities ΔM, $\Delta\Gamma$ and ϕ are measured. It should be stressed that also the sign of $\Delta\Gamma/\Delta M$ is firmly established. Measuring $\operatorname{sign}(\Delta\Gamma/\Delta M)$ is difficult for all meson-antimeson systems. In the neutral Kaon system the measurement of ΔM and $\operatorname{sign}(\Delta\Gamma/\Delta M)$ uses K_{short} *regeneration*: If a K_{long} beam hits a nucleus in a target (the regenerator), strong inelastic scattering changes the $|K_{\mathrm{long}}\rangle$ state into a superposition of $|K_{\mathrm{long}}\rangle$ and $|K_{\mathrm{short}}\rangle$ giving access to observables which are sensitive to ΔM and the abovementioned sign. For details on these experimental aspects I refer to [36].

Finally I discuss $D - \overline{D}$ mixing: Box diagrams in Fig. 1 with one or two internal b quarks are highly CKM-suppressed. The dominant box diagrams with internal d and s quarks suffer from a very efficient GIM suppression proportional to m_s^4/m_c^2. This makes the diagrams sensitive to very low scales and perturbative calculations of ΔM_D, $\Delta\Gamma_D$ and a_{fs}^D are put into doubt. In the effective theory both M_{12} and Γ_{12} are dominated by the bilocal contribution with $H^{|\Delta C|=1}$.
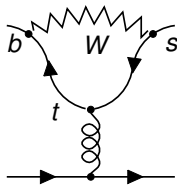
Figure 7: Gluonic penguin diagram with an internal top quark.

The only possible clear prediction is the qualitative statement that all these quantities are very small. Theoretical calculations usually quote numbers for the quantities $x \equiv \Delta M_D/\Gamma_D$ and $y \equiv \Delta\Gamma_D/(2\Gamma_D)$. The theoretical predictions for $|x|, |y|$ cover the range from zero to $|x|, |y| \sim 0.01$ and come without reliable error estimates. Therefore current experimental values are compatible with the SM but may also be dominated by a new physics contribution. A "smoking gun" of new physics, however, would be the discovery of a non-zero CP asymmetry in the D system.

3.4 Mixing-induced *CP* asymmetries

At the end of Sect. 2.3 we have learned that mixing-induced *CP* asymmetries can provide clean information on fundamental *CP* phases in the Lagrangian. These *CP* asymmetries involve the interference between mixing and decay amplitudes as depicted on the right.

In this lecture we restrict the discussion to gold-plated modes which involve a *CP* eigenstate f_{CP} in the final state, cf. Eq. (10).[4] In the B_d and B_s meson systems the mixing-induced *CP* asymmetries are a real gold mine, because there are many decay modes satisfying the condition for a golden decay mode as defined after Eq. (62). Prominent examples are the decays $B_s \to J/\psi\phi$ and $B_d \to J/\psi K_{\mathrm{short}}$, whose decay amplitudes essentially only involve the CKM factor $V_{cs}V_{cb}^*$. To understand this first note that the decay proceeds at tree–level by exchanging a W boson. There are also contributions involving an up, charm or top quark loop, with attached gluons splitting into the charm-anticharm pair hadronising into the J/ψ meson. Such diagrams are called *penguin diagrams*. A penguin diagram in the narrow sense only involves one neutral vector boson (which can be a gluon, photon or Z boson). A gluonic penguin diagram is depicted in Fig. 7. (Yet a J/ψ cannot be produced from a single gluon. One needs a photon or three gluons at least.) In the context of mixing-induced *CP* asymmetries one often speaks of *penguin pollution*, because the penguin diagrams may involve different CKM factors than the tree diagram spoiling the golden-mode property. To estimate the penguin pollution in $B_s \to J/\psi\phi$ and $B_d \to J/\psi K_{\mathrm{short}}$ first use the unitarity relation $V_{ts}V_{tb}^* = -V_{cs}V_{cb}^* - V_{us}V_{ub}^*$ to write

$$H^{|\Delta B|=1} = V_{cs}V_{cb}^* h_c + V_{cs}^* V_{cb} h_c^\dagger + V_{us}V_{ub}^* h_u + V_{us}^* V_{ub} h_u^\dagger. \tag{141}$$

[4]One can also identify gold-plated decays into non-CP eigenstates, important channels are e.g. $B_s \to D_s^\pm K^\mp$.

Here the last two terms are highly suppressed, since $|V_{us}^* V_{ub}| \sim 0.03\,|V_{cs}^* V_{cb}|$. Moreover, h_u has no tree contributions, but solely stems from penguin diagrams with up and top quarks. Since these loop effects involve non-perturbative physics, it is difficult to quantify the loop suppression. Still, the CKM suppression is efficient enough to render the modes gold-plated at the level of a few percent. Since the CKM elements are factored out in Eq. (141), h_c and h_u only contain Wilson coefficients, operators and real constants. Importantly, $h_{u,c}$ and $h_{u,c}^\dagger$ are related by the CP transformation:

$$h_{u,c}^\dagger \;=\; (CP)^\dagger h_{u,c} CP. \tag{142}$$

While I discuss $B_s \to J/\psi\phi$ and $B_d \to J/\psi K_{\mathrm{short}}$ here for definiteness, the results apply to other gold-plated $M \to f_{\mathrm{CP}}$ modes as well, with obvious replacements for the CKM elements. The underlying reason for the cancellation of hadronic uncertainties in gold-plated decays is the CP invariance of QCD: While we cannot compute $\langle f_{\mathrm{CP}}|h_c|B\rangle^5$, we can relate this matrix element to $\langle f_{\mathrm{CP}}|h_c^\dagger|\overline{B}\rangle$ through

$$\langle f_{\mathrm{CP}}|h_{u,c}^\dagger|\overline{B}\rangle \;=\; \langle f_{\mathrm{CP}}|(CP)^\dagger h_{u,c} CP|\overline{B}\rangle \;=\; -\eta_{\mathrm{CP}}\langle f_{\mathrm{CP}}|h_{u,c}|B\rangle, \tag{143}$$

where I just used the CP transformations of Eqs. (9–10) and Eq. (142). We first apply this to the decay mode $B_s \to J/\psi\phi$. The final state consists of two vector mesons. By conservation of angular momentum they can be in states with orbital angular momentum quantum numbers $l = 0, 1$ or 2: The two spin-1 states of the vector mesons can be added to a state of total spin $0, 1$ or 2, which requires an orbital angular momentum of $l = 0, 1$ or 2 to give a $J/\psi\phi$ state with zero total angular momentum. The p-wave state with $l = 1$ is CP-odd and the other two states are CP-even, owing to the parity quantum number $(-1)^l$ of their spatial wave function. Experimentally one separates these states by an angular analysis [37, 38] of the data sample. This can be done including the full time dependence of the decay, so that we can isolate the time-dependent CP asymmetries in the different partial-wave channels. The most-populated state is the CP-even $l = 0$ (i.e. s-wave) state. Writing $f_{\mathrm{CP}} = (J/\psi\phi)_l$ with $\eta_{\mathrm{CP}} = (-1)^l$ we obtain for the amplitudes $A_{f_{\mathrm{CP}}}$ and $\overline{A}_{f_{\mathrm{CP}}}$ (see Eq. (12)):

$$\frac{\overline{A}_{f_{\mathrm{CP}}}}{A_{f_{\mathrm{CP}}}} \;\simeq\; \frac{\langle f_{\mathrm{CP}}|H^{|\Delta B|=1}|\overline{B}_s\rangle}{\langle f_{\mathrm{CP}}|H^{|\Delta B|=1}|B_s\rangle} \;=\; \frac{V_{cs}^* V_{cb}}{V_{cs} V_{cb}^*}\frac{\langle f_{\mathrm{CP}}|h_c^\dagger|\overline{B}_s\rangle}{\langle f_{\mathrm{CP}}|h_c|B_s\rangle} \;=\; -\eta_{\mathrm{CP}}\frac{V_{cs}^* V_{cb}}{V_{cs} V_{cb}^*} \tag{144}$$

Combining this result with Eqs. (47) and (13) we find

$$\lambda_{f_{\mathrm{CP}}} \;=\; \eta_{\mathrm{CP}}\frac{V_{tb}^* V_{ts}}{V_{tb} V_{ts}^*}\frac{V_{cs}^* V_{cb}}{V_{cs} V_{cb}^*} \;=\; \eta_{\mathrm{CP}}\, e^{2i\beta_s}. \tag{145}$$

In the last step I have used the definition of β_s in Eq. (77). With Eq. (145) we can calculate the time-dependent CP asymmetry of Eq. (61). First we verify that our golden mode satisfies $|\lambda_{f_{\mathrm{CP}}}| = 1$, so that A_{CP}^{dir} in Eq. (62) vanishes. The other two quantities in Eq. (61) evaluate with Eq. (145) to $A_{CP}^{\mathrm{mix}} = -\eta_{\mathrm{CP}}\sin(2\beta_s)$ and $A_{\Delta\Gamma} = -\eta_{\mathrm{CP}}\cos(2\beta_s)$, so that (neglecting the tiny $\mathcal{O}(a)$ term)

$$a_{f_{\mathrm{CP}}}(t) = \eta_{\mathrm{CP}}\frac{\sin(2\beta_s)\sin(\Delta M_{B_s} t)}{\cosh(\Delta\Gamma_{B_s} t/2) - \eta_{\mathrm{CP}}\cos(2\beta_s)\sinh(\Delta\Gamma_{B_s} t/2)} \qquad \text{for } f_{\mathrm{CP}} = (J/\psi\phi)_l. \tag{146}$$

---

[5]In flavour physics matrix elements like $\langle f|H^{|\Delta B|=1}|M\rangle$ are always understood to include the strong interaction. This means that the fields are understood as interacting fields in the Heisenberg picture with respect to the strong interaction.
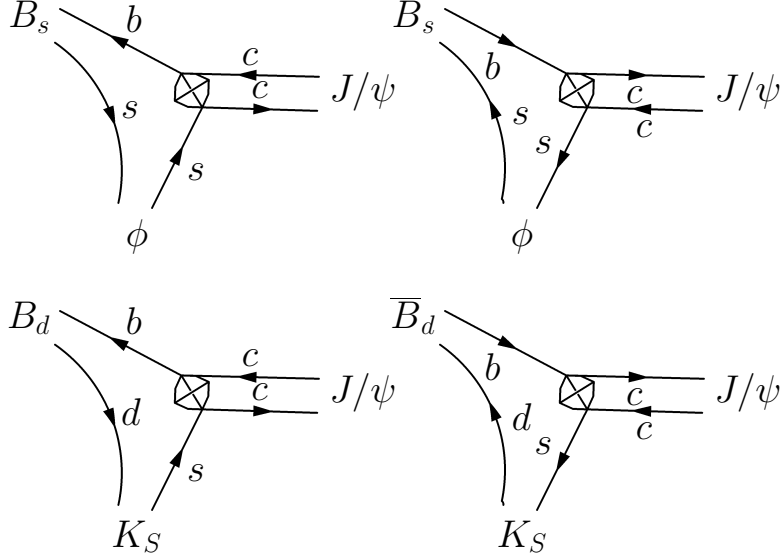
Figure 8: Interfering amplitudes which give rise to mixing-induced CP violation for the two golden modes discussed in the text.

In the SM β_s is small and $a_{(J/\psi\phi)_l}(t)$ is an ideal testing ground to find new physics [27, 38].

Next I discuss $B_d \to J/\psi K_{\text{short}}$. The final state has orbital angular momentum $l = 1$ balancing the spin of the J/ψ. Neglecting the small CP violation in $K - \overline{K}$ mixing we can regard the K_{short} as CP-even. The J/ψ is CP-even as well and the orbital angular momentum contributes a factor of -1 to the total CP quantum number. Thus $\eta_{J/\psi K_{\text{short}}} = -1$. From Fig. 8 we observe a novel feature compared to $B_s \to J/\psi\phi$. The interference of the B_d and $\overline{B}_d$ decays involves $K - \overline{K}$ mixing: The B_d decay involves the K component of K_{short}, while the $\overline{B}_d$ decays into the $\overline{K}$ component of K_{short}. Experimentally the K_{short} is detected via a pair of charged pions whose invariant mass equals M_K, denoted here by $(\pi^+\pi^-)_K$. Therefore we should identify the amplitudes $A_{f_{\text{CP}}=J/\psi K_{\text{short}}}$ and $\overline{A}_{f_{\text{CP}}=J/\psi K_{\text{short}}}$ with $A(B_d \to J/\psi K \to J/\psi(\pi^+\pi^-)_K)$ and $\overline{A}(\overline{B}_d \to J/\psi\overline{K} \to J/\psi(\pi^+\pi^-)_K)$, respectively. Therefore

$$\frac{\overline{A}_{J/\psi K_{\text{short}}}}{A_{J/\psi K_{\text{short}}}} = \frac{V_{cb}V_{cs}^*}{V_{cb}^*V_{cs}}\frac{V_{us}V_{ud}^*}{V_{us}^*V_{ud}}, \qquad \lambda_{J/\psi K_{\text{short}}} = -\frac{V_{tb}^*V_{td}}{V_{tb}V_{td}^*}\frac{V_{cb}V_{cs}^*}{V_{cb}^*V_{cs}}\frac{V_{us}V_{ud}^*}{V_{us}^*V_{ud}} \simeq -e^{-2i\beta} \quad (147)$$

In the last step I have used the definition of β in Eq. (72) and neglected $\arg[-V_{cd}V_{cs}^*/(V_{ud}V_{us}^*)] \simeq A^2\lambda^4\overline{\eta} < 10^{-3}$, so that $\text{Im}\,\lambda_{J/\psi K_{\text{short}}} \simeq \sin(2\beta)$. We may further neglect $\Delta\Gamma_{B_d}$ in Eq. (61) to find the most famous time-dependent CP asymmetry,

$$a_{J/\psi K_{\text{short}}}(t) = \sin(2\beta)\sin(\Delta M_{B_d}t). \quad (148)$$

Finally I give a (very incomplete) list of other golden $M \to f_{\text{CP}}$ decays. The decay $B_s \to J/\psi\phi$ can be substituted for $B_s \to J/\psi\eta^{(\prime)}$, which does not require any angular decomposition.

In a hadron collider experiment η's and η''s are hard to detect, but $B_s \to J/\psi \eta^{(\prime)}$ is interesting for B factories running on the $\Upsilon(5S)$ resonance. While the modes discussed above provide insight into the physics of $B-\overline{B}$ mixing, one can also use mixing-induced CP violation to probe CP phases from new physics in loop-induced B decays such as $B_d \to \phi K_{\mathrm{short}}$ [39]. This mode is triggered by the quark decay $\overline{b} \to \overline{s}s\overline{s}$. The same transition in probed in $B_s \to \phi\phi$. Likewise new physics in the $\overline{b} \to \overline{s}d\overline{d}$ amplitude may reveal itself in $B_s \to K_{\mathrm{short}}K_{\mathrm{short}}$. Gold-plated D^0 decays are $D^0 \to K_{\mathrm{short}}\pi^0$ and $D^0 \to K_{\mathrm{short}}\rho^0$, which are penguin-free $c \to s\overline{d}u$ decays. A gold-plated K decay is $K_{\mathrm{long}} \to \pi^0\nu\overline{\nu}$ [40]. Here no meson-antimeson oscillations are present, but $K-\overline{K}$ mixing nevertheless enters the process through the mass eigenstate K_{long}. The final state $\pi^0\nu\overline{\nu}$ is CP-even and the dominant contribution to the decay involves mixing-induced CP violation, i.e. the decay amplitude is proportional to $\mathrm{Im}\,\lambda_f$ (see e.g. Ref [41]).

3.5 The unitarity triangle

Many measurements contribute to the global fit of the unitarity triangle defined in Eq. (70) and depicted in Fig. 3. Conceptually it is useful to disentangle tree decays from FCNC processes: Tree-level amplitudes are insensitive to new physics and therefore determine the true apex $(\overline{\rho}, \overline{\eta})$ of the unitarity triangle. In principle one could determine the unitarity triangle in this way, insert the result into the SM predictions of the FCNC processes and then assess the possible impact of new physics on the latter. In practice, however, the tree constraints still suffer from large uncertainties, while for example $a_{J/\psi K_{\mathrm{short}}}(t)$ in Eq. (148) and $\Delta M_{B_d}/\Delta M_{B_s}$ in Eq. (114) determine $\sin(2\beta)$ and the side R_t (see Eq. (71)) fairly precisely. Therefore, for the time being, it is best to combine all information into a global fit of the unitarity triangle.

From $b \to c\ell\overline{\nu}$ decays $|V_{cb}| \simeq A\lambda^2$ is precisely determined. Therefore we realise from Eqs. (71) and (76) that any measurement of $|V_{ub}|$ essentially fixes the side R_u of the triangle. $|V_{ub}|$ is determined from (inclusive or exclusive) semileptonic $b \to u$ decays and hadronic uncertainties limit the accuracy of the extracted $|V_{ub}|$ to 8-10%. The theoretical methods used to determine $|V_{cb}|$ and $|V_{ub}|$ are briefly reviewed in Ref. [42]. The angle γ of the unitarity triangle is currently measured in two ways from tree-level decays: First, the interference of the $b \to c\overline{u}s$ and $b \to u\overline{c}s$ amplitudes in $B^\pm \to \overset{(-)}{D}K^\pm$ decays is exploited [43]. Second, one measures mixing-induced CP violation in $B_d \to \pi\pi$, $B_d \to \rho\pi$ or $B_d \to \rho\rho$ decays, which allows to find the angle α of the desired triangle. These modes are not gold-plated and suffer from penguin pollution, which, however, can be eliminated by means of an isospin analysis [44]. While the extracted result for α is sensitive to new physics in $B_d-\overline{B}_d$ mixing, this possible effect can be eliminated if the measured α^{exp} and β^{exp} are combined to give $\gamma^{\mathrm{exp}} = \pi - \alpha^{\mathrm{exp}} - \beta^{\mathrm{exp}}$. Combining the constraints from $|V_{ub}|$, γ and α with those from meson-antimeson mixing discussed in this lecture results in the unitarity triangle shown in Fig. 9.

Suggestions for further reading

There are many good review articles on meson-antimeson mixing and flavour physics in general, putting emphasis on different aspects of the field. A student interested in the theoretical foundation of flavour physics, effective Hamiltonians and higher-order calculations is referred to the lecture in Ref. [48] and the review articles in Refs. [34, 49]. Most reviews and lectures focus on CP violation and I recommend Refs. [47] and [50]. I have only briefly touched $D-\overline{D}$ mixing, two review articles dedicated to D physics are cited in Ref. [51]. Lectures covering
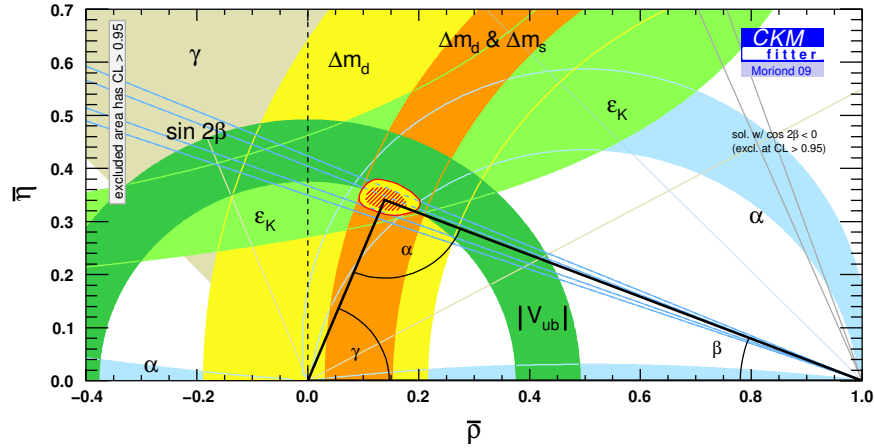
Figure 9: Global fit to the unitarity triangle from the CKMFitter group [45]. A different statistical approach is used by the UTFit group [46].

both K and D physics can be found in Ref. [52]. A concise summary of the physics entering CKM metrology can be found in Ref. [42], a more elaborate article on the subject is Ref. [53]. Standard textbooks on flavour physics are listed in Ref. [54].

Acknowledgements

References

[1] D. J. Gross and F. Wilczek, Phys. Rev. Lett., **30** (1973) 1343.
H. D. Politzer, Phys. Rev. **30** (1973) 1346.

[2] S. L. Glashow, J. Iliopoulos and L. Maiani, Phys. Rev. **D2** (1970) 1285.

[3] M. K. Gaillard and B. W. Lee, Phys. Rev. **D10** (1974) 897.

[4] J. H. Christenson, J. W. Cronin, V. L. Fitch and R. Turlay, Phys. Rev. Lett. **13** (1964) 138; Phys. Rev. **140B** (1965) 74.

[5] S. L. Glashow, Nucl. Phys. **22** (1961) 579. S. Weinberg, Phys. Rev. Lett. **19** (1967) 1264. A. Salam in *Elementary Particle Physics (Nobel Symp. 8)*, ed. N. Svartholm, Almquist and Wilsell, Stockholm, 1968.

[6] M. Kobayashi and T. Maskawa, Progr. Theor. Phys. **49** (1973) 652.

[7] H. Albrecht *et al.* [ARGUS Collaboration], Phys. Lett. B **192** (1987) 245.

[8] C. Amsler *et al.* [Particle Data Group], Phys. Lett. B **667** (2008) 1.

[9] G. Lüders, Dan. Mat. Phys. Medd. **28** (1954) 5; W. Pauli in *Niels Bohr and the Development of Physics*, ed. W. Pauli, L. Rosenfeld and V. Weisskopf (McGraw-Hill, New York, 1955); G. Lüders, Ann. Phys. **2** (1957).

[10] L.A. Khalfin, Zh. Eksp. Teor. Fiz. **33** (1957) 1371.

[11] V.F. Weisskopf and E.P. Wigner, Z. Phys. **63** (1930) 54; **65** (1930) 18; T. D. Lee, R. Oehme and C. N. Yang, Phys. Rev. **106** (1957) 340.

[12] P. K. Kabir, *The CP puzzle: strange decays of the neutral Kaon*, Acad. Pr., London, 1968. O. Nachtmann, *Elementary particle physics : concepts and phenomena*, Springer, Berlin, 1990.

[13] C. B. Chiu and E. C. G. Sudarshan, Phys. Rev. D **42** (1990) 3712.

[14] A. Abulencia *et al.* [CDF Collaboration], Phys. Rev. Lett. **97** (2006) 242003 [arXiv:hep-ex/0609040].

[15] L. Wolfenstein, Phys. Rev. Lett. **51** (1983) 1945.

[16] C. Jarlskog, Phys. Rev. Lett. **55** (1985) 1039.

[17] A. J. Buras, M. E. Lautenbacher, G. Ostermaier, Phys. Rev. D **50** (1994) 3433.

[18] A. J. Buras, M. Jamin and P. H. Weisz, Nucl. Phys. B **347** (1990) 491.

[19] A. J. Buras and P. H. Weisz, Nucl. Phys. B **333** (1990) 66.

[20] V. M. Abazov *et al.* [DØ Collaboration], Phys. Rev. Lett. **97** (2006) 021802 [arXiv:hep-ex/0603029]; DØ Note 5618-CONF.

[21] A. S. Kronfeld and S. M. Ryan, Phys. Lett. B **543** (2002) 59 [arXiv:hep-ph/0206058]. D. Becirevic, S. Fajfer, S. Prelovsek and J. Zupan, Phys. Lett. B **563** (2003) 150 [arXiv:hep-ph/0211271]. V. Gadiyak and O. Loktik, Phys. Rev. D **72** (2005) 114504 [arXiv:hep-lat/0509075]. D. Becirevic, S. Fajfer and J. F. Kamenik, JHEP **0706** (2007) 003 [arXiv:hep-ph/0612224].

[22] M. Jamin and B. O. Lange, Phys. Rev. D **65** (2002) 056005 [arXiv:hep-ph/0108135].

[23] M. Beneke, G. Buchalla and I. Dunietz, Phys. Rev. **D54**, 4419 (1996). A. S. Dighe, T. Hurth, C. S. Kim and T. Yoshikawa, Nucl. Phys. B **624** (2002) 377 [arXiv:hep-ph/0109088].

[24] M. Beneke, G. Buchalla, C. Greub, A. Lenz and U. Nierste, Phys. Lett. B **459** (1999) 631 [arXiv:hep-ph/9808385].

[25] M. Beneke, G. Buchalla, A. Lenz and U. Nierste, Phys. Lett. B **576** (2003) 173 [arXiv:hep-ph/0307344].

[26] M. Ciuchini, E. Franco, V. Lubicz, F. Mescia and C. Tarantino, JHEP **0308** (2003) 031 [arXiv:hep-ph/0308029].

[27] A. Lenz and U. Nierste, JHEP **0706** (2007) 072 [arXiv:hep-ph/0612167].

[28] T. Inami and C. S. Lim, Progr. Theor. Phys. 65 (1981) 297 [Erratum: 65 (1981) 1772].

[29] S. Aoki *et al.* [JLQCD Collaboration], Phys. Rev. Lett. **91** (2003) 212001 [arXiv:hep-ph/0307039]. E. Dalgic *et al.*, arXiv:hep-lat/0610104; J. Shigemitsu for HPQCD Collaboration, talk at LATTICE 2006, http://www.physics.utah.edu/lat06/abstracts/sessions/weak/s1//Shigemitsu_Junko.pdf.

[30] A. I. Vaĭnsteĭn, V. I. Zakharov, V. A. Novikov and M. A. Shifman, Sov. J. Nucl. Phys. 23 (1976) 540. M. I. Vysotskiĭ, Sov. J. Nucl. Phys. 31 (1980) 797. F. J. Gilman and M. B. Wise, Phys. Rev. D27 (1983) 1128. J. M. Flynn, Mod. Phys. Lett. A5 (1990) 877. A. Datta, J. Fröhlich and E. A. Paschos, Z. Phys. C46 (1990) 63.

[31] S. Herrlich and U. Nierste, Nucl. Phys. B **419** (1994) 292.

[32] S. Herrlich and U. Nierste, Phys. Rev. D **52** (1995) 6505; Nucl. Phys. B **476** (1996) 27.

[33] D. J. Antonio *et al.* [RBC Collaboration and UKQCD Collaboration], Phys. Rev. Lett. **100** (2008) 032001 [arXiv:hep-ph/0702042].

[34] K. Anikeev *et al.*, *B physics at the Tevatron: Run II and beyond*, [hep-ph/0201071].

[35] A. J. Buras and D. Guadagnoli, Phys. Rev. D **78** (2008) 033005 [arXiv:0805.3887 [hep-ph]].

[36] Robert E. Marshak, Riazuddin and Ciaran P. Ryan, *Theory of weak interactions in particle physics*, Wiley-Interscience, New York, 1969.

[37] A. S. Dighe, I. Dunietz, H. J. Lipkin and J. L. Rosner, Phys. Lett. B **369** (1996) 144 [arXiv:hep-ph/9511363]. A. S. Dighe, I. Dunietz and R. Fleischer, Eur. Phys. J. C **6** (1999) 647 [arXiv:hep-ph/9804253].

[38] I. Dunietz, R. Fleischer and U. Nierste, Phys. Rev. D **63** (2001) 114015 [arXiv:hep-ph/0012219].

[39] Y. Grossman and M. P. Worah, Phys. Lett. B **395** (1997) 241 [arXiv:hep-ph/9612269].

[40] G. Buchalla and A. J. Buras, Nucl. Phys. B **400** (1993) 225. M. Misiak and J. Urban, Phys. Lett. B **451** (1999) 161 [arXiv:hep-ph/9901278].

[41] Y. Grossman and Y. Nir, Phys. Lett. B **398** (1997) 163 [arXiv:hep-ph/9701313].

[42] U. Nierste, Int. J. Mod. Phys. A **21** (2006) 1724 [arXiv:hep-ph/0511125].

[43] M. Gronau and D. London., Phys. Lett. B **253**, 483 (1991). M. Gronau and D. Wyler, Phys. Lett. B **265**, 172 (1991).

[44] M. Gronau and D. London, Phys. Rev. Lett. **65**, 3381 (1990).

[45] A. Höcker, H. Lacker, S. Laplace and F. Le Diberder, Eur. Phys. J. C **21**, 225 (2001) [arXiv:hep-ph/0104062]. J. Charles *et al.* [CKMfitter Group], Eur. Phys. J. C **41**, 1 (2005) [arXiv:hep-ph/0406184]. `http://ckmfitter.in2p3.fr`

[46] M. Ciuchini *et al.*, JHEP **0107**, 013 (2001)[arXiv:hep-ph/0012308]. M. Bona *et al.* [UTfit Collaboration], arXiv:hep-ph/0509219. `http://utfit.roma1.infn.it`

[47] Y. Nir, arXiv:hep-ph/0510413.

[48] A. J. Buras, arXiv:hep-ph/9806471.

[49] G. Buchalla, A. J. Buras and M. E. Lautenbacher, Rev. Mod. Phys. **68** (1996) 1125 [arXiv:hep-ph/9512380].

[50] R. Fleischer, arXiv:hep-ph/0405091.

[51] G. Burdman and I. Shipsey, Ann. Rev. Nucl. Part. Sci. **53** (2003) 431 [arXiv:hep-ph/0310076]. I. I. Bigi, Nucl. Phys. Proc. Suppl. **185** (2008) 121 [arXiv:0808.1773 [hep-ph]].

[52] G. Buchalla, arXiv:hep-ph/0103166.

[53] A. Ali, arXiv:hep-ph/0312303.

[54] I.I. Bigi and A.I. Sanda, *CP violation*, Cambridge University Press, Cambridge, 2000. G.C. Branco, L. Lavoura and J.P. Silva *CP Violation*, Clarendon Press, Oxford, 1999. Oxford Science Publications.

Electroweak radiative corrections and heavy top

M. I. Vysotsky[1]

[1]ITEP, Moscow, Russia

1 Lecture 1: 5 steps

Why are we going to speak about electroweak radiative corrections (ERC) in the summer 2008?

Practical aspects: SM prediction of the value of M_H from ERC: $M_H = (85 + 30 - 20)$ GeV.

If LHC discovers a heavy Higgs boson, it will mean that new electroweak nonsinglet particle(s) do exist.

Besides Higgs: if other particle(s) are discovered at LHC – their contribution(s) to ERC will be one of the first questions you would like to analyze.

So: ERC will be a hot topic at LHC.

Theoretical aspect: creation of the *renormalizable* theory of weak interactions in the 60's is one of the greatest achievements of theoretical physics in the XX century.

So: an educated person should know how to calculate *radiative corrections* in GWS theory.

Why to discuss ERC at the School on "Heavy Quark Physics"?
Usually (QED, QCD) heavy particle contributions to rad.corr. are damped.
Muon magnetic moment [1] :
$\mu = e/(2m_\mu)[1 + \alpha/(2\pi)(Schwinger) + ... + (m_\mu/\Lambda_0)^2$ (Berestetskii, Krohin, Khlebnikov, 1956)].

By the way, $\mu^{exp} = [1 + (1165920.8 \pm 0.6)10^{-9}]e/(2m_\mu)$, and experimental uncertainty corresponds to $\Lambda_0 > 3$ TeV, just LHC scale...

Nondecoupling.
In electroweak theory heavy particle contributions to radiative corrections are enhanced because of Higgs mechanism of mass generation. Let us estimate leading term in meson-antimeson transition amplitude [2] .
t'Hooft-Landau gauge, $G_H = 1/p^2$
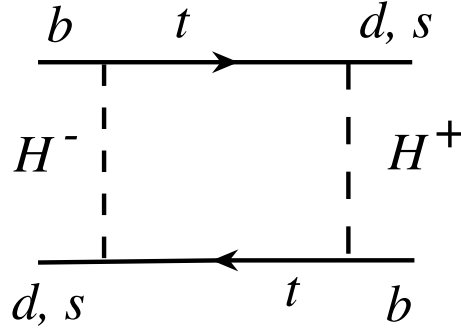
$$(m_t/\eta)^4 \int d^4 p p_\alpha p_\beta / [(p^2 - m_t^2)^2 p^4] =$$
$$\sim m_t^2/\eta^4 \sim G_F^2 m_t^2$$

$M_Z = 91.188(2) GeV; \ \ M_W = 80.400(25) GeV; \Gamma_Z, \ \ Br(Z \to l^+ l^-), \ \ A_{FB}^{l,c,b}$
and other parameters of Z are measured now with the precision better than 0.1 % .

How large are radiative corrections?

$\delta \sim \frac{g^2}{16\pi^2} = \frac{\alpha_W}{4\pi} = \frac{\alpha}{4\pi \sin^2\theta} \approx 0.2\% \Longrightarrow$

one needs to take into account these corrections to deal with experimental data.

Brief reminder.
QED: $\quad L(e_0, m_0)$
At one loop we get:

$$e = e_0[1 + c_e \frac{\alpha}{\pi} \ln \frac{\Lambda^2}{m_e^2}] , \ \ m = m_0[1 + c_m \frac{\alpha}{\pi} \ln \frac{\Lambda^2}{m_e^2}] , \tag{1}$$

where Λ is the ultraviolet cutoff.
e and m are measured with record precision and from (1) we get:
$e_0 \equiv e_0(\Lambda, m, e), \ m_0 \equiv m_0(\Lambda, m, e)$.
The next step is the calculation of some amplitude; say Compton scattering, $e\gamma \to e\gamma$:

$$A = A_0(e_0, m_0) + A_1(e_0, m_0, \Lambda) = A(e, m, s, t)$$

In this way we get a finite expression with one loop radiative corrections taken into account.
QED (quod erat demonstrandum).

$SU(2)_L \otimes U(1)$
The situation differs from QED.

Let us consider a gauge sector:

1. $L(g, g', \eta)$. These coupling constants and Higgs expectation value are not measured directly and are known with rather poor precision;

2. M_Z is known precisely, but it is not a parameter of the Lagrangian...

So, some modifications are needed.
Different approaches to study radiative corrections are possible.

1989 - start of SLC and LEP I;

LEPTOP, 1991 - 1995
Victor Novikov, Lev Okun, Alexander Rozanov, M.V. [3]

(ZFITTER (D.Yu. Bardin et al., Dubna - Zeuten) - was widely used by LEP collaborations to deal with raw data; other approaches can be found in the literature).

5 steps to heaven
1. The best measured observables: G_μ, m_Z, α

2. $G_\mu = G_\mu(g_0, \bar{g}_0, \eta_0; \Lambda)$, $\quad m_Z = ...,\quad \alpha = ...$

3. $g_0 = g_0(G_\mu, m_Z, \alpha; \Lambda)$; $\quad \bar{g}_0 = \bar{g}_0(G_\mu, m_Z, \alpha; \Lambda)$; $\eta_0 = \eta_0(G_\mu, m_Z, \alpha; \Lambda)$

4. $m_W = m_W(g_0, \bar{g}_0, \eta_0; \Lambda)$,

5. $m_W = m_W[g_0(G_\mu, m_Z, \alpha; \Lambda), \bar{g}_0(G_\mu, m_Z, \alpha; \Lambda), \eta_0(G_\mu, m_Z, \alpha; \Lambda); \Lambda]$
Dependence on Λ in the last expression cancels because the theory is renormalizable.
Take other observables
($\Gamma_Z = ...,\quad A_{FB} = ...,\quad ...$)
and repeat items 4 and 5.

This is all what is needed to take into account electroweak radiative corrections at one loop.

QED.

A technical remark: ultraviolet cutoff Λ breaks local gauge invariance. To restore it in QED one subtracts photon mass, which appears to be proportional to $e\Lambda$.
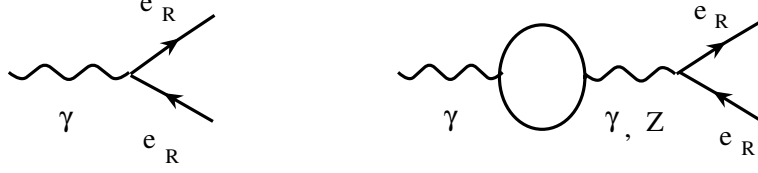In QAD we wish to calculate IVB masses.

The way out: dimensional regularization.
We will calculate integrals in $D = 4 - 2\varepsilon$ dimensional space-time, where they converge and local gauge invariance is not spoiled.

So, in all formulas instead of Λ poles $1/\varepsilon$ will occur. In final formulas which express physical quantities ($M_W, \Gamma_Z, ...$) through G_μ, m_Z, α these poles cancel.

step 2, α

$$\alpha = \frac{e_0^2}{4\pi}[1 - \Pi'_\gamma(0) - 2\frac{s}{c}\frac{\Pi_{\gamma Z}(0)}{M_Z^2}] \ , \tag{2}$$

where Z interaction is given by
$$\bar{g}(T_3 - Qs^2) = -Q\frac{s}{c}e, \quad \bar{g} = g/c = e/(cs)$$

$s \equiv sin\theta$ - the sine of electroweak mixing angle.

$\alpha \to \bar{\alpha}$

The obtained equation for fine structure constant can be used to get formulas for electroweak rad.corr.

However, since $\Pi'_\gamma(0) \sim \alpha \ln(\Lambda^2/m_{l,q}^2)$, where m_l and m_q are the masses of charged leptons and quarks, in final expressions u.v. cutoff Λ will be substituted by M_Z, and logarithmically enhanced rad. corr. will emerge.

Their physical sense is transparent: they correspond to α running from $q^2 = 0$ to the electroweak scale $q^2 = M_Z^2$.

It is very convenient to take this running into account from the very beginning, separating it from proper weak rad. corr.

$$\bar{\alpha} \equiv \alpha(M_Z) = \frac{e_0^2}{4\pi}[1 - \frac{\Pi_\gamma(M_Z^2)}{M_Z^2} - 2\frac{s}{c}\frac{\Pi_{\gamma Z}(0)}{M_Z^2}] \tag{3}$$

This equation will be used to determine the bare parameters of electroweak Lagrangian (remember that $e_0^2 = g_0^2(1 - \frac{g_0^2}{g_0'^2})$).

From Eqs (2,3) one should find the numerical value of $\bar{\alpha}$:

$$\bar{\alpha} = \frac{\alpha}{1 - \delta\alpha} \ , \ \ \delta\alpha = \Pi'_\gamma(0) - \frac{\Pi_\gamma(M_Z^2)}{M_Z^2} \ , \tag{4}$$

and for electron loop one easily obtains:

$$\delta\alpha = \frac{\alpha}{3\pi}\ln(\frac{M_Z^2}{m_e^2}) \ .$$

Substituting it into Eq.(4) we obtain one of the most famous equations in physics: zero charge formula of Landau, Abrikosov, Khalatnikov [4].

Summing up leptonic and hadronic contributions we get:

$$\alpha(M_Z) \equiv \bar{\alpha} = [128.95(5)]^{-1}$$

instead of $\alpha = [137.0359991(5)]^{-1}$.

step 2, M_Z

$$G^Z_{\mu\nu} = \frac{-ig_{\mu\nu}}{k^2 - M^2_{Z_0} + \Pi_Z(k^2)} + ... \ ,$$

The pole position corresponds to the Z-boson mass:

$$M^2_Z = M^2_{Z_0} - \Pi_Z(M^2_Z) , \quad M_{Z_0} = \frac{\bar{g}_0 \eta_0}{2} \ . \tag{5}$$

step 2, G_μ
$\mu \to e\nu_\mu\bar{\nu}_e$

It is convenient to divide rad. corr. into 2 parts: dressing of W - boson propagator, described by $\Pi_W(0)$, and vertexes and boxes, denoted by D:

$$\frac{G_\mu}{\sqrt{2}} = \frac{g^2_0}{8m^2_{W_0}}[1 + \frac{\Pi_W(0)}{M^2_W} + D] = \frac{1}{2\eta^2_0}[1 + \frac{\Pi_W(0)}{M^2_W} + D] \ . \tag{6}$$

What about logarithmic running of the weak charge from $q^2 \approx m^2_\mu$ to $q^2 \approx M^2_W$? $\Pi_W(q^2)$ contains logarithmic term: $\Pi_W(q^2) \sim q^2 \ln \frac{\Lambda^2}{max(q^2, m^2_e)}$. However, due to nonzero mass of IVB running takes place only above this mass.

So, there are two conditions for the charge to run logarithmically:
momentum transfer should be larger than the masses of the particles in the loop *and* larger than the mass of the corresponding vector boson.
Or the distances should be smaller...

That is why in the Z - and W - boson physics the big log occurs only in the running of α.

step 3

$$G_\mu = \frac{1}{\sqrt{2}\eta^2_0}[1 + \frac{\Pi_W(0)}{M^2_W} + D] \ ,$$

$$M^2_Z = \frac{1}{4}\bar{g}^2_0\eta^2_0 - \Pi_Z(M^2_Z) \ ,$$

$$4\pi\bar{\alpha} = g^2_0(1 - \frac{g^2_0}{\bar{g}^2_0})[1 - \frac{\Pi_\gamma(M^2_Z)}{M^2_Z} - 2\frac{s}{c}\frac{\Pi_{\gamma Z}(0)}{M^2_Z}]$$

.

For bare parameters we get:

$$\eta_0^2 = \frac{1}{\sqrt{2}G_\mu}[1 + \frac{\Pi_W(0)}{M_W^2} + D] \ ,$$

$$\bar{g}_0^2 = 4\sqrt{2}G_\mu M_Z^2[1 + \frac{\Pi_Z(M_Z^2)}{M_Z^2} - \frac{\Pi_W(0)}{M_W^2} - D] \ ,$$

and it is convenient to rewrite the equation for g_0 in the following way:

$$\frac{g_0^2}{\bar{g}_0^2}(1 - \frac{g_0^2}{\bar{g}_0^2}) = \frac{\pi\bar{\alpha}}{\sqrt{2}G_\mu M_Z^2}(1 + \frac{\Pi_W(0)}{M_W^2} - \frac{\Pi_Z(M_Z^2)}{M_Z^2} + \frac{\Pi_\gamma(M_Z^2)}{M_Z^2} +$$

$$+ 2\frac{s}{c}\frac{\Pi_{\gamma Z}(0)}{M_Z^2} + D) \ .$$

$sin\theta$

Arithmetic was enough to solve the first 2 equations; for the third one trigonometry is needed.

Let us define an electroweak mixing angle:

$$\sin^2\theta\cos^2\theta = \frac{\pi\bar{\alpha}}{\sqrt{2}G_\mu M_Z^2} \ , \quad \sin^2\theta = 0.2310(1)$$

and solve the third equation:

$$\frac{g_0}{\bar{g}_0} = c[1 + \frac{s^2}{2(c^2 - s^2)}(\frac{\Pi_Z(M_Z^2)}{M_Z^2} - \frac{\Pi_W(0)}{M_W^2} - \frac{\Pi_\gamma(M_Z^2)}{M_Z^2}$$

$$- 2\frac{s}{c}\frac{\Pi_{\gamma Z}(0)}{M_Z^2} - D)] \ .$$

step 4; custodial symmetry

Let us start from the W - boson mass:

$$M_W^2 = M_{W_0}^2 - \Pi_W(M_W^2) \ , \quad M_{W_0} = \frac{g_0\eta_0}{2} \ .$$

At step 2 an analogous equation was written for M_Z; using it we get:

$$\frac{M_W}{M_Z} = \frac{g_0}{\bar{g}_0}[1 + \frac{\Pi_Z(M_Z^2)}{2M_Z^2} - \frac{\Pi_W(M_W^2)}{2M_W^2}] \ .$$

If $U(1)$ charge g_0' were zero, then $g_0 = \bar{g}_0$, and at tree level $M_W = M_Z$, which is a good approximation to the real life: $80 GeV \approx 90 GeV$.

t: *anti*custodial symmetry

What about loops? If $m_{up} = m_{down}$, then $\Pi_Z(M_Z^2) = \Pi_W(M_W^2)$ and IVB stay degenerate.

In the real life top quark is extremely heavy, and the contribution of the (t, b) doublet to the difference of W- and Z- boson masses is enhanced as $m_t^2/M_Z^2 \approx 4$.

step 5, M_W

$$\frac{M_W}{M_Z} = c + \frac{c^3}{2(c^2 - s^2)}\left(\frac{\Pi_Z(M_Z^2)}{M_Z^2} - \frac{\Pi_W(M_W^2)}{M_W^2}\right)+$$

$$+\frac{cs^2}{2(c^2 - s^2)}\left(\frac{\Pi_W(M_W^2)}{M_W^2} - \frac{\Pi_W(0)}{M_W^2} - \frac{\Pi_\gamma(M_Z^2)}{M_Z^2}-\right.$$

$$\left.-2\frac{s}{c}\frac{\Pi_{\gamma Z}(0)}{M_Z^2} - D\right) \ ,$$

UV divergences cancel in the last expression:
*the formula for finite one loop ew rad. corr. to the ratio of IVB masses is obtained!!!*

$Z \to l^+l^-$ Reminding that Z-boson coupling constant is $\bar{g}_0$ and corresponding generator equals
$T_3 - s_0^2 Q$
we get for the decay amplitude at the tree level:

$$A_0 = \frac{\bar{g}_0}{2}\bar{l}\left[-\frac{1}{2}\gamma_\alpha\gamma_5 - \left(\frac{1}{2} - 2s_0^2\right)\gamma_\alpha\right]l \ Z_\alpha \ .$$

Taking into account the expressions for $\bar{g}_0$ and $g_0/\bar{g}_0$ as well as the loop corrections to the tree diagram we straightforwardly obtain the expression for the decay amplitude free from the ultraviolet divergences.
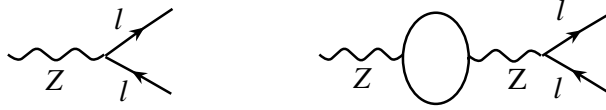
$$A = \sqrt{\sqrt{2}G_\mu M_Z^2}\left[1 + \frac{\Pi_Z(M_Z^2)}{2M_Z^2} - \frac{\Pi_W(0)}{2M_W^2} - \frac{1}{2}D-\right.$$

$$\left.-\frac{1}{2}\Pi_Z'(M_Z^2)\right] \times \left[\left(-\frac{1}{2} + F_A\right)\bar{l}\gamma_\alpha\gamma_5 l+\right.$$

$$+\left(2s^2 - \frac{1}{2} + F_V + 2cs\frac{\Pi_{Z\gamma}(M_Z^2)}{M_Z^2} + \frac{2s^2c^2}{c^2 - s^2}\times\right.$$

$$\times\left(\frac{\Pi_W(0)}{M_W^2} - \frac{\Pi_Z(M_Z^2)}{M_Z^2} + \frac{\Pi_\gamma(M_Z^2)}{M_Z^2} + 2\frac{s}{c}\frac{\Pi_{\gamma Z}(0)}{M_Z^2} + D\right)\right)$$

$$\bar{l}\gamma_\alpha l\Big] \ ,$$

where functions F_A and F_V take into account corrections to Zll vertex.

step 5, g_A and g_V
Let us rewrite the expression for the decay amplitude:

$$A = \sqrt{\sqrt{2}G_\mu M_Z^2}\bar{l}[g_A\gamma_\alpha\gamma_5 + g_V\gamma_\alpha]l \ Z_\alpha \ .$$

The UV finite expressions for axial and vector coupling constants are given by a long formula above.

2 Lecture 2: top and Higgs

Formulas for electroweak radiative corrections obtained in the first lecture are characterized by strong dependence on the top quark mass which helped to find the top at TEVATRON in 1994.

There are two places in ew corrections to IVB parameters where top quark contributions are enhanced:

1. the polarization operators (of nonconserved currents);
2. $Z \to t\bar{t} \to b\bar{b}$ decay amplitude.

Why does current nonconservation matter?
$\Pi_\gamma(q^2)$, $\Pi_{\gamma Z}(q^2) \sim [g_{\mu\nu}q^2 - q_\mu q_\nu](a + bq^2/m_t^2 + ...)$,
while $\Pi_W \sim g_{\mu\nu}(m_t^2 + ...)$.

m_t^2 term from Π's
In the limit $m_t^2 \gg m_W^2, m_Z^2$ we have:
$\Pi(m_V^2) = \Pi(0)$, that is why we get the following relations:

$$\frac{M_W}{M_Z} = c + \frac{c^3}{2(c^2 - s^2)}\left(\frac{\Pi_Z(0)}{M_Z^2} - \frac{\Pi_W(0)}{M_W^2}\right) \ ,$$

$$g_A = -\frac{1}{2} - \frac{1}{4}\left(\frac{\Pi_Z(0))}{M_Z^2} - \frac{\Pi_W(0)}{M_W^2}\right) \ ,$$

$$g_V/g_A = 1 - 4s^2 + \frac{4c^2 s^2}{c^2 - s^2}\left(\frac{\Pi_Z(0)}{M_Z^2} - \frac{\Pi_W(0)}{M_W^2}\right) \ .$$

In order to honestly calculate the m_t dependence of the physical observables one should calculate the top quark contributions to polarization operators:

$$-i\Pi_{\mu\nu}^\psi(q^2) = -$$

$$-\int \frac{d^D k}{(2\pi)^D \mu^{D-4}} \frac{Sp\gamma_\mu(\gamma_5)(\hat{k} + m_1)\gamma_\nu(\gamma_5)(\hat{k} + \hat{q} + m_2)}{(k^2 - m_1^2)((k+q)^2 - m_2^2)} \ ,$$

where we use dimensional regularization of the quadratically divergent expression: $D = 4 - 2\varepsilon$ and the factor μ takes care of the canonical dimension of the integral.
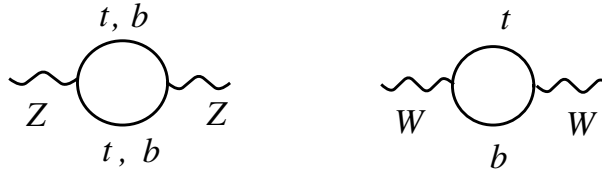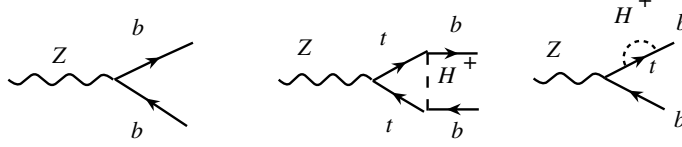

"Back of the envelope" calculation of m_t^2 term:

$$\frac{\Pi_Z^\psi(0)}{M_Z^2} - \frac{\Pi_W^\psi(0)}{M_W^2} = \frac{3\bar{\alpha}}{8\pi c^2 s^2 M_Z^2} \int \frac{dp^2}{(p^2 + m_t^2)^2} \times$$

$$\times \left[p^4/2 + (p^2 + m_t^2)^2/2 - p^2(p^2 + m_t^2)\right] =$$

$$= \frac{3\bar{\alpha}}{16\pi c^2 s^2}(\frac{m_t}{M_Z})^2 \quad .$$

Specific for $Z \to bb$ decay m_t^2 term comes from:

Htb vertex is proportional to m_t, that is why one-loop diagrams produce correction to Zbb coupling enhanced as $(m_t/M_Z)^2$.

To calculate this correction we can neglect Z-boson momentum.

Z-boson coupling is proportional to $T_3 - Qs^2$. The part proportional to b-quark electric charge Q induces vector coupling which is not renormalized by Higgs loop (CVC) - so, at zero momentum transfer $(q_\mu^Z = 0)$ the sum of one loop diagrams is zero.

What remains is T_3 which induces the coupling with b_L and t_L.

And again the vector part is not renormalized, so only axial current remains.

Since Z-boson has only vector coupling with Higgs, we should not calculate corresponding vertex diagram. And only the diagram with Ztt coupling should be taken into account.

Calculating a vertex diagram with UV cutoff Λ we get:

$$\bar{g}/4/(16\pi^2)(\frac{m_t}{\eta/\sqrt{2}})^2 \times$$

$$\times[-1/2 ln(\Lambda^2/m_t^2) + 3/2]\bar{b}\gamma_\alpha \frac{(1+\gamma_5)}{2} b \, Z_\alpha \, ,$$

while (tH) insertions into external legs give:

$$\bar{g}/4/(16\pi^2)(\frac{m_t}{\eta/\sqrt{2}})^2 \times$$

$$\times[1/2 ln(\Lambda^2/m_t^2) + 1/2]\bar{b}\gamma_\alpha \frac{(1+\gamma_5)}{2} b \, Z_\alpha \, .$$

The sum of the two last expressions produces correction to g_L^b:

$$-\bar{g}/2[1 - (\frac{m_t}{\eta/\sqrt{2}})^2/(16\pi^2)]\bar{b}\gamma_\alpha \frac{(1+\gamma_5)}{2} b \, Z_\alpha =$$

$$= -\bar{g}/2[1 - \frac{\alpha}{8\pi c^2 s^2}(\frac{m_t}{M_Z})^2]b\gamma_\alpha \frac{(1+\gamma_5)}{2} b \, Z_\alpha \, ,$$

which reduces $\Gamma_Z(bb)$.

M_H

Electroweak rad. corr. depend on M_H. This is the reason why from precision measurement of Z- and W-boson parameters the value of M_H is extracted.

Which diagrams matter? The radiation of Higgs from the fermion line is proportional to m_f/η, and since $\eta = 1/(\sqrt{\sqrt{2}G_\mu}) = 246 GeV$ even in the case of b-quark it should be neglected.

What remain are the vector boson polarization operators (just as in the case of top, if we forget for the moment $Z \to bb$ decay).

It is convenient to perform calculations in unitary gauge where the nonphysical degrees of freedom $(H^\pm, Im H^0)$ are absent.
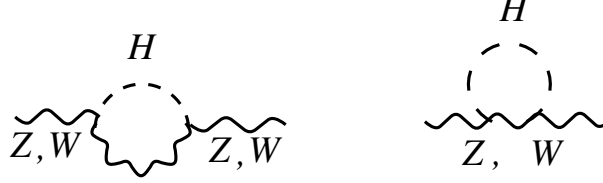
The following substitution allows to extract Higgs interactions with W-boson from W mass term:

$$(\frac{g\eta}{2})^2|W|^2 \to (\frac{g(\eta + H^0)}{2})^2|W|^2 =$$

$$= (\frac{g\eta}{2})^2|W|^2 + \frac{1}{2}g^2\eta H^0|W|^2 + \frac{g^2}{4}H^{0^2}|W|^2 =$$

$$= M_W^2|W|^2 + gM_W H^0|W|^2 + \frac{1}{4}g^2 H^{0^2}|W|^2 \ \ .$$

Analogously from the Z-boson mass term in Lagrangian we can obtain HZZ and $HHZZ$ coupling constants.

A less trivial example is the extraction of $H\gamma\gamma$ vertex from the following one loop effective Lagrangian:

$$L_{eff}(q^2 \ll M^2) = \frac{1}{4}F_{\mu\nu}^2 \times$$

$$\times \sum \frac{b_i e^2}{16\pi^2}log(\frac{\Lambda^2}{M_i^2}) \ \ ,$$

where $b = -4/3$ for a charged lepton, $-4Q^2$ for a (colored) quark, 7 for W-boson are the coefficients of Gell-Mann – Low function. Substituting $M = f(g)\eta(1 + H/\eta)$ and expanding the logarithm we obtain the amplitude of $H \to \gamma\gamma$ decay. The most remarkable in the last formula is the sign of the W loop contribution, opposite to that of the lepton and quark loop, and number 7 as well.

Asymptotic freedom in the USSR, 1965.

Let me start from number 7 obtained by V.S.Vanyashin and M.V.Terentiev in their 1965 ZhETPh paper [5] . At present the easiest way to derive it is the following:

$7 = 11/3C_V - 1/6 - 1/6, C_V = 2$ for $SU(2)$,

where $11/3C_V$ is the contribution of the massless vectors in adjoint representation to the β-function. One factor $1/6$ comes from the Higgs doublet contribution to the same SU(2) β-function, while another $1/6$ is the Higgs doublet contribution to the running of the coupling constant g',

$$1/e = 1/g + 1/g' \ \ .$$

Concerning the sign Vanyashin and Terentiev stressed that it is *opposite* to that which *always* occurs in QFT.

A bit of history: I heard from Terentiev that when he was giving a talk at ITEP seminar on this paper Pomeranchuk said that evidently the theory was not selfconsistent (he relied upon Landau - Pomeranchuk "zero-charge" theorem). At the end of the paper this "wrong sign" behavior of β-function was attributed to nonrenormalizability of the electrodynamic of massive charged vector bosons.

However in the Abstract the anomalous character of the electric charge renormalization was emphasized.

M.V. Terentiev worked at ITEP, V.S. Vanyashin worked and is still working at Dnepropetrovsk Physico-Technical Institute.

It is remarkable that if Higgs boson mass is around 120 GeV (which is quite probable: SM fit, see below) than $H \to \gamma\gamma$ decay will play the important role in Higgs discovery and factor "7" will become known to everybody in hep community 45 years after its first appearance.

Back to Higgs in radiative corrections.

Calculation of W- and Z-boson polarization operators provides us with explicit dependence of physical observables on M_H. In the limit $M_H \gg M_Z$ we get:

$$\Pi_W^H \sim M_H^2 \ln(M_H^2) + M_H^2 + (M_W^2 + q^2)\ln(M_H^2) .$$

In the differences of polarization operators on which physical quantities depend:

$$\frac{\Pi_W(M_W^2)}{M_W^2} - \frac{\Pi_W(0)}{M_W^2} , \quad \frac{\Pi_Z(M_Z^2)}{M_Z^2} - \frac{\Pi_W(M_W^2)}{M_W^2} \quad \text{and}$$

$$\Pi_Z'(M_Z^2)$$

the first two terms cancel and we are left with the logarithmic dependence on Higgs mass .

Heavy top and Higgs asymptotics:

$$\frac{M_W}{M_Z} = c + \frac{3\bar{\alpha}c}{32\pi s^2(c^2 - s^2)}\left[(\frac{m_t}{M_Z})^2 - \frac{11}{9}s^2\ln(\frac{M_H}{M_Z})^2\right],$$

$$g_A = -\frac{1}{2} - \frac{3\bar{\alpha}}{64\pi c^2 s^2}\left[(\frac{m_t}{M_Z})^2 - s^2\ln(\frac{M_H}{M_Z})^2\right],$$

$$\frac{g_V}{g_A} = 1 - 4s^2 + \frac{3\bar{\alpha}}{4\pi(c^2 - s^2)}\left[(\frac{m_t}{M_Z})^2 - (s^2 + \frac{1}{9})\times\right.$$

$$\left.\times \ln(\frac{M_H}{M_Z})^2\right].$$

Since the coefficients multiplied by log are almost equal, without the knowledge of the value of m_t one could not determine the value of M_H.

3 Lecture 3: SM fits; NP contributions

After top discovery at Tevatron in 1994 the electroweak precision data provide information on Higgs mass.

The dependence on M_H is provided by Π's; the "constants" are also very important. The expressions in square brackets at a previous slide are substituted by three functions:

$$V_m(t,h)\,, V_A(t,h)\,, V_R(t,h)\,;$$

$$t \equiv (m_t/M_Z)^2, h \equiv (M_H/M_Z)^2,$$

which take into account all the existing loop calculations ($\alpha_W, \alpha_s\alpha_W,...$, for details see Novikov, Okun, Rozanov, Vysotsky [3] .

Yellow Report

After the first years of LEPI operation it has become clear that the experimental data on Z parameters will have very high accuracy. That is why 4 codes which existed in literature have been compared with the aims to check numerical consistency of the different approaches to radiative corrections calculation and to determine theoretical uncertainties.

The results are published in the CERN Yellow Report 95-03, Editors D.Bardin, W. Hollik, G.Passarino [6] .

From history to our days.
LEPTOP fit of the precision observables (A.Rozanov, Summer 2008).

Observable	Exper. data	LEPTOP fit	Pull
Γ_Z, GeV	2.4952(23)	2.4963(15)	-0.5
σ_h, nb	41.540(37)	41.476(14)	1.8
R_l	20.771(25)	20.743(18)	1.1
A_{FB}^l	0.0171(10)	0.0164(2)	0.8
A_τ	0.1439(43)	0.1480(11)	-0.9
R_b	0.2163(7)	0.2158(1)	0.7
R_c	0.172(3)	0.1722(1)	-0.0
A_{FB}^b	0.0992(16)	0.1037(7)	-2.8
A_{FB}^c	0.0707(35)	0.0741(6)	-1.0
$s_l^2\,(Q_{\mathrm{FB}})$	0.2324(12)	0.2314(1)	0.8

Observable	Exper. data	LEPTOP fit	Pull
A_{LR}	0.1513(21)	0.1479(11)	1.6
A_b	0.923(20)	0.9349(1)	-0.6
A_c	0.670(27)	0.6682(5)	0.1
m_W, GeV	80.398(25)	80.377(17)	0.9
m_t, GeV	172.6(1.4)	172.7(1.4)	-0.1
M_{H}, GeV		84^{+32}_{-24}	
$\hat\alpha_s$		0.1184(27)	
$1/\bar\alpha$	128.954(48)	128.940(46)	0.3
$\chi^2/n_{\mathrm{d.o.f}}$		18.1/12	

With 10 MeV experimental accuracy of M_W the accuracy in M_H will be (+20 -15) GeV, while at the moment $M_H < 140(150)$GeV at 95% C.L., $M_H < 185(200)$GeV at 99.5% C.L.

(numbers in brackets take into account theoretical uncertainty).

This is the end of the Standard Model story.

The main results for other domains of particle physics:

1. QCD: power corrections for Z width into hadrons are definetly negligible; the obtained value of $\hat{\alpha}_s$ appears to be considerably larger than (some) QCD people believed; in particular J/ψ is outside of the perturbative QCD domain;

2. GUT: the precise determination of $sin\theta$ excludes simplest SU(5) unification theory without low energy SUSY.

New Physics.

What if LHC after a couple of months of operation will announce the discovery of 300 GeV (or even heavier) Higgs?

It will definitely mean that beyond Standard Model there are other electroweak nonsinglet particles which contribute to the functions V_i and shift the value of M_H in the minimum of χ^2.

Before discussing New Physics contribution to radiative corrections let me present two popular sets of parameters widely used in literature.

$\varepsilon_1, \varepsilon_2, \varepsilon_3$

A set of three parameters ε_i has been suggested by Altarelli, Barbieri and Jadach for the most general phenomenological analysis of New Physics [7]. These parameters are in one-to-one correspondence with our parameters V_i:

$$\varepsilon_1 \sim \alpha_W V_A$$

$$\varepsilon_2 \sim \alpha_W[(V_A - V_m) - 2s^2(V_A - V_R)]$$

$$\varepsilon_3 \sim \alpha_W(V_A - V_R)$$

Since ε_2 and ε_3 do not contain the leading $\sim m_t^2$ term, their values were useful in search for New Physics before the mass of top quark was measured directly.

S, T, U

These letters, popular in particle physics, were used by Peskin and Takeuchi for the parametrization of the so-called oblique corrections due to New Physics contribution to electroweak observables [8]. Schematically:

$$\delta\varepsilon_1 = \alpha T , \ \ \delta\varepsilon_2 \sim \alpha U , \ \ \delta\varepsilon_3 = \alpha S ,$$

where δ means that only NP contributions should be taken into account.

Literally, Peskin and Takeuchi made one more step. Discussing NP with a scale much larger than M_Z they expanded the polarization operators at $q^2 = 0$, taking into account only the first two terms, $\Pi(0)$ and $\Pi'(0)$, which is the correct approximation as far as higher derivatives are suppressed as $[(M_Z^2)/(M_{NP}^2)]^n$. One can find in the literature (PDG) the allowed domains of S, U and T for a given value of Higgs mass and check, if your favourite NP model falls in these domains.

However, some caution is necessary:

1. if the mass of a new particle is only slightly above $M_Z/2$ then the heavy mass expansion does not work;

2. the allowed domain of S, U and T depends on M_H.

To decouple or to nondecouple?
This is the first question you must ask analyzing NP. The most famous example of NP with decoupling is SUSY.

Why do sleptons and squarks decouple? Because mass splitting within SU(2) doublet is small, while from scalar fields you can organize only vector current, which is conserved. What about charginos and higgsinos? They form vector multiplets (not chiral) which also decouples.

As a result the direct searches of the superpartners push lower limits on their masses so high (hundreds of GeV) that their contributions to rad.corr. are MOSTLY negligible.

Is there any relation between low energy SUSY and rad. corr. except SUSY GUT?

Yes: in all the variants of SUSY the lightest Higgs boson mass appeared to be less than 200 GeV, usually close to 100 GeV, which nicely coincides with the values of M_H obtained from rad. corr.

4 generation [9].
The simplest example of nondecoupled New Physics. It nondecouples just as the third generation with heavy top. Mass of the neutral lepton N should be larger than $M_Z/2$ since Z boson width allows only 3 light neutrino flavors.

Many new parameters: masses of new particles and their mixing with three light generations. For simplicity let us suppose that mixing is small.

At the next two slides the results of data fit by the LEPTOP code performed by Alexander Rozanov in summer 2008 are presented.

4 generation with 120 GeV Higgs
$m_E = 200$GeV, $m_U + m_D = 450$ GeV, $\chi^2/d.o.f. = 17.6/11$, the quality of fit is the same as in SM.

4 generation with 600 GeV Higgs
$m_E = 200$GeV, $m_U + m_D = 450$ GeV, $\chi^2/d.o.f. = 17.4/11$, the quality of the fit is the same as in SM.
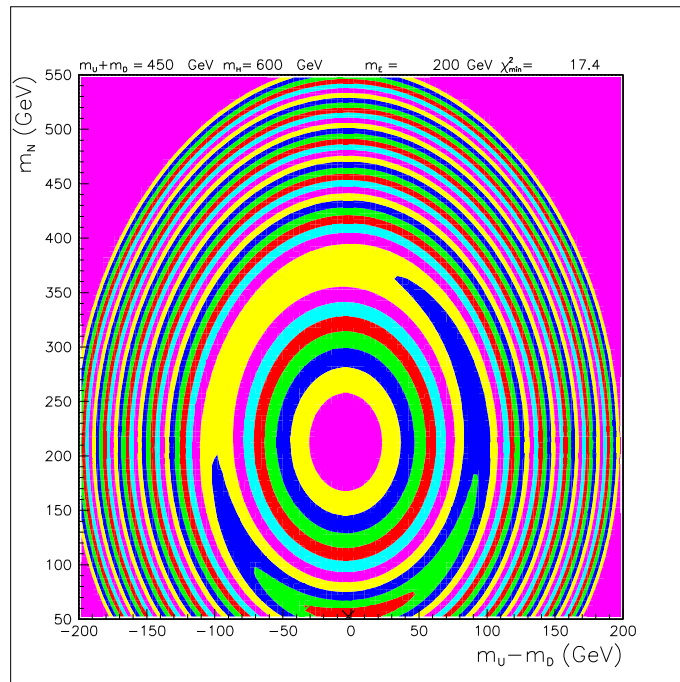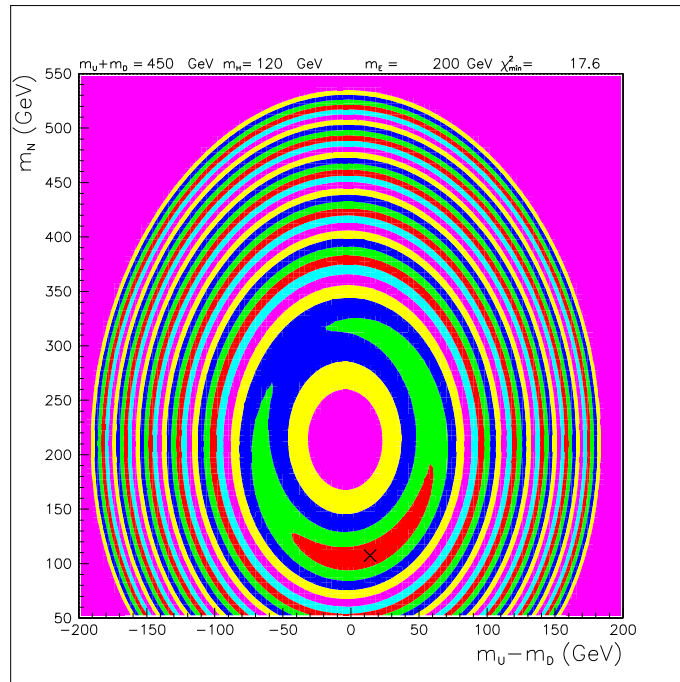
So: Higgs is light ONLY in SM or if NP decouples.

Soon after LHC will start to produce physics the last pages of Electroweak Interactions will be written.

References

[1] V.B. Berestetskii, O.I. Krohin, A.K. Khlebnikov, ZhETF **30** 788 (1956).

[2] M.I. Vysotsky, Yad.Fiz. **31** 1535 (1980).

[3] V.A. Novikov, L.B. Okun, A.N. Rozanov, M.I. Vysotsky,"LEPTOP", hep-ph/9503308; Rep. Prog. Phys. **62**, 1275 (1999).

[4] L.D. Landau , A.A. Abrikosov, I.M. Khalatnikov, DAN USSR **95**, 497, 773, 1117 (1954).

[5] V.S. Vanyashin, M.V. Terentiev, ZhETF **48** 568 (1965).

[6] CERN Yellow Report 95-03(1995), Editors: D.Bardin, W.Hollik, G.Passarino.

[7] G. Altarelli, R. Barbieri, Phys. Lett. **B253** 161 (1991); Nucl. Phys. **B369** 3 (1992).

[8] M. Peskin, T. Takeuchi, Phys. Rev. Lett. **65** 964 (1990); Phys. Rev. **D46** 381 (1992).

[9] M. Maltoni, V.A. Novikov, L.B. Okun, A.N. Rozanov, Phys.Lett. **B476** 107 (2000); V.A. Novikov, L.B. Okun, A.N. Rozanov, JETP Lett. **76** 127 (2002), Pisma v ZhETF **76** 158 (2002).

Higher radiative corrections in HQET

Andrey Grozin

Budker Institute of Nuclear Physics, Novosibirsk 630090, Russia

After a brief introduction to Heavy Quark Effective Theory, we discuss α representation in HQET and methods of calculation of some kinds of HQET diagrams up to three loops.

1 Introduction

Effective field theories are very useful for describing physics at low energies $\ll M$, or large distances $\gg 1/M$, where M is a high energy scale where some new particles or interactions become important. Effective Lagrangians are constructed as series in $1/M$. Coefficients in them are obtained by matching scattering amplitudes in the full theory and in the effective one up to some order in $1/M$. These matching coefficients are the only quantities which depend on M. All calculations inside the effective theory involve only characteristic energy scales (they are $\ll M$) of processes under consideration. The case when there is one such scale is especially simple. We can choose the renormalization scale μ of order of this characteristic energy scale. Then there will be no large logarithms in perturbative series, and truncating such series will produce small errors. If we try to consider the same process in the full theory, there is a second scale M, and no choice of μ allows us to get rid of large logarithms. Also, each extra scale in Feynman diagrams (with loops) makes their calculation much more difficult technically.

Heavy Quark Effective Theory (HQET) is an effective low-energy field theory for some problems in QCD. In many widely-known effective field theories (Heisenberg–Euler theory of low-energy photon interactions, Fermi 4-fermion theory of weak interactions at low energies) the heavy particle (electron or W in these examples) does not appear. In HQET, the heavy quark appears in initial and final states, but is always nearly on-shell and non-relativistic (in some reference frame).

HQET is discussed in textbooks [1, 2] in detail. Here we shall concentrate on methods and results of calculations of multiloop Feynman diagrams in HQET, see e.g. [3]. Various methods of multiloop calculations are presented in the excellent book [4] in great detail, most of these methods are used in HQET.

2 Heavy Quark Effective Theory

2.1 Lagrangian and Feynman rules

We are going to consider a class of QCD problems involving a single heavy quark with (on-shell) mass $m \gg \Lambda_{\rm QCD}$. Namely, we require that there exists a reference frame where it stays nearly at rest all the time. In other words, there exists a 4-velocity v ($v^2 = 1$) such that

$$p = mv + \tilde{p}, \qquad (2.1)$$

and the characteristic residual momentum $\tilde{p}^{\mu} \ll m$. Light quarks and gluons also have characteristic momenta $p_i^{\mu} \ll m$. Such problems can be described, instead of QCD, by a simpler effective field theory called HQET. Its Lagrangian is a series in $1/m$. At the leading order,

$$L = \overline{\tilde{Q}}_v iv \cdot D \tilde{Q}_v + \mathcal{O}\left(\frac{1}{m}\right) + \text{(light fields)} . \tag{2.2}$$

The HQET heavy-quark field satisfies $\slashed{v}\tilde{Q}_v = \tilde{Q}_v$. All light fields are described as in QCD. In the v rest frame,

$$L = \tilde{Q}^{+} i D_0 \tilde{Q} + \mathcal{O}\left(\frac{1}{m}\right) + \text{(light fields)} , \tag{2.3}$$

where $\tilde{Q}$ is a 2-component spinor.

The mass shell of the heavy quark, i.e., the dependence of its residual energy $\tilde{p}_0$ on its momentum $\vec{p}$, is

$$\tilde{p}_0 = p_0 - m = \frac{\vec{p}^{\,2}}{2m} .$$

At the leading order in $1/m$, it becomes $\tilde{p}_0 = 0$. This is exactly what follows from the Lagrangian (2.3).

The HQET Lagrangian (2.2) is not Lorentz-invariant, because it contains a fixed vector v. However, v is not uniquely defined. It can be changed by $\sim \tilde{p}/m$ (see (2.1)). Lagrangians with such different choices of v must produce identical physical predictions. This requirement is called reparametrization invariance, and it restricts $1/m^n$ corrections in the Lagrangian.

The heavy-quark chromomagnetic moment is, by dimensionality, $\sim 1/m$. Therefore, at the leading order the heavy-quark spin does not interact with the gluon field. We may rotate the spin at will without changing physics — heavy-quark spin symmetry. In particular, B and B^* are degenerate and have identical properties, because they can be transformed into each other by rotating the b spin. We can even change the magnitude of the heavy-quark spin (e.g., to switch it off) without changing physics — this supersymmetry group is called superflavour symmetry.

It is difficult to simulate a QCD heavy quark on the lattice because the lattice spacing a must be much less than the minimum characteristic distance of the problem, $1/m$. The HQET Lagrangian does not contain m, and the only applicability condition of its discretization is $a \ll 1/\tilde{p}$. When we investigate the structure of heavy–light hadrons, $\tilde{p} \sim \Lambda_{\text{QCD}}$, and the condition $a \ll 1/\Lambda_{\text{QCD}}$ is the same as for light hadrons.

The Lagrangian (2.2) gives the Feynman rules

$$\underset{\tilde{p}}{\Longrightarrow} = i\,\frac{1+\slashed{v}}{2}\,\frac{1}{\tilde{p} \cdot v + i0}\,, \qquad \overset{a\ \mu}{\Longrightarrow} = igt^a v^{\mu} . \tag{2.4}$$

In the v rest frame, the propagator is (the unit 2×2 spin matrix assumed)

$$i\,\frac{1}{\tilde{p}_0 + i0} . \tag{2.5}$$

In the coordinate space, the heavy quark does not move:

$$\underset{0 \qquad\qquad x}{\Longrightarrow} = -i\theta(x_0)\delta(\vec{x}) . \tag{2.6}$$

HQET-quark loops vanish because the heavy quark propagates only forward in time. We can also see this in the momentum space: all poles of the propagators in such a loop are in the lower $\tilde{p}_0$ half-plane, and closing the integration contour upwards, we get 0.

These Feynman rules can be also obtained from QCD at $m \to \infty$. The QCD massive-quark propagator gives the HQET one:

$$
\underset{mv + \tilde{p}}{\longrightarrow} = \underset{\tilde{p}}{\longrightarrow} + \mathcal{O}\left(\frac{\tilde{p}}{m}\right),
$$
$$
\frac{m + m\not{v} + \not{\tilde{p}}}{(mv + \tilde{p})^2 - m^2 + i0} = \frac{1 + \not{v}}{2} \frac{1}{\tilde{p} \cdot v + i0} + \mathcal{O}\left(\frac{\tilde{p}}{m}\right). \tag{2.7}
$$

The QCD vertex, when sandwiched between two projectors, becomes the HQET one:

$$
\frac{1 + \not{v}}{2} \gamma^\mu \frac{1 + \not{v}}{2} = \frac{1 + \not{v}}{2} v^\mu \frac{1 + \not{v}}{2}. \tag{2.8}
$$

When there is an external leg near a vertex, there is no projector; but we can insert it, and the argument holds.

We have thus proved that at the tree level any QCD diagram is equal to the corresponding HQET diagram up to $\mathcal{O}(\tilde{p}/m)$ corrections. This is not true at loops, because loop momenta can be arbitrarily large. Renormalization properties of HQET (anomalous dimensions, etc.) differ from those in QCD.

2.2 One-loop propagator diagram

Let's calculate the simplest one-loop diagram (Fig. 1)

$$
\frac{1}{i\pi^{d/2}} \int \frac{d^d k}{\left[-2\left(k + \tilde{p}\right) \cdot v - i0\right]^{n_1} \left[-k^2 - i0\right]^{n_2}} =
$$
$$
\frac{1}{i\pi^{d/2}} \int \frac{dk_0 \, d^{d-1}\vec{k}}{\left[-2\left(k_0 + \omega\right) - i0\right]^{n_1} \left[-k_0^2 + \vec{k}^{\,2} - i0\right]^{n_2}} = (-2\omega)^{d - n_1 - 2n_2} I(n_1, n_2). \tag{2.9}
$$

It depends only on the residual energy $\omega = \tilde{p}_0$, not $\vec{\tilde{p}}$; the power of -2ω is clear from dimensional counting.
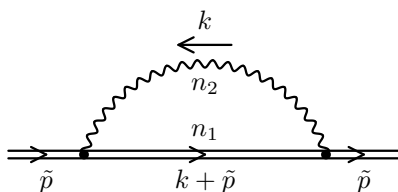

Figure 1: One-loop propagator diagram

If $\omega > 0$, real pair production is possible, and we are on a cut. We shall consider the case $\omega < 0$, when the integral is an analytic function of ω. We'll set $-2\omega = 1$. If n_1 is integer and

$n_1 \leq 0$, $I(n_1, n_2) = 0$ because this is a massless vacuum diagram. If n_2 is integer and $n_2 \leq 0$, $I(n_1, n_2) = 0$ because the diagram contains an HQET loop.

At $\omega < 0$, all poles in the k_0 plane are below the real axis at $k_0 > 0$ and above the real axis at $k_0 < 0$, and we can rotate the integration contour counterclockwise without crossing poles (if $\omega > 0$, we cross the pole at $k_0 = -\omega - i0$). This Wick rotation

$$k_0 = i k_{E0} \tag{2.10}$$

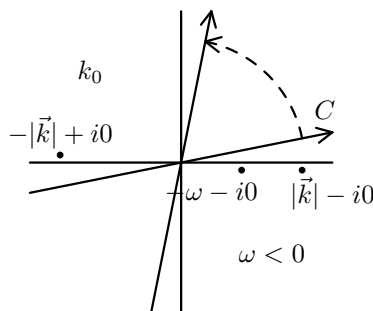(Fig. 2) brings us into Euclidean momentum space ($k^2 = -k_E^2$).

Figure 2: Wick rotation

In the Euclidean space,

$$I(n_1, n_2) = \frac{1}{\pi^{d/2}} \int \frac{dk_{E0}}{\left(1 - 2ik_{E0}\right)^{n_1}} \int \frac{d^{d-1}\vec{k}}{\left(\vec{k}^2 + k_{E0}^2\right)^{n_2}} . \tag{2.11}$$

Using the well-known formula

$$\int \frac{d^d k_E}{(k_E^2 + m^2)^n} = \pi^{d/2} (m^2)^{d/2-n} \frac{\Gamma\left(n - \frac{d}{2}\right)}{\Gamma(n)} \tag{2.12}$$

with $d \to d - 1$, $m^2 \to k_{E0}^2$, $n \to n_2$, we obtain

$$I(n_1, n_2) = \frac{\Gamma\left(n_2 - \frac{d-1}{2}\right)}{\pi^{1/2}\Gamma(n_2)} \int \frac{\left(k_{E0}^2\right)^{(d-1)/2 - n_2} dk_{E0}}{\left(1 - 2ik_{E0}\right)^{n_1}} . \tag{2.13}$$

The integrand is even in k_{E0}, and has cuts at $k_{E0}^2 < 0$ (it would be wrong to write it as $k_{E0}^{d-1-2n_2}$). Deforming the integration contour around the upper cut (Fig. 3), we can express the integral via the discontinuity at this cut:

$$I(n_1, n_2) = 2 \frac{\Gamma\left(n_2 - \frac{d-1}{2}\right)}{\pi^{1/2}\Gamma(n_2)} \cos\left[\pi\left(\frac{d}{2} - n_2\right)\right] \int_0^\infty \frac{k^{d-1-2n_2} dk}{(2k+1)^{n_1}} . \tag{2.14}$$

This integral can be easily calculated in Γ functions:

$$I(n_1, n_2) = \frac{2^{2n_2 - d + 1}}{\pi^{1/2}} \cos\left[\pi\left(\frac{d}{2} - n_2\right)\right] \frac{\Gamma(d - 2n_2)\Gamma(n_1 + 2n_2 - d)\Gamma\left(n_2 - \frac{d-1}{2}\right)}{\Gamma(n_1)\Gamma(n_2)} . \tag{2.15}$$
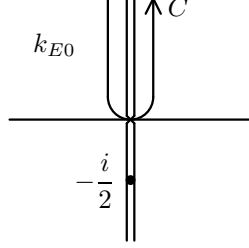
Figure 3: Integration contour

Using the well-known properties of the Γ function

$$\Gamma(2x) = \pi^{-1/2} 2^{2x-1} \Gamma(x) \Gamma\left(x + \tfrac{1}{2}\right), \qquad \Gamma(x)\Gamma(1-x) = \frac{\pi}{\sin \pi x}, \tag{2.16}$$

we can simplify this result:

$$I(n_1, n_2) = \frac{\Gamma(n_1 + 2n_2 - d)\Gamma\left(\frac{d}{2} - n_2\right)}{\Gamma(n_1)\Gamma(n_2)}. \tag{2.17}$$

It is also easy to derive this result in coordinate space [3]. HQET propagators in momentum and coordinate space are related by

$$\int_{-\infty}^{+\infty} \frac{e^{-i\omega t}}{(-2\omega - i0)^n} \frac{d\omega}{2\pi} = \frac{i}{2\Gamma(n)} \left(\frac{it}{2}\right)^{n-1} e^{-0t}\theta(t), \tag{2.18}$$

$$\int_0^{\infty} e^{(i\omega - 0)t} \left(\frac{it}{2}\right)^{n-1} dt = -\frac{2i\Gamma(n)}{(-2\omega - i0)^n}; \tag{2.19}$$

massless propagators — by

$$\int \frac{e^{-ip \cdot x}}{(-p^2 - i0)^n} \frac{d^d p}{(2\pi)^d} = \frac{i}{(4\pi)^{d/2}} \frac{\Gamma(d/2 - n)}{\Gamma(n)} \left(\frac{4}{-x^2 + i0}\right)^{d/2 - n}, \tag{2.20}$$

$$\int \left(\frac{4}{-x^2 + i0}\right)^n e^{ip \cdot x} d^d x = -i(4\pi)^{d/2} \frac{\Gamma(d/2 - n)}{\Gamma(n)} \frac{1}{(-p^2 - i0)^{d/2 - n}}. \tag{2.21}$$

Our diagram in coordinate space (Fig. 4, $x = vt$) is just the product of the heavy propagator (2.18) and the light one (2.20) (where $-x^2/4 = -t^2/4 = (it/2)^2$):

$$-\frac{1}{2} \frac{1}{(4\pi)^{d/2}} \frac{\Gamma(d/2 - n_2)}{\Gamma(n_1)\Gamma(n_2)} \left(\frac{it}{2}\right)^{n_1 + 2n_2 - d - 1} \theta(t).$$

The inverse Fourier transform (2.19) gives our diagram (2.9) in momentum space

$$\frac{i}{(4\pi)^{d/2}} I(n_1, n_2)(-2\omega)^{d - n_1 - 2n_2},$$

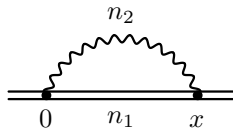where $I(n_1, n_2)$ is given by (2.17).

Figure 4: One-loop propagator diagram in coordinate space

2.3 Renormalization

The Lagrangian contains bare fields and parameters:

$$L = \overline{\tilde{Q}}_{v0} iv \cdot D_0 \tilde{Q}_{v0} \qquad D_{0\mu} = \partial_\mu - ig_0 A_{0\mu}^a t^a \,. \tag{2.22}$$

They are related to the renormalized ones by the renormalization constants:

$$\tilde{Q}_{v0} = \tilde{Z}_Q^{1/2} \tilde{Q}_v \,, \quad A_0 = Z_A^{1/2} A \,, \quad a_0 = Z_A a \,, \quad g_0 = Z_\alpha^{1/2} g \,, \tag{2.23}$$

where a_0 is the gauge-fixing parameter. The ghost field, the light-quark fields (and their masses) are renormalized as in QCD (not written here). Minimal renormalization constants have the structure
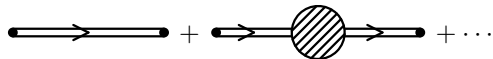
$$Z_i = 1 + \frac{Z_{11}}{\varepsilon} \frac{\alpha_s}{4\pi} + \left(\frac{Z_{22}}{\varepsilon^2} + \frac{Z_{21}}{\varepsilon} \right) \left(\frac{\alpha_s}{4\pi} \right)^2 + \cdots \tag{2.24}$$

They don't contain ε^0 and ε^n ($n > 0$) terms, only negative powers needed to remove divergences, and hence are called minimal. We have to define α_s to be exactly dimensionless. In the $\overline{\text{MS}}$ scheme α_s depends on the renormalization scale μ:

$$\frac{g_0^2}{(4\pi)^{d/2}} = \mu^{2\varepsilon} \frac{\alpha_s(\mu)}{4\pi} Z_\alpha(\alpha_s(\mu)) e^{\gamma_E \varepsilon} \,, \tag{2.25}$$

where γ_E is the Euler constant.

Let's calculate the HQET propagator with one-loop accuracy:

$$i\tilde{S}(\omega) = i\tilde{S}_0(\omega) + i\tilde{S}_0(\omega)(-i)\tilde{\Sigma}(\omega) i\tilde{S}_0(\omega) + \cdots \tag{2.26}$$

where

$$\tilde{S}_0(\omega) = \frac{1}{\omega} \,. \tag{2.27}$$

The one-loop heavy-quark self-energy (Fig. 5) is

$$\tilde{\Sigma}(\omega) = iC_F \int \frac{d^d k}{(2\pi)^d} ig_0 v^\mu \frac{1}{k_0 + \omega} ig_0 v^\nu \frac{-i}{k^2} \left(g_{\mu\nu} - \xi \frac{k_\mu k_\nu}{k^2} \right) \,, \tag{2.28}$$

where $\xi = 1 - a_0$. In the numerator, we may replace $(k \cdot v)^2 = (k_0 + \omega - \omega)^2 \to \omega^2$, because if we cancel $k_0 + \omega$ in the denominator the integral vanishes. Using (2.17), we obtain

$$\tilde{\Sigma}(\omega) = C_F \frac{g_0^2 (-2\omega)^{1-2\varepsilon}}{(4\pi)^{d/2}} \left[2I(1,1) + \frac{\xi}{2} I(1,2) \right]$$

$$= C_F \frac{g_0^2 (-2\omega)^{1-2\varepsilon}}{(4\pi)^{d/2}} \frac{\Gamma(1+2\varepsilon)\Gamma(1-\varepsilon)}{d-4} \left(\xi + \frac{2}{d-3} \right) \,. \tag{2.29}$$
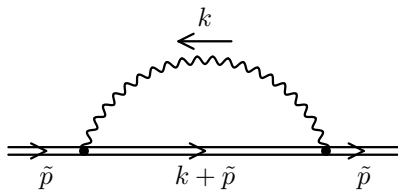
Figure 5: One-loop heavy-quark self-energy

The propagator expressed via renormalized quantities is

$$\omega \tilde{S}(\omega) = 1 + C_F \frac{\alpha_s(\mu)}{4\pi\varepsilon} e^{-2L\varepsilon} \big[3 - a(\mu) + 4\varepsilon + \cdots \big] , \qquad (2.30)$$

where

$$L = \log \frac{-2\omega}{\mu} .$$

It should be equal $\tilde{S}(\omega) = \tilde{Z}_Q \tilde{S}_r(\omega)$, where the renormalized propagator $\tilde{S}_r(\omega)$ is finite at $\varepsilon \to 0$. Therefore,

$$\tilde{Z}_Q = 1 + C_F (3 - a) \frac{\alpha_s}{4\pi\varepsilon} \qquad (2.31)$$

(it is also easy to write $\tilde{S}_r(\omega)$).

The HQET field does not renormalized in the Yennie gauge $a = 3$. This is exactly the reason why this gauge has been introduced in the theory of electrons interacting with soft photons (Bloch–Nordsieck model), which is the Abelian HQET. In the Abelian case, this non-renormalization holds to all orders due to the exponentiation theorem. In HQET, this is only true at one loop.

Now we shall discuss the renormalization of g. Due to the gauge invariance, all g's in the Lagrangian are equal. The coupling of the HQET quark field to gluon is thus identical to the usual QCD coupling, where the HQET heavy flavour is not counted in the number of flavours n_f. In order to find Z_α we need to renormalize the heavy-quark – gluon vertex and all propagators attached to it. We have already calculated $\tilde{Z}_Q$. The renormalization of the gluon propagator is well known (Fig. 6):

$$Z_A = 1 - \left[\frac{C_A}{2} \left(a - \frac{13}{3} \right) + \frac{4}{3} T_F n_f \right] \frac{\alpha_s}{4\pi\varepsilon} . \qquad (2.32)$$
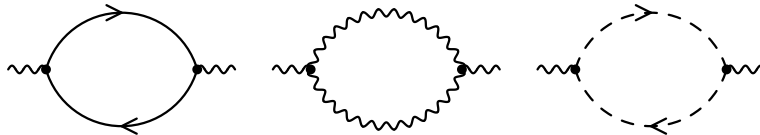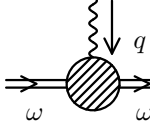

Figure 6: One-loop gluon self-energy

Let's introduce the vertex

$$= ig_0 t^a \tilde{\Gamma}^\mu , \quad \tilde{\Gamma}^\mu = v^\mu + \tilde{\Lambda}^\mu , \tag{2.33}$$

where $\tilde{\Lambda}^\mu$ starts from one loop. When expressed via renormalized quantities, the vertex should be $\tilde{\Gamma} = \tilde{Z}_\Gamma \tilde{\Gamma}_r$, where the renormalized vertex $\tilde{\Gamma}_r$ is finite at $\varepsilon \to 0$. A physical matrix element is obtained from the corresponding vertex by multiplying it by the wave-function renormalization constant $Z_i^{1/2}$ for each external leg. In our case,

$$g_0 \tilde{\Gamma} \tilde{Z}_Q Z_A^{1/2} = g \tilde{\Gamma}_r Z_\alpha^{1/2} \tilde{Z}_\Gamma \tilde{Z}_Q Z_A^{1/2} = \text{finite.}$$

Therefore, $Z_\alpha^{1/2} \tilde{Z}_\Gamma \tilde{Z}_Q Z_A^{1/2}$ must be finite. But the only minimal (2.24) renormalization constant finite at $\varepsilon \to 0$ is 1:

$$Z_\alpha = \left(\tilde{Z}_\Gamma \tilde{Z}_Q \right)^{-2} Z_A^{-1} . \tag{2.34}$$

At one loop the HQET vertex is given by two diagrams (Fig. 7). It is very easy to calculate the first one. It contains two heavy denominators which can be replaced by a difference:

$$\frac{1}{(k_0 + \omega)(k_0 + \omega')} = \frac{1}{\omega' - \omega} \left(\frac{1}{k_0 + \omega} - \frac{1}{k_0 + \omega'} \right) . \tag{2.35}$$

We get the difference of the self-energies:

$$\tilde{\Lambda}_1^\mu = - \left(1 - \frac{C_A}{2C_F} \right) \frac{\tilde{\Sigma}(\omega') - \tilde{\Sigma}(\omega)}{\omega' - \omega} v^\mu . \tag{2.36}$$

This result can also be obtained from the Ward identity. The UV divergence of this contribution is

$$\tilde{\Lambda}_1^\mu = \left(C_F - \frac{C_A}{2} \right) (a - 3) \frac{\alpha_s}{4\pi\varepsilon} v^\mu . \tag{2.37}$$

The second diagram is more difficult. It has been calculated in [5]. Now we only need its UV divergence, and it should be $\sim v^\mu$. We may nullify all external momenta. After that, the diagram will contain no scale and hence vanish. It will contain both UV and IR divergences which cancel. Therefore, we'll have to introduce some IR regularization to get the UV divergence. We have

$$ig_0 \tilde{\Lambda}_2^\mu = \frac{C_A}{2} \int \frac{d^d k}{(2\pi)^d} ig_0 v^{\alpha'} \frac{i}{k \cdot v} ig_0 v^{\beta'}$$
$$\times \frac{-i}{k^2} \left(g_{\alpha\alpha'} - \xi \frac{k_\alpha k_{\alpha'}}{k^2} \right) \frac{-i}{k^2} \left(g_{\beta\beta'} - \xi \frac{k_\beta k_{\beta'}}{k^2} \right) ig_0 V^{\alpha\beta\mu}(k, -k, 0) , \tag{2.38}$$
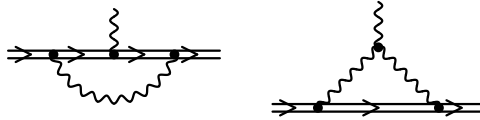

Figure 7: One-loop HQET vertex

where the three-gluon vertex is

$$V^{\mu_1\mu_2\mu_3}(p_1, p_2, p_3) = (p_3 - p_2)^{\mu_1} g^{\mu_2\mu_3} + (p_1 - p_3)^{\mu_2} g^{\mu_3\mu_1} + (p_2 - p_1)^{\mu_3} g^{\mu_1\mu_2} \,. \tag{2.39}$$

It vanishes when contracted with the same vector in all three indices:

$$V^{\mu_1\mu_2\mu_3}(p_1, p_2, p_3) v_{\mu_1} v_{\mu_2} v_{\mu_3} = 0 \,,$$

and when contracted in two indices with the corresponding momenta:

$$V^{\mu_1\mu_2\mu_3}(p_1, p_2, p_3) p_{1\,\mu_1} p_{2\,\mu_2} = 0 \,.$$

Therefore, ξ^0 and ξ^2 terms vanish:

$$\tilde{\Lambda}_2^\mu v_\mu = iC_A g_0^2 \xi \int \frac{d^d k}{(2\pi)^d} \frac{k^2 - (k \cdot v)^2}{(k^2)^3} \,.$$

Averaging over k directions $(k \cdot v)^2 \to k^2/d$, we get

$$\tilde{\Lambda}_2^\mu v_\mu = iC_A g_0^2 \xi \left(1 - \frac{1}{d}\right) \int \frac{d^d k}{(2\pi)^d} \frac{1}{(k^2)^2} \,.$$

The UV divergence of this integral can be obtained by introducing any IR regularization, e.g., an IR cut-off in the Euclidean momentum integral or a small mass:

$$\int \frac{d^d k}{(2\pi)^d} \frac{1}{(k^2)^2}\bigg|_{\text{UV}} = \frac{i}{(4\pi)^{d/2}\varepsilon} \,. \tag{2.40}$$

We arrive at the UV divergence of the second vertex diagram:

$$\tilde{\Lambda}_2^\mu = -\frac{3}{4} C_A (1 - a) \frac{\alpha_s}{4\pi\varepsilon} v^\mu \,. \tag{2.41}$$

From (2.37) and (2.41) we obtain

$$\tilde{Z}_\Gamma = 1 + \left[C_F(a - 3) + C_A \frac{a + 3}{4}\right] \frac{\alpha_s}{4\pi\varepsilon} \,. \tag{2.42}$$

The product which appears in (2.34) is

$$\tilde{Z}_\Gamma \tilde{Z}_Q = 1 + C_A \frac{a + 3}{4} \frac{\alpha_s}{4\pi\varepsilon} \,. \tag{2.43}$$

In the Abelian case $\tilde{Z}_\Gamma \tilde{Z}_Q = 1$ to all orders, due to the Ward identity. This is why we only got the non-abelian colour structure C_A in (2.43). Finally, combining this with (2.32), we see that the a dependence cancels, and

$$Z_\alpha = 1 - \beta_0 \frac{\alpha_s}{4\pi\varepsilon} \,, \quad \beta_0 = \frac{11}{3} C_A - \frac{4}{3} T_F n_f \,. \tag{2.44}$$

Thus we have derived the one-loop β function of QCD (n_f does not include the HQET heavy flavour Q). Most textbooks use the massless-quark – gluon vertex or the ghost – gluon one (see, e.g., [3]). In the later case, calculations are a little shorter. The HQET derivation presented here is as short as the ghost one.

3 α parametrization

3.1 General formulae

α parametrization of Feynman integrals (including those containing numerators) is discussed in many textbooks, see e.g. [6]. Here we shall discuss HQET integrals; all rules can be trivially obtained from [6], though they were not yet explicitly stated in the literature.

First let's calculate the one-loop diagram (2.9) (Fig. 1) using α parametrization

$$\frac{1}{a^n} = \frac{1}{\Gamma(n)} \int_0^\infty d\alpha \, \alpha^{n-1} e^{-a\alpha} \,. \tag{3.1}$$

We get

$$\frac{1}{\Gamma(n_1)\Gamma(n_2)} \int d\alpha \, \alpha^{n_2-1} \, d\beta \, \beta^{n_1-1} \, d^d k \, e^X \,, \quad X = \alpha k^2 + 2\beta(k + \tilde{p}) \cdot v \,.$$

We shift the integration momentum

$$k = k' - \frac{\beta}{\alpha} v$$

to eliminate the linear term in the exponent:

$$X = \alpha k'^2 - \frac{\beta^2}{\alpha} + 2\beta\omega \,.$$

Now it is easy to calculate the momentum integral:

$$\int d^d k \, e^{\alpha k^2} = i \int d^d k_E \, e^{-\alpha k_E^2} = i \left(\frac{\pi}{\alpha}\right)^{d/2} \,. \tag{3.2}$$

Therefore,

$$(-2\omega)^{d-n_1-2n_2} I(n_1, n_2) = \frac{1}{\Gamma(n_1)\Gamma(n_2)} \int d\alpha \, \alpha^{n_2-1} \, d\beta \, \beta^{n_1-1} \, \alpha^{-d/2} \exp\left(-\frac{\beta^2}{\alpha} + 2\beta\omega\right) \,.$$

Now we make the substitution $\beta = \alpha y$ and integrate in α:

$$\frac{\Gamma\left(n_1 + n_2 - \frac{d}{2}\right)}{\Gamma(n_1)\Gamma(n_2)} \int_0^\infty dy \, y^{n_1-1} \left[y(y - 2\omega)\right]^{d/2-n_1-n_2} \,.$$

The HQET Feynman parameter y has the dimensionality of energy and varies from 0 to ∞. The y integral can be easily calculated in Γ functions, and we again obtain (2.17).

Now we shall consider the most general HQET Feynman integral without numerators. Any HQET diagram contains a single heavy line and has the form

$$I = \int \prod \frac{d^d k_i}{i\pi^{d/2}} \frac{1}{\prod L_a^{n_a} \prod H_c^{n_c}} \,, \tag{3.3}$$

where k_i are loop momenta $(i, j \in [1, L])$,

$$L_a = m_a^2 - q_a^2 - i0 \,, \quad H_c = -2q_c \cdot v - i0$$

are light denominators ($a, b \in [1, N_l]$) and heavy ones ($c, d \in [1, N_h]$):

$$q_a = \sum N_{ai}k_i + \sum N_{an}p_n \,, \quad q_c = \sum N_{ci}k_i + \sum N_{cn}p_n \,,$$

p_n are external momenta ($n, m \in [1, N_e - 1]$), and the coefficients N express momenta of propagators via the loop and external momenta (these coefficients are equal to 0 or ± 1). Using the α representation (3.1) for all lines, we obtain

$$I = \frac{1}{\prod \Gamma(n_a) \prod \Gamma(n_c)} \int \prod d\alpha_a \, \alpha_a^{n_a - 1} \prod d\beta_c \, \beta_c^{n_c - 1} \prod \frac{d^d k_i}{i\pi^{d/2}} \, e^X \,,$$
$$X = \sum \alpha_a (q_a^2 - m_a^2) + 2 \sum \beta_c q_c \cdot v \,. \tag{3.4}$$

Dimensionalities of the parameters are $\alpha_a \sim 1/M^2$, $\beta_c \sim 1/M$. The exponent is

$$X = \sum M_{ij} k_i \cdot k_j - 2 \sum Q_i \cdot k_i + Y \,, \tag{3.5}$$

where

$$M_{ij} = \sum \alpha_a N_{ai} N_{aj} \,,$$
$$Q_i = -\sum \alpha_a N_{ai} N_{an} p_n - v \sum \beta_c N_{ci} \,,$$
$$Y = \sum \alpha_a \left(\sum N_{an} p_n \right)^2 + 2 \sum \beta_c N_{cn} p_n \cdot v - \sum \alpha_a m_a^2 \,. \tag{3.6}$$

Now we shift the loop momenta $k_i = k_i' + K_i$ to eliminate linear terms:

$$K_i = \sum M_{ij}^{-1} Q_j \,. \tag{3.7}$$

Then

$$X = \sum M_{ij} k_i' \cdot k_j' - \sum M_{ij}^{-1} Q_i \cdot Q_j + Y \,. \tag{3.8}$$

Performing the Wick rotation to Euclidean k_i' and integration in the loop momenta, we obtain

$$I = \frac{1}{\prod \Gamma(n_a) \prod \Gamma(n_c)} \int \prod d\alpha_a \, \alpha_a^{n_a - 1} \prod d\beta_c \, \beta_c^{n_c - 1} \left[D(\alpha) \right]^{-d/2}$$
$$\times \exp\left[-\frac{A(\alpha) + A_1(\alpha, \beta) + A_2(\alpha, \beta)}{D(\alpha)} - \sum \alpha_a m_a^2 \right] \,, \tag{3.9}$$

where

$$D(\alpha) = \det M \,,$$
$$\frac{A(\alpha)}{D(\alpha)} = \sum M_{ij}^{-1} \alpha_a \alpha_b N_{ai} N_{an} N_{bj} N_{bm} p_n \cdot p_m - \sum \alpha_a N_{an} N_{am} p_n \cdot p_m \,,$$
$$\frac{A_1(\alpha, \beta)}{D(\alpha)} = 2 \sum M_{ij}^{-1} \alpha_a \beta_c N_{ai} N_{an} N_{cj} p_n \cdot v - 2 \sum \beta_c N_{cn} p_n \cdot v \,,$$
$$\frac{A_2(\alpha, \beta)}{D(\alpha)} = \sum M_{ij}^{-1} \beta_c \beta_d N_{ci} N_{dj} \,. \tag{3.10}$$

The polynomials $D(\alpha)$, $A(\alpha)$, $A_1(\alpha,\beta)$, $A_2(\alpha,\beta)$ have dimensionality $1/M^{2L}$. The function $D(\alpha)$ is homogeneous in α_a of degree L. The function $A(\alpha)$ is homogeneous in α_a of degree $L+1$ and linear in $p_n \cdot p_m$. The function $A_1(\alpha,\beta)$ is linear in β_c, of degree L in α_a, and linear in $p_n \cdot v$. The function $A_2(\alpha,\beta)$ is quadratic in β_c and of degree $L-1$ in α_a; it does not contain momenta.

It is always possible to calculate (at least) one integration in (3.9). Let's insert $\delta\left(\sum \alpha_a - \eta\right) d\eta$ under the integral sign, and make the substitution $\alpha_a = \eta x_a$, $\beta_c = \eta y_c$. Then the η integral is a Γ function:

$$I = \frac{\Gamma\left(\sum n_a + \sum n_c - L\frac{d}{2}\right)}{\prod \Gamma(n_a) \prod \Gamma(n_c)} \int \frac{\prod dx_a\, x_a^{n_a-1} \prod dy_c\, y_c^{n_c-1}\, \delta\left(\sum x_a - 1\right)}{[D(x)]^{d/2} \left[\frac{A(x)+A_1(x,y)+A_2(x,y)}{D(x)} + \sum x_a m_a^2\right]^{\sum n_a + \sum n_c - Ld/2}}\,.$$

(3.11)

The ordinary Feynman parameters x_a are dimensionless and vary from 0 to 1; the HQET Feynman parameters y_c have dimensionality of energy and vary from 0 to ∞.

3.2 Graph-theoretical rules

The polynomials $D(\alpha)$, $A(\alpha)$, $A_1(\alpha,\beta)$, $A_2(\alpha,\beta)$ can be extracted directly from the diagram, see [6]. We shall formulate the rules and illustrate them by an example shown in Fig. 8.
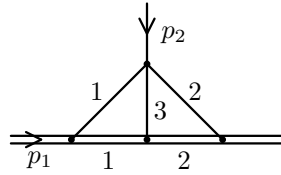
Figure 8: An HQET vertex diagram

1. Cut a few light lines so as to get a connected tree, form the product of α_a of the cut lines. $D(\alpha)$ is the sum of all such products.

$$D = \alpha_1\alpha_2 + \alpha_1\alpha_3 + \alpha_2\alpha_3\,.$$
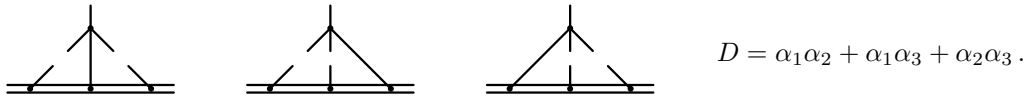
2. Cut a few light lines to get two connected trees (the heavy line is in one of the two parts). Form the product of α_a of the cut lines and multiply it by $(-P^2)$, where P is the momentum flowing from one connected part to the other one. $A(\alpha)$ is the sum of all such terms.

$$A = -p_2^2\alpha_1\alpha_2\alpha_3\,.$$
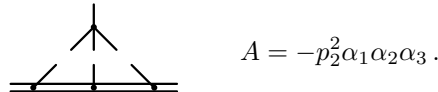
3. Cut a single heavy line and a few light ones to get two connected trees (now the heavy line enters one connected part and leaves the other one). Form the product of β_c of the cut

heavy line and α_a of the cut light ones and multiply by $(-2P \cdot v)$, where P is the momentum flowing from the first connected part to the second one. $A_1(\alpha, \beta)$ is the sum of all such terms.
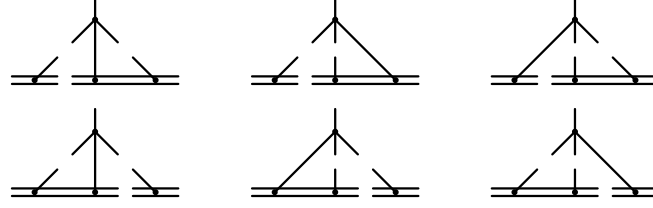
$$A_1 = -2p_1 \cdot v\,\beta_1\alpha_1(\alpha_2 + \alpha_3) - 2(p_1 + p_2) \cdot v\,\beta_1\alpha_2\alpha_3$$
$$- 2(p_1 + p_2) \cdot v\,\beta_2\alpha_2(\alpha_1 + \alpha_3) - 2p_1 \cdot v\,\beta_2\alpha_1\alpha_3\,.$$

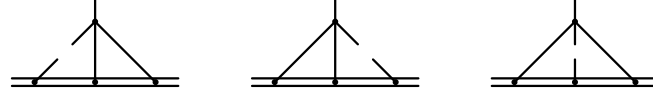**4**. Cut a few light lines to get a connected diagram with a single loop in such a way that this loop contains at least one heavy line. Sum β_c of the heavy lines belonging to the loop, square the sum, and multiply by α_a of the cut light lines. Sum all terms.

$$A_2 = \alpha_1\beta_2^2 + \alpha_2\beta_1^2 + \alpha_3(\beta_1 + \beta_2)^2\,.$$

These rules can be simplified a little. Suppose p_1 is the residual momentum of the incoming heavy line, and let's route it along the heavy line. Then the exponent X (3.4) contains $2p_1 \cdot v \sum \beta_c$. We can add this expression to the exponent in (3.9), and then set $p_1 = 0$ while calculating $A_1(\alpha, \beta)$.

There is an analogy between Feynman diagrams in α representation and electrical circuits (Table 1). The average momentum flowing through a propagator corresponds to current. The first Kirchhoff rule is satisfied: the sum of momenta flowing into a vertex vanishes. Light lines are resistors α_a, and heavy lines — voltage sources $\beta_c v$ (batteries with zero internal resistance, the voltage does not depend on the current). The second Kirchhoff rule says that the sum of voltages along a loop (say, loop i) must vanish. These equations are nothing but the equations $\sum M_{ij}K_j = Q_i$ which determine the average loop momenta K_i (see (3.7)).

	Current	Voltage
a	$\bar{q}_a = \sum N_{ai}K_i + \sum N_{an}p_n$	$\alpha_a\bar{q}_a$
c	$\bar{q}_c = \sum N_{ci}K_i + \sum N_{cn}p_n$	$\beta_c v$

Table 1: Analogy with electrical circuits

The Joule heat $\sum \alpha_a\bar{q}_a^2$ plus 2 times the energy consumption by the voltage sources $\sum \beta_c\bar{q}_c \cdot v$ gives

$$-\frac{A(\alpha) + A_1(\alpha, \beta) + A_2(\alpha, \beta)}{D(\alpha)}\,.$$

The case $\alpha_a \to 0$ or $\beta_c \to 0$ corresponds to a short circuit (line shrinks to a point); the case $\alpha_a \to \infty$ — no contact (the line is removed).

Generalization to integrals with numerators is straightforward [6]. Suppose we have a polynomial $\mathcal{P}(q_a, q_c)$ inserted into the numerator of (3.3). Then we can add

$$2\sum q_a \cdot \xi_a + 2\sum q_c \cdot \eta_c$$

to the exponent X (3.4), and apply the differential operator

$$\mathcal{P}\left(\frac{1}{2}\frac{\partial}{\partial \xi_a}, \frac{1}{2}\frac{\partial}{\partial \eta_c}\right)$$

to the result at $\xi_a = 0$, $\eta_c = 0$. Before this step, the only difference is the substitution $\beta_c v \to \beta_c v + \eta_c$, and the fact that a light line a can be also considered "heavy" in A_1 and A_2 calculations, with ξ_a playing the role of βv. Let's formulate the rules to calculate A_1, A_2.

$\mathbf{3'}$. Cut a single heavy line (say, c) and a few light ones to get two connected trees, and form the product of $-2(\beta_c v + \eta_c) \cdot P$, where P is the momentum flowing from the first connected part to the second one; multiply this product by α_a of all cut light lines. Or cut a single light line (say, a) and a few light ones to get two connected trees, form the product $-2\xi_a \cdot P$, and multiply it by α_b of these additional cut lines. Here the first and the second connected parts are defined by the direction of the momentum of the first cut line (q_c or q_a for a heavy or light line). $A_1(\alpha, \beta, \xi, \eta)$ is the sum of all such terms.

$\mathbf{4'}$. Cut a few light lines to get a connected diagram with a single loop. Sum $\beta_c v + \eta_c$ or ξ_a of the heavy or light lines belonging to the loop, square the sum, and multiply by α_a of the cut light lines. Sum all terms to get $A_2(\alpha, \beta, \xi, \eta)$.

4 HQET propagator diagrams

4.1 Two loops

4.1.1 Diagram 1

We have calculated the one-loop HQET propagator diagram by three different methods (Sects. 2.2 and 3.1). Now we shall consider two-loop propagator diagrams in HQET. There are two generic topologies of such diagrams (Fig. 9). This means that all other possible topologies can be obtained from these ones by shrinking some lines. The method of calculation of these diagrams has been constructed in [7].

The first diagram (Fig. 10) is

$$-\frac{1}{\pi^d}\int \frac{d^d k_1\, d^d k_2}{D_1^{n_1} D_2^{n_2} D_3^{n_3} D_4^{n_4} D_5^{n_5}} = (-2\omega)^{2d-n_1-n_2-2(n_3+n_4+n_5)} I(n_1, n_2, n_3, n_4, n_5)\,, \qquad (4.1)$$

where

$$D_1 = -2(k_{10} + \omega)\,, \quad D_2 = -2(k_{20} + \omega)\,,$$
$$D_3 = -k_1^2\,, \quad D_4 = -k_2^2\,, \quad D_5 = -(k_1 - k_2)^2$$

(the power of -2ω is fixed by dimensionality). It is symmetric with respect to $(1 \leftrightarrow 2, 3 \leftrightarrow 4)$, and vanishes if two adjacent indices are ≤ 0.
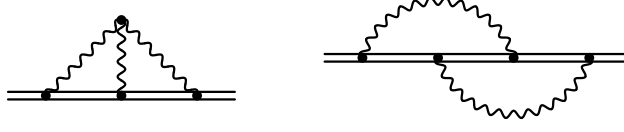
Figure 9: Generic topologies of two-loop propagator diagrams
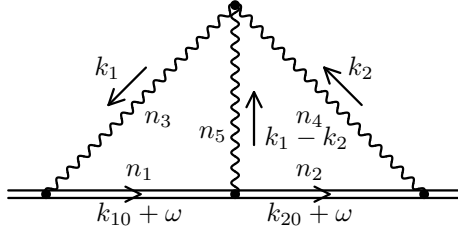
Figure 10: Diagram 1

If $n_5 = 0$, the diagram is the product of two one-loop ones:

$$I(n_1, n_2, n_3, n_4, 0) = \quad = I(n_1, n_3)I(n_2, n_4). \qquad (4.2)$$

If $n_1 = 0$, we first calculate the inner massless loop. The one-loop massless diagram is

$$\frac{1}{i\pi^{d/2}} \int \frac{d^d k}{[-(k+p)^2 - i0]^{n_1} [-k^2 - i0]^{n_2}} = (-p^2)^{d/2 - n_1 - n_2} G(n_1, n_2),$$
$$G(n_1, n_2) = \frac{\Gamma(-d/2 + n_1 + n_2)\Gamma(d/2 - n_1)\Gamma(d/2 - n_2)}{\Gamma(n_1)\Gamma(n_2)\Gamma(d - n_1 - n_2)}. \qquad (4.3)$$

This gives the coefficient $G(n_3, n_5)$, and shifts the power n_4 by $n_3 + n_5 - d/2$:

$$I(0, n_2, n_3, n_4, n_5) = G(n_3, n_5)I(n_2, n_4 + n_3 + n_5 - d/2) \qquad (4.4)$$

(the case $n_2 = 0$ is symmetric). If $n_3 = 0$, we first calculate the inner HQET loop. This gives

the coefficient $I(n_1, n_5)$, and shifts the power n_2 by $n_1 + 2n_5 - d$:

$$I(n_1, n_2, 0, n_4, n_5) = I(n_1, n_5)I(n_2 + n_1 + 2n_5 - d, n_4) \tag{4.5}$$

(the case $n_4 = 0$ is symmetric).

But what can we do if all 5 powers of denominators are positive? We shall use integration by parts [8]. Integral of any full derivative over the whole space of loop momenta is zero. When applied to the integrand of (4.1), the derivative

$$\frac{\partial}{\partial k_2} \rightarrow \frac{n_2}{D_2} 2v + \frac{n_4}{D_4} 2k_2 + \frac{n_5}{D_5} 2(k_2 - k_1).$$

Applying $(\partial/\partial k_2) \cdot k_2$ or $(\partial/\partial k_2) \cdot (k_2 - k_1)$ to the integrand, we obtain zero integral. On the other hand, we can calculate these derivatives explicitly. Using $2k_2 \cdot v = -D_2 - 2\omega$, $2(k_2 - k_1) \cdot k_2 = D_3 - D_4 - D_5$, we see that applying these differential operators is equivalent to inserting

$$d - n_2 - n_5 - 2n_4 - 2\omega \frac{n_2}{D_2} + \frac{n_5}{D_5}(D_3 - D_4),$$

$$d - n_2 - n_4 - 2n_5 + \frac{n_2}{D_2}D_1 + \frac{n_4}{D_4}(D_3 - D_5)$$

under the integral sign. These combinations of integrals vanish. These recurrence relations are usually written as

$$\left[d - n_2 - n_5 - 2n_4 + n_2\mathbf{2}^+ + n_5\mathbf{5}^+(\mathbf{3}^- - \mathbf{4}^-)\right] I = 0, \tag{4.6}$$

$$\left[d - n_2 - n_4 - 2n_5 + n_2\mathbf{2}^+\mathbf{1}^- + n_4\mathbf{4}^+(\mathbf{3}^- - \mathbf{5}^-)\right] I = 0, \tag{4.7}$$

where, for example, $\mathbf{1}^-$ lowers n_1 by 1 and $\mathbf{2}^+$ raises n_2 by 1. Applying $(\partial/\partial k_2) \cdot v$, we obtain a (less useful) relation

$$\left[-2n_2\mathbf{2}^+ + n_4\mathbf{4}^+(\mathbf{2}^- - 1) + n_5\mathbf{5}^+(\mathbf{2}^- - \mathbf{1}^-)\right] I = 0. \tag{4.8}$$

A useful relation can be obtained from homogeneity of the integral (4.1) in ω. Applying $\omega(d/d\omega)$, we get the same integral times its dimensionality $2(d - n_3 - n_4 - n_5) - n_1 - n_2$. On the other hand, we can calculate the derivative explicitly:

$$\left[2(d - n_3 - n_4 - n_5) - n_1 - n_2 + n_1\mathbf{1}^+ + n_2\mathbf{2}^+\right] I = 0. \tag{4.9}$$

This homogeneity relation is not independent: it is the sum of the $(\partial/\partial k_2) \cdot k_2$ relation (4.6) and its mirror-symmetric $(\partial/\partial k_1) \cdot k_1$ one.

A particularly useful relation can be obtained by subtracting the $\mathbf{1}^-$ shifted homogeneity relation (4.9) from the $(\partial/\partial k_2) \cdot (k_2 - k_1)$ relation (4.7):

$$\left[d - n_1 - n_2 - n_4 - 2n_5 + 1 - \left(2(d - n_3 - n_4 - n_5) - n_1 - n_2 + 1\right)\mathbf{1}^- \right.$$
$$\left. + n_4\mathbf{4}^+(\mathbf{3}^- - \mathbf{5}^-)\right] I = 0. \tag{4.10}$$

Solving it for the I with the unshifted indices, we obtain an expression for $I(n_1, n_2, n_3, n_4, n_5)$ via 3 integrals:

$$I = \frac{(2(d - n_3 - n_4 - n_5) - n_1 - n_2 + 1)\mathbf{1}^- + n_4 \mathbf{4}^+ (\mathbf{5}^- - \mathbf{3}^-)}{d - n_1 - n_2 - n_4 - 2n_5 + 1} I\,. \tag{4.11}$$

Each of them has $n_1 + n_3 + n_5$ reduced by 1. Each application of (4.11) moves us closer to the origin (Fig. 11). Therefore, after a finite number of steps, any integral $I(n_1, n_2, n_3, n_4, n_5)$ will be reduced to the trivial cases in which one of the indices vanishes.
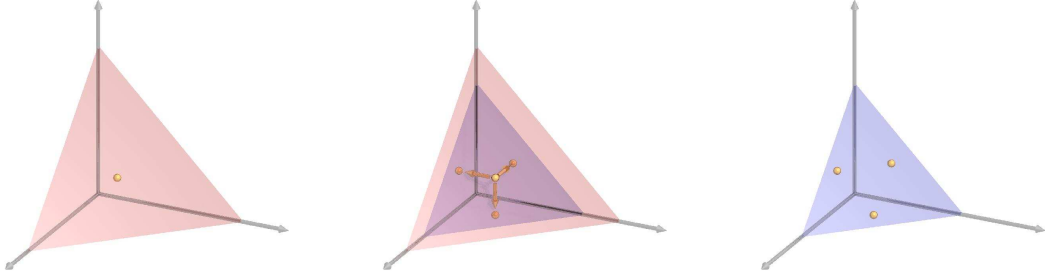
Figure 11: A single step of the integration-by-parts reduction

4.1.2 Diagram 2

The second diagram (Fig. 12) is

$$-\frac{1}{\pi^d} \int \frac{d^d k_1\, d^d k_2}{D_1^{n_1} D_2^{n_2} D_3^{n_3} D_4^{n_4} D_5^{n_5}} = (-2\omega)^{2d - n_1 - n_2 - n_3 - 2(n_4 + n_5)} J(n_1, n_2, n_3, n_4, n_5)\,, \tag{4.12}$$

where

$$D_1 = -2(k_{10} + \omega)\,, \quad D_2 = -2(k_{20} + \omega)\,, \quad D_3 = -2(k_{10} + k_{20} + \omega)\,,$$
$$D_4 = -k_1^2\,, \quad D_5 = -k_2^2$$

(the power of -2ω is fixed by dimensionality). It is symmetric with respect to $(1 \leftrightarrow 2, 4 \leftrightarrow 5)$, and vanishes if $n_4 \leq 0$ or $n_5 \leq 0$ or two adjacent $n_{1...3}$ are ≤ 0.

This integral is trivial if $n_3 = 0$ or $n_{1,2} = 0$. In general, it has 3 linear denominators and only 2 loop momenta; therefore, these denominators are linearly dependent:

$$D_1 + D_2 - D_3 = -2\omega\,. \tag{4.13}$$

Inserting this combination under the integral sign, we obtain

$$J = (\mathbf{1}^- + \mathbf{2}^- - \mathbf{3}^-)J\,. \tag{4.14}$$
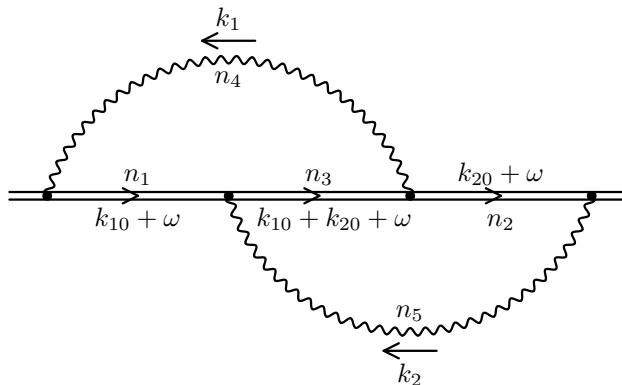
Figure 12: Diagram 2

Each application of this recurrence relation reduces $n_1 + n_2 + n_3$ by 1. Therefore, after a number of such steps any integral will reduce to the trivial cases (Fig. 11).

The integral (4.12) can contain a power of $k_1 \cdot k_2$ in the numerator; this scalar product cannot be expressed via the denominators. However, this is not a serious problem [9].

Let's summarize. All scalar integrals belonging to the two generic topologies of Fig. 9, with any indices n_i (and with any power of $k_1 \cdot k_2$ in the numerator of the second integral) can be reduced to linear combinations of two master integrals

$$\text{\raisebox{-0.5em}{\includegraphics}} = I_1^2 \,, \qquad \text{\raisebox{-0.5em}{\includegraphics}} = I_2 \,, \qquad (4.15)$$

with coefficients being rational functions of d. Here the n-loop HQET sunset integral is

$$\text{\raisebox{-0.5em}{\includegraphics}} = I_n = \frac{\Gamma(1 + 2n\varepsilon)\Gamma^n(1 - \varepsilon)}{(1 - n(d - 2))_{2n}} \,. \qquad (4.16)$$

This reduction can be done using integration by parts [7] (see also [9]).

4.2 Three loops

4.2.1 Reduction

There are 10 generic topologies of three-loop HQET propagator diagrams (Fig. 13).

All these integrals, with any powers of denominators and irreducible numerators, can be
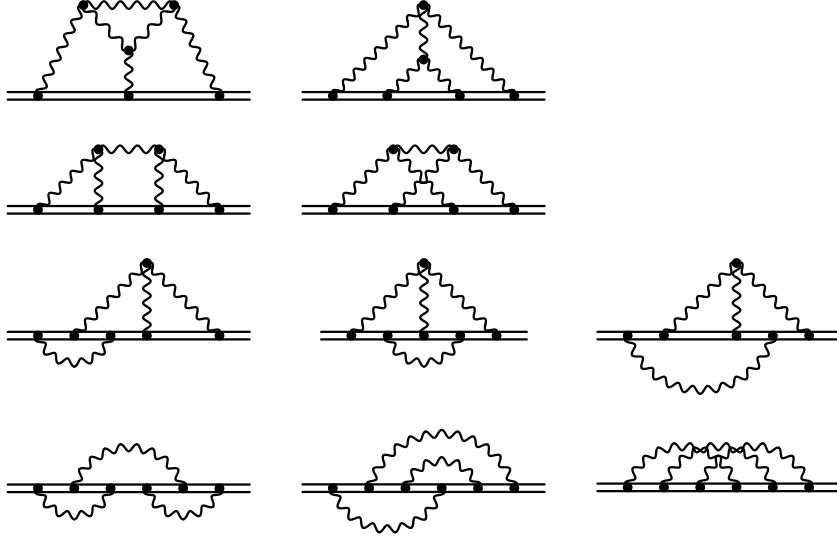
Figure 13: Generic topologies of three-loop propagator diagrams

reduced [9] to 8 master integrals:

$$= I_1^3 \,, \tag{4.17}$$

$$= I_1 I_2 \,, \tag{4.18}$$

$$= I_3 \,, \tag{4.19}$$

$$= \frac{I_1^2 I(6-2d,1)}{I_2 I(5-2d,1)} I_3 = \frac{3d-7}{2d-5} \frac{I_1^2}{I_2} I_3 \,, \tag{4.20}$$

$$= \frac{G_1^2 I(1,4-d)}{G_2 I(1,3-d)} I_3 = -2 \frac{3d-7}{d-3} \frac{G_1^2}{G_2} I_3 \,, \tag{4.21}$$
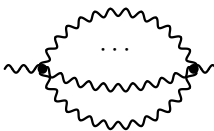
$$= G_1 I(1,1,1,1,2-d/2) \,, \tag{4.22}$$

$$= I_1 J(1,1,3-d,1,1) \,, \tag{4.23}$$

$$= B_8 \,, \tag{4.24}$$

using integration by parts. Here the n-loop HQET sunset I_n is defined by (4.16), and the n-loop massless sunset is

$$= G_n = \frac{1}{\left(n + 1 - n\frac{d}{2}\right)_n \left((n+1)\frac{d}{2} - 2n - 1\right)_n} \frac{\Gamma(1 + n\varepsilon)\Gamma^{n+1}(1 - \varepsilon)}{\Gamma(1 - (n+1)\varepsilon)} \,.$$

$$\tag{4.25}$$

This reduction algorithm has been implemented as a `REDUCE` package `Grinder` [9]. It is analogous to the massless package Mincer [10]. The first 5 master integrals can be easily expressed via Γ functions, exactly in d dimensions. The next two ones reduce to two-loop ones with a single ε-dependent index[1] (Sects. 4.2.2 and 4.2.3). The last one is truly three-loop (Sect. 4.2.4).

4.2.2 $\quad J(1, 1, n, 1, 1)$

Here we shall calculate the integral J (4.12) (Fig. 12) for arbitrary powers of denominators. To this end, we shall first consider the one-loop diagram with two different residual energies ω_1 and ω_2 (Fig. 14a):

$$I = \frac{1}{i\pi^{d/2}} \int \frac{d^d k}{D_1^{n_1} D_2^{n_2} D_3^{n_3}} \,, \tag{4.26}$$

where

$$D_1 = -2(k_0 + \omega_1), \quad D_2 = -2(k_0 + \omega_2), \quad D_3 = -k^2 \,.$$

If $n_{1,2}$ are integer, this integral can be easily calculated by partial fraction decomposition (Sect. 2.3).
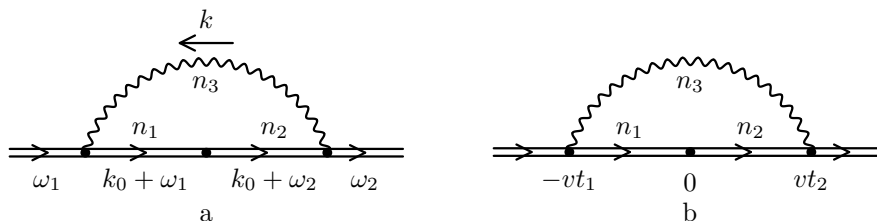
Figure 14: One-loop diagram

Closely following Sect. 2.2, we first integrate in $d^{d-1}\vec{k}$:

$$
\begin{aligned}
I &= \frac{\Gamma\left(n_3 - \frac{d-1}{2}\right)}{\pi^{1/2}\Gamma(n_3)} \int \frac{\left(k_{E0}^2\right)^{(d-1)/2 - n_3} dk_{E0}}{\left(-2\omega_1 - 2ik_{E0}\right)^{n_1} \left(-2\omega_2 - 2ik_{E0}\right)^{n_2}} \\
&= 2\frac{\Gamma\left(n_3 - \frac{d-1}{2}\right)}{\pi^{1/2}\Gamma(n_3)} \cos\left[\pi\left(\frac{d}{2} - n_3\right)\right] \int_0^\infty \frac{k^{d-1-2n_3} dk}{(2k - 2\omega_1)^{n_1}(2k - 2\omega_2)^{n_2}} \,.
\end{aligned}
$$

---

[1] `Grinder` uses $B_4 = I_3 I_1^2 / I2$ and $B_5 = I_3 G_1^2 / G_2$ as elements of its basis instead of (4.20) and (4.21).

We obtain [11]

$$I = I(n_1 + n_2, n_3)\,_2F_1\left(\begin{array}{c} n_1, n_1 + n_2 + 2n_3 - d \\ n_1 + n_2 \end{array}\middle| 1 - \frac{\omega_1}{\omega_2}\right)(-2\omega_2)^{d - n_1 - n_2 - 2n_3}. \qquad (4.27)$$

One can easily check that this result is symmetric with respect to $(\omega_1 \leftrightarrow \omega_2, n_1 \leftrightarrow n_2)$, using properties of hypergeometric function. If $\omega_1 = \omega_2$, it reduces to $I(n_1 + n_2, n_3)$.

Let's also calculate this integral using α representation (Sect. 3.1):

$$I = \frac{1}{\Gamma(n_1)\Gamma(n_2)\Gamma(n_3)} \int d\alpha\, \alpha^{n_3 - 1}\, d\beta_1\, \beta_1^{n_1 - 1}\, d\beta_2\, \beta_2^{n_2 - 1}\, \alpha^{-d/2}$$

$$\times \exp\left[-\frac{(\beta_1 + \beta_2)^2}{\alpha} + 2(\omega_1\beta_1 + \omega_2\beta_2)\right].$$

Now we make the substitution $\beta_{1,2} = \alpha y_{1,2}$ and integrate in α:

$$I = \frac{\Gamma\left(n_1 + n_2 + n_3 - \frac{d}{2}\right)}{\Gamma(n_1)\Gamma(n_2)\Gamma(n_3)} \int dy_1\, y_1^{n_1 - 1}\, dy_2\, y_2^{n_2 - 1}\left[(y_1 + y_2)^2 - 2(\omega_1 y_1 + \omega_2 y_2)\right]^{d/2 - n_1 - n_2 - n_3}.$$

After the substitution $y_1 = yx$, $y_2 = y(1 - x)$, the integral in y can be taken:

$$I = \frac{\Gamma\left(\frac{d}{2} - n_3\right)\Gamma\left(n_1 + n_2 + 2n_3 - \frac{d}{2}\right)}{\Gamma(n_1)\Gamma(n_2)\Gamma(n_3)}$$

$$\times \int_0^1 dx\, x^{n_1 - 1}(1 - x)^{n_2 - 1}\left[-2\omega_1 x - 2\omega_2(1 - x)\right]^{d - n_1 - n_2 - 2n_3}. \qquad (4.28)$$

And we again obtain (4.27).

Finally, we shall derive the same result in coordinate space (Fig. 14b, see Sect. 2.2):

$$I = -\frac{1}{4}\frac{\Gamma\left(\frac{d}{2} - n_3\right)}{\Gamma(n_1)\Gamma(n_2)\Gamma(n_3)} \int dt_1\, dt_2\, e^{i(\omega_1 t_1 + \omega_2 t_2)}\left(\frac{it_1}{2}\right)^{n_1 - 1}\left(\frac{it_2}{2}\right)^{n_2 - 1}\left(\frac{i(t_1 + t_2)}{2}\right)^{2n_3 - d1}.$$

The substitution $t_1 = tx$, $t_2 = t(1 - x)$ reduces this expression to (4.28).

Now we return to our main problem — calculating $J = J(n_1, n_2, n_3, n_4, n_5)$ (Fig. 12) with arbitrary indices. We set $-2\omega = 1$; the power of -2ω can be reconstructed by dimensionality. Substituting the one-loop subdiagram (4.27), we have

$$J = \frac{I(n_1 + n_3, n_4)}{i\pi^{d/2}} \int \frac{d^d k}{(-k^2)^{n_5}(1 - 2k_0)^{n_2}}$$

$$\times (1 - 2k_0)^{d - n_1 - n_3 - 2n_4}\,_2F_1\left(\begin{array}{c} n_1, n_1 + n_3 + 2n_4 - d \\ n_1 + n_3 \end{array}\middle| \frac{-2k_0}{1 - 2k_0}\right)$$

$$= \frac{I(n_1 + n_3, n_4)\Gamma\left(n_5 - \frac{d-1}{2}\right)}{\pi^{d/2}\Gamma(n_5)} \int_{-\infty}^{+\infty} \frac{(k_{E0}^2)^{(d-1)/2 - n_5} dk_{E0}}{(1 - 2ik_{E0})^{n_1 + n_2 + n_3 + 2n_4 - d}}$$

$$\times\,_2F_1\left(\begin{array}{c} n_1, n_1 + n_3 + 2n_4 - d \\ n_1 + n_3 \end{array}\middle| \frac{-2ik_{E0}}{1 - 2ik_{E0}}\right).$$

We can deform the integration contour (Fig. 3, $k_{E0} = iz/2$):

$$J = \frac{I(n_1 + n_3, n_4)\Gamma\left(n_5 - \frac{d-1}{2}\right)}{2^{d-2n_5-1}\pi^{d/2}\Gamma(n_5)} \cos\left[\pi\left(\frac{d}{2} - n_5\right)\right]$$
$$\times \int_0^\infty \frac{z^{d-2n_5-1}dz}{(z+1)^{n_1+n_2+n_3+2n_4-d}} {}_2F_1\left(\begin{array}{c} n_1, n_1+n_3+2n_4-d \\ n_1+n_3 \end{array} \middle| \frac{z}{z+1}\right).$$

Now we substitute the series

$${}_2F_1\left(\begin{array}{c} a,b \\ c \end{array} \middle| x\right) = \frac{\Gamma(c)\Gamma(b)}{\Gamma(a)} \sum_{n=0}^\infty \frac{\Gamma(n+a)\Gamma(n+b)}{\Gamma(n+1)\Gamma(n+c)} x^n,$$

and integrate term by term. The result is

$$J = \frac{I(n_1+n_3, n_4)\Gamma\left(n_5-\frac{d-1}{2}\right)\Gamma(d-2n_5)\Gamma(n_1+n_2+n_3+2n_4+2n_5-2d)}{2^{d-2n_5-1}\pi^{d/2}\Gamma(n_5)\Gamma(n_1+n_2+n_3+2n_4-d)} \cos\left[\pi\left(\frac{d}{2}-n_5\right)\right]$$
$$\times {}_3F_2\left(\begin{array}{c} n_1, n_1+n_3+2n_4-d, d-2n_5 \\ n_1+n_3, n_1+n_2+n_3+2n_4-d \end{array} \middle| 1\right).$$

Using (2.16), we can simplify this result:

$$J(n_1, n_2, n_3, n_4, n_5) =$$
$$\frac{\Gamma\left(\frac{d}{2}-n_4\right)\Gamma\left(\frac{d}{2}-n_5\right)\Gamma(n_1+n_3+2n_4-d)\Gamma(n_1+n_2+n_3+2n_4+2n_5-2d)}{\Gamma(n_4)\Gamma(n_5)\Gamma(n_1+n_3)\Gamma(n_1+n_2+n_3+2n_4-d)}$$
$$\times {}_3F_2\left(\begin{array}{c} n_1, n_1+n_3+2n_4-d, d-2n_5 \\ n_1+n_3, n_1+n_2+n_3+2n_4-d \end{array} \middle| 1\right). \tag{4.29}$$

It was first derived in coordinate space [9, 3]. Checking the symmetry $(n_1 \leftrightarrow n_2, n_4 \leftrightarrow n_5)$ requires using some ${}_3F_2$ identities.

4.2.3 $I(1,1,1,1,n)$

This diagram has been calculated in [12] using Gegenbauer polynomial technique in coordinate space [13]:

$$= I(1,1,1,1,n) = \frac{\Gamma\left(\frac{d}{2}-1\right)\Gamma\left(\frac{d}{2}-n-1\right)}{\Gamma(d-2)}$$
$$\times \left[2\frac{\Gamma(2n-d+3)\Gamma(2n-2d+6)}{(n-d+3)\Gamma(3n-2d+6)}{}_3F_2\left(\begin{array}{c} n-d+3, n-d+3, 2n-2d+6 \\ n-d+4, 3n-2d+6 \end{array} \middle| 1\right)\right.$$
$$\left. - \Gamma(d-n-2)\Gamma^2(n-d+3)\right]. \tag{4.30}$$

Some details of this method are discussed in [3].

4.2.4 Inversion

The last three-loop master integral has been calculated [15] using inversion. We shall first consider inversion relations at one and two loops. The one-loop massive on-shell integral defined by

$$\int \frac{d^d k}{[m^2 - (k + mv)^2 - i0]^{n_1} [-k^2 - i0]^{n_2}} = i\pi^{d/2} m^{d-2(n_1+n_2)} M(n_1, n_2) \qquad (4.31)$$

can be written in terms of the dimensionless Euclidean momentum $K = k_E/m$:

$$\int \frac{d^d K}{(K^2 - 2iK_0)^{n_1} (K^2)^{n_2}} = \pi^{d/2} M(n_1, n_2).$$
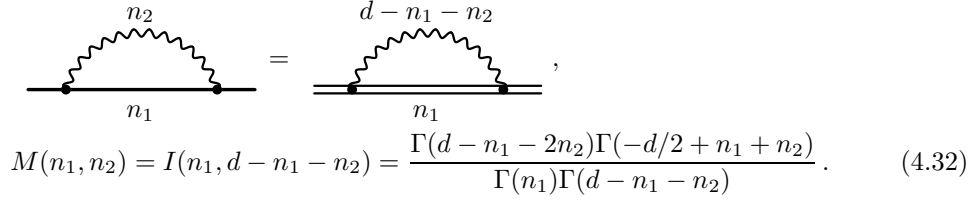
Similarly, the one-loop HQET propagator integral (2.9) expressed via $K = k_E/(-2\omega)$ is

$$\int \frac{d^d K}{(1 - 2iK_0)^{n_1} (K^2)^{n_2}} = \pi^{d/2} I(n_1, n_2).$$

Inversion $K = K'/K'^2$ transforms the massive on-shell denominator into the HQET one:

$$K^2 - 2iK_0 = \frac{1 - 2iK_0'}{K'^2}.$$

Therefore,

$$M(n_1, n_2) = I(n_1, d - n_1 - n_2) = \frac{\Gamma(d - n_1 - 2n_2)\Gamma(-d/2 + n_1 + n_2)}{\Gamma(n_1)\Gamma(d - n_1 - n_2)}. \qquad (4.32)$$

Similarly, at two loops we obtain [14]

This relation is less useful, because the HQET diagram in the right-hand side contains two non-integer indices.

At three loops we have [3]
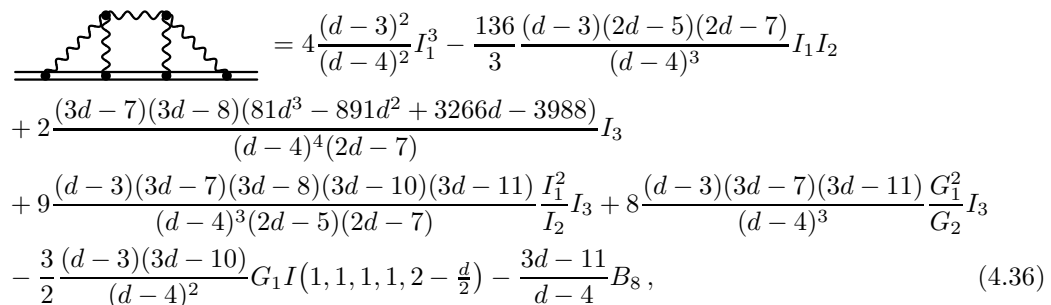
In particular, the HQET ladder diagram with all indices $n_i = 1$ is convergent; its value at $d = 4$ is related [15] to a massive on-shell diagram

 $=$ $= -5\zeta_5 + 12\zeta_2\zeta_3 \,.$ (4.35)

by the second inversion relation. This is one of the on-shell three-loop master integrals, and its value at $d = 4$ is known [16, 17]. Calculating this ladder diagram with `Grinder`:

$$
\text{} = 4\frac{(d-3)^2}{(d-4)^2}I_1^3 - \frac{136}{3}\frac{(d-3)(2d-5)(2d-7)}{(d-4)^3}I_1 I_2
$$
$$
+ 2\frac{(3d-7)(3d-8)(81d^3 - 891d^2 + 3266d - 3988)}{(d-4)^4(2d-7)}I_3
$$
$$
+ 9\frac{(d-3)(3d-7)(3d-8)(3d-10)(3d-11)}{(d-4)^3(2d-5)(2d-7)}\frac{I_1^2}{I_2}I_3 + 8\frac{(d-3)(3d-7)(3d-11)}{(d-4)^3}\frac{G_1^2}{G_2}I_3
$$
$$
- \frac{3}{2}\frac{(d-3)(3d-10)}{(d-4)^2}G_1 I\left(1,1,1,1,2-\tfrac{d}{2}\right) - \frac{3d-11}{d-4}B_8 \,, \tag{4.36}
$$

and solving for the most difficult HQET three-loop master integral B_8 (4.24), we obtain the ε expansion of this integral up to $\mathcal{O}(\varepsilon)$. This concludes the investigation of three-loop master integrals, and allows one to solve three-loop propagator problems in HQET up to terms $\mathcal{O}(1)$.

4.2.5 Applications

Using this technique, the HQET heavy-quark propagator has been calculated up to three loops [18], and the heavy-quark field anomalous dimension (obtained earlier by a completely different method [17]) has been confirmed. The anomalous dimension of the HQET heavy–light quark current has been calculated [18]. The correlator of two heavy–l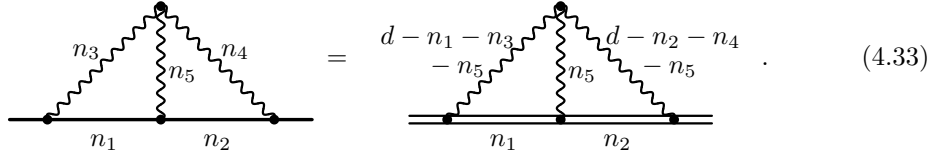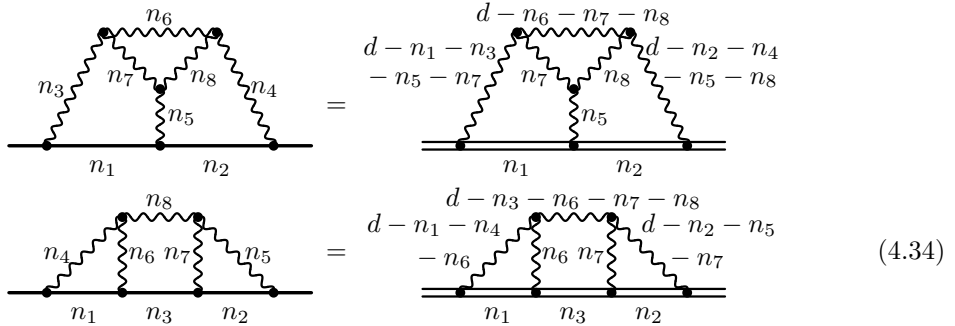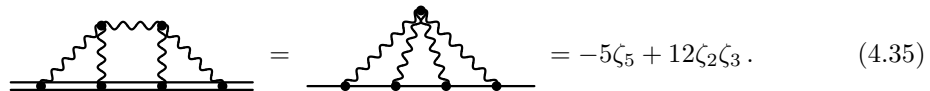ight currents has been found, up to three loops, including light-quark mass corrections of order m and m^2 [19]. The quark-condensate contribution to this correlator has been also calculated up to three loops [19]. Its ultraviolet divergence yields the difference of twice the anomalous dimension of the heavy-quark current and the that of the quark condensate, thus providing a completely independent confirmation of the result obtained in [18]. The gluon-condensate contribution has been calculated up to two loops [19] (at one loop it vanishes).

5 On-shell HQET propagator diagrams with mass

5.1 Two loops

On-shell HQET propagator diagrams vanish if all flavours (except the HQET one) are considered massless, because loop integrals contain no scale. If there is a massive flavour (c in the b-quark HQET), such diagrams are non-zero. They first appear at two loops. They are used, e.g., to calculate on-shell renormalization constants in HQET.

Let's first consider [20] a class of such integrals (Fig. 15)

$$
F(n_1, n_2) = \int \frac{f(k^2)\, d^d k}{D_1^{n_1} D_2^{n_2}} \,, \quad \text{where} \quad D_1 = -2k \cdot v - i0 \,, \quad D_2 = -k^2 - i0 \,, \tag{5.1}
$$
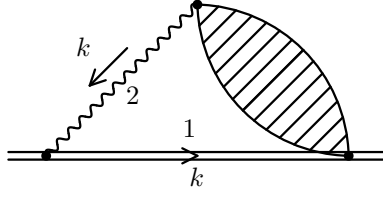
Figure 15: Diagram with a single HQET line

and $f(k^2)$ is an arbitrary function. We can construct an identity in which $f'(k^2)$ terms cancel:

$$\frac{\partial}{\partial k} \cdot \left(k - 2\frac{D_2}{D_1}v \right) \frac{f(k^2)}{D_1^{n_1} D_2^{n_2}} = \left[d - n_1 - 2 - 4(n_1 + 1)\frac{D_2}{D_1^2} \right] \frac{f(k^2)}{D_1^{n_1} D_2^{n_2}} \,. \tag{5.2}$$

Integrating it, we obtain an integration-by-parts relation [20]

$$(d - n_1 - 2)F(n_1, n_2) = 4(n_1 + 1)\mathbf{1}^{++}\mathbf{2}^- F(n_1, n_2) \,. \tag{5.3}$$

Let's call integrals with even n_1 apparently even, and with odd n_1 — apparently odd (they would be even and odd in v if we neglected $i0$ in the denominator). These two classes of integrals are not mixed by the recurrence relation (5.3). We can use this relation to reduce all apparently even integrals to vacuum integrals with $n_1 = 0$ (Fig. 16). Apparently odd integrals with $n_1 < 0$ can be reduced to $n_1 = -1$. Substituting $n_1 = -1$ to (5.3), we see that these integrals vanish, and hence all integrals with odd $n_1 < 0$ vanish too. Apparently odd integrals with $n_1 > 0$ can be reduced to $n_1 = 1$ (Fig. 16); however, they are not related to those with $n_1 = -1$.
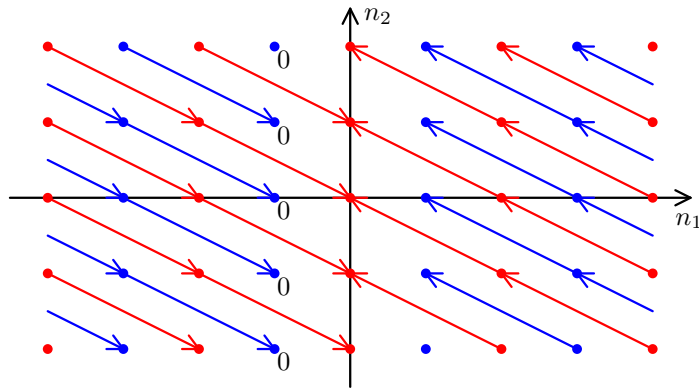
Figure 16: Recurrence relation

The solution of the recurrence relation can thus be written as

$$
F(n_1, n_2) = \begin{cases} (-4)^{-n_1/2} \dfrac{\Gamma\left(\frac{d}{2}\right)}{\Gamma\left(\frac{d-n_1}{2}\right)} \dfrac{\Gamma\left(\frac{1-n_1}{2}\right)}{\Gamma\left(\frac{1}{2}\right)} F\left(0, n_2 + \dfrac{n_1}{2}\right) & \text{even } n_1, \\[3mm] 2^{1-n_1} \dfrac{\Gamma\left(\frac{d-1}{2}\right)}{\Gamma\left(\frac{n_1+1}{2}\right)\Gamma\left(\frac{d-n_1}{2}\right)} F\left(1, n_2 + \dfrac{n_1-1}{2}\right) & \text{odd } n_1 > 0, \\[3mm] 0 & \text{odd } n_1 < 0. \end{cases}
\tag{5.4}
$$

Some of these properties can be understood more directly. If $n_1 < 0$, $i0$ in $D_1^{-n_1}$ can be safely neglected; averaging this factor over k directions, we obtain 0 for odd n_1 and the upper formula in (5.4) for even n_1. It was suggested [21] that this last formula can also be used for even $n_1 > 0$, but the proof (presented here) only appeared in [20].
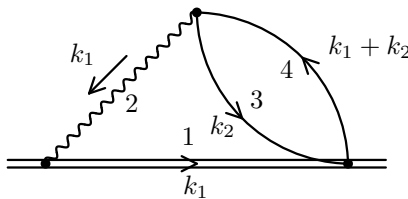
Figure 17: Two-loop diagram

Now let's consider the two-loop diagram (Fig. 17)

$$
F(n_1, n_2, n_3, n_4) = \frac{1}{(i\pi^{d/2})^2} \int \frac{d^d k_1 \, d^d k_2}{D_1^{n_1} D_2^{n_2} D_3^{n_3} D_4^{n_4}}\,,
\tag{5.5}
$$

where

$$
D_1 = -2k_1 \cdot v - i0\,, \quad D_2 = -k_1^2 - i0\,,
$$
$$
D_3 = 1 - k_2^2 - i0\,, \quad D_4 = 1 - (k_1 + k_2)^2 - i0\,.
$$

It is symmetric with respect to $3 \leftrightarrow 4$, and vanishes if n_3 or n_4 is integer and non-positive. It can be calculated using α parametrization [20]:

$$
F(n_1, n_2, n_3, n_4) =
\tag{5.6}
$$
$$
\frac{\Gamma\left(\frac{n_1}{2}\right)\Gamma\left(\frac{d-n_1}{2} - n_2\right)\Gamma\left(\frac{n_1-d}{2} + n_2 + n_3\right)\Gamma\left(\frac{n_1-d}{2} + n_2 + n_4\right)\Gamma\left(\frac{n_1}{2} + n_2 + n_3 + n_4 - d\right)}{2\Gamma(n_1)\Gamma(n_3)\Gamma(n_4)\Gamma\left(\frac{d-n_1}{2}\right)\Gamma(n_1 + 2n_2 + n_3 + n_4 - d)}\,.
$$

In full accordance with (5.4), integrals $F(n_1, n_2, n_3, n_4)$ with even n_1 reduce to $F(0, n_2 + n_1/2, n_3, n_4)$ (this is a well-known two-loop vacuum integral [22]); those with odd $n_1 > 0$ reduce to $F(1, n_2 + (n_1 - 1)/2, n_3, n_4)$; and those with odd $n_1 < 0$ vanish. All apparently even integrals are proportional to the single master integral

$$
I_0^2 = \quad\parbox{2cm}{\vspace{2cm}}\,,
\tag{5.7}
$$

and apparently odd ones — to

$$J_0 = \quad = 2^{4d-9} \pi^2 \frac{\Gamma(5-2d)}{\Gamma^2(2-d/2)} \,. \tag{5.8}$$

Integrals (5.5) can also contain powers of $(2k_2 + k_1) \cdot v$ in the numerator; see [20] for details of their evaluation.

5.2 Three loops

5.2.1 Reduction

There are two generic topologies of three-loop on-shell HQET propagator diagrams with a massive loop (Fig. 18). Algorithms of their reduction to master integrals, using integration by parts identities, have been constructed [20] by Gröbner bases technique [23].
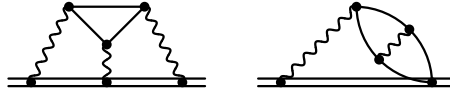
Figure 18: Topologies of three-loop on-shell HQET propagator diagrams with mass

All apparently even integrals of the first topology reduce to
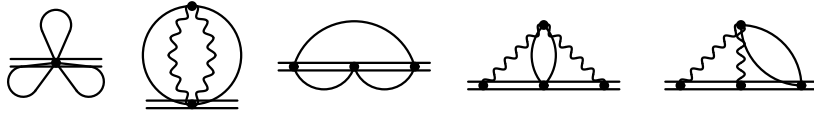
while apparently odd ones to
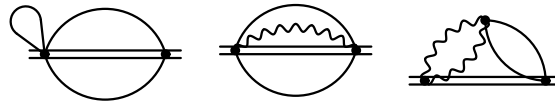
All apparently even integrals of the second topology reduce to
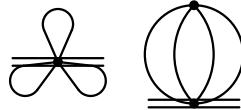
while apparently odd ones to
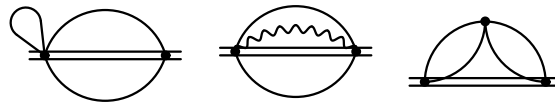
The master integrals
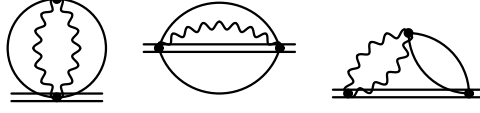
can be easily expressed via Γ functions. The master integral
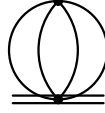
has been investigated in detail [24, 25].

5.2.2 A master integral

Now we shall discuss the integrals

$$I_{n_1 n_2 n_3} = \text{} \tag{5.9}$$

(I_{111} is one of the master integrals). Several approaches have been tried [20, 26]. The best result was obtained [26] using a method similar to [24].

First we consider (following [28]) the one-loop subdiagram

$$I_{n_1 n_2}(p_0) = \text{} = \frac{1}{i\pi^{d/2}} \int \frac{dk_0 \, d^{d-1}\vec{k}}{[-2(k_0 + p_0) - i0]^{n_1}[1 - k^2 - i0]^{n_2}} . \tag{5.10}$$

After the Wick rotation, we integrate in $d^{d-1}\vec{k}$:

$$I_{n_1 n_2}(p_0) = \frac{\Gamma(n_2 - (d-1)/2)}{\pi^{1/2}\Gamma(n_2)} \int_{-\infty}^{+\infty} dk_{E0} \frac{(k_{E0}^2 + 1)^{(d-1)/2 - n_2}}{(-2p_0 - 2ik_{E0})^{n_1}} .$$

If $p_0 < 0$, we can deform the integration contour (Fig. 19):

$$I_{n_1 n_2}(p_0) = 2\frac{\Gamma(n_2 - (d-1)/2)}{\pi^{1/2}\Gamma(n_2)} \cos\left[\pi\left(\frac{d}{2} - n_2\right)\right] \int_1^\infty dk \frac{(k^2 - 1)^{(d-1)/2 - n_2}}{(2k - 2p_0)^{n_1}} .$$

This integral is

$$
\begin{aligned}
I_{n_1 n_2}(p_0) = &\frac{\Gamma(n_1 + n_2 - 2 + \varepsilon)\Gamma(n_1 + 2n_2 - 4 + 2\varepsilon)}{\Gamma(n_2)\Gamma(2(n_1 + n_2 - 2 + \varepsilon))} \\
&\times {}_2F_1\left(\left.\begin{matrix} n_1, n_1 + 2n_2 - 4 + 2\varepsilon \\ n_1 + n_2 - \frac{3}{2} + \varepsilon \end{matrix}\right| \frac{1}{2}(1 + p_0)\right),
\end{aligned}
$$

or, after using a $_2F_1$ identity,

$$
I_{n_1 n_2}(p_0) = \frac{\Gamma(n_1 + n_2 - 2 + \varepsilon)\Gamma(n_1 + 2n_2 - 4 + 2\varepsilon)}{\Gamma(n_2)\Gamma(2(n_1 + n_2 - 2 + \varepsilon))}
$$
$$
\times \, _2F_1\left(\left. \begin{array}{c} \frac{1}{2}n_1, \frac{1}{2}n_1 + n_2 - 2 + \varepsilon \\ n_1 + n_2 - \frac{3}{2} + \varepsilon \end{array} \right| 1 - p_0^2 \right) . \tag{5.11}
$$

This result was obtained [26] using the HQET Feynman parametrization:

$$
I_{n_1 n_2}(p_0) = \frac{\Gamma(n_1 + n_2 - 2 + \varepsilon)}{\Gamma(n_1)\Gamma(n_2)} \int_0^\infty y^{n_1 - 1}(y^2 - 2p_0 y + 1)^{2 - n_1 - n_2 - \varepsilon} \, dy .
$$

This integral at $p_0 < 0$ gives (5.11) (a similar expression has been derived in [27]).
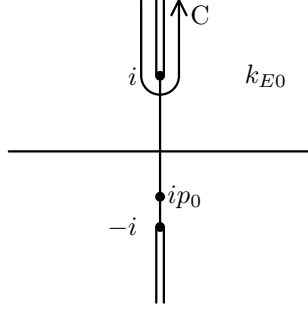
Figure 19: Integration contour

Now we can integrate in $d^{d-1}\vec{p}$ in the three-loop diagram:

$$
I_{n_1 n_2 n_3} = \frac{\Gamma(n_3 - 3/2 + \varepsilon)}{\pi^{1/2}\Gamma(n_3)} \int_{-\infty}^{+\infty} I_{n_1 n_2}^2(ip_{E0})(1 + p_{E0}^2)^{3/2 - n_3 - \varepsilon} dp_{E0} . \tag{5.12}
$$

The square of $_2F_1$ in (5.11) can be expressed via an $_3F_2$ using the Clausen identity. We analytically continue this $_3F_2$ from $1 + p_{E0}^2 > 1$ to $z = 1/(1 + p_{E0}^2) < 1$ and integrate (5.12) term by term. The result contains, in general, three $_4F_3$ of unit argument.

A convergent integral I_{122} is related to the master integral I_{111} by

$$
I_{122} = -\frac{(d-3)^2(d-4)(3d-8)(3d-10)}{8(3d-11)(3d-13)} I_{111} .
$$

For this integral, we obtain [26]

$$
\frac{I_{122}}{\Gamma^3(1+\varepsilon)} = -\frac{1}{2\varepsilon^2}\left[\frac{1}{1+2\varepsilon} \, _4F_3\left(\left. \begin{array}{c} 1, \frac{1}{2} - \varepsilon, 1 + \varepsilon, -2\varepsilon \\ \frac{3}{2} + \varepsilon, 1 - \varepsilon, 1 - 2\varepsilon \end{array} \right| 1 \right) \right.
$$
$$
- \frac{2}{1+4\varepsilon} \frac{\Gamma^2(1-\varepsilon)\Gamma^3(1+2\varepsilon)}{\Gamma^2(1+\varepsilon)\Gamma(1-2\varepsilon)\Gamma(1+4\varepsilon)} \, _3F_2\left(\left. \begin{array}{c} \frac{1}{2}, 1 + 2\varepsilon, -\varepsilon \\ \frac{3}{2} + 2\varepsilon, 1 - \varepsilon \end{array} \right| 1 \right)
$$
$$
\left. + \frac{1}{1+6\varepsilon} \frac{\Gamma^2(1-\varepsilon)\Gamma^4(1+2\varepsilon)\Gamma(1-2\varepsilon)\Gamma^2(1+3\varepsilon)}{\Gamma^4(1+\varepsilon)\Gamma(1+4\varepsilon)\Gamma(1-4\varepsilon)\Gamma(1+6\varepsilon)} \right] . \tag{5.13}
$$

Expansion of this result up to ε^7 agrees with [26]

$$\frac{I_{122}}{\Gamma^3(1+\varepsilon)} = \frac{\pi^2}{3} \frac{\Gamma^3(1+2\varepsilon)\Gamma^2(1+3\varepsilon)}{\Gamma^6(1+\varepsilon)\Gamma(2+6\varepsilon)} \,. \tag{5.14}$$

This equality has also been checked by high precision numerical calculations at some finite ε values. This conjectured hypergeometric identity can also be rewritten in a nice form [28]

$$g_1(\varepsilon)_4F_3 \left(\begin{array}{c} 1, \frac{1}{2}-\varepsilon, 1+\varepsilon, -2\varepsilon \\ \frac{3}{2}+\varepsilon, 1-\varepsilon, 1-2\varepsilon \end{array} \middle| 1 \right) - 2g_2(\varepsilon)_3F_2 \left(\begin{array}{c} \frac{1}{2}, 1+2\varepsilon, -\varepsilon \\ \frac{3}{2}+2\varepsilon, 1-\varepsilon \end{array} \middle| 1 \right) + g_3(\varepsilon) = 0 \,, \tag{5.15}$$

where

$$b(\varepsilon) = \frac{\Gamma(1-\varepsilon)\Gamma(1+2\varepsilon)}{\Gamma(1+\varepsilon)} \,, \quad g_n(\varepsilon) = \frac{b^n(\varepsilon)}{b(n\varepsilon)(1+2n\varepsilon)} \,.$$

We have no analytical proof.

5.2.3 Other master integrals

Other master integrals were calculated [20] using Mellin–Barnes representation (see, e.g., [4]). Now we shall discuss a simple example of this technique. Let's consider the one-loop propagator diagram with two massive lines:

$$\frac{1}{i\pi^{d/2}} \int \frac{d^d k}{[m^2 - k^2]^{n_1}[m^2 - (k+p)^2]^{n_2}} \,.$$

Using Feynman parametrization,

$$= \frac{\Gamma(n_1+n_2)}{\Gamma(n_1)\Gamma(n_2)} \frac{1}{i\pi^{d/2}} \int \frac{dx\, x^{n_2-1}(1-x)^{n_1-1}\, d^d k}{[(m^2-k^2)(1-x)+(m^2-(k+p)^2)x]^{n_1+n_2}}$$

$$= \frac{\Gamma(n_1+n_2)}{\Gamma(n_1)\Gamma(n_2)} \frac{1}{i\pi^{d/2}} \int \frac{dx\, x^{n_2-1}(1-x)^{n_1-1}\, d^d k}{[-k^2 - 2xp\cdot k - xp^2 + m^2]^{n_1+n_2}} \,.$$

After the shift $k = k' - xp$:

$$= \frac{\Gamma(n_1+n_2)}{\Gamma(n_1)\Gamma(n_2)} \frac{1}{i\pi^{d/2}} \int \frac{dx\, x^{n_2-1}(1-x)^{n_1-1}\, d^d k}{[m^2 + x(1-x)(-p^2) - k'^2]^{n_1+n_2}} \,,$$

we can integrate in k':

$$= \frac{\Gamma\left(n_1+n_2-\frac{d}{2}\right)}{\Gamma(n_1)\Gamma(n_2)} \int_0^1 \frac{dx\, x^{n_2-1}(1-x)^{n_1-1}}{[m^2 + x(1-x)(-p^2)]^{n_1+n_2-d/2}} \,.$$

Now we shall use Mellin–Barnes representation

$$\frac{1}{(a+b)^n} = \frac{a^{-n}}{\Gamma(n)} \frac{1}{2\pi i} \int_{-i\infty}^{+i\infty} dz\, \Gamma(-z)\Gamma(n+z) \left(\frac{b}{a}\right)^z \,. \tag{5.16}$$

Here the integration contour is chosen in such a way that all poles of $\Gamma(\cdots + z)$ (they are called *left poles*) are to the left of the contour, and all poles of $\Gamma(\cdots - z)$ (they are called *right poles*)

are to the right of it. It is easy to check (5.16): closing the contour to the right we get the expansion of the left-hand side in b/a; closing it to the left — the expansion in a/b.

We continue our calculation:

$$
= \frac{m^{d-2(n_1+n_2)}}{\Gamma(n_1)\Gamma(n_2)} \frac{1}{2\pi i} \int_{-i\infty}^{+i\infty} dz \Gamma(-z)\Gamma(n_1+n_2+z) \left(\frac{-p^2}{m^2}\right)^z \int_0^1 dx\, x^{n_2+z-1}(1-x)^{n_1+z-1}
$$

$$
= \frac{m^{d-2(n_1+n_2)}}{\Gamma(n_1)\Gamma(n_2)} \frac{1}{2\pi i} \int_{-i\infty}^{+i\infty} dz \frac{\Gamma(-z)\Gamma(n_1+z)\Gamma(n_2+z)\Gamma\left(n_1+n_2-\frac{d}{2}+z\right)}{\Gamma(n_1+n_2+2z)} \left(\frac{-p^2}{m^2}\right)^z .
$$

This means that two massive lines can be replaced by one massless one (raised to the power $-z$) at the price of one extra integration in z:

$$
\text{(diagram)} = \frac{1}{i\pi^{d/2}} \int \frac{d^d k}{[m^2-k^2-i0]^{n_1}[m^2-(k+p)^2-i0]^{n_2}} =
$$

$$
\frac{m^{d-2(n_1+n_2)}}{\Gamma(n_1)\Gamma(n_2)} \frac{1}{2\pi i} \int_{-i\infty}^{+i\infty} dz \frac{\Gamma(-z)\Gamma(n_1+z)\Gamma(n_2+z)\Gamma(n_1+n_2-d/2+z)}{\Gamma(n_1+n_2+2z)}
$$

$$
m^{-2z} \text{(diagram)} \tag{5.17}
$$

This trick allows us to reduce this master integral to a single Mellin–Barnes integral. Using integration by parts, we can kill one of three lines in the left (integer) triangle, and calculate the integrand in Γ functions. This allows us to find several terms of its ε expansion:

$$
\text{(diagram)} = \frac{\Gamma^2(2\varepsilon)\Gamma(3\varepsilon-1)}{4\Gamma(4\varepsilon)} \frac{1}{2\pi i} \int_{-i\infty}^{+i\infty} dz
$$

$$
\frac{\Gamma(1+z)\Gamma(1/2+\varepsilon+z)\Gamma(1+\varepsilon+z)\Gamma(-2\varepsilon-z)\Gamma(-\varepsilon-z)\Gamma(-z)}{\Gamma(3/2+\varepsilon+z)\Gamma(1-2\varepsilon-z)}
$$

$$
= -\Gamma^3(1+\varepsilon)\left[\frac{\pi^2}{9\varepsilon^2} - \frac{6\zeta_3-5\pi^2}{9\varepsilon} + \frac{11}{270}\pi^4 - \frac{10}{3}\zeta_3 + \frac{19}{9}\pi^2\right.
$$

$$
\left. + \left(-\frac{8}{3}\zeta_5 + \frac{8}{9}\pi^2\zeta_3 + \frac{11}{54}\pi^4 - \frac{38}{3}\zeta_3 + \frac{65}{9}\pi^2\right)\varepsilon + \cdots\right]. \tag{5.18}
$$

This master integral has been evaluated in a closed form using Mellin–Barnes in α representation:

$$
\text{(diagram)} = \frac{\Gamma(1/2-\varepsilon)\Gamma(-\varepsilon)\Gamma^2(2\varepsilon)\Gamma(1+\varepsilon)\Gamma(3\varepsilon-1)}{4\Gamma(3/2-\varepsilon)\Gamma(4\varepsilon)}
$$

$$
\times \left[\psi\left(\frac{1}{2}-\varepsilon\right) + \psi\left(1-\varepsilon\right) - 2\log 2 + 2\gamma_E\right]. \tag{5.19}
$$

This master integral can be written as a double Mellin–Barnes integral using (5.17). It

appears possible to calculate one integral:

$$
\begin{aligned}
&\text{[diagram]} = \frac{\pi^{3/2}}{4^\varepsilon \Gamma(3/2-\varepsilon)} \frac{1}{2\pi i} \\
&\int_{-i\infty}^{+i\infty} dz \, \frac{\Gamma(1+z)\Gamma\left(\frac{3}{2}-\varepsilon+z\right)\Gamma(\varepsilon+z)\Gamma\left(-\frac{1}{2}+\varepsilon-z\right)\Gamma\left(-\frac{3}{2}+2\varepsilon-z\right)\Gamma(-z)}{\Gamma\left(\frac{3}{2}+z\right)\Gamma(\varepsilon-z)} \\
&= \Gamma^3(1+\varepsilon)\frac{32}{3}\pi^2 \left[-1+2\left(4\log 2 - \pi - 7\right)\varepsilon + \cdots\right].
\end{aligned}
\tag{5.20}
$$

5.2.4 Applications

Feynman integrals considered here were used [20] for calculating the matching coefficients for the HQET heavy-quark field and the heavy–light quark current between the b-quark HQET with dynamic c-quark loops and without such loops (the later theory is the low-energy approximation for the former one at scales below m_c). Another recent application — the effect of $m_c \neq 0$ on $b \to c$ plus lepton pair at three loops [29]. The method of regions was used; the purely soft region (loop momenta $\sim m_c$) gives integrals of this type. Two extra terms of ε expansion of the master integral of Sect. 5.2.2 were required for this calculation which were not obtained in [20]. This was the initial motivation for [26].

Acknowledgements

References

[1] A.V. Manohar, M.B. Wise, *Heavy Quark Physics*, Cambridge University Press (2000).

[2] A.G. Grozin, *Heavy Quark Effective Theory*, Springer Tracts in Modern Physics **201**, Springer (2004); hep-ph/0008300.

[3] A.G. Grozin, Int. J. Mod. Phys. **A19** (2004) 473 [hep-ph/0307297]; *Lectures on QED and QCD: Practical Calculation and Renormalization of One- and Multi-Loop Feynman Diagrams*, World Scientific (2007).

[4] V.A. Smirnov, *Feynman Integral Calculus*, Springer (2006).

[5] A.I. Davydychev, A.G. Grozin, Eur. Phys. J. **C20** 333 (2001) [hep-ph/0103078].

[6] O.I. Zavialov, *Renormalized Feynman Diagrams*, Nauka, Moscow (1979) (in Russian); *Renormalized Quantum Field Theory*, Kluwer Academic Press (1989).

[7] D.J. Broadhurst, A.G. Grozin, Phys. Lett. **B267** 105 (1991).

[8] K.G. Chetyrkin, F.V. Tkachov, Nucl. Phys. **B192** 159 (1981).

[9] A.G. Grozin, JHEP **03** 013 (2000) [hep-ph/0002266].

[10] S.G. Gorishny, S.A. Larin, F.V. Tkachov, preprint INR P-0330, Moscow (1984); S.G. Gorishny, S.A. Larin, L.R. Surguladze, F.V. Tkachov, Comput. Phys. Commun. **55** 381 (1989); S.A. Larin, F.V. Tkachov, J.A.M. Vermaseren, preprint NIKHEF-H/91-18, Amsterdam (1991).

[11] E. Bagan, P. Ball, P. Gosdzinsky, Phys. Lett. **B301** 249 (1993).

[12] M. Beneke, V.M. Braun, Nucl. Phys. **B426** (1994) 301 [hep-ph/9402364].

[13] K.G. Chetyrkin, A.L. Kataev, F.V. Tkachov, Nucl. Phys. **B174** 345 (1980).

[14] D.J. Broadhurst, A.G. Grozin, in *New Computing Techniques in Physics Research IV*, ed. B. Denby, D. Perret-Gallix, World Scientific (1995), p. 217 [hep-ph/9504400].

[15] A. Czarnecki, K. Melnikov, Phys. Rev. **D66** 011502 (2002) [hep-ph/0110028].

[16] S. Laporta, E. Remiddi, Phys. Lett. **B379** 283 (1996) [hep-ph/9602417].

[17] K. Melnikov, T. van Ritbergen, Nucl. Phys. **B591** 515 (2000) [hep-ph/0005131].

[18] K.G. Chetyrkin, A.G. Grozin, Nucl. Phys. **B666** 289 (2003) [hep-ph/0303113].

[19] K.G. Chetyrkin, A.G. Grozin, unpublished.

[20] A.G. Grozin, A.V. Smirnov, V.A. Smirnov, JHEP **11** 022 (2006) [hep-ph/0609280].

[21] D.J. Broadhurst, A.G. Grozin, Phys. Rev. **D52** 4082 (1995) [hep-ph/9410240].

[22] A.A. Vladimirov, Theor. Math. Phys. **43** 417 (1980).

[23] A.V. Smirnov, V.A. Smirnov, JHEP **01** 001 (2006) [hep-lat/0509187];
A.V. Smirnov, JHEP **04** 026 (2006) [hep-ph/0602078].

[24] D.J. Broadhurst, Z. Phys. **C54** 599 (1992).

[25] D.J. Broadhurst, hep-th/9604128.

[26] A.G. Grozin, T. Huber, D. Maître, JHEP **07** 033 (2007) [arXiv:0705.2609].

[27] J. Zupan, Eur. Phys. J. **C25** 233 (2002) [hep-ph/0202135].

[28] A.G. Grozin, Nucl. Phys. B (Proc. Suppl.) **183** 302 (2008) [arXiv:0805.1474].

[29] A. Pak, A. Czarnecki, Phys. Rev. Lett. **100** 241807 (2008) [arXiv:0803.0960]; arXiv:0808.3509.

Radiative corrections to top quark decays

A. Kadeer[1], J.G. Körner[1]

[1]Institut für Physik, Johannes-Gutenberg-Universität, Staudinger Weg 7, 55099 Mainz, Germany

We provide a pedagogical introduction to the subject of Standard Model decays of unpolarized top quarks into unpolarized and polarized W-bosons including their QCD and electroweak radiative corrections.

1   Introductory remarks

These lectures held by one of us (JGK) at the II Helmholtz International Summer School on Heavy Quark Physics in Dubna, Russia (August 11 - 21 2008) are meant as pedagogical lectures aimed at the level of the audience which, on the participants' side, was composed of graduate students with a few postdoctoral students mixed in. We give many details on the Born level calculation of rates and angular decay distributions which can be profitably used in the higher order radiative correction calculations. The material collected in the write-up of the lectures given by one of us at the International School on Heavy Quark Physics in Dubna, Russia (27 May - 5 Jun 2002) [1] covering similar topics will not always be repeated. In addition to the review [1] we very much recommend the excellent reviews on top quark physics in [2, 3, 4, 5, 6]. One of the main aim of these lectures is to illustrate advanced loop techniques in simple Born term settings. We begin by listing the basic properties of the Standard Model (SM) top quark and its SM decay features.

1.1   Mass of the top quark

In our numerical calculations we always take the top quark mass to be $m_t = 175\,\text{GeV}$. The latest Tevatron combination is $m_t = 173.1 \pm 0.6(stat.) \pm 1.1(syst.)\,\text{GeV}$ [7]. Since all our results are in closed analytical form any other value of the top quark mass can be used as input in these formulas.

There have been suggestions for indirect measurements of the top quark mass through the measurements of dynamic quantities that depend on the value of the top quark mass. For example, the SM $(t\bar{t})$-production rate at e.g. hadron colliders is sensitive to the value of the top quark mass (in particular at the Tevatron II) and thus the $(t\bar{t})$-production rate could be used to "measure" the top quark mass. Another possibility is to accurately measure the longitudinal and transverse-minus helicity decay rates of the top quark. The ratio of the two helicity rates is well suited for an indirect determination of the top quark mass since the ratio depends quadratically on the top quark mass, i.e. $\Gamma_L/\Gamma_- \sim m_t^2/m_W^2$. One should, however, always take into account radiative corrections in such indirect top quark mass measurements. For example, in the latter case the NLO QCD and electroweak radiative corrections have different effects on

the two partial helicity rates which lead to a 3.6% upward shift in the helicity rate ratio Γ_L/Γ_- for top quark masses around 175 GeV [8, 9].

In a third method one measures the mean distance that b-hadrons from $(t\bar{t})$-events travel before they decay [10]. The mean distance is obviously correlated with the value of the top quark mass. Needless to say that all these indirect top quark mass measurements crucially depend on the assumed correctness of the SM.

1.2 Top quark decays before it can hadronize

Singly produced top quarks in hadronic collisions are produced by weak interactions and are almost 100% polarized. The top quark retains its polarization which it has at birth when it decays. The standard argument is that the life time of the top quark ($\tau_t \cong 4.6 \times 10^{-25}s$) is shorter than the hadronization time which is characterized by the inverse of the nonperturbative scale of QCD, i.e.$\Lambda_{QCD}^{-1} \cong 10^{-23}s$.

However, one can do better as pointed out in [11] who extended earlier work on depolarization effects in the bottom sector [12, 13]. Consider a polarized top quark which picks up a s-wave light antiquark of opposite spin direction. This state will be a coherent superposition of the spin 0 and spin 1 mesonic ground states as follows

$$t(\uparrow)\bar{q}(\downarrow) = \frac{1}{\sqrt{2}}\underbrace{\left(\frac{t(\uparrow)\bar{q}(\downarrow) - t(\downarrow)\bar{q}(\uparrow)}{\sqrt{2}}\right)}_{spin\ 0} + \frac{1}{\sqrt{2}}\underbrace{\left(\frac{t(\uparrow)\bar{q}(\downarrow) + t(\downarrow)\bar{q}(\uparrow)}{\sqrt{2}}\right)}_{spin\ 1}. \tag{1}$$

The coherent superposition will become decoherent on two counts. First the system oscillates between the two mass eigenstates with a time scale $t_{\text{decoherence}} \approx 1/\Delta m_T \approx 6 \cdot 10^{-22}s$ characterized by the mass difference $\Delta m_T = m_{T^*} - m_T \approx (m_b/m_t)\Delta m_B \approx 1\text{MeV}$ where $\Delta m_B = m_{B^*} - m_B$. Loss of coherence through the decay $T^* \to T + \gamma$ can be neglected since it sets in much later at a time scale $t_{\text{decay}} \approx 6 \cdot 10^{-17}s$ [11]. Thus the depolarization time scale is set by $t_{\text{decoherence}}$ and is larger than the tradional estimate based on $\Lambda_{QCD}^{-1} \cong 10^{-23}s$ by a factor of 60. Altogether, the top quark has decayed after $\tau_t = 4.6 \cdot 10^{-25}s$ much before depolarization sets in at $t_{\text{decoherence}} \approx 6 \cdot 10^{-22}s$. One concludes that the top quark retains its polarization which it has at birth when it decays.

The decay of polarized top quarks and the corresponding spin-momentum correlations in these decays will not be discussed in these lectures. A discussion of the spin-momentum correlations and their NLO QCD corrections can be found in [8, 14, 15]. We mention that top quarks produced at e^+e^--colliders also possess a high degree of polarization which, in addition, can also be attuned by tuning the beam polarization.

The issue of whether the top quark retains its original polarization when it decays is also of importance in the case of hadronically produced top quark pairs. Although the single top (or antitop) polarization is zero because parity is conserved in the hadronic production process there are sizable spin-spin correlations of the top and antitop quark spins which give important information on the $(t\bar{t})$-production process (see e.g. [4]).

1.3 Dominance of the decay $t \to X_b + W^+$

From the unitarity of the KM–matrix one has the relation

$$\underbrace{|V_{ub}|^2}_{(\approx 0.004)^2} \quad + \quad \underbrace{|V_{cb}|^2}_{(\approx 0.04)^2} \quad + \quad |V_{tb}|^2 = 1 \ . \tag{2}$$

One concludes that $V_{tb} \approx 1$. There are a number of other SM decays such as $t \to X_s + W^+$ which are negligible compared to the dominant mode $t \to X_b + W^+$ [1].

1.4 Rate ratio of $t \to b + W^+ (\to leptons)$ and $t \to b + W^+ (\to hadrons)$

Let us list the possible leptonic and hadronic decay modes of the the W^+. For the leptonic modes one has the three modes

$$W^+ \quad \to \quad (\tau^+ \nu_\tau), \ (\mu^+ \nu_\mu), \ (e^+ \nu_e) \qquad \text{weight}: 3 \tag{3}$$

When listing the weight factor we have neglected lepton mass effects.

For the hadronic modes one has

$$
\begin{aligned}
W^+ \quad &\to \quad c\bar{b}, \ c\bar{s}, \ c\bar{d} \qquad \text{weight}: 1 \otimes 3 \ (colour \ summation) \\
&\to \quad u\bar{b}, \ u\bar{s}, \ u\bar{d} \qquad \text{weight}: 1 \otimes 3 \ (colour \ summation)
\end{aligned}
\tag{4}
$$

Again mass effects have been neglected. In (4) we have summed over the respective three modes using again the unitarity of the KM-matrix $\sum_{j=b,s,d} |V_{cj}|^2 = 1$ and $\sum_{j=b,s,d} |V_{uj}|^2 = 1$. In addition one has to add in a factor of three from colour summation. One thus obtains

$$\frac{\Gamma\big(t \to b + W^+ (\to leptons)\big)}{\Gamma\big(t \to b + W^+ (\to hadrons)\big)} = \frac{3}{6} \ . \tag{5}$$

1.5 Width of the top quark

As mentioned before the top quark decays almost 100% to $t \to b + W^+$ in the SM. The other SM decay modes are negligible. Let us list the theoretical values of the SM decay width and radiative corrections relative to the Born term width ($\Gamma(\text{Born}) = 1.56$ GeV for $m_b = 0$).

$$
\begin{aligned}
\frac{1}{\Gamma(\text{Born})} \, \Gamma_{t \to b + W^+} = \quad & 1 & \text{Born LO} \\
& -0.27\% & \text{Born} \quad m_b \neq 0 \\
& -8.5\% & \text{QCD} \quad \text{NLO} \quad [16] \\
& +1.55\% & \text{electroweak} \quad \text{NLO} \quad [17, 18] \\
& -1.56\% & \text{finite } W^+ - \text{width} \quad [16] \\
& -2.25\% & \text{QCD} \quad \text{NNLO} \quad [19, 20]
\end{aligned}
\tag{6}
$$

The NLO and NNLO QCD corrections and the NLO electroweak corections will be discussed in Sec. 2. The finite width corrections will be discussed in Sec. 5.

---

[1] In order to simplify the notation we shall in the following refer to the decay $t \to X_b + W^+$ as $t \to b + W^+$.

It is interesting to note that the non-SM decay width into a charged Higgs $t \to b + H^+$ can become comparable in size to the SM decay width $t \to b + W^+$ for small and large values of $\tan\beta$ if m_{H^+} is not too close to the phase space boundary (see e.g. [4]). A precise measurement of the top quark decay width could therefore provide stringent exclusion regions in the $(\tan\beta, m_{H^+})$-parameter space of Two-Higgs-Doublet models which contain a charged Higgs boson.

The measurement of the top quark decay width is not simple at hadron colliders. In principle there are two methods to experimentally get a handle on the decay width Γ_t or lifetime $\tau_t = 1/\Gamma_t$ of the top quark. One can attempt to measure the mean decay length in the laboratory which is given by the mean decay length [2]

$$\bar{s} = v_{lab} \cdot \tau_{lab} = \beta\gamma \; c \cdot \tau = \left[\frac{p_{lab}}{m}\right] c \cdot \tau \; . \tag{7}$$

where $v_{lab} = \beta c$ and $\tau_{lab} = \gamma\tau$, and $\beta = p_{lab}c/E_{lab}$ and $\gamma = E_{lab}/(mc^2)$. That this measurement is difficult is illustrated by the following example. Take a top quark width of 1.43 GeV. The laboratory momentum of the top quark p_{lab} must have the astronomically high value of $\approx 10^{15}$ GeV to produce a mean decay length of 1mm. Nevertheless CDF has attempted such a measurement using information on the magnitude of the impact parameter of the charged lepton with respect to the collision vertex. CDF puts a 95% confidence level upper limit of $1.8 \cdot 10^{-13}s$ on the lifetime of the top quark which corresponds to a $3.7 \cdot 10^{-12}$ GeV lower limit on the top quark width [21]. Naturally, this is not a very useful bound. CDF also provides an upper limit on the top quark width by a fit of the reconstructed top quark mass to a Breit-Wigner shape function. The reult is $\Gamma_t < 13.1$ GeV at 95% C.L. [22]. The upper bound is still nine times larger than the expected SM width.

An indirect way of determining the top quark width relies heavily on the validity of the SM. The suggestion is to measure the branching ratio $\mathcal{B}(t \to bW) = \Gamma(t \to bW)/\Gamma(t \to \text{all})$. This could be done e.g. by measuring the rate of top quark pair production followed by their decays $t \to bW$, i.e. by measuring $\sigma_{t\bar{t}} \cdot (\mathcal{B}(t \to bW))^2$. Assuming that one can reliably calculate $\sigma_{t\bar{t}}$ one can then extract $\mathcal{B}(t \to bW)$ (see e.g. [3]). In the simplest version of this approach one takes the SM value $\Gamma(t \to bW)$ to determine the width of the top quark through $\Gamma(t \to \text{all}) = \Gamma(t \to bW)/\mathcal{B}(t \to bW)$. In a more sophisticated approach one uses single-top production to extract the parameters that determine the partial width $\Gamma(t \to bW)$ [23].

We mention that a much improved determination of the top quark width with an uncertainty of $\Delta\Gamma \approx 30$ MeV can be expected from a multi-parameter scan of the threshold region of $(t\bar{t})$-production at the ILC [24].

1.6   Top quark yield

At the LHC top quark pairs will be produced quite copiously in 7 on 7 TeV proton-proton collisions. After a one-year probation run at reduced energies and luminosities starting in the end of 2009 the LHC will start running at full energy in 2010 with a low luminosity run of $L \approx 10^{33} cm^{-2} s^{-1}$. After a luminosity upgrade around the year 2017 the high luminosity run will have $L \approx 10^{34} cm^{-2} s^{-1}$. Multiply these numbers with $\sigma(t\bar{t}) \sim 825\,pb = 825 \times 10^{-36} cm^2$ to obtain $\approx 1\,(10)\,(t\bar{t})$-pairs every second for the low (high) luminosity run.

Top quark pair production at the Tevatron II (1 on 1 TeV $p\bar{p}$-collisions) occurs at a reduced rate. Because the energy of the Tevatron II is lower, the $(t\bar{t})$-production cross section is down

---

[2]We have employed a mixed notation in the last equality of Eq.(7) where we set $c = 1$ for the quantities in the square bracket $[p_{lab}/m]$.

by a factor of ≈ 100. In addition, the Tevatron II luminosity is down by a factor of ≈ 10 compared to the LHC low luminosity run. Taking these two factors into account one has $\approx 1 \times 10^{-3}$ $(t\bar{t})$-pairs per second at the Tevatron II.

In the SM single top production cross section in $(p\bar{p})$- and (pp)-collisions is down by a factor of ≈ 3 compared to top quark pair production. The nice feature of single top production is that the top quarks are polarized since the production of single top quarks proceeds through weak interactions. The polarization can be calculated to be close to 100% (see e.g. [4]).

At the ILC $(t\bar{t})$-production will occur at a somewhat reduced rate compared to the LHC. At 500 GeV the NLO rate is $\sigma(t\bar{t}) \sim 0.5 \, pb = 0.5 \times 10^{-36} cm^2$ (see e.g. [25, 26]) which gives 10^{-2} $(t\bar{t})$-events per second assuming a luminosity of $L \approx 2 \cdot 10^{34} cm^{-2} s^{-1}$.

1.7 Polarization of W^+ gauge boson

The decay $t \to b + W^+$ is weak and therefore the W^+-boson is in general expected to be polarized. We shall refer to the three partial rates that correspond to the three polarization states of the W^+-boson as longitudinal (Γ_L), transverse-plus (Γ_+) and transverse-minus (Γ_-). At leading order (LO) the results for the helicity fractions $\mathcal{G}_i = \Gamma_i/\Gamma$ $(i = L, +, -)$ (or, in another language, for the normalized diagonal density matrix elements of the W^+-boson ρ_{00}, ρ_{++} and ρ_{--}) are[3]

$$\mathcal{G}_L : \mathcal{G}_+ : \mathcal{G}_- = \frac{1}{1 + 2y^2} : 0 : \frac{2y^2}{1 + 2y^2} \,, \tag{8}$$

where $y^2 = m_W^2/m_t^2 = 0.211$ with $m_b = 0$. Numerically one has

$$\mathcal{G}_L : \mathcal{G}_+ : \mathcal{G}_- = 0.703 : 0 : 0.297 \,. \tag{9}$$

Note that $\mathcal{G}_L + \mathcal{G}_+ + \mathcal{G}_- = 1$. In comparison, an unpolarized W^+ would correspond to

$$\mathcal{G}_L : \mathcal{G}_+ : \mathcal{G}_- = 1/3 : 1/3 : 1/3 \,. \tag{10}$$

1.8 Dominance of the longitudinal mode

As $(m_W/m_t) \to 0$ the longitudinal polarization vector becomes increasingly parallel to q^μ (see e.g. [1]), viz.

$$\epsilon_L^\mu = \frac{1}{m_W}\Big(q^\mu + \mathcal{O}(m_W/m_t)\Big) \,. \tag{11}$$

Therefore the longitudinal mode dominates in the large top quark mass limit. In fact, from $q_\mu \bar{u}_b \gamma^\mu (1-\gamma_5) u_t = m_t \bar{u}_b (1+\gamma_5) u_t$ one concludes from dimensional arguments that $\Gamma_L \sim G_F m_t^3$ whereas $\Gamma_\pm \sim G_F m_t m_W^2$ or $\Gamma_\pm/\Gamma_L \sim m_W^2/m_t^2$.

An explicit calculation shows that $\Gamma_+ = 0$ at LO for $m_b = 0$ (see Eq.(8)). Looking at Fig. 1 the vanishing of the LO transverse-plus rate Γ_+ can be understood from angular momentum conservation. First remember that a massless left-chiral fermion is left-handed as drawn in Fig. 1. At LO one has a back-to-back decay configuration. Therefore the W^+-boson cannot be right-handed because the m-quantum numbers in the final state would add up to $3/2$ which cannot be reached by the spin $1/2$ top quark in the initial state. At NLO (or any higher order) the decay $t \to b + g + W^+$ is, in general, no longer back-to-back as illustrated in Fig. 1 and one

---

[3]The helicities of the W-boson are alternatively labelled by $(L, +, -)$, $(0, +1, -1)$ or by (L, T_+, T_-).

anticipates that $\Gamma_+ \neq 0$ at NLO and at any higher order. This is, in fact borne out by the NLO calculation to be described later on. The physics interest lies in the fact that nonvanishing transverse-plus helicity rates can also be generated by non-SM right-chiral $(t\bar{b})$-currents. In order to unambiguously identify non-SM contributions to the transverse-plus helicity rate it is therefore important to get a quantitative handle on the size of the SM higher order radiative correction contributions to the transverse-plus helicity rate.
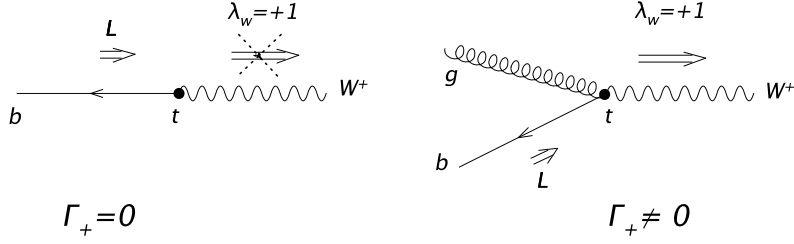
Figure 1: Angular momentum conservation for $t \rightarrow b + W^+$ and for $t \rightarrow b + W^+ + g$.

1.9 Measurement of the helicity fractions of the W^+ through the angular decay distribution in its decay

The W^+ decays weakly to $(l^+\nu_l)$ or to $(\bar{q}_i q_j)$. The angular decay distribution can therefore be utilized to analyze the polarization of the decaying W^+, i.e. the W^+ is self-analyzing.

The W^+ has the three (diagonal) polarization states L, T_+ and T_- the weights of which are determined by the three partial helicity rates Γ_L and $\Gamma_\pm$. As we shall explicitly derive further on, the angular decay distribution for $t \rightarrow b + W^+(\rightarrow l^+ + \nu_l)$ reads
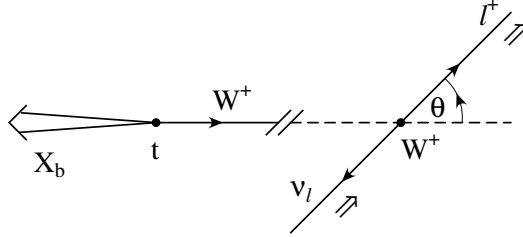
Figure 2: Definition of polar angle θ in the W^+ rest system.

$$\frac{d\Gamma}{d\cos\theta} = \frac{3}{4}\sin^2\theta\ \Gamma_L + \frac{3}{8}(1+\cos\theta)^2\Gamma_+ + \frac{3}{8}(1-\cos\theta)^2\Gamma_-\ , \qquad (12)$$

where the polar angle θ is measured in the W–rest frame as shown in Fig. 2. Integrating over $\cos\theta$ one recovers the total rate $\Gamma = \Gamma_L + \Gamma_+ + \Gamma_-$. If the W^+ were unpolarized one would have $\Gamma_L = \Gamma_+ = \Gamma_- = \Gamma/3$ resulting in a flat decay distribution $d\Gamma/d\cos\theta = \Gamma/2$.

One can also define a forward-backward asymmetry by considering the rate in the forward hemisphere Γ_F and in the backward hemisphere Γ_B in the W^+-rest frame. The forward-backward asymmetry A_{FB} is then given by

$$A_{FB} = \frac{\Gamma_F - \Gamma_B}{\Gamma_F + \Gamma_B} = \frac{3}{4} \frac{\Gamma_+ - \Gamma_-}{\Gamma_L + \Gamma_+ + \Gamma_-} \ . \tag{13}$$

At the Born term level one has

$$A_{FB}(\text{Born}) = -\frac{3}{4} \frac{2y^2}{1 + 2y^2} = -0.22 \ . \tag{14}$$

The forward-backward asymmetry is negative, i.e. one has more leptons in the backward hemisphere than in the forward hemisphere. The numerical value of the forward-backward asymmetry is not very large on account of the dominance of the longitudinal mode.

It is always useful to check on the correctness of the sign of the parity violating term proportional to $(\pm \cos \theta)$ and thereby on the sign of A_{FB}. This is again easily done by considering the collinear cases $\cos \theta = \pm 1$ and appealing to angular momentum conservation. And, in fact, Eq.(12) shows that the mode Γ_- decouples in the forward direction $\cos \theta = 1$ (and vice versa Γ_+ decouples in the backward direction) as can be appreciated from the helicity configurations in Fig. 2. This implies that Γ_+ favours forward leptons ℓ^+ leading to energetic leptons in the t-rest frame whereas Γ_- favours backward ℓ^+ leading to less energetic leptons in the t-rest frame. As we have seen $\Gamma_+ = 0$ at LO so that one expects a softer lepton spectrum in the t-rest frame then in the case of the decay of an unpolarized W^+.

2 Top quark decay rate

2.1 Leading (LO) rate

We shall calculate the leading order rate in three different ways for pedagogical reasons. The first way is the traditional covariant way where no particular sophistication is needed. In the second way we use the helicity methods which has the advantage that by calculating the helicity amplitudes one has the full spin information of the decay at hand. In the third method we use the optical theorem which serves the purpose of introducing rather sophisticated technical material in a simple setting which are needed later on in the higher order calculations.

2.1.1 Covariant method

The matrix element for the decay $t \rightarrow b + W^+$ $(p_t = p_b + q)$ is given by

$$M = -i \frac{g_w}{2\sqrt{2}} V_{tb} \bar{u}_b \gamma^\mu (1 - \gamma_5) u_t \epsilon_\mu^* \ . \tag{15}$$

Upon squaring and summing over the spins one obtains

$$|\overline{M}|^2 = \sum_{spins} \frac{g_w^2}{8} |V_{tb}|^2 \left(\bar{u}_b \gamma^\mu (1 - \gamma_5) u_t \epsilon_\mu^* \right) \left(\bar{u}_b \gamma^\nu (1 - \gamma_5) u_t \epsilon_\nu^* \right)^\dagger , \tag{16}$$

where we write $\sum_{spins} |M|^2 = |\overline{M}|^2$. Use of the completeness relations

$$\sum_{\pm 1/2} u\bar{u} = \not{p} + m \tag{17}$$

and

$$\sum_{0,\pm} \epsilon^\mu(m)\epsilon^{*\nu}(m) = -g^{\mu\nu} + \frac{q^\mu q^\nu}{m_W^2} \tag{18}$$

leads to $(m_b = 0)$

$$\begin{aligned}
|\overline{M}|^2 &= \frac{g_w^2}{8}|V_{tb}|^2 \text{Tr}\left\{ \not{p}_b\gamma^\mu(1-\gamma_5)(\not{p}_t+m_t)\gamma^\nu(1-\gamma_5)\right\}\left(-g_{\mu\nu}+\frac{q_\mu q_\nu}{m_W^2}\right) \\
&= \frac{g_\omega^2}{8}|V_{tb}|^2\, 2\text{Tr}\left\{\not{p}_b\gamma^\mu\not{p}_t\gamma^\nu\right\}\left(-g_{\mu\nu}+\frac{q_\mu q_\nu}{m_W^2}\right) \\
&= \frac{g_w^2}{8}|V_{tb}|^2\, 8\left((p_t p_b)+\frac{1}{m_W^2}2(p_b p_t)\,(p_t q)\right) .
\end{aligned} \tag{19}$$

Using four-momentum conservation $p_t = p_b + q$ and the mass shell conditions $p_b^2 = m_b^2 = 0$ and $q^2 = m_W^2$ one obtains

$$|\overline{M}|^2 = \frac{g_w^2}{8}|V_{tb}|^2\, 4m_t^2\frac{1-y^2}{y^2}(1+2y^2) .$$

The rate can be computed using the two–body decay formula

$$\Gamma = \frac{1}{2s_t+1}R_2\left[|\overline{M}|^2\right] , \tag{20}$$

where R_2 denotes the two-body phase space integral [27]. We symbolically write $R_2\left[|\overline{M}|^2\right]$ for the two-body phase space integration over the squared matrix element $|\overline{M}|^2$, i.e. we write

$$R_2\left[|\overline{M}|^2\right] = \frac{1}{2m_t}\int\frac{1}{(2\pi)^3}\frac{d^3q}{2\,E_W}\int\frac{1}{(2\pi)^3}\frac{d^3p_b}{2\,E_b}\,(2\pi)^4\,\delta^{(4)}(p_t-p_b-q)\,|\overline{M}|^2 . \tag{21}$$

In order to stay general we calculate R_2 for $m_b \neq 0$. The phase space integral will be evaluated in the top quark rest system. We write $1/(2E_W) = \int dE_W\,\delta(q^2-m_W^2) = \int dE_W\,\delta(E_W^2-|\vec{q}|^2-m_W^2)$, where we implicitly take the positive energy solution $E_W = +\sqrt{|\vec{q}|^2+m_W^2}$. The corresponding relation for the bottom quark energy reads $1/(2E_b) = \int dE_b\,\delta(p_b^2-m_b^2)$. Using these two relations one converts the three-dimensional integrations in (21) into four-dimensional integrations. One obtains

$$R_2\left[|\overline{M}|^2\right] = \frac{1}{8\pi^2 m_t}\int d^4q\int d^4p_b\,\delta(q^2-m_W^2)\,\delta(p_b^2-m_b^2)\,\delta^{(4)}(p_t-p_b-q)\,|\overline{M}|^2 . \tag{22}$$

The integration over d^4p_b can be done with the result that the argument of the second δ-function becomes $(p_t-q)^2 - m_b^2 = m_t^2 - 2m_t E_W + m_W^2 - m_b^2$, i.e.

$$R_2\left[|\overline{M}|^2\right] = \frac{1}{8\pi^2 m_t}\int d^4q\,\delta(q^2-m_W^2)\,\delta\left((p_t-q)^2-m_b^2\right)\,|\overline{M}|^2 . \tag{23}$$

Next one integrates over $dE_W = d(2m_t E_W)/2m_t$ with the result that the argument of the remaining δ-function becomes $q^2 - m_W^2 = E_W^2 - |\vec{q}|^2 - m_W^2 \to (m_t^2 + m_W^2 - m_b^2)^2/(4m_t^2) - |\vec{q}|^2 - m_W^2$. The remaining integration over d^3q can be done using spherical coordinates such that $d^3q \to d\Omega |\vec{q}|^2 d|\vec{q}|^2 = \frac{1}{2}|\vec{q}|d|\vec{q}|^2$. The result is

$$R_2\left[\,|\overline{M}|^2\right] = \frac{1}{8\pi}\frac{1}{m_t^2}\,|\vec{q}|\,|\overline{M}|^2\,, \tag{24}$$

where $|\vec{q}| = \sqrt{\lambda(m_t^2, m_W^2, m_b^2)}/(2m_t)$ is the magnitude of the momentum of the W^+-boson in the top quark rest (t–rest) frame and where $\lambda(a,b,c) = (a^2+b^2+c^2-2ab-2ac-2bc)$ is Källén's function. Naturally we could have calculated the two-body phase space R_2 directly without including the squared matrix element $|\overline{M}|^2$ in the integrand as long as the kinematic variables in $|\overline{M}|^2$ are fixed according to four-momentum conservation and the mass-shell conditions.

We now return to the approximation $m_b = 0$ where $|\vec{q}| = m_t(1 - y^2)/2$. Substituting the matrix element squared (19) into the rate formula (20) one obtains

$$\Gamma(\text{Born}) = \Gamma_0\,(1 - y^2)^2(1 + 2y^2)\,, \tag{25}$$

where Γ_0 is the $m_W = 0$ Born term rate $(g_\omega^2/(8m_W^2) = G_F/\sqrt{2})$

$$\Gamma_0 = \frac{G_F m_t^3}{8\pi\sqrt{2}}|V_{tb}|^2\,. \tag{26}$$

2.1.2 Helicity amplitude method

The helicity amplitudes for $t \to b + W^+$ can be calculated from the transition matrix element by using spinors and polarization vectors with definite helicities λ_t, λ_b and λ_W. One needs to calculate (we omit the coupling factor $-i\frac{g_w}{2\sqrt{2}}V_{tb}$)

$$H_{\lambda_t;\lambda_b\lambda_W} = \bar{u}_b(\lambda_b)\gamma^\mu(1 - \gamma_5)u_t(\lambda_t)\epsilon_\mu^*(\lambda_W)\,. \tag{27}$$

We shall work in the t–rest system with the z-axis along the W^+ (see Fig. 3) such that $\lambda_t = -\lambda_b + \lambda_W$. In order to be general we keep $m_b \neq 0$.
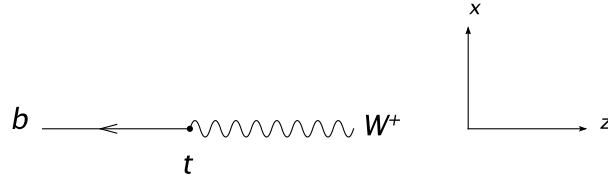
Figure 3: Definition of the the two–body coordinate system in the top quark rest system.

Let us collect the relevant t–rest system spinor and polarization vector expressions. For the helicity spinors one has

$$u_t(1/2) = \sqrt{2m_t}\begin{pmatrix}\chi_+\\0\end{pmatrix}, \qquad u_b(1/2) = \sqrt{E_b + m_b}\begin{pmatrix}\chi_-\\\frac{|\vec{q}|}{E_b+m_b}\chi_-\end{pmatrix},$$

$$u_t(-1/2) = \sqrt{2m_t}\begin{pmatrix}\chi_-\\0\end{pmatrix}, \qquad u_b(-1/2) = \sqrt{E_b + m_b}\begin{pmatrix}-\chi_+\\\frac{|\vec{q}|}{E_b+m_b}\chi_+\end{pmatrix}, \tag{28}$$

where $\chi_\pm$ are Pauli spinors given by $\chi_+ = \begin{pmatrix} 1 \\ 0 \end{pmatrix}$ and $\chi_- = \begin{pmatrix} 0 \\ 1 \end{pmatrix}$.

The helicity polarization four-vectors of the W^+ read

$$\epsilon_\mu^*(\pm 1) = \frac{1}{\sqrt{2}}\,(0; \pm 1, -i, 0)\,,$$

$$\epsilon_\mu^*(0) = \frac{1}{\sqrt{q^2}}\,(|\vec{q}|; 0, 0, -q_0)\,. \tag{29}$$

There are altogether four possible helicity configurations in $t \to b + W^+$ which are listed in Table 1.

λ_t	λ_b	λ_W
1/2	-1/2	0
-1/2	1/2	0
1/2	1/2	1
-1/2	-1/2	-1

Table 1: Helicity configurations in $t \to b + W^+$.

For the helicity amplitudes $H_{\lambda_t; \lambda_b \lambda_W}$ $(Q_\pm = (m_t \pm m_b)^2 - q^2)$ one obtains

$$\sqrt{q^2}\,H_{\frac{1}{2};-\frac{1}{2}0} = -m_t(\sqrt{Q_+} + \sqrt{Q_-}) + m_b(\sqrt{Q_+} - \sqrt{Q_-}) \quad \overset{m_b \to 0}{=} \quad -2m_t^2\sqrt{1-y^2}\,,$$

$$\sqrt{q^2}\,H_{-\frac{1}{2};\frac{1}{2}0} = -m_t(\sqrt{Q_+} - \sqrt{Q_-}) + m_b(\sqrt{Q_+} + \sqrt{Q_-}) \quad \overset{m_b \to 0}{=} \quad 0\,,$$

$$H_{\frac{1}{2};\frac{1}{2}1} = -\sqrt{2}(\sqrt{Q_+} - \sqrt{Q_-}) \quad \overset{m_b \to 0}{=} \quad 0\,,$$

$$H_{-\frac{1}{2};-\frac{1}{2}-1} = -\sqrt{2}(\sqrt{Q_+} + \sqrt{Q_-}) \quad \overset{m_b \to 0}{=} \quad -2\sqrt{2}\,m_t\sqrt{1-y^2}\,, \tag{30}$$

where we have included both the $m_b \neq 0$ and $m_b = 0$ results in (30). The squared matrix element $|\overline{M}|^2$ finally is given by

$$|\overline{M}|^2 = \sum_{\lambda_t = -\lambda_b + \lambda_W} |H_{\lambda_t; \lambda_b \lambda_W}|^2 = \underbrace{|H_{\frac{1}{2};-\frac{1}{2}0}|^2 + |H_{-\frac{1}{2};\frac{1}{2}0}|^2}_{L} + \underbrace{|H_{\frac{1}{2};\frac{1}{2}1}|^2}_{T_+} + \underbrace{|H_{-\frac{1}{2};-\frac{1}{2}-1}|^2}_{T_-}$$

$$= 4m_t^2 \frac{(1-y^2)}{y^2}\Big(\underbrace{1}_{L} + \underbrace{0}_{T_+} + \underbrace{2y^2}_{T_-}\Big)\,, \tag{31}$$

where we have set $m_b = 0$ in the second line of (31). The result agrees with the covariant calculation (see Eq.(19)). The advantage of the helicity method is that one can separately identify the three (diagonal) helicity contributions of the W^+ boson L, T_+ and T_- as indicated in Eq.(31). In fact, the helicity amplitudes contain the complete spin information of the process. Thus one can easily calculate other polarization effects using the helicity amplitudes such as the decay of polarized top quarks, the polarization of the bottom quark and polarization correlation effects. $m_b \neq 0$ effects are easily included by using the $m_b \neq 0$ helicity amplitudes in Eq.(30). One can also define covariant helicity projectors which allow one to directly calculate the longitudinal, the transverse-plus and transverse-minus helicity rates without taking recourse to the helicity amplitudes. This will be described in Sec. 5.

2.1.3 Optical theorem method and cutting rules

In this subsection we shall use yet another method to calculate the leading order rate for $t \rightarrow b + W^+$ using the optical theorem. Whereas the optical theorem method does not offer particular technical advantages in LO calculations it is the method of choice for higher order calculations as e.g. the calculation of the NNLO rate to be described later on. The reason is simply that the phase space integrations in the NNLO radiative correction calculations become prohibitively complicated and cannot be automated as easily as higher order loop calculations. We present the optical theorem method for the LO case for pedagogical reasons because the LO discussion allows us to introduce concepts which are also needed in the NNLO radiative correction calculation to be described later on.
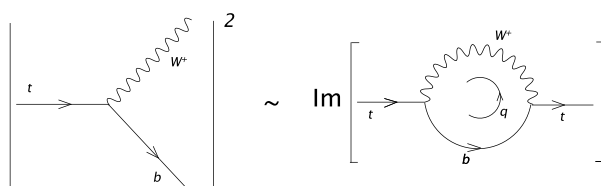
Figure 4: Illustration of the optical theorem method to calculate the LO top quark width.

The optical theorem relates the width Γ of a particle to the imaginary part of the self-energy contribution Σ of the particle. In the top quark case one has [4]

$$\Gamma = \frac{1}{2s_t + 1} \frac{\text{Im}\, \Sigma}{m_t} \,, \tag{32}$$

where, for the present purposes, Σ is the one-loop self-energy of the top quark as illustrated in Fig.4.

Using standard Feynman rules [27, 28] the one-loop self-energy contribution is given by $(p_t = p_b - q)$

$$i\Sigma_{one-loop} = \sum_{s_t} \bar{u}(p_t, s_t) \int \frac{d^4q}{(2\pi)^4} \left(i\frac{g_w}{\sqrt{2}} \gamma^\mu \frac{1 - \gamma_5}{2} V_{tb} \right) \frac{i\slashed{p}_b}{p_b^2 + i\epsilon} \times$$

$$\times \left(i\frac{g_w}{\sqrt{2}} \gamma^\nu \frac{1 - \gamma_5}{2} V_{tb}* \right) \frac{-i \left(g_{\mu\nu} - q_\mu q_\nu / m_W^2 \right)}{q^2 - m_W^2 + i\epsilon} u(p_t, s_t). \tag{33}$$

One can again use the completeness relation $\sum_{\pm 1/2} u_t \bar{u}_t = (\slashed{p}_t + m_t)$ to rewrite Eq.(33) as a trace. The trace can be taken as in Eq.(19) except that one now cannot avail of the mass-shell conditions $q^2 = m_W^2$ and $p_b^2 = 0$. One obtains

$$\Sigma_{one-loop} = \frac{1}{i} \frac{g_w^2}{8} |V_{tb}|^2 \frac{8}{m_W^2} \int \frac{d^4q}{(2\pi)^4} \frac{p_t q (2p_t q + 2q^2 + m_W^2) + m_t^2 m_W^2}{\left[(p_t + q)^2 + i\epsilon \right] \left[q^2 - m_W^2 + i\epsilon \right]} \,. \tag{34}$$

The usual procedure is to expand the q-dependent numerator factors in terms of the q-dependent denominator factors $D_q = q^2 - m_W^2$ and $D_b = (p_t + q)^2$ in order to obtain q-independent

---

[4] A very nice discussion of the optical theorem and related technical material relevant to top quark decays can be found in the thesis of I.R. Blokland [28].

numerator factors (the corresponding integrals are called scalar integrals) after cancellation. We therefore write

$$
\begin{aligned}
p_t q &= -\frac{1}{2}(m_t^2 + m_W^2 + D_q - D_b)\,, \\
q^2 &= m_W^2 + D_q\,.
\end{aligned}
\tag{35}
$$

The contributions proportional to D_q and D_b cancel against the denominator pole factors and their contributions can be dropped when taking the imaginary part since single or zero pole contributions have no imaginary part (see e.g. [28]). We therefore have

$$
\Sigma_{one-loop} = \frac{1}{i}\frac{g_w^2}{8}|V_{tb}|^2 \frac{4m_t^4}{m_W^2}(1-y^2)(1+2y^2)\int \frac{d^4q}{(2\pi)^4}\frac{1}{\left[(p_t+q)^2+i\epsilon\right]\left[q^2-m_W^2+i\epsilon\right]}\,.
\tag{36}
$$

According to the cutting rules the discontinuity of a Feynman graph is obtained by the product of the discontinuities of the pole factors which are being cut, where the discontinuity of a single pole is given by [27, 28]

$$
\text{Disc}\,\frac{1}{p^2-m^2+i\epsilon} = -2\pi i\,\delta(p^2-m^2)\,.
\tag{37}
$$

Furthermore, the imaginary part and the discontinuity of a graph M are related by $2i\,\text{Im}M = \text{Disc}\,M$. One therefore has

$$
\text{Im}\Sigma_{one-loop} = \frac{1}{i}\frac{1}{2i}\frac{g_w^2}{8}|V_{tb}|^2 \frac{4m_t^4}{m_W^2}(1-y^2)(1+2y^2)\int \frac{d^4q}{(2\pi)^4}(-2\pi i)^2\delta\big((p_t+q)^2\big)\delta(q^2-m_W^2)\,.
\tag{38}
$$

In order to exhibit the similarity to the integral (23) we change the integration variable $q \to -q$. One can then use the result of Sec. 2.1.1

$$
\int d^4q\,\delta(q^2-m_W^2)\,\delta\big((p_t-q)^2\big) = \frac{\pi}{2}(1-y^2))
$$

to arrive at

$$
\Gamma(Born) = \Gamma_0(1-y^2)^2(1+2y^2)\,,
\tag{39}
$$

where, as before,

$$
\Gamma_0 = \frac{G_F\,m_t^3}{8\sqrt{2}\pi}|V_{tb}|^2 \quad \text{and} \quad y = \frac{m_W}{m_t}\,.
\tag{40}
$$

As it must be the result agrees with the covariant and helicity amplitude calculations. It is quite reassuring that the decay rate turns out to be positive definite in the end, as it must be, considering all the minus signs and the factors of (i) appearing in the rate calculation using the optical theorem method.

2.1.4 Expansion by regions and the (m_W/m_t)-expansion

In Sec 2.1.3 we have calculated the leading order rate by using the optical theorem and cutting rules to determine the imaginary part of the one-loop self energy diagram. In this subsection we shall go one step further and calculate the leading order rate using a (m_W/m_t)-expansion which allows us to introduce the concepts of expansion by regions and integration-by-parts identities.

All latter three concepts are essential in the calculation of the NLLO rate presented in [19, 20]. As emphasized before we shall pattern the LO rate calculation after the NNLO calculation entirely for pedagogical reasons. In the LO case the follow-up calculations are simple enough to be presented in a few simple lines, whereas they are more involved in the full NNLO calculation.

Let us summarize the main ideas of the NNLO rate calculation presented in [19, 20] which we down-size to the present LO case.

- Reduce the two-mass-scale problem (m_t, m_W) to a one-mass-scale problem (m_t) by expanding in the ratio m_W/m_t. Obtain the results as an expansion in powers of m_W/m_t.

- Use dimensional regularization to regularize the UV and IR/M singularities

- Use the method of expansion by regions to calculate the one-loop integral [29, 30, 31].

One has to consider the two regions [29, 30, 31]:

- Hard region
  The loop momentum is hard and is of $\mathcal{O}(m_t)$. One can then expand the W-propagator as a power series in $m_W^2/m_t^2 \ll 1$:

$$\frac{1}{q^2 - m_W^2} = \frac{1}{q^2} + \frac{m_W^2}{q^4} + \frac{m_W^4}{q^6} + ... = \frac{1}{q^2} \sum_{n=0}^{\infty} \left(\frac{m_W^2}{q^2} \right)^n . \tag{41}$$

  The massive propagator has thereby been converted into a sum of massless propagators.

- Soft region
  The momentum q flowing through the W is soft. One therefore cannot use the above expansion (41) of the W propagator. However, in the soft region one can expand the b-quark propagator, cif.

$$\frac{1}{(p_t + q)^2} = \frac{1}{p_t^2} \sum_{n=0}^{\infty} \left(-\frac{2p_t \cdot q + q^2}{p_t^2} \right)^n . \tag{42}$$

  There is only one denominator factor in the loop integral and its imaginary part vanishes

$$\text{Im} \int \frac{1}{i} \frac{d^4q}{(2\pi)^4} \frac{1}{(q^2 - m_W^2)} = 0 . \tag{43}$$

  Therefore there is no contribution from the soft region in the one-loop case. This is different at NLO and NNLO.

What remains to be done is to evaluate integrals of the form

$$\text{Im} \int \frac{1}{i} \frac{d^4q}{(2\pi)^4} \frac{1}{(q^2)^{n+1}(p_t + q)^2} \tag{44}$$

which result from the m_W^2/q^2 expansion in the hard region. The integrals can all be reduced to one master integral by using integration-by-parts identities.

The first term in the expansion (41), $n = 0$, leads to a two–point one–loop integral of the form

$$\text{Im} \int \frac{1}{i} \frac{d^4q}{(2\pi)^4} \frac{1}{q^2(p_t + q)^2} . \tag{45}$$

We calculate the one-loop integral directly in dimensional regularization ($D = 4 - 2\epsilon$) and take its imaginary part at the end without resorting to the cutting rules. The details of how to evaluate one-loop integrals in dimensional regularization can be found in [27]. One first introduces a one parameter Feynman parametrization, collects terms and performs a shift in the integration variable $(q + xp_t) \to q$, i.e.

$$
\begin{aligned}
\int \frac{d^D q}{(2\pi)^D} \frac{1}{q^2(p_t + q)^2} &= \int \frac{d^D q}{(2\pi)^D} \int_0^1 dx \frac{1}{[(q + p_t)^2 x + q^2(1 - x)]^2} \\
&= \int \frac{d^D q}{(2\pi)^D} \int_0^1 dx \frac{1}{[(q + xp_t)^2 + p_t^2 x(1 - x)]^2} \\
&= \int \frac{d^D q}{(2\pi)^D} \int_0^1 dx \frac{1}{[q^2 + p_t^2 x(1 - x)]^2} \; .
\end{aligned}
\tag{46}
$$

Next we do a Wick rotation $q_0 \to iq_{0E}$. The factor of i from the Wick rotation cancels the factor of i in the denominator of (44). One then does a D-dimensional Euclidean integration over the loop momentum q, and, finally, one integrates over the Feynman parameter x which results in Euler's Beta function $B(1 - \epsilon, 1 - \epsilon)$. The sequence of steps is represented in the following sequence of equations:

$$
\begin{aligned}
\mathrm{Im} \int \frac{1}{i} \frac{d^D q}{(2\pi)^D} \frac{1}{q^2(p_t + q)^2} &= \mathrm{Im} \int_0^1 dx \frac{1}{(4\pi)^{D/2}} \frac{\Gamma(2 - \frac{D}{2})}{\Gamma(2)} \left(\frac{1}{-p_t^2 x(1 - x)} \right)^{2 - \frac{D}{2}} \\
&= \mathrm{Im} \frac{\Gamma(1 + \epsilon)}{(4\pi)^{D/2}} \frac{\Gamma(\epsilon)}{\Gamma(1 + \epsilon)} (-p_t^2)^{-\epsilon} \int_0^1 dx \, x^{-\epsilon} (1 - x)^{-\epsilon} \\
&= \frac{\Gamma(1 + \epsilon)}{(4\pi)^{D/2}} \frac{\Gamma(\epsilon)}{\Gamma(1 + \epsilon)} B(1 - \epsilon, 1 - \epsilon) \mathrm{Im}(-p_t^2)^{-\epsilon} \\
&= \frac{\Gamma(1 + \epsilon)}{(4\pi)^{D/2}} \frac{\Gamma(\epsilon)}{\Gamma(1 + \epsilon)} \frac{\Gamma^2(1 - \epsilon)}{\Gamma(2 - 2\epsilon)} (m_t^2)^{-\epsilon} \sin \pi\epsilon \; .
\end{aligned}
\tag{47}
$$

We retain only the finite term in the last line of (47). One obtains

$$
\mathrm{Im} \int \frac{1}{i} \frac{d^4 q}{(2\pi)^4} \frac{1}{q^2(p_t + q)^2} = \frac{1}{16\pi^2} \, \pi \, .
\tag{48}
$$

We have used

$$
(\frac{-p_t^2}{m_t^2})^{-\epsilon} = e^{\ln(-p_t^2/m_t^2)^{-\epsilon}} = e^{-\epsilon \ln(-p_t^2/m_t^2)} = 1 - \epsilon \ln(p^2/m_t^2) + ...
\tag{49}
$$

which leads to

$$
\mathrm{Im}(\frac{-p_t^2}{m_t^2})^{-\epsilon} = \mathrm{Im}(-1 + i0)^{-\epsilon} = \sin \pi\epsilon = \pi\epsilon + ... \; .
\tag{50}
$$

In addition to the integral (45) with $n = 0$ the imaginary part of which we have just calculated we also need the imaginary parts of the integrals (44) with $n \geq 1$. They can be obtained from the "master integral" (45) by integration-by-parts (IBP) techniques [32, 33]. The general procedure of reducing a set of integrals to a set of simpler integrals is called "reduction to master integrals". In the present case this reduction is quite trivial but can become quite

involved in more general settings. The reduction procedure has been automated by the Laporta algorithm [34, 35].

Technical aside: Integration-by-parts (IBP) identities [32, 33].

In order to calculate the integral corresponding to the second term in the expansion (41) we consider the differential form $(\partial_\mu := \partial/\partial q^\mu)$

$$\partial_\mu \frac{(p_t + q)^\mu}{q^2(p_t + q)^2} = \frac{\partial_\mu(p_t + q)^\mu}{q^2(p_t + q)^2} + \frac{(p_t + q)^\mu}{q^2}\partial_\mu\frac{1}{(p_t + q)^2} + \frac{(p_t + q)^\mu}{(p_t + q)^2}\partial_\mu\frac{1}{q^2}. \tag{51}$$

Differentiate carefully, i.e. $\partial_\mu q^\mu := \frac{\partial q^\mu}{\partial q^\mu} = D = 4 - 2\epsilon$, and drop the "surface term" on the left-hand side. Also use $2p_t q = -m_t^2 - q^2 + (p_t + q)^2$. This gives

$$\frac{1}{q^4(p_t + q)^2} = \frac{1}{m_t^2}\left(\frac{2\epsilon - 1}{q^2(p_t + q)^2} + \frac{1}{q^4}\right). \tag{52}$$

In dimensional regularization massless tadpole (single pole) diagrams are zero, i.e. one can drop the second term on the r.h.s. of (52) after dimensional integration. At the relevant order of ϵ one therefore has

$$\text{Im}\int\frac{1}{i}\frac{d^D q}{(4\pi)^D}\frac{1}{q^4(p_t + q)^2} = -\frac{1}{m_t^2}\text{Im}\int\frac{1}{i}\frac{d^D q}{(4\pi)^D}\frac{1}{q^2(p_t + q)^2}. \tag{53}$$

Going through the same exercise for $\partial_\mu\frac{(p_t+q)^\mu}{(q^2)^{n+1}(p_t+q)^2}$ for $n \geq 2$ one finds

$$\text{Im}\int\frac{1}{i}\frac{d^D q}{(4\pi)^D}\frac{1}{(q^2)^{n+1}(p_t + q)^2} = 0. \qquad \text{for} \quad n \geq 2 \tag{54}$$

Because the higher order terms vanish we only need to sum the first two terms in the expansion (41). The result

$$\text{Im}\int\frac{1}{i}\frac{d^D q}{(4\pi)^D}\frac{1}{(p_t + q)^2}\frac{1}{q^2}\sum_{n=0}^{\infty}\left(\frac{m_W^2}{q^2}\right)^n = \frac{1}{16\pi^2}\left(1 - \frac{m_W^2}{m_t^2}\right)\pi \tag{55}$$

is in agreement with the one in Sec. 2.1.3.

2.2 Next-to-leading order (NLO) QCD corrections

The traditional technique used for NLO calculation is to calculate the one-loop and tree-graph contributions separately. In the present case the UV singularities are regularized by dimensional regularization whereas the IR/M singularities are regularized by introducing gluon and bottom quark masses. The IR/M singularities will eventually appear as $(\ln m_g)-$ and $(\ln m_b)-$ singularities and cancel among the one-loop and tree graph contributions [8, 9, 14, 16, 36]. We mention that the calculation can also be done in dimensional regularization without recourse to the traditional $m_g \neq 0$ and $m_b \neq 0$ regularization [37].

For example, generic diagrams for the QCD NLO calculation are displayed in Fig. 5. Without going into the details of the calculation (see e.g. [8]) we just quote the result of the
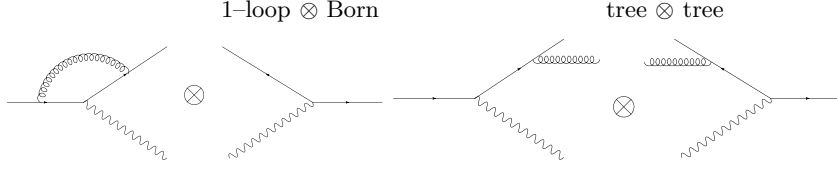
Figure 5: Generic NLO QCD contributions

NLO calculation. For the total rate one obtains ($\hat{\Gamma} = \Gamma/\Gamma(\text{Born})$) (see e.g. [36])

$$
\begin{aligned}
\hat{\Gamma}(NLO) &= 1 + \frac{\alpha_s}{2\pi} C_F \frac{y^2}{(1-y^2)^2(1+2y^2)} \left\{ \frac{(1-y^2)(5+9y^2-6y^4)}{2y^2} - \frac{2(1-y^2)^2(1+2y^2)\pi^2}{3y^2} \right. \\
&\quad - \frac{(1-y^2)^2(5+4y^2)}{y^2}\ln(1-y^2) - \frac{4(1-y^2)^2(1+2y^2)}{y^2}\ln(y)\ln(1-y^2) - 4(1+y^2)\times \\
&\quad \left. \times (1-2y^2)\ln(y) - \frac{4(1-y^2)^2(1+2y^2)}{y^2}\text{Li}_2(y^2) \right\}.
\end{aligned}
\tag{56}
$$

The numerical value of the NLO QCD correction appears in Eq.(6). Our numerical input values are $m_t = 175$ GeV and $m_W = 80.419$ GeV. The strong coupling constant has been evolved from $\alpha_s(M_Z) = 0.1175$ to $\alpha_s(m_t) = 0.1070$ using two-loop running. Numerically one has $\Gamma = \Gamma(\text{Born})(1 - 8.54\%)$. One sees that the NLO QCD corrections reduce the Born term rate by the large amount of 8.5%.

In the limit $y \to 0$ one obtains

$$
\hat{\Gamma}(\text{NLO}) = 1 + \frac{\alpha_s}{2\pi} C_F \left\{ \frac{5}{2} - \frac{2}{3}\pi^2 \right\}, .
\tag{57}
$$

The leading $y \to 0$ contribution reduces the rate by 9.26% which is already quite close to the rate reduction of the full result (8.5%). We shall return to an assessment of the quality of the y-expansion later on. It is curious to note that the radiative QCD corrections reduce the LO rate whereas the radiative QCD corrections to the decay $Z \to q\bar{q}$ enhance the LO rate ratio $\hat{\Gamma}(\text{LO})$ by $\frac{\alpha_s}{2\pi}(6/4)C_F = \alpha_s/\pi$, i.e. $\hat{\Gamma}(\text{NLO}; Z \to q\bar{q}) = 1 + \alpha_s/\pi$.

The NLO rate can also be calculated by the optical theorem method using the y-expansion. At NLO one has contributions both from the soft and the hard region leading to an infinite power series in y and $y \ln y$ where the $(y \ln y)$-contributions come from the interplay of the soft and hard integration regions. The results of the y-expansion have been checked against the exact result Eq.(56) up to $O(y^{16})$ [38] (see also [28]).

2.3 NLO electroweak corrections

In Fig. 6 we have drawn the LO diagram and the four NLO tree-level diagrams that contribute to $t \to b + W^+ + (\gamma)$. We use the Feynman-'tHooft gauge so that one has a NLO contribution from the charged unphysical Higgs boson χ^+ as shown in Fig. 6. Compare the number of four electroweak NLO tree-level diagrams with the two QCD NLO tree-level diagrams. When squaring the tree-level diagrams one would expect a four-fold complexity factor when going
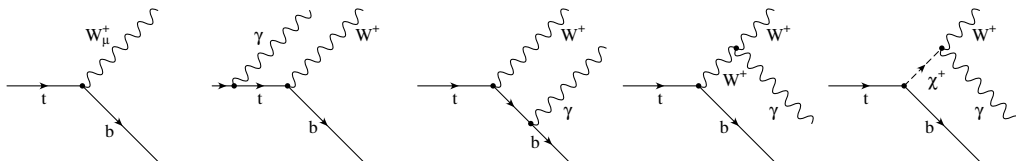
Figure 6: Born and electroweak tree-graph contributions to $t \to b + W^+ \, (\gamma)$. χ^+ denotes the charged Goldstone boson.

from QCD to the electroweak tree-graph corrections. It is therefore quite remarkable that the squared tree graph expressions in both cases are similar in length and structure [9].
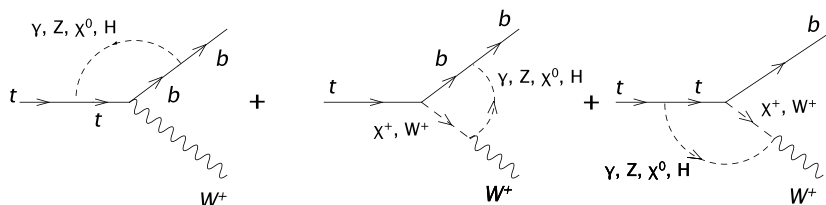
Figure 7: Eighteen electroweak three-point one-loop graphs in Feynman-'tHooft gauge contributing to $t \to b + W^+$.

In addition to the tree graph contributions one has to consider 18 three-point one-loop graphs in the Feynman-'tHooft gauge as shown in Fig. 7. Looking at Fig. 7 one would superficially expect 4+8+8=20 one-loop contributions. However, since there is no $(W^+W^+\chi^0)$–vertex, this number reduces to 18 as stated before. In Fig. 7 $\chi^\pm$ and χ^0 are the charged and neutral unphysical Goldstone bosons, and H is the physical Higgs. The results of calculating the one-loop contributions exist in amplitude form [17]. In the course of calculating the electroweak radiative corrections to the partial helicity rates the results of [17] were recalculated and confirmed by us. In particular we checked the results of [17] numerically with the automated loop calculation program XLOOPS/GiNaC developed at the University of Mainz [39, 40, 41]. In addition to the one-loop three-point functions one has a large number of one-loop two-point functions needed in the one-loop renormalization program. Again these have been reevaluated using XLOOPS/GiNaC.

We have used the so-called G_F–renormalization scheme for the electroweak corrections where G_F, M_W and M_Z are used as input parameters. The G_F–scheme is the appropiate renormalization scheme for processes with mass scales that are much larger than M_W as in the present case. The electroweak radiative corrections are substantially larger in the so-called α–scheme where α, G_F and M_Z are used as input parameters. The numerical results of the electroweak corrections to the rate are given in Eq.(6).

2.4 NNLO QCD corrections

In the NNLO case squaring of the contributing tree and loop diagrams leads to the four generic contributions shown in Fig. 8. However, with present techniques, this method is not viable,
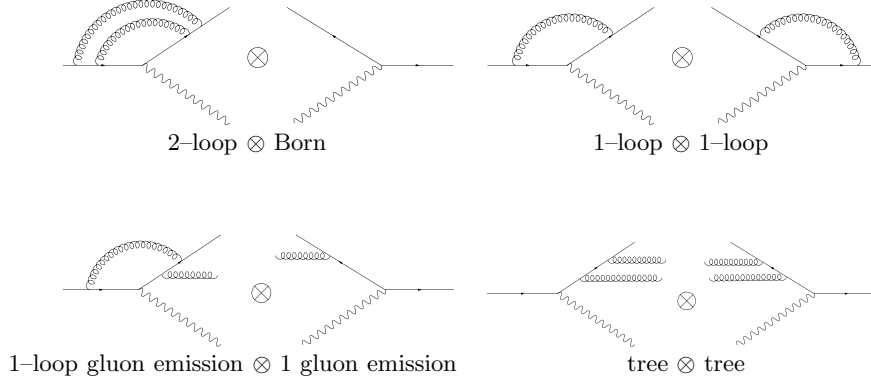
Figure 8: Generic NNLO QCD contributions.

mainly because the NNLO phase space integration become too difficult.

Instead, one resorts again to the optical theorem and calculates the NNLO rate from the three-loop self-energy diagrams according to [19, 20]

$$\Gamma(\text{NNLO}) = \frac{1}{2s_t + 1} \frac{1}{m_t} \text{Im}\Sigma(3 - loop), \tag{58}$$

There are altogether 38 three-loop Feynman diagrams a sample of which are shown in Fig. 9.
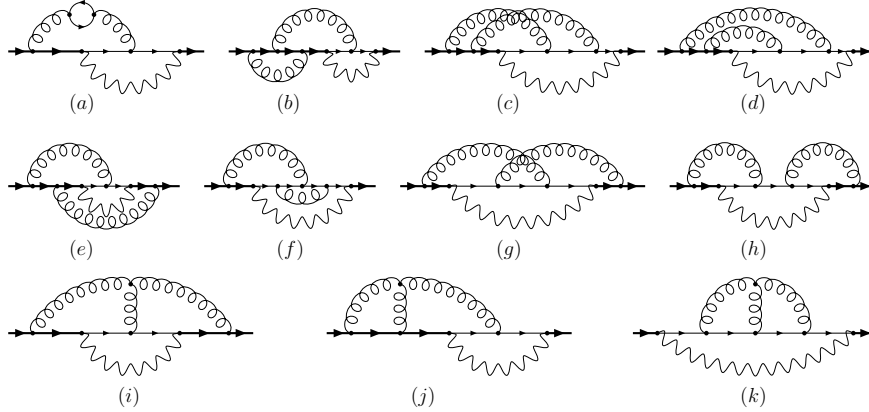
Figure 9: Sample three-loop diagrams whose imaginary parts contribute to the NNLO calculation of the top quark width.

The main ideas of the NNLO calculation of the rate have already been described in the calculation of the Born term rate in Sec. 2.1.3. It turns out that again one only has to consider two momentum regions. In the hard region all loop momenta are hard and the W-propagator can be expanded into a series of massless propagators as in the LO case. In the soft region the gluon momenta are hard but the loop momentum flowing through the W is soft. Differing

from the LO calculation one now also has contributions from the soft region. In the soft region the integrals factorize into two-loop self-energy-type integrals and a one-loop vacuum bubble diagram which are not difficult to integrate. The interplay of the hard and the soft region leads to additional $(y^n \ln y)$-terms in the $y = (m_W/m_t)$-expansion.

One can reduce all integrals to 23 master integrals by integration-by-parts identities. Use was made of Laporta's algorithm in this reduction to master integrals. The imaginary parts of the master integrals were calculated using the cutting rules where care had to be taken that some of the master integrals admitted several ways of cutting them. We mention that the calculation had been done in the general covariant gauge $-g^{\mu\nu} + (\xi - 1)k^\mu k^\nu/k^2$ for the gluon in order to check on gauge invariance. The numerical results on the NNLO QCD corrections are given in Eq.(6).

3 W-helicity fractions in top quark decays

3.1   Angular decay distribution for $t \to b + W^+(\to \ell^+ + \nu_\ell)$ (I)

In Fig. 6 we display the LO amplitude contribution to $t \to b + \ell^+ + \nu_\ell$. On squaring the amplitude and taking the spin sums one is led to the contraction $L_{\mu\nu}H^{\mu\nu}$(Born). For the
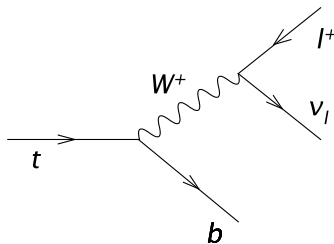
Figure 10: LO Born term contribution to $t \to b + W^+(\to \ell^+ + \nu_\ell)$

lepton tensor we obtain

$$
\begin{aligned}
L^{\mu\nu} &= \frac{1}{8}\mathrm{Tr}\, \slashed{p}_\ell \gamma^\mu(1-\gamma_5)\slashed{p}_\nu \gamma^\nu(1-\gamma_5) \\
&= p_\ell^\mu p_\nu^\nu + p_\ell^\nu p_\nu^\mu - \frac{1}{2}m_W^2 g^{\mu\nu} - i\epsilon^{\mu\nu\alpha\beta}p_{\ell\alpha}p_{\nu\beta} \ .
\end{aligned}
\tag{59}
$$

The LO hadron tensor is given by $(m_b = 0)$

$$
\begin{aligned}
H^{\mu\nu}(\mathrm{Born}) &= \frac{1}{8}\mathrm{Tr}(\slashed{p}_t + m_t)\gamma^\mu(1-\gamma_5)\slashed{p}_b\gamma^\nu(1-\gamma_5) \\
&= p_t^\mu p_b^\nu + p_t^\nu p_b^\mu - p_t\cdot p_b g^{\mu\nu} - i\epsilon^{\mu\nu\alpha'\beta'}p_{t\alpha'}p_{b\beta'} \ .
\end{aligned}
\tag{60}
$$

The factors $1/8$ have been introduced for convenience. The result of contracting the lepton and hadron tensor reads

$$
L_{\mu\nu}H^{\mu\nu}(\mathrm{Born}) = 4(p_t \cdot p_\ell)\,(p_b \cdot p_\nu) = 4(p_t \cdot p_\ell)\,(p_b \cdot (q - p_\ell)) \ .
\tag{61}
$$

Note that one originally had

$$L_{\mu\nu}H^{\mu'\nu'}(\text{Born})(-g_{\mu'}^{\mu} + \frac{q_{\mu'}q^{\mu}}{m_W^2})(-g_{\nu'}^{\nu} + \frac{q_{\nu'}q^{\nu}}{m_W^2}) \qquad (62)$$

which turns into $L_{\mu\nu}H^{\mu\nu}(\text{Born})$ in the zero lepton mass case where $q_{\mu}L^{\mu\nu} = q_{\nu}L^{\mu\nu} = 0$. The lepton mass corrections are of $\mathcal{O}(m_\ell^2/m_t^2)$ and are thus negligible. If one wants to include lepton mass effects one has to retain the full W–projector in (62).

One must evaluate the invariant $L_{\mu\nu}H^{\mu\nu}$ in one frame. Here we choose the rest frame of the top quark. Since we want to evaluate $L_{\mu\nu}H^{\mu\nu}$ in terms of the angle $\cos\theta$ defined in the W^+-rest frame ($W_{r.f.}$) as shown in Fig. 2 we write[5]

$$p_\ell^{\mu}\left(W_{\text{r.f.}}\right) = \frac{m_W}{2}\left(1; \sin\theta\cos\phi, \sin\theta\sin\phi, \cos\theta\right). \qquad (63)$$

We then boost the lepton momentum $p_\ell^{\mu}\left(W_{\text{r.f.}}\right)$ to the top quark rest frame ($t_{\text{r.f.}}$) where the invariants in (61) are to be evaluated. The relevant Lorentz boost matrix reads

$$L(boost) = \frac{1}{m_W}\begin{pmatrix} q_0 & 0 & 0 & |\vec{q}| \\ 0 & m_W & 0 & 0 \\ 0 & 0 & m_W & 0 \\ |\vec{q}| & 0 & 0 & q_0 \end{pmatrix} \qquad (64)$$

such that

$$p_\ell^{\mu}\left(t_{\text{r.f.}}\right) = L(boost)\, p_\ell^{\mu}\left(W_{\text{r.f.}}\right).$$

The boost will not affect the transverse components $\mu = 1, 2$ but only the zero and longitudinal components $\mu = 0, 3$. In Eq.(64) q_0 and $|\vec{q}|$ denote the energy and momentum of the W-boson in the top quark rest frame.

In the following we set $m_b = 0$ such that $q_0 = \frac{m_t}{2}(1 + y^2)$ and $|\vec{q}| = \frac{m_t}{2}(1 - y^2)$. Boosting $p_\ell^{\mu}\left(W_{\text{r.f.}}\right)$ one obtains

$$p_\ell^{\mu}\left(t_{\text{r.f.}}\right) = \frac{m_t}{4}\left((1+y^2)+(1-y^2)\cos\theta;\, 2y\sin\theta\cos\phi,\, 2y\sin\theta\sin\phi,\, (1-y^2)+(1+y^2)\cos\theta\right). \quad (65)$$

The remaining momentum four–vectors in the t–rest frame are given by

$$\begin{aligned} p_t^{\mu} &= m_t(1; 0, 0, 0), \\ p_b^{\mu} &= \frac{m_t}{2}\left(1 - y^2; 0, 0, -(1 - y^2)\right), \\ q^{\mu} &= \frac{m_t}{2}(1 + y^2, 0, 0, 1 - y^2). \end{aligned} \qquad (66)$$

We are now in the position to evaluate the invariants appearing in Eq.(61). We sort the resulting expression in terms of the polar angle factors $\sin^2\theta$ and $(1 \pm \cos\theta)^2/2$. Since we are

---

[5]In Eq.(63) we have specified the azimuthal dependence of $p_\ell^{\mu}\left(W_{\text{r.f.}}\right)$. This is not really needed in the present application because we do not specify a preferred transverse direction. In general, a transverse direction could be defined by the polarization of the top quark or the decay products of the b-quark. In this case one has to retain the azimuthal dependence of the lepton's momentum as done in (63). Whereas the sign of polar angle correlations can always be checked by physics arguments, there are no ready physics arguments to check the signs of the azimuthal correlations. To get the signs of the azimuthal correlations right it is indispensable to use the boosting method as described above (see e.g. [42]).

not interested in the azimuthal angle dependence in the present application we integrate over the azimuthal angle ϕ. One then obtains the angular decay distribution

$$\int_0^{2\pi} d\phi \, L_{\mu\nu} H^{\mu\nu}(\text{Born}) = 2\pi \frac{8}{3} \frac{m_t^4}{4} \Bigg\{ \underbrace{\frac{1}{2}(1-y^2)}_{\sim L} \quad \frac{3}{4} \sin^2\theta$$
$$\underbrace{0}_{\sim T_+} \quad \frac{3}{8}(1+\cos\theta)^2$$
$$+ \underbrace{y^2(1-y^2)}_{\sim T_-} \quad \frac{3}{8}(1-\cos\theta)^2 \Bigg\}, \qquad (67)$$

where, by comparison with Eq.(21), we have identified the three LO hadron contributions proportional to L and $T_\pm$. The normalized helicity fractions $\mathcal{G}_L$ and $\mathcal{G}_\pm$ written down before in Eq.(8) can be read off from Eq.(67). As we shall see later on from an angular momentum analysis, the sorting of the angular contributions in (67) should be done exactly along the three angular factors proportional to $\sin^2\theta$ and $(1\pm\cos\theta)^2/2$ discussed above. The corresponding coefficient factors are then proportional to the partial helicity rates Γ_L and $\Gamma_\pm$, respectively. An untreated and unsorted Mathematica output of $L_{\mu\nu} H^{\mu\nu}$ would, in general, lead to quite lengthy and messy expressions.

Repeating the same exercise for $m_b \neq 0$ one obtains ($x = m_b/m_t$)

$$\int_0^{2\pi} d\phi \, L_{\mu\nu} H^{\mu\nu}(\text{Born}) = 2\pi \frac{8}{3} \frac{m_t^4}{4} \Bigg\{ \underbrace{\frac{1}{2}\Big((1-x^2)^2 - y^2(1+x^2)\Big)}_{\sim L} \quad \frac{3}{4}\sin^2\theta$$
$$+ \underbrace{\frac{1}{2}y^2\Big(1-y^2+x^2-\sqrt{\lambda}\Big)}_{\sim T_+} \quad \frac{3}{8}(1+\cos\theta)^2$$
$$+ \underbrace{\frac{1}{2}y^2\Big(1-y^2+x^2+\sqrt{\lambda}\Big)}_{\sim T_-} \quad \frac{3}{8}(1-\cos\theta)^2 \Bigg\}, \quad (68)$$

where

$$\lambda = \lambda(1, y^2, x^2) = 1 + y^4 + x^4 - 2y^2 x^2 - 2y^2 - 2x^2 . \qquad (69)$$

For the $m_b \neq 0$ normalized helicity fractions one now obtains

$$\mathcal{G}_L = \quad ((1-x^2)^2 - y^2(1+x^2))/N ,$$
$$\mathcal{G}_+ = \quad y^2(1-y^2+x^2-\sqrt{\lambda})/N ,$$
$$\mathcal{G}_- = \quad y^2(1-y^2+x^2+\sqrt{\lambda})/N , \qquad (70)$$

where

$$N = (1-x^2)^2 + y^2(1-2y^2+x^2) . $$

Let us compare the resulting numerical $m_b \neq 0$ values for the normalized helicity fraction with their $m_b = 0$ counterparts. One obtains (we take $m_b = 4.8\,\text{GeV}$ as default value)

$$m_b = 4.8\,\text{GeV}: \qquad \mathcal{G}_L : \mathcal{G}_+ : \mathcal{G}_- = \quad 0.7025 : 0.0004 : 0.2971 ,$$
$$m_b = 0 \qquad : \qquad \mathcal{G}_L : \mathcal{G}_+ : \mathcal{G}_- = \quad 0.7031 : \qquad 0 : 0.2969 . \qquad (71)$$

The effect of including the nonvanishing bottom quark mass can be seen to be quite small.

Although we have derived the decay distributions (67) and (68) for the Born term case, the angular structure is quite general as will be shown in the next subsection. In the general case one has to replace the LO Born term structure function $H^{\mu\nu}(\text{Born})$ in (67) and (68) by their generalized counterparts as e.g. the corresponding NLO or NNLO structure functions.

3.2 Angular decay distribution for $t \to b + W^+(\to \ell^+ + \nu_\ell)$ (II)

The $\cos\theta$ dependence of $L_{\mu\nu}H^{\mu\nu}$ can also be worked out in a more systematic way by using the completeness relation for the polarization four–vectors Eq.(18) [6]. One can then rewrite the contraction of the lepton and hadron tensors $L_{\mu\nu}H^{\mu\nu}$ as

$$
\begin{aligned}
L_{\mu\nu}H^{\mu\nu} &= L^{\mu'\nu'}g_{\mu'\mu}g_{\nu'\nu}H^{\mu\nu} \\
&= \sum_{m,m'} L^{\mu'\nu'}\epsilon_{\mu'}(m)\epsilon_\mu^*(m)\epsilon_{\nu'}^*(m')\epsilon_\nu(m')H^{\mu\nu} \\
&= \sum_{m,m'} \left(L^{\mu'\nu'}\epsilon_{\mu'}(m)\epsilon_{\nu'}^*(m') \right) \left(H^{\mu\nu}\epsilon_\mu^*(m)\epsilon_\nu(m') \right) \\
&= \sum_{m,m'} L_{mm'}H_{mm'} \, .
\end{aligned}
\tag{72}
$$

We have thereby converted the invariant contraction $L_{\mu\nu}H^{\mu\nu}$ into a contraction over the spatial spherical components $L_{mm'}H_{mm'}$ ($m, m' = +, 0, -$), where the spatial spherical components of the lepton and hadron tensors are defined by

$$
\begin{aligned}
L_{mm'} &= L^{\mu\nu}\epsilon_\mu(m)\epsilon_\nu^*(m') \, , \\
H_{mm'} &= H^{\mu\nu}\epsilon_\mu^*(m)\epsilon_\nu(m') \, .
\end{aligned}
\tag{73}
$$

We have again dropped the $q^\mu q^\nu$-terms in the completeness relation in Eq. (18) since $q_\mu L^{\mu'\nu'} = q_\nu L^{\mu'\nu'} = 0$ for massless leptons. The nice feature of the representation (72) is that the left bracket and the right bracket in the next to last row of (72) are separately Lorentz invariant. One can therefore evaluate the left bracket in the W^+ rest frame, and the right bracket in the t–rest system without involving any boost.

Let us now specify the the W^+-rest frame four-vectors that are needed in the W^+-rest frame evaluation of the lepton matrix $L_{mm'}$. In the W^+ rest frame one has

$$
\begin{aligned}
p_\ell^\mu &= m_W/2 \, (1; \quad \sin\theta\cos\phi, \quad \sin\theta\sin\phi, \quad \cos\theta) \, , \\
p_\nu^\mu &= m_W/2 \, (1; -\sin\theta\cos\phi, \, -\sin\theta\sin\phi, \, -\cos\theta) \, ,
\end{aligned}
\tag{74}
$$

and the polarization vectors (in our convention $a^\mu = (a_0, \vec{a})$ and $a_\mu = (a_0, -\vec{a})$)

$$
\begin{aligned}
\epsilon_\mu(L) &= (0; 0, 0, -1) \, , \\
\epsilon_\mu(\pm) &= \frac{1}{\sqrt{2}}(0; \pm 1, i, 0) \, .
\end{aligned}
\tag{75}
$$

It is then straight-forward to evaluate $L_{mm'} = L^{\mu\nu}\epsilon_\mu(m)\epsilon_\nu^*(m')$ using the lepton tensor (59).

---

[6]Since the method is general we can omit the LO specification in $H^{\mu\nu}(\text{Born})$.

The various components of the lepton matrix $L_{mm'}$ can be written in a very compact and suggestive way in terms of Wigner's small d^1-function. One has

$$L_{mm'}(\theta, \phi) = m_W^2 \; d_{m\,1}^1(\theta) d_{m'\,1}^1(\theta) e^{i(m-m')\phi} \,, \tag{76}$$

where the spin one d^1 function is given by (convention of Rose)

$$d_{mm'}^1(\theta) = \begin{pmatrix} \frac{1}{2}(1+\cos\theta) & -\frac{1}{\sqrt{2}}\sin\theta & \frac{1}{2}(1-\cos\theta) \\ \frac{1}{\sqrt{2}}\sin\theta & \cos\theta & -\frac{1}{\sqrt{2}}\sin\theta \\ \frac{1}{2}(1-\cos\theta) & \frac{1}{\sqrt{2}}\sin\theta & \frac{1}{2}(1+\cos\theta) \end{pmatrix} . \tag{77}$$

The rows and columns are labeled in the order $(+1, 0, -1)$. The representation (76) should be of no surprise to anyone who is familiar with the behaviour of angular momentum states under a rotation by the angles θ and ϕ. In the lepton system (x', y', z') the only nonvanishing component of the lepton matrix is $L_{+1,+1} = m_W^2/2$ as the antilepton and the neutrino are both left-handed (see Fig. 2). Eq.(76) represents the rotation of the lepton matrix from the lepton system (x', y', z') to the hadron system (x, y, z). In the case $m_l \neq 0$ one has to augment Eq.(76) by temporal spin 0 components and interference contributions of the temporal spin 0 and spatial spin 1 components [44].

When integrating $L_{\mu\nu} H^{\mu\nu}$ over the azimuthal angle ϕ one remains only with the three diagonal elements of $H_{mm'}$. One has

$$\int d\phi \; L_{\mu\nu} H^{\mu\nu} = 2\pi \, m_W^2 \sum_{m=+1,0,-1} d_{m,+1}^1(\theta) d_{m,+1}^1(\theta) H_{mm}$$

$$= 2\pi \frac{2}{3} m_W^2 \left(\frac{3}{4} \sin^2\theta \, H_{00} + \frac{3}{8}(1+\cos\theta)^2 H_{++} + \frac{3}{8}(1-\cos\theta)^2 H_{--} \right) . \tag{78}$$

By convention one drops one of the double indices in the diagonal elements of the hadronic density matrix H_{mm}, i.e. one replaces $H_{00} \rightarrow H_0$ and $H_{\pm\pm} \rightarrow H_\pm$ as has been done in the rest of this paper. For the LO case one reproduces Eq.(21) using $H_{00}(= H_L) = |H_{\frac{1}{2};-\frac{1}{2}0}|^2 + |H_{-\frac{1}{2};\frac{1}{2}0}|^2$, $H_{++}(= H_+) = |H_{\frac{1}{2};\frac{1}{2}1}|^2$ and $H_{--}(= H_-) = |H_{-\frac{1}{2};-\frac{1}{2}-1}|^2$ from (30).

The advantage of method II is that the method can easily be applied to more complex decay processes involving spin. Also one can easily incorporate lepton mass effects and include polarization effects of initial and final state particles [43, 44]. For example, method II was applied to the full angular analysis of $B \rightarrow D, D^* + \ell + \nu_\ell$ ($\ell = e, \mu, \tau$) [43, 44] and the rare decays $B \rightarrow K, K^* + \ell^+ + \ell^-$ ($\ell = e, \mu, \tau$) [45] including results on the polarisation of the final lepton. Another example is [42] where we have used method II to describe the semileptonic decay process of a polarized Ξ^0, $\Xi^0(\uparrow) \rightarrow \Sigma^+ + l^- + \bar{\nu}_l$ ($l^- = e^-, \mu^-$) followed by the nonleptonic decay $\Sigma^+ \rightarrow p + \pi^0$. In this process the mass difference $M_{\Xi^0} - M_{\Sigma^+} = 125.46\,\text{MeV}$ is comparable to the μ–mass which makes inclusion of lepton mass effects mandatory. In fact one finds $\Gamma(\mu)/\Gamma(e) \approx 1/120$ in this process. A cascade type analysis as used in the method II is ideally suited for Monte Carlo event generators that describe complex cascade decays involving particles with spin. In fact, we wrote a Monte Carlo generator for the above semileptonic Ξ^0 decay process [42] which was profitably used in the analysis of the NA48 data on this process.

3.3 Experimental results on helicity fractions

An early MC study quotes experimental sensitivities of $\delta\mathcal{G}_L = 0.7\,\%$ and $\delta\mathcal{G}_+ = 0.3\,\%$ for an integrated luminosity of $100\,\text{fb}^{-1}$ at Tevatron II energies which corresponds to $\approx 8 \cdot 10^6$

$(t\bar{t})$-pairs [46]. Compare this to the NLO QCD changes $\delta\mathcal{G}_L = 0.7\,\%$ and $\delta\mathcal{G}_+ = 0.1\,\%$ to be discussed later on which shows that the radiative corrections are of the same order as the experimental sensitivities. Much higher event rates can be reached at the LHC in one year. A more recent MC study based on $10\ fb^{-1}$ at the LHC quotes measurement uncertainties of $\delta\mathcal{G}_L = 1.9\,\%$, $\delta\mathcal{G}_+ = 0.22\,\%$ and $\delta\mathcal{G}_- = 1.8\,\%$ [47].

Experimentally, there has been a continuing interest in the measurement of the helicity fractions. Latest measurements are

$$
\begin{aligned}
\text{CDF(2008 [48]) :} \qquad & \mathcal{G}_L = 0.66 \pm 0.16(\text{stat}) \pm 0.05(\text{syst}) \\
& \mathcal{G}_+ = -0.03 \pm 0.06(\text{stat}) \pm 0.03(\text{syst}) \\
\text{DO(2009 [49]) :} \qquad & \mathcal{G}_L = 0.490 \pm 0.106(\text{stat}) \pm 0.085(\text{syst}) \\
& \mathcal{G}_+ = -0.104 \pm 0.076(\text{stat}) \pm 0.066(\text{syst})
\end{aligned}
\tag{79}
$$

All of these measurements are well within the SM predictions.

4   Construction of covariant helicity projectors

In Eq.(73) we have defined the helicity structure functions H_m $(m = L, +, -)$ which multiply the angular factors in the angular decay distribution. According to their definition in Eq.(73) the helicity structure functions H_m can be calculated in a frame-dependent way by use of the frame-dependent polarization vectors (29). It is much more convenient to calculate the helicity structure functions covariantly, and, in fact, a covariant projection is indispensable for the NLO and NNLO calculations. The covariantization is achieved by defining covariant helicity projectors $\mathbb{P}_m^{\mu\nu}$ which covariantly project onto the helicity structure functions via

$$
H_m = \mathbb{P}_m^{\mu\nu} H_{\mu\nu} \qquad (m = L, +, -).
\tag{80}
$$

This definition holds for any general hadron tensor structure irrespective of the fact that we have dealt only with the Born term hadron tensor up to now. To construct the covariant helicity projectors we start with their representation in terms of the t-rest frame polarization vectors (29) according to the definition Eq.(73). One has

$$
\begin{aligned}
\mathbb{P}_L^{\mu\nu} &= \epsilon^{*\mu}(L)\,\epsilon^\nu(L)\,, \\
\mathbb{P}_\pm^{\mu\nu} &= \epsilon^{*\mu}(\pm)\,\epsilon^\nu(\pm).
\end{aligned}
\tag{81}
$$

In covariantizing the forms (81) it helps to remember that the helicity projectors must be four-transverse to the momentum of the W^+, i.e. they must satisfy

$$
q_\mu \mathbb{P}_m^{\mu\nu} = q_\nu \mathbb{P}_m^{\mu\nu} = 0 \ .
\tag{82}
$$

Further, they must satisfy the orthonormality and completeness relations

$$
\begin{aligned}
\text{orthonormality:} \quad & g_{\mu\nu} \mathbb{P}_m^{\mu\nu} = -1 \\
& g_{\alpha\beta} \mathbb{P}_m^{\mu\alpha} \mathbb{P}_n^{\beta\nu} = -\delta_{mn} \mathbb{P}_m^{\mu\nu} \\
\text{completeness} \quad : \quad & \sum_m \mathbb{P}_m^{\mu\nu} := \mathbb{P}_{U+L}^{\mu\nu} = -g^{\mu\nu} + \frac{q^\mu q^\nu}{m_W^2}
\end{aligned}
\tag{83}
$$

As it turns out the covariant projectors can be constructed from the following three projectors

- Projector for the total rate $\mathbb{P}_{U+L}^{\mu\nu}$

$$\mathbb{P}_{U+L}^{\mu\nu} = -g^{\mu\nu} + \frac{q^\mu q^\nu}{m_W^2} \tag{84}$$

- Projector for the longitudinal helicity rate $\mathbb{P}_L^{\mu\nu}$

$$\mathbb{P}_L^{\mu\nu} = \frac{m_W^2}{m_t^2} \frac{1}{|\vec{q}|^2} \left(p_t^\mu - \frac{p_t \cdot q}{m_W^2} q^\mu \right) \left(p_t^\nu - \frac{p_t \cdot q}{m_W^2} q^\nu \right) \tag{85}$$

- Projector for the forward-backward asymmetric helicity rate $\mathbb{P}_F^{\mu\nu} = \mathbb{P}_+^{\mu\nu} - \mathbb{P}_-^{\mu\nu}$
  ($\epsilon_{0123} = 1$)

$$\mathbb{P}_F^{\mu\nu} = \frac{1}{m_t} \frac{1}{|\vec{q}|} i\epsilon^{\mu\nu\alpha\beta} p_{t,\alpha} q_\beta \tag{86}$$

The denominator factor $|\vec{q}|^2$ refers to the top quark rest frame. In invariant form the normalization factor is given by $|\vec{q}|^2 = ((p_t q)^2 - m_W^2 m_t^2)/m_t^2$. Finally, the three projectors read ($H_m = \mathbb{P}_m^{\mu\nu} H_{\mu\nu}$; $m = L, +, -$)

$$\begin{aligned}
\mathbb{P}_L^{\mu\nu} &= \frac{m_W^2}{m_t^2} \frac{1}{|\vec{q}|^2} \left(p_t^\mu - \frac{p_t \cdot q}{m_W^2} q^\mu \right) \left(p_t^\nu - \frac{p_t \cdot q}{m_W^2} q^\nu \right), \\
\mathbb{P}_\pm^{\mu\nu} &= \frac{1}{2} \left(\mathbb{P}_{U+L}^{\mu\nu} - \mathbb{P}_L^{\mu\nu} \pm \mathbb{P}_F^{\mu\nu} \right) .
\end{aligned} \tag{87}$$

It is instructive to check that, in the t-rest frame or in the W^+-rest frames, the covariant helicity projectors in Eq. (87) reduce to the form (81) in terms of the rest frame polarization vectors (29) and (75), respectively. Note, though, that in the W-rest frame the normalization factor $|\vec{q}|$ in Eqs. (85) and (86) has to be replaced by $y|\vec{p_t}|$ where $|\vec{p_t}|$ is the magnitude of the top quark momentum in the W^+-rest frame.

The denominator factors $|\vec{q}|^{-2}$ and $|\vec{q}|^{-1}$ in Eqs. (85) and (86) are needed for the correct normalization of the projectors, *cif.* Eq.(83). As we shall see later on the denominator factors $|\vec{q}|^2$ and $|\vec{q}|$ somewhat complicate the NLO and NNLO calculation of the helicity rates as compared to the total rate.

5   Narrow width approximation

Let us begin with by discussing how to factorize of the three–body rate $\Gamma(t \to b + \ell^+ + \nu_\ell)$ into the two–body rates $\Gamma(t \to b + W^+)$ and $\Gamma(W^+ \to \ell^+ + \nu_\ell)$ using the narrow width approximation for the W-boson. The rate formula for the three body decay $t \to b + \ell^+ + \nu$ reads (see [27])

$$\Gamma_3 = \frac{1}{2m_t} \int \frac{1}{(2\pi)^3} \frac{d^3 p_b}{2\, E_b} \int \frac{1}{(2\pi)^3} \frac{d^3 p_{l+}}{2\, E_{l+}} \int \frac{1}{(2\pi)^3} \frac{d^3 p_{\nu_l}}{2\, E_{\nu_l}} \frac{1}{2} |\overline{M}_3|^2 (2\pi)^4 \delta^{(4)}(p_t - p_b - p_{\ell+} - p_{\nu_l}), \tag{88}$$

which we write as

$$\Gamma_3 = \frac{1}{2} R_3 \left[|\overline{M}_3|^2 \right] . \tag{89}$$

The squared three-body matrix element $|\overline{M}_3|^2$ is given by

$$|\overline{M}_3|^2 = 64 \frac{g_\omega^2}{8} L_{\mu\nu} \frac{g_\omega^2}{8} |V_{tb}|^2 H^{\mu\nu} \left| \frac{1}{q^2 - m_W^2 + im_W\Gamma_W} \right|^2, \tag{90}$$

where we have introduced the Breit-Wigner line shape to account for the finite width of the W^+–boson. We have also reinstituted the factor of $8 \cdot 8 = 64$ in (90) which was introduced earlier for convenience.

Next we introduce the identity

$$1 = \int dq^2 \int \frac{d^3q}{2\,E_W} \delta^{(4)}(q - p_{\ell^+} - p_{\nu_l}), \tag{91}$$

which can be seen to be true in the W^+ rest frame where $q^2 = E_W^2$ and $\int \frac{dE_W^2}{2E_W} \delta(E_W - E_{l^+} - E_{\nu_l}) = 1$. The identity (91) allows one to factorize the three-body phase space integral $R_3(t \to b + \ell^+ + \nu_\ell)$ into the two-body phase space integrals $R_2(t \to b + W^+)$ and $R_2(W^+ \to l^+ + \nu_l)$. One has

$$R_3 = 2m_W \int \frac{dq^2}{(2\pi)} \overbrace{\frac{1}{2m_t} \left\{ \int \frac{1}{(2\pi)^3} \frac{d^3p_b}{2\,E_b} \int \frac{1}{(2\pi)^3} \frac{d^3q}{2\,E_W} (2\pi)^4 \delta^{(4)}(p_t - p_b - q) \right\}}^{R_2(t\to b+W^+)}$$
$$\underbrace{\frac{1}{2m_W} \left\{ \int \frac{1}{(2\pi)^3} \frac{d^3p_{\ell^+}}{2\,E_{\ell^+}} \int \frac{1}{(2\pi)^3} \frac{d^3p_{\nu_l}}{2\,E_{\nu_l}} (2\pi)^4 \delta^{(4)}(q - p_{\ell^+} - p_{\nu_l})) \right\}}_{R_2(W^+\to l^++\nu_l)}. \tag{92}$$

The phase space nicely factorizes. But how about the factorization of the squared three–body matrix element $|\overline{M}_3|^2$? The matrix element squared also factorizes *after angular integration* which can be seen by using the relation

$$\int d\cos\theta\, d\phi\, L_{mn}(\theta, \phi) = \frac{4\pi}{3}\, m_W^2 \delta_{mn} \tag{93}$$

which follows from the explicit representation of $L_{mn}(\theta, \phi)$ given in Eq.(76). In fact, one has

$$\int d\cos\theta\, d\phi \Big(\sum_{m,n} H_{mn} \sum_{m,n} L_{mn}(\theta, \phi) \Big) = \frac{1}{\mathrm{Tr}\,\{\delta_{mn}\}} \Big(\sum_n H_{nn} \Big) \int d\cos\theta\, d\phi \Big(\sum_m L_{mm}(\theta, \phi) \Big). \tag{94}$$

The factor $1/\mathrm{Tr}\,\{\delta_{mn}\} = 1/3$ provides for the crucial statistical factor $1/(2s_W + 1)$ in the W^+ width formula. Note that the explicit angular integrations over $\cos\theta$ and ϕ appearing in (94) are implicit in (92) [7]. One thus finds

$$\begin{aligned} \Gamma(t \to b + \ell^+ + \nu) &= \frac{m_W}{\pi} \int dq^2 \frac{1}{2} R_2 \Big[|\overline{M}|^2(t \to b + W^+) \Big] \\ &\quad \cdot \frac{1}{3} R_2 \Big[|\overline{M}|^2(W^+ \to \ell^+ + \nu) \Big] \left| \frac{1}{q^2 - m_W^2 + im_W\Gamma_W} \right|^2. \end{aligned} \tag{95}$$

---

[7]We mention that an alternative derivation of the appearance of the statistical factor $1/3$ has been given in [50].

The narrow–width approximation consists in the replacement of the Breit-Wigner line shape by a δ–function, *cif*.

$$\left|\frac{1}{q^2 - m_W^2 + im_W\Gamma_W}\right|^2 = \frac{\pi}{m_W\,\Gamma_W}\frac{1}{\pi}\frac{m_W\,\Gamma_W}{(q^2 - m_W^2)^2 + m_W^2\Gamma_W^2} \stackrel{\Gamma_W \to 0}{=} \frac{\pi}{m_W\,\Gamma_W}\delta(q^2 - m_W^2) . \quad (96)$$

Using the narrow-width approximation for the W^+-boson the three-body decay $t \to b + \ell^+ + \nu$ can be seen to factorize, *cif*.

$$\begin{aligned}\Gamma(t \to b + \ell^+ + \nu_\ell) &=& \Gamma(t \to b + W^+)\frac{\Gamma(W^+ \to \ell^+ + \nu_\ell)}{\Gamma_W}\\ &=& \Gamma(t \to b + W^+)\,BR(W^+ \to \ell^+ + \nu_\ell)\end{aligned} \quad (97)$$

which is a result which one expects from physical intuition. Incidentally, the derivation of the factorization formula (97) was posed as one of the problems in the 2004 TASI lectures of T. Han [51]. Judging from the contents of this subsection this was not one of his simpler problems.

The numerical value of the finite-width correction to the total width listed in (6) consists of the replacement of $\delta(q^2 - m_W^2)$ by the Breit–Wigner line shape and integrating over q^2, *cif*.

$$\int_0^{m_t^2} dq^2\,\delta(q^2 - m_W^2) \to \int_0^{m_t^2} dq^2\frac{m_W\Gamma_W}{\pi}\frac{1}{(q^2 - m_W^2)^2 + m_W^2\Gamma_W^2} \quad (98)$$

where Γ_W is the width of the W-boson ($\Gamma_W = 2.12$ GeV).

Numerically the finite-width correction to the total Born term rate amounts to 1.56% (see Eq.(6)) and is of the order of $\Gamma_W/m_W = 2.64\%$ as would be expected. A more extensive discussion on finite width corrections can be found in [50, 52].

6 Higher order corrections to helicity fractions

6.1 NLO QCD and electroweak corrections

As in the calculation of the NLO total rate structure function $H_{U+L} = H_+ + H_- + H_L$ (we call $H_+ + H_- = H_U$ where U stands for the "unpolarized transverse") we have employed the traditional technique when calculating the helicity structure functions H_L and $H_\pm$, i.e. we have separately calculated the hadronic loop and tree contributions after contracting them with the relevant projectors $\mathbb{P}_L^{\mu\nu}$, $\mathbb{P}_\pm^{\mu\nu}$.

As mentioned before, the appearance of the normalization factors $|\vec{q}|^{-1}$ and $|\vec{q}|^{-2}$ in the projectors make the calculation technically more difficult than that for the total rate. For the one-loop contribution the additional normalization factors are of no concern since they appear only as overall factors outside of the one-loop integral. This is different for the phase space integration of the tree-graph contributions where the normalization factors appear under the integral. Typically one of the phase space integrations is over the scaled invariant mass of the bottom quark and the gluon $z = (p_b + p_g)^2/m_t^2$. The normalization factors then appear as overall factors $|\vec{q}|^{-1}$ and $|\vec{q}|^{-2}$ in the phase space integral, where

$$|\vec{q}| = \frac{m_t}{2}\sqrt{\lambda(1, y^2, z)} . \quad (99)$$

The ensuing class of phase space integrals is more general and more difficult than the class of integrals appearing in the total rate calculation. Nevertheless, the phase space integrations can still be done in closed form.

As a sample result we present the $m_b = 0$ result for $\hat{\Gamma}_L = \Gamma_L/\Gamma_{U+L}$(Born). One obtains [8, 14, 36]

$$
\begin{aligned}
\hat{\Gamma}_L(\text{NLO}) \quad = \quad & \frac{1}{(1-y^2)^2(1+2y^2)}\Big((1-y^2)^2 + \frac{\alpha_s}{2\pi}C_F\Big\{(1-y^2)(5+47y^2-4y^4)/2 \\
- \quad & \frac{2\pi^2}{3}(1+5y^2+2y^4)-3(1-y^2)^2\ln(1-y^2) + 16y^2(1+2y^2)\ln(y) - 2(1-y)^2 \\
\times \quad & (2-y+6y^2+y^3)\ln(1-y)\ln(y) - 2(1+y)^2(2+y+6y^2-y^3)\ln(y)\ln(1+y) \\
- \quad & 2(1-y)^2(4+3y+8y^2+y^3)\text{Li}_2(y) - 2(1+y)^2(4-3y+8y^2-y^3)\text{Li}_2(-y)\Big\}\Big) . \quad (100)
\end{aligned}
$$

In the limit $y \to 0$ one finds $\hat{\Gamma}_L(\text{NLO}) = 1 + \alpha_s C_F/(2\pi)(5/2 - 2\pi^2/3)$ and thus $\hat{\Gamma}_L(\text{NLO})$ saturates the total rate $\hat{\Gamma}(\text{NLO})$ (see Eq.(57)) in this limit. This is expected since $\Gamma_U/\Gamma_L \propto m_W^2/m_t^2 = y^2$. Results for the other two NLO QCD helicity rates $\hat{\Gamma}_+$ and $\hat{\Gamma}_-$ can be found in [8, 14, 36]. The NLO electroweak corrections to the helicity rates can be found in [9].

Let us summarize our numerical NLO results on the helicity fractions including also the finite width corrections discussed in Sec.5. We write

$$
\Gamma_i = \Gamma_i(\text{Born}) + \Delta\Gamma_i(\text{QCD}) + \Delta\Gamma_i(\text{EW}) + \Delta\Gamma_i(\text{FW}) + \Delta\Gamma_i(m_b \neq 0) . \quad (101)
$$

As before we normalize the partial rates to the total Born term rate Γ_{U+L}(Born). Thus we write $\hat{\Gamma}_i = \Gamma_i/\Gamma_{U+L}$(Born) $(i = +, -, L)$. For the transverse-minus and longitudinal rates we factor out the normalized partial Born rates $\hat{\Gamma}_i$ and write $(i = -, L)$

$$
\hat{\Gamma}_i = \hat{\Gamma}_i(\text{Born})\Big(1 + \delta_i(\text{QCD}) + \delta_i(\text{EW}) + \delta_i(\text{FW}) + \delta\Gamma_i(m_b \neq 0)\Big) , \quad (102)
$$

where $\delta_i = \Gamma_{U+L}(\text{Born})\,\Delta\Gamma_i/\Gamma_i(\text{Born})$. Writing the result in this way helps to quickly assess the percentage changes brought about by the various corrections.

Numerically one has

$$
\begin{aligned}
\hat{\Gamma}_- \quad = \quad & 0.297\Big(1 - 0.0656(\text{QCD}) + 0.0206(\text{EW}) - 0.0197(\text{FW}) - 0.00172(m_b \neq 0)\Big) \\
= \quad & 0.297(1 - 0.0664) , \quad (103)
\end{aligned}
$$

and

$$
\begin{aligned}
\hat{\Gamma}_L \quad = \quad & 0.703\Big(1 - 0.0951(\text{QCD}) + 0.0132(\text{EW}) - 0.0138(\text{FW}) - 0.00357(m_b \neq 0)\Big) \\
= \quad & 0.703(1 - 0.0993) . \quad (104)
\end{aligned}
$$

It is quite remarkable that the electroweak corrections almost cancel the finite width corrections in both cases.

In the case of the transverse-plus rate the partial Born term rate cannot be factored out because of the fact that Γ_+(Born) is zero. In this case we present our numerical result in the form

$$
\hat{\Gamma}_+ = \Delta\hat{\Gamma}_+(\text{QCD}) + \Delta\hat{\Gamma}_+(\text{EW}) + \Delta\hat{\Gamma}_+(m_b \neq 0). \quad (105)
$$

One has

$$
\begin{aligned}
\hat{\Gamma}_+ &= 0.000927(\text{QCD}) + 0.0000745(\text{EW}) + 0.000358(m_b \neq 0) \\
&= 0.00136.
\end{aligned}
\tag{106}
$$

Note that the finite width correction to the transverse-plus helicity rate is zero. Numerically the NLO corrections to $\hat{\Gamma}_+$ occur only at the pro mille level. It is save to say that, if top quark decays reveal a violation of the SM left-chiral $(V - A)$ current structure that exceeds the 1% level, the violations must have a non-SM origin such as e.g. an admixture of a right-chiral $(V + A)$ current structure in the decay vertex $t \to b + W^+$.

6.2 Quality of the (m_W/m_t)–expansion

In order to check on the quality of the $y = (m_W/m_t)$-expansion we take the known closed form NLO result (100) for $\hat{\Gamma}_L$ and expand it in powers of y^2 and $y^2 \ln y$. The expansion of the curly bracket in (100) reads

$$
\Gamma_L(\alpha_s) = \Gamma_0 \frac{\alpha_s}{2\pi} C_F \{...\} = \Gamma_0 \frac{\alpha_s}{2\pi} C_F \left\{ \left(\frac{5}{2} - \frac{2\pi^2}{3} \right) + \left(40 - \frac{10\pi^2}{3} \right) y^2 \right.
$$
$$
\left. + \frac{1}{9} \left(119 - 12\pi^2 - 6\ln y \right) y^4 + \left(-\frac{253}{90} + \frac{10\ln y}{3} \right) y^6 + ... \right\} . \tag{107}
$$

Note that $\Gamma_L(\alpha_s) \to 0$ as the phase space closes at $y = 1$ $(\text{Li}_2(-1) = -\pi^2/12)$. In Fig. 7 we show a plot of the y-dependence of $\Gamma_L(\alpha_s)$ (in units of $[\Gamma_0 \frac{\alpha_s}{2\pi} C_F]$) for different orders of y^n and for the full result. All curves start at $(5/2 - 2\pi^2/3) = 0.459$ for $y = 0$. The full result goes to zero at $y = 1$ remembering that $\text{Li}_2(-1) = -\pi^2/12$. As Fig. 7 shows the quality of the expansion is already quite good at $O(y^6)$ even for large y-values.

This raises the hope that such a (m_W/m_t)-expansion can also be usefully employed in other contexts. One could think of possible applications of the NNLO calculation of $t \to b + W^+$ discussed earlier (which only exists in expanded form) to processes such as

- $b \to u + \ell^- + \bar{\nu}_\ell$

- $\mu^- \to e^- + \bar{\nu}_e + \nu_\mu$

extending q^2 over the whole kinematical range $0 \leqslant q^2 \leqslant (m_1 - m_2)^2$ in these processes.

The region very close to the upper kinematical limit of q^2 given by $q_{max}^2 = (m_t - m_b)^2$ requires a separate discussion because this region is sensitive to $m_b \neq 0$ effects. The upper kinematical limit is called the zero recoil point since $\vec{q} = 0$ at this point. For example, at zero recoil $(y = 1 - m_b/m_t = 1 - 4.8/175 = 0.973)$ one finds

$$
m_b \neq 0: \qquad \mathcal{G}_L : \mathcal{G}_+ : \mathcal{G}_- = 1/3 : 1/3 : 1/3 \tag{108}
$$

using Eq.(70). The equipartitioned helicity fractions result from the fact that, close to zero recoil, the only surviving transition is the allowed Gamow-Teller s–wave transition. However, for $m_b = 0$ one has the zero recoil ratios at $y = 1$ (see Eq.(8))

$$
m_b = 0: \qquad \mathcal{G}_L : \mathcal{G}_+ : \mathcal{G}_- = 1/3 : \ 0 \ : 2/3 . \tag{109}
$$
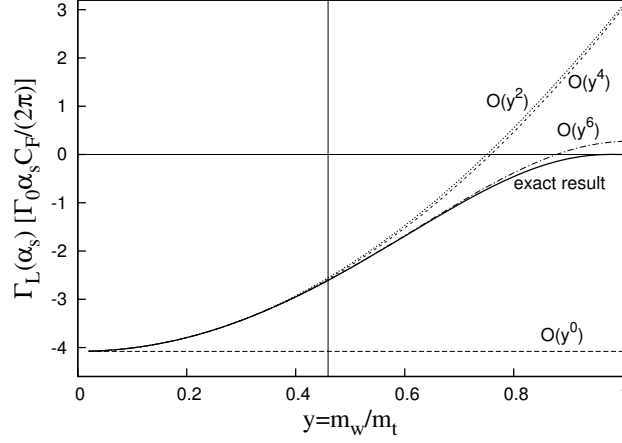
Figure 11: Quality of the y-expansion of the α_s corrections to $\Gamma_L(\alpha_s)$. Shown are different orders of the y-expansion in units of $[\Gamma_0\,\alpha_s\,C_F/2\pi]$. Dashed line: $O(y^0)$; dotted line: $O(y^2)$; dashed line : $O(y^4)$; dash-dotted line: $O(y^6)$; full line: exact result. Vertical line corresponds to the physical point $y = m_W/m_t = 0.459$.

In order to investigate the behaviour of the helicity fractions close to zero recoil, in Fig. 8 we plot the y^2-dependence of the helicity fractions for $m_b \neq 0$ and $m_b = 0$ with zero recoil values at $y = 1 - m_b/m_t$ and $y = 1$, respectively. In the region close to their respective zero recoil points the curves considerably differ from each other. Away from zero recoil the $m_b = 0$ and $m_b \neq 0$ curves very quickly approach each other. Fig. 8 shows that it is safe to use the $m_b = 0$ approximation for y-values below $y \approx 0.9$.
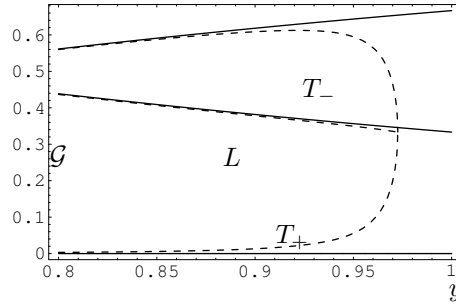
Figure 12: Helicity fractions $\mathcal{G}_L, \mathcal{G}_+$ and $\mathcal{G}_-$ close to zero recoil. Dashed line: $m_b \neq 0$; full line: $m_b = 0$. The kinematical zero recoil point is given by $y = 1$ (full line) and $y = 1 - m_b/m_t$ (dashed line).

6.3 NNLO QCD corrections to helicity fractions

In Sec. 2.4 we have desribed how the total NNLO rate can be calculated in a $y = (m_W/m_t)$-expansion using the optical theorem. Two new features appear in the corresponding NNLO calculation of the helicity rates $\Gamma_{L,\pm}$. First there is a parity violating three-loop contribution which is projected out by the projector $\mathbb{P}_F^{\mu\nu}$. One has to deal with the problem of how to treat γ_5 in the environment of dimensionally regularized loop integrals. We take the prescription of [53] and replace

$$\gamma_\mu\gamma_5 \to \frac{1}{3!}\epsilon_{\mu\alpha\beta\gamma}\gamma^\alpha\gamma^\beta\gamma^\gamma \ . \tag{110}$$

When using this prescription one needs to add finite three-loop counter terms which are given in [54].

The second new feature is related to the normalization factors $|\vec{q}|^{-1}$ and $|\vec{q}|^{-2}$ in the three helicity projectors $\mathbb{P}_{L,\pm}^{\mu\nu}$ which replace the total rate projector $\mathbb{P}_{U+L}^{\mu\nu} = -g^{\mu\nu} + q^\mu q^\nu/m_W^2$. In the hard region one can expand in inverse powers of the (large) propagator pole factor $P = (p_t + q)^2 - m_t^2$.

$$|\vec{q}|^2 = q_0^2 - m_W^2 = \left(\frac{p_t q}{m_t}\right)^2 - m_W^2 \ . \tag{111}$$

One expands in the propagator pole factor $P = (p_t + q)^2 - m_t^2 = 2p_t q + q^2$, i.e. $p_t q = \frac{1}{2}P(1 - m_W^2 P^{-1})$ where one can replace q^2 by m_W^2 since one is cutting through the W-line anyhow. One then has

$$\frac{1}{|\vec{q}|^{\,2}} = \frac{4m_t^2}{P^2}\sum_{n=0}^{\infty}\left(\frac{2m_W^2 P^2 - m_W^4 + 4m_t^2 m_W^2}{P^2}\right)^n \ ,$$

$$\frac{1}{|\vec{q}|} = \frac{2m_t}{P}\sum_{n=0}^{\infty}\binom{2n}{n}\left(\frac{2m_W^2 N - m_W^4 + 4m_t^2 m_W^2}{4\,P^2}\right)^n \ . \tag{112}$$

Thus, the additional propagator-like structures from the projectors are transformed into a scalar on-shell propagator with momentum $p+q$ and mass m_t raised to arbitrary, integer powers. This will eventually lead to twelve additional three-loop master integrals next to the master integrals appearing in the total rate calculation of [19, 20] whose imaginary parts can again be calculated in closed analytical form using the cutting rules.

In the soft region one cannot perform an expansion of $|\vec{q}|$, since $|\vec{q}|^2 = q_0^2 - m_W^2$ and q_0 is of order m_W in the soft region. However, in this region the W boson loop factorizes. Therefore, one only has to replace the usual one-loop vacuum bubble integrals with integrals of the type

$$\int \frac{\mathrm{d}^d q}{(q^2 - m_W^2)\,(q_0^2 - m_W^2)^n} \ , \tag{113}$$

with $n = 1/2$ and 1. These integrals are not difficult to evaluate.

The validity of the treatment of these two new features has been tested against the known NLO results up to $\mathcal{O}((m_W/m_t)^{16})$ [38]. First results of the NNLO calculation have been published in [38]. Complete results on the NNLO calculation of the helicity rates will be published soon [55].

7 Summary and conclusions

We have discussed some of the properties of the top quark with an emphasis on the SM decay properties of the top quark. We have defined partial helicity rates into polarized W^+-bosons and have derived the resulting angular decay distribution of $W^+_{pol} \to l^+\nu$. We have described the LO calculation of the partial helicity rates using several methods including also the optical theorem and a m_W/m_t-expansion as a preparation for the description of the NNLO calculation of the total rate and the partial helicity rates. We have summarily described the main features of NLO QCD and electroweak corrections to the total width and the partial helicity rates.

We are looking forward to the LHC era with its expected wealth of data on the top quark and its decay properties.

Acknowledgements

References

[1] J. G. Körner and M. C. Mauser, "One-loop corrections to polarization observables," Lect. Notes Phys. **647** (2004) 212 [arXiv:hep-ph/0306082].

[2] J. H. Kühn, "Theory of top quark production and decay," arXiv:hep-ph/9707321.

[3] D. Chakraborty, J. Konigsberg and D. L. Rainwater, "Review of top quark physics," Ann. Rev. Nucl. Part. Sci. **53** (2003) 301

[4] W. Bernreuther, "Top quark physics at the LHC," J. Phys. G **35** (2008) 083001 [arXiv:0805.1333 [hep-ph]].

[5] W. Wagner, "Top-quark physics at the Tevatron," Nucl. Phys. Proc. Suppl. **183** (2008) 67.

[6] J. R. Incandela, A. Quadt, W. Wagner and D. Wicke, "Status and Prospects of Top-Quark Physics," arXiv:0904.2499 [hep-ex].

[7] Tevatron Electroweak Working Group for the CDF Collaboration and D0 Collaborations, arXiv:0903.2503 [hep-ex].

[8] M. Fischer, S. Groote, J. G. Körner and M. C. Mauser, Phys. Rev. D **65** (2002) 054036

[9] H. S. Do, S. Groote, J. G. Körner and M. C. Mauser, Phys. Rev. D **67** (2003) 091501

[10] C. S. Hill, J. R. Incandela and J. M. Lamb, Phys. Rev. D **71** (2005) 054029

[11] Y. Grossman and I. Nachshon, JHEP **0807** (2008) 016

[12] F.E. Close, J.G. Körner, R.J.N. Phillips, D.J. Summers, J. Phys. G **18** (1992) 1716.

[13] A. F. Falk and M. E. Peskin, Phys. Rev. D **49** (1994) 3320

[14] M. Fischer, S. Groote, J. G. Körner, M. C. Mauser and B. Lampe, Phys. Lett. B **451** (1999) 406

[15] S. Groote, W. S. Huo, A. Kadeer and J. G. Körner, Phys. Rev. D **76** (2007) 014012

[16] M. Jezabek and J. H. Kühn, Nucl. Phys. B **314** (1989) 1.

[17] A. Denner and T. Sack, Nucl. Phys. B **358** (1991) 46.

[18] G. Eilam, R. R. Mendel, R. Migneron and A. Soni, Phys. Rev. Lett. **66** (1991) 3105.

[19] I. R. Blokland, A. Czarnecki, M. Slusarczyk and F. Tkachov, Phys. Rev. Lett. **93** (2004) 062001

[20] I. R. Blokland, A. Czarnecki, M. Slusarczyk and F. Tkachov, Phys. Rev. D **71** (2005) 054004

[21] CDF-coll, Conf. Note 8104, available from http://www-cdf.fnal.gov/physics/new/top/top.html

[22] T. Aaltonen *et al.* [CDF Collaboration], Phys. Rev. Lett. **102** (2009) 042001

[23] D. O. Carlson and C. P. Yuan, arXiv:hep-ph/9509208.

[24] M. Martinez and R. Miquel, Eur. Phys. J. C **27** (2003) 49

[25] S. Groote, J. G. Körner and M. M. Tung, Z. Phys. C **70** (1996) 281

[26] S. Groote, J. G. Körner and J. A. Leyva, arXiv:0905.4465 [hep-ph]. [27]

[27] M. E. Peskin and D. V. Schroeder, *Reading, USA: Addison-Wesley (1995) 842 p*

[28] I. R. Blokland, "Multiloop calculations in perturbative quantum field theory," Alberta University thesis 2004, UMI-NQ-95909

[29] V. A. Smirnov, Mod. Phys. Lett. A **10** (1995) 1485

[30] V. A. Smirnov, Phys. Lett. B **394** (1997) 205

[31] M. Beneke and V. A. Smirnov, Nucl. Phys. B **522** (1998) 321

[32] F. V. Tkachov, Phys. Lett. B **100** (1981) 65.

[33] K. G. Chetyrkin and F. V. Tkachov, Nucl. Phys. B **192** (1981) 159.

[34] S. Laporta and E. Remiddi, Phys. Lett. B **379** (1996) 283

[35] S. Laporta, Int. J. Mod. Phys. A **15** (2000) 5087

[36] M. Fischer, S. Groote, J. G. Körner and M. C. Mauser, Phys. Rev. D **63** (2001) 031501

[37] A. Czarnecki, Phys. Lett. B **252** (1990) 467.

[38] J. H. Piclum, A. Czarnecki and J. G. Körner, Nucl. Phys. Proc. Suppl. **183** (2008) 48.

[39] A. Frink, J. G. Körner and J. B. Tausk, "Massive two-loop integrals and Higgs physics," arXiv:hep-ph/9709490.

[40] L. Brücher, J. Franzkowski and D. Kreimer, "xloops: Automated Feynman diagram calculation," Comput. Phys. Commun. **115** (1998) 140.

[41] C. W. Bauer, A. Frink and R. Kreckel, "Introduction to the GiNaC Framework for Symbolic Computation within arXiv:cs/0004015.

[42] A. Kadeer, J. G. Körner and U. Moosbrugger, Eur. Phys. J. C **59** (2009) 27

[43] J. G. Körner and G. A. Schuler, Phys. Lett. B **231** (1989) 306.

[44] J. G. Körner and G. A. Schuler, Z. Phys. C **46** (1990) 93.

[45] A. Faessler, T. Gutsche, M. A. Ivanov, J. G. Körner and V. E. Lyubovitskij, Eur. Phys. J. direct C **4** (2002) 18

[46] E. H. Simmons, "Top physics," arXiv:hep-ph/0011244.

[47] J. A. Aguilar-Saavedra, J. Carvalho, N. F. Castro, A. Onofre and F. Veloso, Eur. Phys. J. C **53** (2008) 689

[48] T. Aaltonen *et al.* [CDF Collaboration], Phys. Lett. B **674** (2009) 160

[49] The D0 Collaboration, Model independent measurement of the W boson helicity in top quark decays at D0, D0 note 5722-Conf, 20058 (2008).

[50] C. F. Uhlemann and N. Kauer, Nucl. Phys. B **814** (2009) 195

[51] T. Han, Lectures given at TASI 2004, "Collider phenomenology: Basic knowledge and techniques," arXiv:hep-ph/0508097.

[52] G. Calderon and G. Lopez Castro, Int. J. Mod. Phys. A **23** (2008) 3525.

[53] S. A. Larin, Phys. Lett. B **303** (1993) 113

[54] S. A. Larin and J. A. M. Vermaseren, Phys. Lett. B **259** (1991) 345.

[55] J. H. Piclum, A. Czarnecki and J. G. Körner, to be published

Beauty and charm results from the B factories

Boštjan Golob

Faculty of Mathematics and Physics, University of Ljubljana, Jadranska 19, 1000 Ljubljana, Slovenia
Jožef Stefan Institute, Jamova 39, 1000 Ljubljana, SLovenia

In two lectures we present recent results from the existing B-factories experiments, Belle and BaBar. The discussed topics include short phenomenological motivation, experimental methods and results on B meson oscillations, selected rare B meson decays (leptonic, $b \to s\gamma$ and $b \to s\ell^+\ell^-$), mixing and CP violation in the system of D^0 mesons, and leptonic decays of D_s mesons.

1 Introduction

The lectures presented in this paper are a part of the B-factories lectures prepared in collaboration with A.J. Bevan (also given in the proceedings of the school). To obtain an approximate overview of recent results on flavour physics arising from Belle and BaBar both sets of presentations (each composed of two one-hour lectures) should be consulted.

The lectures presented here include - beside the experimental methods and results - some short phenomenological sketches of motivation and/or interpretation of individual measurements. The author, being an experimentalist, should warn the reader that some examples of phenomenological interpretation are simplified and that serious theoretical treatment requires consultation of references given in the text. Examples are thus to be treated with a grain of salt; to quote the famous poet: *"It is a curious fact that people are never so trivial as when they take themselves seriously." (O. Wilde, 1854 - 1900).*

A large majority of results presented in the lectures arise from the measurements performed with the two experiments taking data at the B-factories, e^+e^- asymmetric colliders running at the center-of-mass (CM) energy $\sqrt{s} = m_{\Upsilon(4S)}c^2$ [1]. $\Upsilon(4S)$, a $b\bar{b}$ bound state with a mass just above the threshold for $\Upsilon(4S) \to B\bar{B}$ decay, is a copious source of B meson pairs. Mesons are produced almost at rest in the CM system, but since the electron beam has an energy higher than the positron one, they are boosted and decay time dependent measurements of meson decays are thus possible. The Belle detector [1], operating at the KEKB collider [2] in Tsukuba, Japan, has so far recorded an integrated luminosity of around 860 fb^{-1}, roughly corresponding to 950×10^6 pairs of B mesons [2]. The BaBar detector [3] at the PEP-II collider in Stanford, USA, has recorded around 550 fb^{-1} of data.

Beside the production of B meson pairs from the $\Upsilon(4S)$ other processes take place in e^+e^- collisions at the given CM energy. For the subject of the lectures the most important is the continuum production of $c\bar{c}$ quark pairs, arising in $e^+e^- \to \gamma^* \to c\bar{c}$. This is sketched in Fig.

---

[1] Here and in the following we adopt a notation where m_X represents a nominal mass value of particle X. If we refer to the reconstructed invariant mass of a system Y we use the notation $m(Y)$.
[2] Both, $B^0\bar{B}^0$ and B^+B^- pairs are produced, at approximately the same rate.

1, where the cross-section for hadron production in electron-positron collisions is plotted as a function of the CM collision energy. The cross-section for the production of $c\bar{c}$ pairs is larger
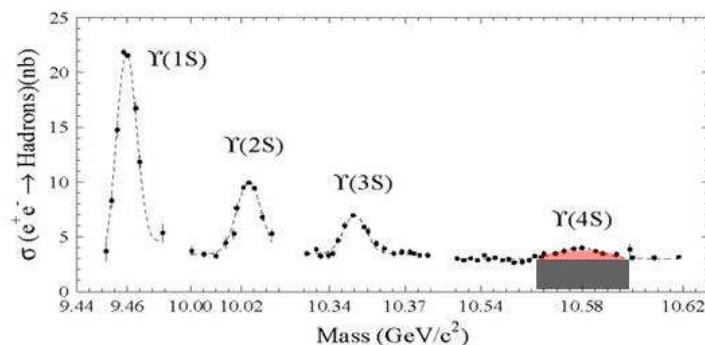
Figure 1: Cross-section for production of hadrons in e^+e^- collisions as a function of $\sqrt{s}$. The resonant production of $\Upsilon(4S) \to B\bar{B}$ is represented as the light shaded area, and the continuum $e^+e^- \to \gamma^* \to q\bar{q}$ as the dark shaded area.

than the one for the B meson production, at the integrated luminosity of KEKB it corresponds to around 1.1×10^9 produced pairs of charmed hadrons.

In the course of the lectures we will mention also some related results from experiments other than B-factories, specifically the ones from the CDF-II experiment at Tevatron [4], recording data in $p\bar{p}$ collisions, and Cleo-c experiment [5] at the e^+e^- collider CESR, running at the $D\bar{D}$ meson pair production threshold. All these experiments provide for a truly diverse experimental environment to study various aspects of heavy flavour physics. *"We all live with the objective of being happy; our lives are all different and yet the same." (A. Frank, 1929 - 1945).*

2 Lecture I

"Never loose an opportunity of seeing anything beautiful, for **beauty** *is God's handwriting."*
(R.W. Emerson, 1803-1882)

2.1 B meson oscillations

The mixing of neutral mesons, that is the transition of a neutral meson P^0 into its antiparticle and vice-versa, appears as a consequence of states of definite flavour (P^0, $\bar{P}^0$) being a linear superposition of the eigenstates of an effective Hamiltonian (states of a simple exponential time evolution) $P_{1,2}$:

$$|P_{1,2}\rangle = p|P^0\rangle \pm q|\bar{P}^0\rangle \quad . \tag{1}$$

For a thorough derivation of the equations describing the oscillations of mesons the reader is advised to follow [6].

While the mass eigenstates have a simple time evolution, the time dependent decay rate of flavour eigenstates depends on the mixing parameters x and y, expressed in terms of the mass

and width difference of $P_{1,2}$ as $x = (m_1 - m_2)/\bar{\Gamma}$ and $y = (\Gamma_1 - \Gamma_2)/2\bar{\Gamma}$. $\bar{\Gamma}$ is the average decay width of the two mass eigenstates. The decay rate of a state initially produced as a P^0 is

$$\frac{d\Gamma(P^0 \to f)}{dt} = e^{-t}\big[\big(|A_f|^2 + |\frac{q}{p}\bar{A}_f|^2\big)\cosh yt + \big(|A_f|^2 - |\frac{q}{p}\bar{A}_f|^2\big)\cos xt$$

$$+ 2\Re\big(\frac{q}{p}A_f^*\bar{A}_f\big)\sinh yt - 2\Im\big(\frac{q}{p}A_f^*\bar{A}_f\big)\sin xt\big] . \tag{2}$$

In the above equation t is a dimensionless decay time, defined in terms of a proper decay time t' as $t = t'\bar{\Gamma}$. The notation A_f, $\bar{A}_f$ is used to represent instantaneous amplitudes for $P^0 \to f$ and $\bar{P}^0 \to f$ decays. It is obvious from Eq. (2) that using the decay time distribution of experimentally accessible flavour eigenstates one can determine the mixing parameters x and y. Moreover, the effect of the mixing parameters on $d\Gamma/dt$ depends on the chosen decay channel $(A_f, \bar{A}_f)$. The decay time distribution of an initially produced $\bar{P}^0$ is obtained from Eq. (2) by replacing $A_f \leftrightarrow \bar{A}_f$ and $q/p \to p/q$. The decay time distributions for decays to conjugated final state $\bar{f}$ are obtained by a simple $f \to \bar{f}$ transformation. The above decay rates are illustrated in Fig. 2 for several values of x and y.
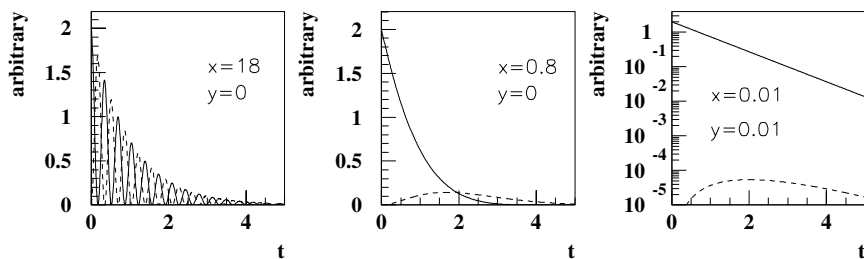
Figure 2: Probability for an initially produced meson P^0 to decay at time t as P^0 (full curve) or $\bar{P}^0$ (dashed curve). Qualitatively the left example roughly corresponds to the case of B_s^0 mesons, the middle one to the case of B^0 mesons and the right one to the case of D^0 mesons. Note the logarithmic scale on the right plot.

The neutral B meson pairs[3] from $\Upsilon(4S)$ decays are produced in a quantum coherent state with the quantum numbers corresponding to that of the $\Upsilon(4S)$. Before the coherence is disturbed by a decay of one of the mesons, the pair is always in a $B^0 - \bar{B}^0$ state. The decay rates given above are valid only after the first of the two mesons decays. To be used in measurements of B^0 mesons produced from $\Upsilon(4S)$, the decay time t in Eq. (2) should thus be changed to Δt, the difference between the decay times of the first and the second neutral B meson (and the exponential factor should include $|\Delta t|$ instead of t).

The experimental method of measuring B^0 meson oscillation frequency[4] x relies on a similar method as the one used for measuring the CP violation (see lectures by A.J. Bevan). However, instead of CP specific final states, flavour specific final states of B meson decays are used (like

---

[3]We will use notation B^0 for B_d^0 mesons, while for the strange B mesons we will use a strict B_s^0 notation.

[4]Strictly speaking experiments in B system measure the mass difference between the two eigenstates, Δm. However, since the dimensionless mixing parameter $x = \Delta m/\bar{\Gamma}$ can be more directly compared for different meson species, we prefer to use this. Similarly as for the notation of B mesons, we use Δm and x for the B_d^0 mesons and Δm_s and x_s for B_s^0 mesons. In lecture II we will use x_D and y_D to denote the corresponding mixing parameters in the D^0 system.

$B^0 \to J/\psi K^{*0}$, $K^{*0} \to K^+\pi^-$), which allow to determine the flavour of the decaying B meson. The method is sketched in Fig. 3. The measured t distribution deviates from Eq. (2) due to several reasons: usage of flavour specific final state ($\bar{A}_f = A_{\bar{f}} = 0$), negligible decay width difference ($y \ll 1$), probability of wrong flavour tagging (w) and finite accuracy in determination of Δt (resolution function $R_{\text{sig}}(\Delta t)$). Taking into account these corrections, the final expected decay time distributions are

$$\frac{d\Gamma(B^0 \to f)}{d\Delta t} = e^{-|\Delta t|}|A_f|^2\big[1 + (1-2w)\cos(x\Delta t)\big] \otimes R_{\text{sig}}(\Delta t)$$

$$\frac{d\Gamma(\bar{B}^0 \to f)}{d\Delta t} = e^{-|\Delta t|}|A_f|^2\big[1 - (1-2w)\cos(x\Delta t)\big] \otimes R_{\text{sig}}(\Delta t) \quad , \qquad (3)$$

where the $\otimes$ sign denotes a convolution. The resolution function is composed as a convolution of several Gaussian functions [7]. The average accuracy of Δt determination is around 1.4 ps (the lifetime of B^0 mesons is 1.53 ps [8]).
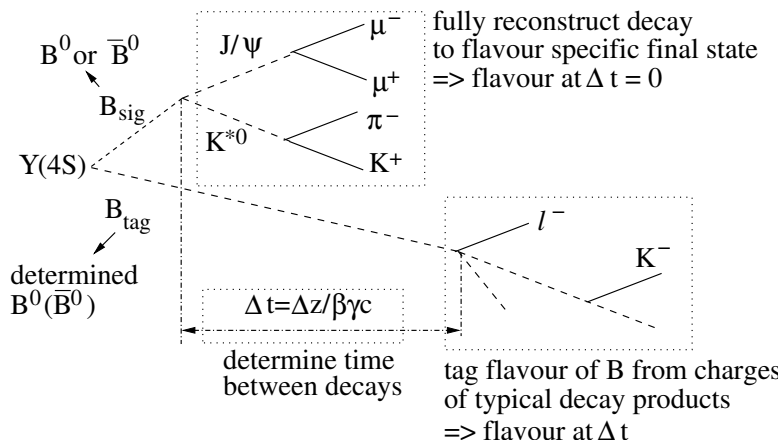
Figure 3: Illustration of the method used to measure the B^0 oscillation frequency x.

The most precise single measurement of x [9] uses several flavour specific final states to reconstruct the signal B^0 meson decays. Results are presented in Fig. 4 (left) in form of the asymmetry

$$\frac{d\Gamma(B^0 \to f)/d\Delta t - d\Gamma(\bar{B}^0 \to f)/d\Delta t}{d\Gamma(B^0 \to f)/d\Delta t + d\Gamma(\bar{B}^0 \to f)/d\Delta t} = (1-2w)\cos x\Delta t \otimes R_{\text{sig}}(\Delta t) \quad . \qquad (4)$$

The average value of existing Δm measurements [10], expressed in terms of $x = \Delta m/\bar{\Gamma}$, is $x = 0.776 \pm 0.008$.

Calculation of $\langle \bar{B}^0|H_{eff}|B^0\rangle$ matrix element, visualized by the loop diagram of Fig. 4 (right), results in [11]

$$\Delta m_q = 2\frac{G_F^2 m_W^2 \eta_B m_{B_q} B_{B_q} f_{B_q}^2}{12\pi^2} S_0(m_t^2/m_W^2)|V_{tq}^* V_{tb}|^2\big(1 + \mathcal{O}(\frac{m_b^2}{m_t^2})\big) \quad . \qquad (5)$$

The equation is written using a subscript q to emphasize that the same relation is also appropriate for the system of B_s^0 mesons. Using the measured value of the oscillation frequency for
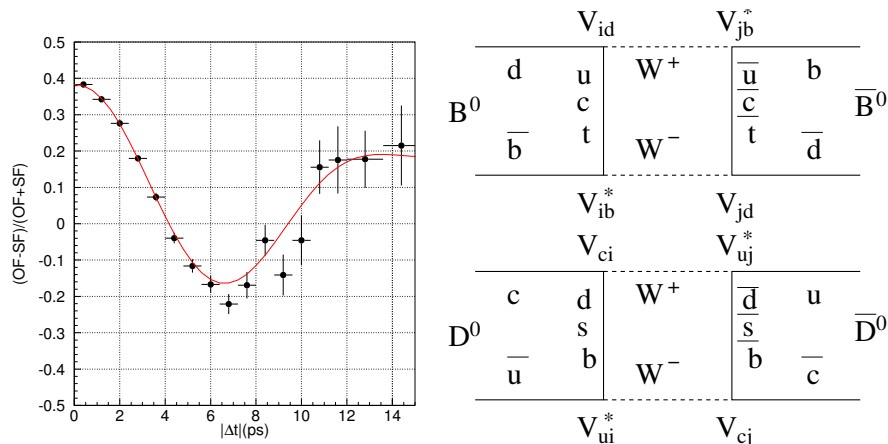
Figure 4: Left: Result of B^0 oscillation frequency measurement [9] shown in the form of the asymmetry (4). Right: Loop diagram describing the $B^0 \to \bar{B}^0$ transition (top) and the short distance contribution to $D^0 \to \bar{D}^0$ (bottom) transition.

B^0 mesons one can determine elements of the Cabibbo-Kobayashi-Maskawa (CKM) matrix, if the QCD parameters η_B, B_{B_q}, f_{B_q} are known[5]. Due to their non-perturbative nature these quantities are difficult to estimate (usualy the lattice QCD calculations, LQCD, are exploited) and result in a large uncertianty of CKM elements determination. The constraints from the measured value of Δm on parameters $(\bar{\rho}, \bar{\eta})$ used to parametrize the CKM matrix [12] are shown in Fig. 5 (left) [13]. Since 2006 the oscillation frequency is measured also in the system of B_s^0 mesons, $x_s = 25.5 \pm 0.6$ [14]. In the ratio of $\Delta m_s / \Delta m$ the QCD uncertainties cancel to a large extent. The measured ratio $\Delta m_s / \Delta m$ is thus much more constraining than Δm constraint alone (Fig. 5 (left)), and actually at the moment represents the most constraining measurement for the $\bar{\rho}$ among various flavour physics studies.

2.2 Leptonic B meson decays

Measurements of charged B meson leptonic decays are interesting for several reasons: theoretically they are easier to interpret compared to semileptonic and hadronic decays, within the SM the measured rates can potentially yield the value of the least known CKM element V_{ub}, and they are sensitive to possible contributions of processes beyond the SM. A Feynman diagram of an arbitrary pseudoscalar meson leptonic decay is shown in Fig. 5 (right). The QCD effects are described by a single parameter f_P, the meson decay constant describing the overlap of the two quarks wave function. The leptonic decays of a pseudoscalar mesons are helicity suppressed, the expected ratios of decay widths are $1 : 4 \times 10^{-3} : 10^{-7}$ for the τ, μ and e decays, respectively. Despite the problems due to at least two undetected neutrinos in the final state the decays to τ leptons are the only decays observed so far.

The method of measurement consist of fully (partially) reconstructing the accompanying B meson using a large number of hadronic (semileptonic) decay modes. After the particles assigned to the tagging meson are successfully identified one searches for one or three charged

---

[5]Function $S_0(x)$ is known.
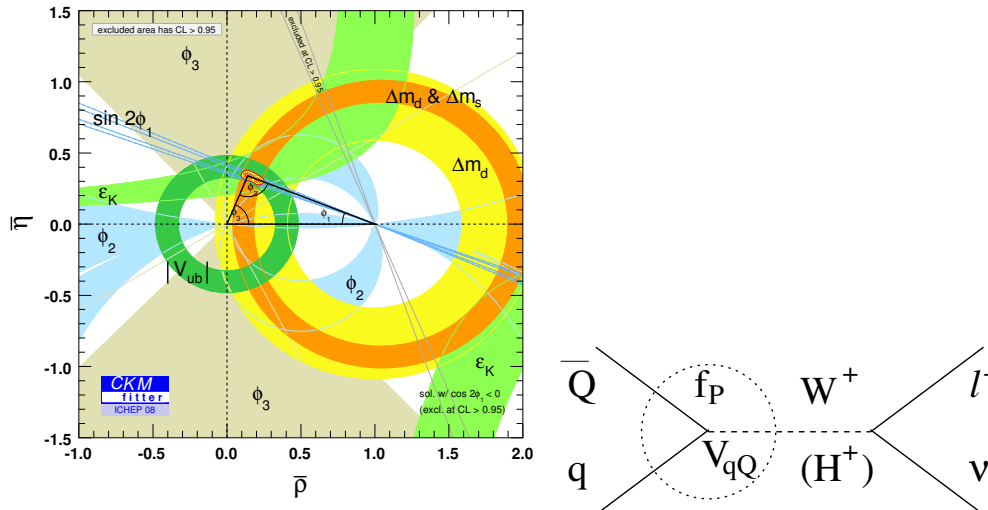
Figure 5: Left: Constraints in the $(\bar{\rho}, \bar{\eta})$ plane arising from various measurement [13]. The light shaded region denoted by Δm_d represents the constraint from the B^0 oscillation frequency, and the dark shaded region denoted by $\Delta m_d \& \Delta m_s$ the constraint from the ratio of B^0 and B^0_s oscillation frequencies. Right: Feynman diagram of a pseudoscalar meson leptonic decay. The QCD effects are described by the decay constant f_P. Beside the SM W^+ contribution also particles not included in the SM (like the charged Higgs boson) may contribute.

tracks originating from the τ decay. Finally the energy in the electromagnetic calorimeter (E_{ECL}) not assigned to the particles used in the previous reconstruction is examined. Signal decays with only neutrinos left in the final state are expected to peak at $E_{ECL} \sim 0$. The E_{ECL} distribution of selected events in the measurement by Belle [15] is shown in Fig. 6 (left). The excess of events above the expectation from MC simulation at low values of E_{ECL} is the signal for the $B^+ \rightarrow \tau^+ \nu_\tau$ decays. From the fit to the distribution the branching fraction $Br(B^+ \rightarrow \tau^+ \nu_\tau) = (1.65 \pm_{0.37}^{0.38} \pm_{0.37}^{0.35}) \times 10^{-4}$ is obtained, where the main contribution to the systematic error arises from the uncertainties in the shape of the E_{ECL} signal and background distributions. A similar measurement performed by BaBar [16] yields $Br(B^+ \rightarrow \tau^+ \nu_\tau) = (1.2 \pm 0.4 \pm 0.4) \times 10^{-4}$, and the average of all measurements provided by Heavy Flavour Averaging Group is $Br(B^+ \rightarrow \tau^+ \nu_\tau) = (1.51 \pm 0.33) \times 10^{-4}$ [10].

Calculation of $\Gamma(B^+ \rightarrow \tau^+ \nu_\tau)$ yields [17]

$$\Gamma(B^+ \rightarrow \tau^+ \nu_\tau) = \frac{G_F^2}{8\pi} |V_{ub}|^2 f_B^2 m_B m_\tau^2 (1 - \frac{m_\tau^2}{m_B^2}) \left[1 - \frac{m_B^2}{m_H^2} \tan^2 \beta\right]^2 \ , \tag{6}$$

where the last factor in brackets is a correction due to a possible contribution of the charged Higgs boson. The measured value is in agreement with the SM expectation (using LQCD prediction $f_B = (216 \pm 22)$ MeV [18], and $|V_{ub}| = (3.9 \pm 0.5) \times 10^{-3}$ [17]) and allows to put constraints on the parameters $(m_H, \tan \beta)$ in the two Higgs doublet models (m_H is the charged Higgs boson mass and $\tan \beta$ is the ratio of the vacuum expectation values). The constraints
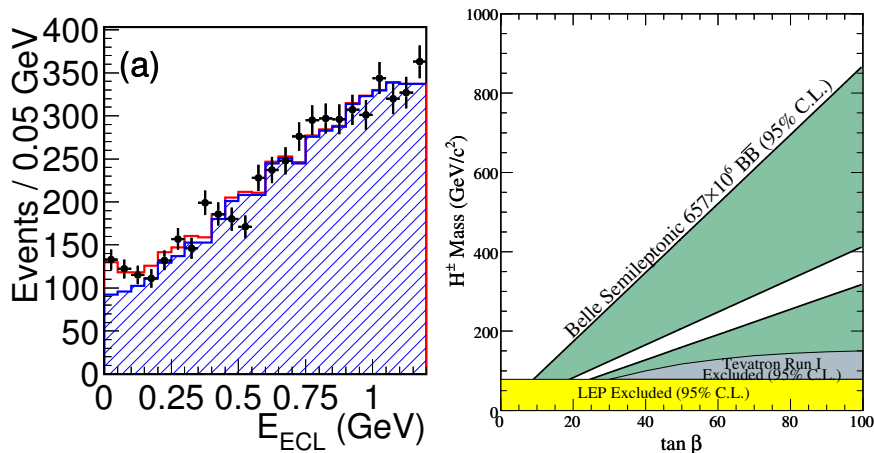
Figure 6: Left: Distribution of the energy in the electromagnetic calorimeter for selected $B^+ \to \tau^+ \nu_\tau$ candidate events. The excess of data (points with error bars) above the expectation from simulation (histogram) is the signal. Right: Excluded region (shaded) in the $(m_H, \tan\beta)$ plane arising from the measurement of $Br(B^+ \to \tau^+ \nu_\tau)$ [15].

arising from the Belle measurement are shown in Fig. 6 (right).

2.3 $b \to s\gamma$ decays

Decays involving the $b \to s\gamma$ transition cannot occur at the tree level in SM. Such a flavor changing neutral current (FCNC) is only possible as a higher order process and is thus sensitive to possible contributions of New Physics (NP). Some possible diagrams, within and beyond the SM, are shown in Fig. 7 (left). At the parton level the photon energy in the CM frame is approximately half of the b quark mass. Also at the hadron level E_γ is sensitive to m_b, which is important for determination of $|V_{ub}|$ and $|V_{cb}|$ from semileptonic B decays.

There are both, theoretical and experimental difficulties in the measurements. The former arise since in all experimental methods there is a lower cut-off applied to E_γ. To determine the branching fraction, for example, one has to extrapolate the partial rate for $E_\gamma > E_{\text{cut}}$ to the full energy region using models, which introduces theoretical uncertainties. On the experimental side the efforts are being made to lower the cut-off, but this makes problems due to the huge backgrounds even more severe (see Fig. 7 (right)). The name of the game is thus to suppress the backgrounds to an acceptable level; *"Your background and environment is with you for life. No question about that." (S. Connery, 1930).* Methods of reconstruction may be divided into inclusive, semi-inclusive and exclusive ones. In an inclusive measurement only the photon is reconstructed. From the total E_γ distribution of events recorded at the $\Upsilon(4S)$ peak an analogous distribution of events, recorded 60 MeV below the peak is subtracted. The latter represents only the photons arising from $e^+e^- \to q\bar{q}$ (continuum) events, and if the distribution is scaled according to the integrated luminosity of both samples, the remainder after the subtraction represents the energy distribution of photons from B meson decays. A search is made for photon pairs consistent with π^0 or η decays and such γ's are removed from the selected sample. The remaining background is estimated using simulated samples but normalized using data
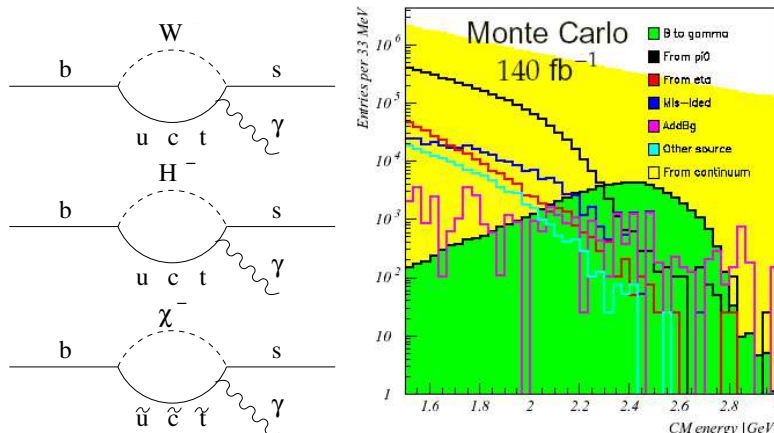
Figure 7: Left: SM (top) and some NP (middle and bottom) contributions to the $b \to s\gamma$ process. Right: Simulated photon energy distributions from various processes. The smallest shaded region is the contribution of $b \to s\gamma$ (note the logarithmic scale).

control samples.

Result of such an inclusive method is shown in Fig. 8 (left) [19]. E_γ distribution peaks at
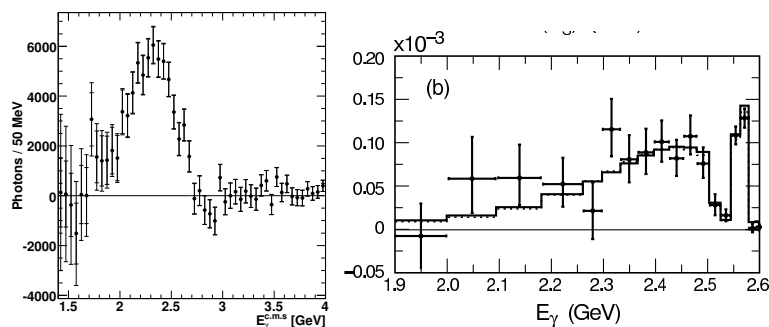
Figure 8: Left: Raw CM system photon energy distribution for inclusively reconstructed $b \to s\gamma$ decays [19]. Right: Differential branching fraction of $B \to X_s\gamma$ as a function of E_γ obtained in semi-inclusive measurement [20].

around half of the b quark mass and is consistent with zero above the kinematic limit for $B \to K\gamma$ decays, confirming the correctness of the subtraction procedure. To determine the branching fraction and the correct shape of the energy distribution one has to apply a deconvolution method to the raw spectrum, correct it for the efficiency of reconstruction, subtract a simulated contribution of $b \to d\gamma$ decays ($\sim 4\%$) and make the transformation to the B meson rest frame. The partial branching fraction in the interval $E_\gamma > 1.7$ GeV is found to be $Br(b \to s\gamma) = (3.31 \pm 0.19 \pm 0.37 \pm 0.01) \times 10^{-4}$. The last uncertainty is due to the boost from the CM to the B meson frame, and the largest systematic uncertainty arises from the normalization of backgrounds other than π^0 and η.

As an example of a semi-inclusive measurement we present the analysis of $B \to X_s \gamma$ by BaBar collaboration [20], where X_s represent a sum of various decay modes with $K^{\pm}$, K_S, $\pi^{\pm}$ and η mesons in the final state. The photon energy is in this method calculated from the invariant mass of the hadronic system $m(X_s)$ which results in a better resolution compared to the measured photon energy in the electromagnetic calorimeter. The background is suppressed using neural network for the rejection of continuum events and vetoes for γ's from π^0 and η mesons. To calculate the branching fraction for $B \to X_s \gamma$ the number of observed events must be corrected for the fraction of decays not taken into account in the reconstruction (25% at low $m(X_s)$ due a to non-inclusion of K_L, and higher at higher masses). The resulting differential branching fraction for $E_\gamma > 1.9$ GeV is shown in Fig. 8 (right). The integral rate in the $E_\gamma > 1.9$ GeV interval is found to be $Br(b \to s\gamma) = (3.27 \pm 0.18 \pm_{0.40}^{0.55} \pm_{0.12}^{0.04}) \times 10^{-4}$, where the last error is due to the QCD parameters affecting the efficiency.

The measured branching fractions impose limits on possible contribution of charged Higgs boson. The world average of inclusive branching fraction is $Br(b \to s\gamma) = (3.52 \pm 0.23 \pm 0.09) \times 10^{-4}$ [10]. The 95% C.L. limit following from [21] is $m_H > 300$ GeV for any value of $\tan \beta$. In all measurements also the first and the second moment of the photon energy spectra are determined. These can be expressed with the same QCD parameters entering also the determination of $|V_{ub}|$ and $|V_{cb}|$ in inclusive semileptonic B decays. Details of a simultaneous fit performed to photon energy spectrum in $b \to s\gamma$ and lepton momentum and hadronic mass spectra in semileptonic decays to determine the elements of CKM matrix is described in [10].

2.4 $b \to s\ell^+\ell^-$ decays

Decays involving the $b \to s\ell^+\ell^-$ parton process are another example of a FCNC transition. From that point of view they are interesting for the same reasons as the $b \to s\gamma$ decays. Again, the inclusive decays are theoretically easier to interpret than the exclusive ones. Nevertheless, a lot of work has been done in identifying the observables in exclusive decays, especially $B \to K^*\ell^+\ell^-$, for which the theoretical uncertainties are small [22]. Feynman diagrams contributing to $b \to s\ell^+\ell^-$ are shown in Fig. 9 (left). The differential decay rate $d\Gamma/dq^2$, where q^2 is the
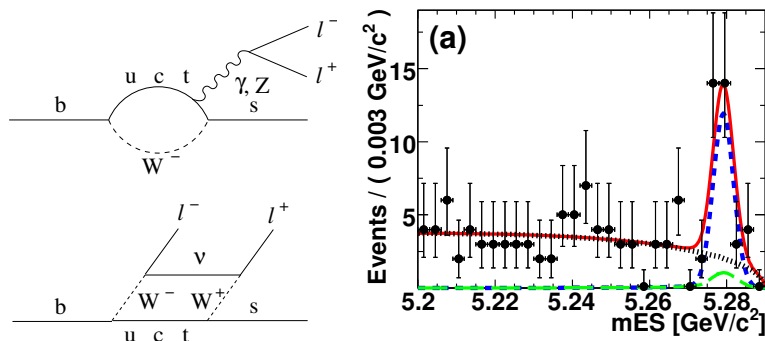
Figure 9: Left: SM Feynman diagrams for $b \to s\ell^+\ell^-$. Right: Energy substituted B meson mass for reconstructed $B \to K^*\ell^+\ell^-$ decays. The distribution is shown for a part of the full sample with low q^2 [24].

invariant mass of the lepton pair, can be described in terms of effective Wilson coefficients

C_7^{eff}, C_9^{eff} and C_{10}^{eff}, which include the perturbative part of the process and thus dependence on heavy masses of SM particles m_W, m_t, as well as on possible NP masses m_{NP}. The absolute value of the coefficient C_7^{eff} can be constrained from the measured rate of $b \to s\gamma$ process, while in $b \to s\ell^+\ell^-$ additional information (on sign of C_7^{eff}, as well as C_9^{eff}, C_{10}^{eff}) can be obtained due to the interference of the two amplitudes shown in Fig. 9 (left). NP could change the values of the Wilson coefficients as well as add new operators causing the transition. In exclusive $B \to K^*\ell^+\ell^-$ decays the theoretical description includes beside the Wilson coefficients also the non-perturbative part expressed by the form factors which are predicted with an accuracy of around 30% [23]. This uncertainty is significantly reduced in some observables arising from the study of angular distributions, like the lepton forward-backward asymmetry (A_{FB}) and the fraction of longitudinally polarized K^*'s (F_L).

BaBar performed a study of $B \to K^*\ell^+\ell^-$ decays in [24]. The reconstruction proceeds through identification of a lepton pair ($\mu^+\mu^-$ or e^+e^-) with invariant mass not in the range of charmonium states J/ψ or $\psi(2S)$. The K^* can be either charged or neutral, reconstructed through $K\pi$, $K\pi^0$ and $K_S\pi$ final states. The signal can be seen in the energy substituted B meson mass, $M_{ES} = (E_{CM}/2)^2 - (\sum_i \vec{p}_i)^2$, where $\vec{p}_i$ and E_{CM} are the B decay products momenta and e^+e^- collision energy, respectively, calculated in the CM frame (Fig. 9 (right)). The background is composed of combinatorial one (described by reconstructing events with $\mu^\pm e^\mp$ lepton pairs), hadrons misidentified as muons (in $\mu^\pm\mu^\mp$ channel) and peaking background from $B \to D\pi$ decays where the charmed meson decays to $K^*\pi$ (vetoed by requiring the invariant mass of $K^*\pi$ not to be consistent with a D meson).

For the reconstructed events the distribution of the kaon helicity angle in the rest frame of K^* is investigated to obtain the fraction of longitudinally polarized K^*'s (F_L). F_L value is then used as an input to the fit to the distribution of the angle between the lepton and K^* in the $\ell^+\ell^-$ rest frame. This angle follows a $1 + 3F_L + (1 - F_L)\cos^2\theta_\ell + (8/3)A_{FB}\cos\theta_\ell$ distribution. The A_{FB} is the lepton forward-backward asymmetry which can be predicted in terms of the Wilson coefficients. In Fig. 10 (left) measured A_{FB} is shown as a function of q^2 for the measurement by BaBar as well as the most recent measurement by Belle collaboration [25]. The measured values are compared to the SM prediction and the expectation for the Wilson coefficient C_7^{eff} of reversed sign. In general the measurements seems to be shifted to larger asymmetry values than predicted.

Similarly as for the $b \to s\gamma$ decays, also for $b \to s\ell^+\ell^-$ semi-inclusive measurements have been performed by summing up various hadronic decay modes of the strange quark system (K_S or $K^\pm$ with 0 to 4 pions) accounting for around 70% of the total decay rate. The average of the branching fraction measurements is $Br(B \to X_s\ell^+\ell^-) = (4.50\pm^{1.03}_{1.01}) \times 10^{-6}$ [10].

Various measurements of FCNC can be combined to put constraints on possible NP contribution to Wilson coefficients. Within a Minimal Flavour Violation scenario these constraints are presented in Fig. 10 (right) [26]. Measurements of $Br(B \to X_s\gamma)$, $Br(B \to X_s\ell^+\ell^-)$, $Br(K \to \pi\nu\nu)$ and $Br(B_s \to \mu\mu)$ are used as the input. The combination of measurements is consistent with the SM ($\delta C_i = 0$) although there are large areas corresponding to non-SM contributions possible.

3 Lecture II

"**Charm** *is...a way of getting the answer yes without having to ask any clear question.*" (A. Camus, 1913-1960)
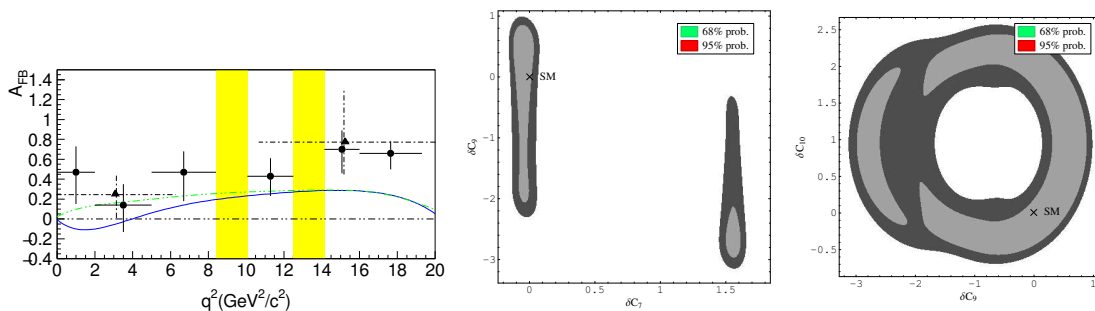
Figure 10: Left: Measured A_{FB} as a function of q^2 in $B \to K^* \ell^+ \ell^-$ decays. The data points marked with triangles (dashed-dotted error bars) are from [24] and circular data points (full error bars) from [25]. The shaded regions represent q^2 intervals not included in the measurement (J/ψ, $\psi(2S)$ regions). Full line represents the SM prediction and the dashed curve prediction with $C_7^{\mathrm{eff}} = -C_7^{\mathrm{SM, eff}}$. Right: Constraints on NP contributions to Wilson coefficients arising from measurements of various FCNC processes [26]. The SM corresponds to $\delta C_i = 0$. Light shaded areas represent the 68% C.L. and dark shaded the 95% C.L. region.

3.1 D meson oscillations

The second lecture is devoted to results in physics of charmed hadrons from B-factories. Charm physics in recent years gained in interest of both, experimental and theoretical physicists, mainly due to new interesting results from Belle and BaBar. Both experiments are not only factories of B mesons but also of charmed hadrons (see Section 1 and Fig. 1). Contemporary charm physics has a twofold impact: as a ground of theory predictions tests, mainly tests of LQCD, and as a self-standing field of SM measurements and NP searches. An example of the first kind are the measurements of charmed meson decay constants, to be compared to LQCD calculations, to verify those and thus enable a more reliable estimates of the CKM matrix elements from the measurements in the B meson sector. The outstanding examples of the second group of measurements are recent observations of D^0 mixing and searches for the CP violation in processes involving charmed hadrons.

Neutral D mesons are the only neutral meson system composed of up-like quarks. Hence a different contribution of virtual new particles than in the mixing of other neutral mesons is possible in the loops of diagrams describing the $D^0 \leftrightarrow \bar{D}^0$ transition (Fig. 4 (right)). However, the short distance contribution to the mixing rate, illustrated by the box diagram, is extremely small. The reason is the effective GIM suppression; calculation of the amplitude for this transition reveals [27] that it is proportional to $V_{cs}^* V_{cd}^* V_{ud} V_{us} (m_s^2 - m_d^2)/m_c^2$. Hence the amplitude is doubly Cabibbo suppressed, and furthermore arises only as a consequence of SU(3) flavour symmetry breaking. The resulting oscillation frequency defined in Sect. 2.1 is $|x_D| = \mathcal{O}(10^{-5})$. This unobservable effect is hindered by long distance contribution to the transition amplitude, for example from states accessible to both, D^0 and $\bar{D}^0$ (e.g. $D^0 \to K^+ K^- \to \bar{D}^0$). This contribution is difficult to estimate. Current calculations [28] within the SM predict $|x_D|$, $|y_D| \lesssim \mathcal{O}(10^{-2})$. The result illustrates the order of magnitude of the mixing parameters to be expected in the D^0 system (compare to measured values of x, x_s given in Sect. 2.1) as well as the large theoretical uncertainty of the predictions.

The time evolution of an initially produced D^0 meson follows Eq. (2) with the simplification

due to $|x_D|$, $|y_D| \ll 1$:

$$\frac{d\Gamma(D^0 \to f)}{dt} = e^{-t}|A_f + \frac{q}{p}\frac{ix_D + y_D}{2}A_{\bar{f}}|^2 + \mathcal{O}(x_D^3, \ y_D^3) \ . \tag{7}$$

The time integrated rate for an initially produced D^0 meson to decay as a $\bar{D}^0$, $R_M = (x_D^2 + y_D^2)/2 \sim 10^{-4}$, is small and represents the reason for a 31 years time span between the discovery of D^0 mesons and the experimental observation of the D^0 mixing. According to the famous writer, *"The duration of passion is proportionate with the original resistance of the woman."* *(H. de Balzac, 1799 - 1850)*, this was a further motivation to perform such a measurement.

There are several methods and selection criteria common to various measurements of D^0 mixing. Tagging of the flavour of an initially produced D^0 meson is achieved by reconstruction of decays $D^{*+} \to D^0\pi_s^+$ or $D^{*-} \to \bar{D}^0\pi_s^-$. The charge of the characteristic low momentum pion π_s determines the tag. The energy released in the D^* decay, $q = m(D^*) - m(D^0) - m_\pi$, has a narrow peak for the signal events and thus helps in rejecting the combinatorial background. D^0 mesons produced in B decays have a different decay length distribution and kinematic properties than the mesons produced in fragmentation. In order to obtain a sample of neutral mesons with uniform properties one selects D^* mesons with momentum above the kinematic limit for the B meson decays. The decay time is obtained from the reconstructed momentum and decay length of D^0 meson, and the latter is obtained from a common vertex of D^0 decay products and an intersection point of D^0 momentum vector and the e^+e^- interaction region.

Methods of measuring the mixing parameters as well as sensitivities depend on specific final states chosen. The first to be described are decays to CP eigenstate f_{CP}. In the limit of negligible CP symmetry violation (CPV, described in Section 3.2) the mass eigenstates $D_{1,2}$ coincide with the CP eigenstates (in case of no CPV $q/p = 1$, see Eq. (1)). In decays $D^0 \to f_{CP}$ only the mass eigenstate component of D^0 with the CP eigenvalue equal to the one of f_{CP} contributes. By measuring the lifetime of D^0 in decays to f_{CP} one thus determines the corresponding $1/\Gamma_1$ or $1/\Gamma_2$. On the other hand, flavour specific final states like $K^-\pi^+$ have a mixed CP symmetry. The measured value of the effective lifetime in these decays corresponds to a mixture of $1/\Gamma_1$ and $1/\Gamma_2$. The relation between the two lifetimes can be written as [29]

$$\tau(f_{CP}) = \frac{\tau(D^0)}{1 + \eta_f y_{CP}} \ , \tag{8}$$

where $\tau(f_{CP})$ and $\tau(D^0)$ are the lifetimes measured in $D^0 \to f_{CP}$ and $D^0 \to K^-\pi^+$, respectively. $\eta_f = \pm 1$ denotes the CP eigenvalue of f_{CP}. The relative difference of the lifetimes is described by the parameter y_{CP}. Expressed in terms of the mixing parameters, y_{CP} reads [29] $y_{CP} = y_D \cos\phi - (1/2)A_M x_D \sin\phi$, with A_M and ϕ describing the CPV in mixing and in interference between mixing and decays, respectively. In case of no CPV, $A_M = \phi = 0$ and $y_{CP} = y_D$.

The measurement of y_{CP} by Belle [30] represents the first evidence of D^0 mixing [6]. Number of reconstructed decays to CP-even states K^+K^- and $\pi^+\pi^-$ were 110×10^3 and 50×10^3, with purities of 98% and 92%, respectively. A simultaneous fit to the decay time distributions of KK, $\pi\pi$ and $K\pi$ decays was performed with y_{CP} as a common free parameter. In order to perform a precision measurement of lifetime in each of the decay modes a special care should

---

[6]Published simultaneously with the measurement of $D^0 \to K^+\pi^-$ decays by BaBar [31] which also gives evidence of the mixing.

be devoted to a proper description of t resolution function in various data-taking periods (for details the reader is referred to the original publication). The t distributions and the result of the fit are presented in Fig. 11. The quality of the fit ($\chi^2/n.d.f. = 313/289$) confirms an accurate description of the resolution effects. The measured value of y_{CP} is $(1.31\pm0.32\pm0.25)\%$
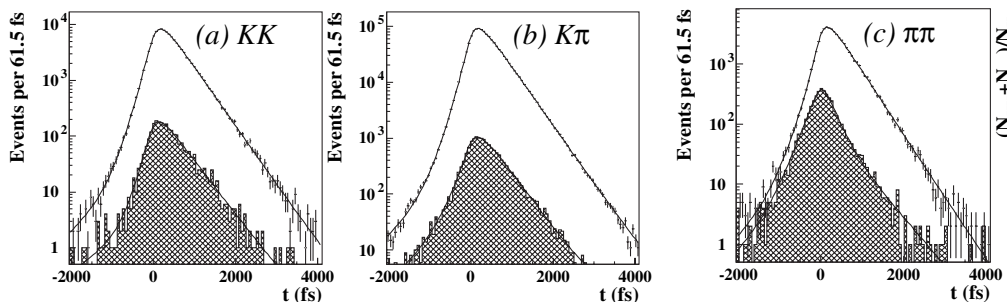
Figure 11: Decay time distributions of $D^0 \to h^+h^-$ ($h = K$, π) [30]. Hatched histogram is the contribution of background obtained from $m(h^+h^-)$ sidebands. Full line is the result of a simultaneous fit to all three distributions with y_{CP} as a common free parameter.

and the largest contribution to the systematic uncertainty arises due to a possible small detector induced bias in the decay time determination. y_{CP} deviates from the null value by more than three standard deviations including the systematic uncertainty. This evidence is confirmed by a similar measurement performed by the BaBar collaboration [32], finding $y_{CP} = (1.24\pm0.30\pm0.13)\%$.

Another possibility to look for the effect of mixing represent decays of initially produced D^0's to a wrong-sign final state $K^+\pi^-$. While the more abundant D^0 decays lead to the $K^-\pi^+$ charge combination, the wrong-sign combination can be reached through doubly Cabibbo suppressed (DCS) decays or through a $D^0 \to \bar{D}^0$ mixing followed by a Cabibbo favored (CF) $\bar{D}^0$ decay. In order to separate the mixing contribution from the DCS decays an analysis of the decay time distribution must be performed. The t-dependent decay rate, $d\Gamma(D^0 \to K^+\pi^-) \propto [R_D + \sqrt{R_D}y'_D t + (1/4)(x'^2_D + y'^2_D)t^2]e^{-t}$, consists of three terms corresponding to DCS term (R_D), mixing term ($x'^2_D + y'^2_D$) and the interference between the two. Additional complication in the interpretation of the result arises since the decay rate depends on parameters x' and y' which are the mixing parameters rotated by a strong phase difference between the amplitudes of CF and DCS decays. In [31] BaBar collaboration fitted the t distribution of around 4000 reconstructed wrong-sign decays. Result of the fit is presented in Fig. 12 (left) in terms of the allowed region in (x'^2, y') plane. While the central value is in the physically forbidden region ($x'^2 < 0$) the no-mixing point $((x'^2, y') = (0, 0))$ is excluded by a confidence level corresponding to 3.9 standard deviations. Numerically they find $x'^2 = (-0.22 \pm 0.33 \pm 0.21) \times 10^{-3}$ and $y' = (0.97 \pm 0.44 \pm 0.31)\%$.

The method which allows for a direct determination of both mixing parameters, x_D and y_D, is the study of decays into self conjugated multi-body final states. Several intermediate resonances can contribute to such a final state. In the recent measurement by Belle [33] the $K_S\pi^+\pi^-$ final state was analyzed, where contributions from CF decays (e.g. $D^0 \to K^{*-}\pi^+$), DCS decays (e.g. $D^0 \to K^{*+}\pi^-$) and decays to CP eigenstates (e.g. $D^0 \to \rho^0 K_S$) are present. Individual contributions can be identified by analyzing the Dalitz distribution of the decay.
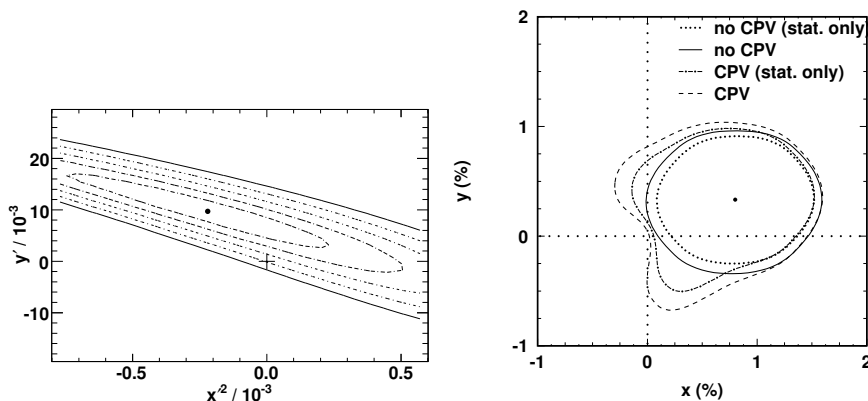
Figure 12: Left: Likelihood contours in (x'^2, y') plane arising from the measurement of $D^0 \to K^+\pi^-$ decays [31]. The lines correspond to 1-5 σ C.L., the dot represents the central value and the cross the no-mixing point. Right: 95% C.L. contour of (x_D, y_D) as determined in the time-dependent Dalitz study of $D^0 \to K_S\pi^+\pi^-$ [33]. Regions arising from the fit with neglected and allowed CPV, as well as neglecting or incorporating the systematic uncertainty are shown.

Due to the interference among different types of decays it is possible to determine their relative phases (unlike in $D^0 \to K^+\pi^-$ decays where the relative phase between DCS and CF decays cannot be determined). And most importantly, since these types of intermediate states also exhibit a specific time evolution one can determine directly the mixing parameters x_D and y_D by studying the time evolution of the Dalitz distribution. The signal p.d.f. for a simultaneous fit to the Dalitz and decay-time distribution is

$$|\langle K_S\pi^+\pi^-|D^0(t)\rangle|^2 = |\frac{1}{2}\mathcal{A}(m_-^2, m_+^2)\left[e^{-i\lambda_1 t} + e^{-i\lambda_2 t}\right] + \frac{1}{2}\overline{\mathcal{A}}(m_-^2, m_+^2)\left[e^{-i\lambda_1 t} - e^{-i\lambda_2 t}\right]|^2 \quad , \quad (9)$$

composed of an instantaneous amplitude for D^0 decay, $\mathcal{A}(m_-^2, m_+^2)$, and an amplitude for the $\bar{D}^0$ decay, $\bar{\mathcal{A}}(m_-^2, m_+^2)$, arising due to a possibility of mixing. They both depend on the Dalitz variables $m_-^2 = m^2(K_S\pi^-)$ and $m_+^2 = m^2(K_S\pi^+)$. The dependence on the mixing parameters is hidden in $\lambda_{1,2} = m_{1,2} - i\Gamma_{1,2}/2$. If CPV is neglected the amplitude for $\bar{D}^0$ tagged decays is $|\langle K_S\pi^+\pi^-|\bar{D}^0(t)\rangle|^2(m_+^2, m_-^2, t) = |\langle K_S\pi^+\pi^-|D^0(t)\rangle|^2(m_-^2, m_+^2, t)$. As in the case of B^0 oscillation measurements the p.d.f. of Eq. (9) must be corrected to include the finite resolution on the decay time.

Based on $\sim 500 \times 10^3$ reconstructed decays with a purity of 95% Belle obtained a good description of the Dalitz distribution using 18 different resonant intermediate states and a non-resonant contribution. A simultaneous fit to m_-^2, m_+^2 and t yielded mixing parameters $x_D = (0.80 \pm 0.29\pm_{0.16}^{0.13})\%$, $y_D = (0.33 \pm 0.24\pm_{0.14}^{0.10})\%$. This represents by far the most constraining determination of x_D up to date. Contour of allowed (x_D, y_D) values at 95% C.L. is shown in Fig. 12 (right).

3.2 CP violation in the system of neutral D mesons

A general, easy to reach expectation is that possible CPV in processes involving charmed hadrons must be small within the SM. This arises due to the fact that such processes involve the

first two generations of quarks for which the elements of the CKM matrix are almost completely real. Typical CKM factor entering both the short distance box diagram as well as the decays to real states accessible to both, D^0 and $\bar{D}^0$, is $V_{cs}^* V_{us}$. Using CKM matrix unitarity this can be expressed as $-V_{cd}^* V_{ud}[1+(V_{cb}^* V_{ub})/(V_{cd}^* V_{ud})]$. Considering the small absolute value of the second term one can see that $\arg(V_{cs}^* V_{us}) \approx \Im((V_{cb}^* V_{ub})/(V_{cd}^* V_{ud})) \sim 7 \times 10^{-4}$. This is the typical value of the weak phase in charmed hadron processes which determines the size of the CPV effects in the SM. For example, CPV asymmetries like A_Γ discussed below, are typically of the order of $x_D \sin\phi$, where ϕ is the weak phase considered, and hence $A_\Gamma \sim \mathcal{O}(10^{-5})$. Deviation of $|q/p|$ value from unity, which also represents the CP violation, is roughly expected to be of the order of $\sin\phi \sim 10^{-3}$. These values are all below the current experimental sensitivity and any positive experimental signature would be a clear sign of some contribution beyond the SM.

All three distinct types of CP violation, CPV in decays, in mixing and in the interference between decays with and without mixing (see lectures by A.J. Bevan) can in principle be present in the D^0 system. They are parameterized by A_D, A_M and ϕ according to

$$\frac{A_f}{\bar{A}_{\bar{f}}} = 1 + \frac{A_D}{2}; \quad (A_D \neq 0, \ CPV \text{ in decay})$$

$$|\frac{q}{p}| = 1 + \frac{A_M}{2}; \quad (A_M \neq 0, \ CPV \text{ in mixing})$$

$$\frac{q}{p}\frac{\bar{A}_f}{A_f} = -\frac{(1 + A_M/2)\sqrt{R_D}}{1 + A_D/2} e^{i(\phi - \delta_f)}; \quad (\phi \neq 0, \ CPV \text{ in interference}) \ . \tag{10}$$

In the above equations $\sqrt{R_D}$ is the ratio of amplitude magnitudes $|\bar{A}_f/A_f|$ and δ_f is the strong phase difference between the two.

In all mentioned mixing parameter measurements also a search for possible CPV has been performed [7].

In decays to CP eigenstates ($D^0 \to KK, \ \pi\pi$) one measures lifetimes separately for D^0 and $\bar{D}^0$ tagged events. A measurable asymmetry

$$A_\Gamma = \frac{\tau(\bar{D}^0 \to f_{CP}) - \tau(D^0 \to f_{CP})}{\tau(\bar{D}^0 \to f_{CP}) + \tau(D^0 \to f_{CP})} \tag{11}$$

is related to the mixing and CPV parameters as [29] $A_\Gamma = (1/2)A_M y_D \cos\phi - x_D \sin\phi$ and equals zero in the case of no CPV. The measured values by Belle [30] and Babar [32] are $A_\Gamma = (0.01 \pm 0.30 \pm 0.15)\%$ and $A_\Gamma = (0.26 \pm 0.36 \pm 0.08)\%$, respectively. Hence there is no sign of the CP violation at the sensitivity level of around 0.3%.

In $D^0 \to K^+\pi^-$ decays the decay time distribution is also fitted separately for D^0 mesons and their anti-particles. There are six observables, $x'^\pm$, $y'^\pm$, $R_D^\pm$, where the $\pm$ superscripts denote the observables for D^0 and $\bar{D}^0$ subsamples. They are related to the parameters of Eq. (10) by $A_D = (R_D^+ - R_D^-)/(R_D^+ + R_D^-)$, $R_M^\pm = (x'^{\pm 2} + y'^{\pm 2})/2$ and $A_M = (R_M^+ - R_M^-)/(R_M^+ + R_M^-)$. From such fits the results of the search for CPV in mixing and in decay are $A_M = 0.1 \pm 2.9$, $A_D = (-2.1 \pm 5.4)\%$ [31] or $A_M = 0.67 \pm 1.2$, $A_D = (-2.3 \pm 4.7)\%$ [36] (errors here include statistical and systematic uncertainties). There is no hint of a direct CPV at the level of 5%.

In the t-dependent analysis of $D^0 \to K_S\pi\pi$ Dalitz distribution the possibility of CPV is included by additional two free parameters in the fit, A_M and ϕ. Also the direct CPV can

---

[7]Note that both, mixing and CPV searches can also be performed using the time-integrated quantities, for example the rate of wrong-sign semileptonic decays $D^0 \to \bar{D}^0 \to \ell^- K^+ \nu$ [34] or the CP asymmetry $(\Gamma(D^0 \to f) - \Gamma(\bar{D}^0 \to \bar{f}))/(\Gamma(D^0 \to f) + \Gamma(\bar{D}^0 \to \bar{f}))$ [35].

be checked by allowing the contributions of various intermediate states to be different for D^0 and $\bar{D}^0$ Dalitz distributions. The latter was not observed within the statistical uncertainties. Parameters of CPV in mixing and interference are found to be $A_M = -0.26 \pm 0.60 \pm 0.20$ and $\phi = (-0.24 \pm 0.31 \pm 0.09) \ rad$. The contours of (x_D, y_D) arising from the fit allowing for the CPV are presented in Fig. 12 (right).

3.3 Average of D^0 mixing parameters

To make conclusions arising from a variety of results on D^0 mixing and CPV searches the Heavy Flavour Averaging Group performs an average of various measurements including correlations among the measured variables [10]. An illustration of (x_D, y_D) constraints imposed by individual measurements is shown in Fig. 13 (left). World average of mixing and CPV parameters for the D^0 system is presented in Tab. 1. The results are presented graphically
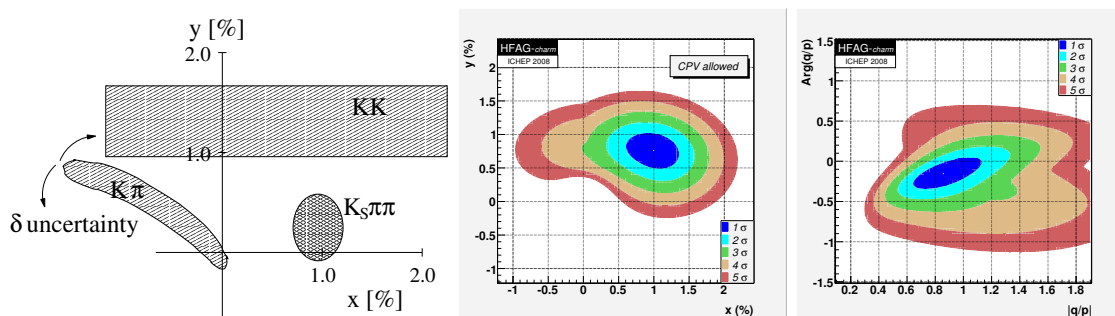
Figure 13: Left: Illustration of constraints on (x_D, y_D) values arising from various measurements. Middle: Probability contours for (x_D, y_D) corresponding to 1-5 σ C.L. from the average of measurements [10]. Right: Probability contours for CPV parameters $(|q/p|, \phi)$ corresponding to 1-5 σ C.L. from the average of measurements [10].

Parameter	Value	Parameter	Value
x_D	$(1.00\pm^{0.24}_{0.26})\%$	A_D	$(-2.1 \pm 2.4)\%$
y_D	$(0.76\pm^{0.17}_{0.18})\%$	$|q/p|$	$0.86\pm^{0.17}_{0.15}$
R_D	$(0.336 \pm 0.009)\%$	ϕ	$-8.8°\pm^{7.6°}_{7.2°}$

Table 1: Average of D^0 mixing (left) and CPV (right) parameters [10].

in Figs. 13 (middle) and 13 (right) as contours in (x_D, y_D) and $(|q/p|, \phi)$ planes. The mixing phenomena in the neutral D meson system is firmly established, with the mixing parameters x_D and y_D of the order of 1%. The oscillation frequency can be compared to the values for other neutral meson systems, $x \approx 0.8$ (B^0), $x_K \approx 1$ (K^0) and $x_s \approx 25$ (B_s^0). Since both parameters, x_D and y_D, appear to be positive, it seems that the CP-even state of neutral charmed mesons is shorter-lived (like in the K^0 system) and also heavier (unlike in the K^0 system). At the moment there is no sign of CPV in the D^0 system, at the level of one standard deviation of the world average results.

Results in the D^0 mixing impose some stringent constraints on the parameters of various NP models [37]. As an example we quote the R-parity violating Supersymmetry models, where an enhancement of x_D could arise from an exchange of down-like squarks or sleptons in the loop of the box diagram. The exclusion region of possible values of the squark mass and R-parity violating coupling constants for various upper limits on x_D is presented in Fig. 14 (left). Planned Super B-factory, which would accumulate data corresponding to an integrated
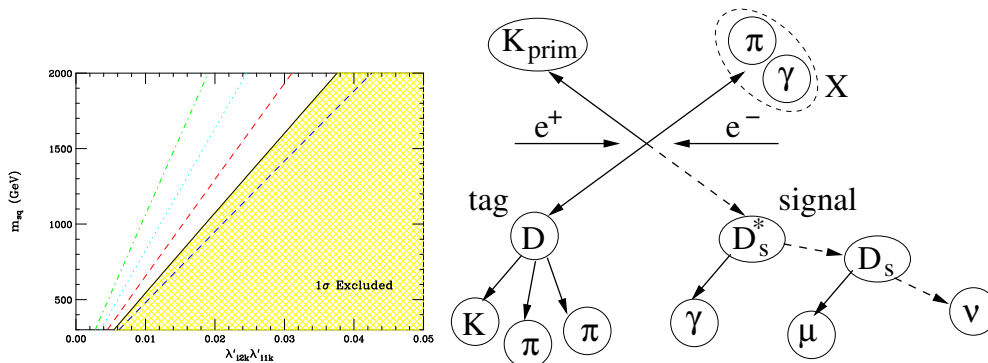
Figure 14: Left: Constraints on the values of squark mass and R-parity violating coupling constants arising from $x_D < 1\%$ (hatched region is excluded). Dashed lines represent boundaries of the exclusion region for $x_D < 1.5\%$, 0.8%, 0.5% and 0.3% [37]. Right: Sketch of a method to measure $Br(D_s^+ \rightarrow \mu^+\nu)$ [38]. Full lines represent particles detected in the detector or exclusively reconstructed, and dashed lines particles reconstructed in the recoil (from the known momenta of incident beams and detected particles).

luminosity of 50 ab^{-1} (compared to the current 0.8 ab^{-1} at KEKB), would of course yield results on D^0 mixing and CPV of much better precision. The extrapolated accuracies are $\sigma(x_D) \sim 0.1\%$, $\sigma(y_D) \sim 0.06\%$, $\sigma(|q/p|) \sim 0.05$ and $\sigma(\phi) \sim 3°$. This would allow to severely constrain relations among parameters of various NP parameters and to search for possible CPV phenomena in the region where a large number of these models predict an observable effect. However, one should not forget the words "Prediction is very difficult, especially of the future." (N. Bohr, 1885 - 1962).

3.4 D_s leptonic decays

Charmed mesons leptonic decays are analogous to the leptonic decays of B mesons (Sect. 2.2). By measuring the rate of such decays one would hope to determine the decay constant of the corresponding meson, see Eq. (6), and by that test the predictions of LQCD. Both Belle and BaBar performed measurements of $Br(D_s^+ \rightarrow \mu^+\nu)$. Cleo-c collaboration measured decays $D_s^+ \rightarrow \tau\nu$ as well.

In [38] Belle measured the absolute branching fraction of $D_s^+ \rightarrow \mu^+\nu$ using a method illustrated in Fig. 14 (right). Events of the type $e^+e^- \rightarrow D_s^* D^{\pm,0} K^{\pm,0} X$ are used, where X can be any number of additional pions from fragmentation, and up to one photon. An event is divided into a tag side, where a full reconstruction of D and a primary K meson is performed, and a signal side where the decay chain $D_s^{*+} \rightarrow D_s^+\gamma$, $D_s^+ \rightarrow \mu^+\nu_\mu$ is searched for. Tag side charged and neutral D mesons are reconstructed in $D \rightarrow Kn\pi$ decays. For all possible combinations

of particles in X, the signal side D_s^{*+} meson is identified by reconstruction of the recoil mass $m_{\rm rec}(DKX)$, using the known beam momentum and four-momentum conservation. The recoil mass $m_{\rm rec}(Y)$ is calculated as the magnitude of the four-momentum $p_{\rm beams} - p_Y$. The next step in the event reconstruction is a search for a photon for which the recoil mass $m_{\rm rec}(DKX\gamma)$ is consistent with the nominal mass of D_s^+. The sample of D_s^+ mesons reconstructed using this procedure represent an inclusive sample of decays, among which the leptonic decays are searched for. If an identified muon is found among the tracks so far not used in the reconstruction, the square of the recoil mass $m_{\rm rec}^2(DKX\gamma\mu)$ is calculated. For signal decays this mass corresponds to the mass of the final state neutrino and hence peaks at zero.

Final distribution of $m_{\rm rec}^2(DKX\gamma\mu)$ is shown in Fig. 15 (left) where a clear signal of leptonic decays can be seen. Majority of background can be described using reconstructed $D_s^+ \to e^+\nu$ decays where due to the helicity suppression no signal is expected. Number of reconstructed signal decays is found to be $N(D_s^+ \to \mu^+\nu) = 169 \pm 16 \pm 8$. Comparing to the number of inclusively reconstructed D_s^+ decays and correcting for the efficiency of muon reconstruction one obtains the branching fraction $Br(D_s^+ \to \mu^+\nu) = (6.44 \pm 0.76 \pm 0.56) \times 10^{-3}$. The largest contribution to the systematic uncertainty arises from a limited number of simulated decays used to describe the shape of the signal distribution. Using Eq. (6) (without the factor arising from the charged Higgs contribution) and the value of $|V_{cs}|$ as determined in a global fit to the CKM elements applying the unitarity of the matrix [8], one determines the value of D_s meson decay constant, $f_{D_s} = (275 \pm 16 \pm 12)$ MeV.

BaBar [39] used a somewhat different approach by measuring the yield of $D_s^+ \to \mu^+\nu$ relative to the $D_s^+ \to \phi\pi$ decays. The branching fraction determined in this way is a relative measurement normalized to the $Br(D_s^+ \to \phi\pi)$. While this method enables a larger statistics of the reconstructed sample it suffers from a hard-to-estimate systematic uncertainty in the normalization mode ($\phi\pi$ state is actually an intermediate state of the $K^+K^-\pi^+$ final state and can be influenced by the interference among various intermediate states). The neutrino momentum is determined from the missing momentum in an event. The resolution is improved by constraining the ν and the reconstructed muon momentum to yield the nominal mass of D_s meson. Fig. 15 (right) shows the distribution of the reconstructed mass difference between the D_s^* and D_s meson, where the signal of leptonic decays consist of 489 ± 55 events (the error is statistical only). Calculation of the decay constant yields a value of $f_{D_s} = (283 \pm 17 \pm 7 \pm 14)$ MeV, where the last error is due to the uncertainty of $Br(D_s^+ \to \phi\pi)$.

How do the measured values compare to the LQCD calculations? The average of absolute measurements (beside the described Belle measurement these include measurements by Cleo-c collaboration in muon and tau decay modes [41]) is $f_{D_s} = (274 \pm 10)$ MeV [17]. The recent LQCD result exhibits a huge improvement in the accuracy compared to previous determinations of the D_s meson decay constant: $f_{D_s} = (241 \pm 3)$ MeV [40]. The discrepancy between the two values is more than 3 standard deviations. While the fact that for the D^+ decay constant experimental results confirm the calculation (albeit within larger errors) may point to some intervention of NP [42] one should probably wait for a) confirmation of the LQCD estimate (and especially its uncertainty) and b) more accurate experimental measurements before making any conclusion [8].

---

[8]For D^+ decays the $H^\pm$ contribution is proportional to $(m_D^2/m_H^2)(m_d/m_c)\tan^2\beta$ while for D_s^+ decays it is proportional to $(m_{D_s}^2/m_H^2)(m_s/m_c)\tan^2\beta$ [43]. See also Eq. (6), where for B^+ decays, due to $m_b \gg m_u$, the correction is simply $(m_B^2/m_H^2)\tan^2\beta$.
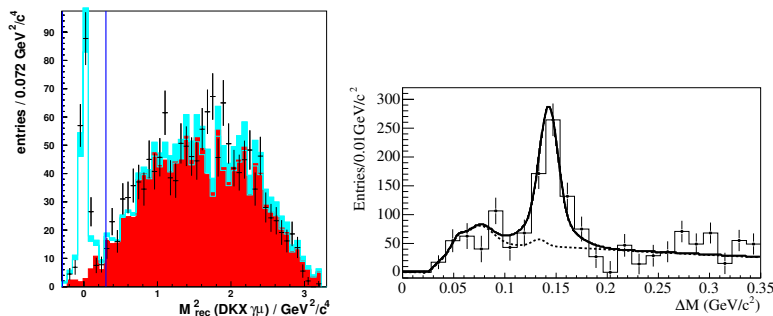
Figure 15: Left: Distribution of $m_{rec}^2(DKX\gamma\mu)$ for $D_s^+ \to \mu^+\nu$ candidate events [38]. The peak at zero corresponds to the signal decays. Right: $m(D_s^*) - m(D_s)$ distribution for $D_s^+ \to \mu^+\nu$ candidate events [39]. Signal peaks at the nominal mass difference.

4 Summary

Although in the lectures we were able to present only a small fraction of exciting physics results that arose from the B-factories over almost a decade of operation, we hope the selected examples demonstrate the following:

- B-factories have successfully performed precision measurements in identification of SM processes and determination of SM parameters, as well as a complement to direct NP searches that are soon to be started at the LHC;

- experimental tests in general confirm predictions of the SM, although several hints of discrepancies at the level of 3 standard deviations exist;

- B-factories have outreached their program as foreseen at the startup.

Specifically related to the presented measurements one should note

- B oscillations in conjunction with a breakthrough in B_s oscillations confirm the SM to a high accuracy;

- leptonic and radiative B meson decays constrain possible contribution of NP but large room for improvement remains for the Super B-factory;

- important results in charm physics complement the results in the B meson sector;

- measurements of D^0 mixing and search for the CPV represent another achieved milestone in particle physics, more precise measurements and theoretical predictions are needed;

- D_s leptonic decays may test predictions of LQCD once the results are confirmed.

4.1 Acknowledgments

The author wishes to thank the organizers of the school for the great summer school atmosphere and a very pleasant stay in Dubna. Most of the measurements presented in the lectures are

the result of a splendid work of the Belle and BaBar collaboration members and of the superb performance of the KEKB and PEP-II accelerators.

The credit for the quotes used goes to:
Oscar Wilde, Irish playwright, poet, 1854-1900.
Anne Frank, Jewish girl, author of the famous diary, 1929-1945.
Ralph Waldo Emerson, American Poet and Essayist, 1803-1882.
Sir Sean Connery, Scottish actor and producer, 1930.
Albert Camus, Algerian-born French writer, 1913-1960.
Honore de Balzac, French novelist and playwright, 1799-1850.
Niels Bohr, Danish physicist, 1885-1962.

References

[1] A. Abashian *et al.* (Belle Coll.), Nucl. Instr. Meth. A**479**, 117 (2002).

[2] S. Kurokawa, E. Kikutani, Nucl. Instr. Meth. A**499**, 1 (2003), and other papers in this volume.

[3] B. Aubert *et al.* (BaBar Coll.), Nucl. Instr. Meth. A**479**, 1 (2002).

[4] D. Acosta *et al.* (CDF Coll.), Phys. Rev. D**71**, 032001 (2005).

[5] D. Peterson *et al.*, Nucl. Instr. Meth. A**478**, 142 (2002); Y. Kubota *et al.* (CLEO Coll.), Nucl. Instr. Meth. A**320**, 66 (1992).

[6] D. Kirkby, Y. Nir, review *CP Violation in Meson Decays*, in C. Amsler *et al.*, Phys. Lett. B**667**, 1 (2008), and references therein.

[7] H. Tajima *et al.*, Nucl. Instr. Meth. A**533**, 370 (2004).

[8] C. Amsler *et al.*, Phys. Lett. B**667**, 1 (2008).

[9] K. Abe *et al.* (Belle Coll.), Phys. Rev. D**71**, 072003 (2005).

[10] E. barberio *et al.* (HFAG), arXiv:0808.1297, and updates at http://www.slac.stanford.edu/xorg/hfag/

[11] A.J. Buras *et al.*, Nucl. Phys. B**245**, 369 (1984).

[12] J. Charles *et al.* (CKMfitter group), Eur. Phys. J. C**41**, 1 (2005).

[13] http://ckmfitter.in2p3.fr

[14] A. Abulencia *et al.* (CDF Coll.), Phys. Rev. Lett. **97**, 242003 (2006).

[15] K. Ikado *et al.* (Belle Coll.), Phys. Rev. Lett. **97**, 251802 (2006); update of measurement at ICHEP'08, presentation by K. Hara, http://ichep08.com/

[16] B. Aubert *et al.* (BaBar Coll.), Phys. Rev. D**76**, 052002 (2007).

[17] See J. Rosner, S. Stone, review *Decay Constants of Charged Pseudoscalar Mesons*, in C. Amsler *et al.*, Phys. Lett. B**667**, 1 (2008), and references therein.

[18] A. Gray *et al.* (HPQCD Coll.), Phys. Rev. Lett. **95**, 212001 (2005).

[19] K. Abe *et al.* (Belle Coll.), arXiv:0804.1580.

[20] B. Aubert *et al.* (BaBar Coll.), Phys. Rev. D**72**, 052004 (2005).

[21] M. Misiak *et al.*, Phys. Rev. Lett. **98**, 022002 (2007).

[22] U. Egede *et al.*, arXiv:0807.2589, and references therein.

[23] A. Ali *et al.*, Phys. rev. D**66**, 034002 (2002).

[24] B. Aubert *et al.* (BaBar Coll.), arXiv:0804.4412.

[25] I. Adachi *et al.* (Belle Coll.), arXiv:0810.0335.

[26] T. Hurth *et al.*, arXiv:0807.5039.

[27] G. Burdman, I. Shipsey, Ann. Rev. Nucl. Sci. **53**, 431 (2005).

[28] I.I. Bigi, N. Uraltsev, Nucl. Phys. B**592**, 92 (2001); A.F. Falk *et al.*, Phys. Rev. D**69**, 114021 (2004).

[29] S. Bergmann *et al.*, Phys. Lett. B **486**, 418 (2000).

[30] M. Starič *et al.* (Belle Coll.), Phys. Rev. Lett. **98**, 211803 (2007).

[31] B. Aubert *et al.* (BaBar Coll.), Phys. Rev. Lett. **98**, 211802 (2007).

[32] B. Aubert *et al.* (BaBar Coll.), Phys. Rev. D**78**, 011105 (2008).

[33] L.M. Zhang *et al.* (Belle Coll.), Phys. Rev. Lett. **99**, 131803 (2007).

[34] U. Bitenc *et al.* (Belle Coll.), Phys. Rev. D**77**, 112003 (2008).

[35] B. Aubert *et al.* (BaBar Coll.), Phys. Rev. Lett. **100**, 061803 (2008).

[36] L.M. Zhang *et al.* (Belle Coll.), Phys. Rev. Lett. **96**, 151801 (2006).

[37] E. Golowich *et al.*, Phys. Rev. D**76**, 095009 (2007).

[38] L. Widhalm *et al.* (Belle Coll.), Phys. Rev. Lett. **100**, 241801 (2008).

[39] B. Aubert *et al.* (BaBar Coll.), Phys. Rev. Lett. **98**, 141801 (2007).

[40] E. Follana *et al.* (HPQCD and UKQCD Coll.), Phys. Rev. Lett. **100**, 062002 (2008).

[41] M. Artuso *et al.* (Cleo-c Coll.), Phys. Rev. Lett. **99**, 071802 (2007); K.M. Ecklund *et al.* (Cleo-c Coll.), Phys. Rev. Lett. **100**, 161801 (2008).

[42] B.A. Dobrescu, A.S. Kronfeld, Phys. Rev. Lett. **100**, 241802 (2008).

[43] W.S. Hou, Phys. Rev. D**48**, 2342 (1993).

Results from the B factories

Adrian Bevan[1]

[1]Department of Physics, Queen Mary, University of London, London E14NS, UK

These proceedings are based on lectures given at the Helmholtz International Summer School Heavy Quark Physics at the Bogoliubov Laboratory of Theoretical Physics, Dubna, Russia, during August 2008. I review the current status of CP violation in B meson decays from the B factories. These results can be used, along with measurements of the sides of the Unitarity Triangle, to test the CKM mechanism. In addition I discuss experimental studies of B decays to final states with 'spin-one' particles.

1 Introduction

In 1964 Christenson *at al.* discovered CP violation in weak decay [1]. Shortly afterward Sakharov noted that CP violation was a crucial ingredient to understanding how our matter dominated universe came into existence [2]. It was not until 1972 when Kobayashi and Maskawa extended Cabibbo's work on quark mixing to three generations that CP violation was introduced into the theory of weak interactions [3, 4]. The resulting three generation quark mixing matrix is called the CKM matrix and this has a single CP violating phase. Once the magnitude of the elements of this matrix have been measured, and the CP violating phase was parameterized by measurement of CP violation in kaon decays, the CKM matrix could be used to predict CP violating effects in other processes. The CKM matrix is

$$V_{\mathrm{CKM}} = \left(\begin{array}{ccc} V_{\mathrm{ud}} & V_{\mathrm{us}} & V_{\mathrm{ub}} \\ V_{\mathrm{cd}} & V_{\mathrm{cs}} & V_{\mathrm{cb}} \\ V_{\mathrm{td}} & V_{\mathrm{ts}} & V_{\mathrm{tb}} \end{array} \right),$$

and it describes the couplings of the u, c and t quarks to d, s, and b quarks, through transitions mediated by the exchange of a W boson. In 1981 Bigi and Sanda noted that there could be large CP violating effects in a number of B meson decays, and in particular in the decay of $B^0 \to J/\psi K_S^0$ [5][1]. At first it was not obvious how to experimentally test these ideas, that is until Oddone realized that the effects could be observed using data from collisions at an asymmetric e^+e^- collider [6]. Two asymmetric energy e^+e^- colliders called B factories were built to probe CP violation in B meson decays, and in doing so, to test the theory behind the CKM matrix. Recently Kobayashi and Maskawa have been awarded the 2008 Nobel Prize for Physics[2] for their contribution to the CKM mechanism.

The remainder of these proceedings describe the accelerators and detectors called B factories, tests of the CKM theory through studies of the unitarity triangle via CP violation and CKM matrix element measurements, tests of CPT, and studies of B mesons decay to final states with

---

[1]Charge conjugation is implied throughout these proceedings.

[2]The 2008 prize was awarded to Nambu, Kobayashi and Maskawa for work on broken symmetries. See http://nobelprize.org/nobel_prizes/physics/laureates/2008/.

two spin-one particles. In these proceedings I summarise one half of the lectures on experimental results from the B factories, and the contribution from Bostjan Golob covers the second half.

2 The B factories

The need to test CKM theory in B decays led to at least 21 different concepts for B factories to be proposed [7]. Of these only two were built: The *BABAR* experiment [8] and PEP-II accelerator [9] at the Stanford Linear Accelerator Center in the USA and the Belle experiment [10] and KEKB accelerator [11] at KEK in Japan. The B factories are similar in design and operation and started to collect data in 1999, quickly exceeding their original design goals by a large factor. Table 1 shows the integrated luminosity recorded at *BABAR* and Belle at various centre of mass energies $\sqrt{s}$. *BABAR* finished collecting data in 2008 having recorded 433fb^{-1} of data (465×10^6 $B\overline{B}$ pairs), and at the time of writing these proceedings Belle was still taking data having recorded 1171fb^{-1} of data (1257×10^6 $B\overline{B}$ pairs). These proceedings discuss experimental measurements made using data taken at the $\Upsilon(4S)$. The physics process of interest here is $e^+e^- \to \Upsilon(4S) \to B\overline{B}$.

	BABAR (fb^{-1})	Belle (fb^{-1})	Total (fb^{-1})
$\Upsilon(5S)$	. . .	24	24
$\Upsilon(4S)$	433	738	1171
$\Upsilon(3S)$	30	. . .	30
$\Upsilon(2S)$	14.5	. . .	14.5
$\Upsilon(1S)$	. . .	7	7
Off-resonance	54	75	129

Table 1: Luminosity of data recorded at different $\sqrt{s}$.

In addition to this *interesting* process, there is also a significant cross section for e^+e^- decay into $q\overline{q}$ where q is a quark lighter than the b quark, and into di-lepton pairs. These other processes are backgrounds when studying the decays of B mesons. However, copious amounts of D mesons and τ leptons are also created at a B factory: In fact a B factory is really a *flavour* factory.

For time-dependent CP asymmetry measurements, such as those described in Section 3.1, the B^0 and $\overline{B}^0$ created in the $\Upsilon(4S)$ decay are in a P wave correlated state. Neutral B mesons can mix[3], and until one of the B mesons decays, we have only one B^0 and one $\overline{B}^0$ event in the decay. This EPR correlation stops at the instant one of the B mesons in the event decays. After that time t_1, the other B in the event oscillates between a B^0 and a $\overline{B}^0$ state until it decays at some time t_2. The difference between these two decay times is used to extract information about CP violation. In a symmetric e^+e^- collider time difference corresponds to a spatial separation Δz of $30\mu m$ between the B meson vertices which is too small to be measured in a detector. In an asymmetric energy collider the spatial separation of vertices is approximately $200\mu m$ which is measurable in a detector. The need to resolve the two B vertices in an event is the reason why PEP-II and KEK-B are asymmetric energy e^+e^- colliders.

---

[3]See the contribution of U. Nierst to these proceedings.

A B meson that decays into an *interesting* final state such as $J/\psi K_S^0$ is called the B_{rec}. The other B meson in the event is called the B_{tag} which is used to determine or *tag* the flavour of B_{rec} at the time that the first B meson decay occurs. We don't know which of the B_{rec} or B_{tag} decay first, and so the proper time difference between the decay of the B_{rec} and B_{tag} is a signed quantity related to the measured Δz by $\Delta t \simeq \Delta z / c\beta\gamma$.

3 Unitarity triangle physics

The CKM matrix is unitary, so $V_{\text{CKM}} V_{\text{CKM}}^\dagger = I$, which leads to six complex relations that can each be represented as closed triangles in the Standard Model (SM). The equation $V_{\text{ud}} V_{\text{ub}}^* + V_{\text{td}} V_{\text{tb}}^* + V_{\text{cd}} V_{\text{cb}}^* = 0$ is the one related to the so-called unitarity triangle (shown in Figure 1). This triangle can be completely parameterised by any two of the three angles α, β, γ, by measuring the sides, or by constraining the coordinates of the apex. If we are able to measure more than two of these quantities we can over-constrain the theory. Sections 3.1.1 through 3.1.4 discuss measurements of the angles, and section 3.2 discusses measurements related to the sides of the triangle. The angles of the unitarity triangle are given by

$$\alpha \equiv \arg\left[-V_{\text{td}} V_{\text{tb}}^* / V_{\text{ud}} V_{\text{ub}}^*\right], \tag{1}$$

$$\beta \equiv \arg\left[-V_{\text{cd}} V_{\text{cb}}^* / V_{\text{td}} V_{\text{tb}}^*\right], \tag{2}$$

$$\gamma \equiv \arg\left[-V_{\text{ud}} V_{\text{ub}}^* / V_{\text{cd}} V_{\text{cb}}^*\right], \tag{3}$$

and the apex of the unitarity triangle is given by

$$\overline{\rho} + i\overline{\eta} \equiv -\frac{V_{\text{ud}} V_{\text{ub}}^*}{V_{\text{cd}} V_{\text{cb}}^*}.$$

At the current level of experimental precision, we use $V_{\text{ub}} = |V_{\text{ub}}| e^{i\gamma}$ and $V_{\text{td}} = |V_{\text{td}}| e^{i\beta}$.
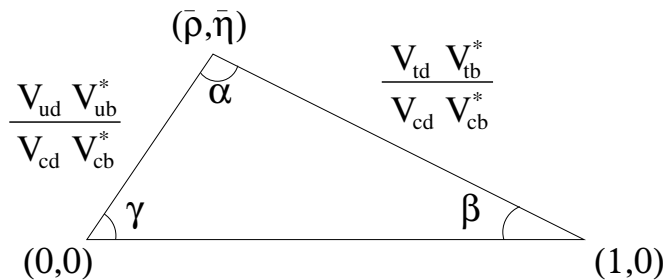
Figure 1: The unitarity triangle.

3.1 CP violation measurements

The signal decay-rate distribution of a CP eigenstate decay, $f_+(f_-)$ for $B_{\text{tag}} = B^0$ $(\overline{B}^0)$, is given by:

$$f_\pm(\Delta t) = \frac{e^{-|\Delta t|/\tau}}{4\tau}[1 \mp \Delta\omega \pm (1 - 2\omega)(-\eta_f S \sin(\Delta m_d \Delta t) \mp C \cos(\Delta m_d \Delta t))] \otimes \mathcal{R}(\Delta t, \sigma(\Delta t)),$$

where η_f is the CP eigenvalue of the final state f, $\tau = 1.530 \pm 0.009$ps is the mean B^0 lifetime and $\Delta m_d = 0.507 \pm 0.005$ps^{-1} is the $B^0 - \overline{B}^0$ mixing frequency [13]. The physical decay rate is convoluted with the detector resolution $\mathcal{R}(\Delta t, \sigma(\Delta t))$. As $\Delta\Gamma$ is expected to be small in the SM, it is assumed that there is no difference between B^0 lifetimes, i.e. $\Delta\Gamma = 0$. The parameters S and C are defined as:

$$S = \frac{2Im\lambda}{1 + |\lambda|^2}, \qquad C = \frac{1 - |\lambda|^2}{1 + |\lambda|^2},$$

where $\lambda = \frac{q}{p}\frac{\overline{A}}{A}$ is related to the level of B^0-$\overline{B}^0$ mixing (q/p), and the ratio of amplitudes of the decay of a $\overline{B}^0$ or B^0 to the final state under study $(\overline{A}/A)$. Sometimes we assign the wrong flavour to B_{tag}. The probability for this to happen is given by the mis-tag fraction ω, where $\Delta\omega$ is the difference between the mistag probability of B^0 and $\overline{B}^0$ decays.

CP violation is probed by studying the time-dependent decay-rate asymmetry

$$\mathcal{A} = \frac{R(\Delta t) - \overline{R}(\Delta t)}{R(\Delta t) + \overline{R}(\Delta t)} = -\eta_f S \sin(\Delta m_d \Delta t) - C \cos(\Delta m_d \Delta t),$$

where $R(\overline{R})$ is the decay-rate for B^0 ($\overline{B}^0$) tagged events. The Belle Collaboration use a different convention to that of the *BABAR* Collaboration with $C = -A_{CP}$. Here all results are quoted using the S and C convention.

In the case of charged B-meson decays (and $\pi^0\pi^0$ as there is no vertex information) one can study a time integrated charge asymmetry

$$A_{CP} = \frac{\overline{N} - N}{\overline{N} + N},$$

where N ($\overline{N}$) is the number of B ($\overline{B}$) decays to the final state. A non-zero measurement of S, C or A_{CP} is a clear indication of CP violation.

In order to quantify the mistag probabilities and resolution function parameters, the B factories study decay modes to flavour specific final states. These states form what is usually referred to as the B_{flav} sample of events. The following decay modes are included in the B_{flav} sample: $B \to D^{(*)-}\pi^+$, $D^{(*)-}\rho^+$, and $D^{(*)-}a_1^+$. It is assumed that the mistag probabilities and resolution function parameters determined for the B_{flav} sample are the same as those for the signal B_{rec} decays.

There are three types of CP Violation that can occur: (i) CP Violation in mixing, which requires $|q/p| \neq 1$, (ii) CP Violation in decay (also called direct CP violation) where $|\overline{A}/A| \neq 1$, and (iii) CP violation in the interference between mixing and decay amplitudes.

3.1.1 The angle β

The golden channel predicted to be the best one to observe CP violation in B meson decays through the measurement of $\sin 2\beta$ is $B^0 \to J/\psi K_S^0$ [5]. The phase β comes from the V_{tb} vertices of the $B^0 - \overline{B}^0$ mixing amplitudes. This is just one of the theoretically clean $b \to c\overline{c}s$ Charmonium decays, where the measurement of S is a direct measurement of $\sin 2\beta$, neglecting the small effect of mixing in the neutral kaon system. The other theoretically clean decays include $\psi(2S)K_S^0$, $\chi_{1c}K_S^0$, $\eta_c K_S^0$, and $J/\psi K^{*0}$. Figure 2 shows the mixing and tree diagrams
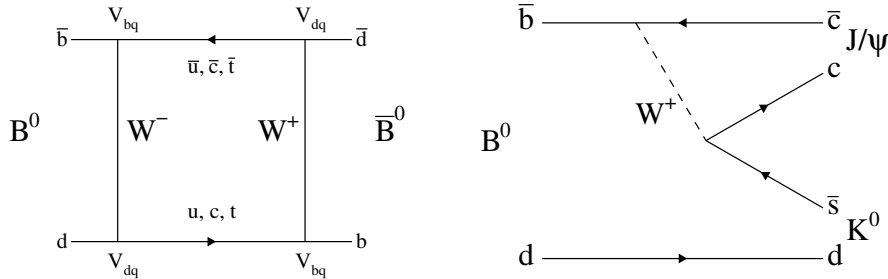
Figure 2: The (left) mixing and (right) tree contributions to Charmonium decays.

relevant for $b \rightarrow c\bar{c}s$ Charmonium decays. There are several calculations of the level of SM uncertainty on the measurement of $\sin 2\beta$ in $b \rightarrow c\bar{c}s$ decays which include theoretical and data driven phenomenological estimates of this uncertainty [14, 15, 16]. The data driven method uses $B^0 \rightarrow J/\psi\pi^0$ to limit the SM uncertainties at a level of 10^{-2}, and the theoretical calculations limit these uncertainties to be $\mathcal{O}(10^{-3})$ to $\mathcal{O}(10^{-4})$. *BABAR* found a signal for CP violation in B meson decay in 2001 [17] and this result was confirmed two weeks later by Belle [18]. The latest analyses from the B factories provide the most precise test of CKM theory [19, 20]. These results are summarised in Table 2 where the *BABAR* result uses B decays to $J/\psi K^0$, $\psi(2S)K_S^0$, $\chi_{1c}K_S^0$, $\eta_c K_S^0$, and $J/\psi K^{*0}$ to measure $\sin 2\beta$. Belle use $J/\psi K^0$, and $\psi(2S)K_S^0$ final states for their measurement.

When converting the measured value of $\sin 2\beta$ to a value of β we obtain a four fold ambiguity on β. The four solutions for beta are $21.1°$, $68.9°$, $201.1°$, and $248.9°$. The two solutions $68.9°$ and $248.9°$ are disfavoured by $\cos 2\beta$ measurements from decays such as $B^0 \rightarrow J/\psi K^*$ [21], $D^*D^*K_S^0$ [22] and

Experiment	$\sin 2\beta$
BABAR	$0.691 \pm 0.029(\text{stat.}) \pm 0.014(\text{syst.})$
Belle	$0.650 \pm 0.029(\text{stat.}) \pm 0.018(\text{syst.})$
World Average	0.671 ± 0.024

Table 2: Experimental results for $\sin 2\beta$ from the B factories.

$D^{*0}h^0$ [23]. The only solution for β that is consistent with the Standard Model is $\beta = (21.1 \pm 0.9)°$. This result corresponds to the first test of the CKM mechanism as the apex of the unitarity triangle can be constrained using Eq. 1. In order to fully constrain the theory, we need a second measurement from one of the observables described below.

As can be seen from Table 2, the precision of the $\sin 2\beta$ result from the B factories is still limited by statistics. This measurement will be refined by the next generation of experiments, including LHCb [24], SuperB [25] and SuperKEKB [26]. For example, the measurement of $\sin 2\beta$ with 75ab^{-1} from SuperB will be systematics limited and have a precision of ± 0.005 [25].

3.1.2 The angle α

The measurement of α is not as straight forward as β. All of the decay channels that are sensitive to α have potentially large contributions from loop amplitudes[4], in addition to the leading order tree and mixing contributions. Figure 3 shows these tree and loop contributions. In the absence of a loop contribution, the interference between tree and mixing amplitudes would result in $S = \sin(2\alpha)$. Here the weak phase[5] measured is $\alpha = \pi - \beta - \gamma$ where β comes from the V_{td} vertices of the mixing amplitudes, and γ comes from the V_{ub} vertex of the tree amplitude. However, the loop contributions have a different weak phase to the tree contribution, so they 'pollute' the measurement of α. There are two schemes used in order to determine the loop pollution $\delta\alpha$: (i) use $SU(2)$ relations [28], and (ii) use $SU(3)$ relations [32] to constrain the effect of loop amplitudes on the extraction of α from measurements of B meson decays to h^+h^- final states, where $h = \pi, \rho$. The effect of loop amplitudes is $\delta\alpha = \alpha - \alpha_{\text{eff}}$, where α_{eff} is related to the measured S and C via $S = \sqrt{1 - C^2}\sin(2\alpha_{\text{eff}})$.
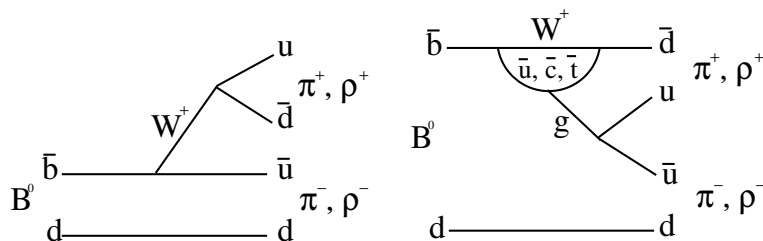
Figure 3: The tree (left) and gluonic loop (right) contributions to $B \to h^+h^-$ decays.

One can use $SU(2)$ isospin to relate the amplitudes of B decays to $\pi\pi$ final states [28]. This results in two relations:

$$\frac{1}{\sqrt{2}}A^{+-} = A^{+0} - A^{00}, \qquad \frac{1}{\sqrt{2}}\overline{A}^{+-} = \overline{A}^{-0} - \overline{A}^{00},$$

where A^{ij} ($\overline{A}^{ij}$) are the amplitudes of B ($\overline{B}$) decays to the final state with charge ij. These two relations correspond to triangles in a complex plane with a common base given by $|A^{+0}| = |\overline{A}^{-0}|$ neglecting electroweak loop contributions. There are three such relations for $\rho\rho$ decays, one for each of the transversity states (Section 5). The extraction of α from $\rho\pi$ decays is complicated by the fact that the final state is not a CP eigenstate [29, 30]. A more detailed overview of the experimental methods used for $\pi\pi$, $\rho\rho$, and $\rho\pi$ decays is given in Ref. [31].

The experimental results for $B \to \pi\pi$ [34, 35], $B \to \rho\rho$ [36, 37, 38, 39, 41, 40], and $B \to \rho\pi$ [42, 43] decays can be combined together in order to constrain α. This constraint is shown in Figure 4 for the $SU(2)$ approach. The solution compatible with the SM is $\alpha = (91 \pm 8)°$ [33] which provides a second reference point to test the CKM mechanism.

Beneke *at al.* proposed the use of $SU(3)$ to relate the loop component of $B^+ \to \rho^- K^{*0}$ to the loop component of $B^0 \to \rho^+\rho^-$ [32]. In order to do this, one has to measure the branching

---

[4]These loop amplitudes are often called 'penguins' in B physics literature. This nomenclature stems from a lost bet as described in Ref. [27].

[5]A weak phase is one that changes sign under CP. The angles of the unitarity triangle are weak phases.

fractions and fractions of longitudinally polarized signal in both decay channels, as well as S and C for the longitudinal polarization of $B^0 \to \rho^+\rho^-$. On doing this, *BABAR* finds that $\alpha = (89.8^{+7.0}_{-6.4})°$, where the corresponding loop to tree ratio measured is $0.10^{+0.03}_{-0.04}$ [37].

The strongest constraint on α comes from the study of $B \to \rho\rho$ decays and this measurement is currently limited by statistics. The next generation of experiments will be able to refine our knowledge of α: LHCb will be able to measure this to $\mathcal{O}(5°)$ [44] with 10fb^{-1} of data using $B \to \rho\pi$ decays, but will not be able to measure all of the necessary inputs for the $\pi\pi$ and $\rho\rho$ measurements. The SuperB experiment will be able to measure α to a level that will be limited by systematic and theoretical uncertainties: $\mathcal{O}(1-2°)$ [25] with a data sample of 75ab^{-1}.

It is also possible to constrain α using $SU(3)$ based approaches for decays such as $B \to a_1\pi$, and $a_1\rho$. Even though these decays are experimentally challenging to measure, the time-dependent analysis of $B \to a_1\pi$ decays has been performed [45]. Additional experimental constraints, such as the branching fractions of $K_1\pi$ decays, are required to interpret those results as a measurement on α. Only a branching fraction upper limit exists for $B^0 \to a_1^\pm \rho^\mp$ [46].

Figure 4: The constraint on α from an isospin analysis of $B \to hh$ decays. Constraints are made on the magnitude of the penguin to tree ratio for $B \to \pi\pi$ decays when making this plot. This figure is reproduced from UT fit [33]. The shaded regions correspond to the allowed solutions for α.

3.1.3 The angle γ

There are several promising methods being pursued in order to constrain γ or $\sin(2\beta+\gamma)$, however none of these provides as stringent a bound as those for β and α. Here I discuss three methods used to constrain γ: these are called Gronau-London-Wyler (GLW) [47], Attwood-Dunietz-Soni (ADS) [48] and Giri-Grossman-Soffer-Zupan (GGSZ) [49]. These three methods are theoretically clean, and use B decays to $D^{(*)}K^{(*)}$ final states to measure γ.

The GLW method [47] uses $B^+ \to D^0_{CP}X^+$ and $B^+ \to \overline{D}^0_{CP}X^+$ where X^+ is a strangeness one state, and D^0_{CP} is a D^0 decay to a CP eigenstate (similarly for $\overline{D}^0_{CP}$) to extract γ. The CP-even eigenstates used are $D^0_{CP} \to h^+h^-$ where $h = \pi, K$, and the CP-odd eigenstates used are $D^0_{CP} \to K^0_S\pi^0, K^0_S\omega$, and $K^0_S\phi$. The ratio of Cabibbo allowed to Cabibbo suppressed decays is given by the parameter r_B. The experimentally determined value is $r_B \sim 0.1$ which leads to a relatively a large uncertainty on γ extracted using this method. A similar measurement has been performed using $D^{*0}_{CP}K$ decays, where r_B^* is found to be $0.22 \pm 0.09 \pm 0.03$, and only weak constraints can be placed on γ [52, 51].

The ADS method [48] uses the doubly Cabibbo suppressed decays $B^+ \to D^{*0}K^{(*)\pm}$ where the interference between amplitudes with a D and a $\overline{D}$ decaying into a $K^+\pi^-$ final state is

sensitive to γ. As with the GLW method, the ADS method requires more statistics than are currently available in order to measure γ [53, 54].

The GGSZ method [49] uses B decays to $D^{(*)0}K^{(*)}$ final states where the $D^{(*)}$ subsequently decays to $K_S^0 h^+ h^-$ ($h = \pi, K$)to constrain γ. This method is self tagging either by the charge of the reconstructed $B^\pm$ meson, or by the charge of the reconstructed $K^{(*)}$ for neutral B decays. One has to understand the D Dalitz decay distribution to determine γ. Using this method Belle measure $\gamma = (76^{+12}_{-13} \pm 4 \pm 9)^\circ$ [55] where the errors are statistical, systematic and model dependent. The corresponding $BABAR$ measurement is $\gamma = (76^{+23}_{-24} \pm 5 \pm 5)^\circ$ [56]. The difference in statistical uncertainties of these measurements comes from the fact that Belle measure a larger value of r_B than $BABAR$.

Figure 5 shows the experimental constraint on γ where the total precision on this angle is 20° with a central value of 71°. The next generation of experiments will be able to refine our knowledge of γ: LHCb will be able to measure this to $\mathcal{O}(2^\circ)$ [44] with $10\mathrm{fb}^{-1}$ of data. The SuperB experiment will be able to measure γ to $\mathcal{O}(1^\circ)$ [25] with a data sample of $75\mathrm{ab}^{-1}$.
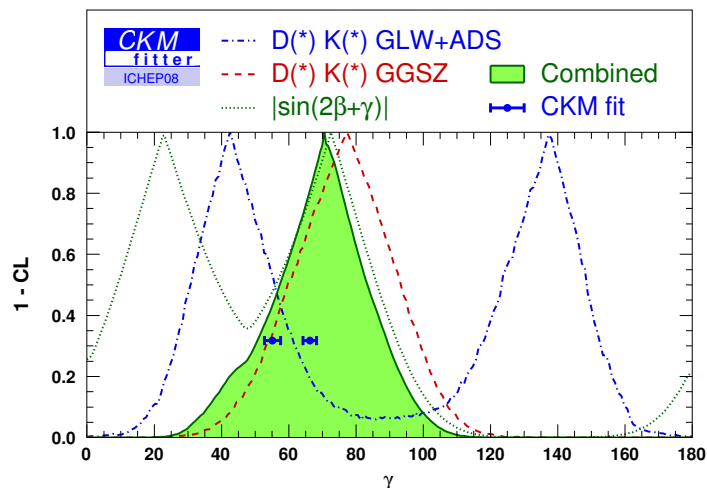
Figure 5: The experimental constraint on γ. This figure is from CKM Fitter [50].

3.1.4 Angle constraints on the CKM theory

The angle measurements described in the previous sections individually constrain CKM theory by restricting the allowed values of $\overline{\rho}$ and $\overline{\eta}$. The individual and combined constraints of these measurements are shown in Fig. 6. The angle constraints are consistent with CKM theory at the current level of precision. Combining the angle measurements: $\beta = (21.1 \pm 0.9)^\circ$, $\alpha = (89.9^{+7.0}_{-6.4})^\circ$, and $\gamma = (71 \pm 20)^\circ$, we obtain $\overline{\rho} = 0.13 \pm 0.04$ and $\overline{\eta} = 0.34 \pm 0.02$. The the precision on these constraints is dominated by our knowledge of α and β. CKM theory requires that $\alpha + \beta + \gamma = 180^\circ$. The B factory measurements give $\alpha + \beta + \gamma = (190 \pm 21)^\circ$ where the precision of this test is limited by our knowledge of γ.
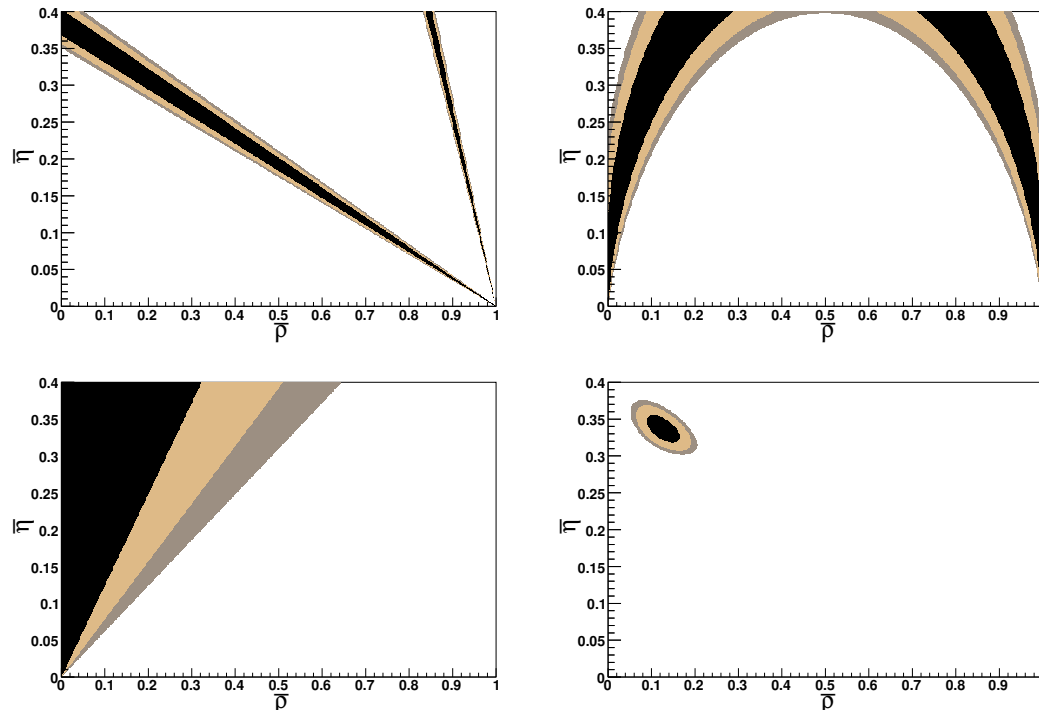
Figure 6: Angle constraints on $\overline{\rho}$ and $\overline{\eta}$ from (top left) β, (top right) α, (bottom left) γ, and (bottom right) combined. The shaded contours show the 68% (black), 90% (light) and 95% (medium) confidence levels.

3.1.5 Direct CP violation

Direct CP violation was established by the NA48 and KTeV experiments in 1999 [57, 58] through the measurement of a non-zero value of the parameter ϵ'/ϵ. This phenomenon was confirmed 45 years after CP violation was discovered in kaon decays. In contrast to this in B meson decay direct CP violation was observed only a few years after

Experiment	A_{CP}
BABAR	$-0.107 \pm 0.016^{+0.006}_{-0.004}$ [61]
Belle	$-0.094 \pm 0.018 \pm 0.008$ [60]
CDF	$-0.086 \pm 0.023 \pm 0.009$ [62]
CLEO	$-0.04 \pm 0.16 \pm 0.02$ [63]

Table 3: Experimental results for A_{CP}, where the first error quoted is statistical and the second is systematic.

CP violation was established. The first observation of direct CP violation in B decays was made via the measurement of a non-zero A_{CP} in $B^0 \to K^\pm \pi^\mp$ decays in 2007 by *BABAR* [59]. The following year Belle confirmed this result [60]. The latest results of this measurement are summarised in Table 3. It has been suggested that the difference in the direct CP violation observed in $B^0 \to K^\pm \pi^\mp$ and $B^+ \to K^+ \pi^0$ could be due to new physics (See Ref. [59] and

references therein). A more plausible explanation is that the difference arises from final state interactions [64].

3.1.6 Searching for new physics

The B factories have seen evidence for, or have observed indirect CP violation in $B^0 \to J/\psi K^0$, $B^0 \to J/\psi \pi^0$, $B^0 \to \psi(2S)K_S^0$, $B^0 \to \eta_{1c}K_S^0$, $B^0 \to \eta'K^0$, $B^0 \to f_0^0(980)K_S^0$, $B^0 \to K^+K^-K^0$, $B^0 \to D^{*+}D^{*-}$, and $B^0 \to \pi^+\pi^-$. They have also seen evidence for or observed direct CP violation in $B^0 \to \pi^+\pi^-$, $B^0 \to \eta K^{*0}$, $B^0 \to \rho^\pm \pi^\mp$, $B^0 \to K^\pm \pi^\mp$, $B^\pm \to \rho^0 K^\mp$, $B \to D_{CP+}^0 K$, $B \to D^{(*)0}K^*$. All of the measurements of CP violating asymmetries to date are consistent with CKM theory. It is possible that there is more to CP violation than the CKM theory and the rest of this section discusses one way to search for effects beyond CKM.

A large number of rare B decays are sensitive to β however as these measurements are not necessarily clean we call the phase measured β_{eff}. These fall into two categories: those that are loop dominated; and those that have a loop and a tree contribution. The SM loop amplitude can be replaced by a corresponding amplitude with unknown heavy particles, for example the SUSY partners of the SM loop constituents, so the loops are sensitive to the presence of new physics. The consequence of this is that if there are new heavy particles that contribute to the loop, the SM calculated expectation for observables
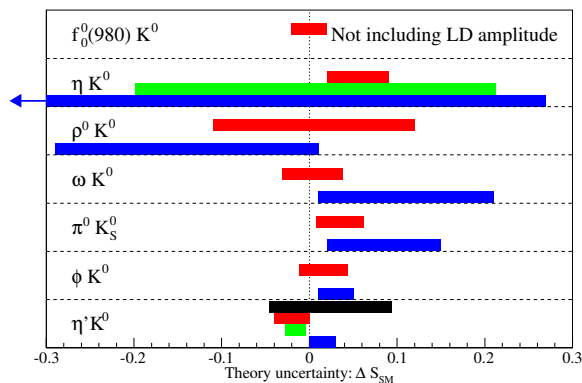
Figure 7: Theoretical estimates of ΔS_{SM}.

will differ from experimental measurements of the observables. $\sin 2\beta$ has been measured to an accuracy of $1°$ using tree dominated $c\bar{c}s$ decays and this can be used as a reference point to test for deviations from the SM. If we measure $\sin 2\beta_{\text{eff}}$ for a rare decay, then $\Delta S = \sin 2\beta_{\text{eff}} - \sin 2\beta - \Delta S_{\text{SM}}$ is zero in the absence of new physics. Here ΔS_{SM} is a term that accounts for the effect of possible higher order SM contributions to a process that would lead to the measured $\sin 2\beta_{\text{eff}}$ differing from the $c\bar{c}s$ measurement. Such effects include contributions from long distance scattering (LD), annihilation topologies and other often neglected terms. There has been considerable theoretical effort in recent years to try and constrain ΔS_{SM} which is summarised in Figure 7. The figure is divided into decay modes, and each decay mode has up to four error bands drawn on it. These error bands come from (top to bottom) calculations by Beneke *at al.* [65], Williamson and Zupan [66], Cheng *at al.* [67], and Gronau *at al.* [68]. It is clear from this work that some of the decay modes are clean, and the SM expectation of $\sin 2\beta_{\text{eff}}$ is essentially the same as the expectation for $\sin 2\beta$ from $c\bar{c}s$. However some modes have a significant contribution to ΔS from ΔS_{SM}. The experimental situation is shown in Figure 8 [69].

154

The most precisely determined $\sin 2\beta_{\text{eff}}$ from a $b \to s$ loop process is that of $B^0 \to \eta' K^0$. This is also one of the theoretically cleanest channels, and is consistent with the SM expectation of $\Delta S = 0$ at the current precision. In recent years it has been frequently noted that the average value of $\sin 2\beta_{\text{eff}} - \sin 2\beta$ is less than zero with a significance of between two and three standard deviations. However as discussed above, it is not correct to compare the average of any set of processes unless the value of ΔS_{SM} is the same for that set. If one wants to make a comparison at the percent level, it has to be done on a mode-by-mode basis, and to do that we need to build a next generation of experiments to record and analyse $\mathcal{O}(50-100)\text{ab}^{-1}$ of data. The two proposed experiments SuperB and SuperKEKB will be able to make such measurements. If one compares the measured values of $\sin 2\beta_{\text{eff}} - \sin 2\beta$ for the $b \to d$ processes which have a tree and a loop contribution it is clear that they are consistent with the SM expectation. At future B factories it will be possible to extend this approach to making comparisons of the precision measurements of α and γ from different decay channels.
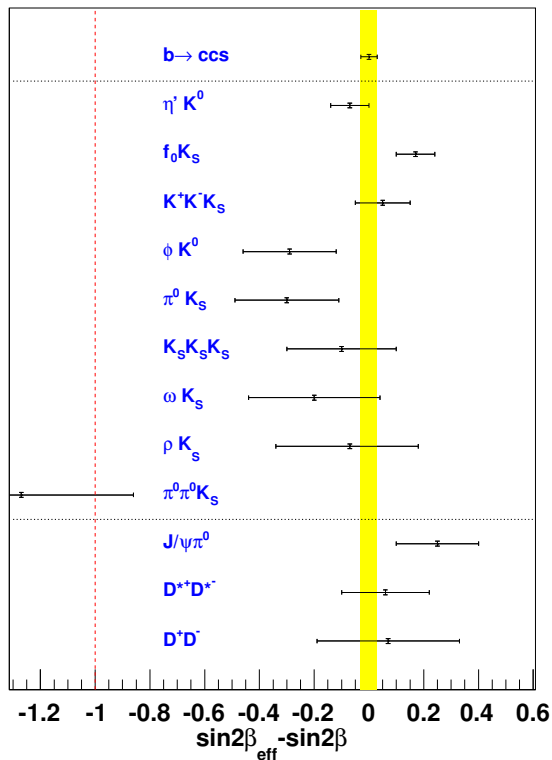
Figure 8: Measurements of $\sin 2\beta_{\text{eff}}$-$\sin 2\beta$. The top part and vertical band show the reference measurement from $c\bar{c}s$ decays (See Sec. 3.1.1), the middle part shows measurements from $b \to s$ loop processes, and the part section shows measurements from $b \to d$ processes with loop and tree contributions. All results shown are averages of measurements from *BABAR* and Belle.

3.2 Side measurements

This section discusses the measurements of $|V_{\text{ub}}|$, $|V_{\text{cb}}|$, and $|V_{\text{td}}/V_{\text{ts}}|$ in turn. All of these quantities are can be used to constrain the unitarity triangle. The measurements of $|V_{\text{ub}}|$ and $|V_{\text{cb}}|$ use the semi-leptonic decays $B \to X\ell\nu$ where $X = X_u$ or X_c and it is possible to put constraints on $|V_{\text{td}}/V_{\text{ts}}|$ by measuring $B \to X_{d,s}\gamma$ decays.

3.2.1 Measuring $|V_{\text{ub}}|$

The branching ratios of B decays to $u\ell\nu$ semi-leptonic final states are proportional to $|V_{ub}|$ for a limited region of phase space. In order to reduce backgrounds in these measurements, both B mesons in the event are reconstructed using the so-called *recoil* method. This involves reconstructing the inclusive or exclusive $b \to u\ell\nu$ signal, as well as reconstructing everything else in the event into a fully reconstructed final state (i.e. one with no missing energy). If this is done correctly for a $B\overline{B}$ event, then the missing 4-momentum in the centre of mass will correspond to the 4-momentum of the undetected ν from the signal decay. The recoil method results in low signal efficiencies, typically a few percent, however most of the non-B background will have been rejected from the selected sample of events and the signal sample is relatively clean. Once isolated, it is possible to measure the partial branching fraction of a decay as a function of a phase space variable, including the q^2 of the $\ell\nu$ in the final state, the invariant mass of the X_u, missing mass (corresponding to the neutrino), or energy of the lepton.

Figure 9: Constraints on $|V_{ub}|$ compiled by HFAG [71].

Given the partial branching fraction measurement, theoretical input is required in order to compute $|V_{ub}|$. There are several schemes available to convert the partial branching fraction to a measurement of $|V_{ub}|$ (ADFR, BLNP, BLL, DGE, GGOU, LLR, and LNP), and all of these schemes [70] give compatible results [71]. Figure 9 shows the different values of $|V_{ub}|$ extracted from the data for the different schemes where the LLR and LNP schemes use $B \to X_u\ell\nu$ decays normalised to $B \to X_s\gamma$ decays in order to determine $|V_{ub}|$.

3.2.2 Measuring $|V_{cb}|$

The recoil method discussed above is also used in order to isolate signals in the measurement of $|V_{cb}|$. Only two decay channels are considered (i) $B \to D\ell^+\overline{\nu}$ and (ii) $B^+ \to D^{*0}\ell^+\overline{\nu}$ where the partial branching fraction of these decays is proportional to $|V_{cb}|$ up to some form factor.

The partial branching fraction of $B \to D\ell^+\overline{\nu}$ is proportional to $G^2|V_{cb}|^2$, where G is a form factor that depends on kinematic quantities. As the measurement is statistically limited, seven (nine) different D^0 (D^+) daughter decays into final states with neutral and charged pions and kaons are reconstructed. The results obtained using a combined fit to all data are $G(1)|V_{cb}| = (43.0 \pm 1.9 \pm 1.4) \times 10^{-3}$, where $|V_{cb}| = (39.8 \pm 1.8 \pm 1.3 \pm 0.9) \times 10^{-3}$ [71] where this result is dominated by *BABAR* [72, 73]. Errors are statistical, systematic and from the form

factor dependence. Figure 10 shows the distribution of $G(1)|V_{cb}|$ versus ρ^2 obtained, where the form factor G depends on the shape parameter ρ^2.

The partial branching fraction of $B^+ \to D^{*0}\ell^+\overline{\nu}$ is proportional to $F^2|V_{cb}|^2$, where F is a form factor that depends on kinematic quantities. The measurement of $|V_{ub}|$ using this mode is systematically limited, and as a result the only D^{*0} daughter decay channel considered is to a $D^0\pi$ final state, where the D meson subsequently decays to $K^+\pi^-$. The values of $F(1)|V_{cb}|$ and the slope parameter ρ^2 are extracted from a three dimensional fit to data, where the discriminating variables in the fit are the mass difference between the reconstructed D^* and D meson masses Δm, the angle between the B and the $Y = D^*\ell$ in the centre of mass θ^*_{BY} and an estimator for the dot product of the four velocities of the B and the D^*. The results obtained are $F(1)|V_{cb}| = (35.97 \pm 0.53) \times 10^{-3}$ and $|V_{cb}| = (38.7 \pm 0.6 \pm 0.9) \times 10^{-3}$, where the first uncertainty is experimental and the second is theoretical [71] where this result is dominated by Belle and *BABAR* [73, 74, 75, 76]. Figure 10 shows the distribution of $F(1)|V_{cb}|$ versus ρ^2.
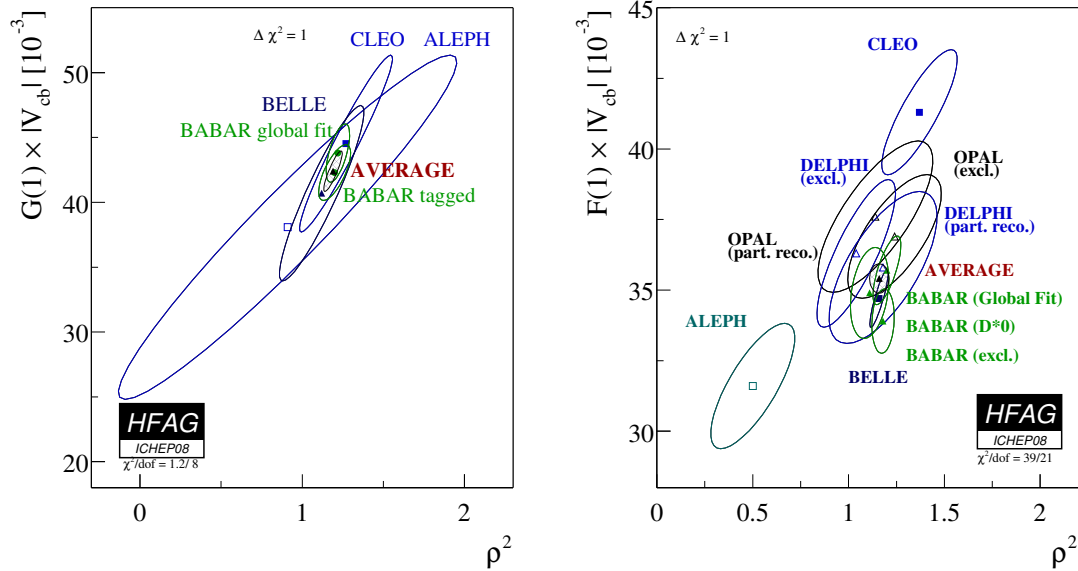
Figure 10: Measurements of (left) $G(1)|V_{cb}|$ and (right) $F(1)|V_{cb}|$ versus the slope ρ^2 obtained from $D^{(*)}\ell\overline{\nu}$ decays. These plots are from Ref. [71].

3.2.3   Measuring $|V_{td}/V_{ts}|$

It is possible to measure the ratio $|V_{td}/V_{ts}|$ using $B \to X_d\gamma$ and $B \to X_s\gamma$ decays as outlined by Ali, Asatrian and Greub [77]. The branching fractions of these processes depend on $|V_{td}|$ and $|V_{ts}|$, respectively. These are Flavour Changing Neutral Currents that are sensitive to new physics, where the leading order contributions are electroweak loop amplitudes. *BABAR* perform an inclusive analysis of $B \to X_d\gamma$ decays where X_d is reconstructed from between two and four π mesons, or a $\pi^+\eta$ final state, and extract a branching fraction in two regions of the invariant

mass m_X of X_d [78]. Belle perform an exclusive analysis and reconstruct X_d in ρ and ω final states [79]. The branching fractions measured are summarised in Table 4.

Experiment	Region/mode	$\mathcal{B}$ ($\times 10^{-6}$)
BABAR	$0.6 < m_X < 1.0\ GeV/c^2$	$1.2 \pm 0.5 \pm 0.1$
BABAR	$1.0 < m_X < 1.8\ GeV/c^2$	$2.7 \pm 1.2 \pm 0.4$
Belle	$B^+ \to \rho^+\gamma$	$0.87^{+0.29\ +0.09}_{-0.27\ -0.11}$
Belle	$B^0 \to \rho^0\gamma$	$0.78^{+0.17\ +0.09}_{-0.16\ -0.10}$
Belle	$B^0 \to \omega\gamma$	$0.40^{+0.19\ +0.09}_{-0.17\ -0.10}$

Table 4: Branching fraction ($\mathcal{B}$) measurements for $B \to X_d\gamma$. Inclusive measurements shown are from *BABAR*, and exclusive measurements shown are from Belle.

The constraint on $|V_{\mathrm{td}}/V_{\mathrm{ts}}|$ obtained using these measurements are $0.195^{+0.020}_{-0.019}$(expt) $\pm$ 0.015(theory) and 0.177 ± 0.043(expt) ± 0.001(theory) from Belle and *BABAR*, respectively. The small theoretical uncertainty on the *BABAR* measurement is the result of the method used to determine $|V_{\mathrm{td}}/V_{\mathrm{ts}}|$ from data.

4   Tests of CPT

The combined symmetry of C, P and T otherwise written as CPT is conserved in locally gauge invariant quantum field theory. The role of CPT in our understanding of physics is described in more detail in Refs. [80, 81, 82, 83] and an observation of CPT violation would be a sign of new physics. CPT violation could be manifest in neutral meson mixing, so the B factories are well suited to test this symmetry. The contribution to these proceedings by Nierst describes the phenomenon of neutral meson mixing in detail in terms of the complex parameters p and q. It is possible to extend the formalism used by Nierst to allow for possible CPT violation, and in doing so the heavy and light mass eigenstates of the B^0 meson B_{H} and B_{L} become

$$|B_{\mathrm{L,H}}\rangle = p\sqrt{1 \mp z}|B^0\rangle \pm q\sqrt{1 \pm z}|\overline{B}^0\rangle,$$

where B^0 and $\overline{B}^0$ are the strong eigenstates of the neutral B meson. If we set $z = 0$ we recover the CPT conserving solution and if CP and CPT are conserved in mixing then $|q|^2 + |p|^2 = 1$.

Two types of analysis have been performed by *BABAR* to test CPT. The first of these uses the B_{flav} sample that characterises the dilution and resolutions for the Charmonium $\sin 2\beta$ analysis discussed in Section 3.1 along with the Charmonium CP eigenstates $B^0 \to J/\psi K^0$, $\psi(2S)K_S^0$, and $\chi_{1c}K_S^0$ to extract z [86]. This analysis also uses control samples of charged B decays: $B^+ \to \overline{D}^{(*)0}\pi^+$, $J/\psi K^{(*)+}$, $\psi(2S)K^+$, and $\chi_{1c}K^+$ to obtain

$$\left|\frac{q}{p}\right| = 1.029 \pm 0.013(\mathrm{stat.}) \pm 0.011(\mathrm{syst.}),$$
$$(\mathrm{Re}\lambda_{\mathrm{CP}}/|\lambda_{\mathrm{CP}}|)\mathrm{Re}z = 0.014 \pm 0.035(\mathrm{stat.}) \pm 0.034(\mathrm{syst.}),$$
$$\mathrm{Im}z = 0.038 \pm 0.029(\mathrm{stat.}) \pm 0.025(\mathrm{syst.}),$$

which is compatible with no CP violation in $B^0 - \overline{B}^0$ mixing and CPT conservation.

The second and more powerful type of analysis uses di-lepton events where both B mesons in an event decay into an $X^{\mp}\ell^{\pm}\nu$ final state tests CPT. Di-lepton events can be grouped by lepton charge into three types: $++$, $+-$ and $--$ where the numbers of such events N^{++}, N^{+-} and N^{--} are related to $\Delta\Gamma$ and z as a function of Δt as described in Ref. [89]. Using these distributions we can construct two asymmetries: the first is a T/CP asymmetry

$$\mathcal{A}_{T/CP} = \frac{P(\overline{B}^0 \to B^0) - P(B^0 \to \overline{B}^0)}{P(\overline{B}^0 \to B^0) + P(B^0 \to \overline{B}^0)} = \frac{N^{++} - N^{--}}{N^{++} - N^{--}} = \frac{1 - \left|\frac{q}{p}\right|^4}{1 + \left|\frac{q}{p}\right|^4},$$

and the second is a CPT asymmetry

$$\mathcal{A}_{CPT}(\Delta t) = \frac{N^{+-}(\Delta t > 0) - N^{+-}(\Delta t < 0)}{N^{+-}(\Delta t > 0) + N^{+-}(\Delta t < 0)} \simeq 2\frac{\mathrm{Im}z\sin(\Delta m_d \Delta t) - \mathrm{Re}z\sinh\left(\frac{\Delta\Gamma\Delta t}{2}\right)}{\cosh\left(\frac{\Delta\Gamma\Delta t}{2}\right) + \cos(\Delta m_d \Delta t)},$$

where $\mathcal{A}_{CPT}(\Delta t)$ is sensitive to $\Delta\Gamma \times \mathrm{Re}z$. In the Standard Model $\mathcal{A}_{T/CP} \sim 10^{-3}$ and $\mathcal{A}_{CPT} = 0$ [84, 85]. *BABAR* measure [87]

$$\left|\frac{q}{p}\right| - 1 = (-0.8 \pm 2.7(\text{stat.}) \pm 1.9(\text{syst.})) \times 10^{-3},$$
$$\mathrm{Im}z = (-13.9 \pm 7.3(\text{stat.}) \pm 3.2(\text{syst.})) \times 10^{-3},$$
$$\Delta\Gamma \times \mathrm{Re}z = (-7.1 \pm 3.9(\text{stat.}) \pm 2.0(\text{syst.})) \times 10^{-3},$$

which is compatible with no CP violation in $B^0 - \overline{B}^0$ mixing and CPT conservation. It is possible to study variations as a function of sidereal time, where 1 sidereal day is approximately 0.99727 solar days [88] where z depends on the four momentum of the B candidate. *BABAR* re-analysed their data to and find that it is consistent with $z = 0$ at 2.8 standard deviations [89]. The constraint on z is shown in Figure 11.
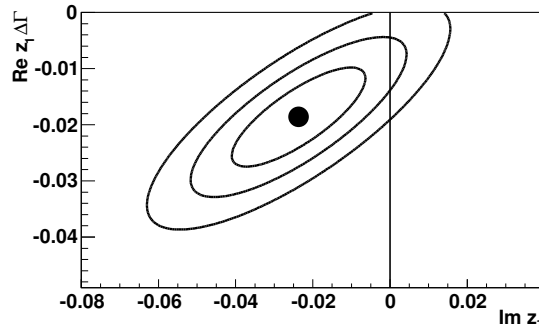
Figure 11: Constraints on the imaginary part of z and $\Delta\Gamma \times \mathrm{Re}z$ using dilepton events at *BABAR*. This figure is reproduced from Ref. [89].

5 B decays to spin one particles

Decays of B mesons to final states with two vector ($J^P = 1^-$) or axial-vector ($J^P = 1^+$) particles have a number of interesting kinematic observables that can be used to test theoretical understanding of heavy flavour. The angular distribution of such a process where the spin one particles decay into two daughters is a function of three variables: ϕ, θ_1 and θ_2, where ϕ is the angle between the decay planes of the spin one particles, and θ_i are the angles between the spin one particle decay daughter momentum and the direction opposite to that of the B^0 in the spin one particle rest frame. The θ_i are often referred to as helicity angles. Figure 12 illustrates these three angles for the decay $B^0 \to \rho^+\rho^-$.

Figure 12: A schematic of the decay of a B meson via two ρ mesons to a four pion final state. The ρ meson final states are shown in their rest frames, and ϕ is the angle between the decay planes of the ρ mesons.

It is only possible to perform a full angular analysis if we have sufficient data to constrain the unknown observables. When we search for a rare decay it is normal to perform a simplified angular analysis in terms of the helicity angles, having first integrated over ϕ. On doing this one obtains

$$\frac{d^2\Gamma}{\Gamma\, d\cos\theta_1\, d\cos\theta_2} = \frac{9}{4}\left[f_{\mathrm{L}}\cos^2\theta_1\cos^2\theta_2 + \frac{1}{4}(1 - f_{\mathrm{L}})\sin^2\theta_1\sin^2\theta_2\right]$$

where the parameter f_{L} is referred to as the fraction of longitudinally polarized events which is given by

$$\frac{\Gamma_L}{\Gamma} = \frac{|H_0|^2}{|H_0|^2 + |H_{+1}|^2 + |H_{-1}|^2} = f_{\mathrm{L}},$$

where the H_i are helicity amplitudes. It is convenient to analyse the data using the transversity basis when performing time-dependent CP studies where the transversity amplitudes are $A_0 = H_0$, $A_\perp = (H_{+1} - H_{-1})/\sqrt{2}$ and $A_{||} = (H_{+1} + H_{-1})/\sqrt{2}$ [90]. A_0 and $A_{||}$ are CP even and $A_\perp$ is CP odd. Helicity suppression arguments lead to the expectation of the following hierarchy:

$$A_0 : A_{||} : A_\perp \sim \mathcal{O}\left(1\right) : \mathcal{O}\left(\frac{m_R}{m_B}\right) : \mathcal{O}\left(\frac{m_R}{m_B}\right)^2,$$

where m_R is the mass of the spin one resonance and m_B is the B meson mass. This hierarchy predicts that $f_{\mathrm{L}} = 1 - m_R^2/m_B^2$ [91, 92, 93, 94]. The B factories have measured the fraction of longitudinally polarized events in a number of different channels, the results of which are shown in Table 5.

It is clear that the helicity suppression argument works for a number of the decay modes studied. These are all tree dominated processes such as $B \to \rho^+\rho^-$. It is also clear that there are several decay modes that do not behave in the same way. The most precisely measured channel that disagrees with the helicity suppression argument is $B^0 \to \phi K^{*0}$, where $f_{\mathrm{L}} \sim 0.5$. This discrepancy is often called the 'polarization puzzle' in the literature. Several papers for example Ref. [92] have highlighted the possibility that new physics could be the source of the difference, however final state interactions or refined calculations could also account for the difference. The

Decay Mode	*BABAR*	Belle
$B^0 \to \phi K^{*0}$ [95, 96]	$0.494 \pm 0.34 \pm 0.013$	$0.45 \pm 0.05 \pm 0.02$
$B^+ \to \phi K^{*+}$ [97, 96]	$0.49 \pm 0.05 \pm 0.03$	$0.52 \pm 0.08 \pm 0.03$
$B^0 \to \rho^+ \rho^-$ [37, 41]	$0.992 \pm 0.024^{+0.026}_{-0.013}$	$0.941^{+0.034}_{-0.040} \pm 0.030$
$B^0 \to \rho^0 \rho^0$ [38, 40]	$0.75^{+0.11}_{-0.14} \pm 0.05$	. . .
$B^+ \to \rho^0 \rho^-$ [36, 39]	$0.905 \pm 0.042^{+0.023}_{-0.027}$	$0.95 \pm 0.11 \pm 0.02$
$B^0 \to \omega K^{*0}$ [98]	. . .	$0.56 \pm 0.29^{+0.18}_{-0.08}$
$B^+ \to \omega \rho^{*+}$ [99]	$0.82 \pm 0.11 \pm 0.02$	. . .
$B^0 \to K^{*0}\overline{K}^{*0}$ [100]	$0.80^{+0.10}_{-0.12} \pm 0.06$	. . .
$B^0 \to \rho^0 K^{*0}$ [101]	$0.57 \pm 0.09 \pm 0.08$	. . .
$B^+ \to \rho^0 K^{*+}$ [101]	$0.96^{+0.04}_{-0.15} \pm 0.05$	. . .
$B^+ \to \rho^+ K^{*0}$ [101, 102]	$0.52 \pm 0.10 \pm 0.04$	$0.43 \pm 0.11^{+0.05}_{-0.02}$

Table 5: Experimental results for f_L from B meson decays to two vector meson final states. The first uncertainty is statistical and the second is systematic.

decay modes that do not follow the naive helicity suppression argument are all loop dominated. In addition to studying B decays to final states with two vector particles, it is possible to study vector axial-vector and two axial-vector final states. Measurements of these decays could help refine our understanding of the source of the polarization puzzle. There are a number of rare decays that have suppressed standard model topologies, for example $B \to \phi\phi$ and $B \to \phi\rho$. Experimental limits on these decays are at the level of a few 10^{-7} [103]. These decays could be significantly enhanced by new physics, and Gronau and Rosner recently suggested that $\phi - \omega$ mixing could result in a significant enhancement of the $B \to \phi\rho^+$ decay [104].

6 Summary

The B factories have produced a large number of results in many areas of flavour physics. The ability of the B factories to quickly crosscheck each others results has been extremely beneficial to the development of experimental measurements and techniques over the past decade. Only a small number of these results have been discussed here: those pertaining to testing the unitarity triangle, CPT, and B decays to final states with two spin one particles. These results are consistent with the CKM theory for CP violation in the Standard Model. There are a number of measurements sensitive to new physics contributions that can be made at future experiments such as SuperB in Italy and Super KEK-B in Japan [25, 26]. Such precision tests of flavour physics could be used to elucidate the flavour structure beyond the Standard Model.

7 Acknowledgments

References

[1] J.H. Christenson, J.W. Cronin, V.L. Fitch, and R. Turlay, Phys. Rev. Lett. **13** 138-140 (1964).

[2] A. D. Sakharov, Pis'ma Zh. Eksp. Teor. Fiz. **5** 32 (1967) [JETP Lett. **5** 24 (1967)].

[3] N. Cabibbo, Phys. Rev. Lett. **10** 531 (1963).

[4] M. Kobayashi and T. Maskawa, Prog. Theor. Phys **49** 652 (1973).

[5] I. Bigi and A. Sanda, Nucl. Phys. **B193** 85 (1981).

[6] P. Oddone, *Detector Considerations*, Workshop on Conceptual Design of a Test Linear Collider: Possibilities for a B Anti-B Factory, Los Angeles, California, pp 423-446 (1987).

[7] J. Dorfan, B-Factory Symposium, Stanford, 17th October 2008.

[8] *BABAR* Collaboration, Nucl. Instrum. Meth. Phys. Res., Sec. A **479** 1 (2002).

[9] PEP-II Conceptual Design Report, SLAC-R-418 (1993).

[10] Belle Collaboration, Nucl. Instrum. Meth. Phys. Res., Sec. A **479** 117 (2002).

[11] KEKB B-factory Design Report, KEK Report 95-7 (1995).

[12] *BABAR* Collaboration, Nucl. Instrum. Meth. Phys. Res., Sec. A **479**, 1 (2002).

[13] C. Amsler *at al..*, Phys. Lett. B **667** 1 (2008).

[14] H. Li and S. Mishima, JHEP **0703** 009 (2007).

[15] H. Boos, J. Reuter, and T. Mannel, Phys. Rev. D **70**, 036006 (2006).

[16] M. Ciuchini, M. Pierini, and L. Silvestrini, Phys. Rev. Lett. **95**, 221804 (2005).

[17] *BABAR* Collaboration, Phys. Rev. Lett. **87** 091801 (2001).

[18] Belle Collaboration, Phys. Rev. Lett. **87** 091802 (2001).

[19] *BABAR* Collaboration, SLAC-PUB-13324; *BABAR* Collaboration, Phys. Rev. Lett. **99**, 171803.

[20] Belle Collaboration, Phys. Rev. Lett. **98**, 031802 (2007); Belle Collaboration, Phys. Rev. D **77**, 091103 (2008).

[21] *BABAR* Collaboration, Phys. Rev. D **71** 032005 (2005); Belle Collaboration, Phys. Rev. Lett. **95** 091601 (2005).

[22] *BABAR* Collaboration, Phys. Rev. D **71** 032005 (2005); Belle Collaboration, Phys. Rev. Lett. **95** 091601 (2005).

[23] *BABAR* Collaboration, Phys. Rev. Lett. **99** 081801 (2007).

[24] LHCb: `http://lhcb.web.cern.ch/lhcb/`.

[25] SuperB: Conceptual Design Report, arXiv:0709.0451; Valencia Physics Workshop, arXiv:0810.1312. `http://www.pi.infn.it/SuperB/`.

[26] Super KEK-B: `http://superb.kek.jp/`.

[27] M. Shifman, ITEP Lectures in Particle Physics and Field Theory. **1** pp v-xi (1999); e-Print: hep-ph/9510397.

[28] M. Gronau and D. London, Phys. Rev. Lett. **65**, 3381 (1990).

[29] H. Lipkin *at al.*, Phys. Rev. D **44**, 1454 (1991).

[30] A. Snyder and H. Quinn, Phys. Rev. D **48**, 2139 (1993); H. Quinn and J. Silva, Phys. Rev. D **62**, 054002 (2000).

[31] A. Bevan, Mod. Phys. Lett. A**21** 305-318 (2006).

[32] M. Beneke *at al.*, Phys. Lett. B **638** 68 (2006).

[33] UTfit Collaboration, `http://www.utfit.org/`.

[34] Belle Collaboration, Phys. Rev. Lett. **98**, 211801 (2007).

[35] *BABAR* Collaboration, arXiv:0807.4226.

[36] *BABAR* Collaboration, Phys. Rev. Lett. **97**, 261801 (2006).

[37] *BABAR* Collaboration, Phys. Rev. D **76**, 052007 (2007); *BABAR* Collaboration, Phys. Rev. Lett. **93** 231801 (2004).

[38] *BABAR* Collaboration, arXiv:0807.4977.

[39] Belle Collaboration, Phys. Rev. Lett. **91**, 221801 (2003).

[40] Belle Collaboration, arXiv:0708.2006.

[41] Belle Collaboration, Phys. Rev. D **76**, 011104 (2007).

[42] *BABAR* Collaboration, Phys. Rev. D **76** 012004 (2007).

[43] Belle Collaboration, Phys. Rev. D **77** 072001 (2008).

[44] T. Nakada, Acta Phys. Polon. **B38** 299 (2007).

[45] *BABAR* Collaboration, Phys. Rev. Lett. **98**, 181803 (2007).

[46] *BABAR* Collaboration, Phys. Rev. D **74** 031104 (2006).

[47] M. Gronau, D. London, and D. Wyler, Phys. Lett. B **253** 483 (1991).

[48] M. Attwood, I. Dunietz, and A. Soni, Phys. Rev. Lett. **78** 3257 (1997).

[49] A. Giri, Y. Grossman, A. Soffer, and J. Zupan, Phys. Rev. D **68** 054018 (2003).

[50] CKMfitter Group, Eur. Phys. J. C**41** 1-131 (2005), updates available at http://ckmfitter.in2p3.fr.

[51] Belle Collaboration, Phys. Rev. D **73**, 051106 (2006).

[52] *BABAR* Collaboration, Phys. Rev. D **72**, 071103 (2005); *BABAR* Collaboration, Phys. Rev. D **77**, 111102 (2008); *BABAR* Collaboration, arXiv:0807.2408.

[53] Belle Collaboration, Phys. Rev. D **78** 071901 (2008).

[54] *BABAR* Collaboration, Phys. Rev. D **72**, 032004 (2005); *BABAR* Collaboration, Phys. Rev. D **72**, 071104 (2005); *BABAR* Collaboration, Phys. Rev. D **76**, 111101 (2007).

[55] Belle Collaboration, arXiv:0803.3375.

[56] *BABAR* Collaboration, Phys. Rev. D **78** 034023 (2008).

[57] V. Fanti *at al.*, Phys. Lett. B **465** 335 (1999).

[58] A. Alavi-Harati *at al.*, Phys. Rev. Lett. **83** 22 (1999).

[59] *BABAR* Collaboration, Phys. Rev. Lett. **99** 021603 (2007).

[60] Belle Collaboration, Nature **452** 332 (2008).

[61] *BABAR* Collaboration, arXiv:0807.4226.

[62] CDF Collaboration, hep-ex/0612018.

[63] CLEO Collaboration, Phys. Rev. Lett. **85** 525 (2000).

[64] C. K. Chua, Phys. Rev. D **78** 076002 (2008).

[65] M. Beneke *at al.*, Phys. Lett. B**620** 143 (2005).

[66] A. Williamson and J. Zupan, Phys. Rev. D **74** 014003 (2006).

[67] H.Y.Cheng *at al.*, Phys. Rev. D **72** 014006 (2005).

[68] M. Gronau *at al.*, Phys. Rev. D **74** 093003 (2006).

[69] Belle Collaboration, Phys. Rev. D **77**, 071101 (2008); *BABAR* Collaboration, Phys. Rev. Lett. **101**, 021801 (2008); Belle Collaboration, Phys. Rev. Lett. **98**, 221802 (2007); Belle Collaboration, Phys. Rev. Lett. **98**, 031802 (2007); *BABAR* Collaboration, arXiv:0809.1174; *BABAR* Collaboration, Phys. Rev. Lett. **99**, 161802 (2007); *BABAR* Collaboration, Phys. Rev. D **76**, 091101 (2007); *BABAR* Collaboration, arXiv:0708.2097; Belle Collaboration, Phys. Rev. D **76**, 091103 (2007); *BABAR* Collaboration, Phys. Rev. Lett. **99**, 161802 (2007); Belle Collaboration, arXiv:0708.1845; *BABAR* Collaboration, Phys. Rev. D **76**, 071101 (2007); *BABAR* Collaboration, Phys. Rev. Lett. **99**, 161802 (2007).

[70] B. Lange *at al.*, Phys. Rev. D **72** 073006 (2005); J. R. Anderson and E. Gardi, JHEP 0601: 097 (2006); E. Gardi arXiv:0806.4524; P. Gambino *at al.*, JHEP 0710 058 (2007); U. Aglietti *at al.*, arXiv:0711.0860; C. W. Bauer *at al.*, Phys. Rev. D **64** 113004 (2001); A. Leibovich *at al.*, Phys.Rev. D61 (2000) 053006; B. Lange *at al.*, JHEP 0510 084 (2005).

[71] HFAG Group, arXiv:0704.3575, partial update online at `http://www.slac.stanford.edu/xorg/hfag`.

[72] *BABAR* Collaboration, arXiv:0807.4978.

[73] *BABAR* Collaboration, arXiv:0809.0828.

[74] Belle Collaboration, Phys. Lett. B **526**, p247 (2002).

[75] *BABAR* Collaboration, Phys. Rev. Lett. **100** 231803 (2008).

[76] *BABAR* Collaboration, Phys. Rev. D **77** 032002 (2008).

[77] A. Ali *at al.*, Phys. Lett. B **429** 87 (1998).

[78] *BABAR* Collaboration, arXiv:0708.3702.

[79] Belle Collaboration, Phys. Rev. Lett. **95** 241801 (2005).

[80] G. Lüders, Mat. Fys. Medd. **28** 5 (1954).

[81] R. Jost, Helv. Phys. Acta **30** 409 (1957).

[82] W. Pauli, Nuovo Cimento **6** 204 (1957).

[83] F. Dyson, Phys. Rev. **110** 579 (1958).

[84] M. Beneke *at al.*, Phys. Lett. B **576** 173 (2003).

[85] M. Ciuchini *at al.*, JHEP **0308** 031 (2003).

[86] *BABAR* Collaboration, Phys. Rev. D **70** 012007 (2004).

[87] *BABAR* Collaboration, Phys. Rev. Lett. **96** 251802 (2006).

[88] V.A. Kostelecky, Phys. Rev. Lett. **80** 1818 (1998).

[89] *BABAR* Collaboration, Phys. Rev. Lett. **100** 131802 (2008).

[90] I. Dunietz *at al.*, Phys. Rev. D **43** 2193 (1991).

[91] A. Ali *at al.*, Phys. Rev. D **58** 094009 (1998).

[92] A. Kagan, Phys. Lett. B **601** 151-163 (2004).

[93] G. Kramer and W. Palmer, Phys. Rev. D **45** 193 (1992).

[94] M. Suzuki, Phys. Rev. D **66** 054018 (2002).

[95] *BABAR* Collaboration, arXiv:0808.3586.

[96] Belle Collaboration, Phys. Rev. Lett. **94** 221804 (2005).

[97] *BABAR* Collaboration, Phys. Rev. Lett. **99** 201802 (2007).

[98] Belle Collaboration, arXiv:0807.4271.

[99] *BABAR* Collaboration, Phys. Rev. D **74** 051102 (2006).

[100] *BABAR* Collaboration, Phys. Rev. Lett. **100** 081801 (2008).

[101] *BABAR* Collaboration, Phys. Rev. Lett. **97** 201801 (2006).

[102] Belle Collaboration, Phys. Rev. Lett. **95** 141801 (2005).

[103] *BABAR* Collaboration, arXiv:0807.3935.

[104] M. Gronau and J. Rosner, arXiv:0806.3584.

Lepton-number violating meson decays in theories beyond the Standard Model

Anatoly Borisov

Faculty of Physics, Moscow State University, 119991 Moscow, Russia

After discussion of mechanisms of lepton number violation, we consider meson decays $K^+ \to \pi^- \ell^+ \ell'^+$ and $D^+ \to K^- \ell^+ \ell'^+$ ($\ell, \ell' = e, \mu$) with $\Delta L = 2$ in the Standard Model extended by massive Majorana neutrinos and in a supersymmetric extension of the Standard Model with explicit breaking of R-parity by trilinear or bilinear Yukawa couplings in the superpotential. We give estimates of the branching ratios for these decays and compare the effectiveness of various decay mechanisms taking into account present experimental bounds on lepton mixing, masses of neutrinos and superparticles, and R-parity violating couplings.

1 Introduction

In the Standard Model (SM), the lepton L and baryon B numbers are conserved due to the accidental $U(1)_L \times U(1)_B$ symmetry. But the L and B nonconservation is a generic feature of various extensions of the SM. That is why lepton-number violating processes are sensitive tools for testing theories beyond the SM.

The following $\Delta L \neq 0$ processes have been extensively studied: neutrinoless double beta decay $(A, Z) \to (A, Z + 2) + e^- + e^-$ [1, 2, 3]; rare meson decays $M^+ \to M'^- \ell^+ \ell'^+$ ($\ell, \ell' = e, \mu$) ($K^+ \to \pi^- \mu^+ \mu^+$ etc.) [4, 5, 6, 7]; same-sign dilepton production in high-energy hadron-hadron and lepton-hadron collisions: $pp \to \ell^\pm \ell'^\pm X$ [8, 9, 10], $e^\pm p \to \overset{(-)}{\nu_e} \ell^\pm \ell'^\pm X$ [11, 12]; (μ^-, e^+) conversion in nuclei $(A, Z) + \mu_b^- \to e^+ + (A, Z - 2)^*$ [13].

The SM is based on the gauge group

$$G_{\mathrm{SM}} = SU(3)_c \times SU(2)_I \times U(1)_Y \tag{1}$$

with the subscripts c, I, and Y denoting color, weak isospin and hypercharge, respectively, and three fermion generations (families, $f = 1, 2, 3$), each of them is consisted of 5 different representations of G_{SM}:

$$L_L^f(\mathbf{1}, \mathbf{2}, -1) = (\nu_{eL}, e_L)^T, (\nu_{\mu L}, \mu_L)^T, (\nu_{\tau L}, \tau_L)^T;$$
$$Q_L^f(\mathbf{3}, \mathbf{2}, 1/3) = (u_L, d_L)^T, (c_L, s_L)^T, (t_L, b_L)^T;$$
$$E_R^f(\mathbf{1}, \mathbf{1}, -2) = e_R, \mu_R, \tau_R; \ U_R^f(\mathbf{3}, \mathbf{1}, 4/3) = u_R, c_R, t_R; \ D_R^f(\mathbf{3}, \mathbf{1}, -2/3) = d_R, s_R, b_R. \tag{2}$$

The fermion interactions are mediated by 12 ($= 8_c + 3_I + 1_Y$) gauge vector bosons.

In addition, the SM contains a *single* Higgs boson doublet $\varphi(\mathbf{1}, \mathbf{2}, 1)$. Its *nonzero* vacuum expectation value $\langle \varphi \rangle$ *spontaneously breaks* the gauge symmetry and *yields masses* to weak

bosons (as well as to charged fermions and the Higgs boson itself):

$$\langle\varphi\rangle = (0, v/\sqrt{2}\,)^T \Rightarrow \quad G_{\mathrm{SM}} \to SU(3)_c \times U(1)_Q, \tag{3}$$

where the electric charge $Q = I_3 + Y/2$.

The Higgs boson is the only piece of the SM which is not confirmed experimentally up to now!

2 Lepton numbers and mechanisms of their violation

So there are three lepton families (generations) in the SM (see Eq. (2)). By definition, the *lepton family number* (LFN) $L_\ell = +1(-1)$ for particles $\ell = e^-, \nu_e, \ldots$ (for antiparticles $\bar{\ell} = e^+, \bar{\nu}_e, \ldots$), and $L_\ell = 0$ for leptons $\ell' \neq \ell, \bar{\ell}' \neq \bar{\ell}$. The *total lepton number* (LN)

$$L = L_e + L_\mu + L_\tau, \tag{4}$$

so that $L = +1(-1)$ for each ℓ ($\bar{\ell}$) and $L = 0$ for other particles (*nonleptons*).

In the minimal SM (with *massless* neutrinos), each LFN is *conserved separately*. For example, in the muon decay $\mu^- \to e^- + \bar{\nu}_e + \nu_\mu$: $L_e = 0 = 1 + (-1) + 0$, $L_\mu = 1 = 0 + 0 + 1$, $L = 1 = 1 + (-1) + 1$.

The SM has three *active* neutrinos $\nu_{\ell L}(\ell = e, \mu, \tau)$ taking part in charged current (CC) and neutral current (NC) weak interactions mediated by the massive charged $W^\pm$ and neutral Z bosons:

$$\mathcal{L}_{\mathrm{CC}} = -\frac{g}{\sqrt{2}} \sum_\ell \left(\bar{\ell}_L \gamma^\mu \nu_{\ell L} W_\mu^- + \bar{\nu}_{\ell L} \gamma^\mu \ell_L W_\mu^+\right), \ \mathcal{L}_{\mathrm{NC}} = -\frac{g}{2\cos\theta_W} \sum_\ell \bar{\nu}_{\ell L} \gamma^\mu \nu_{\ell L} Z_\mu, \tag{5}$$

where the weak-mixing angle is defined by $\tan\theta_W = g'/g$ with g and g' being the the $SU(2)_I$ and $U(1)_Y$ gauge couplings, respectively. The SM contains no *sterile* neutrinos $\nu_{\ell R}$.

In the SM, the lepton family L_ℓ and baryon B numbers are conserved to all orders of perturbation theory due to the *accidental* global symmetry:

$$G_{\mathrm{SM}}^{\mathrm{global}} = U(1)_{L_e} \times U(1)_{L_\mu} \times U(1)_{L_\tau} \times U(1)_B, \tag{6}$$

existing at the level of *renormalizable operators*. The symmetry (6) is called *accidental* because we do not impose it *intentionally*. It is a *direct consequence* of the gauge symmetry and the choice of the representations of the physical fields.

The SM is a *chiral* gauge theory, since there are L-doublets and R-singlets of the gauge group $SU(2)_I$ (they have *different* electroweak interactions, see Eqs. (2) and (5)).

The left-handed and right-handed chiral components of a Dirac field ψ are defined as:

$$\psi_L = P_L \psi, \quad \psi_R = P_R \psi, \quad \psi = \psi_L + \psi_R,$$

where the chirality projection operators

$$P_{L,R} = (1 \mp \gamma^5)/2 = P_{L,R}^2, \quad P_L P_R = 0, \quad \gamma^5 = i\gamma^0 \gamma^1 \gamma^2 \gamma^3.$$

Chirality is eigenvalue of the operator γ^5: $\gamma^5 \psi_L = -\psi_L$, $\gamma^5 \psi_R = +\psi_R$.

Taking into account the relations:

$$\bar{\psi}\gamma^\mu\partial_\mu\psi = \bar{\psi}_L\gamma^\mu\partial_\mu\psi_L + \bar{\psi}_R\gamma^\mu\partial_\mu\psi_R; \ \ \bar{\psi}\psi = \bar{\psi}_R\psi_L + \bar{\psi}_L\psi_R,$$

where $\bar{\psi}_{L,R} = \overline{P_{L,R}\psi} = \bar{\psi}P_{R,L}, \ \bar{\psi} = \psi^+\gamma^0$, we see:

• chiral components interact with gauge fields *independently*;

• the Dirac mass term $(\mathcal{L}_D = -m_D\bar{\psi}\psi)$ in the Lagrangian relates *different* chiral components and *violates* chirality conservation that takes place for *massless* (Weyl) fermions.

In the SM, neutrinos are massless due to absence of $\nu_{\ell R}$. The only possible neutrino mass term $\mathcal{L}_{ML} = -\frac{1}{2}m_L(\bar{\nu}_L\nu_L^c + \bar{\nu}_L^c\nu_L)$ *violates* the lepton number: $\Delta L = \pm 2$. The global symmetry (6) prevents generation of the Majorana mass term $\mathcal{L}_{ML}$ by loop corrections.

The $B - L$-violating terms *cannot be induced even nonperturbatively* because the $U(1)_{B-L}$ subgroup of the group (6) is *non-anomalous*.

Discovery of neutrino oscillations (1998–2002) (predicted by B. Pontecorvo in 1957 [14]),

$$\nu_\ell \to \nu_{\ell'} \ (\ell \neq \ell'),$$

has clearly demonstrated the LFN violation: $\Delta L_{\ell'} = -\Delta L_\ell = 1$. Here ν_ℓ is the neutrino of flavor $\ell = e, \mu, \tau$. It is created in association with the charged lepton ℓ^+ in the decay $W^+ \to \ell^+ + \nu_\ell$.

Up to now the oscillations have been observed unambiguously for solar ($\nu_e \to \nu_\mu(\nu_\tau)$), atmospheric ($\nu_e \to \nu_\mu(\nu_\tau)$), reactor ($\bar{\nu}_e \to \bar{\nu}_\mu$), and accelerator ($\nu_\mu \to \nu_\tau$) neutrinos (for a review, see [15]).

The neutrino oscillations imply that *neutrinos are massive and mixed particles*, i.e. the neutrino flavor state is a coherent superposition of neutrino mass eigenstates:

$$|\nu_\ell\rangle = \sum_i U_{\ell i}^* |\nu_i\rangle \quad (\ell = e, \mu, \tau). \tag{7}$$

Here $U = (U_{\ell i}) \equiv U_{PMNS}$ is the Pontecorvo–Maki–Nakagawa–Sakata lepton mixing matrix [14, 16], ν_is are neutrinos with definite masses m_i, and the neutrino mass spectrum is *nontrivial*: $\Delta m_{jk}^2 \equiv m_j^2 - m_k^2 \neq 0$.

So neutrino oscillations *require extension* of the SM (New Physics) to include nonzero neutrino masses and violation of LFNs. One of the main unsolved questions of particle physics is the nature of neutrino masses: to be Dirac or Majorana type? It should be noted that the neutrino oscillations do not probe the nature of the mass.

The Dirac neutrino carries the lepton number which distinguishes it from the antineutrino. The Dirac neutrino mass term $\mathcal{L}_D$ is generated just like the quark and charged lepton masses via the standard Higgs mechanism (see Eq. (3)) with addition of right-handed neutrinos $\nu_{\ell R}$:

$$-\mathcal{L}_{\text{Yuk}} = y_{\ell\ell'}\bar{L}_\ell\tilde{\varphi}\nu_{\ell' R} + \text{H.c.}, \ \ \bar{L}_\ell = (\bar{\ell}_{\ell L}, \bar{\nu}_{\ell L}), \quad \tilde{\varphi} = i\tau_2\varphi \Rightarrow \tilde{\varphi}_0 = (v/\sqrt{2}, 0)^T,$$
$$-\mathcal{L}_{Yuk} \Rightarrow -\mathcal{L}_D = (M_D)_{\ell\ell'}\bar{\nu}_{\ell L}\nu_{\ell' R} + \text{H.c.}, \tag{8}$$

where $y_{\ell\ell'}$ are Yukawa couplings. The Dirac mass matrix is complex and *nondiagonal*: $(M_D)_{\ell\ell'} = y_{\ell\ell'}v/\sqrt{2}$. Therefore $\mathcal{L}_D$ *violates* LFNs L_e, L_μ, L_τ, but it *conserves* the total LN (4). The standard diagonalization gives $\mathcal{L}_D = -\sum_i m_i\bar{\nu}_i\nu_i$, where ν_i is the 4-component field of Dirac neutrinos with mass m_i, and flavor fields in Eqs. (5)

$$\nu_{\ell L}(x) = \sum_i U_{\ell i}\nu_{iL}(x),$$

U is the PMNS mixing matrix (see Eq. (7)).

The Majorana neutrino is a true neutral particle identical to its antiparticle [17]. There are two types of Majorana mass terms (we consider a simple case of one flavor):

$$\mathcal{L}_{ML} = -\frac{1}{2}m_L(\bar{\nu}_L^c \nu_L + \bar{\nu}_L \nu_L^c), \quad \mathcal{L}_{MR} = -\frac{1}{2}m_R(\bar{\nu}_R^c \nu_R + \bar{\nu}_R \nu_R^c). \tag{9}$$

Here the *charge conjugated* fields are defined as follows:

$$\psi^c = C\bar{\psi}^T = C\gamma^{0T}\psi^*(\psi^* = (\psi^+)^T), \quad \bar{\psi}^c \equiv \overline{\psi^c} = \psi^T C = -\psi^T C^{-1}, \quad C = i\gamma^2\gamma^0,$$

and useful relations are valid: $\psi_L^c \equiv (\psi_L)^c = P_R\psi^c = (\psi^c)_R$, $\psi_R^c \equiv (\psi_R)^c = P_L\psi^c = (\psi^c)_L$.

The Majorana mass term *violates lepton number by two units*, $\Delta L = \pm 2$.

The total Dirac–Majorana mass term is given by (see Eqs. (8) and (9))

$$\mathcal{L}_{D+M} = \mathcal{L}_D + \mathcal{L}_{ML} + \mathcal{L}_{MR}, \tag{10}$$

and after diagonalization it takes the form

$$\mathcal{L}_{D+M} = -\frac{1}{2}\sum_k m_k(\bar{\nu}_{kL}^c \nu_{kL} + \bar{\nu}_{kL}\nu_{kL}^c) = -\frac{1}{2}\sum_k m_k\bar{\nu}_k\nu_k,$$

where two mass eigenstates, $\nu_k = \nu_{kL} + \nu_{kL}^c = \nu_k^c$, are Majorana neutrinos.

From experimental data, we know that the masses of observed neutrinos are much smaller than those of charged leptons (m_ℓ) and quarks (m_q): 0.04 eV < Mass [Heaviest ν_i] < (0.07 ÷ 0.7) eV [15]. The dominant paradigm for the origin of *finite but tiny* neutrino mass is the *seesaw mechanism* (for a review, see [18]): beyond the SM (at ultra-high energies) there exists a mechanism generating the *right-handed Majorana mass term*, and the Dirac mass term is generated through the standard Higgs mechanism, so that in Eq. (10)

$$m_R \gg m_D \sim m_\ell \text{ or } m_q, \ m_L = 0. \tag{11}$$

The neutrino ν_R is *completely neutral* under the SM gauge group (1), and m_R is *not connected* with the SM symmetry breaking scale $v = \left(\sqrt{2}G_F\right)^{-1/2} \simeq 246$ GeV, but is associated to a different higher mass scale, e.g., the GUT-scale: $m_R \sim \Lambda_{\text{GUT}} \sim 10^{15} \div 10^{16}$ GeV $\gg m_D$. There exists a large number of seesaw models in which both m_D and m_R vary over many orders of magnitude, with m_R ranging somewhere between the TeV scale and the GUT-scale [19].

Diagonalization of the mass term (10) of the type (11) gives two mass eigenstates, which are light ν_1 and heavy ν_2 Majorana neutrinos:

$$m_1 \simeq m_D^2/m_R \ll m_D, \quad m_2 \simeq m_R \gg m_D;$$

$$\nu_L = i\nu_{1L}\cos\theta + \nu_{2L}\sin\theta, \ \nu_R^c = -i\nu_{1L}\sin\theta + \nu_{2L}\cos\theta, \ \tan 2\theta = 2m_D/m_R \ll 1,$$

so that $\nu_L \simeq i\nu_{1L}$, $\nu_R^c \simeq \nu_{2L}$.

In the general case of an *arbitrary* number $n_s(\geq 3)$ of *electroweak-singlet (sterile)* neutrinos, the seesaw mass term is

$$-\mathcal{L}_{D+MR} = \bar{\nu}_L M_D \nu_R + \frac{1}{2}\bar{\nu}_R^c M_R \nu_R + \text{H.c.}, \tag{12}$$

where M_D is a $3 \times n_s$ Dirac mass matrix and M_R is a $n_s \times n_s$ Majorana mass matrix. Its diagonalization by means of a unitary $(3 + n_s) \times (3 + n_s)$ matrix V gives 3 light and n_s heavy Majorana neutrinos:

$$\nu_{\ell L} = \sum_{k=1}^{3} V_{\ell k}\nu_{kL}^{\text{light}} + \sum_{k=4}^{n_s+3} V_{\ell k}\nu_{kL}^{\text{heavy}}. \tag{13}$$

A possible scenario of the generation of the Dirac-Majorana mass term $\mathcal{L}_{D+MR}$ suitable for the seesaw mechanism may look as follows: the grand unified group $G_{\mathrm{GUT}} = SO(10)$ can be *broken* to the SM group G_{SM} (1) through the chain

$$SO(10) \xrightarrow{\Lambda_{\mathrm{GUT}}} G_{\mathrm{SM}} \times U(1)_{B-L} \xrightarrow{V} G_{\mathrm{SM}} \xrightarrow{v} SU(3)_c \times U(1)_Q,$$

with the *breaking scales* Λ_{GUT}, $V (\sim 1 \div 10 \text{ TeV})$ and v. The generated mass matrices in Eq. (12) are $M_R = YV/\sqrt{2}$ and $M_D = yv/\sqrt{2}$, where Y and y are the matrices of corresponding Yukawa couplings.

Probable mechanisms of LN violation may include exchange by:

• Majorana neutrinos [18] (the preferred mechanism after the discovery of neutrino oscillations [15]: SM + ν_M);

  • SUSY particles (RPV MSSM [20]: neutralinos, sleptons, squarks, gluinos);

  • scalar bilinears [21] (the component ξ^{--} of the $SU(2)_I$ triplet Higgs scalar, doubly charged dileptons etc.);

  • leptoquarks [22] (in various extensions of the SM: scalar or vector particles carrying both L and B numbers);

  • right-handed W_R bosons in the *left-right symmetric* models [23] based on the gauge group $G_{LR} = SU(3)_c \times SU(2)_L \times SU(2)_R \times U(1)_{B-L}$ ($\rightarrow G_{\mathrm{SM}} \rightarrow SU(3)_c \times U(1)_Q$), ν_R's and the seesaw mechanism are needed);

  • other (Kaluza–Klein sterile singlet neutrinos in theories with large extra dimensions [24]: an infinite tower of KK neutrino mass eigenstates, ...).

3 Semileptonic Decays of pseudoscalar mesons with $\Delta L = 2$

As examples of the processes with LN violation we consider the rare meson decays

$$K^+ \rightarrow \pi'^- \ell^+ \ell'^+, \quad D^+ \rightarrow K'^- \ell^+ \ell'^+ \quad (\ell, \ell' = e, \mu, \tau) \tag{14}$$

mediated by Majorana neutrinos or supersymmetric particles.

3.1 Decays via exchange by Majorana neutrinos

The lowest order amplitude of the process is given by the sum of the tree and box diagrams shown in Fig. 1 (there are also two crossed diagrams with interchanged lepton lines).
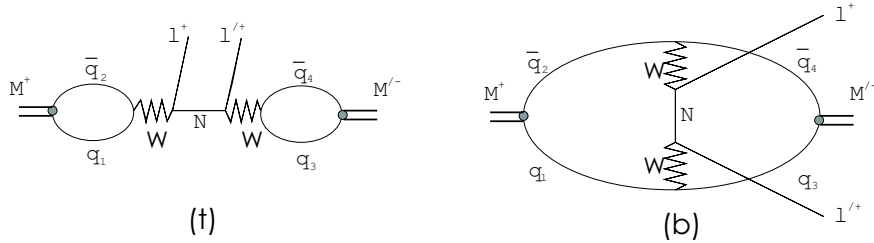
Figure 1: Feynman diagrams for the decay $M^+ \rightarrow M'^- \ell^+ \ell'^+$. Here N is a Majorana neutrino, bold vertices correspond to Bethe–Salpeter amplitudes for mesons as bound states of a quark and an antiquark.

The width of the decay $M^+(P) \to M'^-(P')\ell^+(p)\ell'^+(p')$ is given by

$$\Gamma_{\ell\ell'} = \left(1 - \frac{1}{2}\delta_{\ell\ell'}\right) \int (2\pi)^4 \delta^{(4)}(P' + p + p' - P)\frac{|A_t + A_b|^2}{2m_M} \frac{d^3P' d^3p d^3p'}{2^3(2\pi)^9 P'^0 p^0 p'^0},$$

where A_t (A_b) is the tree(box)-diagram amplitude expressed in the Bethe–Salpeter formalism of Ref. [25] as

$$A_i = (2\pi)^{-8} \int d^4q d^4q' H^{(i)}_{\mu\nu} L_i^{\mu\nu} \quad (i = t, b).$$

Here the lepton tensors

$$L_i^{\mu\nu} = \frac{g^4}{4} \frac{g^{\mu\alpha}}{p_i^2 - m_W^2} \frac{g^{\nu\beta}}{p_i'^2 - m_W^2} \sum_N U_{\ell N} U_{\ell' N} \eta_N m_N$$

$$\times \left(\bar{v}^c(p) \left[\frac{\gamma_\alpha \gamma_\beta}{(p_i - p)^2 - m_N^2} + \frac{\gamma_\beta \gamma_\alpha}{(p_i - p')^2 - m_N^2}\right] P_L v(p')\right) \quad (i = t, b), \tag{15}$$

where η_N is the charge conjugation phase factor of the field of Majorana neutrinos with mass m_N: $N = \eta_N N^c$, $|\eta_N| = 1$; $p_t = P$, $p_t' = P'$; $p_b = \frac{1}{2}(P - P') + q' - q$, $p_b' = \frac{1}{2}(P - P') - q' + q$; the hadron tensors

$$H^{(t)}_{\mu\nu} = \text{Tr}\left[\chi_P(q)V_{12}\gamma_\mu P_L\right]\text{Tr}\left[\bar{\chi}_{P'}(q')V_{43}\gamma_\nu P_L\right], \;\; H^{(b)}_{\mu\nu} = \text{Tr}\left[\chi_P(q)V_{13}\gamma_\mu P_L \bar{\chi}_{P'}(q')V_{42}\gamma_\nu P_L\right]$$

are expressed in terms of the elements V_{jk} of the CKM matrix and the model-dependent Bethe–Salpeter (BS) amplitudes for the mesons [25]

$$\chi_P(q) = \int d^4x e^{iq\cdot x}\chi_P(x) = \gamma^5(1 - \delta_M \hat{P})\phi_P(q), \tag{16}$$

where $\delta_M = (m_1 + m_2)/m_M^2$, m_M is the mass of a meson made of a quark q_1 and an antiquark $\bar{q}_2$ with *current* masses m_1 and m_2, $q = (p_1 - p_2)/2$ is the relative 4-momentum, $P = p_1 + p_2$ is the total 4-momentum of the meson, $\hat{P} = \gamma^\mu P_\mu$; the function $\phi_P(q)$ is *model dependent*. The tree amplitude is expressed in a *model independent* way in terms of the decay constants of the initial and final meson, f_M and $f_{M'}$, as follows:

$$A_t = -\frac{1}{4}f_M f_{M'} V_{12} V_{43} P_\mu P_\nu' L_t^{\mu\nu}.$$

The box amplitude depends (in general) on the *details of hadron dynamics*

$$A_b = 2V_{13}V_{42}\delta_M \delta_{M'}(P_\mu P_\nu' + P_\nu P_\mu' - g_{\mu\nu}P \cdot P' + i\varepsilon_{\mu\nu\alpha\beta}P^\alpha P'^\beta)$$

$$\times \int \frac{d^4q}{(2\pi)^4}\frac{d^4q'}{(2\pi)^4}\phi_P(q)\phi_{P'}(q')L_b^{\mu\nu}(q - q', p, p'; P - P').$$

We use the leading current-current approximation in the lepton tensors (15) due to relative smallness of the meson masses, $m_M \ll m_W$, and the expression of the meson decay constant f_M through the function $\phi_P(q)$ in the BS amplitude (16):

$$f_M = 4\sqrt{N_c}\delta_M \int \frac{d^4q}{(2\pi)^4}\phi_P(q),$$

where $N_c = 3$ is the number of quark colors. For the function $\phi_P(q)$, the relativistic Gaussian model has been used [25]:

$$\phi_P(q) = \frac{4\pi}{\alpha^2} \left(1 - \mu^2\right)^{-1/2} \exp\left\{-\frac{1}{2\alpha^2}\left[2\left(\frac{P \cdot q}{m_M}\right)^2 - q^2\right]\right\},$$

$$\alpha^2 = \frac{\pi}{4\sqrt{N_c}}\left(1 - \mu^2\right)^{1/2}\frac{f_M}{\delta_M}, \;\; \mu = m_M\delta_M = \frac{m_1 + m_2}{m_M}. \tag{17}$$

The branching ratios (BRs)

$$B_{\ell\ell'} = \Gamma(M^+ \to M'^- \ell^+\ell'^+)/\Gamma(M^+ \to \text{all}) \tag{18}$$

have been calculated for two limiting cases of *heavy* $(m_N \gg m_M)$ and *light* $(m_N \ll m_\ell, \; m_{\ell'})$ Majorana neutrinos (see Eqs. (13), (15) and Ref. [5] for details):

$$B_{\ell\ell'}^{\text{heavy}} = C_{\ell\ell'}^{\text{heavy}}\left|\langle m_{\ell\ell'}^{-1}\rangle\right|^2, \;\; B_{\ell\ell'}^{\text{light}} = C_{\ell\ell'}^{\text{light}}\left|\langle m_{\ell\ell'}\rangle\right|^2, \tag{19}$$

where the *effective* Majorana masses are defined as follows:

$$\langle m_{\ell\ell'}^{-1}\rangle = \sum_N U_{\ell N}U_{\ell' N}\eta_N m_N^{-1}, \;\; \langle m_{\ell\ell'}\rangle = \sum_N U_{\ell N} U_{\ell' N}\eta_N m_N. \tag{20}$$

Here the coefficients $C_{\ell\ell'}^{\text{heavy}}$ are expressed model independently through the meson decay constants, and $C_{\ell\ell'}^{\text{light}}$'s are calculated with use of the model function (17). The following values of the parameters have been used in numerical calculations: $(f_\pi, f_K, f_D) = (130.7, 159.8, 228)$ MeV; $(m_u, m_d, m_s, m_c) = (4, 7, 150, 1.26 \times 10^3)$ MeV. The results are shown in the third and fifth columns of Table 1. The second column of this table shows the present direct experimental upper bounds on the BRs [15] which are too weak to set reasonable limits on the effective Majorana masses (20). So we have derived the *indirect* bounds on the BRs (19) using the limits

Rare decay	Exp. upper bound on $B_{\ell\ell'}$	$C_{\ell\ell'}^{\text{heavy}}$ (MeV^2)	Ind. bound on $B_{\ell\ell'}^{\text{heavy}}$	$C_{\ell\ell'}^{\text{light}}$ (MeV^{-2})	Ind. bound on $B_{\ell\ell'}^{\text{light}}$
$K^+ \to \pi^- e^+ e^+$	6.4×10^{-10}	8.5×10^{-10}	5.9×10^{-32}	4.4×10^{-20}	2.3×10^{-33}
$K^+ \to \pi^- \mu^+ \mu^+$	3.0×10^{-9}	2.4×10^{-10}	1.1×10^{-24}	1.2×10^{-20}	6.2×10^{-34}
$K^+ \to \pi^- e^+ \mu^+$	5.0×10^{-10}	1.0×10^{-9}	5.1×10^{-24}	8.8×10^{-20}	2.0×10^{-33}
$D^+ \to K^- e^+ e^+$	4.5×10^{-6}	2.2×10^{-9}	1.5×10^{-31}	4.5×10^{-21}	2.4×10^{-34}
$D^+ \to K^- \mu^+ \mu^+$	1.3×10^{-5}	2.0×10^{-9}	8.9×10^{-24}	4.1×10^{-21}	2.2×10^{-34}
$D^+ \to K^- e^+ \mu^+$	1.3×10^{-4}	4.2×10^{-9}	2.1×10^{-23}	9.1×10^{-21}	2.0×10^{-34}

Table 1: Experimental and indirect upper bounds on the branching ratios $B_{\ell\ell'}$ for the rare meson decays with $\Delta L = 2$ mediated by heavy or light Majorana neutrinos.

on the masses (20) obtained from the precision electroweak measurements, neutrino oscillation experiments, searches for the neutrinoless double beta decay and cosmological data:

$$\left|\langle m_{ee}^{-1}\rangle\right| < \left(1.2 \times 10^8 \text{ GeV}\right)^{-1}, \left|\langle m_{\mu\mu}^{-1}\rangle\right| < \left(1.5 \times 10^4 \text{ GeV}\right)^{-1}, \left|\langle m_{e\mu}^{-1}\rangle\right| < \left(1.4 \times 10^4 \text{ GeV}\right)^{-1};$$

$$\left|\langle m_{\ell\ell}\rangle\right| < 0.23 \text{ eV } (\ell = e, \; \mu), \;\; \left|\langle m_{e\mu}\rangle\right| < 0.15 \text{ eV}. \tag{21}$$

These indirect bounds (see the forth and sixth columns of Table 1) are greatly more stringent than the direct ones.

3.2 Decays in the MSSM with explicit R-parity violation

Here we consider another mechanism of the $\Delta L = 2$ rare decays (14) based on R-parity violating supersymmetry (SUSY) (for a review, see Ref. [20]). The minimal supersymmetric extension of the SM (MSSM) includes the fields of the two-Higgs-doublet extension of the SM and those of the corresponding *supersymmetric partners*. Each fermion (boson) has a superpartner of spin 0 (1/2). R-parity is defined as $R = (-1)^{3(B-L)+2S}$, where S, L, and B are the spin, the lepton and baryon numbers, respectively. In the MSSM, R-parity conservation is imposed to prevent the L and B violation; it also leads to the production of superpartners in pairs and ensures the stability of the lightest superparticle. However, *neither gauge invariance nor supersymmetry require R-parity conservation*. There are many generalizations of the MSSM with explicitly or spontaneously broken R-symmetry [20]. We consider a SUSY theory with the minimal particle content of the MSSM and explicit R-parity violation ($R\!\!\!/$MSSM).

The most general form for the R-parity and lepton number violating part of the superpotential is given by

$$W_{R\!\!\!/} = \varepsilon_{\alpha\beta}\left(\frac{1}{2}\lambda_{ijk}L_i^\alpha L_j^\beta \bar{E}_k + \lambda'_{ijk}L_i^\alpha Q_j^\beta \bar{D}_k + \epsilon_i L_i^\alpha H_u^\beta\right). \tag{22}$$

Here $i, j, k = 1, 2, 3$ are generation indices, L and Q are $SU(2)$ doublets of left-handed lepton and quark superfields ($\alpha, \beta = 1, 2$ are isospinor indices), $\bar{E}$ and $\bar{D}$ are singlets of right-handed superfields of leptons and down quarks, respectively; H_u is a doublet Higgs superfield (with hypercharge $Y = 1$); $\lambda_{ijk} = -\lambda_{jik}$, λ'_{ijk} and ϵ_i are constants.

In the superpotential (22) the trilinear ($\propto \lambda$, λ') and bilinear ($\propto \epsilon$) terms are present. At first, we assume that the bilinear terms are absent at tree level ($\epsilon = 0$). They will be generated by quantum corrections [20], but it is expected that the phenomenology will still be dominated by the tree-level trilinear terms.

The leading order amplitude of the process $K^+ \to \pi^- + \ell^+ + \ell'^+$ in the $R\!\!\!/$MSSM is described by three types of diagrams shown in Fig. 2. For the numerical estimates of the branching
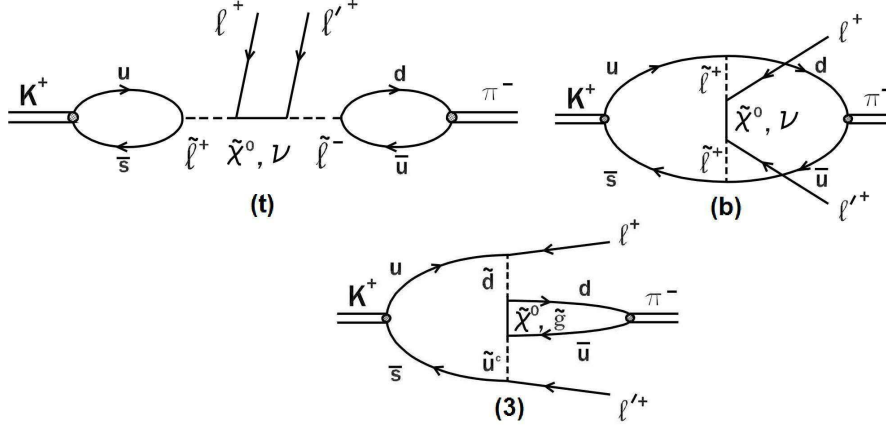
Figure 2: Feynman diagrams for the decay $K^+ \to \pi^- + \ell^+ + \ell'^+$ mediated by Majorana neutrinos ν, neutralinos $\tilde{\chi}^0$, gluinos $\tilde{g}$ with $\tilde{f}$ being the scalar superpartners of the corresponding fermions $f = \ell, u, d$ (leptons and quarks).

ratios (18), we have used the known values for the couplings, decay constants, meson, lepton

and current quark masses [15], and a typical set of the MSSM parameters and the elements of the 4×4 neutralino mixing matrix from Ref. [26]. In addition, we have taken all the masses of superpartners to be equal with a common value m_{SUSY}. Taking into account the present bounds on the effective Majorana masses (21), we find that the main contribution to the decay width comes from the exchange by neutralinos and gluinos (see Fig. 2). The results of the calculations for the decays $K^+ \to \pi^- \ell^+ \ell^+$ and $D^+ \to K^- \ell^+ \ell'^+$ are shown in Table 2 (here $m_{200} = m_{SUSY}/(200 \text{ GeV})$) [6].

For upper bounds on the trilinear couplings (from analysis of a number of other processes [20]) $|\lambda'\lambda'| \lesssim 5 \times 10^{-6}$, we obtain an estimate of the BRs:

$$B_{\ell\ell'}(\text{tri}\slashed{R}) \lesssim 10^{-28} m_{200}^{-10}. \quad (23)$$

This estimate is much smaller than the corresponding direct experimental bounds and lies between (except for the ee decay mode) the indirect bounds

Rare decay	$B_{\ell\ell'} \times m_{200}^{10}$
$K^+ \to \pi^- e^+ e^+$	$1.3 \times 10^{-17} \lvert\lambda'_{111}\lambda'_{112}\rvert^2$
$K^+ \to \pi^- \mu^+ \mu^+$	$4.7 \times 10^{-18} \lvert\lambda'_{211}\lambda'_{212}\rvert^2$
$K^+ \to \pi^- e^+ \mu^+$	$4.3 \times 10^{-18} \lvert\lambda'_{111}\lambda'_{212} + \lambda'_{211}\lambda'_{112}\rvert^2$
$D^+ \to K^- e^+ e^+$	$1.4 \times 10^{-18} \lvert\lambda'_{122}\lambda'_{111} - 0.39\lambda'_{121}\lambda'_{112}\rvert^2$
$D^+ \to K^- \mu^+ \mu^+$	$1.3 \times 10^{-18} \lvert\lambda'_{222}\lambda'_{211} - 0.39\lambda'_{221}\lambda'_{212}\rvert^2$
$D^+ \to K^- e^+ \mu^+$	$6.5 \times 10^{-19} \lvert(\lambda'_{122}\lambda'_{211} + \lambda'_{222}\lambda'_{111})$ $-0.39(\lambda'_{121}\lambda'_{212} + \lambda'_{221}\lambda'_{112})\rvert^2$

Table 2: The branching ratios $B_{\ell\ell'}$ for the meson decays mediated by trilinear Yukawa couplings in the $\slashed{R}$MSSM.

based on the mechanisms of the decays mediated by heavy and light Majorana neutrinos (see Table 1).

For the case of tree-level bilinear couplings ($\epsilon \neq 0, \lambda = 0, \lambda' = 0$ in Eq. (22)), trilinear couplings cannot be generated via radiative corrections [20]. The bilinear terms in the superpotential induce mixing between the SM leptons and the MSSM charginos and neutralinos in the mass-eigenstate basis and lead to the $\Delta L = \pm 1$ lepton-quark interactions, in particular, giving rise to the meson decays (14). For this bilinear decay mechanism, the order-of-magnitude estimate of the BRs is given by [7]

$$B_{\ell\ell'}(\text{bi}\slashed{R}) \lesssim 10^{-48} m_{200}^{-10}, \quad (24)$$

which is twenty orders of magnitude smaller than that for the trilinear mechanism (23).

4 Conclusion

In the minimal SM (with massless neutrinos), each lepton family number L_ℓ and the baryon number B are conserved due to the accidental global symmetry (6).

The unambiguous observation of neutrino oscillations implies nonzero neutrino masses and lepton mixing and clearly demonstrates the LFN violation (with conservation of the total LN).

It is natural to believe that the neutrino mass is the first evidence of New Physics.

The LN violation is a generic feature of theories beyond the SM, and searching $\Delta L \neq 0$ processes is a way to test these theories.

The semileptonic rare meson decays (RMDs) with $\Delta L = 2$ were investigated in the SM extended by Majorana neutrinos and in the MSSM with explicit R-parity violation. The indirect bounds on the RMD branching ratios have been derived from the precision electroweak measurements, neutrino oscillation experiments, searches for the $0\nu2\beta$ decay, cosmological data, and bounds on R-parity violating couplings. These indirect bounds are *greatly more stringent*

than the bounds from direct searching RMDs. So the RMDs will hardly be seen in the nearest future.

The neutrinoless double beta decay and the production of same-sign dileptons at colliders (like the LHC) look substantially more promising for observation.

Acknowledgments

References

[1] W.H. Furry, Phys. Rev. **56** 1184 (1939).

[2] S.R. Elliot and P. Vogel, Ann. Rev. Nucl. Part. Sci. **52** 115 (2002); J.D. Vergados, Phys. Rep. **361** 1 (2002); P. Vogel, arXiv:hep-ph/0611243 (2006).

[3] A. Ali, A.V. Borisov and D.V. Zhuridov, Phys. Rev. **76** 093009 (2007).

[4] A. Ali, A.V. Borisov and N.B. Zamorin, Eur. Phys. J. **C21** 123 (2001).

[5] A. Ali, A.V. Borisov and M.V. Sidorova, Phys. Atom. Nucl. **69** 475 (2006).

[6] A. Ali, A.V. Borisov and M.V. Sidorova, Moscow Univ. Phys. Bull. **62 (1)** 6 (2007).

[7] A. Ali, A.V. Borisov and M.V. Sidorova, arXiv:0801.2517 [hep-ph] (2008).

[8] A. Ali, A.V. Borisov and N.B. Zamorin, Proc. 10th Lomonosov Conf. on Elementary Particle Physics "Frontiers of Particle Physics", Moscow, 2001, Ed. A.I. Studenikin (World Sci., Singapore, 2003), p. 74.

[9] O. Panella, M. Cannoni, C. Carimalo and Y.N. Srivastava, Phys. Rev. **D65** 035005 (2002).

[10] C.-S. Chen, C.-Q. Geng and D.V. Zhuridov, arXiv:0801.2011 [hep-ph] (2008).

[11] W. Rodejohann and K. Zuber, Phys. Rev. **D62** 094017 (2000).

[12] A. Ali, A.V. Borisov and D.V. Zhuridov, Phys. Atom. Nucl. **68** 2061 (2005).

[13] P. Domin, S. Kovalenko, A. Faessler and F. Šimkovic, Phys. Rev. **C70** 065501 (2004).

[14] B. Pontecorvo, Zh. Eksp. Teor. Fiz. **33** 549 (1957), **34** 247 (1958).

[15] Particle Data Group: C. Amsler *et al.*, Phys. Lett. **B667** 1 (2008).

[16] Z. Maki, M. Nakagawa and S. Sakata, Prog. Theor. Phys. **28** 870 (1962); B. Pontecorvo, Zh. Eksp. Teor. Fiz. **53** 1717 (1967).

[17] E. Majorana, Nuovo Cim., **5** 171 (1937).

[18] C. Giunti and C. W. Kim, *Fundamentals of Neutrino Physics and Astrophysics* (Oxford Univ. Press, New York, 2007)

[19] P. Langacker, Nucl. Phys. (Proc. Suppl.) **B100** 383 (2001).

[20] R. Barbier *et al.*, Phys. Rep. **420** 1 (2005).

[21] H.V. Klapdor-Kleingrothaus and U. Sarkar, Phys. Lett. **B554** 45 (2003).

[22] M. Hirsch, H.V. Klapdor-Kleingrothaus and S.G. Kovalenko, Phys. Rev. **D54** 4207 (1996).

[23] R.N. Mohapatra, *Unification and Supersymmetry: The Frontiers of Quark-Lepton Physics* (Springer-Verlag, New York, 2003).

[24] G. Bhattacharyya, H.V. Klapdor-Kleingrothaus, H. Päs and A. Pilaftsis, arXiv:hep-ph/0402071 (2004).

[25] G. Esteve, A. Morales and R. Núñes-Lagos, J. Phys. **G9** 357 (1983).

[26] B.C. Allanach, A. Dedes and H.K. Dreiner, Phys. Rev. **D69** 115002 (2004).

B-meson form factors

M.A. Ivanov

JINR, 141980 Dubna, Russia

The results for *B*-meson heavy-to-light transition form factors calculated using the study of Dyson-Schwinger equations in QCD are reviewed. In this relativistic approach, which realises confinement and dynamical chiral symmetry breaking, all physical values of momentum transfer in the transition form factors are simultaneously accessible. These results can be useful in the analysis and correlation of the large body of data being accumulated at extant facilities, and thereby in probing the Standard Model and beyond.

1   Introduction

Transition form factors that characterise the decays of *B*-mesons into light pseudoscalar and vector mesons, the so-called heavy-to-light decays, are basic to an understanding of this heavy-meson's exclusive semi-leptonic and rare radiative decays. These form factors also provide the factorisable amplitudes that appear in *B*-meson exclusive nonleptonic charmless decays. An understanding of all these processes is essential to the reliable determination of CKM matrix elements, and transitions mediated by electroweak and gluonic penguin operators. Moreover, they should provide a means of searching for non Standard Model effects and CP violation. Considering all these factors, it is not surprising that heavy-light form factors are the subject of much experimental and theoretical scrutiny, as evidenced by the discussion in Ref. [1].

The analysis of heavy-to-light processes has two facets. One is factorisation; viz., the feature that in exclusive decays of *B*-mesons there exist strong interaction effects that do not correspond to form factors. These may be radiative corrections to purely hadronic operators in the weak effective Lagrangian or final state interactions between daughter hadrons. The development of soft collinear effective-field theory (SCET) is providing a means of simplifying that problem, yielding factorisation theorems which enable a systematic approximation to be developed for a given process in terms of products of soft and hard matrix elements (see, e.g. [2]). Analyses relevant to the processes we consider herein may be found in Refs. [3, 4, 5, 6, 7] where the semileptonic B-decay, rare $B \to (K, K^*)l^+l^-$, $B \to V\gamma$ decay amplitudes were expressed in terms of the $B \to P(V)$ form factors, light-front distribution amplitudes of the heavy- and light-mesons and hard scattering kernels that can be evaluated perturbatively.

The second facet, once factorisation for a given process is assumed or proved, is to evaluate the hadronic transition form factors. Naturally, they cannot be calculated in perturbation theory. The relevant matrix elements involve single hadrons in the initial and final states. Hence, their calculation requires information about the structure of both heavy- and light-mesons. A variety of theoretical approaches have been applied to this problem, recent amongst which are analyses using light-cone sum rules [8, 9], light-front quark models [10], a constituent-quark model in a dispersion relation formulation [11], and relativistic quark models – e.g., Refs. [12, 13, 14]. It is notable that while the methods of Refs. [8, 9, 10] can only provide access

to the form factors on a domain of small timelike q^2, the entire range of physical momenta is directly accessible in Refs. [11, 12, 13, 14]. The latter is also true of the method employed in our approach.

In the present context it is worth explaining that the relativistic constituent quark model introduced in Ref. [15] has been applied to the description of B and B_c transition form factors [13, 14] using a small set of variable parameters. The model's starting point is an interaction Lagrangian that describes the correlation of constituent-quarks within a meson and represents the system by a bound-state amplitude. The so-called compositeness condition plays a key role in the consistent formulation of the model. In these studies the propagation of constituent-quarks is described by a free-particle Green function; i.e., $S(k) = 1/(m_Q - \not{k})$, wherein m_Q is a light or heavy constituent-quark mass. In order to avoid unphysical thresholds in transition amplitudes, it is necessary that for a meson of mass m_H composed of quarks Q_1 and Q_2, $m_H < m_{Q_1} + m_{Q_2}$. This poses problems for a description of light vector mesons (ρ, K^*), heavy flavoured vector mesons (D^*,B^*) and for P-wave and excited charmonium states. To sidestep this, in the evaluation of matrix elements Refs. [14] employed identical masses for all heavy pseudoscalar and vector flavored mesons; viz., $m_{B^*} = m_B$, $m_{D^*} = m_D$, and for all P-wave and excited charmonium states. This is probably a reliable approximation for the heavy mesons because the corresponding mass splittings are small. However, it is merely a stopgap measure for the light vector mesons, and one of the motivations for this article is to remedy that situation. We implement confinement of light-quarks, in a manner which we shall subsequently elucidate.

Models based on results obtained via QCD's Dyson-Schwinger equations (DSEs) have also been employed [16, 17, 18, 19]. These studies possess the feature that quark propagation is described by fully dressed Schwinger functions. That dressing has a material impact on light-quark characteristics and, e.g., eliminates the threshold problem just described in connection with Refs. [13, 14]. Within this framework, as we have shown [16, 17, 18, 19] and shall see again herein, constant mass approximation can nevertheless be justified for b-quarks and to some extent also for c-quarks. The results for B-meson heavy-to-light transition form factors calculated using the study of Dyson-Schwinger equations in QCD and published in[16] are reviewed herein. In this relativistic approach, which realises confinement and dynamical chiral symmetry breaking, all physical values of momentum transfer in the transition form factors are simultaneously accessible. These results can be useful in the analysis and correlation of the large body of data being accumulated at extant facilities, and thereby in probing the Standard Model and beyond.

2   Heavy to light transitions

Herein our primary subjects are the following matrix elements, which can be expressed in Minkowski space via dimensionless form factors:

$$< P(p_2) \, | \, \bar{q} \, \gamma_\mu \, b \, | B(p_1) >= F_+(q^2) P_\mu + F_-(q^2) q_\mu \, ,$$

$$< P(p_2) \, | \, \bar{q} \, \sigma_{\mu\alpha} q^\alpha \, b \, | \, B(p_1) >= \frac{i}{m_1 + m_2} \left\{ q^2 \, P_\mu - Pq \, q_\mu \right\} F_T(q^2) \, ,$$

$$< V(p_2, \epsilon_2) \, | \, \bar{q} \, \gamma_\mu (1 - \gamma_5) \, b \, | \, B(p_1) >=$$
$$= \frac{i}{m_1 + m_2} \, \epsilon_2^{\dagger\nu} \left\{ -g_{\mu\nu} \, Pq \, A_0(q^2) + P_\mu P_\nu \, A_+(q^2) + q_\mu P_\nu \, A_-(q^2) + i\varepsilon_{\mu\nu\alpha\beta} P^\alpha q^\beta \, V(q^2) \right\} \, ,$$

$$< V(p_2, \epsilon_2) \, | \, \bar{q} \, \sigma_{\mu\nu} q^\nu (1 + \gamma_5) \, b \, | \, B(p_1) >= \epsilon_2^{\dagger\nu} \left\{ - \left(g_{\mu\nu} - q_\mu q_\nu / q^2 \right) \, Pq \, a_0(q^2) \right.$$
$$\left. + \left(P_\mu - q_\mu \, Pq/q^2 \right) \, P_\nu \, a_+(q^2) + i\varepsilon_{\mu\nu\alpha\beta} P^\alpha q^\beta \, g(q^2) \right\} \tag{1}$$

For reference it is useful to relate the form factors we have defined to those used, e.g., in Ref. [8], which are denoted by a superscript c in the following formulae:

$$
\begin{aligned}
F_+ &= f_+^c \, , & F_- &= -\frac{m_1^2 - m_2^2}{q^2} (f_+^c - f_0^c) \, , & F_T &= f_T^c \, , \\
A_0 &= \frac{m_1 + m_2}{m_1 - m_2} A_1^c \, , & A_+ &= A_2^c \, , & A_- = \frac{2m_2(m_1 + m_2)}{q^2} (A_3^c - A_0^c) \, , & V &= V^c \, , \\
a_0 &= T_2^c \, , & g &= T_1^c \, , & a_+ = T_2^c + \frac{q^2}{m_1^2 - m_2^2} T_3^c \, .
\end{aligned}
\tag{2}
$$

We note in addition that the form factors $A_i^c(q^2)$ satisfy the constraints: $A_0^c(0) = A_3^c(0)$ and

$$2m_2 A_3^c(q^2) = (m_1 + m_2) A_1^c(q^2) - (m_1 - m_2) A_2^c(q^2) \, . \tag{3}$$

The leading term in a systematic and symmetry preserving truncation of the DSEs yields a generalised impulse approximation to the matrix elements expressed in Eq. (1), which is depicted in Fig. 1. This diagram represents an amplitude via a single integral written in Euclidean metrics:

$$\mathcal{A}(p_1, p_2) = \mathrm{tr}_{CD} \int \frac{d^4 k}{(2\pi)^4} \bar{\Gamma}_{P(V)}(k; -p_2) S_{f_l}(k + p_2) \Gamma_I(p_2, p_1) S_b(k + p_1) \Gamma_B(k; p_1) S_u(k) \, , \tag{4}$$

where the trace is over colour and Dirac-spinor indices. Equation (4) makes plain that our calculations require information about dressed-quark propagators – $S(p)$, meson Bethe-Salpeter amplitudes – $\Gamma(k; P)$, and interaction vertices – $\Gamma_I(p, q)$. We discuss these later on.

In order to provide a well-constrained analysis of the matrix elements in Eqs. (1), we calculate simultaneously the leptonic decay constants of all participating mesons. $w_1 + w_2 = 1$, whereas for vector mesons, For the Bethe-Salpeter amplitudes appearing in these expressions, the canonical
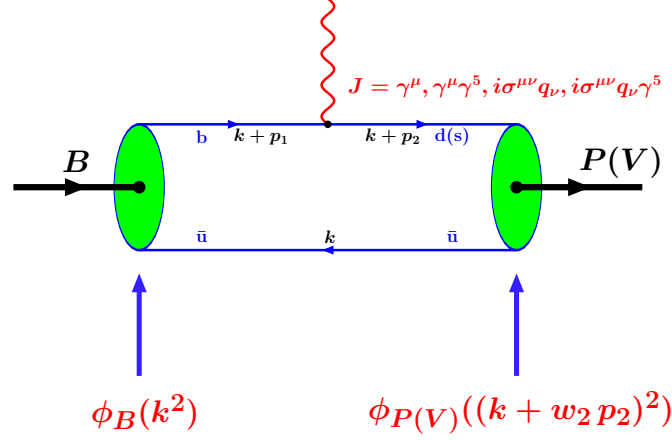
Figure 1: Diagrammatic representation of the matrix elements in Eq. (1). The solid lines denote dressed-quark propagators; the filled ellipses, meson Bethe-Salpeter amplitudes ; and the connection of the undulating line with the dressed-quark propagator, an interaction vertex.

normalisation condition is accepted,

$$2P_\mu \;=\; \left[\frac{\partial}{\partial K_\mu}\Pi(P,K)\right]_{K=P}^{P^2=-m_{0^-}^2} \tag{5}$$

$$\Pi(P,K) \;=\; \mathrm{tr}_{CD}\int\frac{d^4k}{(2\pi)^4}\,\bar\Gamma_{0^-}(k;-P)S_{f_1}(k+w_1K)\Gamma_{0^-}(k;P)S_{f_2}(k-w_2K)\,.$$

The expression for vector mesons is analogous and is given explicitly in Ref. [19].

For any quark flavour, the dressed-quark propagator has the general form

$$S(p) = -i\gamma\cdot p\,\sigma_V(p^2) + \sigma_S(p^2) = 1/[i\gamma\cdot p\,A(p^2) + B(p^2)]. \tag{6}$$

An efficacious parametrisation of $S(p)$, which exhibits the features of the numerical solutions of the quark DSE , has been employed in Ref. [19] and is expressed in an algebraic form via entire functions:

$$\bar\sigma_S(x) \;=\; 2\,\bar m\,\mathcal{F}(2(x+\bar m^2)) + \mathcal{F}(b_1x)\,\mathcal{F}(b_3x)\,[b_0 + b_2\mathcal{F}(\epsilon x)]\,,$$

$$\bar\sigma_V(x) \;=\; \frac{1}{x+\bar m^2}\left[1 - \mathcal{F}(2(x+\bar m^2))\right]\,, \tag{7}$$

with $x = p^2/\lambda^2$, $\bar m = m/\lambda$, $\mathcal{F}(x) = (1-e^{-x})/x$, $\bar\sigma_S(x) = \lambda\,\sigma_S(p^2)$ and $\bar\sigma_V(x) = \lambda^2\,\sigma_V(p^2)$. The parameter values were fixed in Ref. [19] by requiring a least-squares fit to a wide range of light- and heavy-meson observables, and take the values:

f	$\bar m_f$	b_0^f	b_1^f	b_2^f	b_3^f
$u=d$	0.00948	0.131	2.94	0.733	0.185
s	0.210	0.105	3.18	0.858	0.185

(8)

The mass-scale $\lambda = 0.566\,\mathrm{GeV}$, with which value the current-quark masses are $m_u = 5.4\,\mathrm{MeV}$, $m_s = 119\,\mathrm{MeV}$.

Equations (7) – (8) provide an algebraic form for $S(p)$ that combines the effects of confinement and DCSB with free-particle behaviour at large spacelike p^2.

As has been shown in [19] it is reasonable for the c-quark and for the b-quark,sensible, to employ a constituent-quark propagator; viz.,

$$S_Q(k) = \frac{1}{i\gamma \cdot k + \hat{M}_Q}\,, \ Q = c, b, \tag{9}$$

where the values $\hat{M}_c = 1.32\,\text{GeV}$ and $\hat{M}_b = 4.65\,\text{GeV}$, were fixed in the same least-squares fit as the light-quark parameters in Eq. (8) [19].

The meson Bethe-Salpeter amplitudes, which appear in Fig. 1 and are consistent with the generalised impulse approximation. The solution of this equation requires a simultaneous solution of the quark DSE. However, since we have already chosen to simplify the calculations by parametrising $S(p)$, we follow Ref. [19] and also employ that expedient with $\Gamma_{P(V)}$.

Dynamical chiral symmetry breaking and the axial-vector Ward-Takahashi identity have a big impact on the structure and properties of light pseudoscalar mesons. In fact, the quark-level Goldberger-Treiman relations motivate and support the following efficacious parametrisation of light pseudoscalar meson Bethe-Salpeter amplitudes:

$$\Gamma_P(k; P) = i\gamma_5\,\mathcal{E}_P(k^2)\,, \qquad \mathcal{E}_P(k^2) = \frac{\sqrt{2}}{f_P}\,B_P(k^2)\,, \qquad P = \pi, K, \tag{10}$$

where $B_P := B_u|_{b_0^u \to b_0^P}$ is obtained from Eqs. (6), (7), (7) via the replacements $b_0^u \to b_0^\pi = 0.204$, and $b_0^u \to b_0^K = 0.319$. as appropriate.

It is reasonable to parametrise vector meson Bethe-Salpeter amplitudes as follows:

$$\Gamma_\mu^V(k; p) = \frac{1}{\mathcal{N}_V}\left(\gamma_\mu + p_\mu\,\frac{\gamma \cdot p}{M_V^2}\right)\varphi(k^2)\,, \qquad \varphi(k^2) = \exp(-k^2/\omega_V^2)\,; \tag{11}$$

namely, a function whose support is concentrated in the infrared. Clearly, $p_\mu\Gamma_\mu^V(k; p) = 0$. An *ansatz* in Eq.(11) is little different to that used in Ref. [19]. The one parameter is a mass-scale ω_V, which specifies the momentum space width of the amplitude. The normalisation is calculated via the analogues of Eqs. (5) and (6).

For heavy mesons we write [19]

$$\Gamma_H(k; p) = \frac{1}{\mathcal{N}_H}\,\gamma_H\,\varphi_H(k^2)\,, \tag{12}$$

where $\gamma_P = i\,\gamma_5$, $\gamma_V = \gamma \cdot \epsilon_V$, $\varphi_H(k^2) = \exp\left(-k^2/\omega_H^2\right)$ and $\mathcal{N}_H$ is fixed by Eqs. (5) and (6). In common with Ref. [19], we assume that the width parameters are spin independent; i.e., $\omega_{B^*} = \omega_B$, $\omega_{D^*} = \omega_D$, as would be the case were heavy-quark symmetry to be realised exactly. On the other hand, we allow full flavour-dependence, since high precision experiments related to heavy-quark systems are becoming available. Thus we fit with ω_D, ω_{D_s}, ω_B, ω_{B_s} treated as independent parameters.

Manifest Poincaré covariance is a feature of the direct application of DSEs to the calculation of hadron observables. The manifest covariance is only possible if the complete and complicated structure of hadron bound-state amplitudes is retained. That can impose numerical costs since, e.g., the complete vector meson Bethe-Salpeter amplitude involves eight Poincaré covariants.

Herein, we use simple one-covariant models for the amplitudes with a goal of describing

simultaneously a wide range of phenomena. With the omission of the full structure of amplitudes, however, comes the complication that our results can be sensitive to the definition of the relativistic relative momentum. *Every* study that fails to retain the full structure of the Bethe-Salpeter amplitude shares this complication.

Hence to proceed we must specify the relative momentum. In common with Refs. [19, 17, 18], when a heavy-quark line is involved, we allocate all the heavy-light-meson's momentum to that heavy-quark and choose the single covariant in the heavy-light-meson's Bethe-Salpeter amplitude to be a function of only the light-quark momentum. This is evident in Fig. 1.

For the light mesons, our choice is clearly depicted in Fig. 1; viz., a quark with momentum k_1 and antiquark with momentum k_2 are bound into a system with total momentum p, with the relative momentum $k = w_2 k_1 + w_1 k_2$, where $w_1 + w_2 = 1$. In Refs. [17, 18, 19], and in other phenomenological DSE studies, $w_2 = 1/2$ is usually implicit. Herein we allow w_2 to vary and do not require $w_2^{ud} = w_2^{us}$.

We re-emphasise that the existence of optimal values for these parameters is a consequence of the truncations employed in setting up the bound state model. No dependence would exist in an *ab initio* study, which is possible. However, for the breadth of application herein, an *ab initio* study is beyond *our* capacity.

We parametrise the dressed-quark-photon vertex as was done in Ref. [22] and employ the Ball-Chiu *Ansatz* [23]:

$$i\Gamma_\nu^f(\ell_1, \ell_2) = i\Sigma_A(\ell_1^2, \ell_2^2)\,\gamma_\mu + (\ell_1 + \ell_2)_\mu \left[\frac{1}{2} i\gamma \cdot (\ell_1 + \ell_2)\,\Delta_A(\ell_1^2, \ell_2^2) + \Delta_B(\ell_1^2, \ell_2^2)\right], \qquad (13)$$

where

$$\Sigma_F(\ell_1^2, \ell_2^2) = \frac{1}{2}\left[F(\ell_1^2) + F(\ell_2^2)\right], \qquad \Delta_F(\ell_1^2, \ell_2^2) = \frac{F(\ell_1^2) - F(\ell_2^2)}{\ell_1^2 - \ell_2^2},$$

with $F = A_f, B_f$; i.e., the scalar functions in Eq. (6) evaluated with the appropriate dressed-quark propagator. It is critical that this *Ansatz* satisfies the Ward-Takahashi identity.

It is noteworthy that for heavy-quarks, since from Eq. (9) one has $A_Q(k^2) \equiv 1$ and $M_Q(k^2) \equiv \hat{M}_Q$, Eq. (13) yields

$$\Gamma_\mu^Q(\ell_1, \ell_2) = \gamma_\mu\,; \qquad (14)$$

namely, the correct heavy-quark limit. With algebraic parametrisations of each of the pieces that comprise a matrix element one can obtain simple formulae that express the heavy-quark symmetry limits of these matrix elements. References [17, 18, 19] detail the results of such analysis. In particular, Sec. VI of Ref. citemishasvy provides a complete discussion of the heavy-quark symmetry limits of numerous matrix elements.

To highlight a couple of results relevant to our present discussion, we observe that the leptonic and semileptonic decays of heavy mesons were considered in Ref. [17]. In accord with heavy-quark effective theory [20], it was shown [17] that in the heavy-quark limit the leptonic decay constants evolve as $(\hat{M}_Q)^{-1/2}$ and the matrix elements describing semileptonic heavy-heavy decays can be expressed in terms of a single universal function, ξ. The calculated result for this function can be written

$$\xi(w) = \frac{N_c}{4\pi^2}\,\kappa_1\kappa_2 \int_0^1 d\tau\,\frac{1}{W}\int_0^\infty du\,\varphi_H^2(z_W)\left[\sigma_S(z_W) + \sqrt{\frac{u}{W}}\sigma_V(z_W)\right], \qquad (15)$$

with $\kappa^2 = 1/[m_H \mathcal{N}_H^2]$, $W = 1 + 2\tau(1 - \tau)(w - 1)$, $z_W = u - 2E_H\sqrt{u/W}$, and $w = -v_{H_1} \cdot v_{H_2}$ where $v_H = p_H/m_H$. Owing to the canonical normalisation of the Bethe-Salpeter amplitudes,

	This work	Other	Reference
f_ρ	209	209(2)	PDG [1]
f_{K^*}	217	217(5)	PDG [1]
f_D	223	$222.6\,(16.7)^{+2.8}_{-3.4}$	CLEO [26, 27, 25]
f_{D_s}	281	280(12)(6)	CLEO [26, 27, 25]
f_{D^*}	321	$245\,(20)^{+3}_{-2}$	LAT [29]
$f_{D_s^*}$	364	$272\,(16)^{+3}_{-20}$	LAT [30]
f_B	176	$229^{+36}_{-31}\,(\text{stat})^{+34}_{-37}\,(\text{syst})$	BELLE[31]
f_{B_s}	211	259(32)	HPQCD LAT [32]
f_{B^*}	198	$196\,(24)^{+39}_{-2}$	LAT [29]
$f_{B_s^*}$	235	$229\,(20)^{+41}_{-16}$	LAT [29]

Table 1: Leptonic decay constants f_H (MeV) calculated using the parameter values listed in connection with Eq. (16). Data and selected calculations are provided for comparison.

$\xi(w = 1) = 1$.

In addition to reproducing the results of heavy-quark symmetry, it is an important feature of the DSEs that one can examine the fidelity of the formulae obtained in the heavy-quark limit; viz., elucidate the extent to which they are physically realised. Reference [19] provides a unified and uniformly accurate description of a broad range of light- and heavy-meson observables. It concludes that corrections to the heavy-quark symmetry limit of $\lesssim 30\%$ are encountered in $b \to c$ transitions and that these corrections can be as large as a factor of 2 in $c \to d$ transitions.

3   Calculated results

In the framework we have set up there are eight variable parameters: The widths of the light-vector-meson Bethe-Salpeter amplitudes – ω_ρ, ω_{K^*}, the widths of the heavy-meson Bethe-Salpeter amplitudes – ω_D, ω_{D_s}, ω_B, ω_{B_s}, and the light-quark momentum partitioning parameters – w_2^{ud}, w_2^{us}. All other parameters, including the quark masses, are taken as reported in Ref. [19]. We observe that in the widespread application of this framework and variants thereupon, calculations, when they can be compared with observables, are accurate to a root-mean-square (rms) deviation of 15%. The current application is not different in principle and hence this value should provide a reasonable estimate of our theoretical error.

We determine our parameters through a least-squares fit to meson leptonic decay constants. The parameter values obtained via this procedure are $w_2^{\text{ud}} = 0.377$, $w_2^{\text{us}} = 0.316$ and, in GeV:

$$
\begin{array}{|c|c|c|c|c|c|}
\hline
\omega_\rho & \omega_{K^*} & \omega_D & \omega_{D_s} & \omega_B & \omega_{B_s} \\
\hline
0.561 & 0.611 & 1.50 & 1.97 & 1.37 & 1.63 \\
\hline
\end{array}. \tag{16}
$$

The calculated values of observables are: $\rho \to \pi\pi$ coupling constant $g_{\rho\pi\pi} = 4.62$ [expt. =5.92(2)] and $K^* \to K\pi$ coupling $g_{K^*K\pi} = 4.55$ [expt. =4.67(4)], expressions for which are provided in Ref. [19], plus the leptonic decay constants listed in Table 1. Our calculated light-meson leptonic decay constants are unchanged from Ref. [19]: $f_\pi = 146\,\text{MeV}$; $f_K = 178\,\text{MeV}$ – cf. expt.: 131 MeV and 161 MeV, respectively.
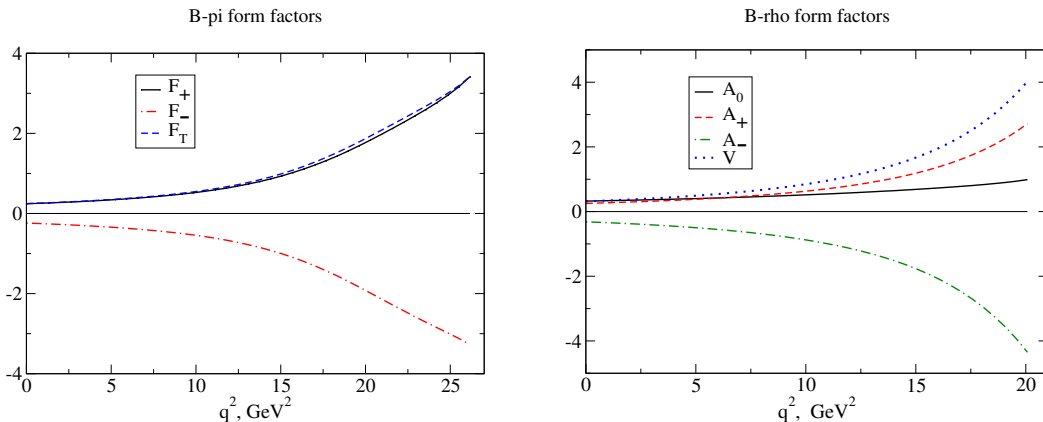
Figure 2: Our results for the $B \to \pi, \rho$ form factors.

With all parameters fixed, we now proceed to the calculation of the $B \to P(V)$ heavy-to-light transitions depicted in Fig. 1. Before reporting the predictions, we offer a technical remark. Calculation of the generalised impulse approximation to the transitions involves the numerical evaluation of a four-dimensional integral whose integrand is the convolution of entire functions and functions with a simple pole. The straightforward use of spherical coordinates in the Euclidean loop integral and the choice of the B-meson rest-frame works well only for $p_1^2 \le M_b^2$. When $p_1^2 > M_b^2$ one needs to shift the integration contour into the complex plane. Since that is not easily done numerically, we employ an alternate representation that can be used straightforwardly for any p_1^2. Namely, with $p_1^2 = -m_1^2$, $p_2^2 = -m_2^2$ and $(p_1 - p_2)^2 = -q^2$:

$$\int \frac{d^4 k}{\pi^2} \frac{F(k^2) \, \phi\Big((k + w_2 p_2)^2\Big) \sigma\Big((k + p_2)^2\Big)}{M_b^2 + (k + p_1)^2} = \frac{1}{\pi} \int\limits_0^\infty du \int\limits_0^1 dv \int\limits_0^\pi d\theta F(z_1) \, \phi(y_2) \, \sigma(z_2) \,,$$

$$z_1 = u + \frac{1-v}{v} [M_b^2 - v m_1^2] \,,$$

$$y_2 = z_1 + 2i\sqrt{uv} \cos\theta \, w_2 m_2 + (1-v) \, w_2 \, (m_1^2 + m_2^2 - q^2) - w_2^2 \, m_2^2 \,,$$

$$z_2 = z_1 + 2i\sqrt{uv} \cos\theta \, m_2 + (1-v) \, (m_1^2 + m_2^2 - q^2) - m_2^2 \,.$$

Figure 2 shows our calculated $B \to \pi$ form factors for $q^2 \in [0, q_{\max}^2]$, with $q_{\max}^2 = (m_B - m_\pi)^2$; viz., on the complete, relevant physical domain. It is noteworthy and phenomenologically important that in our DSE-based approach all form factors can be calculated on the entire domain of physically accessible momenta. Moreover, the chiral limit is directly accessible and the consequences of Goldstone's theorem are manifest, so that both pseudoscalar and vector light-quark mesons are realistically described. No extrapolation in any quantity is required.

Our calculated results are satisfactorily *interpolated* by the simple function

$$F(q^2) = \frac{F(0)}{1 - as + bs^2} \,, \qquad s = q^2 / m_B^2 \,. \tag{17}$$

We list the values of the form factors at the maximum recoil point, $q^2 = 0$, and the parameters a and b in Tables 2 and 3. Analytically, $a_0(0) = a_+(0) = g(0)$, a result preserved by the

	F_+	F_-	F_T	A_0	A_+	A_-	V	a_0	a_+	g
$F(0)$	0.24	-0.24	0.24	0.32	0.25	-0.32	0.32	0.25	0.26	0.26
a	1.87	1.97	1.92	1.16	2.08	2.27	2.21	1.26	2.10	2.21
b	0.93	1.04	1.00	0.32	1.14	1.38	1.30	0.48	1.16	1.29

Table 2: $B \to \pi(\rho)$ form factors: values of the parameters in Eq. (17).

	F_+	F_-	F_T	A_0	A_+	A_-	V	a_0	a_+	g
$F(0)$	0.29	-0.28	0.32	0.40	0.30	-0.38	0.37	0.30	0.30	0.30
a	1.85	1.95	1.90	0.98	1.92	2.10	2.05	1.04	1.95	2.05
b	0.96	1.09	1.02	0.034	0.97	1.19	1.13	0.16	1.00	1.12

Table 3: $B \to K(K^*)$ form factors: values of the parameters in Eq. (17).

interpolation function. We provide the interpolations so that our results may readily be adapted as input for other analyses.

In Table 4 we collect our predictions for the form factors at the maximum recoil point and provide a comparison with extant results obtained within other frameworks. The figures and tables highlight the wide range of phenomena accessible within our approach. That is equalled in the table by Refs. [8, 10, 11].

4   Summary

We presented a wide-ranging analysis of B-meson exclusive semileptonic and rare radiative decays using a phenomenological framework whose elements are based on Dyson-Schwinger equation (DSE) studies in QCD. Confinement and dynamical chiral symmetry breaking are expressed within this approach. Moreover, in the present context it is a particular feature of the method that all transition form factors are directly calculable on the entire physical domain of accessible momentum transfer. This may be contrasted with numerical simulations of lattice regularised QCD, which are currently restricted to the domain of intermediate timelike q^2 (e.g., [36] $q^2 \in [11, 18]\,\mathrm{GeV}^2$) and QCD Sum Rules, which are directly applicable only on the domain of small timelike q^2 (e.g., [8] $q^2 \in [0, 10]\,\mathrm{GeV}^2$).

The results presented herein represent a well-constrained calculation. Improvement over an earlier study [19] was made possible by: the appearance of additional data and lattice results in the interim; and technical improvements in our treatment of the loop integrals. Our results should thus prove valuable in the analysis and correlation of the rapidly accumulating body of information on charmless B-decays. To assist with this, we provided pointwise accurate parametrisations of our calculated transition form factors.

	This work	LCSR [8]	LCSR [9]	LCQM [10]	DQM [11]	RQM [12]
$f^+_{B\pi}(0)$	0.24	0.25±0.05	0.258±0.031	0.25	0.29	0.22
$f^+_{BK}(0)$	0.30	0.31±0.04	0.331±0.041	0.30	0.36	
$f^T_{B\pi}(0)$	0.25	0.21±0.04	0.253±0.028	0.25	0.28	
$f^T_{BK}(0)$	0.32	0.27±0.04	0.358±0.037	0.33	0.35	
$V^{B\rho}(0)$	0.31	0.32±0.10		0.30	0.31	0.30
$V^{BK^*}(0)$	0.37	0.39±0.11		0.34	0.44	
$A^{B\rho}_1(0)$	0.24	0.24±0.08		0.23	0.26	0.27
$A^{BK^*}_1(0)$	0.29	0.30±0.08		0.25	0.36	
$A^{B\rho}_2(0)$	0.25	0.21±0.09		0.22	0.24	0.28
$A^{BK^*}_2(0)$	0.30	0.26±0.08		0.23	0.32	
$T^{B\rho}_1(0)$	0.26	0.28±0.09		0.26	0.27	
$T^{BK^*}_1(0)$	0.30	0.33±0.10		0.29	0.39	

Table 4: Our calculated values of $B \to \pi, K$ and $B \to \rho, K^*$ form factors at the maximum recoil point compared with the results obtained by other authors. Based on the widespread application of our approach herein and elsewhere, we estimate that the relative systematic uncertainty in our calculated results is $\sim 15\%$.

Acknowledgments

References

[1] W. M. Yao *et al.* [Particle Data Group], J. Phys. **G33**, 1 (2006).

[2] Th. Feldmann, "Recent developments in soft-collinear effective theory," hep-ph/0610192.

[3] A. Ali, P. Ball, L. T. Handoko and G. Hiller, Phys. Rev. **D61** 074024 (2000).

[4] A. Ali, E. Lunghi, C. Greub and G. Hiller, Phys. Rev. **D66** 034002 (2002).

[5] A. Ali, G. Kramer and G. h. Zhu, Eur. Phys. J. **C47** 625 (2006).

[6] M. Beneke, T. Feldmann and D. Seidel, Eur. Phys. J. **C41**, 173 (2005).

[7] T. Becher, R. J. Hill and M. Neubert, Phys. Rev. **D72**, 094017 (2005).

[8] A. Khodjamirian, T. Mannel and N. Offen, Phys. Rev. **D75**, 054013 (2007).

[9] P. Ball and R. Zwicky, Phys. Rev. **D71**, 014015 (2005).

[10] C. D. Lu, W. Wang and Z. T. Wei, Phys. Rev. **D76**, 014013 (2007).

[11] D. Melikhov, N. Nikitin and S. Simula, Phys. Rev. **D57**, 6814 (1998).

[12] D. Ebert, R. N. Faustov and V. O. Galkin, Phys. Rev. **D75**, 074008 (2007).

[13] A. Faessler, T. Gutsche, M. A. Ivanov, J. G. Körner and V. E. Lyubovitskij, Eur. Phys. J. direct **C4**, 18 (2002).

[14] M. A. Ivanov, J. G. Körner and P. Santorelli, Phys. Rev. **D63**, 074010 (2001); Phys. Rev. **D71**, 094006 (2005) [Erratum-ibid. **D75**, 019901 (2007)]; Phys. Rev. **D73**, 054024 (2006).

[15] G. V. Efimov and M. A. Ivanov, "The Quark confinement model of hadrons", *Bristol, UK: IOP (1993) 177 p.*; Int. J. Mod. Phys. **A4**, 2031 (1989); M. A. Ivanov, M. P. Locher and V. E. Lyubovitskij, Few Body Syst. **21**, 131 (1996).

[16] M. A. Ivanov, J. G. Körner, S. G. Kovalenko, C. D. Roberts, Phys. Rev. **D76**, 034018 (2007).

[17] M. A. Ivanov, Yu. L. Kalinovsky, P. Maris, C. D. Roberts, Phys. Lett. **B416**, 29 (1998).

[18] M. A. Ivanov, Yu. L. Kalinovsky, P. Maris, C. D. Roberts, Phys. Rev. **C57**, 1991 (1998).

[19] M. A. Ivanov, Yu. L. Kalinovsky, C. D. Roberts, Phys. Rev. **D60**, 034018 (1999).

[20] M. Neubert, Phys. Rept. **245**, 259 (1994).

[21] C. D. Roberts and A. G. Williams, Prog. Part. Nucl. Phys. **33**, 477 (1994).

[22] C. D. Roberts, Nucl. Phys. **A605**, 475 (1996).

[23] J. S. Ball and T.-W. Chiu, Phys. Rev. **D22**, 2542 (1980).

[24] P. Zweber, "Charm leptonic and semileptonic decays," hep-ex/0701018.

[25] M. Artuso *et al.* [CLEO Collaboration], Phys. Rev. Lett. **95**, 251801 (2005).

[26] M. Artuso *et al.* [CLEO Collaboration], "Measurement of $D_s^+ \to \mu^+\nu$ and the decay constant f_{D_s}," hep-ex/0607074.

[27] S. Stone, "Measurement of $D_s^+ \to \ell^+\nu$ and the decay constant f_{D_s}," hep-ex/0610026.

[28] B. Aubert *et al.* [BABAR Collaboration], Phys. Rev. Lett. **98**, 141801 (2007).

[29] D. Becirevic, P. Boucaud, J. P. Leroy, V. Lubicz, G. Martinelli, F. Mescia and F. Rapuano, Phys. Rev. **D60**, 074501 (1999).

[30] C. Aubin *et al.*, Phys. Rev. Lett. **95** (2005) 122002.

[31] K. Ikado *et al.*, Phys. Rev. Lett. **97**, 251802 (2006).

[32] A. Gray *et al.* [HPQCD Collaboration], Phys. Rev. Lett. **95** (2005) 212001.

[33] L. Lellouch and C. J. D. Lin [UKQCD Collaboration], Phys. Rev. **D64**, 094501 (2001).

[34] X. H. Guo and M. H. Weng, Eur. Phys. J. **C50**, 63 (2007).

[35] M. Wingate, C. T. H. Davies, A. Gray, G. P. Lepage and J. Shigemitsu, Phys. Rev. Lett. **92**, 162001 (2004).

[36] D. Becirevic, V. Lubicz and F. Mescia, Nucl. Phys. **B769**, 31 (2007).

Heavy hadron molecules

Amand Faessler, Thomas Gutsche, Valery E. Lyubovitskij[*]

Institut für Theoretische Physik, Universität Tübingen,
Kepler Center for Astro and Particle Physics,
Auf der Morgenstelle 14, D–72076 Tübingen, Germany

We discuss a possible interpretation of $D_{s0}^*(2317)$, $D_{s1}(2460)$, $B_{s0}^*(5725)$, $B_{s1}(5778)$ and $X(3872)$ mesons as hadronic molecules. Using an effective Lagrangian approach we calculate their weak, strong and radiative decays. The new impact of molecular structure of these states is the presence of $u(d)$ quarks in K, $D^{(*)}$ and $B^{(*)}$ mesons which give rise to the direct strong isospin-violating transitions $D_{s0}^*(B_{s0}^*) \to D_s(B_s) + \pi^0$ and $D_{s1}(B_{s1}) \to D_s^*(B_s^*) + \pi^0$ in addition to the modes generated by $\eta - \pi^0$ mixing as was considered before in the literature.

1 Introduction

Nowadays there is strong interest to study newly observed mesons and baryons in the context of a hadronic molecule interpretation [1]. As stressed for example in Ref. [2] the scalar $D_{s0}^*(2317)$ and axial $D_{s1}(2460)$ mesons could be candidates for a scalar DK and a axial D^*K molecule because of a relatively small binding energy of ~ 50 MeV. These states were discovered and confirmed just a few years ago by the Collaborations BABAR at SLAC, CLEO at CESR and Belle at KEKB [3]. In the interpretation of these experiments it was suggested that the $D_{s0}^*(2317)$ and $D_{s1}(2460)$ mesons are the P-wave charm-strange quark states with spin-parity quantum numbers $J^P = 0^+$ and $J^P = 1^+$, respectively.

The next important question concerns the possible structure of the $D_{s0}^*(2317)$ and $D_{s1}(2460)$ mesons. The simplest interpretation of these states is that they are the missing $j_s = 1/2$ (j_s is the angular momentum of the s-quark) members of the $c\bar{s}$ $L = 1$ multiplet. However, this standard quark model scenario is in disagreement with experimental observation, since the $D_{s0}^*(2317)$ and $D_{s1}(2460)$ states are narrower and their masses are lower when compared to theoretical predictions (see e.g. discussion in Ref. [1]). Therefore, in addition to the standard quark-antiquark picture alternative interpretations of the $D_{s0}^*(2317)$ and $D_{s1}(2460)$ mesons have been suggested: four-quark states, mixing of two- and four-quark states, two-diquark states and two-meson molecular states. Up to now strong and radiative decays of the $D_{s0}^*(2317)$ and $D_{s1}(2460)$ mesons have been calculated using different approaches [4]-[28]: quark models, effective Lagrangian approaches, QCD sum rules, lattice QCD, etc.

A new feature related to the molecular $D^{(*)}K$ structure of the $D_{s0}^*(2317)$ and $D_{s1}(2460)$ mesons is that the presence of $u(d)$ quarks in the $D^{(*)}$ and K mesons gives rise to direct strong isospin-violating transitions $D_{s0}^* \to D_s\pi^0$ and $D_{s1} \to D_s^*\pi^0$ in addition to the decay mechanism induced by $\eta - \pi^0$ mixing, as considered previously.

---

[*]On leave of absence from Department of Physics, Tomsk State University, 634050 Tomsk, Russia

In the present paper we will consider the strong, radiative and leptonic decays of the $D_{s0}^*(2317)$ and $D_{s1}(2460)$ meson using an effective Lagrangian approach. The approach is based on the hypothesis that the D_{s0}^* and D_{s1} are bound states of D, K and D^*, K mesons, respectively. In other words, we investigate the position that the D_{s0}^* and D_{s1} are (DK) and (D^*K) hadronic molecules. Their couplings to the constituents are described by effective Lagrangians. The corresponding coupling constants $g_{D_{s0}^*DK}$ and $g_{D_{s1}D^*K}$ are determined by the compositeness condition $Z = 0$ [29, 30], which implies that the renormalization constant of the hadron wave function is set equal to zero. Note, that this condition was originally applied to the study of the deuteron as a bound state of proton and neutron [29]. Then it was extensively used in low-energy hadron phenomenology as the master equation for the treatment of mesons and baryons as bound states of light and heavy constituent quarks (see Refs. [30, 31]). Recently the compositeness condition was used to study the light scalar mesons a_0 and f_0 as $K\bar{K}$ molecules [32]. A new impact of the molecular structure of the $D_{s0}^*(2317)$ and $D_{s1}(2460)$ mesons is that the presence of $u(d)$ quarks in the D^* and K meson gives rise to the direct strong isospin-violating transitions $D_{s0}^* \to D_s \pi^0$ and $D_{s1} \to D_s^* \pi^0$ in addition to the decay induced by $\eta - \pi^0$ mixing considered before in the literature. We show that the direct transition dominates over the $\eta - \pi^0$ mixing transitions. The obtained results for the partial decay widths are consistent with previous calculations. We also extend our formalism to the bottom sector, that is to the $B_{s0}^*(5725)$ and $B_{s1}(5778)$ states and to the charmonium-like states: $X(3872)$, $Z(4433$, etc. See details in Refs. [21]-[26].

2   Approach: basic notions and results

In this section we briefly discuss the formalism for the study of hadronic molecules. For example, we consider the $D_{s0}^{*\pm}(2317)$ meson as a bound state of D and K mesons. Extension to other states is straightforward. First of all we specify the quantum numbers of the $D_{s0}^{*\pm}(2317)$ mesons. We use the current results for the quantum numbers of isospin, spin and parity: $I(J^P) = 0(0^+)$ and mass $m_{D_{s0}^*} = 2.3173\,\text{GeV}$ [3]. Our framework is based on an effective interaction Lagrangian describing the coupling between the $D_{s0}^*(2317)$ meson and their constituents - D and K mesons:

$$\mathcal{L}_{D_{s0}^*}(x) = g_{D_{s0}^*} D_{s0}^{*-}(x) \int dy \Phi_{D_{s0}^*}(y^2) D(x + w_{KD}y) K(x - w_{DK}y) + \text{H.c.} \tag{1}$$

where D and K are the corresponding meson doublets, $w_{ij} = m_i/(m_i + m_j)$ is a kinematic variable, m_D and m_K are the masses of D and K mesons. The correlation function $\Phi_{D_{s0}^*}$ characterizes the finite size of the $D_{s0}^*(2317)$ meson as a $D\,K$ bound state and depends on the relative Jacobi coordinate y with x being the center of mass (CM) coordinate. In the numerical calculations we employ the Gaussian form for $\Phi_{D_{s0}^*}$. Its Fourier transform reads as $\tilde{\Phi}_{D_{s0}^*}(p_E^2) = \exp(-p_E^2/\Lambda_{D_{s0}^*}^2)$, where p_E is the Euclidean Jacobi momentum. Here $\Lambda_{D_{s0}^*}$ is a size parameter, which parametrizes the distribution of D and K mesons inside the D_{s0}^* molecule. The coupling constant $g_{D_{s0}^*}$ is determined by the compositeness condition [29, 30], which implies that the renormalization constant of the hadron wave function is set equal to zero: $Z_{D_{s0}^*} = 1 - \Sigma'_{D_{s0}^*}(m_{D_{s0}^*}^2) = 0$, where $\Sigma'_{D_{s0}^*}$ is the derivative of the D_{s0}^* meson mass operator.

The effective Lagrangian (1) is the starting point for the study of the decays of hadronic molecules. It defines the transition of the molecule into its constituents. Then we should specify the Lagrangian which describes the interaction of the constituents with external fields

(hadrons and gauge bosons) and the diagrams which contribute to the matrix elements of physical processes. All further details can be found in Refs. [21]-[24].

3 Results

Below, in Tables 1 – 4, we display our results for the strong $\Gamma(D_{s0}^*(D_{s1}) \to D_s(D_s^*)\pi)$ and radiative $D_{s0}^*(D_{s1}) \to D_s^*(D_s)\gamma$ decay widths and their ratios $R_{D_{s0}^*} = \Gamma(D_{s0}^* \to D_s^*\gamma)/\Gamma(D_{s0}^* \to D_s\pi)$ and $R_{D_{s1}} = \Gamma(D_{s1} \to D_s\gamma)/\Gamma(D_{s1} \to D_s^*\pi)$, including the extension to the bottom sector, and compare them with the predictions of other approaches.

In the heavy quark limit (when masses of charm and bottom quark/mesons go to infinity) we deduce relations between the couplings of strong decays

$$\frac{G_{B_{s0}^* B_s \pi}}{G_{D_{s0}^* D_s \pi}} \sim \frac{m_b}{m_c}\,, \qquad \frac{G_{B_{s1} B_s^* \pi}}{G_{D_{s1} D_s^* \pi}} \sim \frac{m_b}{m_c}\,. \tag{2}$$

and decay widths of radiative decays:

$$\frac{\Gamma(D_{s1} \to D_s\gamma)}{\Gamma(D_{s0}^* \to D_s^*\gamma)} = \frac{1}{3}\left(\frac{m_{D_{s1}}^2 - m_{D_s}^2}{m_{D_{s0}^*}^2 - m_{D_s^*}^2}\right)^3 \left(\frac{m_{D_{s0}^*}}{m_{D_{s1}}}\right)^3 \simeq 3.80\,, \tag{3}$$

$$\frac{\Gamma(B_{s1} \to B_s\gamma)}{\Gamma(B_{s0}^* \to B_s^*\gamma)} = \frac{1}{3}\left(\frac{m_{B_{s1}}^2 - m_{B_s}^2}{m_{B_{s0}^*}^2 - m_{B_s^*}^2}\right)^3 \left(\frac{m_{B_{s0}^*}}{m_{B_{s1}}}\right)^3 \simeq 0.74\,, \tag{4}$$

and

$$\frac{\Gamma(B_{s0}^* \to B_s^*\gamma)}{\Gamma(D_{s0}^* \to D_s^*\gamma)} = \left(\frac{m_{B_{s0}^*}^2 - m_{B_s^*}^2}{m_{D_{s0}^*}^2 - m_{D_s^*}^2}\right)^3 \left(\frac{m_{D_{s0}^*}}{m_{B_{s0}^*}}\right)^3 \simeq 3.74\,, \tag{5}$$

$$\frac{\Gamma(B_{s1} \to B_s\gamma)}{\Gamma(D_{s1} \to D_s\gamma)} = \left(\frac{m_{B_{s1}}^2 - m_{B_s}^2}{m_{D_{s1}}^2 - m_{D_s}^2}\right)^3 \left(\frac{m_{D_{s1}}}{m_{B_{s1}}}\right)^3 \simeq 0.73\,. \tag{6}$$

Relation (3) is confirmed by the full analysis done in our framework and in other theoretical approaches (see compilation of the results in Refs. [21, 23]). E.g. the relation explains why most of the approaches predict that the decay width $\Gamma(D_{s1} \to D_s\gamma)$ is approximately $3 - 5$ times larger than $\Gamma(D_{s0}^* \to D_s^*\gamma)$. The other relations (4)-(6) help to give predictions for the decay widths of the bottom partners. In particular, we arrive at the conclusion that our full predictions for $\Gamma(B_{s0}^* \to B_s^*\gamma)$ and $\Gamma(B_{s1} \to B_s\gamma)$ – a few keV – are well justified.

Also, we present our results for the leptonic decay constants: $f_{D_{s0}^*} = 67.1$ MeV and $f_{D_{s1}} = 144.5$ MeV. In Table 5 we summarize the present results for $f_{D_{s0}^*}$ and $f_{D_{s1}}$ obtained in different approaches (either on the basis of hadronic models or from the analysis of experimental data on two-body B-meson decays). Our results are in agreement with the predictions of Refs. [4, 33, 34, 35], especially with the lower limits derived from an analysis of the branching ratios of $B \to D^{(*)} D_{s0}^*(D_{s1})$ decays [33, 35].

Using the predicted decay constants $f_{D_{s0}^*}$ and $f_{D_{s1}}$ we calculate the branching ratios of $B \to D^{(*)} D_{s0}^*(D_{s1})$ decays. For this purpose we use the leptonic decay constants $f_{D_{s0}^*}$, $f_{D_{s1}}$ and, in addition, model-independent results for the form factors of $B \to D^{(*)} \ell \bar\nu_\ell$ transitions obtained by Caprini, Lellouch and Neubert (CLN) [36]. Latter derivations are based on heavy quark spin

Table 1: Strong decay widths in keV.

Approach	$\Gamma(D_{s0}^* \to D_s\pi)$	$\Gamma(D_{s1} \to D_s^*\pi)$
Ref. [14]	6 ± 2	
Ref. [7]	7 ± 1	7 ± 1
Ref. [18]	8.69	11.41
Ref. [6]	10	10
Ref. [8]	16	32
Ref. [5]	21.5	21.5
Ref. [17]	32	35
Ref. [13]	39 ± 5	43 ± 8
Ref. [4]	$10 - 100$	
Ref. [9]	155 ± 70	155 ± 70
Ref. [10]	129 ± 43	187 ± 73
Ref. [28]	140	140
Our results [21, 23]	$46.7 - 75$	$50.1 - 79.2$

Table 2: Radiative decay widths in keV.

Approach	$\Gamma(D_{s0}^* \to D_s^*\gamma)$	$\Gamma(D_{s1} \to D_s\gamma)$
Ref. [8]	0.2	
Ref. [27]	0.49	
Ref. [7]	0.85 ± 0.05	
Ref. [12]	1	≤ 7.3
Ref. [15]	≈ 1.1	$0.6 - 2.9$
Ref. [20]	$1.3 - 9.9$	$5.5 - 31.2$
Ref. [10]	≤ 1.4	≈ 2
Ref. [16]	1.6	6.7
Ref. [5]	1.74	5.08
Ref. [6]	1.9	6.2
Ref. [11]	$4 - 6$	$19 - 29$
Ref. [28]	< 7	$\simeq 43.6$
Ref. [9]	21	93
Our results [21, 23]	$0.47 - 0.63$	$2.37 - 3.73$

Table 3: Ratios $R_{D_{s0}^*}$ and $R_{D_{s1}}$.

Approach	$R_{D_{s0}^*}$	$R_{D_{s1}}$
Ref. [8]	0.01	
Ref. [10]	≤ 0.02	0.01 - 0.02
Ref. [28]	< 0.05	$\simeq 0.31$
Ref. [5]	0.08	0.24
Ref. [11]	$0.11 - 0.14$	
Ref. [6]	0.19	0.62
Ref. [9]	0.09 - 0.25	0.41 - 1.09
Ref. [16]	0.16	0.67
Data [3]	≤ 0.059	0.44 ± 0.09
Our results [21, 23]	$\simeq 0.01$	$\simeq 0.05$

Table 4: Decay widths of $B_{s0}^*(5725)$ and $B_{s1}(5778)$ in keV.

Approach	$\Gamma(B_{s0}^* \to B_s\pi)$	$\Gamma(B_{s1} \to B_s^*\pi)$	$\Gamma(B_{s0}^* \to B_s^*\gamma)$	$\Gamma(B_{s1} \to B_s\gamma)$
Refs. [18, 19]	7.92	10.36		
Our results [24]	$55.2 - 89.9$	$57.4 - 94.7$	$3.07 - 4.06$	$2.01 - 2.67$

Table 5: Leptonic decay constants $f_{D_{s0}^*}$ and $f_{D_{s1}}$.

Approach	$f_{D_{s0}^*}$ (MeV)	$f_{D_{s1}}$ (MeV)
Ref. [11]	225 ± 25	225 ± 25
Ref. [37]	206 ± 120	
Ref. [38]	200 ± 50	
Ref. [39]	170 ± 20	247 ± 37
Ref. [40]	138 ± 16	259 ± 13
Ref. [41]	110 ± 18	233 ± 31
Ref. [33]	$> (74 \pm 11)/|a_1|$	$> (166 \pm 20)/|a_1|$
Ref. [34]	71	117
Ref. [34]	60 ± 13	150 ± 40
Ref. [35]	$> (58 - 86)/|a_1|$	$> (90 - 228)/|a_1|$
Ref. [4]	67 ± 13	
Ref. [42]	44	41
Our results [22]	67.1 ± 4.5	144.5 ± 11.1

Table 6: Branching ratios of $B \to D^{(*)} D_{s0}^*(D_{s1})$ decays (in units of 10^{-3}).

Mode	Data (averaged) [3]	BABAR [43]	Our results [22]
$B^- \to D_{s0}^{*-} D^0$	$> 0.74^{+0.23}_{-0.19}$		1.03 ± 0.14
$\bar{B}^0 \to D_{s0}^{*-} D^+$	$> 0.97^{+0.41}_{-0.34}$		0.96 ± 0.13
$B^- \to D_{s1}^- D^0$	$> 1.4^{+0.6}_{-0.5}$	$4.3 \pm 1.6 \pm 1.3$	2.54 ± 0.39
$\bar{B}^0 \to D_{s1}^- D^+$	$> 2.0^{+0.6}_{-0.5}$	$2.6 \pm 1.5 \pm 0.74$	2.36 ± 0.36
$B^- \to D_{s0}^{*-} D^{*0}$	$> 0.9 \pm 0.6^{+0.4}_{-0.3}$		0.50 ± 0.07
$\bar{B}^0 \to D_{s0}^{*-} D^{*+}$	$> 1.5 \pm 0.4^{+0.5}_{-0.4}$		0.47 ± 0.06
$B^- \to D_{s1}^- D^{*0}$	$> 5.5 \pm 1.2^{+2.2}_{-1.6}7.6$	$11.2 \pm 2.6 \pm 2.0$	7.33 ± 1.12
$\bar{B}^0 \to D_{s1}^- D^{*+}$	$> 7.6 \pm 1.7^{+3.2}_{-2.4}$	$8.8 \pm 2.0 \pm 1.4$	6.85 ± 1.05

Table 7: Ratios $MD^*/MD = \Gamma(B \to MD^*)/\Gamma(B \to MD)$ for $M = D_{s0}^*, D_{s1}$.

Mode	Data [35]	CLF [35]	Our results [22]
$D_{s0}^{*-} D^{*0}/D_{s0}^{*-} D^0$	0.91 ± 0.73	0.49	0.48
$D_{s0}^{*-} D^{*+}/D_{s0}^{*-} D^+$	0.59 ± 0.26	0.49	0.48
$D_{s1}^- D^{*0}/D_{s1}^- D^0$	3.4 ± 2.4	3.6	2.9
$D_{s1}^- D^{*+}/D_{s1}^- D^+$	2.6 ± 1.5	3.6	2.9

Table 8: Decay width of $X(3872) \to \gamma J/\psi$ in keV.

Approach	$\Gamma(X(3872) \to \gamma J/\psi)$
$[c\bar{c}]$, Ref. [44]	11
$[c\bar{c}]$, Ref. [45]	71
$[c\bar{c}]$, Ref. [45]	139
[molecule], Ref. [45]	8
Our results	124.8 - 231.3 ($\epsilon = 0.7$ MeV) 129.8 - 239.1 ($\epsilon = 1$ MeV) 138.0 - 251.4 ($\epsilon = 1.5$ MeV)

symmetry, dispersive constraints, including short-distance and power corrections. In Table 6 we present our predictions for the branching ratios of two-body decays $B \to D^{(*)} D_{s0}^*(D_{s1})$. For the data we use the averaged lower limits from PDG [3] and in addition for the modes with a $D_{s1}(2460)$ meson in the final state the direct results of the BABAR Collaboration. Our predictions are in good agreement with the experimental data except for the marginal situation in the case of the $\bar{B}^0 \to D_{s0}^{*-} D^{*+}$ decay, where our prediction is slightly lower than the experimental limit. In Table 7 we present the results for the ratios $\Gamma(B \to D^* D_{s0}^*)/\Gamma(B \to DD_{s0}^*)$ and $\Gamma(B \to D^* D_{s1})/\Gamma(B \to DD_{s1})$. We also use the compilation of experimental data and theoretical results within the covariant light-front (CLF) approach [34] summarized in Table 10 of Ref. [35]. Here, our predictions are in good agreement with the existing experimental data. In comparison with the CLF approach our predictions are lower, although not significantly.

Finally we consider $X(3872)$ resonance as a hadronic molecule, a loosely–bound state of charmed D^0 and D^{*0} mesons, since its mass is very close to the $D^{*0}\bar{D}^0$ threshold. Assuming structure and quantum numbers of $X(3872)$ as $(D^0\bar{D}^{*0} - D^{*0}\bar{D}^0)/\sqrt{2}$ and $J^{PC} = 1^{++}$, we calculate the $X(3872) \to \gamma J/\psi$ decay width. We also estimate the contribution of an additional $c\bar{c}$ component in the $X(3872)$ to this decay width, which is shown to be suppressed relative to the one of the molecular configuration.

In Table 8, we list our results for the decay width $\Gamma(X(3872) \to \gamma J/\psi)$ at the following values of binding energy $\epsilon = 0.7, 1, 1.5$ MeV. The range of values for our results is due to the variation of the scale parameter Λ_X from 2 to 3 GeV. Although the resulting decay width is not very sensitive to a change in the binding energy ϵ, the result depends stronger on the variation of Λ_X. The latter result is consistent with the conclusion of Ref. [45], where the $\Gamma(X(3872) \to \gamma J/\psi)$ decay width is also very sensitive to details of the wave function or finite–size effects. We obviously need more data to constrain our model parameter Λ_X. We therefore consider the present results as an estimate. For comparison we also present the results of Refs. [44, 45]. As was stressed in [45], in the framework of the charmonium picture there is a strong sensitivity to the model details, e.g. to the choice of binding potential, leading to a variation of the predictions from 11 keV [44] to 139 keV [45]. On the other hand, our result is larger than the prediction $\Gamma(X(3872) \to \gamma J/\psi) = 8$ keV of the other molecular approach [45]. Therefore, a future precise measurement of $\Gamma(X(3872) \to \gamma J/\psi)$ will be a crucial check for theoretical approaches.

4   Summary

We studied the new charm-strange mesons $D_{s0}^*(2317)$ and $D_{s1}(2460)$ in the hadronic molecule interpretation, considering DK and D^*K bound states, respectively. Using an effective Lagrangian approach we calculated their weak, strong and radiative decays. A new impact of their molecular structure is that the presence of $u(d)$ quarks in the $D^{(*)}$ and K meson loops gives rise to direct strong isospin-violating transitions $D_{s0}^* \to D_s\pi^0$ and $D_{s1} \to D_s^*\pi^0$, in addition to the decay mechanism induced by $\eta - \pi^0$ mixing as was considered before in the literature. Also, we extend our formalism to the bottom sector: that is $B_{s0}^*(5725)$ and $B_{s1}(5778)$ states. We calculated weak decay properties of $D_{s0}^*(2317)$ and $D_{s1}(2460)$: the leptonic decay constants $f_{D_{s0}^*}$, $f_{D_{s1}}$ and branching ratios of the two-body bottom meson decays $B \to D^{(*)} D_{s0}^*(D_{s1})$. Also we estimated the $X(3872) \to \gamma J/\psi$ decay width.

Acknowledgements

References

[1] J. L. Rosner, Phys. Rev. D **74** 076006 (2006)

[2] T. Barnes, F. E. Close and H. J. Lipkin, Phys. Rev. D **68** 054006 (2003)

[3] C. Amsler *et al.* (Particle Data Group), Phys. Lett. B **667** 1 (2008)

[4] H. Y. Cheng and W. S. Hou, Phys. Lett. B **566** 193 (2003)

[5] W. A. Bardeen, E. J. Eichten and C. T. Hill, Phys. Rev. D **68** 054024 (2003)

[6] S. Godfrey, Phys. Lett. B **568** 254 (2003)

[7] P. Colangelo and F. De Fazio, Phys. Lett. B **570** 180 (2003)

[8] Fayyazuddin and Riazuddin, Phys. Rev. D **69** 114008 (2004)

[9] S. Ishida, M. Ishida, T. Komada, T. Maeda, M. Oda, K. Yamada and I. Yamauchi, AIP Conf. Proc. **717** 716 (2004)

[10] Y. I. Azimov and K. Goeke, Eur. Phys. J. A **21** 501 (2004)

[11] P. Colangelo, F. De Fazio and A. Ozpineci, Phys. Rev. D **72** 074004 (2005)

[12] F. E. Close and E. S. Swanson, Phys. Rev. D **72** 094004 (2005)

[13] W. Wei, P. Z. Huang and S. L. Zhu, Phys. Rev. D **73** 034004 (2006)

[14] M. Nielsen, Phys. Lett. B **634** 35 (2006)

[15] X. Liu, Y. M. Yu, S. M. Zhao and X. Q. Li, Eur. Phys. J. C **47** 445 (2006)

[16] J. Vijande, F. Fernandez and A. Valcarce, Phys. Rev. D **73** 034002 (2006) [Erratum-ibid. D **74** 059903 (2006)]

[17] J. Lu, X. L. Chen, W. Z. Deng and S. L. Zhu, Phys. Rev. D **73** 054012 (2006)

[18] F. K. Guo, P. N. Shen, H. C. Chiang and R. G. Ping, Phys. Lett. B **641** 278 (2006)

[19] F. K. Guo, P. N. Shen and H. C. Chiang, Phys. Lett. B **647** 133 (2007)

[20] Z. G. Wang, Phys. Rev. D **75** 034013 (2007)

[21] A. Faessler, T. Gutsche, V. E. Lyubovitskij, and Y. L. Ma, Phys. Rev. D **76** 014005 (2007)

[22] A. Faessler, T. Gutsche, S. Kovalenko and V. E. Lyubovitskij, Phys. Rev. D **76** 014003 (2007)

[23] A. Faessler, T. Gutsche, V. E. Lyubovitskij, and Y. L. Ma, Phys. Rev. D **76** 114008 (2007)

[24] A. Faessler, T. Gutsche, V. E. Lyubovitskij, and Y. L. Ma, Phys. Rev. D **77** 114013 (2008)

[25] A. Faessler, T. Gutsche and V. E. Lyubovitskij, Prog. Part. Nucl. Phys. **61** 127 (2008)

[26] Y. B. Dong, A. Faessler, T. Gutsche and V. E. Lyubovitskij, Phys. Rev. D **77** 094013 (2008)

[27] D. Gamermann, L. R. Dai, and E. Oset, Phys. Rev. C **76** 055205 (2007)

[28] M. F. M. Lutz and M. Soyeur, Nucl. Phys. A **813** 14 (2008)

[29] S. Weinberg, Phys. Rev. **130** 776 (1963) A. Salam, Nuovo Cim. **25** 224 (1962)

[30] G. V. Efimov and M. A. Ivanov, *The Quark Confinement Model of Hadrons* (IOP Publishing, Bristol & Philadelphia, 1993).

[31] M. A. Ivanov, M. P. Locher and V. E. Lyubovitskij, Few Body Syst. **21** 131 (1996); M. A. Ivanov, V. E. Lyubovitskij, J. G. Körner and P. Kroll, Phys. Rev. D **56** 348 (1997); M. A. Ivanov, J. G. Körner, V. E. Lyubovitskij and A. G. Rusetsky, Phys. Rev. D **60** 094002 (1999); A. Faessler, T. Gutsche, M. A. Ivanov, J. G. Körner and V. E. Lyubovitskij, Phys. Lett. B **518** 55 (2001); A. Faessler, T. Gutsche, M. A. Ivanov, J. G. Körner, V. E. Lyubovitskij, D. Nicmorus and K. Pumsa-ard, Phys. Rev. D **73** 094013 (2006); A. Faessler, T. Gutsche, B. R. Holstein, V. E. Lyubovitskij, D. Nicmorus and K. Pumsa-ard, Phys. Rev. D **74** 074010 (2006); A. Faessler, T. Gutsche, B. R. Holstein, M. A. Ivanov, J. G. Korner and V. E. Lyubovitskij, Phys. Rev. D **78** 094005 (2008)

[32] V. Baru, J. Haidenbauer, C. Hanhart, Yu. Kalashnikova, and A. E. Kudryavtsev, Phys. Lett. B **586** (2004) 53; C. Hanhart, Y. S. Kalashnikova, A. E. Kudryavtsev, and A. V. Nefediev, Phys. Rev. D **75** 074015 (2007)

[33] D. S. Hwang and D. W. Kim, Phys. Lett. B **606** 116 (2005)

[34] H. Y. Cheng, C. K. Chua and C. W. Hwang, Phys. Rev. D **69** 074025 (2004)

[35] H. Y. Cheng and C. K. Chua, Phys. Rev. D **74** 034020 (2006)

[36] I. Caprini, L. Lellouch and M. Neubert, Nucl. Phys. B **530** 153 (1998)

[37] F. Jugeau, A. Le Yaouanc, L. Oliver and J. C. Raynal, Phys. Rev. D **72** 094010 (2005)

[38] G. Herdoiza, C. McNeile and C. Michael [UKQCD Collaboration], Phys. Rev. D **74** 014510 (2006)

[39] P. Colangelo, G. Nardulli, A. A. Ovchinnikov and N. Paver, Phys. Lett. B **269** 201 (1991).

[40] R. C. Hsieh, C. H. Chen and C. Q. Geng, Mod. Phys. Lett. A **19** 597 (2004)

[41] S. Veseli and I. Dunietz, Phys. Rev. D **54** 6803 (1996)

[42] A. Le Yaouanc, L. Oliver, O. Pene, J. C. Raynal and V. Morenas, Phys. Lett. B **520** 59 (2001)

[43] B. Aubert *et al.* [BABAR Collaboration], Phys. Rev. D **74** 031103 (2006)

[44] T. Barnes and S. Godfrey, Phys. Rev. D **69** 054008 (2004)

[45] E. S. Swanson, Phys. Lett. B **598** 197 (2004)

$B^0 - \bar{B}^0$ mixing: hadronic matrix elements beyond factorization in QCD sum rules analysis

Alexei A. Pivovarov

Institute for Nuclear Research, 117312 Moscow, Russia

The analysis of B-meson mixing within sum rules technique is presented. It is shown that the factorization results are reproduced at the diagram level. The non-factorizable contributions due to non-perturbative vacuum condensates to bag parameters are small.

1 Flavordynamics in Standard Model

There are three generations of matter fields (fermions) in the Standard Model

$$\text{quarks}: \quad \begin{pmatrix} u \\ d \end{pmatrix}, \begin{pmatrix} c \\ s \end{pmatrix}, \begin{pmatrix} t \\ b \end{pmatrix} \quad + \quad \text{leptons}$$

where $u, d, c \dots$ are flavors of quarks. Yukawa interaction with Higgs boson H gives masses to originally massless fermions:

$$\lambda_f H \bar{f} f \to m_f \bar{f} f, \quad m_f = \lambda_f \langle H \rangle$$

where λ_f is the coupling constant and $\langle H \rangle$ is the vacuum expectation value of the Higgs field. Gauge interaction of up, $U_i = (u, c, t)_L$, and down, $D_j = (d, s, b)_L$, quarks with W-bosons includes CKM matrix V [1] in such a way that its entries V_{ij} are effectively the coupling constants $V_{ij} \cdot \bar{U}_i \gamma_\mu D_j W^\mu$. The interaction with nonvanishing elements V_{ij} initiates transitions between quark flavors $b \to c, \quad s \to u, \quad c \leftrightarrow d, \dots$ The CKM entries V_{ij} and quark masses m_f are parameters of SM: their numerical values are to be found from data. Masses of quarks (or Yukawa couplings) are quite different numerically

$$m_{u,d} \sim 5 \times 10^{-3} \text{ GeV}, \quad m_s = 0.1 \text{ GeV}$$

$$m_c = 1.3 \text{ GeV}, \; m_b = 4.2 \text{ GeV}, \; m_t = 175 \text{ GeV}$$

that leads to a variety of flavor changing decays which are kinematically allowed. The parameters V_{ij} are also different numerically: their hierarchy is governed by $\lambda = V_{us} \approx 0.22$

$$V \simeq \begin{pmatrix} 1 - \frac{1}{2}\lambda^2 & \lambda & A\lambda^3 (\rho - i\eta) \\ -\lambda(1 + iA^2\lambda^4\eta) & 1 - \frac{1}{2}\lambda^2 & A\lambda^2 \\ A\lambda^3 (1 - \rho - i\eta) & -A\lambda^2 & 1 \end{pmatrix} \tag{1}$$

This matrix determines the rates of flavor changing transitions.

In contrast to leptons (τ, μ decays, neutrino mixing) no "free" quarks have been detected in experiments so far but only hadrons. The observed transitions are therefore between flavored
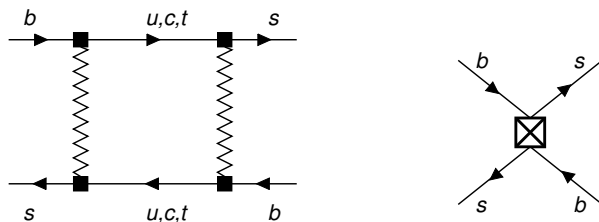
Figure 1: Transition operator

hadrons, i.e. $b \to s$ means $B \to K$ or $B \to X_s$. Here QCD enters the game: it constitutes the most difficult part of the analysis of EW flavor structure of quark sector in SM.

A specific class of $\Delta F = 2$ transitions is represented by mixing of different flavored mesons [2]

$$sd: \ K^0 - \bar{K}^0; \quad cu: \ D^0 - \bar{D}^0; \quad bd, bs: \ B^0 - \bar{B}^0$$

and is important as a source of CP violation studies.

2 Phenomenological description of $B^0 - \bar{B}^0$ system

The time evolution of $(B^0, \bar{B}^0)$ system is given by

$$i\frac{d}{dt} \left(\begin{array}{c} B^0 \\ \bar{B}^0 \end{array} \right) = H_{eff} \left(\begin{array}{c} B^0 \\ \bar{B}^0 \end{array} \right)$$

where H_{eff} is a 2×2 mass operator $H_{eff} = (M - i\Gamma/2)_{ij}, \quad i, j = 1, 2$. The non-diagonal elements M_{12} and Γ_{12} are effective $\Delta B = 2$ interactions not present in the SM Lagrangian and calculable. Observables of $B^0 - \bar{B}^0$ system are: the mass difference $\Delta m = M_{heavy} - M_{light} \approx 2|M_{12}|$ and the decay rate difference $\Delta\Gamma = \Gamma_L - \Gamma_H \approx -2|\Gamma_{12}|\cos\arg(-M_{12}/\Gamma_{12})$. These observables can be used to extract the CKM parameters provided that theory is able to compute them. What are theoretical formulae?

3 $B^0 - \bar{B}^0$ mixing in SM: operators and B_B parameters

Theoretically, at the quark level in SM the $\Delta B = 2$ processes go through a box diagram that produces a complicated, non-local transition operator called an effective Hamiltonian, Fig. 1 [3]. It however simplifies, i.e. reduces to local operators because of mass and CKM hierarchies.

The reduction mechanisms are different for Δm and $\Delta\Gamma$.

In the Δm case $V_{tb} \gg V_{cb}, V_{ub}$, the top quark contribution saturates the loop in the box diagram and because of $m_t \gg m_b$ the loop localizes. This reduces the transition effective Hamiltonian to a local operator. The result is known with NLO accuracy in the strong coupling constant. It reads

$$M_{12} = \frac{G_F^2 M_W^2}{4\pi^2} \left(V_{tb}^* V_{td}\right)^2 \eta_B S_0(x_t) \left[\alpha_s^{(5)}(\mu)\right]^{-6/23} \left[1 + \frac{\alpha_s^{(5)}(\mu)}{4\pi} J_5\right] \langle \bar{B}^0 | Q(\mu) | B^0 \rangle$$

where $\eta_B = 0.55 \pm 0.1$, $J_5 = 1.627$ in the NDR scheme, $S_0(x_t)$ is the short distance function, $x_t = m_t^2/m_W^2$, and $Q(\mu) = (\bar{b}_L\gamma_\sigma d_L)(\bar{b}_L\gamma^\sigma d_L)(\mu)$ is the local four-quark operator.

For the width difference one has $\Delta\Gamma \sim \Gamma_{12} \sim \langle\bar{B}_s|\mathcal{T}|B_s\rangle$. Final states in B_s^0 decays are (c, u) "quarks". Because $m_b \gg m_c, m_u$ the Heavy Quark Expansion in $1/m_b$ is used [4]

$$\langle\bar{B}_s|\mathcal{T}|B_s\rangle = \sum_n \frac{C_n}{m_b^n}\langle\bar{B}_s|\mathcal{O}_n^{\Delta B=2}|B_s\rangle$$

with C_n being calculable in PT. NonPT physics is contained in ME of local operators $\mathcal{O}_n^{\Delta B=2}$. At LO in $1/m_b$ two four-quark operators in $\mathcal{T}$ are $Q = (\bar{b}_i s_i)_{V-A}(\bar{b}_j s_j)_{V-A}$ and $Q_S = (\bar{b}_i s_i)_{S-P}(\bar{b}_j s_j)_{S-P}$. At NLO the most important new operators are [5]

$$R_2 = \frac{1}{m_b^2}(\bar{b}_i \overleftarrow{D}_\mu D^\mu s_i)_{V-A}(\bar{b}_i s_i)_{V-A}, \quad R_3 = \frac{1}{m_b^2}(\bar{b}_i D_\mu D^\mu s_i)_{S-P}(\bar{b}_i s_i)_{S-P}.$$

Thus, M_{12} and Γ_{12} reduce to the evaluation of $\langle\bar{B}|Q_i|B\rangle$ in QCD that is a genuine nonPT task. No direct techniques of such evaluation is known at present. In phenomenological applications one usually uses the factorization approximation. Indeed, since $Q_i \sim J \cdot J$ with $J \sim \bar{s}b$ and with understanding that the state $|B\rangle$ is somehow made from the quarks $|s\bar{b}\rangle$ it is tempting "to factorize" the matrix element in the following way $\langle\bar{B}|Q_i|B\rangle = \langle\bar{B}|J \cdot J|B\rangle = C_{\text{comb}}\langle\bar{B}|J|0\rangle\langle0|J|B\rangle$ with C_{comb} being a combinatorial factor. For $J \sim \bar{b}_L\gamma_\mu d_L$ the matrix element is parametrized through $\langle0|\bar{b}_L\gamma_\mu d_L|B^0(\mathbf{p})\rangle = ip_\mu f_B/2$ where f_B is decay constant into leptons. Clearly, this approximation is rather naive and the main problem is to evaluate its accuracy in some regular way. Still, the factorization formulae can be used for parametrization of IR dynamics. Writing $\langle\bar{B}_s|Q_i|B_s\rangle = B_i\langle\bar{B}_s|Q_i|B_s\rangle^{fac}$ one introduces bag parameters B_i which are genuine dynamical QCD quantities controlling the accuracy of the factorization [6].

Thus, the factorization for operators Q_i reads

$$\langle\bar{B}|Q|B\rangle = f_B^2 M_B^2 2\left(1 + \frac{1}{N_c}\right)B, \quad \langle\bar{B}|Q_S|B\rangle = -f_B^2 M_B^2 \frac{M_B^2}{(m_b+m_s)^2}\left(2 - \frac{1}{N_c}\right)B_S$$

at the leading order and

$$\langle\bar{B}|R_2|B\rangle = -f_B^2 M_B^2\left(\frac{M_B^2}{m_b^2} - 1\right)\left(1 - \frac{1}{N_c}\right)B_2, \langle\bar{B}|R_3|B\rangle = f_B^2 M_B^2\left(\frac{M_B^2}{m_b^2} - 1\right)\left(1 + \frac{1}{2N_c}\right)B_3$$

at the subleading order.

It turns out that the main theoretical uncertainties in Δm and $\Delta\Gamma$ are related to ME of local operators $\mathcal{O}_i \in \{Q, Q_S, R_2, R_3\}$, or equivalently, the bag parameters B_i. The evaluation of bag B_B parameters (as well as B_K of $K^0 - \bar{K}^0$ mixing) has long history (factorization, quark models, large N_c, lattice,...). In my talk I present an approach based on OPE and QCD sum rules. The general features are:

- close in spirit to lattice computations, which is a first-principles method. QCD sum rule approach relies on asymptotic expansions of a Green's function (analytically in a small parameter) while on the lattice the whole function can be found (numerically)

- sum rule techniques provide a consistent way of treating perturbative corrections which is needed to retain RG invariance of physical observables usually violated in other approximations (factorization)

4 OPE and sum rules analysis

The starting point of the analysis is a three-point correlator

$$T(p_1, p_2) = i^2 \int d^4x d^4y e^{ip_1 x - ip_2 y} \langle Tj(x)\mathcal{O}(0)j(y)\rangle$$

where $\mathcal{O} \in \{Q, Q_S, R_2, R_3\}$ is a generic four-quark operator and j can be either AV or PS current $j_5^\mu = \bar{s}\gamma^\mu\gamma_5 b$ (AV), and $j_5 = \bar{s}i\gamma_5 b$ (PS) with a nonvanishing overlap between the vacuum and the B-meson state $\langle 0|\bar{s}\gamma_\mu\gamma_5 b(0)|\bar{B}(p)\rangle = if_B p_\mu$ and $\langle 0|\bar{s}i\gamma_5 b(0)|\bar{B}(p)\rangle = f_B M_B^2/(m_b + m_s)$.

The dispersion relation determines the spectral density $\rho(s_1, s_2)$

$$T(p_1, p_2) = \int ds_1 ds_2 \frac{\rho(s_1, s_2)}{(s_1 - p_1^2)(s_2 - p_2^2)}$$

that is evaluated in two ways. In hadronic picture through the model B-meson pole plus continuum

$$\rho^{\text{had}}(s_1, s_2) = f_B^2 \delta(s_1 - M_B^2)\delta(s_2 - M_B^2)\langle\bar{B}|\mathcal{O}|B\rangle + \rho^{\text{cont}}(s_1, s_2)$$

or theoretically in QCD using OPE that gives $\rho^{\text{OPE}}(s_1, s_2)$.

The general idea of QCD sum rules is to use the quark-hadron duality in a sense that the sum of hadronic contributions is equal to that of quarks and gluons

$$\int ds_1 ds_2 \, \rho_i^{\text{had}}(s_1, s_2) = \int ds_1 ds_2 \, \rho_i^{\text{OPE}}(s_1, s_2).$$

In practice various "flavors" of sum rules usually used:
1. Finite Energy sum rules with the duality region Δ being the square $m_b^2 < s_i < s_0$ in the (s_1, s_2) plane [7, 8, 9]

$$f_B^2 \langle\bar{B}|\mathcal{O}|B\rangle = \int_\Delta ds_1 ds_2 \, \rho^{\text{OPE}}(s_1, s_2)$$

2. Borel sum rule with modeling the hadronic continuum with the OPE prediction and using Borel transform [10, 11, 12, 13]

$$f_B^2 \langle\bar{B}|\mathcal{O}|B\rangle e^{-\frac{M_B^2}{M_1^2} - \frac{M_B^2}{M_2^2}} = \int_\Delta ds_1 ds_2 \, e^{-\frac{s_1}{M_1^2} - \frac{s_2}{M_2^2}} \rho^{\text{OPE}}(s_1, s_2)$$

4.1 Factorization in sum rules

The OPE diagrams show that one can split the three-point correlator into two pieces $T(p_1, p_2) = T_{\text{fac}}(p_1, p_2) + \Delta T(p_1, p_2)$. The factorized part has an explicit form $T_{fac}(p_1, p_2) = \text{const} \times \Pi(p_1)\Pi(p_2)$ with the "const" and the $\Pi(p_i)$ specific to the operator involved. For the operators of V-A structure one finds

$$T_{\text{fac}}^{\text{AV}}(p_1, p_2) = 2\left(1 + \frac{1}{N_c}\right)\Pi^V(p_1)\Pi^V(p_2)$$

with $p^\alpha \Pi^V(p) = i \int dx e^{ipx}\langle Tj(x)\bar{b}\gamma^\alpha(1 - \gamma_5)s(0)\rangle$. Sum rule for the factorized piece T_{fac} yields the factorization approximation value for the bag parameters $B = 1$.
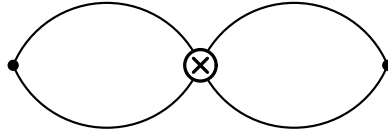
Figure 2: PT diagram at LO

At LO in pQCD the three-point function factorizes $T(p_1, p_2) = T_{\text{fac}}(p_1, p_2)$, $\quad \Delta T(p_1, p_2) = 0$ and $T^{\text{LO}}(p_1, p_2) = T_{\text{fac}}^{\text{LO}}(p_1, p_2) = \text{const} \times \Pi^{\text{LO}}(p_1)\Pi^{\text{LO}}(p_2)$. This corresponds to the naive quark picture and one reproduces the result $B = 1$ that is expected for the LO analysis. However one can do better than that even at higher orders. Some diagrams build up the full function $\Pi(p_1)$ and $T_{\text{fac}}(p_1, p_2) = \text{const} \times \Pi(p_1)\Pi(p_2)$. Indeed, the NLO factorizable contributions are given by
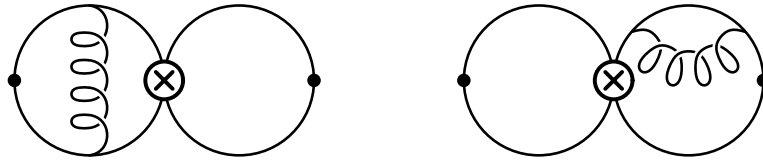
Figure 3: Factorizable diagrams at NLO

the product of two-point correlation functions

$$\Pi_{\text{NLO}}^f = \frac{8}{3}(p_1.p_2)\{\Pi_{\text{LO}}(p_1^2)\Pi_{\text{NLO}}(p_2^2) + \text{symm}(p_1, p_2)\}$$

Since the spectral density of $\Pi_{\text{NLO}}(p^2)$ is known analytically the problem of the NLO analysis in factorization approximation can readily be solved.

Within OPE analysis one has to take into account the condensate contributions. The relevant diagrams can also be classified as factorizable and nonfactorizable ones. The leading condensate contribution is given by the gluon condensate represented by the diagram on Fig. 4
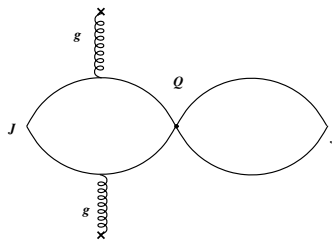
Figure 4: A factorizable gluon condensate diagram
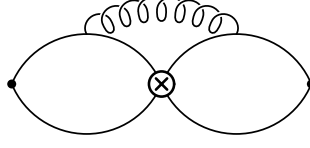
Figure 5: A non-factorizable diagram at NLO of pQCD

Factorizable diagrams form a subset of all contributions which is gauge and RG invariant.

Non-factorizable contributions in pQCD are first given by the diagram presented in Fig. 5. Thus the NLO analysis of non-factorizable contributions within perturbation theory amounts to the calculation of a set of three-loop diagrams [14, 15].

Non-factorizable condensate contributions are given on Fig. 6. They are technically simpler to compute. In my present talk I discuss sum rule analysis with nonPT terms only [16].

4.2 Condensate corrections to factorization

The leading nonPT term is given by the gluon condensate defined through the vacuum matrix element

$$\langle G^a_{\mu\nu} G^b_{\alpha\beta} \rangle = \frac{\delta^{ab}}{12(N_c^2 - 1)} (g_{\mu\alpha} g_{\nu\beta} - g_{\mu\beta} g_{\nu\alpha}) \langle GG \rangle.$$

Dimension-five contributions are proportional to the mixed quark-gluon condensate, which is defined through the matrix element

$$\langle \bar{s}_\alpha i g_s G^a_{\beta\eta} t^a s_\rho \rangle = \frac{(i\sigma_{\beta\eta})_{\rho\alpha}}{48} \langle \bar{s} G s \rangle.$$

Dimension-six contributions involve four-quark matrix elements $\langle \bar{s} \Gamma_1 s \bar{s} \Gamma_2 s \rangle$. Thus, OPE result for the spectral density is

$$\Delta \rho_i(s_1, s_2) = \Delta \rho_i^{\text{GG}}(s_1, s_2) \langle GG \rangle + \Delta \rho_i^{\text{sGs}}(s_1, s_2) \langle \bar{s} G s \rangle + \ldots$$

for each of the eight cases (AV or PS) current for Q, Q_S, R_2, R_3 operators.
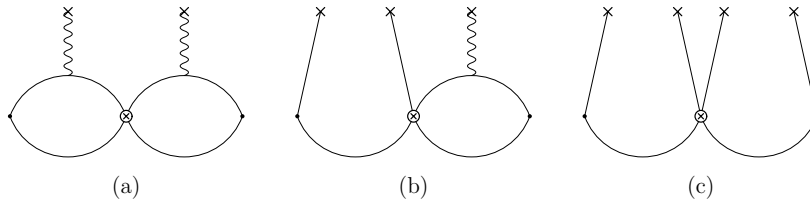
Figure 6: Non-factorizable contributions: (a) $\langle GG \rangle$, (b) $\langle \bar{s} G s \rangle$, and (c) the $\langle \bar{s} s \bar{s} s \rangle$ condensate.

As an example here is an explicit expression for the spectral density for Q_S operator with PS current ($z_i = m_b^2/s_i$)

$$\Delta\rho_{\mathrm{PS}}(s_1, s_2) = \frac{1}{48\pi^2}\langle\frac{\alpha_s}{\pi}GG\rangle\frac{1}{s_1 s_2}(\frac{s_1 s_2}{2}(6 - 3z_1 - 3z_2 + z_1 z_2) + (p_1 p_2)^2 z_1 z_2)$$

$$+ \frac{m_b}{16\pi^2}\langle\bar{s}Gs\rangle\left((-2 + z_1)\delta(s_2 - m_b^2) + (-2 + z_2)\delta(s_1 - m_b^2)\right).$$

To show how SR analysis works I consider a case of the operator Q in HQET approximation within finite energy sum rules for simplicity.

The hadron spectral density for this case reads $\rho^B(s) = f_B^2\delta(s_1 - M_B^2)\delta(s_2 - M_B^2)\langle\bar{B}|Q|B\rangle$. The HQET limit is obtained by using the substitution $s_i = (m_b + E_i)^2$ and expanding in E_i/m_b. Thus, the OPE spectrum in HQET limit reads

$$\Delta\rho^{OPE}(s_1, s_2) = \frac{1}{48\pi^2}\frac{\langle g_s^2 G^2\rangle}{4\pi^2}\frac{1}{m_b^2}(-6).$$

We write the bag parameter explicitly as $B = 1 + \Delta B$ and find the sum rule ($s_0 = (m_b + E_0)^2$)

$$\frac{8}{3}\Delta B(2\pi f_B)^4 = -2\langle g_s^2 G^2\rangle\frac{E_0^2}{m_b^2}.$$

The problem is now how to fix E_0? One can do that using the two-point correlator that gives the relation between $(2\pi f_B)^2$ and E_0 in the form [17, 18]

$$(2\pi f_B)^2 = \frac{8}{m_b}E_0^3.$$

For $f_{B_s} = 240$ MeV and $m_b = 4.8$ GeV [19, 20, 21] that gives $E_0 = 1.1$ GeV. Using this relation one finds

$$\Delta B = -\frac{3}{256}\frac{\langle g_s^2 G^2\rangle}{E_0^4} = -\frac{3}{16}\frac{\langle g_s^2 G^2\rangle}{[(2\pi f_B)^2 m_b]^4}.$$

The result for the non-perturbative bag parameter is independent of m_b, as it should be in the HQET limit, where dynamical quantities depend on soft physics only. The scaling relation $f_B \sim 1/\sqrt{m_b}$ is respected by the result from two point correlator as well. For $\langle g_s^2 G^2\rangle = 0.48$ GeV^4 = (0.83 GeV)^4 we have $\Delta B = -0.006$, at $E_0 = 1$ GeV, which shows that the non-factorizable contribution to the matrix element is tiny. Why is ΔB so small? It is because the scale $(2\pi f_B)^2 m_b = (2E_0)^3 = (2.2$ GeV)^3 is much larger than the scale of the gluon condensate (0.83 GeV)^4. The result for ΔB is proportional to the fourth power of a small number

$$\Delta B = -3\left(\frac{0.83 \text{ GeV}}{4E_0}\right)^4 \approx -3\left(\frac{0.83 \text{ GeV}}{4 \text{ GeV}}\right)^4 = -3(0.21)^4 = -3 \times 0.002$$

with $E_0 = 1$ GeV. This example shows that FESR are simple and give reasonable results. However one can use a bit more sophisticated analysis based on Borel sum rules.
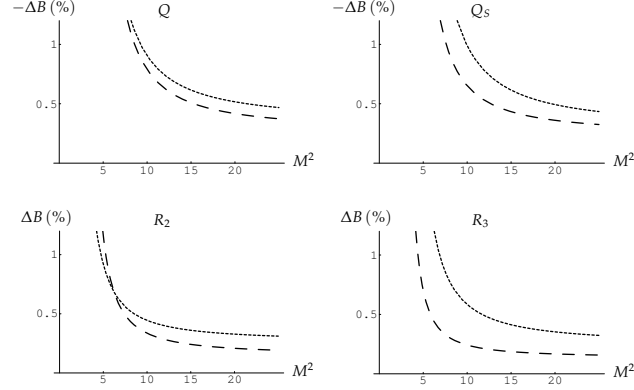
Figure 7: ΔB vs. M^2 (GeV^2) for Q, Q_S, R_2, R_3 with the Borel sum rules in full QCD.

The results of the Borel QCD sum rules for ΔB are shown in Fig. 7. The short-dashed lines are for AV current, and the long-dashed lines for PS current with the parameters $m_b = 4.2$ GeV, $f_{B_s} = 240$ MeV, $s_0 = 36$ GeV^2. The numerical prediction is $|\Delta B| = 0.5\%$ in all considered cases.

Because the b-quark is heavy one can also use HQET approximation on the theory side. The Borel sum rule results in HQET approximation are given in Fig. 8. We take $\bar{\Lambda} = 600$ MeV, $m_b = 4.8$ GeV, $f_{B_s} = 240$ MeV, $2E_0 = 2.5$ GeV. The short-dashed lines are obtained using an axial vector interpolating current, and the long-dashed lines using a pseudoscalar current. The
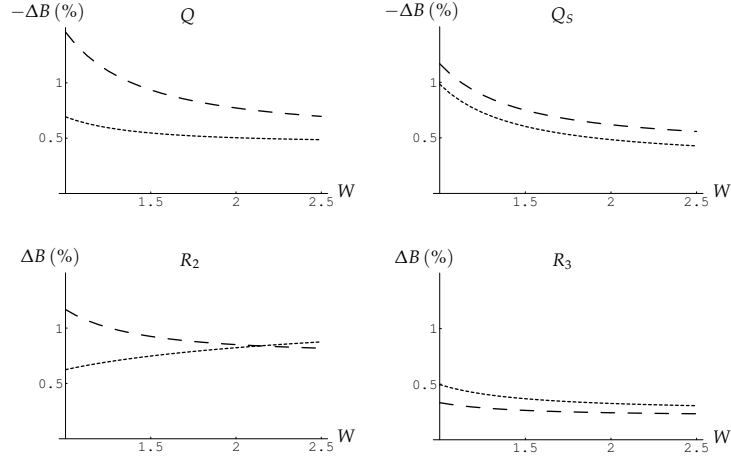
Figure 8: Plots of $(-)\Delta B$ vs. W (GeV) obtained with the Borel sum rules in HQET.

numerical predictions are quite consistent and give $|\Delta B| = (0.5 - 1)\%$ in all cases. However for the operator R_2 the convergence in $1/m_b$ is slow.

Operator	$\Delta B(\%)$ QCD	$\Delta B(\%)$ HQET
R_2	0.3 ± 0.3	0.8 ± 0.7
R_3	0.3 ± 0.2	0.3 ± 0.2

Table 1: A summary of the results.

Numerical results for the most interesting operators at subleading order R_2 and R_3 are presented in Table 1. The analysis of the uncertainties of our typical prediction is given in Fig. 9 for Q_S operator, AV current, in the HQET sum rule. We used the following parameters: $210 \,\text{MeV} < f_{B_s} < 270 \,\text{MeV}$, $m_b = 4.8 \,\text{GeV}$, $1 \,\text{GeV} < E_0 < 1.5 \,\text{GeV}$. Condensates are varied by $\pm 30\%$. The largest errors are due to f_B. The uncertainty due to the condensates is comparable with that due to f_B.
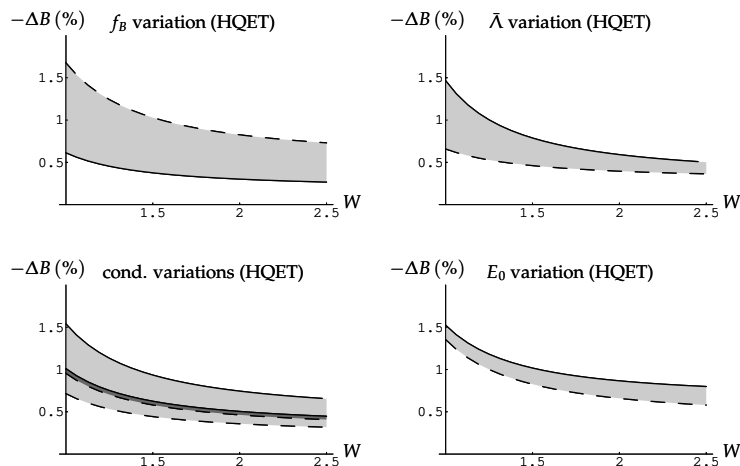
Figure 9: $-\Delta B$ for Q_S operator, AV current, in the HQET sum rule. For the condensate variations, the dark-gray band corresponds to the gluon condensate and the larger light-gray band to the quark-gluon condensate variation.

5 Summary

To summarize, we demonstrated that

- Sum Rules technique is a powerful tool for analysing ME of local operators relevant to flavor physics. Factorization results are reproduced at diagram level

- Non-factorizable contributions due to nonPT condensates to bag parameters are small: $\Delta B_i = (0.5 - 1)\%$ for all operators $\{Q, Q_S, R_2, R_3\}$ relevant to theoretical description of $B_s^0 - \bar{B}_s^0$ mixing

- Non-factorizable PT terms involve three-loop diagrams and their computation is a nontrivial task. Some preliminary results are nonetheless available for the operator Q.

6 Acknowledgments

References

[1] M. Kobayashi and T. Maskawa, Prog. Theor. Phys. **49**, 652 (1973).

[2] S. L. Glashow, J. Iliopoulos and L. Maiani, Phys. Rev. D **2**, 1285 (1970).

[3] A. Lenz and U. Nierste, JHEP **0706**, 072 (2007) [arXiv:hep-ph/0612167]. A. Lenz, Int. J. Mod. Phys. A **23**, 3321 (2008) [arXiv:0710.0940 [hep-ph]].

[4] A. V. Manohar and M. B. Wise, Camb. Monogr. Part. Phys. Nucl. Phys. Cosmol. **10**, 1 (2000).

[5] M. Beneke, G. Buchalla, I. Dunietz, Phys. Rev. D **54**, 4419 (1996).

[6] M. Gaillard and B. Lee, Phys. Rev. D **10**, 897 (1974).

[7] N. V. Krasnikov, A. A. Pivovarov and A. N. Tavkhelidze, Pisma Zh. Eksp. Teor. Fiz. **36**, 272 (1982), Z. Phys. C **19**, 301 (1983); A. A. Pivovarov, Z. Phys. C **53**, 461 (1992).

[8] K. G. Chetyrkin et al., Phys. Lett. B, **174**, 104 (1986).

[9] A. A. Ovchinnikov, A. A. Pivovarov, Phys. Lett. B, **207**, 333 (1988).

[10] M. A. Shifman, A. I. Vainshtein and V. I. Zakharov, Nucl. Phys. B **147**, 448 (1979).

[11] A. Pich, Phys. Lett. B **206** (1988) 322.

[12] L. J. Reinders and S. Yazaki, Phys. Lett. B **212**, 245 (1988).

[13] C. S. Huang, A. Zhang and S. L. Zhu, Eur. Phys. J. C **21** (2001) 313 [arXiv:hep-ph/0011145].

[14] S. Narison and A. A. Pivovarov, Phys. Lett. B **327**, 341 (1994).

[15] J. G. Körner, A. I. Onishchenko, A. A. Petrov and A. A. Pivovarov, Phys. Rev. Lett. **91**, 192002 (2003).

[16] T. Mannel, B. D. Pecjak and A. A. Pivovarov, arXiv:hep-ph/0703244.

[17] N. V. Krasnikov and A. A. Pivovarov, Phys. Lett. B **112**, 397 (1982); A. A. Pivovarov, Yad. Fiz. **62**, 2077 (1999) .

[18] V. A. Nesterenko and A. V. Radyushkin, Phys. Lett. B **115**, 410 (1982); S. V. Mikhailov and A. V. Radyushkin, Phys. Rev. D **45**, 1754 (1992); A. P. Bakulev and A. V. Radyushkin, Phys. Lett. B **271**, 223 (1991).

[19] W.-M. Yao et al., Journal of Physics G **33**, 1 (2006).

[20] J. H. Kühn, A. A. Penin and A. A. Pivovarov, Nucl. Phys. B **534**, 356 (1998); A. A. Penin and A. A. Pivovarov, Phys. Lett. B **435**, 413 (1998), Nucl. Phys. B **549**, 217 (1999).

[21] A. Pineda and A. Signer, Phys. Rev. D **73**, 111501 (2006) [arXiv:hep-ph/0601185].

Rare radiative leptonic decays of B mesons: A review

D. Melikhov[1], N. Nikitin[1], D. Tlisov[1], K. Toms[1]

[1]Lomonosov Moscow State University Skobeltsyn Institute of Nuclear Physics (MSU SINP), 1(2), Leninskie gory, GSP-1, Moscow 119991, Russian Federation

In this article we present few physical aspects of a rare radiative semileptonic decays of B-mesons in the framework of the Standard Model. We concider the corresponding transition form factors properties and contirbutions from a various processes to the decay amptlitudes. Finally we present a few estimates for a branching ratios of such decays.

1 INTRODUCTION

Rare radiateve decays of B–mesons ($B_{d,s} \to \gamma \ell^+ \ell^-$) are produced by $b \to d, s$ quark transitions (so-called Flavor Changing Neutral Currents). Such currents are forbidden at the tree level in the framework of the Standard Model (SM) and occur starting from the lowest order only through the one-loop "penguin" and "box" diagrams (Fig 1). The branching ratios of these decays are very small (order of $10^{-8} - 10^{-15}$). This makes certain parameters of these decays very sensitive to Beyond the Standard Model physics (SUSY, Extra Dimensions, LR-models, Two Higgs–doublet models and others), and provide us with a precision set of tests for SM itself in a high perturbative order.
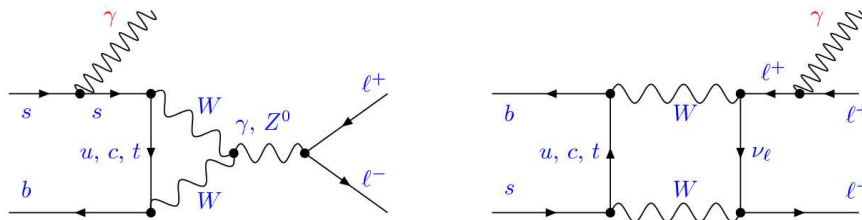
Figure 1: The lowest order Standard Model contribution to $B_s^0 \to \gamma \ell^+ \ell^-$

Because of the top-quark dominance in the loops it is possible to find the values of $|V_{ts}|$ and $|V_{td}|$ CKM matrix elements. Also, these rare decays can provide us with a new information of the long-distance QCD effects in a matrix elements of the effective tensor and pseudotensor currents between initial and final hadronic states. And finally, some rare decays could provide essential background for other rare decays with smaller branching ratios, especially, $B_s^0 \to \gamma \mu^+ \mu^-$ decay will be very important for studies of pure muonic B–meson decay $B_s^0 \to \mu^+ \mu^-$ at LHC.

Naive estimate gives us a ratio $\frac{Br(B_{d,s}^0 \to \gamma \ell^+ \ell^-)}{Br(B_{d,s}^0 \to \ell^+ \ell^-)} \approx \frac{M_B^2}{m_\ell^2} \frac{\alpha_{em}}{4\pi}$. The ratio $\frac{M_B^2}{m_\ell^2}$ corresponds to the helicity-suppressed factor in the decay $B_s^0 \to \ell^+ \ell^-$ (like in the decay $\pi \to \mu\nu_\mu$). Decays $B_{d,s}^0 \to \gamma \ell^+ \ell^-$ are not helicity-suppressed, because in the final state we have a photon. The constant α_{em} corresponds to an additional γ–emission. The factor 4π corresponds to the ratio of two-body ($\ell^+ \ell^-$) and three-body ($\gamma \ell^+ \ell^-$) phase spaces. Numerically:

1) $Br(B_q^0 \to e^+ e^-) \ll Br(B_q^0 \to e^+ e^- \gamma)$, because $M_{B_q^0}^2/m_e^2 \sim 10^8 \gg 4\pi/\alpha_{em} \sim 10^3$

2) $Br(B_q^0 \to \mu^+ \mu^-) \sim Br(B_q^0 \to \mu^+ \mu^- \gamma) \approx Br(B_q^0 \to e^+ e^- \gamma)$, because $M_{B_q^0}^2/m_\mu^2 \sim 2.5 \times 10^3 \sim 4\pi/\alpha_{em}$ and $Br(B_q^0 \to \tau^+ \tau^- \gamma) \sim \alpha_{em} Br(B_q^0 \to \tau^+ \tau^-)$.

2 THEORETICAL FRAMEWORK

2.1 Theoretical description

From the theoretical point of view, $b \to d, s$ transitions are concidered using the effective Hamiltonian [1]:

$$H^{eff}(b \to q) = \frac{G_F}{\sqrt{2}} V_{tb} V_{tq}^* \sum_i C_i(\mu) O_i(\mu) \qquad (1)$$

in the form of Wilson expansion. The set of Wilson coefficients $C_i(\mu)$ depends on the current model and contains the lowest order model contributions and perturbative QCD corrections [1]. The scale parameter μ is approximately equal to the mass of b-quark and is about 5 GeV. This parameter separates the perturbative and nonperturbative contributions of the strong interactions. The nonperturbative contribution is contained in the matrix elements of basis operators $O_i(\mu)$ between the initial and final hadronic states. For the calculation of these matrix elements it is necessarily to use different nonperturbative methods. The accuracy of nonperturbative calculations depends on a method, and is typically about 15%. The accuracy of the Wilson coefficients for SM with NLO (NNLO) QCD-corrections [1] is not greater than 15% (7%) if parameter $\mu \in [m_b/2, 2m_b]$.

The nonperturbative contribution of the strong interactions are contained in the matrix elements of these operators: $\langle$ final states $|O_i(\mu)|$ initial states $\rangle$. These matrix elements can be described in the terms of Lorentz-invariant form factors and structures constructed using 4-momenta of initial and final particles, tensors $g^{\mu\nu}$ and $\varepsilon_{abcd} \equiv \varepsilon_{\alpha\beta\mu\nu} a^\alpha b^\beta c^\mu d^\nu$, where $\varepsilon^{0123} = -1$. For the decays $\bar{B}_{d,s}^0 \to \gamma \ell^+ \ell^-$ all of the basic operators have the same form $Q_i(\mu) = H_i^{\cdots} L_{i\,\ldots}$. Therefore, the matrix elements for these decays have the form:

$$\sum_i \langle \gamma(k, \epsilon) | H_i^{\cdots} | \bar{B}_q^0(p) \rangle \, \bar{\ell}(p_2) L_{i\,\ldots} \ell(-p_1).$$

The coefficient $C_{9V}^{\text{eff}}(\mu, q^2)$ in the Hamiltonian $H_{eff}^{b \to q \ell^+ \ell^-}$ [1] includes long-distance effects related to the $\bar{u}u$ and $\bar{c}c$ resonances in the q^2–channel.

3   FORM FACTORS CALCULATIONS

3.1 F_V and F_{TV} form factors

For the transition to a real photon, matrix elements of the vector and tensor currents are given by the following formulas[1]

$$\langle\gamma(k,\,\epsilon)|\bar{q}\gamma_\mu b|\bar{B}_q^0(p)\rangle \;=\; e\,\epsilon^{*\,\alpha}\,\varepsilon_{\mu\alpha\xi\eta}p^\xi k^\eta\,\frac{F_V(q^2)}{M_B},$$

$$\langle\gamma(k,\,\epsilon)|\bar{q}\sigma_{\mu\nu}b|\bar{B}_q^0(p)\rangle\,(p-k)^\nu \;=\; i\,e\,\epsilon^{*\,\alpha}\varepsilon_{\mu\alpha\xi\eta}p^\xi k^\eta\,F_{TV}(q^2,0).$$

We treat the penguin form factor $F_{TV}(q_1^2,q_2^2)$ as a functions of two variables: q_1 is the momentum of the photon emitted from the $b\to q$ vertex, and q_2 is the momentum of the photon emitted from the valence quark of the $\bar{B}_q^0$ meson.

In the region where $E_\gamma\gg\Lambda_{\rm QCD}$, the form factors obey the LEET relation, which is valid to $O(\Lambda_{\rm QCD}/m_b)$, $O(\Lambda_{\rm QCD}/E_\gamma)$, and $O(\alpha_s)$ accuracy:

$$F_V \simeq F_{TV} \propto \frac{f_B M_B}{E_\gamma}.$$

Near $q^2=M_B^2$ these form factors have a pole at $q^2=M_{B^*}^2$. This pole is located very close to the upper boundary of the physical region, $q^2=M_B^2$, since $M_{B^*}-M_B=45$ MeV $\sim O(\Lambda_{\rm QCD}^2/m_b)$.

In the heavy quark limit $m_b\to\infty$ form factors F_V and F_{TV} should be approximately equal. Therefore, at $q^2=M_B^2$ (i.e. at small E_γ) $F_V\simeq F_{TV}$.

The calculations of F_A and F_{TA} form factors are very similar. For the details see the paper [2, 3].

We proposed a simple parametrization for the form factors:

$$F_i(E_\gamma)=\beta_i\frac{M_B f_B}{\Delta_i+E_\gamma},\qquad i=A,V,TA,TV.$$

The numerical parameters were calculated using the dispersion approach of the quark model [4].

3.2   Calculations for the tensor currents

In this subsection we present the simple example of the matrix element composition. The common formula for $\bar{B}_q^0\to\gamma^*$ transition through the tensor current have the form:

$$\begin{aligned}\langle\gamma^*(k,\,\epsilon)|\bar{q}\sigma_{\mu\nu}b|\bar{B}_q^0(p)\rangle \;=\;& i\,e\,\epsilon^{*\,\alpha}\,\big[\varepsilon_{\mu\nu\alpha\beta}p^\beta g_1(q^2)+\varepsilon_{\mu\nu\alpha\beta}k^\beta g_2(q^2)+\\ &+\; p_\alpha\varepsilon_{\mu\alpha\xi\eta}p^\xi k^\eta g_0(q^2)+k_\alpha\varepsilon_{\mu\alpha\xi\eta}p^\xi k^\eta g_3(q^2)\big]\end{aligned}$$

The gauge invariance

$$k^\alpha\left[\varepsilon_{\mu\nu\alpha\beta}p^\beta g_1(q^2)+\varepsilon_{\mu\nu\alpha\beta}k^\beta g_2(q^2)+p_\alpha\varepsilon_{\mu\alpha\xi\eta}p^\xi k^\eta g_0(q^2)+k_\alpha\varepsilon_{\mu\alpha\xi\eta}p^\xi k^\eta g_3(q^2)\right]=0$$

---

[1] In our paper we use the following descriptions for the γ-matrix: $\gamma^5=i\gamma^0\gamma^1\gamma^2\gamma^3$, $\sigma_{\mu\nu}=\frac{i}{2}[\gamma_\mu,\gamma_\nu]$, $e=\sqrt{4\pi\alpha_{\rm em}}$, $O_\mu=\gamma_\mu(1-\gamma_5)$. and kinematics: $p=p_1+p_2+k,=q+k$, $p^2=M_B^2$, $k^2=0$, $p_1^2=p_2^2=m_\ell^2$ and $m_\ell^2\le q^2\le M_B^2$. In the rest frame of the $\bar{B}_q^0$ meson the photon energy is: $E_\gamma=\frac{M_B}{2}\left(1-\frac{q^2}{M_B^2}\right)$.

gives the following relation between the form factors:

$$k^2 \, g_3(q^2) \; = \; g_1(q^2) \; - \; (pk) \, g_0(q^2).$$

Therefore we have:

$$
\begin{aligned}
\langle \gamma^*(k,\,\epsilon)|\bar{q}\sigma_{\mu\nu}b|\bar{B}_q^0(p)\rangle &= ie\epsilon^{*\alpha}\left[\left(\varepsilon_{\mu\nu\alpha\beta}p^\beta - \frac{k_\alpha}{k^2}\varepsilon_{\mu\nu\sigma\rho}k^\sigma p^\rho\right)g_1 + \varepsilon_{\mu\nu\alpha\beta}k^\beta g_2 \right. \\
&\quad + \left. \left(p_\alpha - \frac{k\cdot p}{k^2}k_\alpha\right)\varepsilon_{\mu\nu\rho\sigma}p^\rho k^\sigma g_0\right].
\end{aligned}
$$

Multiplying this equation by $p^\nu - k^\nu = q^\nu$ we have:

$$\langle \gamma^*(k,\,\epsilon)|\bar{q}\sigma_{\mu\nu}b|\bar{B}_q^0(p)\rangle\,(p-k)^\nu \; = \; i\,e\,\epsilon^{*\alpha}\,\varepsilon_{\mu\alpha\xi\eta}p^\xi k^\eta\left(-\,g_1(q^2)\,-\,g_2(q^2)\right).$$

For the real photon $k^2 = 0$ and therefore $g_1(q^2) \; = \; (pk)\,g_0(q^2)$. Finaly, we have

$$\langle \gamma(k,\,\epsilon)|\bar{q}\sigma_{\mu\nu}b|\bar{B}_q^0(p)\rangle\,(p-k)^\nu \; = \; i\,e\,\epsilon^{*\,\alpha}\varepsilon_{\mu\alpha\xi\eta}p^\xi k^\eta\,F_{TV}(q^2,0),$$

where

$$F_{TV}(q^2,0) = -\,g_2(q^2)\,-\,(pk)\,g_0(q^2).$$

4 Decay amplitude contributions

4.1 Emission of a real photon from valence quarks
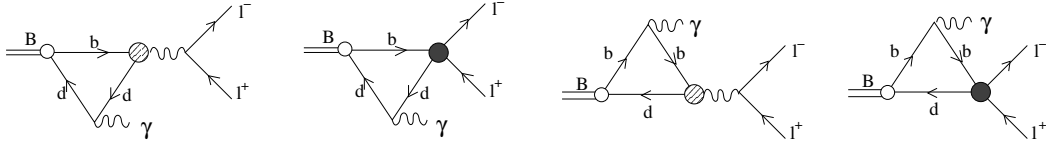
Figure 2: Real fotons direct emission from the valence quarks.

On the fig.2 the real photon is directly emitted from the valence b or q quarks. Dashed circles denote the virtual photonic penguin contribution. Solid circles denote the Z-penguin and box contributions from $H_{eff}^{b\to q\ell^+\ell^-}$ effective Hamiltonian.

For the description of this photon emission we use four form factors: $F_V(q^2)$, $F_A(q^2)$, $F_{TV}(q^2,0)$ and $F_{TA}(q^2,0)$.

On the fig. 3 the valence quarks directly emit the virtual photon which later goes into the final $\ell^+\ell^-$ pair. Dashed circles denote the $b \to q\gamma$ operator from $H_{eff}^{b\to q\gamma}$ effective Hamiltonian. The corresponding amplitude has the same structure as a photonic penguin amplitude with $F_{TA,TV}(q^2,0)$ replaced by $F_{TA,TV}(0,q^2)$.

The form factors $F_{TA,TV}(0,q^2)$ for the necessary timelike momentum transfers are not known. The difficulty with these form factors comes from neutral light vector mesons, ρ^0 and ω for B_d decay and ϕ for B_s decay, which appear in the physical $B \to \gamma\ell^+\ell^-$ decay region. These resonances emerge in the amplitude of the subprocess when the photon is emitted from the light valence d or s quark.
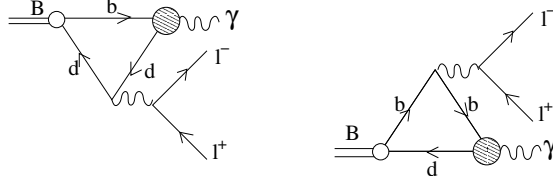
Figure 3: Virtual fotons emission from the valence quarks.

We obtain the form factors $F_{TA,TV}(0, q^2)$ for $q^2 > 0$, using the gauge-invariant version of the vector meson dominance (see [5]). This allows us to express the form factors $F_{TA,TV}(0, q^2)$ in terms of the $B \to V$ transition form factors at zero momentum transfer and leptonic constants f_V of vector mesons:

$$F_{TV,TA}(0, q^2) = F_{TV,TA}(0, 0) - \sum_V 2 f_V g_+^{B \to V}(0) \frac{q^2/M_V}{q^2 - M_V^2 + i M_V \Gamma_V},$$

where M_V and Γ_V are the mass and the width of the vector meson resonance.

4.2 Weak annihilation and bremsstrahlung

The weak annihilation amplitude is given by a triangle diagrams when the u and c quarks in the loop, but here it is suppressed by a power of a heavy quark mass compared to the previous contributions of the real and virtual photon emission from valence quarks.

The final state photon emission from leptons (bremsstrahlung) can be described in the standard way.

5 SOME APPLICATIONS

5.1 $B_{d,s} \to \ell^+ \ell^- \gamma$ decay rates

Let's consider the $B_{d,s} \to \ell^+ \ell^- \gamma$ decay rates as functions of the minimal photon energy E_{min}^γ. The region of the J/ψ and ψ' resonances was excluded, that corresponds to the experimental procedure adopted at LHC. As we can see from the following table, the branching ratio of the decays for e and μ are 10 times large than naive estimations:

$$Br(B_s^0 \to \mu^+ \mu^- \gamma) \approx Br(B_s^0 \to e^+ e^- \gamma) \sim Br(B_s^0 \to \mu^+ \mu^-) \approx 10^{-9}$$

m_ℓ	m_e			m_μ			m_τ		
E_{min}^γ (MeV)	20	50	80	20	50	80	20	50	80
$Br(B_d \to \ell^+ \ell^- \gamma) \times 10^{10}$	3.95	3.95	3.95	1.34	1.32	1.31	3,39	2.37	1.87
$Br(B_s \to \ell^+ \ell^- \gamma) \times 10^9$	24.6	24.6	24.6	18,9	18.8	18.8	11.6	8.10	6.42
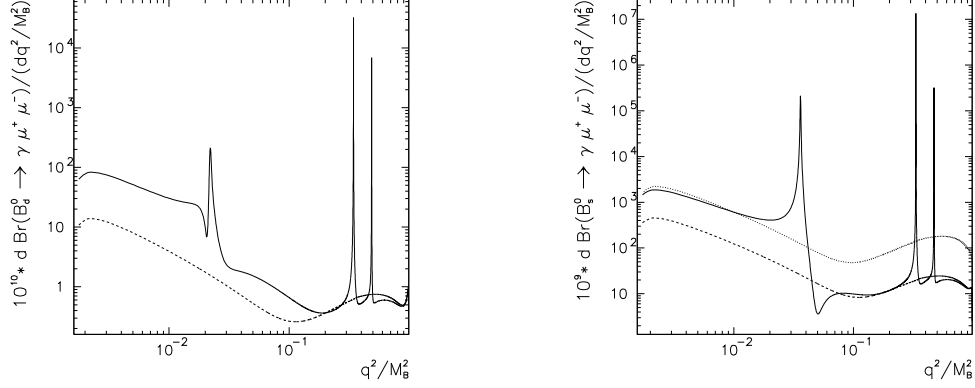
Figure 4: Dilepton mass spectrum in decays: $B_d \to \mu^+\mu^-\gamma$ (left) and $B_s \to \mu^+\mu^-\gamma$ (right) for $E^\gamma_{min} = 20$ MeV. Solid line – our result, dashed line – [6] dotted line – [7]

5.2 Invariant lepton pair mass spectrum

On the figure 4 we present the dilepton mass spectrum for the decays $B_d \to \mu^+\mu^-\gamma$ (left) and $B_s \to \mu^+\mu^-\gamma$ (right) for $E^\gamma_{min} = 20$ MeV.

In the small $q^2 = (p_{\ell^+} + p_{\ell^-})^2$ region, where $\ell = \{e, \mu\}$ the photonic-penguin diagram (like for the rare semileptonic B-decays) and vector mesons (ρ, ϕ) resonant contributions (strongly different from rare semileptonic decays) are absolutely dominating. In the high q^2 region the Z-penguin diagram contribution and Bremsstrahlung contribution from the leptons in the final state start to play an important role. The box diagram with two W-bosons is suppressed by a factor of $M_W^2/m_t^2 \approx 0.2$ with respect to the Z-penguin diagram. In the medium q^2 region the $c\bar{c}$ vector mesons contribution are dominating. This region is excluded from numerical calculations and from the experimental studies.

References

[1] A. Buras, M. Munz, Phys. Rev. **D52** 186 (1995); C. Bobeth et al., JHEP **0404** 071 (2004).

[2] F. Kruger, D. Melikhov, Phys Rev **D67** 034002 (2003).

[3] D. Melikhov, N. Nikitin, Phys Rev **D70** 114028 (2004).

[4] D. Melikhov, Phys Rev **D53** 2460 (1996); Phys Rev **D56** 7089 (1997).

[5] D.Melikhov, O.Nachtmann, V.Nikonov, T.Paulus, EPJ **C34** 345 (2004)

[6] C.Q.Geng et al., Phys Rev **D62** 074017 (2000),

[7] Yu.Dincer and L.M.Sehgal, Phys Lett **B521** 7 (2001).

Heavy quark and quarkonium production in the k_T−factorization approach

S.P. Baranov[1], A.V. Lipatov[2], <u>N.P. Zotov[2]</u>

[1]Lebedev Physics Institute, 119991 Moscow, Russia
[2]SINP, Moscow State Universuty, 119991 Moscow, Russia

We present results of study of the heavy quark and quarkonium production in the framework of the k_T-factorization approach at energies of modern colliders.

1   Introduction

Heavy quark and quarkonium production at high energies is a subject of intense study on both theoretical and experimental sides. First measurements [1] of the b-quark production cross sections at HERA were significantly higher than QCD predictions calculated at next-to-leading order (NLO). Similar observations were made in hadron-hadron collisions at the Tevatron [2] and also in photon-photon interactions at LEP2 [3]. In last case, the theoretical NLO QCD predictions are more than three standard deviations below the experimental data. At the Tevatron, the overall description of the data has been achieved [4] by adopting the non-perturbative fragmentation function of the b-quark into B-meson only. H1 and ZEUS collaborations have reported important data [5, 6, 7] on the beauty photoproduction (both inclusive and associated with hadronic jets) in electron-proton collisions at HERA which refer to small values of the Bjorken scaling variable x. These data are in a reasonable agreement with NLO QCD predictions or somewhat higher. Some disagreement is observed [7] mainly at small decay muon and/or associated jet transverse momenta. But the large excess of the first measurements over NLO QCD, reported [1] by the H1 collaboration, is not confirmed.

In the case of quarkonium production and polarization at the Tevatron energies, the situation is more dramatic (see Sec. 6).

In the present lecture we will apply the k_T-factorization [8, 9, 10] approach of QCD to analyze the HERA and Tevatron data. The k_T-factorization approach is based on the Balitsky-Fadin-Kuraev-Lipatov (BFKL) [11] (or Ciafaloni-Catani-Fiorani-Marchesini (CCFM) [12]) gluon evolution which is valid at small x. The basic dynamical object of the k_T-factorization approach is the so-called unintegrated ($\mathbf{k}_T$-dependent) gluon distribution (UGD) $\mathcal{A}(x, \mathbf{k}_T^2, \mu^2)$ which determines the probability to find a gluon carrying the longitudinal momentum fraction x and transverse momentum $\mathbf{k}_T$ at the probing scale μ^2. The UGD can be obtained from the analytical or numerical solution of the BFKL (or CCFM) evolution equations. Similar to DGLAP, to calculate the cross sections of any physical process the unintegrated gluon density $\mathcal{A}(x, \mathbf{k}_T^2, \mu^2)$ has to be convoluted with the relevant partonic cross section $\hat{\sigma}$. But as the virtualities of the interacting gluons are no longer negligible, the partonic cross section has to be taken off mass shell ($\mathbf{k}_T$-dependent). It is in clear contrast with the DGLAP scheme (so-called collinear factorization). Since the gluons in the initial state are not on-shell and are characterized by virtual

masses (proportional to their transverse momentum), it also assumes a modification of their polarization density matrix [11, 10, 8, 9]. In particular, the polarization vector of a gluon is no longer purely transversal, but acquires an admixture of longitudinal and temporal components.

Some applications of the k_T−factorization approach to the b−quark production at high energies have been discussed in [13, 14, 15, 16, 17, 18, 19, 20, 21, 22, 23] (see also [24, 25, 26]). It was shown [15, 16, 17, 18, 19] that the beauty cross section at the Tevatron can be consistently described in the framework of this approach. Substantial discrepancy between the theory and experiment found [20, 21, 22] for the b-quark production in $\gamma\gamma$ collisions at LEP2, is not confirmed in the comparison between the k_T- factorization results [23] and the last experimental data obtained by ALEPH Collaboration [27]. At HERA, the production of beauty by quasi-real photons and in DIS have been investigated in Refs [28] and a comparison with the ZEUS [6] and H1 [7] measurements has been done in more detail. It was concluded that the k_T-factorization approach provides a reasonable description of the HERA data (see [29]).

In next Sections we present the results from Ref. [28, 17, 30].

2 Basic formulas

We start from the gluon-gluon fusion subprocess. Let p_e and p_p be the four-momenta of the initial electron and proton, k_1 and k_2 the four-momenta of the incoming off-shell gluons, and p_b and $p_{\bar{b}}$ the four-momenta of the produced beauty quarks. In our analysis below we will use the Sudakov decomposition, which has the following form:

$$p_b = \alpha_1 p_e + \beta_1 p_p + p_{b\,T}, \quad p_{\bar{b}} = \alpha_2 p_e + \beta_2 p_p + p_{\bar{b}\,T}, \ k_1 = x_1 p_e + k_{1T}, \quad k_2 = x_2 p_p + k_{2T}, \quad (1)$$

where k_{1T}, k_{2T}, $p_{b\,T}$ and $p_{\bar{b}\,T}$ are the transverse four-momenta of the corresponding particles. It is important that $\mathbf{k}_{1T}^2 = -k_{1T}^2 \neq 0$ and $\mathbf{k}_{2T}^2 = -k_{2T}^2 \neq 0$. If we make replacement $k_1 \to p_e$ and set $x_1 = 1$ and $k_{1T} = 0$, then we easily obtain simpler formulas for the photon-gluon fusion subprocess. The Sudakov variables are defined as follows:

$$\alpha_1 = \frac{m_{b\,T}}{\sqrt{s}} \exp(y_b), \quad \alpha_2 = \frac{m_{\bar{b}\,T}}{\sqrt{s}} \exp(y_{\bar{b}}), \ \beta_1 = \frac{m_{b\,T}}{\sqrt{s}} \exp(-y_b), \quad \beta_2 = \frac{m_{\bar{b}\,T}}{\sqrt{s}} \exp(-y_{\bar{b}}), \quad (2)$$

where $m_{b\,T}$ and $m_{\bar{b}\,T}$ are the transverse masses of the produced quarks, and y_b and $y_{\bar{b}}$ are their rapidities (in the ep center-of-mass frame). From the conservation laws we can easily obtain the following relations:

$$x_1 = \alpha_1 + \alpha_2, \quad x_2 = \beta_1 + \beta_2, \quad \mathbf{k}_{1T} + \mathbf{k}_{2T} = \mathbf{p}_{b\,T} + \mathbf{p}_{\bar{b}\,T}. \quad (3)$$

The variable x_γ^{obs} is often used in the analysis of the data which contain dijet samples. This variable, which is the fraction of the photon momentum contributing to the production of two hadronic jets with transverse energies $E_T^{\mathrm{jet}_1}$ and $E_T^{\mathrm{jet}_2}$, is defined experimentally [6, 7] as

$$x_\gamma^{\mathrm{obs}} = (E_T^{\mathrm{jet}_1} e^{-\eta^{\mathrm{jet}_1}} + E_T^{\mathrm{jet}_2} e^{-\eta^{\mathrm{jet}_2}})/(2yE_e), \quad (4)$$

where yE_e is the initial photon energy and η^{jet_i} are the pseudo-rapidities of the jets. The pseudo-rapidities η^{jet_i} are defined as $\eta^{\mathrm{jet}_i} = -\ln\tan(\theta^{\mathrm{jet}_i}/2)$, where θ^{jet_i} are the polar angles of the jets with respect to the proton beam. Note that the selection of $x_\gamma^{\mathrm{obs}} > 0.75$ and $x_\gamma^{\mathrm{obs}} < 0.75$ yields samples enriched in direct and resolved photon processes, respectively.

The main formulas for the total and differential beauty production cross sections were obtained in the papers [17, 22]. Here we recall some of them. In general case, the cross section σ according to k_T-factorization theorem can be written as a convolution

$$\sigma = \sigma_0 \int \frac{dz}{z} \, d\mathbf{k}_T^2 \, C(x/z, \mathbf{k}_T^2, \mu^2) \mathcal{A}(x, \mathbf{k}_T^2, \mu^2), \tag{5}$$

where $C(x, \mathbf{k}_T^2, \mu^2)$ is the coefficient function corresponding to the relevant partonic subprocess under consideration. The direct photon contribution to the differential cross section of $\gamma p \to b\bar{b} + X$ process is given by

$$\frac{d\sigma^{(\text{dir})}(\gamma p \to b\bar{b} + X)}{dy_b \, d\mathbf{p}_{bT}^2} = \int \frac{|\bar{\mathcal{M}}(\gamma g^* \to b\bar{b})|^2}{16\pi(x_2 s)^2(1 - \alpha_1)} \mathcal{A}(x_2, \mathbf{k}_{2T}^2, \mu^2) d\mathbf{k}_{2T}^2 \frac{d\phi_2}{2\pi} \frac{d\phi_b}{2\pi}, \tag{6}$$

where $|\bar{\mathcal{M}}(\gamma g^* \to b\bar{b})|^2$ is the squared off-shell matrix element which depends on the transverse momentum $\mathbf{k}_{2T}^2$, ϕ_2 and ϕ_b are the azimuthal angles of the initial virtual gluon and the produced quark, respectively.

The formula for the resolved photon contribution can be obtained in a similar way. But the convolution in (5) should be made also with the UGD $\mathcal{A}_\gamma(x, \mathbf{k}_T^2, \mu^2)$ in the photon. The final expression for the differential cross section reads

$$\frac{d\sigma^{(\text{res})}(\gamma p \to b\bar{b} + X)}{dy_b \, d\mathbf{p}_{bT}^2} = \int \frac{|\bar{\mathcal{M}}(g^* g^* \to b\bar{b})|^2}{16\pi(x_1 x_2 s)^2} \times$$
$$\times \mathcal{A}_\gamma(x_1, \mathbf{k}_{1T}^2, \mu^2) \mathcal{A}(x_2, \mathbf{k}_{2T}^2, \mu^2) d\mathbf{k}_{1T}^2 d\mathbf{k}_{2T}^2 dy_{\bar{b}} \frac{d\phi_1}{2\pi} \frac{d\phi_2}{2\pi} \frac{d\phi_b}{2\pi}, \tag{7}$$

where ϕ_1 is the azimuthal angle of the initial virtual gluon having the fraction x_1 of the initial photon longitudinal momentum. It is important that squared off-shell matrix element $|\bar{\mathcal{M}}(g^* g^* \to b\bar{b})|^2$ depends on the transverse momenta $\mathbf{k}_{1T}^2$ and $\mathbf{k}_{2T}^2$. The analytic expressions for the $|\bar{\mathcal{M}}(\gamma g^* \to b\bar{b})|^2$ and $|\bar{\mathcal{M}}(g^* g^* \to b\bar{b})|^2$ have been evaluated in the papers [17, 22]. Note that if we average (7) and (8) over $\mathbf{k}_{1T}$ and $\mathbf{k}_{2T}$ and take the limit $\mathbf{k}_{1T}^2 \to 0$ and $\mathbf{k}_{2T}^2 \to 0$, then we obtain well-known formulas corresponding to the leading-order (LO) QCD calculations.

The gluon-gluon fusion subprocess $g * g* \to b\bar{b}$ is described by three Feynman diagrams, which correspond to the following matrix elements:

$$M_1 = \bar{u}(p_1) \, (-ig\gamma^\mu) \, \varepsilon_\mu(q_1) \, i \frac{\hat{p}_1 - \hat{q}_1 + m}{(p_1 - q_1)^2 - m^2} \, (-ig\gamma^\nu) \, \varepsilon_\nu(q_2) \, v(p_2),$$

$$M_2 = \bar{u}(p_1) \, (-ig\gamma^\nu) \, \varepsilon_\nu(q_2) \, i \frac{\hat{p}_1 - \hat{q}_2 + m}{(p_1 - q_2)^2 - m^2} \, (-ig\gamma^\mu) \, \varepsilon_\mu(q_1) \, v(p_2),$$

$$M_3 = \bar{u}(p_1) \, C^{\mu\nu\lambda}(-q_1, -q_2, q_1 + q_2) \frac{g^2 \, \varepsilon_\mu(q_1) \, \varepsilon_\nu(q_2)}{(q_1 + q_2)^2} \, \gamma_\lambda \, v(p_2),$$

where $\varepsilon_\mu(q_1)$ and $\varepsilon_\nu(q_2)$ are the polarization vectors of the initial gluons, $C^{\mu\nu\lambda}(q_1, q_2, q_3)$ is the standard QCD three gluon vertex:

$$C^{\mu\nu\lambda}(q_1, q_2, q_3) = i((q_2 - q_1)^\lambda) \, g^{\mu\nu} + (q_3 - q_2)^\mu \, g^{\nu\lambda} + (q_1 - q_3)^\nu \, g^{\lambda\mu}).$$

The differential cross section of the process $p\bar{p} \to b\bar{b}X$ has the form of Eq. (7) with the replacements $\gamma \to p$ and $\mathcal{A}_\gamma(x_1, \mathbf{k}_{1T}^2, \mu^2) \to \mathcal{A}(x_1, \mathbf{k}_{1T}^2, \mu^2)$. For a more detailed discussion of the k_T-factorization and nontrivial problems of gauge invariance in the k_T-factorization approach, especially in the hadroproduction of heavy quarks, we refer to [8, 24, 25, 31].

3 Unintegrated gluon distributions (UGD)

Here we discuss various parametrizations of the UGD used in our calculations (see review in [24]).

1) JB parametrization [32]. In this case The UGD is calculated as a convolution of collinear gluon density $G(x, \mu^2)$ with universal weight factors:

$$\mathcal{A}(x, \mathbf{q}_T^2, \mu^2) = \int\limits_x^1 \varphi(\eta, \mathbf{q}_T^2, \mu^2) \, \frac{x}{\eta} \, G\left(\frac{x}{\eta}, \, \mu^2\right) \, d\eta,$$

where

$$\varphi(\eta, \mathbf{q}_T^2, \mu^2) = \begin{cases} \dfrac{\bar{\alpha}_S}{\eta \, \mathbf{q}_T^2} J_0 \left(2\sqrt{\bar{\alpha}_S \ln(1/\eta) \ln(\mu^2/\mathbf{q}_T^2)}\right), & if \ \mathbf{q}_T^2 \leq \mu^2, \\[2mm] \dfrac{\bar{\alpha}_S}{\eta \, \mathbf{q}_T^2} I_0 \left(2\sqrt{\bar{\alpha}_S \ln(1/\eta) \ln(\mathbf{q}_T^2/\mu^2)}\right), & if \ \mathbf{q}_T^2 > \mu^2, \end{cases}$$

where J_0 and I_0 are Bessel functions (of real and imaginary arguments, respectively), and $\bar{\alpha}_s = \alpha_s/3\pi$. The value of $\bar{\alpha}_S$ is connected with the Pomeron intercept: $\Delta = 4\bar{\alpha}_S \ln 2 = 0.53$ at the LO, and $\Delta = 4\bar{\alpha}_S \ln 2 - N\bar{\alpha}_S^2$ at the NLO, with $N \sim 18$. However, some resummation procedures proposed in the last years lead to positive values: $\Delta \sim 0.2 - 0.3$ [33, 11]. We used $\Delta = 0.35$, obtained from the description of the p_T spectrum of D^* electroproduction at HERA [34].

2) KMS parametrization [35]. It was obtained from a unified BFKL and DGLAP description of F_2 data and includes the so called consistency constraint [36]. The consistency constraint introduces a large correction to the LO BFKL equation; about 70% of the full NLO corrections to the BFKL exponent Δ are effectively included in this constraint [37].

3) DGRV parametrization is obtained from conventional gluon density $xG(x, Q^2)$ by taking the Q^2-derivative: $\mathcal{A}(x, q_T^2) = d \, xG(x, Q^2)/dQ^2|_{Q^2=q_T^2}$.

These UGD take into account the different logs terms: $\ln^n(1/x), \ln^n(1/x) ln^n(Q^2/\Lambda_{\mathrm{QCD}}^2)$ and $ln^n(Q^2/\Lambda_{\mathrm{QCD}}^2)$ accodingly.

4) KMR parametrization. In Kimber-Martin-Ryskin approach [38] the UPD is constructed from the known conventional parton distribution function. The μ dependence of the UPD $\mathcal{A}(x, \mathbf{k}_T^2, \mu^2)$ enters at the last step of evolution. The parameter μ plays a dual role: it acts as the factorization scale and also controls the angular ordering of the radiated partons. Therefore a single scale evolution equation (DGLAP or unified DGLAP-BFKL in the KMS form) can be used up to last step. This results in a form similar to the differenial form of the CCFM equation (with angular ordering) with the splitting function P(z) taken as in the DGLAP or DGLAP-BFKL expression. We used the last version of KMRW UPD obtained from DGLAP equations [39]. The KMR UPD $\mathcal{A}_a(x, \mathbf{k}_T^2, \mu^2)$ is defined in all $\mathbf{k}_T^2$ region.

5) J2003 parametrization. In this case the CCFM evolution equations have been solved numerically using a Monte-Carlo method [40]. According to the CCFM equations, the emission of gluons during the initial cascade is only allowed in the angular-ordered region of the phase space. The maximal allowed angle Ξ for any gluon emission sets the scale μ and is defined by the hard scattering quark box. The free parameters of the starting gluon distribution were fitted to the structure function $F_2(x, Q^2)$ (as in the KMS UPD) in the range $x < 10^{-2}$ and $Q^2 > 5$ GeV^2. Here last versions of the UPD J2003 are used from Ref. [19].

4 Numerical results

4.1 Beauty photoproduction at HERA

The most significant theoretical uncertainties in our results are connected with the choice of the UGD and with the factorization and renormalization scales. We chose $\mu_R = \mu_F = \mu = \sqrt{m_b^2 + \langle \mathbf{p}_T^2 \rangle}$, where $\langle \mathbf{p}_T^2 \rangle$ is set to the average $\mathbf{p}_T^2$ of the beauty quark and antiquark. We used a special choice $\mu^2 = \mathbf{k}_T^2$ in the case of KMS gluon, as it was originally proposed in [35]. We took the b-quark mass $m_b = 4.75$ GeV and used the LO formula for the coupling constant $\alpha_s(\mu^2)$ with $n_f = 4$ active quark flavours at $\Lambda_{\text{QCD}} = 200$ MeV, such that $\alpha_s(M_Z^2) = 0.1232$.

The ZEUS data [5, 6] refer to the kinematic region defined by $|\eta^b| < 2$ and $Q^2 < 1$ GeV^2, where η^b is the beauty pseudo-rapidity, the fraction y of the electron energy transferred to the
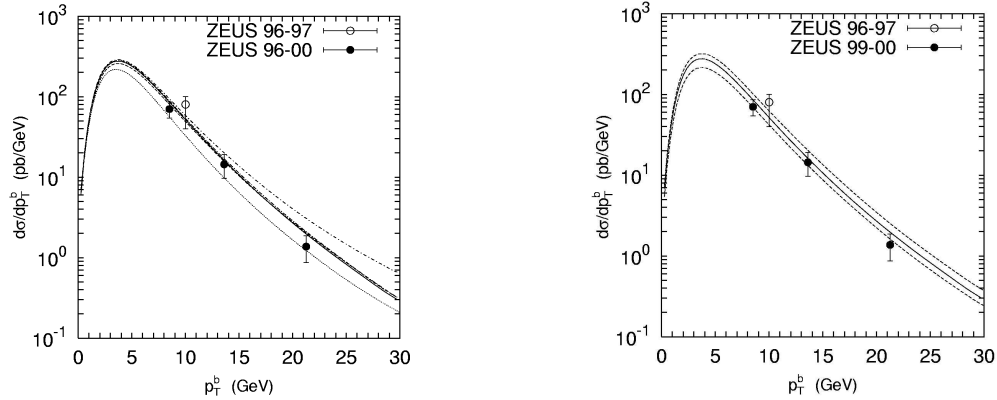
Figure 1: Differential cross section $d\sigma/dp_T^b$ of inclusive $b-$production
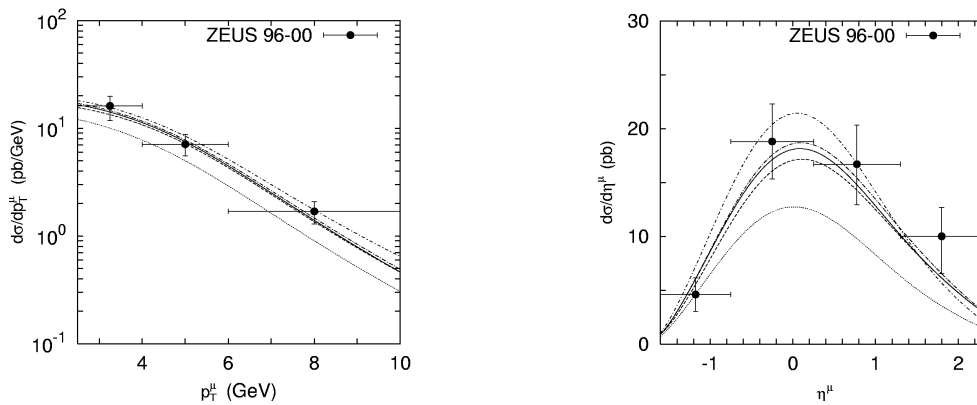
Figure 2: Differential cross section $d\sigma/dp_T^\mu$ (left panel) and $d\sigma/d\eta^\mu$ (right panel) of dijets with an associated muon from b decay.

photon is restricted to the range $0.2 < y < 0.8$. Fig. 1 (left panel) shows our predictions in comparison with these ZEUS data. The solid, dashed, dash-dotted, dotted, and short dash-dotted curves correspond to the results obtained with the J2003 sets $1 - 3$, KMR and KMS unintegrated gluon densities, respectively. One can see that the overall agreement between our predictions and experimental data is very good. All the three sets of J2003 distribution, as well as KMS gluon density, give results which are rather close to each other (except the large p_T^b region where the KMS density predicts harder spectrum). We find also some enhancement of the estimated cross sections as compared with the collinear NLO QCD calculations which lie somewhat below the measurements but still agree with the data within the scale uncertainties. This enhancement comes, in particular, from the non-zero transverse momentum of the incoming off-shell gluons. Note that the KMR gluon distribution gives results which lie below the ZEUS data and which are very similar to the NLO QCD predictions. Fig. 1 (right panel) shows the results corresponding to the J2003 UGD at $\mu^2 = 4m_{bT}^2, m_{bT}^2, (1/4)m_{bT}^2$.

The experimental data [6, 7] on the beauty and associated dijet production at HERA come from both H1 and ZEUS collaborations. The ZEUS data [6] refer to the kinematic region defined by $0.2 < y < 0.8$, $Q^2 < 1$ GeV^2 and given for jets with $p_T^{\text{jet}_1} > 7$ GeV, $p_T^{\text{jet}_2} > 6$ GeV and $|\eta^{\text{jet}}| < 2.5$. The measured cross sections are presented for muons coming from semileptonic b decays in dijet events with $p_T^\mu > 2.5$ GeV and $-1.6 < \eta^\mu < 2.3$. To produce muons from b-quarks in our theoretical calculations, we first convert b-quarks into B-hadrons using the Peterson fragmentation function [41] (our default set of the fragmentation parameter is $\epsilon_b = 0.0035$) and then simulate their semileptonic decay according to the standard electroweak theory. Figs. 2 show the transverse momentum and pseudo-rapidity distributions of the b-quark decay muon in comparison with the ZEUS data. One can see that the calculated cross sections (using the J2003 and KMS unintegrated gluon densities) agree very well with the experimental data.

The ZEUS collaboration have presented the data on the transverse momentum and pseudo-rapidity distributions of jets associated with a muon (so-called μ-jet) or B-hadron (b-jet). The μ-jet is defined as a jet containing a B-hadron that decays into a muon. Similarly, the b-jet is defined as a jet containing B (or $\bar{B}$) hadron. Figs. 3 show our predictions for the transverse momentum distribution of the b-jet (left panel) and the x_γ^{obs} distribution (right panel). One
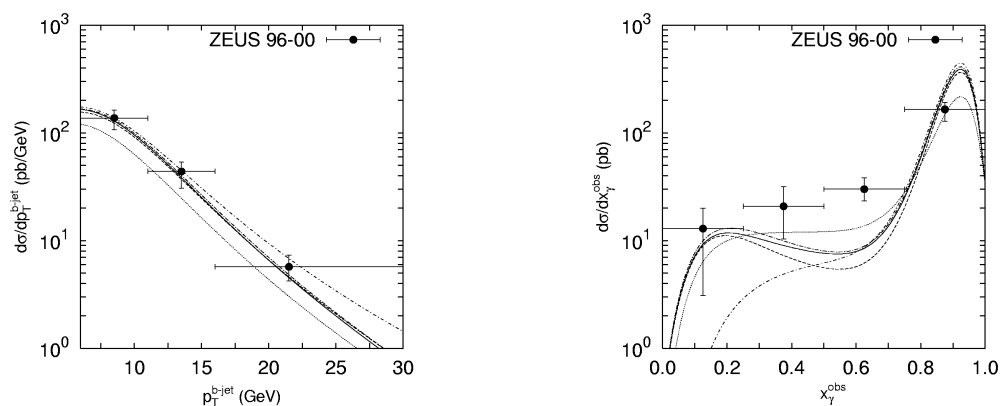
Figure 3: Differential cross section of inclusive $b-$production $d\sigma/dx_\gamma^{obs}$ (right panel) of dijets with an associated muon from b decay.

can see that J2003 and KMS gluon densities give results which agree well with the ZEUS data for the transverse momentum distribution. The J2003 and KMS gluon UPD give a reasonable description of the data but tend to slightly underestimate them at middle and low x_γ^{obs}. In the case of KMS gluon this discrepancy is more significant since the contribution from the gluon-gluon fusion subprocess (in the resolved photon part) are not taken into account here.

4.2 Beauty production at Tevatron

The problem of the b-quark hadroproduction in the framework of the k_T-factorization approach has been solved in Refs. [15, 16, 17, 19, 20]. Figs.4 show the $B-$meson production cross section at the Tevatron in comparison with the CDF data.

In the papers by S. Baranov et al. [14, 17] it has been emphasized that the azimutal $b\bar{b}-$correlations manifest the effects og the inital state gluon off-shellness. Taking into account the non-vanishing initial gluon transverse momenta k_{1T} and k_{2T} leads to the violation of the back-to-back symmetry in the k_T-factorization approach even in the LO approximation.

5 Quarkonium production in $p\bar{p}$ collisions

The production mechanism of heavy quarkonium states involves the physics of both short and long distances, and so, appeals to both perturbative and nonperturbative methods of QCD.

This feature gives rise to two competing theoretical approaches known in the literature as the color-singlet [42] and color-octet [43] models. According to the color-singlet approach, the formation of a colorless final state takes place already at the level of the hard partonic subprocess (which includes the emission of hard gluons when necessary). In the color-octet model, also known as nonrelativistic QCD (NRQCD), the formation of a meson starts from a color-octet $Q\bar{Q}$ pair and proceeds via the emission of soft nonperturbative gluons.

Originally, the color-octet model was introduced to overcome the discrepancy between the large J/ψ production cross section measured in pp interactions at the Tevatron and the results of
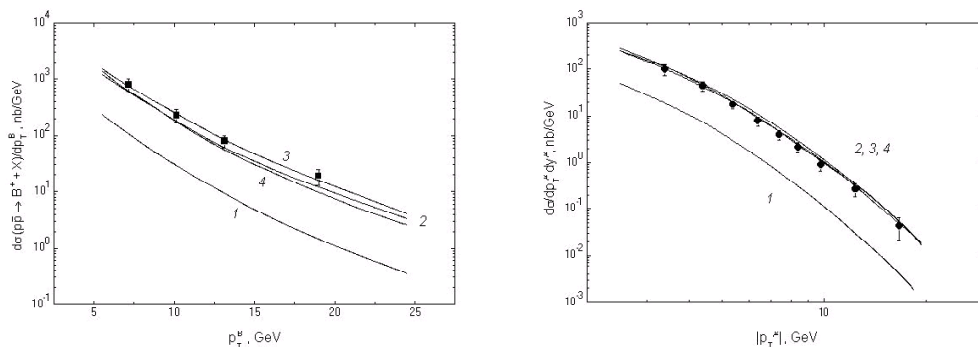
Figure 4: Differential cross section of the $B-$meson production at $\sqrt{s} = 1.8$ TeV (left panel) and μ-distribution (right panel). The curves 1, 2, 3, 4 corerspond to the GRV, KMS, JB and DGRV gluon densities.

theoretical calculations based on the standard perturbative QCD. The problem was apparently solved by attributing the discrepancy to the hypothetical contributions from the intermediate color-octet states, which must obey certain hierarchy in powers of the relative velicity of the quarks in a bound system. However, the numerical estimates of these contributions extracted from the analysis of the Tevatron data are at odds with the HERA data, especially as far as the inelasticity parameter $z = E_{J/\psi}/E_{\gamma}$ is concerned [44]. In the NRQCD approach, the problem of quarkonium polarization remains unsolved [43] also. In Ref. [45] it was emphasised that the off-shellness of the initial gluons, the intrinsic feature of the k_T-factorization approach, has an immediate consequence in the longitudinal polarization of the final state mesons.

The production of Υ mesons in pp collisions can proceed via either direct gluon-gluon fusion or the production of P-wave states χ_b followed by their radiative decays $\chi_b \rightarrow \Upsilon(1S) + \gamma$. The direct mechanism corresponds to the partonic subprocess $g + g \rightarrow \Upsilon(1S) + g$ with hard gluon in the final state. The production of P-wave mesons in the k_T-factorization approach is given by $g + g \rightarrow \chi_b$, and there is no emission of any additional gluons. In order to estimate the degree of theoretical uncertainty connected with the choice of UGD, we use the DGRV and JB parametrizations. All the other parameters are the same as in our first paper from [30]. The polarization state of a vector meson is characterized by the spin alignment parameter α which is defined as a function of any kinematic variable as $\alpha(p_T) = (d\sigma/dp_T - 3d\sigma_L/dp_T)/(d\sigma/dp_T + d\sigma_L/dp_T)$, where σ is the reaction cross section and σ_L is the part of cross section corresponding to mesons with longitudinal polarization (zero helicity state). The limiting values $\alpha = 1$ and $\alpha = -1$ refer to the totally transverse and totally longitudinal polarizations. The experimental definition of α is based on measuring the angular distributions of the decay leptons $d\Gamma(\Upsilon \rightarrow \mu^+ \mu^-)/d\cos\theta \sim 1 + \alpha\cos^2\theta$, where θ is the polar angle of the final state muon measured in the decaying meson rest frame. Fig.5 (left panel) shows our results [30] in comparison with the data on the spin alignment of $\Upsilon(1S)$ mesons obtained by the D0 collaboration [46]. A state with purely direct production mechanism in the bottomonium family is the $\Upsilon(3S)$ meson. The calculations presented here are also valid for this state. In our second paper from [30] the predictions for the spin alignment parameter of Υ have been done in more detail (see Fig.5
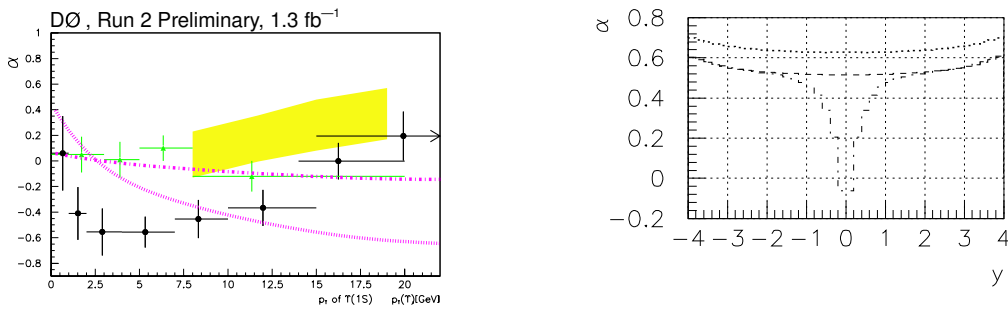
Figure 5: Spin alignment parameter α of $\Upsilon(1S)$ mesons at the Tevatron (left panel). Solid curve, quark spin conservation hypothesis; dash-dotted curves, full depolarization hypothesis; band - NRQCD predictions. Black points, D0 Run 2 experimental data. Rapidity dependence of the parameter α in different helisity frames (right panel): dash-dotted histograms - recoil, dashed - target, dotted - Collins-Soper systems.

(righ panel)). At the LHC energies, the theoretical predictions possess less sensitivity to the choice of UGDs [30].

6 Acknowledgments

References

[1] C. Adloff *et al.* (H1 Collab.), Phys. Lett. **B467** 156 (1999); Erratum: *ibid* **B518** 331 (2001).

[2] F. Abe *et al.* (CDF Collab.), Phys. Rev. **D55** 2546 (1997);
D. Acosta *et al.* (CDF Collab.), Phys. Rev. **D65** 052002 (2002);
S. Abachi *et al.* (D0 Collab.), Phys. Lett. **B487** 264 (2000).

[3] M. Acciari *et al.* (L3 Collab.), Phys. Lett. **B503** 10 (2001);
P. Achard *et al.* (L3 Collab.), Phys. Lett. **B619** 71 (2005);
G. Abbiendi *et al.* (OPAL Collab.), Eur. Phys. J. **C16** 579 (2000).

[4] M. Cacciari and P. Nason, Phys. Rev. Lett. **89** 122003 (2002);
M. Cacciari, S. Frixione, M.L. Mangano, P. Nason and G. Ridolfi, JHEP **0407** 033 (2004).

[5] J. Breitweg *et al.* (ZEUS Collab.), Eur. Phys. J. **C18** 625 (2001).

[6] S. Chekanov *et al.* (ZEUS Collab.), Phys. Rev. **D70** 012008 (2004).

[7] A. Aktas *et al.* (H1 Collaboration), Eur. Phys. J. C **41** 453 (2005).

[8] S. Catani, M. Ciafoloni and F. Hautmann, Nucl. Phys. **B366** 135 (1991).

[9] J.C. Collins and R.K. Ellis, Nucl. Phys. **B360** 3 (1991).

[10] L.V. Gribov, E.M. Levin, and M.G. Ryskin, Phys. Rep. **100** 1 (1983);
E.M. Levin, M.G. Ryskin, Yu.M. Shabelsky and A.G. Shuvaev, Sov. J. Nucl. Phys. **53** 657 (1991).

[11] E.A. Kuraev, L.N. Lipatov, and V.S. Fadin, Sov. Phys. JETP **44** 443 (1976);
E.A. Kuraev, L.N. Lipatov, and V.S. Fadin, Sov. Phys. JETP **45** 199 (1977);
I.I. Balitsky and L.N. Lipatov, Sov. J. Nucl. Phys. **28** 822 (1978).

[12] M. Ciafaloni, Nucl. Phys. **B296** 49 (1988);
S. Catani, F. Fiorani, and G. Marchesini, Phys. Lett. **B234** 339 (1990);
S. Catani, F. Fiorani, and G. Marchesini, Nucl. Phys. **B336** 18 (1990);
G. Marchesini, Nucl. Phys. **B445** 49 (1995).

[13] M.G. Ryskin and Yu.M. Shabelsky, Z. Phys. **C61** 517 (1994);
M.G. Ryskin, Yu.M. Shabelsky and A.G. Shuvaev, Z. Phys. **C69** 269 (1996).

[14] S.P. Baranov and M. Smizanska, Phys. Rev. **D62** 014012 (2000).

[15] Ph. Hägler *et al*, Phys. Phys. Rev. **D62** 071502 (2000).

[16] H. Jung, Phys. Rev. **D65** 034015 (2002).

[17] N.P. Zotov, A.V. Lipatov and V.A. Saleev, Phys. Atom. Nucl. **66** 786 (2003); arXiv:hep-ph/0112114;
S.P. Baranov, N.P. Zotov and A.V. Lipatov, Phys. Atom. Nucl. **67**, 834 (2004).

[18] A.V. Lipatov, L. Lönnblad, and N.P. Zotov, JHEP **0401**, 010 (2004).

[19] H. Jung, Mod. Phys. Lett. **A19** 1 (2004).

[20] L. Motyka and N. Timneanu, Eur. Phys. J. **C27** 73 (2003).

[21] M. Hansson, H. Jung, and L. Jönsson, arXiv:hep-ph/0402019.

[22] A.V. Lipatov and N.P. Zotov, Eur. Phys. J. **C41** 163 (2005).

[23] A.V. Lipatov and N.P. Zotov, JETP Lett. **87** 7 (2008).

[24] B. Andersson *et al.* (Small-*x* Collab.), Eur. Phys. J. **C25** 77 (2002).

[25] J. Andersen *et al.* (Small-*x* Collab.), Eur. Phys. J. **C35** 67 (2004).

[26] J. Andersen *et al.* (Small-*x* Collab.), Eur. Phys. J. **C48** 53 (2006).

[27] S. Shael *et al.* (ALEPH Collab.), JHEP **0709** 102 (2007).

[28] A.V. Lipatov and N.P. Zotov, Phys. Rev. **D73** 114018 (2006); JHEP **0608** 043 (2006).

[29] U. Karshon, I. Schienbein, P. Thompson, *Proccedings of the 14th Intern. Workshop "Deep inelastic scattering",* Tsukuba, Japan (2006) p. 894.

[30] S.P. Baranov and N.P. Zotov, JETP Lett. **86** 435 (2007); *ibid* **88** (2008).

[31] R.D. Ball, Nucl. Phys. **796** 137 (2008).

[32] J. Blumlein, J. Phys. **G19** 1623 91993); arXiv:hep-ph/9506403.

[33] G. Salam, JHEP **9807** 019 (1998); S. Brodsky *et al*, JETP Lett. **70** 155 (1999).

[34] S.P. Baranov and N.P. Zotov, Phys. Lett. **B458** 389 (1999); *ibid* **B491** 111 (2000).

[35] J. Kwiecinski, A.D. Martin and A.M. Stasto, Phys. Rev. **D56** 3991 (1997).

[36] J. Kwiecinski, A.D. Martin and A. Sutton, Phys. Rev. **D52** 1445 (1995); Z. Phys. **C71** 585 (1996).

[37] J. Kwiecinski, A.D. Martin and J. Outhwaite, Eur. Phys. J. **C9** 611 (2001).

[38] M.A. Kimber, A.D. Martin and M.G. Ryskin, **D63**, 114027 (2001).

[39] G. Watt, A.D. Martin and M.G. Ryskin, Eur. Phys. J. **C31** 73 (2003).

[40] H. Jung, G. Salam, Eur. Phys. J. **C19** 351 (2001); H. Jung, Coput. Phys. Comm. **143** 100 (2002).

[41] C. Peterson, D. Schlatter, I. Schmitt and P. Zerwas, Phys. Rev. **D27** 105 (1983).

[42] C.-H.Chang, Nucl Phys. **B172** 425 (1980); R. Baier and R. Rückl, Phys. Lett. **B102** 364 (1981);
E.L. Berger and D. Jones, Phys. Rev. **D23** 1521 (1981);
S.S. Gershtein, A.K. Likhoded and S.R. Slabospitsky, Sov. J. Nucl. Phys. **34** 128 (1981).

[43] G.T. Bodwin, E. Braaten, and G.P. Lepage, Phys. Rev. **D51** 1125 (1995);
E. Braaten and S. Fleming, Phys. Rev. Lett. **74** 3327 (1995);
P. Cho and A.K. Leibovich, Phys. Rev. **D53** 150 (1995); *ibid.* **D53** 6203 (1196).

[44] B. Kniehl, L. Zwirner, Nucl. Phys. **B621** 337 (2002).

[45] S.P. Baranov, Phys. Rev. **D66** 114003 (2002).

[46] D0 Collaboration, V. M. Abazov *at.al.*(DO Collab.), arXiv:0804.2799[hep-ex].

****

Relativistic Description of Heavy Tetraquarks

D. Ebert[1], R. N. Faustov[2], V. O. Galkin[2]

[1]Institut für Physik, Humboldt–Universität zu Berlin, Newtonstr. 15, D-12489 Berlin, Germany
[2]Dorodnicyn Computing Centre, Russian Academy of Sciences, Vavilov Str. 40, 119991 Moscow, Russia

The masses of excited heavy tetraquarks with hidden charm are calculated within the relativistic diquark-antidiquark picture. New experimental data on charmonium-like states above open charm threshold are discussed. The obtained results indicate that $X(3872)$, $Y(4260)$, $Y(4360)$, $Z(4248)$, $Z(4433)$ and $Y(4660)$ could be tetraquark states with hidden charm.

Recently, significant experimental progress has been achieved in charmonium spectroscopy. Several new states, such as $X(3872)$, $Y(4260)$, $Y(4360)$, $Y(4660)$, $Z(4248)$, $Z(4430)$, etc., were observed [1] which cannot be simply accommodated in the quark-antiquark ($c\bar{c}$) picture. These states and especially the charged ones can be considered as indications of the possible existence of exotic multiquark states [2, 3]. In papers [4, 5] we calculated masses of the ground state heavy tetraquarks in the framework of the relativistic quark model based on the quasipotential approach in quantum chromodynamics and then we extend this analysis to the consideration of the excited tetraquark states with hidden charm [6]. As previously, we use the diquark-antidiquark picture to reduce a complicated relativistic four-body problem to the subsequent two more simple two-body problems. The first step consists in the calculation of masses, wave functions and form factors of the diquarks, composed from light and heavy quarks. At the second step, a heavy tetraquark is considered to be a bound diquark-antidiquark system. It is important to emphasize that we do not consider the diquark as a point particle but explicitly take into account its structure by calculating the form factor of the diquark-gluon interaction in terms of the diquark wave functions.

In the quasipotential approach and diquark-antidiquark picture of heavy tetraquarks the interaction of two quarks in a diquark and the diquark-antidiquark interaction in a tetraquark are described by the diquark wave function (Ψ_d) of the bound quark-quark state and by the tetraquark wave function (Ψ_T) of the bound diquark-antidiquark state, respectively. These wave functions satisfy the quasipotential equations of the Schrödinger type [7]

$$\left(\frac{b^2(M)}{2\mu_R} - \frac{\mathbf{p}^2}{2\mu_R}\right)\Psi_{d,T}(\mathbf{p}) = \int \frac{d^3q}{(2\pi)^3} V_{d,T}(\mathbf{p},\mathbf{q};M)\Psi_{d,T}(\mathbf{q}), \tag{1}$$

where the relativistic reduced mass is

$$\mu_R = \frac{E_1 E_2}{E_1 + E_2} = \frac{M^4 - (m_1^2 - m_2^2)^2}{4M^3}, \tag{2}$$

and E_1, E_2 are given by

$$E_1 = \frac{M^2 - m_2^2 + m_1^2}{2M}, \quad E_2 = \frac{M^2 - m_1^2 + m_2^2}{2M}. \tag{3}$$

Here, $M = E_1 + E_2$ is the bound-state mass (diquark or tetraquark), $m_{1,2}$ are the masses of quarks (q and Q) which form the diquark or of the diquark (d) and antiquark ($\bar{d}'$) which form the heavy tetraquark (T), and $\mathbf{p}$ is their relative momentum. In the center-of-mass system the relative momentum squared on mass shell reads

$$b^2(M) = \frac{[M^2 - (m_1 + m_2)^2][M^2 - (m_1 - m_2)^2]}{4M^2}. \tag{4}$$

The kernel $V_{d,T}(\mathbf{p}, \mathbf{q}; M)$ in Eq. (1) is the quasipotential operator of the quark-quark or diquark-antidiquark interaction. It is constructed with the help of the off-mass-shell scattering amplitude, projected onto the positive-energy states. In the following analysis we closely follow the similar construction of the quark-antiquark interaction in mesons which were extensively studied in our relativistic quark model [7, 8]. For the quark-quark interaction in a diquark we use the relation $V_{qq} = V_{q\bar{q}}/2$ arising under the assumption of an octet structure of the interaction from the difference in the qq and $q\bar{q}$ colour states. An important role in this construction is played by the Lorentz structure of the confining interaction. In our analysis of mesons, while constructing the quasipotential of the quark-antiquark interaction, we assumed that the effective interaction is the sum of the usual one-gluon exchange term and a mixture of long-range vector and scalar linear confining potentials, where the vector confining potential contains the Pauli term. We use the same conventions for the construction of the quark-quark and diquark-antidiquark interactions in the tetraquark. The quasipotential is then defined as follows [9, 8].

(a) For the quark-quark (Qq) interactions, $V_d(\mathbf{p}, \mathbf{q}; M)$ reads

$$V_d(\mathbf{p}, \mathbf{q}; M) = \bar{u}_1(p)\bar{u}_2(-p)\mathcal{V}(\mathbf{p}, \mathbf{q}; M)u_1(q)u_2(-q), \tag{5}$$

with

$$\mathcal{V}(\mathbf{p}, \mathbf{q}; M) = \frac{1}{2}\left[\frac{4}{3}\alpha_s D_{\mu\nu}(\mathbf{k})\gamma_1^\mu\gamma_2^\nu + V_{\mathrm{conf}}^V(\mathbf{k})\Gamma_1^\mu(\mathbf{k})\Gamma_{2;\mu}(-\mathbf{k}) + V_{\mathrm{conf}}^S(\mathbf{k})\right].$$

Here, α_s is the QCD coupling constant; $D_{\mu\nu}$ is the gluon propagator in the Coulomb gauge,

$$D^{00}(\mathbf{k}) = -\frac{4\pi}{\mathbf{k}^2}, \quad D^{ij}(\mathbf{k}) = -\frac{4\pi}{k^2}\left(\delta^{ij} - \frac{k^i k^j}{\mathbf{k}^2}\right), \quad D^{0i} = D^{i0} = 0, \tag{6}$$

and $\mathbf{k} = \mathbf{p} - \mathbf{q}$; γ_μ and $u(p)$ are the Dirac matrices and spinors,

$$u^\lambda(p) = \sqrt{\frac{\epsilon(p) + m}{2\epsilon(p)}}\left(\begin{array}{c} 1 \\ \frac{\boldsymbol{\sigma} \cdot \mathbf{p}}{\epsilon(p) + m} \end{array}\right)\chi^\lambda, \tag{7}$$

with $\epsilon(p) = \sqrt{\mathbf{p}^2 + m^2}$.

The effective long-range vector vertex of the quark is defined [8] by

$$\Gamma_\mu(\mathbf{k}) = \gamma_\mu + \frac{i\kappa}{2m}\sigma_{\mu\nu}\tilde{k}^\nu, \qquad \tilde{k} = (0, \mathbf{k}), \tag{8}$$

where κ is the Pauli interaction constant characterizing the anomalous chromomagnetic moment of quarks. In configuration space the vector and scalar confining potentials in the nonrelativistic limit [10] reduce to

$$
\begin{aligned}
V_{\mathrm{conf}}^V(r) &= (1 - \varepsilon)V_{\mathrm{conf}}(r), \\
V_{\mathrm{conf}}^S(r) &= \varepsilon V_{\mathrm{conf}}(r),
\end{aligned} \tag{9}
$$

with

$$V_{\text{conf}}(r) = V_{\text{conf}}^S(r) + V_{\text{conf}}^V(r) = Ar + B, \tag{10}$$

where ε is the mixing coefficient.

(b) For the diquark-antidiquark $(d\bar{d}')$ interaction, $V_T(\mathbf{p}, \mathbf{q}; M)$ is given by

$$\begin{aligned}
V_T(\mathbf{p}, \mathbf{q}; M) &= \frac{\langle d(P)|J_\mu|d(Q)\rangle}{2\sqrt{E_d E_d}} \frac{4}{3} \alpha_s D^{\mu\nu}(\mathbf{k}) \frac{\langle d'(P')|J_\nu|d'(Q')\rangle}{2\sqrt{E_{d'} E_{d'}}} \\
&\quad + \psi_d^*(P)\psi_{d'}^*(P') \left[J_{d;\mu}J_{d'}^\mu V_{\text{conf}}^V(\mathbf{k}) + V_{\text{conf}}^S(\mathbf{k}) \right] \psi_d(Q)\psi_{d'}(Q'), \tag{11}
\end{aligned}$$

where $\langle d(P)|J_\mu|d(Q)\rangle$ is the vertex of the diquark-gluon interaction which takes into account the finite size of the diquark and is discussed below $\left[P^{(')} = (E_{d^{(')}}, \pm\mathbf{p}) \text{ and } Q^{(')} = (E_{d^{(')}}, \pm\mathbf{q}), \right.$ $E_d = (M^2 - M_{d'}^2 + M_d^2)/(2M) \text{ and } E_{d'} = (M^2 - M_d^2 + M_{d'}^2)/(2M) \left. \right]$.

The diquark state in the confining part of the diquark-antidiquark quasipotential (11) is described by the wave functions

$$\psi_d(p) = \begin{cases} 1 & \text{for a scalar diquark,} \\ \varepsilon_d(p) & \text{for an axial-vector diquark,} \end{cases} \tag{12}$$

where the four-vector

$$\varepsilon_d(p) = \left(\frac{(\boldsymbol{\varepsilon}_d \cdot \mathbf{p})}{M_d}, \boldsymbol{\varepsilon}_d + \frac{(\boldsymbol{\varepsilon}_d \cdot \mathbf{p})\mathbf{p}}{M_d(E_d(p) + M_d)} \right), \qquad \varepsilon_d^\mu(p)p_\mu = 0, \tag{13}$$

is the polarization vector of the axial-vector diquark with momentum $\mathbf{p}$, $E_d(p) = \sqrt{\mathbf{p}^2 + M_d^2}$, and $\varepsilon_d(0) = (0, \boldsymbol{\varepsilon}_d)$ is the polarization vector in the diquark rest frame. The effective long-range vector vertex of the diquark can be presented in the form

$$J_{d;\mu} = \begin{cases} \dfrac{(P+Q)_\mu}{2\sqrt{E_d E_d}} & \text{for a scalar diquark,} \\ -\dfrac{(P+Q)_\mu}{2\sqrt{E_d E_d}} + \dfrac{i\mu_d}{2M_d}\Sigma_\mu^\nu \tilde{k}_\nu & \text{for an axial-vector diquark.} \end{cases} \tag{14}$$

Here, the antisymmetric tensor Σ_μ^ν is defined by

$$(\Sigma_{\rho\sigma})_\mu^\nu = -i(g_{\mu\rho}\delta_\sigma^\nu - g_{\mu\sigma}\delta_\rho^\nu), \tag{15}$$

and the axial-vector diquark spin $\mathbf{S}_d$ is given by $(S_{d;k})_{il} = -i\varepsilon_{kil}$; μ_d is the total chromomagnetic moment of the axial-vector diquark.

The constituent quark masses $m_c = 1.55$ GeV, $m_u = m_d = 0.33$ GeV, $m_s = 0.5$ GeV and the parameters of the linear potential $A = 0.18$ GeV^2 and $B = -0.3$ GeV are fixed from previous consideration of meson properties [8] and have values typical in quark models. The value of the mixing coefficient of vector and scalar confining potentials $\varepsilon = -1$ has been determined from the consideration of charmonium radiative decays [7] and the heavy-quark expansion [11]. The universal Pauli interaction constant $\kappa = -1$ has been fixed from the analysis of the fine splitting of heavy quarkonia ^3P_J - states [7]. In this case, the long-range chromomagnetic interaction of quarks vanishes in accordance with the flux-tube model.
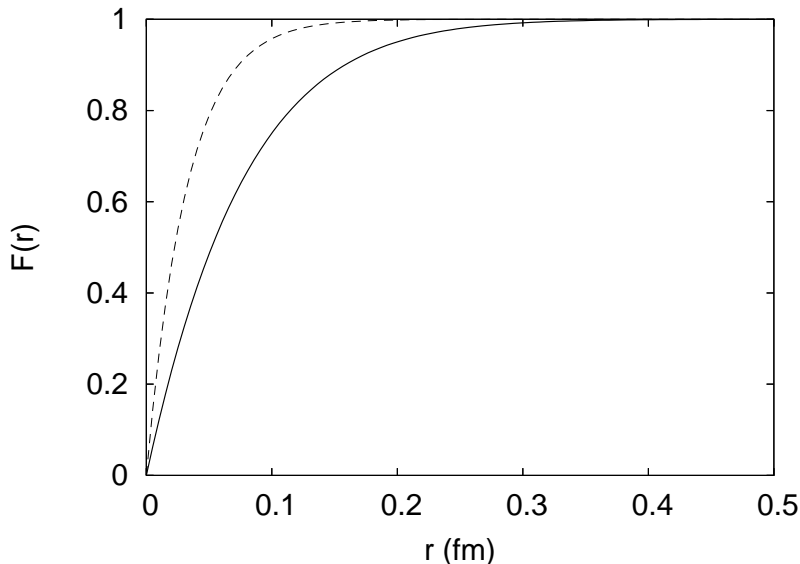
Figure 1: The form factors $F(r)$ for $\{c, q\}$ (solid line) and $\{b, q\}$ (dashed line) axial vector diquarks.

At the first step, we calculate the masses and form factors of the heavy-light diquark. As it is well known, the light quarks are highly relativistic, which makes the v/c expansion inapplicable and thus, a completely relativistic treatment of the light quark dynamics is required. To achieve this goal, we closely follow our consideration of diquarks in heavy baryons and adopt the same procedure to make the relativistic potential local by replacing $\epsilon_{1,2}(p) = \sqrt{m_{1,2}^2 + \mathbf{p}^2} \to E_{1,2} = (M^2 - m_{2,1}^2 + m_{1,2}^2)/2M$. Solving numerically the quasipotential equation (1) with the complete relativistic potential, which depends on the diquark mass in a complicated highly nonlinear way [12], we get the diquark masses and wave functions. In order to determine the diquark interaction with the gluon field, which takes into account the diquark structure, we calculate the corresponding matrix element of the quark current between diquark states. Such calculation leads to the emergence of the form factor $F(r)$ entering the vertex of the diquark-gluon interaction [12]. This form factor is expressed through the overlap integral of the diquark wave functions. Our estimates show that this form factor can be approximated with a high accuracy by the expression

$$F(r) = 1 - e^{-\xi r - \zeta r^2}. \tag{16}$$

The values of the masses and parameters ξ and ζ for heavy-light scalar diquark $[\cdots]$ and axial vector diquark $\{\cdots\}$ ground states are given in Table 1. In Fig. 1 we plot the functions $F(r)$ for $\{Q, q\}$ axial vector diquarks.

At the second step, we calculate the masses of heavy tetraquarks considered as the bound states of a heavy-light diquark and antidiquark. For the potential of the diquark-antidiquark

Table 1: Masses M and form factor parameters of charmed diquarks. S and A denote scalar and axial vector diquarks which are antisymmetric $[\cdots]$ and symmetric $\{\cdots\}$ in flavour, respectively.

Quark content	Diquark type	M (MeV)	ξ (GeV)	ζ (GeV^2)
$[c,q]$	S	1973	2.55	0.63
$\{c,q\}$	A	2036	2.51	0.45
$[c,s]$	S	2091	2.15	1.05
$\{c,s\}$	A	2158	2.12	0.99

interaction (11) we get [5]

$$
\begin{aligned}
V_T(r) &= \hat{V}_{\text{Coul}}(r) + V_{\text{conf}}(r) + \frac{1}{2}\Bigg\{\left[\frac{1}{E_1(E_1+M_1)} + \frac{1}{E_2(E_2+M_2)}\right]\frac{\hat{V}'_{\text{Coul}}(r)}{r} - \left[\frac{1}{M_1(E_1+M_1)}\right. \\
&\quad + \left.\frac{1}{M_2(E_2+M_2)}\right]\frac{V'_{\text{conf}}(r)}{r} + \frac{\mu_d}{2}\left(\frac{1}{M_1^2}+\frac{1}{M_2^2}\right)\frac{V'^V_{\text{conf}}(r)}{r}\Bigg\}\mathbf{L}\cdot(\mathbf{S}_1+\mathbf{S}_2) \\
&\quad + \frac{1}{2}\Bigg\{\left[\frac{1}{E_1(E_1+M_1)} - \frac{1}{E_2(E_2+M_2)}\right]\frac{\hat{V}'_{\text{Coul}}(r)}{r} - \left[\frac{1}{M_1(E_1+M_1)} - \frac{1}{M_2(E_2+M_2)}\right] \\
&\quad \times \frac{V'_{\text{conf}}(r)}{r} + \frac{\mu_d}{2}\left(\frac{1}{M_1^2}-\frac{1}{M_2^2}\right)\frac{V'^V_{\text{conf}}(r)}{r}\Bigg\}\mathbf{L}\cdot(\mathbf{S}_1-\mathbf{S}_2) \\
&\quad + \frac{1}{E_1 E_2}\Bigg\{\mathbf{p}\left[\hat{V}_{\text{Coul}}(r)+V^V_{\text{conf}}(r)\right]\mathbf{p} - \frac{1}{4}\Delta V^V_{\text{conf}}(r) + \hat{V}'_{\text{Coul}}(r)\frac{\mathbf{L}^2}{2r} \\
&\quad + \frac{1}{r}\left[\hat{V}'_{\text{Coul}}(r) + \frac{\mu_d}{4}\left(\frac{E_1}{M_1}+\frac{E_2}{M_2}\right)V'^V_{\text{conf}}(r)\right]\mathbf{L}\cdot(\mathbf{S}_1+\mathbf{S}_2) \\
&\quad + \frac{\mu_d}{4}\left(\frac{E_1}{M_1}-\frac{E_2}{M_2}\right)\frac{V'^V_{\text{conf}}(r)}{r}\mathbf{L}\cdot(\mathbf{S}_1-\mathbf{S}_2) \\
&\quad + \frac{1}{3}\left[\frac{1}{r}\hat{V}'_{\text{Coul}}(r) - \hat{V}''_{\text{Coul}}(r) + \frac{\mu_d^2}{4}\frac{E_1 E_2}{M_1 M_2}\left(\frac{1}{r}V'^V_{\text{conf}}(r) - V''^V_{\text{conf}}(r)\right)\right] \\
&\quad \times \left[\frac{3}{r^2}(\mathbf{S}_1\cdot\mathbf{r})(\mathbf{S}_2\cdot\mathbf{r}) - \mathbf{S}_1\cdot\mathbf{S}_2\right] \\
&\quad + \frac{2}{3}\left[\Delta\hat{V}_{\text{Coul}}(r) + \frac{\mu_d^2}{4}\frac{E_1 E_2}{M_1 M_2}\Delta V^V_{\text{conf}}(r)\right]\mathbf{S}_1\cdot\mathbf{S}_2\Bigg\},
\end{aligned}
\tag{17}
$$

where

$$
\hat{V}_{\text{Coul}}(r) = -\frac{4}{3}\alpha_s\frac{F_1(r)F_2(r)}{r}
$$

is the Coulomb-like potential which takes into account the structure of the diquark and antidiquark through the corresponding form factors $F_{1,2}(r)$. Here, $\mathbf{S}_{1,2}$ and $\mathbf{L}$ are the spin operators

of diquark and antidiquark and the operator of the relative orbital angular momentum. In the following we choose the total chromomagnetic moment of the axial-vector diquark $\mu_d = 0$. Such a choice appears to be natural, since the long-range chromomagnetic interaction of diquarks proportional to μ_d then also vanishes in accordance with the flux-tube model.

In the diquark-antidiquark picture of heavy tetraquarks both scalar S (antisymmetric in flavour $(Qq)_{S=0} = [Qq]$) and axial vector A (symmetric in flavour $(Qq)_{S=1} = \{Qq\}$) diquarks are considered. Therefore we get the following structure of the $(Qq)(\bar{Q}\bar{q}')$ ground $(1S)$ states (C is defined only for $q = q'$):

- Two states with $J^{PC} = 0^{++}$:

$$X(0^{++}) = (Qq)_{S=0}(\bar{Q}\bar{q}')_{S=0}$$
$$X(0^{++\prime}) = (Qq)_{S=1}(\bar{Q}\bar{q}')_{S=1}$$

- Three states with $J = 1$:

$$X(1^{++}) = \frac{1}{\sqrt{2}}[(Qq)_{S=1}(\bar{Q}\bar{q}')_{S=0} + (Qq)_{S=0}(\bar{Q}\bar{q}')_{S=1}]$$
$$X(1^{+-}) = \frac{1}{\sqrt{2}}[(Qq)_{S=0}(\bar{Q}\bar{q}')_{S=1} - (Qq)_{S=1}(\bar{Q}\bar{q}')_{S=0}]$$
$$X(1^{+-\prime}) = (Qq)_{S=1}(\bar{Q}\bar{q}')_{S=1}$$

- One state with $J^{PC} = 2^{++}$:

$$X(2^{++}) = (Qq)_{S=1}(\bar{Q}\bar{q}')_{S=1}.$$

The orbitally excited $(1P, 1D \ldots)$ states are constructed analogously, as a result we find a rich set of tetraquark states. However the number of states in the considered diquark-antidiquark picture is significantly less than in the genuine four-quark approach.

The diquark-antidiquark model of heavy tetraquarks predicts the existence of a flavour $SU(3)$ nonet of states with hidden charm ($Q = c$): four tetraquarks $[(Qq)(\bar{Q}\bar{q}), q = u, d]$ with neither open or hidden strangeness, which have electric charges 0 or ± 1 and isospin 0 or 1; four tetraquarks $[(Qs)(\bar{Q}\bar{q})$ and $(Qq)(\bar{Q}\bar{s}), q = u, d]$ with open strangeness ($S = \pm 1$), which have electric charges 0 or ± 1 and isospin $\frac{1}{2}$; one tetraquark $(Qs)(\bar{Q}\bar{s})$ with hidden strangeness and zero electric charge. Since we neglect in our model the mass difference of u and d quarks and electromagnetic interactions, the corresponding tetraquarks will be degenerate in mass. A more detailed analysis [13] predicts that the tetraquark mass differences can be of a few MeV so that the isospin invariance is broken for the $(Qq)(\bar{Q}\bar{q})$ mass eigenstates and thus in their strong decays. The (non)observation of such states will be a crucial test of the tetraquark model.

The calculated masses of the heavy tetraquark ground $(1S)$ states and the corresponding open charm thresholds are shown in Tables 2, 3. Note that most of the tetraquark states were predicted to lie either above or only slightly below corresponding open charm thresholds. We also calculated masses of orbitally and radially excited tetraquark states with hidden charm. Excitations only of the diquark-antidiquark system are considered. The mass spectrum of excited tetraquark states is shown in Table 4.

In Table 5 we compare our results (EFG) for the masses of the ground and excited charm diquark-antidiquark bound states with the predictions of Refs. [13, 14, 15, 16] and with the

Table 2: Masses of charm diquark-antidiquark ground ($1S$) states (in MeV) calculated in [4]. S and A denote scalar and axial vector diquarks.

State J^{PC}	Diquark content	Mass		
		$cq\bar{c}\bar{q}$	$cs\bar{c}\bar{s}$	$cq\bar{c}\bar{s}$
0^{++}	SS	3812	4051	3922
$1^{+\pm}$	$(S\bar{A} \pm \bar{S}A)/\sqrt{2}$	3871	4113	3982
0^{++}	$A\bar{A}$	3852	4110	3967
1^{+-}	$A\bar{A}$	3890	4143	4004
2^{++}	$A\bar{A}$	3968	4209	4080

Table 3: Thresholds for open charm decays and nearby hidden-charm thresholds.

Channel	Threshold (MeV)	Channel	Threshold (MeV)	Channel	Threshold (MeV)
$D^0\bar{D}^0$	3729.4	$D_s^+D_s^-$	3936.2	$D^0D_s^\pm$	3832.9
D^+D^-	3738.8	$\eta' J/\psi$	4054.7	$D^\pm D_s^\mp$	3837.7
$D^0\bar{D}^{*0}$	3871.3	$D_s^\pm D_s^{*\mp}$	4080.0	$D^{*0}D_s^\pm$	3975.0
$\rho J/\psi$	3872.7	$\phi J/\psi$	4116.4	$D^0 D_s^{*\pm}$	3976.7
$D^\pm D^{*\mp}$	3879.5	$D_s^{*+}D_s^{*-}$	4223.8	$K^{*\pm} J/\psi$	3988.6
$\omega J/\psi$	3879.6			$K^{*0} J/\psi$	3993.0
$D^{*0}\bar{D}^{*0}$	4013.6			$D^{*0}D_s^{*\pm}$	4118.8

masses of the recently observed highly-excited charmonium-like states [1, 17, 18, 19, 20, 21, 22, 23, 24, 25, 26]. We assume that the excitations occur only between the bound diquark and antidiquark. Possible excitations of diquarks are not considered. Our calculation of the heavy baryon masses supports such a scheme [12]. In this table we give our predictions only for some of the masses of the orbitally and radially excited states for which possible experimental candidates are observed. The differences in some of the presented theoretical mass values can be attributed to the substantial distinctions in the used approaches. We describe the diquarks dynamically as quark-quark bound systems and calculate their masses and form factors, while in Refs.[13, 14, 15, 16] they are treated only phenomenologically. Then we consider the tetraquark as purely the diquark-antidiquark bound system. In distinction, Maini et al. consider a hyperfine interaction between all quarks which, e.g., causes the splitting of 1^{++} and 1^{+-} states arising from the SA diquark-antidiquark compositions. From Table 5 we see that our dynamical calculation supports the assumption [13] that $X(3872)$ can be the axial vector 1^{++} tetraquark state composed from the scalar and axial vector diquark and antidiquark in the relative $1S$ state. Recent Belle and BaBar results indicate the existence of a second $X(3875)$ particle a few MeV above $X(3872)$. This state could be naturally identified with the second neutral particle predicted by the tetraquark model [14]. On the other hand, in our model the lightest scalar 0^{++} tetraquark is predicted to be above the open charm threshold $D\bar{D}$ and thus to be broad, while in the model [13] it lies a few MeV below this threshold, and thus is predicted to be narrow. Our 2^{++} tetraquark also lies higher than the one in Ref.[13], thus making its identification with $Y(3943)$ less probable, especially if one averages the original Belle result with the recent BaBar value which is somewhat lower.

The recent discovery in the initial state radiation at B-factories of the $Y(4260)$, $Y(4360)$ and $Y(4660)$ indicates an overpopulation of the expected charmonium 1^{--} states [1, 19, 20, 22,

Table 4: Masses of charm diquark-antidiquark excited $1P$, $2S$ states (in MeV). S and A denote scalar and axial vector diquarks; $\mathcal{S}$ is the total spin of the diquark and antidiquark.

State	Diquark		Mass		
J^{PC}	content	$\mathcal{S}$	$cq\bar{c}\bar{q}$	$cs\bar{c}\bar{s}$	$cq\bar{c}\bar{s}$
$1P$					
1^{--}	$S\bar{S}$	0	4244	4466	4350
$0^{-\pm}$	$(S\bar{A} \pm \bar{S}A)/\sqrt{2}$	1	4269	4499	4381
$1^{-\pm}$	$(S\bar{A} \pm \bar{S}A)/\sqrt{2}$	1	4284	4514	4396
$2^{-\pm}$	$(S\bar{A} \pm \bar{S}A)/\sqrt{2}$	1	4315	4543	4426
1^{--}	$A\bar{A}$	0	4350	4582	4461
0^{-+}	$A\bar{A}$	1	4304	4540	4419
1^{-+}	$A\bar{A}$	1	4345	4578	4458
2^{-+}	$A\bar{A}$	1	4367	4598	4478
1^{--}	$A\bar{A}$	2	4277	4515	4393
2^{--}	$A\bar{A}$	2	4379	4610	4490
3^{--}	$A\bar{A}$	2	4381	4612	4492
$2S$					
0^{++}	$S\bar{S}$	0	4375	4604	4481
$1^{+\pm}$	$(S\bar{A} \pm \bar{S}A)/\sqrt{2}$	1	4431	4665	4542
0^{++}	$A\bar{A}$	0	4434	4680	4547
1^{+-}	$A\bar{A}$	1	4461	4703	4572
2^{++}	$A\bar{A}$	2	4515	4748	4625

23, 24]. Maini et al. [16] argue that $Y(4260)$ is the 1^{--} $1P$ state of the charm-strange diquark-antidiquark tetraquark. We find that $Y(4260)$ cannot be interpreted in this way, since the mass of such ($[cs]_{S=0}[\bar{c}\bar{s}]_{S=0}$) tetraquark is found to be ~ 200 MeV higher. A more natural tetraquark interpretation could be the 1^{--} $1P$ state ($[cq]_{S=0}[\bar{c}\bar{q}]_{S=0}$) ($S\bar{S}$) which mass is predicted in our model to be close to the mass of $Y(4260)$ (see Table 5). Then the $Y(4260)$ would decay dominantly into $D\bar{D}$ pairs. The other possible interpretations of $Y(4260)$ are the 1^{--} $1P$ states of $(S\bar{A} - \bar{S}A)/\sqrt{2}$ and $A\bar{A}$ tetraquarks which predicted masses have close values. These additional tetraquark states could be responsible for the mass difference of $Y(4260)$ observed in different decay channels. As we see from Table 5, the recently discovered resonances $Y(4360)$ and $Y(4660)$ in the $e^+e^- \to \pi^+\pi^-\psi'$ cross section can be interpreted as the excited 1^{--} $1P$ ($A\bar{A}$) and $2P$ ($S\bar{S}$) tetraquark states, respectively. The peak $X(4630)$ very recently observed by Belle in $e^+e^- \to \Lambda_c^+\Lambda_c^-$ [26] is consistent with a 1^{--} resonance $Y(4660)$ and therefore has the same interpretation in our model.

Recently the Belle Collaboration reported the observation of a relatively narrow enhancement in the $\pi^+\psi'$ invariant mass distribution in the $B \to K\pi^+\psi'$ decay [1, 25]. This new resonance, $Z^+(4430)$, is unique among other exotic meson candidates, since it is the first state with a non-zero electric charge. Different theoretical interpretations were suggested [1]. Maiani et al. [15] give qualitative arguments that the $Z^+(4430)$ is the first radial excitation ($2S$) of a diquark-antidiquark $X^+_{u\bar{d}}(1^{+-}; 1S)$ state ($A\bar{A}$) with mass 3882 MeV. Our calculations indicate that the $Z^+(4430)$ could be the 1^+ $2S$ $[cu][\bar{c}\bar{d}]$ tetraquark state, namely the first radial excitation of the ground state $(S\bar{A} - \bar{S}A)/\sqrt{2}$ degenerate with $X(3872)$. The other possible interpretation is the 0^+ $2S$ $[cu][\bar{c}\bar{d}]$ tetraquark state ($A\bar{A}$) which has a very close mass. Measurement of the

Table 5: Comparison of theoretical predictions for the masses of the ground and excited charm diquark-antidiquark states (in MeV) and possible experimental candidates.

State J^{PC}	Diquark content	Theory		Experiment	
		EFG	[13, 14, 15]	state	mass
1S					
0^{++}	$S\bar{S}$	3812	3723		
1^{++}	$(S\bar{A} + \bar{S}A)/\sqrt{2}$	3871	$3872^{\dagger}$	$\begin{cases} X(3872) \\ X(3876) \end{cases}$	$\begin{cases} 3871.4 \pm 0.6 \text{ [1]} \\ 3875.2 \pm 0.7^{+0.9}_{-1.8} \text{ [1]} \end{cases}$
1^{+-}	$(S\bar{A} - \bar{S}A)/\sqrt{2}$	3871	3754		
0^{++}	$A\bar{A}$	3852	3832		
1^{+-}	$A\bar{A}$	3890	3882		
2^{++}	$A\bar{A}$	3968	3952	$Y(3943)$	$\begin{cases} 3943 \pm 11 \pm 13 \text{ [16]} \\ 3914.3^{+4.1}_{-3.8} \text{ [17]} \end{cases}$
1P					
1^{--}	$S\bar{S}$	4244		$Y(4260)$	$\begin{cases} 4259 \pm 8^{+2}_{-6} \text{ [18]} \\ 4247 \pm 12^{+17}_{-32} \text{ [19]} \end{cases}$
1^{-}	$S\bar{S}$	4244			
0^{-}	$(S\bar{A} \pm \bar{S}A)/\sqrt{2}$	4267		$Z(4248)$	$4248^{+44+180}_{-29-35}$ [20]
1^{--}	$(S\bar{A} - \bar{S}A)/\sqrt{2}$	4284			
1^{--}	$A\bar{A}$	4277		$Y(4260)$	$4284^{+17}_{-16} \pm 4$ [21]
1^{--}	$A\bar{A}$	4350		$Y(4360)$	$\begin{cases} 4361 \pm 9 \pm 9 \text{ [22]} \\ 4324 \pm 24 \text{ [23]} \end{cases}$
2S					
1^{+}	$(S\bar{A} \pm \bar{S}A)/\sqrt{2}$	4431			
0^{+}	$A\bar{A}$	4434		$Z(4430)$	$4433 \pm 4 \pm 2$ [24]
1^{+}	$A\bar{A}$	4461	~ 4470		
2P					
1^{--}	$S\bar{S}$	4666		$\begin{cases} Y(4660) \\ X(4630) \end{cases}$	$\begin{cases} 4664 \pm 11 \pm 5 \text{ [22]} \\ 4634^{+8+5}_{-7-8} \text{ [25]} \end{cases}$

† input

$Z^{+}(4430)$ spin will discriminate between these possibilities.

Encouraged by this discovery, the Belle Collaboration performed a study of $\bar{B}^{0} \to K^{-}\pi^{+}\chi_{c1}$ and observed a double peaked structure in the $\pi^{+}\chi_{c1}$ invariant mass distribution [21]. These two charged states, $Z(4051)$ and $Z(4248)$, are explicitly exotic. We find no tetraquark candidates for the $Z(4051)$ peak. On the other hand, we see from Table 5 that $Z(4248)$ can be interpreted in our model as the charged partner of the 1^{-} $1P$ state of the $S\bar{S}$ tetraquark or as the 0^{-} $1P$ state of the $(S\bar{A} \pm \bar{S}A)/\sqrt{2}$ tetraquark.

In summary, we calculated the masses of excited heavy tetraquarks with hidden charm in the diquark-antidiquark picture. In contrast to previous phenomenological treatments, we used the dynamical approach based on the relativistic quark model. Both diquark and tetraquark masses were obtained by numerical solution of the quasipotential wave equation with the corresponding relativistic potentials. The diquark structure was taken into account in terms of diquark wave

functions. It is important to emphasize that, in our analysis, we did not introduce any free adjustable parameters but used their values fixed from our previous considerations of heavy and light hadron properties. It was found that the $X(3872)$, $Z(4248)$, $Y(4260)$, $Y(4360)$, $Z(4430)$ and $Y(4660)$ exotic meson candidates could be tetraquark states with hidden charm.

References

[1] For recent reviews see e.g. G. V. Pakhlova talk at 34th International Conference on High Energy Physics (ICHEP 08), Jule 28-August 5, 2008, Philadelphia, USA, arXiv:0810.4114 [hep-ex]; S. Godfrey and S. L. Olsen, arXiv:0801.3867 [hep-ph]; E. S. Swanson, Phys. Rept. **429**, 243 (2006).

[2] R. L. Jaffe, Phys. Rev. D **15**, 267 (1977); Phys. Rev. Lett. **38**, 195 (1977); V. A. Matveev and P. Sorba, Lett. Nuovo Cim. **20**, 443 (1977).

[3] A. M. Badalyan, B. L. Ioffe and A. V. Smilga, Nucl. Phys. B **281**, 85 (1987); A. B. Kaidalov, Surveys in High Energy Physics **13**, 265 (1999).

[4] D. Ebert, R. N. Faustov and V. O. Galkin, Phys. Lett. B **634**, 214 (2006).

[5] D. Ebert, R. N. Faustov, V. O. Galkin and W. Lucha, Phys. Rev. D **76**, 114015 (2007).

[6] D. Ebert, R. N. Faustov and V. O. Galkin, Eur. Phys. J. C **58**, 399 (2008).

[7] D. Ebert, R. N. Faustov and V. O. Galkin, Phys. Rev. D **67**, 014027 (2003).

[8] D. Ebert, V. O. Galkin and R. N. Faustov, Phys. Rev. D **57**, 5663 (1998); **59**, 019902(E) (1999).

[9] D. Ebert, R. N. Faustov, V. O. Galkin and A. P. Martynenko, Phys. Rev. D **66**, 014008 (2002).

[10] D. Ebert, R. N. Faustov and V. O. Galkin, Phys. Rev. D **62**, 034014 (2000).

[11] R. N. Faustov and V. O. Galkin, Z. Phys. C **66**, 119 (1995); D. Ebert, R. N. Faustov and V. O. Galkin, Phys. Rev. D **73**, 094002 (2006).

[12] D. Ebert, R. N. Faustov and V. O. Galkin, Phys. Rev. D **72**, 034026 (2005); Phys. Lett. B **659**, 612 (2008).

[13] L. Maiani, F. Piccinini, A. D. Polosa and V. Riquer, Phys. Rev. D **71**, 014028 (2005).

[14] L. Maiani, A. D. Polosa and V. Riquer, Phys. Rev. Lett. **99**, 182003 (2007).

[15] L. Maiani, A. D. Polosa and V. Riquer, arXiv:0708.3997 [hep-ph].

[16] L. Maiani, F. Piccinini, A. D. Polosa and V. Riquer, Phys. Rev. D **72**, 031502(R) (2005).

[17] S.-K. Choi *et al.* [Belle Collaboration], Phys. Rev. Lett. **94**, 182002 (2005).

[18] B. Aubert *et al.* [BaBar Collaboration], arXiv:0711.2047 [hep-ex].

[19] B. Aubert *et al.* [BABAR Collaboration], Phys. Rev. Lett. **95**, 142001 (2005).

[20] C. Z. Yuan *et al.* [Belle Collaboration], Phys. Rev. Lett. **99**, 182004 (2007).

[21] R. Mizuk *et al.* [Belle Collaboration], arXiv:0806.4098 [hep-ex].

[22] Q. He *et al.* [CLEO Collaboration], Phys. Rev. D **74**, 091104 (2006).

[23] X. L. Wang *et al.* [Belle Collaboration], Phys. Rev. Lett. **99**, 142002 (2007).

[24] B. Aubert *et al.* [BABAR Collaboration], Phys. Rev. Lett. **98**, 212001 (2007).

[25] K. Abe *et al.* [Belle Collaboration], Phys. Rev. Lett. **100**, 142001 (2008).

[26] G. Pakhlova *et al.* [Belle Collaboration], arXiv:0807.4458 [hep-ex].

Heavy Baryons in the Relativistic Quark Model

D. Ebert[1], R. N. Faustov[2], V. O. Galkin[2]

[1]Institut für Physik, Humboldt–Universität zu Berlin, Newtonstr. 15, D-12489 Berlin, Germany
[2]Dorodnicyn Computing Centre, Russian Academy of Sciences, Vavilov Str. 40, 119991 Moscow, Russia

The masses of the ground state and excited heavy baryons consisting of two light (u, d, s) and one heavy (c, b) quarks are calculated. The heavy-quark–light-diquark picture is used within the relativistic quark model. The semileptonic heavy-to-heavy decay rates of these baryons are also calculated both in the heavy quark limit and with inclusion of first order $1/m_Q$ corrections. An overall good agreement of the obtained predictions with available experimental data is found.

During last few years a significant experimental progress has been achieved in studying heavy baryons with one heavy quark. At present masses of all ground states of charmed baryons as well as of their excitations are known experimentally with rather good precision [1]. The bottom sector is significantly less studied. Only half of the ground state bottom baryon masses are known now. The rate of the semileptonic decay $\Lambda_b \to \Lambda_c e\nu$ has been also measured. The Large Hadron Collider (LHC) will provide us with much more data on properties of ground state and excited bottom baryons. Here we review our studies of masses of the ground state and excited heavy baryons containing one heavy quark and their semileptonic decays. All calculations [2, 3, 4] were performed in the framework of the relativistic quark model based on the quasipotential approach in QCD. We used the heavy-quark–light-diquark approximation to reduce a complicated relativistic three-body problem to the subsequent solution of two more simple two-body problems. The first step is the calculation of the masses, wave functions and form factors of the diquarks, composed from two light quarks. Next, at the second step, a heavy baryon is treated as a relativistic bound system of a light diquark and heavy quark. It is important to emphasize that we do not consider a diquark as a point particle but explicitly take into account its structure through the diquark-gluon vertex expressed in terms of the diquark wave functions.

In the adopted approach the diquark is described by the wave function (Ψ_d) of the two-quark bound state and the baryon is described by the wave function (Ψ_B) of the quark-diquark bound state, satisfying the quasipotential equations of the Schrödinger type

$$\left(\frac{b^2(M)}{2\mu_R} - \frac{\mathbf{p}^2}{2\mu_R}\right)\Psi_{d,B}(\mathbf{p}) = \int \frac{d^3q}{(2\pi)^3} V_{d,B}(\mathbf{p}, \mathbf{q}; M)\Psi_{d,B}(\mathbf{q}), \qquad (1)$$

where the relativistic reduced mass is

$$\mu_R = \frac{M^4 - (m_1^2 - m_2^2)^2}{4M^3}, \qquad (2)$$

and the on-mass-shell relative momentum squared

$$b^2(M) = \frac{[M^2 - (m_1 + m_2)^2][M^2 - (m_1 - m_2)^2]}{4M^2}. \qquad (3)$$

Table 1: Masses of light ground state diquarks (in MeV). S and A denotes scalar and axial vector diquarks antisymmetric $[q, q']$ and symmetric $\{q, q'\}$ in flavour, respectively.

Quark content	Diquark type	Mass				
		[2] our	[7] NJL	[8] BSE	[9] BSE	[10] Lattice
$[u, d]$	S	710	705	737	820	694(22)
$\{u, d\}$	A	909	875	949	1020	806(50)
$[u, s]$	S	948	895	882	1100	
$\{u, s\}$	A	1069	1050	1050	1300	
$\{s, s\}$	A	1203	1215	1130	1440	

The kernel $V_{d,B}(\mathbf{p}, \mathbf{q}; M)$ in Eq. (1) is the QCD motivated operator of the quark-quark (d) or quark-diquark (B) interaction. It is constructed with the help of the off-mass-shell scattering amplitude, projected onto the positive energy states. In the following analysis we closely follow the similar construction of the quark-antiquark interaction in mesons which were extensively studied in our relativistic quark model [5]. For the quark-quark interaction in a diquark we use the relation $V_{qq} = V_{q\bar{q}}/2$ arising under the assumption about the octet structure of the colour quark interaction. An important role in this construction is played by the Lorentz-structure of the nonperturbative confining interaction. In our analysis of mesons we adopted that the effective quark-antiquark interaction is the sum of the one-gluon exchange term and the mixture of long-range vector and scalar linear confining potentials with the vector confining potential containing the Pauli term. We use the same conventions for the construction of the quark-quark and quark-diquark interactions in the baryon. The explicit expressions for the quasipotential of the quark-quark (qq) interaction in the diquark and quark-diquark (Qd) interaction in the baryon are given in Refs. [2, 3]. The values of model parameters can be also found in these references.

At the first step, we calculate the masses and form factors of the light diquark. As it is well-known, the light quarks are highly relativistic, which makes the v/c expansion inapplicable and thus, a completely relativistic treatment is required. To achieve this goal in describing light diquarks, we closely follow our recent consideration of the spectra of light mesons [6] and adopt the same procedure to make the relativistic quark potential local by replacing $\epsilon_{1,2}(p) = \sqrt{m_{1,2}^2 + \mathbf{p}^2} \to E_{1,2} = (M^2 - m_{2,1}^2 + m_{1,2}^2)/(2M)$ (see discussion in Ref. [6]).

The quasipotential equation (1) is solved numerically for the complete relativistic potential which depends on the diquark mass in a highly nonlinear way [2]. The obtained ground state masses of scalar and axial vector light diquarks are presented in Table 1. These masses are in good agreement with values found within the Nambu–Jona-Lasinio model [7], by solving the Bethe-Salpeter equation with different types of the kernel [8, 9] and in quenched lattice calculations [10]. It follows from Table 1 that the difference between the scalar and vector diquark masses decreases from ~ 200 to ~ 120 MeV, when one of the u, d quarks is replaced by the s quark in accord with the statement of Ref. [11].

In order to determine the diquark interaction with the gluon field, which takes into account the diquark structure, it is necessary to calculate the corresponding matrix element of the quark current between diquark states. Such calculation leads to the emergence of the form factor $F(r)$ entering the diquark-gluon vertex [2]. This form factor is expressed through the overlap integral of the diquark wave functions.

At the second step, we calculate the masses of heavy baryons as bound states of a heavy quark and light diquark. For the potential of the heavy-quark–light-diquark interaction we use the expansion in p/m_Q. The light diquark should be treated fully relativistically. To simplify the potential we follow the same procedure, which was used for light quarks in a diquark, and replace the diquark energies $E_d(p) = \sqrt{\mathbf{p}^2 + M_d^2}$ by $E_d = (M^2 - m_Q^2 + M_d^2)/(2M)$ in expressions for the quark-diquark quasipotential. This substitution makes the Fourier transform of the potential local. At leading order in p/m_Q the resulting quasipotentials can be presented in the following forms:
for the scalar diquark

$$V^{(0)}(r) = \hat{V}_{\mathrm{Coul}}(r) + V_{\mathrm{conf}}(r), \qquad (4)$$

and for the axial vector diquark

$$
\begin{aligned}
V^{(0)}(r) &= \hat{V}_{\mathrm{Coul}}(r) + V_{\mathrm{conf}}(r) + \frac{1}{M_d(E_d + M_d)}\frac{1}{r}\left[\frac{M_d}{E_d}\hat{V}'_{\mathrm{Coul}}(r)\right.\\
&\left.- V'_{\mathrm{conf}}(r) + \mu_d\frac{E_d + M_d}{2M_d}V'^V_{\mathrm{conf}}(r)\right]\mathbf{LS}_d,
\end{aligned}
\qquad (5)
$$

$$\hat{V}_{\mathrm{Coul}}(r) = -\frac{4}{3}\alpha_s\frac{F(r)}{r}, \qquad V_{\mathrm{conf}}(r) = Ar + B, \qquad V^V_{\mathrm{conf}}(r) = (1 - \varepsilon)(Ar + B),$$

where $\hat{V}_{\mathrm{Coul}}(r)$ is the smeared Coulomb potential (with the account of the diquark structure). Note that both the one-gluon exchange and confining potentials contribute to the diquark spin-orbit interaction. In the heavy quark limit the heavy baryon levels are degenerate doublets with respect to the heavy quark spin, since the heavy quark spin-orbit and spin-spin interactions arise only at first order in p/m_Q. Solving Eq. (1) numerically we get the heavy quark spin-independent part of the baryon wave function Ψ_B. Then the total baryon wave function is a product of Ψ_B and the spin-dependent part U_B [12].

The leading order degeneracy of heavy baryon states is broken by the p/m_Q corrections. The explicit expression for the quark-diquark potential up to the second order in p/m_Q is given in Ref. [3].

The calculated values of the ground state and excited baryon masses are given in Tables 2-5 in comparison with available experimental data. In the first two columns we put the baryon quantum numbers and the state of the heavy-quark–light-diquark bound system (in usual notations nL), while in the rest columns our predictions for the masses and experimental data are shown.

At present the best experimentally studied quantities are the mass spectra of the Λ_Q and Σ_Q baryons, which contain the light scalar or axial vector diquarks, respectively. They are presented in Tables 2, 3. Masses of the ground states are measured both for charmed and bottom Λ_Q and Σ_Q baryons. Recently the masses of the ground state Σ_b and Σ_b^* baryons were first reported by CDF [16]: $M_{\Sigma_b^+} = 5807.5^{+1.9}_{-2.2} \pm 1.7$ MeV, $M_{\Sigma_b^-} = 5815.2^{+1.0}_{-0.9} \pm 1.7$ MeV, $M_{\Sigma_b^{*+}} = 5829.0^{+1.6}_{-1.7} \pm 1.7$ MeV, $M_{\Sigma_b^{*-}} = 5836.7^{+2.0}_{-1.8} \pm 1.7$ MeV. CDF also significantly improved the precision of the Λ_b mass [13]. For charmed baryons the masses of several excited states are also known. It is important to emphasize that the J^P quantum numbers for most excited heavy baryons have not been determined experimentally, but are assigned by PDG on the basis of quark model predictions. For some excited charm baryons such as the $\Lambda_c(2765)$,

Table 2: Masses of the Λ_Q ($Q = c, b$) heavy baryons (in MeV).

$I(J^P)$	Qd state	$Q = c$		$Q = b$		
		M	M^{exp} [1]	M	M^{exp} [1]	M^{exp} [13]
$0(\frac{1}{2}^+)$	$1S$	2297	2286.46(14)	5622	5624(9)	5619.7(2.4)
$0(\frac{1}{2}^-)$	$1P$	2598	2595.4(6)	5930		
$0(\frac{3}{2}^-)$	$1P$	2628	2628.1(6)	5947		
$0(\frac{1}{2}^+)$	$2S$	2772	2766.6(2.4)?	6086		
$0(\frac{3}{2}^+)$	$1D$	2874		6189		
$0(\frac{5}{2}^+)$	$1D$	2883	2882.5(2.2)?	6197		
$0(\frac{1}{2}^-)$	$2P$	3017		6328		
$0(\frac{3}{2}^-)$	$2P$	3034		6337		

$\Lambda_c(2880)$ and $\Lambda_c(2940)$ it is even not known if they are excitations of the Λ_c or Σ_c. [1] Our calculations show that the $\Lambda_c(2765)$ can be either the first radial ($2S$) excitation of the Λ_c with $J^P = \frac{1}{2}^+$ containing the light scalar diquark or the first orbital excitation ($1P$) of the Σ_c with $J^P = \frac{3}{2}^-$ containing the light axial vector diquark. The $\Lambda_c(2880)$ baryon in our model is well described by the second orbital ($1D$) excitation of the Λ_c with $J^P = \frac{5}{2}^+$ in agreement with the recent spin assignment [15] based on the analysis of angular distributions in the decays $\Lambda_c(2880)^+ \to \Sigma_c(2455)^{0,++}\pi^{+,-}$. Our model suggests that the charmed baryon $\Lambda_c(2940)$, recently discovered by BaBar[14] and then also confirmed by Belle [15], could be the first radial ($2S$) excitation of the Σ_c with $J^P = \frac{3}{2}^+$ which mass is predicted slightly below the experimental value. If this state proves to be an excited Λ_c, for which we have no candidates around 2940 MeV, then it will indicate that excitations inside the diquark should be also considered. [2] The $\Sigma_c(2800)$ baryon can be identified in our model with one of the orbital ($1P$) excitations of the Σ_c with $J^P = \frac{1}{2}^-, \frac{3}{2}^-$ or $\frac{5}{2}^-$ which predicted mass differences are less than 15 MeV. Thus masses of all these states are compatible with the experimental values within errors.

Mass spectra of the Ξ_Q baryons with the scalar and axial vector light (qs) diquarks are given in Tables 4, 5. Experimental data here until recently were available only for charm-strange baryons. In 2007 the D0 Collaboration [18] reported the discovery of the Ξ_b^- baryon with the mass $M_{\Xi_b} = 5774 \pm 11 \pm 15$ MeV. The CDF Collaboration [19] confirmed this observation and gave the more precise value $M_{\Xi_b} = 5792.9 \pm 2.5 \pm 1.7$ MeV. Our model prediction $M_{\Xi_b} = 5812$ MeV is in a reasonable agreement with these new data. In the excited charmed baryon sector we can identify the $\Xi_c(2790)$ and $\Xi_c(2815)$ with the first orbital ($1P$) excitations of the Ξ_c with $J^P = \frac{1}{2}^-$ and $J^P = \frac{3}{2}^-$, respectively, containing the light scalar diquark, which is in agreement with the PDG [1] assignment. Recently Belle [20] reported the first observation of two baryons $\Xi_c(2980)$ and $\Xi_c(3077)$, which existence was also confirmed by BaBar [21]. The $\Xi_c(2980)$ can be interpreted in our model as the first radial ($2S$) excitation of the Ξ_c with $J^P = \frac{1}{2}^+$ containing the light axial vector diquark. On the other hand the $\Xi_c(3077)$ corresponds to the second orbital ($1D$) excitation in this system with $J^P = \frac{5}{2}^+$. Very recently the BaBar Collaboration [17] announced observation of two new charmed baryons $\Xi_c(3055)$ with the mass

---

[1]In Tables 2, 3 we mark with ? the states which interpretation is ambiguous.

[2]The Λ_c baryon with the first orbital excitation of the diquark is expected to have a mass in this region.

Table 3: Masses of the Σ_Q $(Q=c,b)$ heavy baryons (in MeV).

$I(J^P)$	Qd state	$Q=c$				$Q=b$		
		M	$M^{\exp}$ [1]	$M^{\exp}$ [14]	$M^{\exp}$ [15]	M	$M^{\exp}$ [16]	$M^{\exp}$ [16]
$1(\frac{1}{2}^+)$	$1S$	2439	2453.76(18)			5805	5807.5(2.6)	5815.2(2.0)
$1(\frac{3}{2}^+)$	$1S$	2518	2518.0(5)			5834	5829.0(2.4)	5836.7(2.6)
$1(\frac{1}{2}^-)$	$1P$	2805				6122		
$1(\frac{1}{2}^-)$	$1P$	2795				6108		
$1(\frac{3}{2}^-)$	$1P$	2799	2802($\frac{4}{7}$)			6106		
$1(\frac{3}{2}^-)$	$1P$	2761	2766.6(2.4)?			6076		
$1(\frac{5}{2}^-)$	$1P$	2790				6083		
$1(\frac{1}{2}^+)$	$2S$	2864		2846(13)		6202		
$1(\frac{3}{2}^+)$	$2S$	2912		2939.8(2.3)?	2938($\frac{3}{5}$)?	6222		
$1(\frac{1}{2}^+)$	$1D$	3014				6300		
$1(\frac{3}{2}^+)$	$1D$	3005				6287		
$1(\frac{3}{2}^+)$	$1D$	3010				6291		
$1(\frac{5}{2}^+)$	$1D$	3001				6279		
$1(\frac{5}{2}^+)$	$1D$	2960				6248		
$1(\frac{7}{2}^+)$	$1D$	3015				6262		

$M = 3054.2 \pm 1.2 \pm 0.5$ MeV and $\Xi_c(3123)$ with the mass $M = 3122.9 \pm 1.3 \pm 0.3$ MeV. These states can be interpreted in our model as the second orbital ($1D$) excitations of the Ξ_c with $J^P = \frac{5}{2}^+$ containing scalar and axial vector diquarks, respectively. Their predicted masses are 3042 MeV and 3123 MeV.

For the Ω_Q baryons only masses of the ground-state charmed baryons are known. The Ω_c^* baryon was recently discovered by BaBar [22]. The measured mass difference of the Ω_c^* and Ω_c baryons of $(70.8 \pm 1.0 \pm 1.1)$ MeV is in very good agreement with the prediction of our model 70 MeV [2].

The detailed comparison of our predictions for the heavy baryon mass spectra with results of other calculations can be found in Refs. [2, 3].

In order to calculate the exclusive semileptonic decay rate of the heavy baryon, it is necessary to determine the corresponding matrix element of the weak current between baryon states. In the quasipotential approach, the matrix element of the weak current $J_\mu^W = \bar{Q}'\gamma_\mu(1 - \gamma_5)Q$, associated with the heavy-to-heavy quark $Q \to Q'$ $(Q = b$ and $Q' = c)$ transition, between baryon states with masses M_{B_Q}, $M_{B_{Q'}}$ and momenta p_{B_Q}, $p_{B_{Q'}}$ has the form

$$\langle B_{Q'}(p_{B_{Q'}})|J_\mu^W|B_Q(p_{B_Q})\rangle = \int \frac{d^3p\, d^3q}{(2\pi)^6} \bar{\Psi}_{B_{Q'}\,\mathbf{p}_{B_{Q'}}}(\mathbf{p})\Gamma_\mu(\mathbf{p},\mathbf{q})\Psi_{B_Q\,\mathbf{p}_{B_Q}}(\mathbf{q}), \qquad (6)$$

where $\Gamma_\mu(\mathbf{p},\mathbf{q})$ is the two-particle vertex function and $\Psi_{B\,\mathbf{p}_B}$ are the baryon $(B = B_Q, B_{Q'})$ wave functions projected onto the positive energy states of quarks and boosted to the moving reference frame with momentum $\mathbf{p}_B$.

The wave function of the moving baryon $\Psi_{B_{Q'}\,\boldsymbol{\Delta}}$ is connected with the wave function in the

Table 4: Masses of the Ξ_Q $(Q = c, b)$ heavy baryons with scalar diquark (in MeV).

$I(J^P)$	Qd state	$Q = c$			$Q = b$	
		M	$M^{\exp}$ [1]	$M^{\exp}$ [17]	M	$M^{\exp}$[19]
$\frac{1}{2}(\frac{1}{2}^+)$	$1S$	2481	2471.0(4)		5812	5792.9(3.0)
$\frac{1}{2}(\frac{1}{2}^-)$	$1P$	2801	2791.9(3.3)		6119	
$\frac{1}{2}(\frac{3}{2}^-)$	$1P$	2820	2818.2(2.1)		6130	
$\frac{1}{2}(\frac{1}{2}^+)$	$2S$	2923			6264	
$\frac{1}{2}(\frac{3}{2}^+)$	$1D$	3030			6359	
$\frac{1}{2}(\frac{5}{2}^+)$	$1D$	3042		3054.2(1.5)	6365	
$\frac{1}{2}(\frac{1}{2}^-)$	$2P$	3186			6492	
$\frac{1}{2}(\frac{3}{2}^-)$	$2P$	3199			6494	

rest frame ($\boldsymbol{\Delta} = 0$) $\Psi_{B_{Q'}, \mathbf{0}} \equiv \Psi_{B_{Q'}}$ by the transformation

$$\Psi_{B_{Q'} \boldsymbol{\Delta}}(\mathbf{p}) = D_{Q'}^{1/2}(R_{L_{\boldsymbol{\Delta}}}^W) D_d^{\mathcal{I}}(R_{L_{\boldsymbol{\Delta}}}^W) \Psi_{B_{Q'}, \mathbf{0}}(\mathbf{p}), \qquad \mathcal{I} = 0, 1, \tag{7}$$

where R^W is the Wigner rotation, $L_{\boldsymbol{\Delta}}$ is the Lorentz boost from the baryon rest frame to a moving one, $D^{1/2}(R)$ and $D^{\mathcal{I}}(R)$ are rotation matrices of the heavy quark and light diquark spins, respectively.

The hadronic matrix elements for the semileptonic decay $\Lambda_Q \to \Lambda_{Q'}$ are parameterized in terms of six invariant form factors:

$$\langle \Lambda_{Q'}(v', s')|V^\mu|\Lambda_Q(v, s)\rangle = \bar{u}_{\Lambda_{Q'}}(v', s')\Big[F_1(w)\gamma^\mu + F_2(w)v^\mu + F_3(w)v'^\mu\Big]u_{\Lambda_Q}(v, s),$$

$$\langle \Lambda_{Q'}(v', s')|A^\mu|\Lambda_Q(v, s)\rangle = \bar{u}_{\Lambda_{Q'}}(v', s')\Big[G_1(w)\gamma^\mu + G_2(w)v^\mu + G_3(w)v'^\mu\Big]\gamma_5 u_{\Lambda_Q}(v, s), \quad \text{(8)}$$

where $u_{\Lambda_Q}(v, s)$ and $u_{\Lambda_{Q'}}(v', s')$ are Dirac spinors of the initial and final baryon with four-velocities v and v', respectively; $q = M_{\Lambda_{Q'}} v' - M_{\Lambda_Q} v$, and $w = v \cdot v'$. In the heavy quark limit $m_Q \to \infty$ $(Q = b, c)$ the form factors (8) can be expressed through the single Isgur-Wise function $\zeta(w)$ [23]

$$F_1(w) = G_1(w) = \zeta(w); \quad F_2(w) = F_3(w) = G_2(w) = G_3(w) = 0. \tag{9}$$

At subleading order of the heavy quark expansion two additional types of contributions arise [24]. The first one parameterizes $1/m_Q$ corrections to the heavy quark effective theory (HQET) current and is proportional to the product of the parameter $\bar{\Lambda} = M_{\Lambda_Q} - m_Q$, which is the difference of the baryon and heavy quark masses in the infinitely heavy quark limit, and the leading order Isgur-Wise function $\zeta(w)$. The second one comes from the kinetic energy term in $1/m_Q$ correction to the HQET Lagrangian and introduces the additional function $\chi(w)$. Therefore the form factors are given by [24]

$$F_1(w) = \zeta(w) + \left(\frac{\bar{\Lambda}}{2m_Q} + \frac{\bar{\Lambda}}{2m_{Q'}}\right)[2\chi(w) + \zeta(w)],$$

$$G_1(w) = \zeta(w) + \left(\frac{\bar{\Lambda}}{2m_Q} + \frac{\bar{\Lambda}}{2m_{Q'}}\right)\left[2\chi(w) + \frac{w-1}{w+1}\zeta(w)\right],$$

Table 5: Masses of the Ξ_Q ($Q = c, b$) heavy baryons with axial vector diquark (in MeV).

$I(J^P)$	Qd state	M	M^{exp} [1]	M^{exp} [20]	M^{exp} [21, 17]	M
			$Q = c$			$Q = b$
$\frac{1}{2}(\frac{1}{2}^+)$	$1S$	2578	2578.0(2.9)			5937
$\frac{1}{2}(\frac{3}{2}^+)$	$1S$	2654	2646.1(1.2)			5963
$\frac{1}{2}(\frac{1}{2}^-)$	$1P$	2934				6249
$\frac{1}{2}(\frac{1}{2}^-)$	$1P$	2928				6238
$\frac{1}{2}(\frac{3}{2}^-)$	$1P$	2931			2931(6)	6237
$\frac{1}{2}(\frac{3}{2}^-)$	$1P$	2900				6212
$\frac{1}{2}(\frac{5}{2}^-)$	$1P$	2921				6218
$\frac{1}{2}(\frac{1}{2}^+)$	$2S$	2984		2978.5(4.1)	2967.1(2.9)	6327
$\frac{1}{2}(\frac{3}{2}^+)$	$2S$	3035				6341
$\frac{1}{2}(\frac{1}{2}^+)$	$1D$	3132				6420
$\frac{1}{2}(\frac{3}{2}^+)$	$1D$	3127				6410
$\frac{1}{2}(\frac{3}{2}^+)$	$1D$	3131				6412
$\frac{1}{2}(\frac{5}{2}^+)$	$1D$	3123			3122.9(1.4)	6403
$\frac{1}{2}(\frac{5}{2}^+)$	$1D$	3087		3082.8(3.3)	3076.4(1.0)	6377
$\frac{1}{2}(\frac{7}{2}^+)$	$1D$	3136				6390

$$\begin{aligned}
F_2(w) &= G_2(w) = -\frac{\bar{\Lambda}}{2m_{Q'}}\frac{2}{w+1}\zeta(w), \\
F_3(w) &= -G_3(w) = -\frac{\bar{\Lambda}}{2m_Q}\frac{2}{w+1}\zeta(w).
\end{aligned} \tag{10}$$

In our model we obtain the following expressions for the semileptonic decay $\Lambda_Q \to \Lambda_{Q'}$ form factors up to subleading order in $1/m_Q$

$$\begin{aligned}
F_1(w) &= \zeta(w) + \left(\frac{\bar{\Lambda}}{2m_Q} + \frac{\bar{\Lambda}}{2m_{Q'}}\right)[2\chi(w) + \zeta(w)] \\
&\quad + 4(1-\varepsilon)(1+\kappa)\left[\frac{\bar{\Lambda}}{2m_{Q'}}\frac{1}{w-1} - \frac{\bar{\Lambda}}{2m_Q}(w+1)\right]\chi(w), \\
G_1(w) &= \zeta(w) + \left(\frac{\bar{\Lambda}}{2m_Q} + \frac{\bar{\Lambda}}{2m_{Q'}}\right)\left[2\chi(w) + \frac{w-1}{w+1}\zeta(w)\right] \\
&\quad - 4(1-\varepsilon)(1+\kappa)\frac{\bar{\Lambda}}{2m_Q}w\chi(w), \\
F_2(w) &= -\frac{\bar{\Lambda}}{2m_{Q'}}\frac{2}{w+1}\zeta(w) \\
&\quad - 4(1-\varepsilon)(1+\kappa)\left[\frac{\bar{\Lambda}}{2m_{Q'}}\frac{1}{w-1} + \frac{\bar{\Lambda}}{2m_Q}w\right]\chi(w), \\
G_2(w) &= -\frac{\bar{\Lambda}}{2m_{Q'}}\frac{2}{w+1}\zeta(w) - 4(1-\varepsilon)(1+\kappa)\frac{\bar{\Lambda}}{2m_{Q'}}\frac{1}{w-1}\chi(w), \\
F_3(w) &= -G_3(w) = -\frac{\bar{\Lambda}}{2m_Q}\frac{2}{w+1}\zeta(w) + 4(1-\varepsilon)(1+\kappa)\frac{\bar{\Lambda}}{2m_Q}\chi(w),
\end{aligned} \tag{11}$$

where the leading order Isgur-Wise function of heavy baryons

$$\zeta(w) = \lim_{m_Q \to \infty} \int \frac{d^3p}{(2\pi)^3} \Psi_{\Lambda_{Q'}} \left(\mathbf{p} + 2\epsilon_d(p)\sqrt{\frac{w-1}{w+1}} \ \mathbf{e_\Delta} \right) \Psi_{\Lambda_Q}(\mathbf{p}), \tag{12}$$

and the subleading function

$$\chi(w) = -\frac{w-1}{w+1} \lim_{m_Q \to \infty} \int \frac{d^3p}{(2\pi)^3} \Psi_{\Lambda_{Q'}} \left(\mathbf{p} + 2\epsilon_d(p)\sqrt{\frac{w-1}{w+1}} \ \mathbf{e_\Delta} \right) \frac{\bar{\Lambda} - \epsilon_d(p)}{2\bar{\Lambda}} \Psi_{\Lambda_Q}(\mathbf{p}), \tag{13}$$

here $\mathbf{e_\Delta} = \mathbf{\Delta}/\sqrt{\mathbf{\Delta^2}}$ is the unit vector in the direction of $\mathbf{\Delta} = M_{\Lambda_{Q'}} \mathbf{v}' - M_{\Lambda_Q} \mathbf{v}$. It is important to note that in our model the expressions for the Isgur-Wise functions $\zeta(w)$ (12) and $\chi(w)$ (13) are determined in the whole kinematic range accessible in the semileptonic decays in terms of the overlap integrals of the heavy baryon wave functions, which are known from the baryon mass spectrum calculations. Therefore we do not need to make any assumptions about the baryon wave functions or/and to extrapolate our form factors from the single kinematic point, as it was done in most of previous calculations.

For $(1 - \varepsilon)(1 + \kappa) = 0$ the HQET results (10) are reproduced. This can be achieved either setting $\varepsilon = 1$ (pure scalar confinement) or $\kappa = -1$. In our model we need a vector confining contribution and therefore use the latter option. This consideration gives us an additional justification, based on the HQET, for fixing one of the main parameters of the model κ. In the heavy quark limit the wave functions of the initial Ψ_{Λ_Q} and final baryon $\Psi_{\Lambda_{Q'}}$ coincide, and thus the HQET normalization condition $\zeta(1) = 1$ is exactly reproduced. The subleading function $\chi(w)$ vanishes for $w = 1$. The function $\chi(w)$ is very small in the whole accessible kinematic range, since it is roughly proportional to the ratio of the heavy baryon binding energy to the baryon mass.

The $\Lambda_b \to \Lambda_c$ differential decay rate at zero recoil ($w = 1$) [24]:

$$\lim_{w \to 1} \frac{1}{\sqrt{w^2 - 1}} \frac{d\Gamma(\Lambda_b \to \Lambda_c e\nu)}{dw} = \frac{G_F^2 |V_{cb}|^2}{4\pi^3} M_{\Lambda_c}^3 (M_{\Lambda_b} - M_{\Lambda_c})^2 |G_1(1)|^2 \tag{14}$$

is governed by the square of the axial current form factor G_1, which near this point has the following expansion

$$G_1(w) = 1 - \hat{\rho}^2(w - 1) + \hat{c}(w - 1)^2 + \cdots, \tag{15}$$

where in our model with the inclusion of the first order heavy quark corrections (11)

$$\hat{\rho}^2 = 1.51, \qquad \text{and} \qquad \hat{c} = 2.03.$$

This value of the slope parameter of the Λ_b-baryon decay form factor is in agreement with the recent experimental value obtained by the DELPHI Collaboration [25]

$$\hat{\rho}^2 = 2.03 \pm 0.46^{+0.72}_{-1.00}$$

and lattice QCD [26] estimate

$$\hat{\rho}^2 = 1.1 \pm 1.0.$$

Our prediction for the branching ratio of the semileptonic decay $\Lambda_b \to \Lambda_c e\nu$ for $|V_{cb}| = 0.041$ and $\tau_{\Lambda_b} = 1.23 \times 10^{-12}$s [1]

$$Br^{\text{theor}}(\Lambda_b \to \Lambda_c l\nu) = 6.9\%$$

Table 6: Comparison of different theoretical predictions for semileptonic decay rates Γ (in $10^{10} \mathrm{s}^{-1}$) of bottom baryons.

Decay	this work	[27]	[28]	[29]	[30]	[31]	[32]	[33]	[34]
$\Lambda_b \to \Lambda_c e\nu$	5.64	5.9	5.1	5.14	5.39	6.09	5.08 ± 1.3	5.82	5.4 ± 0.4
$\Xi_b \to \Xi_c e\nu$	5.29	7.2	5.3	5.21	5.27	6.42	5.68 ± 1.5	4.98	
$\Sigma_b \to \Sigma_c e\nu$	1.44	4.3			2.23	1.65			
$\Xi'_b \to \Xi'_c e\nu$	1.34								
$\Omega_b \to \Omega_c e\nu$	1.29	5.4	2.3	1.52	1.87	1.81			
$\Sigma_b \to \Sigma_c^* e\nu$	3.23				4.56	3.75			
$\Xi'_b \to \Xi_c^* e\nu$	3.09								
$\Omega_b \to \Omega_c^* e\nu$	3.03			3.41	4.01	4.13			

is in agreement with available experimental data

$$Br^{\exp}(\Lambda_b \to \Lambda_c l\nu) = \left\{ \begin{array}{ll} \left(5.0^{+1.1+1.6}_{-0.8-1.2}\right)\% & \text{DELPHI [23]} \\ \left(8.1 \pm 1.2^{+1.1}_{-1.6} \pm 4.3\right)\% & \text{CDF [25]} \end{array} \right. \tag{16}$$

and the PDG branching ratio [1]

$$Br^{\exp}(\Lambda_b \to \Lambda_c l\nu + \text{anything}) = (9.1 \pm 2.1)\%. \tag{17}$$

The comparison of our model predictions with other theoretical calculations [27, 28, 29, 30, 31, 32, 33, 34] is given in Table 6. In nonrelativistic quark models [27, 28, 29] form factors of the heavy baryon decays are evaluated at the single kinematic point of zero recoil and then different form factor parameterizations (pole, dipole) are used for decay rate calculations. The relativistic three-quark model [30], Bethe-Salpeter model [31] and light-front constituent quark model [32] assume Gaussian wave functions for heavy baryons. The nonrelativistic quark model [33] uses for the form factor evaluations the set of variational wave functions, obtained from baryon spectra calculations without employing the quark-diquark approximation. Finally, Ref. [34] presents the recent QCD sum rule prediction. Calculations of Refs. [29, 30, 31] are done in the heavy quark limit only, while the rest include first order $1/m_Q$ corrections for the decays of Λ-type baryons. From Table 6 we see that all theoretical models give close predictions for the semileptonic decays of heavy baryons with scalar diquark ($\Lambda_b \to \Lambda_c e\nu$ and $\Xi_b \to \Xi_c e\nu$), which are consistent with the available experimental data (16) and (17) for the $\Lambda_b \to \Lambda_c e\nu$ semileptonic decay. Thus one can conclude that the precise measurement of the semileptonic $\Lambda_b \to \Lambda_c e\nu$ decay rate will allow an accurate determination of the CKM matrix element V_{cb} with small theoretical uncertainties.

All predictions for heavy baryon decays with the axial vector diquark listed in Table 6 were obtained in the heavy quark limit. Here the differences between predictions are larger. The nonrelativistic quark model [27] gives for these decay rates the values more than two times larger than other estimates. Our model values for these decay rates are the lowest ones. Among the relativistic quark models the closest to our predictions are given in [31]. Unfortunately, it will be difficult to measure such decays experimentally. Only Ω_b will decay predominantly weakly and thus has sizable semileptonic branching ratios, since a scalar ss diquark is forbidden by the Pauli principle. All other baryons with the axial vector diquark will decay predominantly strongly or electromagnetically and thus their weak branching ratios will be very small.

In summary, we find that all presently available experimental data for the masses of the ground state and excited heavy baryons can be accommodated in the picture treating a heavy baryon as the composite system of the light diquark and heavy quark, experiencing orbital and radial excitations only between these constituents. The data on semileptonic decays of heavy baryons are also well described in this approach.

References

[1] C. Amsler *et al.* [Particle Data Group], Phys. Lett. B **667**, 1 (2008).

[2] D. Ebert, R. N. Faustov and V. O. Galkin, Phys. Rev. D **72**, 034026 (2005).

[3] D. Ebert, R. N. Faustov and V. O. Galkin, Phys. Lett. B **659**, 612 (2008).

[4] D. Ebert, R. N. Faustov and V. O. Galkin, Phys. Rev. D **73**, 094002 (2006).

[5] D. Ebert, V. O. Galkin, and R. N. Faustov, Phys. Rev. D **57**, 5663 (1998); Phys. Rev. D **62**, 034014 (2000); Phys. Rev. D **67**, 014027 (2003).

[6] D. Ebert, R. N. Faustov, V. O. Galkin, Mod. Phys. Lett. A **20**, 1887 (2005); Eur. Phys. J. C **47**, 745 (2006).

[7] D. Ebert, T. Feldmann, C. Kettner, and H. Reinhardt, Z. Phys. C **71**, 329 (1996).

[8] C. J. Burden et al., Phys. Rev. C **55**, 2649 (1997).

[9] P. Maris, Few Body Syst. **32**, 41 (2002).

[10] M. Hess et al., Phys. Rev. D **58**, 111502 (1998).

[11] R. L. Jaffe, Phys. Rep. **409**, 1 (2005).

[12] D. Ebert, R. N. Faustov, V. O. Galkin, and A. P. Martynenko, Phys. Rev. D **70**, 014018 (2004); Phys. Rev. D **66**, 014008 (2002).

[13] D. Acosta *et al.* [CDF Collaboration], Phys. Rev. Lett. **96**, 202001 (2006).

[14] B. Aubert *et al.* [BABAR Collaboration], Phys. Rev. Lett. **98**, 012001 (2007).

[15] R. Mizuk *et al.* [BELLE Collaboration], arXiv:hep-ex/0608043.

[16] I. V. Gorelov [CDF Collaboration], arXiv:hep-ex/0701056.

[17] B. Aubert *et al.* [BaBar Collaboration], arXiv:0710.5763 [hep-ex].

[18] V. M. Abazov *et al.* [D0 Collaboration], Phys. Rev. Lett. **99**, 052001 (2007).

[19] T. Aaltonen *et al.* [CDF Collaboration], Phys. Rev. Lett. **99**, 052002 (2007).

[20] R. Chistov *et al.* [BELLE Collaboration], Phys. Rev. Lett. **97**, 162001 (2006).

[21] B. Aubert *et al.* [BABAR Collaboration], arXiv:hep-ex/0607042.

[22] B. Aubert *et al.* [BaBar Collaboration], Phys. Rev. Lett. **97**, 232001 (2006).

[23] N. Isgur and M. B. Wise, Nucl. Phys. B **348**, 276 (1991).

[24] M. Neubert, Phys. Rep. **245**, 259 (1994); A. Falk and M. Neubert, Phys. Rev. D **47**, 2982 (1993).

[25] J. Abdallah et al. [DELPHI Collaboration], Phys. Lett. B **585**, 63 (2004).

[26] K. C. Bowler et al., Phys. Rev. D **57**, 6948 (1998).

[27] R. Singleton, Jr., Phys. Rev. D **43**, 2939 (1991).

[28] H.-Y. Cheng and B. Tseng, Phys. Rev. D **53**, 1457 (1996).

[29] J. G. Körner, M. Krämer and D. Pirjol, Prog. Part. Nucl. Phys. **33**, 787 (1994).

[30] M. A. Ivanov, V. E. Lyubovitskij, J. G. Körner and P. Kroll, Phys. Rev. D **56**, 348 (1997).

[31] M. A. Ivanov, J. G. Körner, V. E. Lyubovitskij and A. G. Rusetsky, Phys. Rev. D **59**, 074016 (1999).

[32] F. Cardarelli and S. Simula, Phys. Rev. D **60**, 074018 (1999).

[33] C. Albertus, E. Hernández and J. Nieves, Phys. Rev. D **71**, 014012 (2005).

[34] M.-Q. Huang, H.-Y. Jin, J. G. Körner and C. Liu, Phys. Lett. B **629**, 27 (2005).

Heavy-quark contributions to the ratio F_L/F_2 at low values of the Bjorken variable x

A.Yu. Illarionov[1], B.A. Kniehl[2], A.V. Kotikov[3]

[1]SISSA, via Beirut, 2-4, 34014 Trieste and INFN, Sezione di Trieste, Trieste, Italy
[2]II. Institut für Theoretische Physik, Universität Hamburg, 22761 Hamburg, Germany
[3]BLThPh, JINR, 141980 Dubna (Moscow resion), Russia

We study the heavy-quark contributions to the proton structure functions $F_2^i(x, Q^2)$ and $F_L^i(x, Q^2)$, with $i = c, b$, for small values of Bjorken's x variable and provide compact formulas for their ratios $R_i = F_L^i/F_2^i$ that are useful to extract $F_2^i(x, Q^2)$ from measurements of the doubly differential cross section of inclusive deep-inelastic scattering at DESY HERA. Our approach naturally explains why R_i is approximately independent of x and the details of the parton distribution functions in the low-x regime.

1 Introduction

The totally inclusive cross section of deep-inelastic lepton-proton scattering (DIS) depends on the square s of the centre-of-mass energy, Bjorken's variable $x = Q^2/(2pq)$, and the inelasticity variable $y = Q^2/(xs)$, where p and q are the four-momenta of the proton and the virtual photon, respectively, and $Q^2 = -q^2 > 0$. The doubly differential cross section is parameterized in terms of the structure function F_2 and the longitudinal structure function F_L, as

$$\frac{d^2\sigma}{dx\,dy} = \frac{2\pi\alpha^2}{xQ^4}\{[1 + (1-y)^2]F_2(x, Q^2) - y^2 F_L(x, Q^2)\}, \tag{1}$$

where α is Sommerfeld's fine-structure constant. At small values of x, F_L becomes non-negligible and its contribution should be properly taken into account when the F_2 is extracted from the measured cross section. The same is true also for the contributions F_2^i and F_L^i of F_2 and F_L due to the heavy quarks $i = c, b$.

Recently, the H1 [1, 2, 3] and ZEUS [4, 5, 6] Collaborations at HERA presented new data on F_2^c and F_2^b. At small x values, of order 10^{-4}, F_2^c was found to be around 25% of F_2, which is considerably larger than what was observed by the European Muon Collaboration (EMC) at CERN [7] at larger x values, where it was only around 1% of F_2. Extensive theoretical analyses in recent years have generally served to establish that the F_2^c data can be described through the perturbative generation of charm within QCD (see, for example, the review in Ref. [8] and references cited therein).

In the framework of Dokshitzer-Gribov-Lipatov-Altarelli-Parisi (DGLAP) dynamics [9], there are two basic methods to study heavy-flavour physics. One of them [10] is based on the massless evolution of parton distribution functions (PDF) and the other one on the photon-gluon fusion (PGF) process [11]. There are also some interpolating schemes (see Ref. [12] and references cited therein). The present HERA data on F_2^c [2, 3, 5, 6] are in good agreement with the modern theoretical predictions.

In earlier HERA analyses [1, 4], F_L^c and F_L^b were taken to be zero for simplicity. Four years ago, the situation changed: in the papers [2, 3, 5, 6], the F_L^c contribution at next-to-leading order (NLO) was subtracted from the data.

In this paper, we present compact low-x approximation formulae [13] for the ratio $R_i = F_L^i/F_2^i$ at leading order (LO) and NLO, which greatly simplify the extraction of F_2^i from measurements of $d^2\sigma^{i\bar{i}}/(dx\,dy)$.

2 Parton distribution functions at small x

The standard program to study the small x behavior of quarks and gluons is carried out by comparison of the data with the numerical solution of the DGLAP equations fitting the parameters of the x profile of partons at some initial Q_0^2 and the QCD energy scale Λ (see, for instance, [14, 15]). However, in analyzing exclusively the small x region ($x \leq 0.01$), there is the alternative of doing a simpler analysis by using some of the existing analytical solutions of DGLAP in the small x limit (see [16] for review). It was done in Refs. [17]-[19], where it was pointed out that the HERA small x data can be interpreted in the so called doubled asymptotic scaling (DAS) approximation related to the asymptotic behavior of the DGLAP evolution discovered in [20] many years ago.

Here we illustrate results obtained in [18, 19]: the small x asymptotic PDF form in the framework of the DGLAP equation starting at some Q_0^2 with the flat function:

$$x f_a(x, Q_0^2) \;=\; A_a \quad (\text{hereafter } a = q, g), \tag{2}$$

where $x f_a$ are the leading-twist PDF parts and A_a are unknown parameters that have to be determined from data. We neglect the non-singlet quark component at small x.

We would like to note that HERA data [21] show a rise of F_2 at low Q^2 values ($Q^2 < 1\text{GeV}^2$) when $x \to 0$. This rise can be explained naturally by incorporation of higher-twist terms in the analysis (see [19] and Fig.1).

We shortly compile the LO results (the NLO ones may be found in [18, 19]), which are:

$$f_a(x, Q^2) \;=\; f_a^+(x, Q^2) + f_a^-(x, Q^2) \,, \tag{3}$$

$$f_g^+(x, Q^2) \;=\; \left(A_g + \frac{4}{9}A_q\right) I_0(\sigma)\, e^{-\overline{d}_+(1)s} \;+\; O(\rho) \quad, \tag{4}$$

$$f_q^+(x, Q^2) \;=\; \frac{f}{9}\left(A_g + \frac{4}{9}A_q\right)\rho\, I_1(\sigma)\, e^{-\overline{d}_+(1)s} \;+\; O(\rho)\,, \tag{5}$$

$$f_g^-(x, Q^2) \;=\; -\frac{4}{9}A_q e^{-d_-(1)s} \;+\; O(x), \tag{6}$$

$$f_q^-(x, Q^2) \;=\; A_q e^{-d_-(1)s} \;+\; O(x)\,, \tag{7}$$

where where $e = (\sum_1^f e_i^2)/f$ is the average charge square and $\overline{d}_+(1) = 1 + 20f/(27\beta_0)$ and $d_-(1) = 16f/(27\beta_0)$ are the regular parts of d_+ and d_- anomalous dimensions, respectively, in the limit $n \to 1$ [1]. The functions I_ν ($\nu = 0, 1$) are the modified Bessel functions I_ν and the

---

[1] For a quantity $k(n)$ we use the notation $\hat{k}(n)$ for the singular part when $n \to 1$ and $\overline{k}(n)$ for the corresponding regular part.
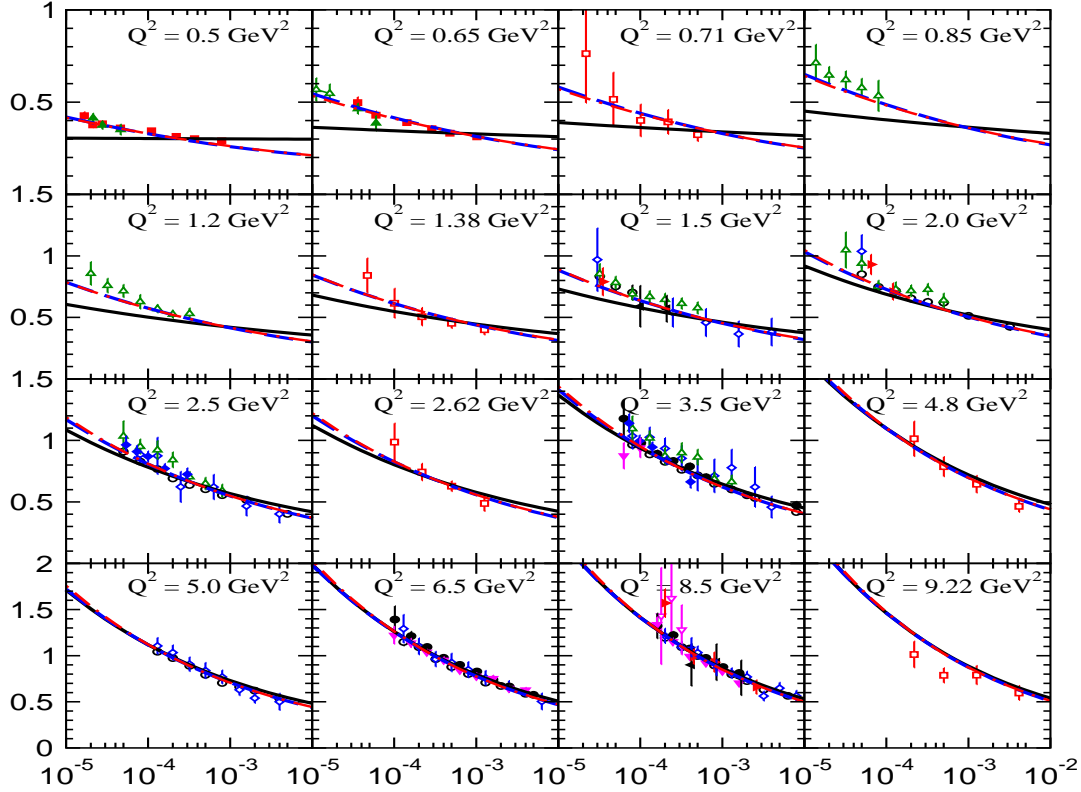
Figure 1: The structure function F_2 as a function of x for different Q^2 bins. The solid and dashed lines are obtained without and with higher-twist terms, respectively.

variables σ and ρ are given by

$$\sigma = 2\sqrt{\hat{d}_+ s \ln(x)}, \quad \rho = \sqrt{\frac{\hat{d}_+ s}{\ln(x)}} = \frac{\sigma}{2\ln(1/x)}, \quad \hat{d}_+ = -\frac{12}{\beta_0}, \tag{8}$$

where β_0 is the first coefficient of the QCD beta function and $s = \ln[a_s(Q_0)/a_s(Q)]$, with Q_0 being the initial scale of the DGLAP evolution, and $a_s(\mu) = \alpha_s(\mu)/(4\pi)$ is the couplant with the renormalization scale μ.

3 Master formula

We now derive our master formula for $R_i(x, Q^2)$ appropriate for small values of x, which has the advantage of being independent of the PDFs $f_a(x, Q^2)$. In the low-x range, where only the gluon and quark-singlet contributions matter, while the non-singlet contributions are negligibly

small, we have[2]

$$F_k^i(x, Q^2) = \sum_{l=+,-} C_{k,g}^l(x, Q^2) \otimes x f_g^l(x, Q^2), \tag{9}$$

where $l = \pm$ labels the usual $+$ and $-$ linear combinations of the gluon contributions, $C_{k,g}^l(x, Q^2)$ are the DIS coefficient functions, which can be calculated perturbatively in the parton model of QCD, and the symbol $\otimes$ denotes convolution according to the usual prescription, $f(x) \otimes g(x) = \int_x^1 (dy/y) f(y) g(x/y)$. Massive kinematics requires that $C_{k,g}^l = 0$ for $x > b_i = 1/(1 + 4a_i)$, where $a_i = m_i^2/Q^2$. We take m_i to be the solution of $\overline{m}_i(m_i) = m_i$, where $\overline{m}_i(\mu)$ is defined in the modified minimal-subtraction ($\overline{\text{MS}}$) scheme.

Exploiting the low-x asymptotic behaviour of $f_a^l(x, Q^2)$ [22],

$$f_a^l(x, Q^2) \overset{x \to 0}{\to} \frac{1}{x^{1+\delta_l}} \tilde{f}_a^l(x, Q^2), \tag{10}$$

where the rise of $\tilde{f}_a^l(x, Q^2)$ as $x \to 0$ is less than any power of x, Eq. (9) can be rewritten as [23, 24]

$$F_k^i(x, Q^2) \approx \sum_{l=+,-} M_{k,g}^l(1 + \delta_l, Q^2) x f_g^l(x, Q^2), \tag{11}$$

where

$$M_{k,a}^l(n, Q^2) = \int_0^{b_i} dx\, x^{n-2} C_{k,a}^l(x, Q^2) \tag{12}$$

is the Mellin transform, which is to be analytically continued from integer values n to real values $1 + \delta_l$ [25].

In the DAS approach [3], one has $M_{k,a}^+(1, Q^2) = M_{k,a}^-(1, Q^2)$ if $M_{k,a}^l(n, Q^2)$ are devoid of singularities in the limit $\delta_l \to 0$, as we assume for the time being. Such singularities actually occur at NLO, leading to modifications to be discussed in Section 5. Defining $M_{k,a}(1, Q^2) = M_{k,a}^\pm(1, Q^2)$ and using (9), Eq. (11) may be simplified to become

$$F_k^i(x, Q^2) \approx M_{k,g}(1, Q^2)\, x f_g(x, Q^2). \tag{13}$$

In fact, the non-perturbative input $f_g(x, Q^2)$ does cancels in the ratio

$$R_i(x, Q^2) \approx \frac{M_{L,g}(1, Q^2)}{M_{2,g}(1, Q^2)}, \tag{14}$$

which is very useful for practical applications. Through NLO, $M_{k,g}(1, Q^2)$ exhibits the structure

$$M_{k,g}(1, Q^2) = e_i^2 a_s(\mu) \left\{ M_{k,g}^{(0)}(1, a_i) + a_s(\mu) \left[M_{k,g}^{(1)}(1, a_i) + M_{k,g}^{(2)}(1, a_i) \ln \frac{\mu^2}{m_i^2} \right] \right\} + \mathcal{O}(a_s^3). \tag{15}$$

where Inserting Eq. (15) into Eq. (14), we arrive at our master formula

$$R_i(x, Q^2) \approx \frac{M_{L,g}^{(0)}(1, a_i) + a_s(\mu) \left[M_{L,g}^{(1)}(1, a_i) + M_{L,g}^{(2)}(1, a_i) \ln(\mu^2/m_i^2) \right]}{M_{2,g}^{(0)}(1, a_i) + a_s(\mu) \left[M_{2,g}^{(1)}(1, a_i) + M_{2,g}^{(2)}(1, a_i) \ln(\mu^2/m_i^2) \right]} + \mathcal{O}(a_s^2). \tag{16}$$

---

[2] Here and in the following, we suppress the variables μ and m_i in the argument lists of the structure and coefficient functions for the ease of notation. Moreover, a further simplification is obtained by neglecting the contributions due to incoming light quarks and antiquarks in Eq. (9), which is justified because they vanish at LO and are numerically suppressed at NLO for small values of x. One is thus left with the PGF contribution.

[3] The singular PDF behavior has been considered recently in [26].

We observe that the right-hand side of Eq. (16) is approximately independent of x, a remarkable feature that is automatically exposed by our procedure. In the next two sections, we present compact analytic results for the LO ($j = 0$) and NLO ($j = 1, 2$) coefficients $M_{k,g}^{(j)}(1, a_i)$, respectively.

4   LO results

The LO coefficient functions of PGF can be obtained from the QED case [27] by adjusting coupling constants and colour factors, and they read [28, 29]

$$
\begin{aligned}
C_{2,g}^{(0)}(x,a) &= -2x\{[1-4x(2-a)(1-x)]\beta - [1-2x(1-2a)+2x^2(1-6a-4a^2)]L(\beta)\}, \\
C_{L,g}^{(0)}(x,a) &= 8x^2[(1-x)\beta - 2axL(\beta)],
\end{aligned}
\tag{17}
$$

where

$$
\beta(x) = \sqrt{1 - \frac{4ax}{1-x}}, \qquad L(\beta) = \ln\frac{1+\beta}{1-\beta}.
\tag{18}
$$

Performing the Mellin transformation in Eq. (12), we find (see details in [13])

$$
M_{2,g}^{(0)}(1,a) = \frac{2}{3}[1+2(1-a)J(a)], \quad M_{L,g}^{(0)}(1,a) = \frac{4}{3}b[1+6a-4a(1+3a)J(a)], \tag{19}
$$

where

$$
J(a) = -\sqrt{b}\ln t, \qquad t = \frac{1-\sqrt{b}}{1+\sqrt{b}},
\tag{20}
$$

At LO, the low-x approximation formula thus reads

$$
R_i \approx 2b_i \frac{1+6a_i-4a_i(1+3a_i)J(a_i)}{1+2(1-a_i)J(a_i)}.
\tag{21}
$$

5   NLO results

The NLO coefficient functions of PGF are rather lengthy and not published in print; they are only available as computer codes [30]. For the purpose of this letter, it is sufficient to work in the high-energy regime, defined by $x \ll 1$, where they assume the compact form [31]

$$
C_{k,g}^{(j)}(x,a) = \beta R_{k,g}^{(j)}(1,a),
\tag{22}
$$

with

$$
\begin{aligned}
R_{2,g}^{(1)}(1,a) &= \frac{8}{9}C_A[5+(13-10a)J(a)+6(1-a)I(a)], \quad R_{k,g}^{(2)}(1,a) = -4C_A M_{k,g}^{(0)}(1,a), \\
R_{L,g}^{(1)}(1,a) &= -\frac{16}{9}C_A b\{1-12a-[3+4a(1-6a)]J(a)+12a(1+3a)I(a)\},
\end{aligned}
\tag{23}
$$

where $C_A = N$ for the colour gauge group SU(N), $J(a)$ is defined by Eq. (20), and

$$
I(a) = -\sqrt{b}\left[\zeta(2) + \frac{1}{2}\ln^2 t - \ln(ab)\ln t + 2\operatorname{Li}_2(-t)\right].
\tag{24}
$$

Here, $\zeta(2) = \pi^2/6$ and $\text{Li}_2(x) = -\int_0^1 (dy/y) \ln(1 - xy)$ is the dilogarithmic function.

As already mentioned in Section 3, the Mellin transforms of $C_{k,g}^{(j)}(x,a)$ exhibit singularities in the limit $\delta_l \to 0$, which lead to modifications in our formalism, namely in Eqs. (13) and (16). As was shown in Refs. [24, 18, 19], the terms involving $1/\delta_l$ depend on the exact form of the subasymptotic low-x behaviour encoded in $\tilde{f}_g^l(x, Q^2)$, as

$$\frac{1}{\delta_l} = \frac{1}{\tilde{f}_g^l(\hat{x}, Q^2)} \int_{\hat{x}}^1 \frac{dy}{y} \tilde{f}_g^l(y, Q^2), \tag{25}$$

where $\hat{x} = x/b$. In the generalized DAS regime, given by Eqs. (3)-(7), we have

$$\frac{1}{\delta_+} \approx \frac{1}{\hat{\rho}} \frac{I_1(\sigma(\hat{x}))}{I_0(\sigma(\hat{x}))}, \qquad \frac{1}{\delta_-} \approx \ln \frac{1}{\hat{x}}. \tag{26}$$

Because the ratio $f_g^-(x, Q^2)/f_g^+(x, Q^2)$ is rather small at the Q^2 values considered, Eq. (13) is modified to become

$$F_k^i(x, Q^2) \approx \tilde{M}_{k,g}(1, Q^2) x f_g(x, Q^2), \tag{27}$$

where $\tilde{M}_{k,g}(1, Q^2)$ is obtained from $M_{k,g}(n, Q^2)$ by taking the limit $n \to 1$ and replacing $1/(n - 1) \to 1/\delta_+$. Consequently, one needs to substitute

$$M_{k,g}^{(j)}(1, a) \to \tilde{M}_{k,g}^{(j)}(1, a) \quad (j = 1, 2) \tag{28}$$

in the NLO part of Eq. (16). Using the identity

$$\frac{1}{I_0(\sigma(\hat{x}))} \int_{\hat{x}}^1 \frac{dy}{y} \beta\left(\frac{x}{y}\right) I_0(\sigma(y)) \approx \frac{1}{\delta_+} - \ln(ab) - \frac{J(a)}{b}, \tag{29}$$

we find the Mellin transform (12) of Eq. (22) to be

$$\tilde{M}_{k,g}^{(j)}(1, a) \approx \left[\frac{1}{\delta_+} - \ln(ab) - \frac{J(a)}{b} \right] R_{k,g}^{(j)}(1, a) \quad (j = 1, 2). \tag{30}$$

The rise of the NLO terms as $x \to 0$ is in agreement with earlier investigations [32].

6 Results

As for our input parameters, we choose [13] $Q_0^2 = 0.306$ GeV^2, $m_c = 1.25$ GeV and $m_b = 4.7$ GeV. While the LO result for R_i in Eq. (21) is independent of the unphysical mass scale μ, the NLO formula (16) does depend on it, due to an incomplete compensation of the μ dependence of $a_s(\mu)$ by the terms proportional to $\ln(\mu^2/Q^2)$, the residual μ dependence being formally beyond NLO. In order to estimate the theoretical uncertainty resulting from this, in [13] we put $\mu^2 = \xi Q^2$ and vary ξ. Besides our default choice $\xi = 1 + 4a_i$, we also considered the extreme choice $\xi = 100$, which is motivated by the observation that NLO corrections are usually large and negative at small x values [33]. A large ξ value is also advocated in Ref. [34], where the choice $\xi = 1/x^\Delta$, with $0.5 < \Delta < 1$, is proposed.

We now extract $F_2^i(x, Q^2)$ $(i = c, b)$ from the H1 measurements of the cross sections in Eq. (1) at low $(12 < Q^2 < 60$ GeV$^2)$ [3] and high $(Q^2 > 150$ GeV$^2)$ [2] values of Q^2 using

Q^2	x	$F_2^c(x,Q^2)\cdot 10^3$ (H1)	$F_2^c(x,Q^2)\cdot 10^3$	$F_2^b(x,Q^2)\cdot 10^4$ (H1)	$F_2^b(x,Q^2)\cdot 10^4$
12	0.197	435 ± 78	431	45 ± 27	45
12	0.800	186 ± 24	185	48 ± 22	48
25	0.500	331 ± 43	329	123 ± 38	123
25	2.000	212 ± 21	212	61 ± 24	61
60	2.000	369 ± 40	368	190 ± 55	190
60	5.000	201 ± 24	200	130 ± 47	130
200	0.500	202 ± 46	202	413 ± 128	400
200	1.300	131 ± 32	130	214 ± 79	212
650	1.300	213 ± 57	214	243 ± 124	238
650	3.200	92 ± 28	91	125 ± 55	125

Table 1: Values of $F_2^c(x,Q^2)$ and $F_2^b(x,Q^2)$ extracted from the H1 measurements of $\tilde{\sigma}^{c\bar{c}}$ and $\tilde{\sigma}^{b\bar{b}}$ at low [3] and high [2] values of Q^2 (in GeV^2) at various values of x (in units of 10^{-3}) using our approach at NLO for $\mu^2 = \xi Q^2$ with $\xi = 1 + 4a_c$. The LO results agree with the NLO results within the accuracy of this table. For comparison, also the results determined in Refs. [2, 3] are quoted.

the LO and NLO results for R_i derived in Sections 4 and 5, respectively. Our NLO results for $\mu^2 = \xi Q^2$ with $\xi = 1 + 4a_i$ are presented for $i = c, b$ in Table 1, where they are compared with the values determined by H1. We refrain from showing our results for other popular choices, such as $\mu^2 = 4m_i^2, Q^2$ and even $\mu^2 = 100Q^2$ because they are very similar. We observe that the theoretical uncertainty related to the freedom in the choice of μ is negligibly small and find good agreement with the results obtained by the H1 Collaboration using a more accurate, but rather cumbersome procedure [2, 3].

In order to assess the significance of and the theoretical uncertainty in the NLO corrections to R_i, we show in Fig. 2 the Q^2 dependences of R_c, R_b, and R_t evaluated at LO from Eq. (21) and at NLO from Eq. (16) with $\mu^2 = 4m_i^2, Q^2 + 4m_i^2$. We observe from Fig. 2 that the NLO predictions are rather stable under scale variations and practically coincide with the LO ones in the lower Q^2 regime. On the other hand, for $Q^2 \gg 4m_i^2$, the NLO predictions overshoot the LO ones and exhibit a strong scale dependence. We encounter the notion that the fixed-flavour-number scheme used here for convenience is bound to break down in the large-Q^2 regime due to unresummed large logarithms of the form $\ln(Q^2/m_i^2)$. In our case, such logarithms do appear linearly at LO and quadratically at NLO. In the standard massless factorization, such terms are responsible for the Q^2 evolution of the PDFs and do not contribute to the coefficient functions. In fact, in the variable-flavour-number scheme, they are $\overline{\text{MS}}$-subtracted from the coefficient functions and absorbed into the Q^2 evolution of the PDFs. Thereafter, the asymptotic large-Q^2 dependences of R_i at NLO should be proportional to $\alpha_s(Q^2)$ and thus decreasing. This is familiar from the Callan-Gross ratio $R = F_L/(F_2 - F_L)$, as may be seen from its (x, Q^2) parameterizations in Ref. [35]. Fortunately, this large-Q^2 problem does not affect our results in Table 1 because the bulk of the H1 data is located in the range of moderate Q^2 values.

The ratio R_c was previously studied in the framework of the k_t-factorization approach [29] and found to weakly depend on the choice of unintegrated gluon PDF and to be approximately x independent in the low-x regime (see Fig. 8 in Ref. [29]). Both features are inherent in our approach, as may be seen at one glance from Eq. (16). The prediction for R_c from Ref. [29], which is included in Fig. 2 for comparison, agrees well with our results in the lower Q^2 range,
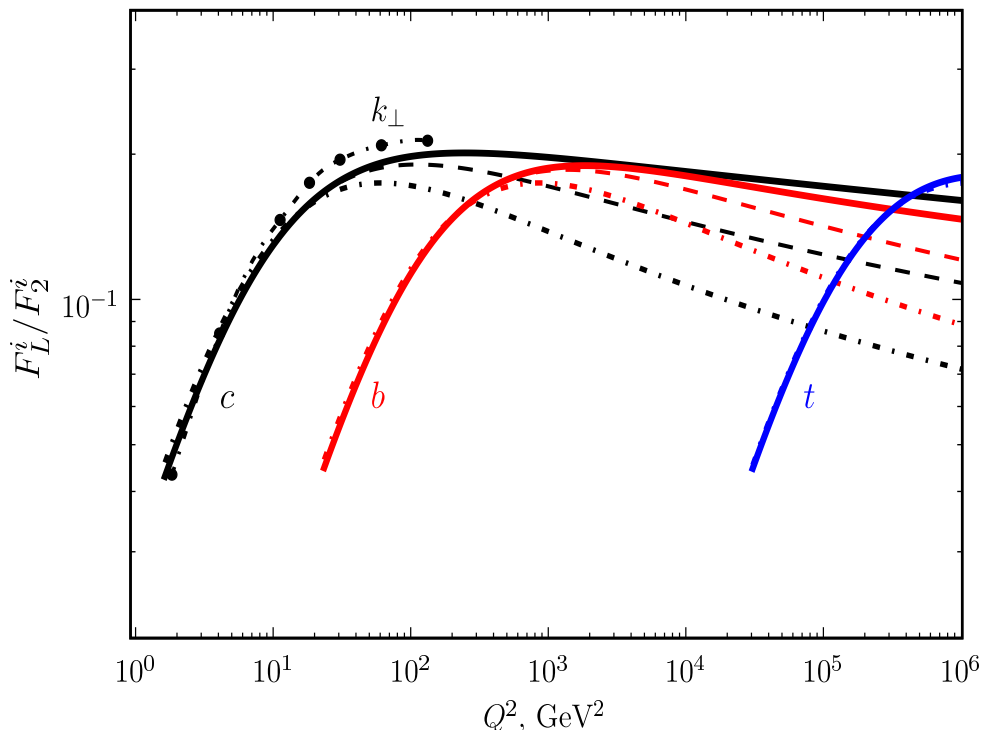
Figure 2: R_c, R_b, and R_t evaluated as functions of Q^2 at LO from Eq. (21) (dot-dashed lines) and at NLO from Eq. (16) with $\mu^2 = 4m_i^2$ (dashed lines) and $\mu^2 = Q^2 + 4m_i^2$ (solid lines). For comparison, the prediction for R_c in the k_t-factorization approach (dot-dot-dashed line) [29] is also shown.

which supports the notion that the k_t-factorization approach partially accounts for the higher-order contributions in the low-x regime.

7   Conclusions

In this paper, we observed a compact formula [13] for the ratio $R_i = F_L^i/F_2^i$ of the heavy-flavour contributions to the proton structure functions F_2 and F_L valid through NLO at small values of Bjorken's x variable. We demonstrated the usefulness of this formula by extracting F_2^c and F_2^b from the doubly differential cross section of DIS recently measured by the H1 Collaboration [2, 3] at HERA. These results agree with those extracted in Refs. [2, 3] well within errors. In the Q^2 range probed by the H1 data, NLO predictions agree very well with the LO ones and are rather stable under scale variations. Since we worked in the fixed-flavour-number scheme, our results are bound to break down for $Q^2 \gg 4m_i^2$, which manifests itself by appreciable QCD correction factors and scale dependences. As is well known, this problem is conveniently solved by adopting the variable-flavour-number scheme, which we leave for future work. Our approach also simply explains the feeble dependence of R_i on x and the details of the PDFs in the low-x

regime.

References

[1] C. Adloff *et al.*, Z. Phys. **C72** 593 (1996); Phys. Lett. **B393** 452 (1997); Nucl. Phys. **B545** 21 (1999).

[2] A. Aktas *et al.*, Eur. Phys. J. **C40** 349 (2005).

[3] A. Aktas *et al.*, Eur. Phys. J. **C45** 23 (2006).

[4] J. Breitweg *et al.*, Phys. Lett. **B407** 402 (1997); Eur. Phys. J. **C12** 35 (2000).

[5] S. Chekanov *et al.*, Phys. Rev. **D69** 012004 (2004).

[6] S. Chekanov *et al.*, JHEP **0707** 074 (2007).

[7] J.J. Aubert *et al.*, Nucl. Phys. **B213** 31 (1983); Phys. Lett. **B110** 73 (1982); Phys. Lett. **B94** 96 (1980).

[8] A.M. Cooper-Sarkar *et al.*, Int. J. Mod. Phys. **A13** 3385 (1998)

[9] V.N. Gribov and L.N. Lipatov, Sov. J. Nucl. Phys. **15** 438, 675 (1972); L.N. Lipatov, Sov. J. Nucl. Phys. **20** 94 (1975); G. Altarelli and G. Parisi, Nucl. Phys. **B126** 298 (1977); Yu.L. Dokshitzer, Sov. Phys. JETP **46** 641 (1977).

[10] B.A. Kniehl *et al.*, Z. Phys. **C76** 689 (1997); J. Binnewies *et al.*, Z. Phys. **C76** 677 (1997); Phys. Rev. **D58** 014014 (1998); Phys. Rev. **D58** 034016 (1998).

[11] S. Frixione *et al.*, Phys. Lett. **B348** 633 (1995); Nucl. Phys. **B454** 3 (1995).

[12] F.I. Olness and W.K. Tung, Nucl. Phys. **B308** 813 (1988); M.A.G. Aivazis *et al.*, Phys. Rev. **D50** 3085 (1994); Phys. Rev. **D50** 3102 (1994); R.S. Thorne and R.G. Roberts, Phys. Rev. **57** 6871 (1998); Phys. Lett. **B421** 303 (1998); Eur. Phys. J. **C19** 339 (2001); W.K. Tung *et al.*, J. Phys. **G28** 983 (2002).

[13] A.Y. Illarionov *et al.*, Phys. Lett. **B663** 66 (2008).

[14] A.D. Martin *et al.*, Eur. Phys. J **C23** 73 (2002); CTEQ Collab.: J. Pumplin *et al.*, JHEP **0207** 012 (2002); M. Gluck *et al.*, Eur. Phys. J **C5** 461 (1998); **C40** 515 (2005).

[15] A.V. Kotikov *et al.*, Z. Phys. **C58** 465 (1993); G. Parente et al., Phys.Lett. **B333** 190 (1994); A.L. Kataev et al., Phys.Lett. **B388** 179 (1996); Phys. Lett. **B417** 374 (1998); Nucl. Phys. Proc. Suppl. **64** 138 (1998); Nucl. Phys. **B573** 405 (2000); V.G. Krivokhizhin and A.V. Kotikov, Phys.Atom.Nucl. **68** 1873 (2005) (hep-ph/0108224).

[16] A.V. Kotikov, Phys. Part. Nucl. **38** 1 (2007) [Erratum-ibid. **38** 828 (2007)].

[17] R.D. Ball and S. Forte, Phys.Lett. **B336** 77 (1994); L. Mankiewicz et al., Phys.Lett. **B393** 175 (1997).

[18] A.V. Kotikov and G. Parente, Nucl. Phys. **B549** 242 (1999).

[19] A.Y. Illarionov et al., Phys. Part. Nucl. **39** 307 (2008).

[20] A. De Rújula et al., Phys.Rev. **D10** 1649 (1974);

[21] C. Adloff et al., Eur. Phys. J. **C21** 33 (2001); Eur. Phys. J. **C13** 609 (2000); S. Chekanov et al., Eur. Phys. J. **C21** 443 (2001); J. Breitweg et al., Phys.Lett. **B478** 53 (2000).

[22] H. Abramowicz et al., Phys. Lett. **B269** 465 (1991); A.V. Kotikov, Mod. Phys. Lett. **A11** 103 (1996); Phys. Atom. Nucl. **59** 2137 (1996).

[23] C. Lopez and F.J. Yndurain, Nucl. Phys. **B171** 231 (1980); Nucl. Phys. **B183** 157 (1981).

[24] A.V. Kotikov, Phys. Rev. **D49** 5746 (1994); Phys. Atom. Nucl. **59** 2137 (1996).

[25] D.I. Kazakov and A.V. Kotikov, Nucl. Phys. **B307** 721 (1988) [Erratum-ibid. **B345** 299 (1990)]; A.V. Kotikov and V.N. Velizhanin, arXiv:hep-ph/0501274 (2005)

[26] N.Y. Ivanov and B.A. Kniehl, arXiv:0806.4705 [hep-ph] (2008).

[27] V.N. Baier et al., Sov. Phys. JETP **23** 104 (1966); V.G. Zima, Yad. Fiz. **16** 1051 (1972); V.M. Budnev et al., Phys. Rept. **15** 181 (1974).

[28] E. Witten, Nucl. Phys. **B104** 445 (1976); J.P. Leveille and T.J. Weiler, Nucl. Phys. **B147** 147 (1979); V.A. Novikov et al., Nucl. Phys. **B136** 125 (1978) 125.

[29] A.V. Kotikov et al., Eur. Phys. J. **C26** 51 (2002).

[30] E. Laenen et al., Nucl. Phys. **B392** 162, 229 (1993).

[31] S. Catani et al., Preprint CERN-Th.6398/92, in Proceeding of the Workshop on Physics at HERA (Hamburg, 1991), Vol. 2., p. 690; S. Catani and F. Hautmann, Nucl. Phys. **B427** 475 (1994); S. Riemersma et al., Phys. Lett. **B347** 143 (1995).

[32] P. Nason et al., Nucl. Phys. **B303** 607 (1988).

[33] G.P. Salam, JHEP **9807** 019 (1998); S.J. Brodsky et al., JETP Lett. **70** 155 (1999); B. Andersson et al., Eur. Phys. J. **C25** 77 (2002).

[34] Yu.L. Dokshitzer and D.V. Shirkov, Z. Phys. **C67** 449 (1995); A.V. Kotikov, Phys. Lett. **B338** 349 (1994).

[35] A. Gonzalez-Arroyo et al., Phys. Lett. **B98** 215 (1981); A.V. Kotikov, Sov. J. Nucl. Phys. **49** 1068 (1989).

Production of Colored Scalar Particles in pp-Collisions and Possible Mass Limits for Scalar Gluons from LHC

M.V. Martynov[1], A.D. Smirnov[2]

[1]Yaroslavl State University, E-mail: martmix@mail.ru
[2]Yaroslavl State University, E-mail: asmirnov@univ.uniyar.ac.ru

Cross sections of the colored scalar particle production in pp-collisions are calculated and differential and total cross sections of the corresponding parton subprocesses are obtained. The total cross section of scalar gluon production in pp-collisions at the LHC is estimated and the dominant decays of scalar gluons are discussed. The production cross section of scalar gluons F with masses $m_F \lesssim 1300$ GeV is shown to be sufficient for the effective production of these particles at the LHC.

The search for new physics beyond the Standard Model induced by higher symmetries (supersymmetry, left-right symmetry, etc.) is one of the modern research directions in elementary particle physics. One such symmetry possibly existing in nature is the four-color symmetry of quarks and leptons, where leptons are considered as the fourth color [1].

Under its own minimal unification with the symmetry of the Standard Model based on the gauge group

$$SU_V(4) \times SU_L(2) \times U_R(1) \tag{1}$$

(the minimal quark-lepton-symmetric model - MQLS-model [2]), the four-color symmetry under the Higgs mechanism of quark and lepton mass splitting predicts, in particular, new scalar particles, $SU_c(3)$ octets and $SU_L(2)$ doublets, the so-called scalar gluons $F_{a'i}$ ($a' = 1, 2$, $i = 1..8$ are $SU_L(2)$ and $SU_c(3)$ indices respectively) [2, 3].

By virtue of their Higgs origin, these particles have quark coupling constants proportional to the ratio of quark masses to vacuum expectation value of SM η and, hence, the values of these constants are known (correct to within the quark mixing parameter), thus determining their interaction with gluons by the known strong coupling constant g_{st}. This makes it possible to quantitatively estimate the cross sections of processes in which these particles participate. Estimates of contributions by the scalar gluon doublets $F_{a'i}$ to the Peskin-Takeuchi S-,T-,U-parameters of radiative corrections, and their comparisons with experimental data on S-,T-,U show that these scalar gluons may be relatively light (with masses of order 1 TeV or less) [4, 5]. Scalar gluons with such masses, being colored objects of the $SU_c(3)$ group, can be pair produced in pp-collisions through gluon fusion and, partly, through quark-antiquark pair annihilation. The scalar $SU_c(3)$-octets with natural suppression of FCNC have been considered in Ref. [6]. The production of scalar $SU_c(3)$-octets at LHC were considered in Refs.[6, 7]. The light colored scalar octets in context of Adjoint $SU(5)$ unification have been discussed in Ref. [8]. In the case of the scalar gluons $F_{a'i}$ of MQLS-model the dominant decays of these particles are known [9, 10], which gives the possibility of search for these particles through their decays at LHC.

In the present paper we calculate the production cross sections of scalar particles of an arbitrary color representation in pp-collisions, and estimate these cross sections for $F_{a'i}$-scalar gluons at LHC energies with discussing the possible constraints on the masses of these particles from future LHC data with account of their dominant decay modes.

Interactions of colored scalar particles Φ_i with gluons is contained in lagrangian

$$\mathcal{L}_{\Phi\Phi g} = \sum_{scalars} \left[\left(D^\mu_{ij} \Phi^j \right)^\dagger \left(D^{ik}_\mu \Phi_k \right) - M^2_\Phi \Phi^{i\dagger} \Phi_i \right], \tag{2}$$

$$D^{ij}_\mu \Phi_j = \left(\partial_\mu \delta^{ij} - ig_s G^a_\mu T^{ij}_a \right) \Phi_j, \tag{3}$$

where T^{ij}_a are the generators of the group representation $SU_c(N)$ ($a=1,2..d_A$, d_A - dimension of the adjoint representation of $SU_c(N)$), realized by the multiplets Φ_i, i,j - color index; in particular (for $N=3$) $i,j = 1,2,3$ for scalar leptoquarks and $i,j = 1,2,..8$ for scalar gluons. The interactions of scalar leptoquark and scalar gluon doublets with fermions in MQLS-model can be found in Refs. [9, 10].

In pp-collisions colored particles can be pair produced through gluon fusion and through quark-antiquark pair annihilation. Contributions to the total production cross section for $\Phi\Phi^*$ pairs are given by the parton subprocess diagrams shown in Fig. 1, 2. Diagrams of the type 2-b give a small contribution to the cross section since the corresponding constants for scalar-fermion interactions with ordinary quarks and leptons in MQLS are small [9, 10].

The differential and total $\Phi\Phi^*$ pair production cross sections in gluon fusion are

$$\frac{d\sigma_{gg\to\Phi\Phi^*}}{dt} = \frac{2\pi\alpha_s^2 d_\Phi}{d_A^2 \hat{s}^2} C_2(\Phi) \left(C_2(\Phi) - \frac{\hat{u}\hat{t}}{\hat{s}^2} C_2(A) \right) \left[1 - 2\frac{\hat{s}M_\Phi^2}{\hat{u}\hat{t}} + 2\left(\frac{\hat{s}M_\Phi^2}{\hat{u}\hat{t}} \right)^2 \right], \tag{4}$$

$$\sigma_{gg\to\Phi\Phi^*} = \frac{\pi\alpha_s^2}{6\hat{s}} \frac{d_\Phi C_2(\Phi)}{d_A^2} \Big[C_2(A)\beta(3 - 5\beta^2) - 12C_2\beta(\beta^2 - 2) +$$
$$+ \ln\left|\frac{\beta+1}{\beta-1}\right| \left(6C_2(\Phi)(\beta^4 - 1) - 3C_2(A)(\beta^2 - 1)^2 \right) \Big], \tag{5}$$

where $\beta = \sqrt{1 - 4M_\Phi^2/s}$ is the velocity of scalar particle in the center of mass frame, and $\hat{s}$ is the squared energy in the center of momentum frame of the partons, d_Φ, d_A are the dimensions of the representation the field Φ and of the adjoint representation and $C_2(\Phi)$ and $C_2(A)$ are the corresponding eigenvalues of Casimir operator. Expressions (4) and (5) agree with the corresponding results of [6] and have the more simple form.

From formula (5) for the $SU(3)$ group ($C_2(A) = 3$, $d_A = 8$) for $C_2(\Phi) = 4/3$ and $d_\Phi = 3$, we obtain the total production cross section of scalar leptoquarks S which coincides with that of Ref. [11]; and for $C_2(\Phi) = 3$, $d_\Phi = 8$, we obtain the total production cross section of scalar gluons F'_a in the form

$$\sigma_{gg\to F_a F_a^*} = \frac{3\pi\alpha_s^2}{16s} \Big[\beta(27 - 17\beta^2) + 3\ln\left|\frac{\beta+1}{\beta-1}\right| (\beta^4 + 2\beta^2 - 3) \Big]. \tag{6}$$

The production of the scalar particles Φ in quark-antiquark pair annihilation are described by the diagram shown in Fig.2-a (the contribution of diagram 2-b from scalar leptoquark and scalar gluon doublets of MQLS - model are small). The corresponding cross sections are

$$\frac{d\sigma_{q\bar{q}\to\Phi\Phi^*}}{d\cos\theta} = \frac{C(\Phi)\pi\alpha_s^2}{9s}\sin^2\theta\,\beta^3, \tag{7}$$

$$\sigma_{q\bar{q}\to\Phi\Phi^*} = \frac{4C(\Phi)\pi\alpha_s^2}{27s}\beta^3, \tag{8}$$

here $C(\Phi)$ are the normalization constants of the generators for the representation Φ: $Tr(T^aT^b) = C(\Phi)\delta^{ab}$, $C(\Phi) = 3$ for scalar gluons and $C(\Phi) = 1/2$ for scalar leptoquarks. For the scalar leptoquarks, expressions (7–8) coincide with the corresponding expressions in [11], but for scalar gluons they give cross sections 6 times larger (having the same masses) than those for scalar leptoquarks.

The total production cross section of scalar particles $\Phi\Phi^*$ in pp-collisions at LHC energy $\sigma_{tot} = \sigma(pp \to \Phi\Phi^*)$ was calculated using the parton densities [12] in the leading order (LO) approximation with a fixed number of quark flavors. The total cross sections of scalar leptoquark production $\sigma_{tot} = \sigma(pp \to SS^*)$ and that of scalar gluon production $\sigma_{tot} = \sigma(pp \to FF^*)$ for LHC energy as functions of scalar particle masses are shown in Fig. 3. Here and below FF^* denotes $F_1F_1^*$ or $F_2F_2^*$ pairs without their summing.

In particular, we have found that for scalar leptoquark and scalar gluon masses

$$m_S = 870^{+50}_{-60}\,\text{GeV}, \tag{9}$$

$$m_F = 1300^{+100}_{-130}\,\text{GeV} \tag{10}$$

the corresponding cross sections are $\sigma(pp \to SS^*) = \sigma(pp \to FF^*) = 0.01\,\text{pb}$ (the horizontal dashed line in Fig. 3), which gives the number of events with production of SS^* or FF^* pairs $N_{events} = 100$ for a luminosity $L = 10\,\text{fb}^{-1}$. The errors indicated in (9) and (10) arise from errors in the distribution functions [12]. The result (9) for scalar leptoquarks S agrees with the estimate from [11].

Among all the possible fermionic decays of the scalar gluons F_1, $F_2 = (\varphi_1 + i\varphi_2)/\sqrt{2}$ of MQLS-model, the most probable are the decays

$$F_1 \to t\tilde{b},\ \ F_2 \to t\tilde{t}\ \ (\varphi_1,\,\varphi_2 \to t\tilde{t}) \tag{11}$$

with the production of the third-generation quarks [9, 10]. In the case where mass splitting inside the scalar doublets Δm is small enough ($\Delta m < m_W$), the modes (11) are dominant with widths of order of ten GeVs and with corresponding branching ratios close to unity $Br(F_1 \to t\tilde{b}) \approx Br(F_2 \to t\tilde{t}) \approx 1$ [9, 10]. If $\Delta m > m_W$, then the weak decays

$$F \to F'W$$

are also possible with widths comparable to those of the decays (11).

Thus, observations of scalar gluons will be possible through the dominant events $t\tilde{t}b\tilde{b}$, $t\tilde{t}t\tilde{t}$, $WWt\tilde{t}b\tilde{b}$ (or $WWt\tilde{t}t\tilde{t}$). Note that the SM background, for example, to the $t\tilde{t}b\tilde{b}$ events is of about $\sigma_{SM}(t\tilde{t}b\tilde{b}) \approx 8$ pb [13] (the darkened stripe in Fig. 3). So, the use of the appropriate cuts can give the possibility to detect the events arising from the decays of the scalar gluons with their masses of order (10) or below.

In conclusion, we resume the results of the work.

The cross sections of the scalar color particle production in pp-collisions are investigated. Differential and total cross sections of the corresponding parton subprocesses ($gg \to \Phi\Phi^*$) and

$(q\bar{q} \to \Phi\Phi^*)$ are obtained. The total cross sections of production of scalar leptoquarks S and of scalar gluons F in pp-collisions at the LHC are estimated and the dominant scalar gluon decay modes are discussed. The production cross section of scalar gluons with masses $m_F \lesssim 1300$ GeV is shown to be sufficient for the effective production ($N_{events} \gtrsim 100$ for $L = 10\,\text{fb}^{-1}$) of these particles at the LHC.
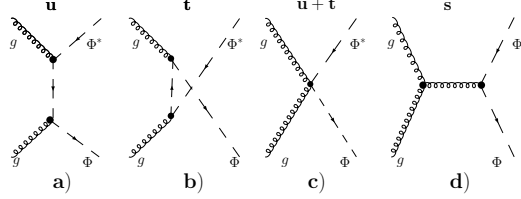

Figure 1: Diagrams of the colored scalar particle production in gg-fusion.
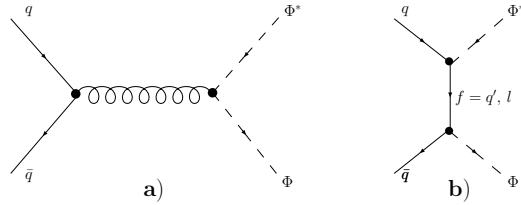
Figure 2: Diagrams of the colored scalar particle production in $q\bar{q}$-annihilation.

References

[1] J. C. Pati and A. Salam, Phys. Rev. D **10**, 275 (1974).

[2] A. D. Smirnov, Phys. Lett. B **346**, 297 (1995), hep-ph/9503239.

[3] A.V. Povarov and A. D. Smirnov, YaF. **64**, 78 (2001). (Physics of Atomic Nuclei **64**, No.1, 74 (2001).)

[4] A. D. Smirnov, Phys. Lett. B **513**, 237 (2002).

[5] A.V. Povarov and A.D. Smirnov YaF. **66**, No.12, 2259 (2003). (Physics of Atomic Nuclei **66**, No.12, 2208 (2003).)

[6] A. V. Manohar, M. B. Wise, Phys. Rev. D **74**, 035009 (2006), hep-ph/0606172.

[7] M. I. Gresham, M. B. Wise, Phys. Rev. D **76**, 075003 (2007), arXiv.org:0706.0909.; M. Gerbush et. al., arXiv.org:0710.3133.; A. R. Zerwekh, C. O. Dib, R. Rosenfeld, arXiv.org:0802.4303.

[8] P. F. Perez, H. Iminniyaz, G. Rodrigo, arXiv.org:0803.4156.

[9] P. Yu. Popov, A. V. Povarov, A. D. Smirnov, Mod. Phys. Lett. A **20**, 3003 (2005), hep-ph/0511149

[10] A. V. Povarov, P. Yu. Popov, A. D. Smirnov, YaF. **70**, 771 (2007); (Physics of Atomic Nuclei **70**, 739 (2007)).

[11] J. Blümlein, E. Boos, A. Kryukov, Z.Phys. **C76**, 137 (1997); hep-ph/9610408.

[12] S. Alekhin, Phys. Rev. D **67**, 014002 (2003)

[13] B. P. Kersevan, E. Richter-Was, Comput. Phys. Commun. **149**, 142 (2003), hep-ph/0201302

Figure 3: The total cross sections of pair production of scalar gluons (1) and of scalar lepto-quarks (2) at LHC, $\sqrt{s} = 14\,TeV$. The dashed lines denote errors arising from pdfs. Th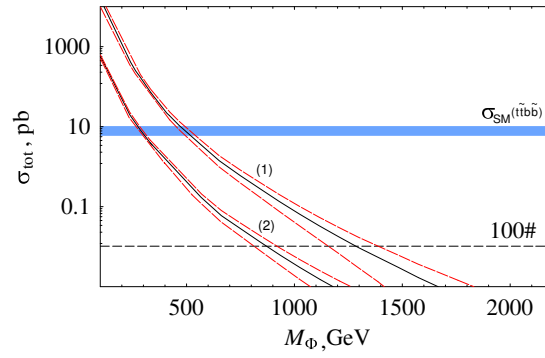e horizontal dashed line shows $\sigma_{tot} = 0.01$ pb which gives $N_{events} = 100$ for a luminosity $L = 10\,\text{fb}^{-1}$. The horizontal darkened stripe shows the SM background for $t\tilde{t}b\tilde{b}$ events.

Double charmonium production in exclusive processes.

V.V.Braguta[1]

[1]IHEP, Protvino, Russia

In this report hard exclusive charmonia production is considered within light cone formalism. The key ingredient of this formalism is the distribution amplitudes, which parameterize nonperturbative effects of hardronization. The properties of S-wave charmonia distribution amplitudes are reviewed and the models for these amplitudes are built. As an example of the application of these models double charmonium production at B-factories is considered.

1 Distribution amplitudes.

Exclusive charmonia production are very interesting both from theoretical and experimental points of view. Commonly, theoretical approach to the description of such processes [1] is based on the factorization theorem. Within this theorem the amplitude of hard exclusive process can be separated into two peaces. The first one is partons production at very small distances, which can be treated within perturbative QCD. The second peace is hardronization of the partons at larger distances. This peace contains information about nonperturbative dynamic of strong interaction. For hard exclusive processes it can be parameterized by process independent distribution amplitudes (DA), which can be considered as hadron's wave functions at light like separation between the partons in the hadron.

DA is the key ingredient of the calculation of any hard exclusive process. For this reason let us begin from the definition of DAs of S-wave charmonium states. There is one leading twist light cone wave function (DA) of $^1S_0$ meson $\phi_0(\xi,\mu)$ and there are two leading twist DAs of $^3S_1$ meson $\phi_L(\xi,\mu)$, $\phi_T(\xi,\mu)$. The function $\phi_L(\xi,\mu)$ is twist two DA of longitudinally polarized $^3S_1$ meson. The function $\phi_T(\xi,\mu)$ is twist two DA of transversely polarized $^3S_1$ meson. These DAs can be defined as follows [1]

$$\langle 0|\bar{Q}(z)\gamma_\alpha\gamma_5[z,-z]Q(-z)|P(p)\rangle_\mu \;=\; if_\eta p_\alpha \int_{-1}^{1} d\xi\, e^{i(pz)\xi}\phi_0(\xi,\mu),$$

$$\langle 0|\bar{Q}(z)\gamma_\alpha[z,-z]Q(-z)|V(\epsilon_{\lambda=0},p)\rangle_\mu \;=\; f_L p_\alpha \int_{-1}^{1} d\xi\, e^{i(pz)\xi}\phi_L(\xi,\mu),$$

$$\langle 0|\bar{Q}(z)\sigma_{\alpha\beta}[z,-z]Q(-z)|V(\epsilon_{\lambda=\pm1},p)\rangle_\mu \;=\; f_T(\mu)(\epsilon_\alpha p_\beta - \epsilon_\beta p_\alpha)\int_{-1}^{1} d\xi\, e^{i(pz)\xi}\phi_T(\xi,\mu),$$

where the following designations are used: x_1, x_2 are the fractions of momentum of the whole meson carried by quark and antiquark correspondingly, $\xi = x_1 - x_2$, p is the momentum of the corresponding meson, μ is the energy scale at which DAs are defined. The factor $[z,-z]$, makes

the matrix elements to be gauge invariant [1]. The dependence of the DAs $\phi_{0,L,T}(x,\mu)$ on scale μ can be found in [1].

Commonly, charmonium mesons are considered as a nonrelativistic bound states of quark-antiquark pair. At leading order approximation in relative velocity of quark-antiquark pair $^{1}S_{0}$ and $^{3}S_{1}$ mesons cannot be distinguished. So within this approximation $^{1}S_{0}$ and $^{3}S_{1}$ mesons have identical DAs at scale $\mu \sim M_{c}$

$$\phi_{0}(\xi,\mu) = \phi_{L}(\xi,\mu) = \phi_{T}(\xi,\mu) = \phi(\xi,\mu). \tag{1}$$

One can expect that in the case of $2S$ mesons corrections to this approximation can be large. However, present accuracy does not allow one to distinguish DAs $\phi_{0,L,T}(x,\mu)$. For this reason the approximation (1) will be used.

In this report DAs will be parameterized by their moments at some scale: $\langle \xi_{0,L,T}^{n} \rangle$. It is worth noting that, the DAs $\phi_{0,L,T}(\xi,\mu)$ are ξ-even. Thus all odd moments $\langle \xi_{0,L,T}^{2k+1} \rangle$ equal zero and one needs to calculate only even moments.

2 Study of charmonium distribution amplitudes.

There are two approaches to the study of DAs. The first one is a functional approach. It is based on Bethe-Salpeter equation. The second approach is an operator approach. It is based on the possibility to parameterize DA by matrix elements of some QCD operators. In this report these matrix elements will be studied within NRQCD or QCD sum rules.

2.1 Functional approach.

It is known that in the center mass frame Bether-Salpeter equation of nonrelativistic system can be reduced to Schrodinger equation. Now the question arises if the solution of Schrodinger equation is known how it is possible to find DA. The answer to this question is given by Brodsky-Huang-Lepage (BHL) [2] which can be written [3] as

$$\phi(\xi) \quad \sim \quad (1 - \xi^{2}) \int dt \; \psi\left(t + \frac{\xi^{2} M_{c}^{2}}{1 - \xi^{2}}\right). \tag{2}$$

Here M_{c} is a quark mass in potential model. If the DA is known than it is not difficult to find the moments. It should be noted here that the larger the power of the moment the larger the contribution coming from the end point regions ($x \sim 0$ and $x \sim 1$) to this moment. From formula (2) one sees that the motion of quark-antiquark pair in these regions is relativistic and cannot be considered reliably in the framework of potential models. Thus it is not possible to calculate higher moments within potential models. Due to this fact the calculations have been restricted by few first moments.

2.2 Operator approach: NRQCD.

As was noted above: it is possible to parameterize DA by matrix elements of some QCD operators. For nonrelativistic system such as charmonium these operators can be expended in relative velocity. At leading order approximation one can get simple formula that allows one to

$\langle \xi^n \rangle$	Buchmuller-Tye model	Cornell model	NRQCD	QCD sum rules
$\langle \xi^2 \rangle_{1S}$	0.086	0.084	0.075 ± 0.011	0.070 ± 0.007
$\langle \xi^2 \rangle_{2S}$	0.16	0.16	0.22 ± 0.14	$0.18 \, ^{+0.05}_{-0.07}$
$\langle \xi^4 \rangle_{1S}$	0.020	0.019	0.010 ± 0.003	0.012 ± 0.002
$\langle \xi^4 \rangle_{2S}$	0.042	0.046	0.085 ± 0.110	$0.051 \, ^{+0.031}_{-0.031}$
$\langle \xi^6 \rangle_{1S}$	0.0066	0.0066	0.0017 ± 0.0007	0.0032 ± 0.0009
$\langle \xi^6 \rangle_{2S}$	0.015	0.016	0.039 ± 0.077	$0.017 \, ^{+0.016}_{-0.014}$

Table 1: The moments of DAs of $1S$ and $2S$ charmonium states obtained within different approaches. In the second and third columns the moments calculated in the framework of Buchmuller-Tye and Cornell potential models are presented. In the fourth column NRQCD predictions for the moments are presented. In last column contains the results obtained within QCD sum rules.

connect the moments of DA with matrix element of NRQCD operators

$$\langle \xi^n \rangle = \frac{\langle v^n \rangle}{n+1}, \quad \langle v^{2k} \rangle = \frac{\langle 0 | \chi^+ ((i\overleftrightarrow{\mathbf{D}})^2)^k \psi | \eta_c(p) \rangle}{\langle 0 | \chi^+ \psi | \eta_c(p) \rangle}. \tag{3}$$

Recently the matrix elements of NRQCD operators was studied in paper [4] where the following results were obtained $\langle v^n \rangle = \gamma^n$. The constant γ can be expressed through the value of the matrix element $\langle v^2 \rangle$. Substituting the last formula into (3) one has the following expression for the moments at leading order approximation in relative velocity $\langle \xi^n \rangle = \gamma^n/(n+1)$. It is not difficult to show that this result for the moments can be reproduced by the following DA

$$\phi(\xi) = \frac{1}{2\gamma} \theta(\gamma - |\xi|), \tag{4}$$

which can be considered as a DA of nonrelativistic meson at leading order approximation in relative velocity.

2.3   Operator approach: QCD sum rules.

Another approach to the calculation of the moments is based on QCD sum rules [5]. The application of QCD sum rules for the study of DAs was developed by Chernyak and Zhitnitsky [1, 6]. In this report this approach will not be considered in detail. The details can be found in papers [3, 7, 8]. Here it should be noted that the main advantage of QCD sum rules in comparison to the approaches considered above is that in the framework of QCD sum rules one does not treat quarkonium as a nonrelativistic system. This allows one to avoid the main source of uncertainty – the relativistic corrections. For this reason, QCD sum rules is the most accurate approach to the calculation of the moments.

$H_1 H_2$	$\sigma_{Belle} \times Br_{H_2 \to charged > 2}(fb)$[10]	$\sigma_{BaBar} \times Br_{H_2 \to charged > 2}(fb)$[11]	$\sigma(fb)$
$\Psi(1S)\eta(1S)$	$25.6 \pm 2.8 \pm 3.4$	$17.6 \pm 2.8^{+1.5}_{-2.1}$	17.1 ± 11.3
$\Psi(2S)\eta(1S)$	$16.3 \pm 4.6 \pm 3.9$	$-$	11.9 ± 8.5
$\Psi(1S)\eta(2S)$	$16.5 \pm 3.0 \pm 2.4$	$16.4 \pm 3.7^{+2.4}_{-3.0}$	14.1 ± 11.3
$\Psi(2S)\eta(2S)$	$16.0 \pm 5.1 \pm 3.8$	$-$	9.5 ± 8.4

Table 2: In the first and second columns the cross sections measured at Belle and BaBar collaborations are shown. In the third column the results of the calculation are shown.

2.4 Models for the distribution amplitudes.

Numerical results of the calculation are collected in Table I. As it was shown in papers [3, 7, 8] these results can be represented by the following models of DAs:

$$\phi_{1S}(\xi, \mu \sim m_c) \sim (1 - \xi^2) \, \mathrm{Exp}\left[-\frac{\beta}{1 - \xi^2}\right]$$

$$\phi_{2S}(\xi, \mu \sim m_c) \sim (1 - \xi^2)(\alpha + \xi^2) \, \mathrm{Exp}\left[-\frac{\beta}{1 - \xi^2}\right] \tag{5}$$

For $1S$ charmonium state the constant β can vary within the interval 3.8 ± 0.7. For $2S$ charmonium state the constants α and β can vary within the intervals $0.03^{+0.32}_{-0.03}$ and $2.5^{+3.2}_{-0.8}$ correspondingly.

In papers [3, 7, 8] it was shown that due to evolution DAs of nonrelativistic systems have very interesting property. Because of the rapid evolution the accuracy of the any model becomes better at large scales. Due to this property the uncertainty in the calculation of the hard amplitudes is not very large.

3 Application of the models of DAs for double charmonia production at B-factories.

In this section the amplitude of the process $e^+ e^- \to VP$, where V and P are vector and pseudoscalar mesons, will be considered. The only formfactor $F(s)$ that parameterizes electromagnetic production of vector and pseudoscalar mesons can be defined as

$$\langle V(p_1, \lambda) P(p_2) | J_\mu^{em} | 0 \rangle = i q_c \, F(s) \, e_{\mu\nu\rho\sigma} \epsilon_\lambda^\nu p_1^\rho p_2^\sigma, \tag{6}$$

where q_c is the charge of c quark, ϵ_λ^ν is the polarization vector of meson $V(p_1, \lambda)$. The cross section of the process $e^+ e^- \to VP$ can be expressed through this formfactor [9]

$$\sigma(e^+ e^- \to VP) = \frac{\pi \alpha^2 q_c^2}{6} \left(\frac{2|\mathbf{p}|}{\sqrt{s}}\right)^3 |F(s)|^2. \tag{7}$$

In paper [9] the expression for this formfactor was derived. In the calculation this expression with DAs (5) will be used. Thus one gets the predictions for the cross sections of double S-wave charmonium production at B-factories Table 2. In the first and second columns the cross

sections measured at Belle and BaBar collaborations are shown. In the third column the results of the calculation are shown. It is seen from this table that the results are in agreement with the experiments. More details of the calculation can be found in paper [12].

References

[1] V. L. Chernyak and A. R. Zhitnitsky, Phys. Rept. **112**, 173 (1984).

[2] S. J. Brodsky, T. Huang and G. P. Lepage, In *Banff 1981, Proceedings, Particles and Fields 2*, 143-199.

[3] V. V. Braguta, A. K. Likhoded and A. V. Luchinsky, Phys. Lett. B **646**, 80 (2007) [arXiv:hep-ph/0611021].

[4] G. T. Bodwin, D. Kang and J. Lee, Phys. Rev. D **74**, 014014 (2006) [arXiv:hep-ph/0603186].

[5] M. A. Shifman, A. I. Vainshtein and V. I. Zakharov, Nucl. Phys. B **147**, 448 (1979).

[6] V. L. Chernyak and A. R. Zhitnitsky, Nucl. Phys. B **201**, 492 (1982)

[7] V. V. Braguta, Phys. Rev. D **75**, 094016 (2007) [arXiv:hep-ph/0701234].

[8] V. V. Braguta, arXiv:0709.3885 [hep-ph].

[9] A. E. Bondar and V. L. Chernyak, Phys. Lett. B **612**, 215 (2005) [arXiv:hep-ph/0412335].

[10] K. Abe *et al.* [Belle Collaboration], Phys. Rev. D **70**, 071102 (2004), hep-ex/0407009.

[11] B. Aubert [BABAR Collaboration], hep-ex/0506062.

[12] V.V. Braguta, to be published

An alternative approach to the isobar model for $B \to K\pi\pi$ decays

B. El-Bennich[1], A. Furman[2], R. Kamiński[3], L. Leśniak[3], B. Loiseau[4] and B. Moussallam[5]

[1] Physics Division, Argonne National Laboratory, Argonne, IL 60439, USA
[2] ul. Bronowicka 85/26, 30-091 Kraków, Poland
[3] Division of Theoretical Physics, The Henryk Niewodniczański Institute of Nuclear Physics, Polish Academy of Sciences, 31-342 Kraków, Poland
[4] LPNHE, Groupe Théorie, Université Pierre et Marie Curie, 4 place Jussieu, 75252 Paris, France
5 Institut de Physique Nucléaire, CNRS/Univ. Paris-Sud 11 (UMR 8608), 91406 Orsay Cedex, France

We analyze the contributions of hadronic final-state interactions to the strong phases generated in $B \to K\pi\pi$ decays. To this end, we develop an alternative approach, based upon scalar and vector πK form factors, to the usually employed isobar model.

1 Introduction

An accurate knowledge of *strong* phases in weak decays is crucial in order to determine CP-violating observables with high precision. In B decays, hadronic contributions of non-perturbative nature are still the main source of theoretical uncertainties. This includes strong phases which originate in heavy-to-light transition form factors, annihilation topologies as well as mesonic final-state interactions. In this talk, we concentrate on the latter hadronic contribution and investigate pion-kaon interactions motivated by recent experimental data on $B \to K\pi\pi$ decays [1–5]. In experimental analyses, these three-body decays are commonly analyzed within the isobar model. Several resonances are observed in the experimental effective $\pi\pi$ and πK mass distributions, where, in the $m_{\pi\pi}$ spectrum, we point out the $f_0(980)$ and $\rho(770)^0$ and the importance of the decay channel $B^\pm \to \rho(770)^0 K^\pm, \rho(770)^0 \to \pi^+\pi^-$ for which *direct CP* violation is now firmly established [2, 3]. In this contribution, we concentrate on the invariant πK mass distribution and in particular the $K_0^*(1430)$ and $K^*(892)$ resonances. The invariant $\pi\pi$ mass on the Dalitz plot of $B \to K\pi\pi$ decays was treated analogously in Ref. [6].

2 Scalar and vector form factors and πK interactions

The assumption is that QCD factorization is applicable in the kinematical configuration where one pion and the kaon form a quasi colinear pair in the center-of-mass frame of the B; their interaction with the second pion emitted in backward direction is suppressed in the $\Lambda_{\rm QCD}/m_b$ expansion. We derive weak decay amplitudes for a quasi two-body state in analogy with the usual QCD factorization approach [7]. Therefore, the decay amplitude $B \to R\pi$, where R is the πK resonance in the s-channel, factorizes into two hadronic currents to which non-factorizable

radiative corrections in $\alpha_s(\mu)$ can be systematically added. The subsequent creation of a pion-kaon pair in an S or a P wave from vacuum is mediated by the current $\langle(\pi K)_{S,P}|\bar{s}\gamma_\mu(1-\gamma_5)d|0\rangle$ and can be described by appropriate scalar or vector form factors. They are derived from unitary coupled-channel equations, constrained by chiral perturbation theory at low energy and experimental data on πK phase shifts and inelasticities via dispersion relations [8].

In the πK mass range below 2 GeV, the resonances $K^*(892)$ and $K_0^*(1430)$ dominate the πK vector and scalar form factors, respectively. We consider two contributions to $B \to K\pi\pi$ decay amplitudes: the QCD factorization amplitudes of weak $b \to s\bar{d}d$ ($B^\pm$ decays) or $b \to s\bar{u}u$ (B^0 decays) transitions and a phenomenological long-distance amplitude with either a c- or u-quark in the loop of the penguin topology [9], also referred to as charming penguins. We include the latter due to the observation in Ref. [7] that the calculated $\mathcal{O}(\alpha_s)$ and $1/m_b$ corrections are insufficient to explain the experimental branching fractions and CP violation for $B \to K^*\pi$. The $B^- \to (K^-\pi^+)_S\pi^-$ decay amplitude reads,

$$
\begin{aligned}
A_S = \frac{G_F}{\sqrt{2}}(M_B^2 - m_\pi^2)\frac{m_K^2 - m_\pi^2}{q^2}F_0^{B^- \to \pi^-}(q^2) \\
\times f_0^{K^-\pi^+}(q^2)\bigg\{\lambda_u\left(a_4^u(S) - \frac{a_{10}^u(S)}{2} + c_4^u\right) + \lambda_c\left(a_4^c(S) - \frac{a_{10}^c(S)}{2} + c_4^c\right) \\
- \frac{2q^2}{(m_b - m_d)(m_s - m_d)}\left[\lambda_u\left(a_6^u(S) - \frac{a_8^u(S)}{2} + c_6^u\right) + \lambda_c\left(a_6^c(S) - \frac{a_8^c(S)}{2} + c_6^c\right)\right]\bigg\}, \quad (1)
\end{aligned}
$$

and the P-wave contribution $B^- \to (K^-\pi^+)_P\pi^-$ is

$$
\begin{aligned}
A_P = 2\sqrt{2}G_F \, \mathbf{p}_{\pi^-} \cdot \mathbf{p}_{\pi^+} \, F_1^{B^- \to \pi^-}(q^2) \\
\times f_1^{K^-\pi^+}(q^2)\bigg\{\lambda_u\left(a_4^u(P) - \frac{a_{10}^u(P)}{2} + c_4^u\right) + \lambda_c\left(a_4^c(P) - \frac{a_{10}^c(P)}{2} + c_4^c\right) \\
+ 2\frac{m_{K^*}}{m_b}\frac{f_V^\perp}{f_V}\left[\lambda_u\left(a_6^u(P) - \frac{a_8^u(P)}{2} + c_6^u\right) + \lambda_c\left(a_6^c(P) - \frac{a_8^c(P)}{2} + c_6^c\right)\right]\bigg\}. \quad (2)
\end{aligned}
$$

Here, $q^2 = (p_{\pi^+} + p_{K^-})^2$ is the effective $K^-\pi^+$ mass squared, $F_0^{B \to \pi}(q^2)$ is the scalar and $F_1^{B \to \pi}(q^2)$ the vector $B \to \pi$ transition form factor and $f_0^{K^-\pi^+}(q^2)$ and $f_1^{K^-\pi^+}(q^2)$ denote the scalar and vector $K^-\pi^+$ form factors, respectively. The coefficients $a_i^{u,c}$ are combinations of short-distance Wilson coefficients which include $\mathcal{O}(\alpha_s)$ vertex and penguin corrections in the quasi two-body approximation of the scalar-pseudoscalar ($a_i^{u,c}(S)$) and pseudoscalar-vector ($a_i^{u,c}(P)$) final states. G_F is the Fermi coupling constant and the factors λ_i are products of CKM matrix elements, $\lambda_u = V_{ub}V_{us}^*$ and $\lambda_c = V_{cb}V_{cs}^*$. The term proportional to $f_V^\perp/f_V$ has been inferred from a similar term which arises at order α_s in the $B \to PV$ amplitudes [7]. The long-distance penguin amplitudes are parametrized by four complex parameters $c_i^k, i = 4, 6, k = u, c$. We stress that the form factors, $f_0^{K^-\pi^+}(q^2)$ and $f_1^{K^-\pi^+}(q^2)$, are the main ingredients which allow for decay amplitudes describing in a unitary way the *entire* $m_{\pi K}$ range below 2 GeV considered by us in $B \to K\pi\pi$ decays. Note also that the q^2 dependence of the S wave, in the third line of Eq. (1), has important consequences on the behaviour of the effective mass distribution. The CP-conjugate amplitudes $B^+ \to (K^+\pi^-)_{S,P}\pi^+$ are obtained from complex conjugation of λ_u and λ_c in Eqs. (1) and (2).

3 Separation of πK resonant scattering from background

There is some ambiguity in the separation between resonant and background contributions due to how these different contributions are parametrized in the isobar model. It is well known from the analytical properties of the scattering matrix, though, that a resonance can be associated with a pole in the complex energy plane of its second Rieman sheet (see, e.g., Ref. [10]). Naturally, this pole also shows up in form factors and correlation functions. We make use of the analytical properties of the form factors, $f_0^{K^-\pi^+}(q^2)$ and $f_1^{K^-\pi^+}(q^2)$, to isolate the scalar and vector resonances $K_0^*(1430)$ and $K^*(892)$, respectively. In the following, we sketch the derivation of the pole for the S wave. All details and the analogous procedure for the P wave are presented in Refs. [8, 11].

We want to define the extrapolation to the second Riemann sheet in the complex $t = q^2$ variable. In Ref. [8, 11], it was assumed that πK scattering is elastic up to the $\eta' K$ threshold and that this channel dominates the S wave, as experimentally confirmed [12]. Thus, a 2×2 T-matrix was constructed for the channels $\pi K \to \pi K$ and $\pi K \to \pi\eta'$. The scalar form factor is related to this T-matrix via unitary coupled-channel equations and dispersion relations (called Mushkelishvili-Omnès equations [13]). The discontinuity of the form factor is,

$$
\begin{aligned}
f_0^{K\pi}(t+i\epsilon) - f_0^{K\pi}(t-i\epsilon) &= -2\sigma_{\pi K}(t+i\epsilon)T_{11}^S(t+i\epsilon)f_0^{K\pi}(t-i\epsilon) , \\
\text{with } \sigma_{\pi K}(t) &= \sqrt{((m_K+m_\pi)^2 - t)(t - (m_K - m_\pi)^2)}/t ,
\end{aligned}
\tag{3}
$$

for t real and in the range $(m_\pi + m_K)^2 \leq t \leq (m_{\eta'} + m_K)^2$. Here, T_{11}^S is the S-wave $\pi K \to \pi K$ T-matrix element, which satisfies a discontinuity equation similar to Eq. (3),

$$
T_{11}^S(t+i\epsilon) - T_{11}^S(t-i\epsilon) = -2\sigma_{\pi K}(t+i\epsilon)T_{11}^S(t+i\epsilon)T_{11}^S(t-i\epsilon) .
\tag{4}
$$

Thus, Eqs. (3) and (4) allow us to find the extension of $f_0^{K\pi}$ on the second Riemann sheet,

$$
f_0^{\mathrm{II}}(t) = \frac{f_0^{K\pi}(t)}{1 - 2\sigma_{\pi K}(t)T_{11}^S(t)} ,
\tag{5}
$$

which, by definition, must satisfy $f_0^{\mathrm{II}}(t - i\epsilon) = f_0^{K\pi}(t + i\epsilon)$ along the cut. We deduce from Eq. (5) that $f_0^{\mathrm{II}}(t)$ displays a pole whenever the denominator function

$$
D(t) = 1 - 2\sigma_{\pi K}(t)T_{11}^S(t)
\tag{6}
$$

becomes zero. In a similar way, one can define the extension to the second sheet of $(T_{11}^S)^{\mathrm{II}}$ which, by virtue of Eq. (4), has exactly the same denominator function $D(t)$. A point t_0 such that $D(t_0) = 0$ corresponds to a pole of $(T_{11}^S)^{\mathrm{II}}$ and can be associated with a resonance [10]. From this, it is simple to isolate the pole part of the form factor

$$
f_0^{\mathrm{pole}}(t) = \frac{f_0^{K\pi}(t_0)}{\alpha\,(t - t_0)} ,
\tag{7}
$$

where $\alpha = dD(t)/dt$ for $t = t_0$. In the numerator, $f_0^{K\pi}(t_0)$ can be computed using its dispersive representation. In practice, we must have $T_{11}^S(t)$ for complex values of t. In Ref. [11], we defined $T_{11}^S(t)$ on the real axis in the range $1.25 \leq \sqrt{t} \leq 2.5$ GeV from a 2×2 K matrix fit to the experimental data. By construction, the elements of the K-matrix have no branch cut on the positive real axis. The meromorphic function parametrization we use should be valid in some
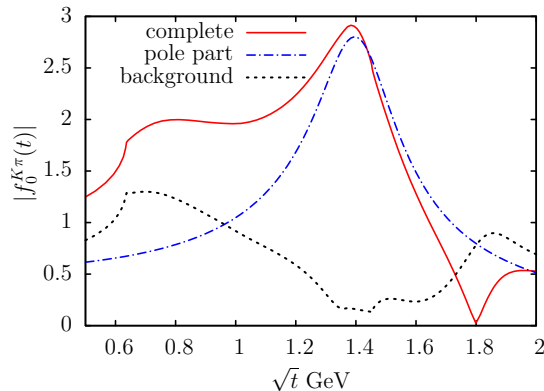
Figure 1: Modulus of the scalar form factor $f_0^{K\pi}(t)$ compared with its pole part.

complex domain of the t variable. It seems reasonable to assume that it remains reliable in the region of the $K_0^*(1430)$, since its pole lies rather close to the real axis.

Numerically, the location of the pole is found to be at $\sqrt{t_0} = (1.403 - i\,0.136)$ GeV. This result compares reasonably well with the values of the mass $M_R = 1.414 \pm 0.006$ GeV and the half-width $\Gamma_R/2 = 0.145 \pm 0.011$ GeV of the $K^*(1430)$, as listed in the Particle Data Group review [14]. The other quantities that determine $f_0^{\rm pole}(t)$ are $f_0^{K\pi}(t_0) = -0.341 - i\,1.506$ and $\alpha = (0.838 + i\,1.171)$ GeV^{-2}. In Figure 1, the modulus of $f_0^{\rm pole}(t)$ is compared with the moduli of $f_0^{K\pi}(t)$ and of the "background" which we may define as the difference $f_0^{\rm b.g.}(t) = f_0^{K\pi}(t) - f_0^{\rm pole}(t)$.

4 Concluding discussion

Once we are in the position to separate the pole from the background contribution, we are left with an S- and P-wave amplitudes completely dominated by the $K_0^*(1430)$ and $K^*(892)$. We may then compare the pole contribution to branching fractions and CP-violating asymmetries with that obtained from experimental parametrizations of the $K_0^*(1430)$ and $K^*(892)$, commonly taken to be Breit-Wigner type amplitudes determined in fits to the Dalitz plot and integrated over the complete $m_{\pi K}$ range. We recall that experimental analyses write the non-resonant πK amplitude separately from the coherent sum of (partially modified) Breit-Wigner terms.

When considering the decays $B^\pm \to K^\pm \pi^\mp \pi^\pm$, $\bar{B}^0 \to \bar{K}^0 \pi^- \pi^+$ and $B^0 \to K^0 \pi^+ \pi^-$, the body of available experimental data by Belle and BaBar [2, 3, 4, 5] is comprised of branching ratios, CP-violating asymmetries, effective πK mass and helicity angle distributions as well as a preliminary result for the phase difference, $\Delta\Phi_0$, between the decay amplitudes of $B^0 \to K^{*+}(892)\pi^-$ and $\bar{B}^0 \to K^{*-}(892)\pi^+$. For the latter we use the preliminary result of Ref. [15]. Our theoretical QCD factorization amplitudes, without charming penguin contributions, predict branching fractions for the $B \to K^*(892)\pi$ and $B \to K_0^*(1430)\pi$ decays too small by factors of about 5 and 2, respectively. Thus, these amplitudes are short of reproducing the experimental values despite the additional strong phases from the scalar πK form factors. If we neglect the penguin corrections $c_{4,6}^{u,c}$ in Eqs. (1) and (2), the mass distribution $m_{\pi K}$ is altered due to the
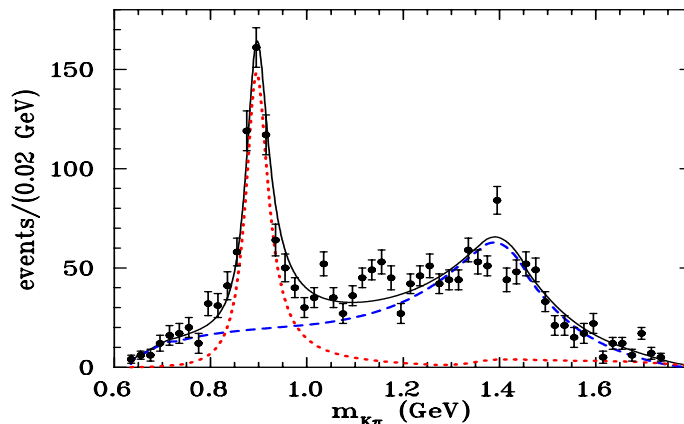
Figure 2: Average $K\pi$ effective mass distributions for $B^{\pm} \to K^{\pm}\pi^{\mp}\pi^{\pm}$ decays. The dashed line corresponds to the S-wave, the dotted line to the P-wave and the solid one to the total amplitude. The data are from [3].

q^2 dependence of the A_S amplitude: the peaks of the $K^*(892)$ and $K_0^*(1430)$ are at the right position but their respective heights do not correspond to those of the data bins.

In Figure 2, we display an example of our results on πK effective mass distributions. More details can be found in Ref. [11]. The mass distributions are averaged over charge conjugate states. In both cases, our model describes quite well the $m_{\pi K}$ distributions in the $K^*(892)$ and $K_0^*(1430)$ regions. It also signals a sizable enhancement below 1 GeV related to the $K^*(800)$ state, also referred to as κ. Integrating over the appropriate πK mass ranges for each resonance, we can calculate branching ratios and CP asymmetries for $B \to K^*(892)\pi$ and $B \to K_0^*(1430)\pi$ which compare well with the experimental ones [11].

References

[1] K. Abe et al. [Belle Collaboration], hep-ex/0509001 (2005).

[2] B. Aubert *et al.* [BaBar Collaboration], *Phys. Rev.* **D72**, 072003 (2005); *erratum-ibid.*, **D74**, 099903 (2006).

[3] A. Garmash *et al.* [Belle Collaboration], *Phys. Rev. Lett.* **96**, 251803 (2006).

[4] A. Garmash *et al.* [Belle Collaboration], *Phys. Rev.* **D75** 012006 (2007).

[5] B. Aubert *et al.* [BaBar Collaboration], *Phys. Rev.* **D71**, 092003 (2005); *ibid.* **D73** 031101(R) (2006).

[6] B. El-Bennich, A. Furman, R. Kamiński, L. Leśniak and B. Loiseau, *Phys. Rev.* **D74**, 114009 (2006).

[7] M. Beneke and M. Neubert, *Nucl. Phys.* **B675**, 333 (2003).

[8] B. Moussallam, Eur. Phys. J. **C53**, 401 (2008).

[9] M. Ciuchini, E. Franco, G. Martinelli and L. Silvestrini, *Nucl. Phys.* **B501**, 271 (1997).

[10] J. R. Taylor, *Scattering theory*, Wiley, New York (1972).

[11] B. El-Bennich, A. Furman, R. Kamiński, L. Leśniak, B. Loiseau and B. Moussallam, work in progress.

[12] D. Aston *et al.*, Phys. Lett. **B 201**, 169 (1988).

[13] N. I. Muskhelishvili, *Singular integral equations*, P. Noordhof (1953).

[14] C. Amsler et al. (Particle Data Group), *Review of particle physics*, Phys. Lett. B 667, 1 (2008).

[15] B. Aubert, *et al.* (BaBar Collaboration), arXiv:0708.2097 [hep-ex].

Quarkonium dissociation in a thermal medium

Jakub Jankowski[1] and David Blaschke[1,2]

[1]Institute for Theoretical Physics, University of Wroclaw, 50-204 Wroclaw, Poland
[2]Bogoliubov Laboratory for Theoretical Physics, JINR, 141980 Dubna, Russia

We investigate the Mott effect for heavy quarkonia due to Debye screening of the heavy quark potential in a plasma of massless quarks and antiquarks. The influence of residual color correlation is investigated by coupling the light quark sector to a temporal gauge field driven by the Polyakov loop potential. This leads to an increase of the Mott dissociation temperatures for quarkonia states which stabilizes in particular the excited states, but has marginal effect on the ground states.

1   Introduction

Since the suggestion of J/ψ suppression as a signal of quark-gluon plasma (QGP) formation by Matsui and Satz [1] in 1986 the problem of quarkonium dissociation in hot and dense strongly interacting matter has played a key role for QGP diagnostics in relativistic heavy-ion collision experiments. The original idea was that in a QGP the string tension of the confining potential vanishes and the residual one-gluon exchange interaction undergoes a Debye screening by the color charges of the plasma. When the temperature dependent Debye radius $r_D(T)$ (the inverse of the Debye mass $m_D(T)$) becomes shorter than the Bohr radius of the charmonium ground state (J/ψ) then the Mott effect [2] (bound state dissociation) occurs and the corresponding temperature is $T_{\text{Mott}}^{J/\psi}$. This simple idea grew up to a multifacetted research direction when not only in the first light ion - nucleus collisions at the CERN NA38 experiment, but also in proton - nucleus collisions at Fermilab J/ψ suppression has been found so that there is not only a QGP but also a cold nuclear matter effect on charmonium production, see [3] for a recent review.

If one wants to explore the question of screening in a plasma more in detail then a variety of appraoches is available in the literature, from the original Debye-Hückel approach [4] where one can study any vacuum potential (for example the Cornell potential) and see its medium modification, over the thermodynamic Green functions approach to the ab-initio studies of heavy-quark potentials in lattice QCD. With the obtained medium-dependent potentials one can then study the bound state problem by solving the nonrelativistic Schrödinger equation or, more systematically, the thermodynamic T - matrix for quarkonia [5].

On the other hand one may calculate proper correlators directly from lattice QCD and extract from them spectral functions [6]. There is an intriguing disagreement between the Mott temperatures deduced from these spectral functions and those of the potential models: the latter are much smaller than the former! From the lattice data for quarkonium correlators one has extracted $T_{J/\psi}^{\text{Mott}} \approx 1.9 T_c$ while in potential model calculations $T_{J/\psi}^{\text{Mott}} \approx 1.2 T_c$. This problem has lead to the discussion of the proper thermodynamical function to be used as a potential in the Schrödinger equation. Should it be the free energy or the internal energy? We will not follow this question in the present work, but refer to [3, 7] and references therein.

Here we examine a simple model of screening as derived from one-loop calculations in thermal quantum field theory, and make a small extension of this result by putting the internal fermion lines in a constant temporal gauge field which mimics confining gluon dynamics (Polyakov-loop potential). In our approach the medium is made of plasma of massless quarks, described by the chirally symmetric phase of the Nambu–Jona-Lasinio (NJL) model of QCD [8]. Confinement is implemented in the most simple way by coupling the system to the Poyakov loop variable - resulting in the so called Polakov loop NJL-model (or PNJL model). Recently it has been successfully used to reproduce lattice data [9] or to describe light meson physics at finite temperatures and densities [10].

2   Debye-screening in a PNJL quark plasma

Given the self energy (polarization function) of a boson that mediates the interaction, the screened potential is given by a resummation of one-particle irreducible diagrams ("bubble" resummation = RPA) [11]

$$V_{\rm sc}(q) = V(q)/[1 + F(0; \mathbf{q})/q^2] \ , \tag{1}$$

where we take $V(q) = -\frac{4}{3}g^2/q^2$, $q^2 = |\mathbf{q}|^2$ as the unscreened vacuum potential. The longitudinal gluon polarization function $F(0; \mathbf{q}) = -\Pi_{00}(0; \mathbf{q})$ in the finite T case can be calculated within perturbative thermal field theory where it takes the form

$$\Pi_{00}(i\omega_l; \mathbf{q}) = Tg^2 \sum_{n=-\infty}^{\infty} \int \frac{d^3p}{(2\pi)^3} \ {\rm Tr}[\gamma^0 S_\Phi(i\omega_n; \mathbf{p})\gamma^0 S_\Phi(i\omega_n - i\omega_l; \mathbf{p} - \mathbf{q})] \ , \tag{2}$$

where $\omega_l = 2\pi l T$ are the bosonic and $\omega_n = (2n+1)\pi T$ are the fermionic Matsubara frequencies of the imaginary-time formalism. The symbol Tr stands for traces in color, flavor and Dirac spaces. S_Φ is the propagator of a massless fermion coupled to the homogeneous static gluon background field φ_3. Its inverse is given by [9, 10]

$$S_\Phi^{-1}(\mathbf{p}; \omega_n) = \gamma \cdot \mathbf{p} + \gamma_0 i\omega_n - \lambda_3 \varphi_3 \ , \tag{3}$$

where φ_3 is related to the Polyakov loop variable defined by [9]

$$\Phi(T) = \frac{1}{3}{\rm Tr}_c(e^{i\beta\lambda_3\varphi_3}) = \frac{1}{3}(1 + 2\cos(\beta\varphi_3)) \ .$$

The physics of $\Phi(T)$ is governed by the temperature-dependent Polyakov loop potential $\mathcal{U}(\Phi)$, which is fitted to describe the lattice data for the pressure of the pure glue system [9]. After performing the color-, flavor- and Dirac traces and making the fermionic Matsubara summation, we obtain in the static, long wavelength limit

$$\Pi_{00}(0; \mathbf{q}) = \frac{2N_{\rm dof}g^2}{\pi^2} \int_0^\infty dp\, p^2 \frac{\partial f_\Phi}{\partial p} = -\frac{4N_{\rm dof}g^2}{\pi^2} \int_0^\infty dp\, p f_\Phi(p) = -\frac{N_{\rm dof}g^2 T^2}{3} I(\Phi) = -m_D^2(T) \ . \tag{4}$$

where $m_D(T)$ is the Debye mass, the number of degrees of freedom is $N_{\rm dof} = N_c\, N_f = 6$ and $f_\Phi(p)$ is quark distribution function [10]. The screened potential is thus

$$V_{\rm sc}(q) = -4\pi\alpha/[q^2 + m_D^2(T)] \ . \tag{5}$$

In comparison to the free fermion case [11, 12] the coupling to the Polyakov loop variable $\Phi(T)$ gives rise to a modification of the Debye mass, given by the integral

$$I(\Phi) = \frac{12}{\pi^2} \int_0^\infty dx \, x \frac{\Phi(1 + 2e^{-x})e^{-x} + e^{-3x}}{1 + 3\Phi(1 + e^{-x})e^{-x} + e^{-3x}}. \tag{6}$$

In the limit of deconfinement ($\Phi = 1$), the case of a massless quark gas is obtained ($I(1) = 1$) while for confinement ($\Phi = 0$) one finds that $I(0) = 1/9$. For the temperature dependence of $\Phi(T)$ we employ in the following chapter the results of a nonlocal PNJL model [13].

3 Variational ansatz and estimation of Mott temperatures

Here we will use the derived potential in the quantum mechanical way to estimate the dissociation temperature. With the trial wave function for the 1S state

$$\psi_{1S}(r; \gamma) = \sqrt{\frac{\gamma^3}{\pi}} \exp(-\gamma r) \tag{7}$$

and the non-relativistic two-body Hamiltonian

$$H = -\frac{\nabla^2}{m_Q} - \frac{\alpha}{r} e^{-m_D(T)r} \ , \tag{8}$$

where the potential term is the Fourier transform of screened Coulomb potential (5), we obtain the energy functional for the Ritz variational principle

$$E_{1S}(\gamma, T) = \langle \psi_{1S}(\gamma) \mid H \mid \psi_{1S}(\gamma) \rangle = \frac{\gamma^2}{m_Q} - \frac{4\alpha\gamma^3}{(m_D(T) + 2\gamma)^2} \ . \tag{9}$$

Simultaneously satisfying the conditions for the ground state energy $dE_{1S}(\gamma, T)/d\gamma = 0$ and for a vanishing binding energy (Mott effect), $E_{1S}(\gamma, T^{\text{Mott}}) = 0$, provides us with an analytic expression for the critical Debye mass $m_D(T_{1S}^{\text{Mott}}) = 2\gamma$. Using once again the condition $E_{1S}(\gamma, T^{\text{Mott}}) = 0$, results in the Mott condition for the Debye potential [2]

$$r_D(T_{1S}^{\text{Mott}}) = a_0 \ , \tag{10}$$

where $a_0 = 2/(\alpha m_Q) = 1/\sqrt{\varepsilon_0 m_Q}$ is the Bohr radius and $\varepsilon_0 = \alpha^2 m_Q/4$ the binding energy of ground state in the vacuum ($m_D = 0$). Due to the temperature dependence of the Debye mass, we obtain the Mott dissociation temperature in the massless quark gas (for $\Phi = 1$)

$$T^{\text{Mott}} = \sqrt{3\varepsilon_0 m_Q/N_{\text{dof}}}/g = \sqrt{\sqrt{\varepsilon_0 m_Q^3}/(2\pi N_{\text{dof}})} \ . \tag{11}$$

In Tab. 1 we give the parameter values according to set (i) of Ref. [14]. The Poyakov loop variable contribution considered in previous section affects the Mott temperature in Eq. (10) and gives the following formula

$$T^{\text{Mott},\Phi} = T^{\text{Mott}}/\sqrt{I(\Phi)} \ . \tag{12}$$

Table 1: Mott temperatures T^{Mott} ($T^{\mathrm{Mott},\Phi}$) according to Eq. (11) (Eq. (12)) for a massless ideal quark gas (PNJL model). The critical temperature is $T_c = 202$ MeV [13]. The parameters are fixed to reproduce quarkonium states in vacuum as Coulombic bound states [14]. In the charmonium (bottomonium) system the heavy quark mass m_Q is $m_c = 1.94$ GeV ($m_b = 5.1$ GeV) and the ground state binding energy ε_0 is 0.78 GeV (0.75 GeV).

	T^{Mott}/T_c	$T^{\mathrm{Mott},\Phi}/T_c$
J/ψ	1.25	1.37
χ_c	0.83	1.11
ψ'	0.66	0.99
Υ	2.50	2.50
χ_b	1.72	1.73
Υ'	1.28	1.39
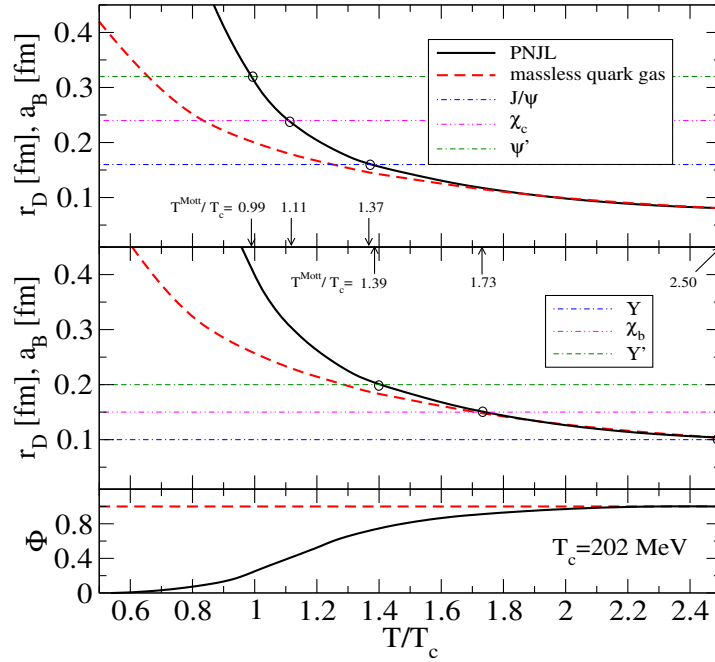
Figure 1: Temperature dependence of the Debye screening radius $r_D(T)$ for charmonium (upper panel) and bottomonium (middle panel) with (solid lines) and without (dashed lines) coupling to the Polyakov loop $\Phi(T)$ shown in the lower panel (from [13]). Sequential dissociation of quarkonia states occurs at the Mott temperatures T^{Mott} for which their Bohr radius equals $r_D(T)$.

This means that in the case of confining color correlations ($0 \leq \Phi < 1$) the Debye screening radius is larger than in a free quark gas at the same temperature, so that bound states get stabilized against thermal dissociation by color screening.

The influence of the Poyakov loop variable on the dissociation temperature is summarized in Figure 1 which shows the temperature dependence of the Debye radius $r_D(T) = 1/m_D(T)$ compared to the Bohr radii of the low-lying states of the charmonium and bottomonium family, respectively. Due to its larger mass and smaller Bohr radius, the Υ dissociates at higher temperatures than the J/ψ, where the free quark gas case is almost reached and the Mott temperatures which almost coincide for the cases with and without coupling to the Polyakov

loop field. For the lighter J/ψ there is a noticeable stabilization due to the coupling to the Polyakov loop potential which results in an increase of the Mott dissociation temperature from 1.25 T_c to 1.37 T_c, still more similar to results of nonrelativistic potential models rather than the still higher dissociation temperatures conjectured from the spectral functions deduced from lattice data for heavy quarkonium correlators by the maximum entropy method. For estimating the Mott temperatures of the excited quarkonia states we have employed the scaling of bound state radii: $r_{\chi_c} = 1.5 \ r_{J/\psi}$, $r_{\psi'} = 2.0 \ r_{J/\psi}$ as obtained in the Cornell-type potential model [7].

4 Conclusions

We have applied the methods of thermal field theory to estimate the effects of Debye screening on heavy quarkonia bound state formation. In order to account for residual effects of confining color correlations in the deconfined phase, we have used the PNJL model in the evaluation of the one-loop polarization function. As expected, a stabilization of bound states in the vicinity of the critical temperature for $T > T_c$ is obtained. We applied Ritz' variational principle to derive an analytical formula for the Mott criterion for heavy quarkonia ground states. The Mott temperatures for excited states are obtained here from a criterion based on their Bohr radii, in good agreement with results from the numerical solution Schrödinger equation for the screened Cornell potential using the here derived Debye mass as screening parameter [15].

Acknowledgments

References

[1] T. Matsui and H. Satz, Phys. Lett. B **178** 416 (1986).

[2] N. F. Mott, Rev. Mod. Phys. **40** 677 (1968).

[3] R. Rapp, D. Blaschke and P. Crochet, arXiv:0807.2470 [hep-ph] (2008).

[4] V. V. Dixit, Mod. Phys. Lett. A **5** 227 (1990).

[5] D. Cabrera and R. Rapp, Phys. Rev. D **76** 114506 (2007);
    C. Y. Wong, Phys. Rev. C **72** 034906 (2005).

[6] M. Asakawa, T. Hatsuda and Y. Nakahara, Prog. Part. Nucl. Phys. **46** 459 (2001);
    A. Jakovac, P. Petreczky, K. Petrov and A. Velytsky, Phys. Rev. D **75** 014506 (2007).

[7] H. Satz, J. Phys. G **32** R25 (2006).

[8] S. P. Klevansky, Rev. Mod. Phys. **64** (1992) 649.

[9] C. Ratti, M. A. Thaler and W. Weise, Phys. Rev. D **73** 014019 (2006).

[10] H. Hansen *et al.*, Phys. Rev. D **75** 065004 (2007).

[11] J. I. Kapusta and C. Gale, *Finite-Temperature Field Theory*, Cambridge University Press (2006).

[12] A. Beraudo, J. P. Blaizot and C. Ratti, Nucl. Phys. A **806** 312 (2008).

[13] D. Blaschke, M. Buballa, A. E. Radzhabov and M. K. Volkov, Yad. Fiz. **71**, 2012 (2008).

[14] F. Arleo, P. B. Gossiaux, T. Gousset and J. Aichelin, Phys. Rev. D **65** 014005 (2002).

[15] J. Jankowski, D. Blaschke and H. Grigorian, arXiv:0911.1534 [hep-ph].

Charmonium in a hot, dense medium

David Blaschke[1,2]

[1]*Institute for Theoretical Physics, University of Wrocław, 50-204 Wrocław, Poland*
[2]*Bogoliubov Laboratory for Theoretical Physics, JINR, 141980 Dubna, Russia*

In this lecture we apply a thermodynamic Green function formalism developed in the context of nonrelativistic plasma physics for the case of heavy quarkonia states in strongly correlated quark matter. Besides the traditional explanation of charmonium suppresion by Debye screening of the strong interaction, we discuss further effects of relevance when heavy quarkonia states propagate in a medium where strong correlations persist in the form of hadronic resonances. These effects may be absorbed in the definition of a plasma Hamiltonian, which was the main result of this work. This plasma Hamiltonian governs the in-medium modification of the bound state energy levels as well as the lowering of the continuum edge which leads not only to the traditional Mott effect for the dissociation of bound states in a plasma, but can also be applied for a consistent calculation of the in-medium modification of quarkonium dissociation rates.

1   Introduction

In developing a theoretical approach to heavy quarkonia as messengers of the deconfinement/ hadronization transition of a quark-gluon plasma formed in a heavy-ion collision, we should aim at a unifying description where hadrons appear as bound states (clusters) of quarks and gluons. The situation is analoguous to the problem of two-particle states in QED plasmas where a well-developed theory in the framework of the Green function technique exists. These methods have been widely developed for the case of the hydrogen plasma, where the electrons and protons as the elementary constituents can form hydrogen atoms as bound states of the attractive Coulomb interaction. The problem is tractable analytically for the isolated two-particle system, with a discrete energy spectrum of bound states and a continuous spectrum of scattering states. Higher complexes, such as molecular hydrogen can also be formed.

In a many-particle system, the problem of bound state formation needs to account for medium effects. They give contributions to a plasma Hamiltonian

$$H^{\mathrm{pl}} = H^{\mathrm{Hartree}} + H^{\mathrm{Fock}} + H^{\mathrm{Pauli}} + H^{\mathrm{MW}} + H^{\mathrm{Debye}} + H^{\mathrm{pp}} + H^{\mathrm{vdW}} + \dots, \qquad (1)$$

where the first three effects, the Hartree- and Fock energies of one-particle states and the Pauli blocking for the two-particle states, are of first order with respect to the interaction and determine the mean-field approximation. The following two terms of the plasma Hamiltonian are the Montroll-Ward term giving the dynamical screening of the interaction in the self-energy, and the dynamical screening (Debye) of the interaction between the bound particles. These contributions are related to the polarization function and are of particular interest for plasmas due to the long-range character of the Coulomb interaction. In a consistent description, both

terms should be treated simultaneously. The last two contributions to the plasma Hamiltonian are of second order with respect to the fugacity: the polarization potential, describing the interaction of a bound state with free charge carriers, and the van der Waals interaction, accounting for the influence of correlations (including bound states) in the medium on the two-particle system under consideration, see [1, 2].

Approximations to medium effects in the self-energy and the effective interaction kernel have to be made in a consistent way, resulting in predictions for the modification of one-particle and two-particle states. On this basis, the kinetics of bound state formation and breakup processes can be described, establishing the ionization equilibrium under given thermodynamical conditions [3]. Coulomb systems similar to the hydrogen plasma are electron-hole plasmas in semiconductors [4], where excitons and biexitons play the role of the atoms and molecules. Other systems which have been widely studied are expanded fluids like alkali plasmas or noble gas plasmas, see [1] and references therein. Applications of the plasma physics concepts for cluster formation and Mott effect to the rather short-ranged strong interactions have been given, e.g., in [5, 6] for nuclear matter and in [7, 8] for quark matter.

In this subsection, we want to discuss basic insights from these investigations of bound state formation in plasmas, as far as they can concern our discussion of heavy quarkonia formation in hot and dense matter. Before going more into the details, let us mention them. Bound state properties remain rather inert to changes of the medium since the self-energy and interaction effects partially compensate each other in lowest order of density. Also, the smaller size of the bound states matters in this respect. The compensation does not hold for continuum states, being influenced by self-energy effects only, so that a lowering of the in-medium ionization threshold must occur which leads to a strong enhancement of the rate coefficients for bound-free transitions and to a sequential "melting" of different bound state excitation levels into the continuum of scattering states at corresponding critical plasma parameters (Mott effect [9]), until even the ground state becomes unbound.

The theory of strongly coupled plasmas has been developed also for strong nonideality, where the formation of clusters in the medium need to be taken into account. This situation is similar to that of a hadronizing quark-gluon plasma and we will therefore refer to cluster expansion techniques as the theoretical basis.

2 Bethe-Salpeter equation and plasma Hamiltonian

The most systematic approach to the description of bound states in plasmas uses the Bethe-Salpeter equation (BSE) for the thermodynamic (Matsubara-) two-particle Green function

$$G_{ab} = G_{ab}^0 + G_{ab}^0 \ K_{ab} \ G_{ab} = G_{ab}^0 + G_{ab}^0 \ T_{ab} \ G_{ab}^0 \ , \qquad (2)$$

which is equivalent to the use of the two-particle T-matrix T_{ab} and has to be solved in conjunction with the Dyson equation for the full one-particle Green function,

$$G_a = G_a^0 + G_a^0 \Sigma_a G_a \ , \qquad (3)$$

defined by the dynamical self-energy $\Sigma_a(p, \omega)$ and the free one-particle Green function $G_a^0(p, \omega) = [\omega - \varepsilon_a(p)]^{-1}$ for a particle of species a with the dispersion relation $\varepsilon_a(p) = \sqrt{p^2 + m_a^2} \approx m_a + p^2/(2m_a)$, see Fig. 1.

The BSE contains all information about the spectrum of two-particle bound as well as scattering states in the plasma. A proper formulation of the plasma effects on the two-particle

Figure 1: The two-particle problem in the medium. Dyson equation (left) and Bethe-Salpeter equation (right) need to be solved in consistent (conserving) approximations for self-energy (Σ) and interaction kernel (K).

spectrum is essential to understand why bound and scattering states are influenced in a different way by the surrounding medium, leading to the Mott-effect for bound states. We give here the essence of a detailed discussion to be found in Ref. [2].

The homogeneous BSE associated with (2) can be given the form of an effective Schrödinger equation for the wave function $\psi_{ab}(p_1, p_2, z)$ of two-particle states in the medium [4]

$$\sum_q \left\{ [\varepsilon_a(p_1) + \varepsilon_b(p_2) - z] \delta_{q,0} - V_{ab}(q) \right\} \psi_{ab}(p_1 + q, p_2 - q, z) =$$

$$= \sum_q H_{ab}^{\mathrm{pl}}(p_1, p_2, q, z) \psi_{ab}(p_1 + q, p_2 - q, z), \tag{4}$$

where a, b denote a pair of particles with 3-momenta p_1 and p_2 which transfer a 3-momentum $2q$ in their free-space interaction $V_{ab}(q)$ and z is a complex two-particle energy variable. The in-medium effects described by (2) have been singled out in the definition of a plasma Hamiltonian, containing all modifications beyond the two-body problem in free space [2, 4]

$$H_{ab}^{\mathrm{pl}}(p_1, p_2, q, z) = \underbrace{V_{ab}(q) [N_{ab}(p_1, p_2) - 1]}_{\text{(i) Pauli blocking}} - \underbrace{\sum_{q'} V_{ab}(q') [N_{ab}(p_1 + q', p_2 - q') - 1] \delta_{q,0}}_{\text{(ii) Exchange self−energy}}$$

$$+ \underbrace{\Delta V_{ab}(p_1, p_2, q, z) N_{ab}(p_1, p_2)}_{\text{(iii) Dynamically screened potential}} - \underbrace{\sum_{q'} \Delta V_{ab}(p_1, p_2, q', z) N_{ab}(p_1 + q', p_2 - q') \delta_{q,0}}_{\text{(iv) Dynamical self−energy}} . \tag{5}$$

Here, $\Delta V_{ab}(p_1, p_2, q, z) = K_{ab}(p_1, p_2, q, z) - V_{ab}(q)$ stands for the in-medium modification of the bare interaction potential to a dynamically screened interaction kernel $K_{ab}(p_1, p_2, q, z)$. The effects of phase space occupation are encoded in the function $N_{ab}(p_1, p_2)$, which for the case of an uncorrelated fermionic medium takes the form of the Pauli blocking factor $N_{ab}(p_1, p_2) = 1 - f_a(p_1) - f_b(p_2)$, where $f_a(p) = \{\exp[(\varepsilon_a(p) - \mu_a)/T] + 1\}^{-1}$ is the Fermi distribution and μ_a the chemical potentential of the species a. Eq. (4) is a generalization of the two-particle Schrödinger equation, where on the left-hand side the isolated two-particle problem is described while many-body effects due to the surrounding medium are given on the right-hand side. The in-medium effects named in the plasma Hamiltonian (1) can be obtained from the one derived in the Bethe-Salpeter approach (5) upon proper choice of the interaction kernel K_{ab} so that Eq. (1) appears a sa special case of Eq. (5).

The influence of the plasma Hamiltonian on the spectrum of bound and scattering states can be qualitatively discussed in perturbation theory. Since bound states are localized in coordinate space, their momentum space wave functions extend over a finite range Λ and we may assume them to be q-independent: $\psi_{ab}(p_1 + q, p_2 - q, z = E_{nP}) \approx \psi_{ab}(p_1, p_2, z = E_{nP})$ for small momentum transfer $q < \Lambda$ and to vanish otherwise. Assuming further a flat momentum

dependence of the Pauli blocking factors $N_{ab}(p_1 + q, p_2 - q) \approx N_{ab}(p_1, p_2)$ for small q where the interaction is strong, we obtain a cancellation of the Pauli blocking term (i) by the exchange self energy (ii) and of the dynamically screened potential (iii) by the dynamical self-energy (iv). Therefore, the bound states remain largely unmodified by medium effects. For scattering states which are extended in coordinate space and can be represented by a delta function in momentum space, the above cancellations do not apply and a shift of the two-particle continuum threshold results. For this mechanism to work it is important that approximation schemes for the self-energy and the interaction kernel have to be consistent as, e.g., in the conserving scheme of Φ-derivable theories [10].

Summarizing the discussion of the plasma Hamiltonian: bound state energies remain unshifted to lowest order in the charge carrier density while the threshold for the continuum of scattering states is lowered. The intersection points of bound state energies and continuum threshold define the Mott densities (and temperatures) for bound state dissociation.

When applying this approach to heavy quarkonia in a medium where heavy quarks (either free or bound in heavy hadrons) are rare, then $N_{ab} = 1$ so that both, (i) and (ii) can be safely neglected. The effects (iii) and (iv) stem from the dynamical coupling of the two-particle state to collective excitations (plasmons) in the medium. In the screened potential approximation, the interaction kernel is represented by $V_{ab}^S(p_1 p_2, q, z) = V_{ab}^S(q, z)\delta_{P, p_1 + p_2}\delta_{2q, p_1 - p_2}$ with

$$V_{ab}^S(q, z) = V_{ab}(q) + V_{ab}(q)\Pi_{ab}(q, z)V_{ab}^S(q, z) = V_{ab}(q)[1 - \Pi_{ab}(q, z)V_{ab}(q)]^{-1} , \qquad (6)$$

with the total momentum P and the momentum transfer $2q$ in the two-particle system. The most frequently used approximation for the here introduced polarization function $\Pi_{ab}(q, z)$, or for the equivalent dielectric function $\varepsilon_{ab}(q, z) = 1 - \Pi_{ab}(q, z)V_{ab}(q)$, is the random phase approximation (RPA). In the next two paragraphs we discuss the static, long wavelength limit of the RPA and its generalization for a clustered medium.

Example 1: statically screened Coulomb potential. The systematic account of the modification of the interaction potential between charged particles a and b by polarization of the medium is taken into account in the dynamical polarization function $\Pi_{ab}(q, z)$, which in RPA reads [2]

$$\Pi_{ab}^{\mathrm{RPA}}(q, z) = 2\delta_{ab} \int \frac{d^3 p}{(2\pi)^3} \frac{f_a(E_p^a) - f_a(E_{p-q}^a)}{E_p^a - E_{p-q}^a - z} . \qquad (7)$$

For the Coulomb interaction, corresponding to the exchange of a massless vector boson, the potential is obtained from the longitudinal propagator in the Coulomb gauge is $V_{ab}(q) = e_a e_b/q^2$. For a recent discussion in the context of heavy quark correlators and potentials see, e.g., [11, 12]. Due to the large masses of the constitutents in the heavy quarkonium case, one may use a Born-Oppenheimer expansion to replace the dynamically screened interaction by its static ($z = 0$) and long-wavelength ($q \to 0$) limit. For nondegenerate systems the distribution functions are Boltzmann distributions and their difference can be expanded as

$$f_a(E_p^a) - f_a(E_{p-q}^a) = \mathrm{e}^{-E_p^a/T}\left(1 - \mathrm{e}^{-(E_{p-q}^a - E_p^a)/T}\right) \approx -f_a(E_p^a)(E_p^a - E_{p-q}^a - z)/T , \qquad (8)$$

so that the energy denominator gets compensated and the polarization function becomes

$$\Pi_{ab}^{\mathrm{RPA}}(q, z) = -2\frac{\delta_{ab}}{T} \int \frac{d^3 p}{(2\pi)^3} f_a(E_p^a) = -\delta_{ab}\frac{n_a(T)}{T} . \qquad (9)$$

The corresponding dielectric function $\varepsilon_{ab}^{\mathrm{RPA}}(q,\omega)$ takes the form

$$\lim_{q \to 0} \varepsilon^{\mathrm{RPA}}(q,0) = 1 + \frac{\mu_D^2}{q^2} \ , \quad \mu_D^2 = \frac{1}{T} \sum_a e_a^2 n_a(T) \ . \tag{10}$$

The screened Coulomb potential in this approximation is therefore $V_{ab}^S(q) = V_{ab}(q)/\varepsilon^{\mathrm{RPA}}(q,0) = e_a e_b/(q^2 + \mu_D^2)$. In this "classical" example of the statically screened Coulomb interaction, the contribution to the plasma Hamiltonian is real and in coordinate representation it is given by

$$\Delta V_{ab}(r) = -\frac{\alpha}{r}(\mathrm{e}^{-\mu_D r} - 1) \approx \alpha \mu_D - \frac{\alpha}{2}\mu_D^2 r \ , \tag{11}$$

where $\alpha = e^2/(4\pi)$ is the fine structure constant. For the change in the Hartree self-energy of one-particle states due to Debye screening we can perform an estimate in momentum space

$$\Sigma_a = \frac{4\pi\alpha}{(2s_a + 1)} \int \frac{d^3q}{(2\pi)^3} \left[\frac{1}{q^2 + \mu_D^2} - \frac{1}{q^2} \right] f_a(E_q^a) \approx -\frac{\alpha\mu_D^2}{\pi} \int_0^\infty \frac{dq}{q^2 + \mu_D^2} = -\frac{\alpha\mu_D}{2} \ . \tag{12}$$

This entails that to lowest order in the density the shift of the one-particle energies (continuum edge of unbound states) $\Sigma_a + \Sigma_b = -\alpha\mu_D$ compensates the contribution due to the screening of the interaction (11)

$$\Delta_{ab} \approx \alpha\mu_D = \mathcal{O}(\sqrt{na_{\mathrm{B},0}^3}) \ , \tag{13}$$

in the wave equation (4). For the shift of the bound state energy levels follows [2, 13]

$$\Delta E_{\mathrm{nl}} \approx -\frac{\alpha}{2}\mu_D^2 \langle r \rangle_{\mathrm{nl}} = \mathcal{O}(na_{\mathrm{B},0}^3) \ , \tag{14}$$

where $a_{\mathrm{B},0} = 1/(\alpha\, m)$ is the Bohr radius.

The Debye mass μ_D, equivalent to the inverse of the Debye radius r_{D} characterizing the effective range of the interaction, depends on the square root of the density $n(T)$ of charge carriers. It is this different response of bound states and scattering continuum to an increase of density and temperature in the medium which leads to the Mott effect (see, e.g., Refs. in [9] and [1]) for electrons in an insulator: bound states of the Debye potential can only exist when the Debye radius is larger than $r_{\mathrm{D,Mott}} = 0.84\, a_{\mathrm{B},0}$ [14]. This entails that above a certain density even the ground state electrons become unbound and form a conduction band, resulting in an insulator-metal transition also called Mott-transition. Further details concerning this example can be found in Ref. [15].

In complete analogy to this electronic Mott effect it is expected that in hadronic matter under compression the hadrons as bound states of quarks undergo a Mott transition which results in a phase transition from the color insulating phase of hadronic matter to a color conducting or even color superconducting phase of deconfined quark matter. This applies to light hadrons as well as to heavy quarkonia, whereby due to the different scales of Bohr radii the Mott dissociation of heavy quarkonia occurs at higher densities than for light hadrons.

In most approaches the quark self energy effects are neglected and one is left with the only medium effect due to a statically screened potential. This has the consequence that in such a picture the continuum edge of the scattering states remains unshifted and due to the lack of compensation the effective interaction leads to a strong medium dependence of the bound state energies (masses). For the electron-hole plasma in highly excited semiconductors it could be

shown experimentally, however, that the compensation picture is correct and the bound state energies remain almost unshifted [16].

One may of course absorb the self-energy effects into a redefinition of the effective interaction, by adding a homogeneous mean-field contribution. This is equivalent to the use of the Ecker-Weitzel potential [17]

$$V_{\text{Ecker}-\text{Weitzel}}(r) = -\frac{\alpha}{r}\text{e}^{-\mu_D r} - \alpha\mu_D \ . \tag{15}$$

It is interesting to note that recent investigations of the screening problem in the context of Debye-Hückel theory [18] and $Q\bar{Q}$ correlators [11, 12] have obtained this continuum shift $(-\alpha\mu_D)$ as a homogeneous background field contribution. According to the above lesson from plasma physics, however, this contribution should be attributed to the self-energy of the constituents rather than to the interaction kernel, since it determines the shift of the continuum edge.

For the development of a comprehensive approach to heavy quarkonia in hadronizing hot, dense QCD matter another insight from plasma physics may be of relevance and will be discussed next: the effect of strong correlations (bound states) in the medium. To this end, the bound states will be treated like a new species occuring in the system. Accordingly, additional diagrams have to be taken into account which stem from a cluster expansion of the interaction kernel K_{ab} and the corresponding self-energy Σ_a, see Figs. 2-4. This leads in the plasma Hamiltonian H^{pl} to a generalization of the self-energy contributions (cluster-Hartree-Fock approximation), the distribution functions in the Pauli-blocking factors and the dynamical screening (cluster-RPA). The van-der-Waals interaction in Eq. (1) appears naturally as a contribution in the cluster expansion, describing polarization effects due to bound states in the medium.

3 Cluster expansion for quarkonia in correlated medium

In the vicinity of the plasma phase transition, correlations play an important role and their proper accounting requires rather sophisticated theoretical methods such as cluster expansion techniques. For the problem of charmonium in dense hadronic matter at the deconfinement transition, i.e. in the strong coupling case, we suggest a systematic Born series expansion of collisions with free and bound states in the surrounding matter so that all terms linear in the density of free particles and bound states are taken into account.

We describe the cluster expansion here in terms of its diagrammatic expressions for the interaction kernel and the corresponding self-energy. The 1st Born approximation diagrams of this expansion are given in Fig. 2, see also the monograph [2]. The wavy line denotes the dynamically screened interaction V_{ab}^{S}, which in a strongly correlated plasma receives contributions from the polarization of the medium beyond the RPA, denoted as generalized (cluster-) RPA in Fig. 4, see Ref. [19]. Bound and scattering states are described consistently in the two-particle T-matrices. For a generalization to higher n-particle correlations, see [6, 20] and the monograph [2]. The diagrams containing T-matrices do not contribute to the charmonium spectrum as long as the densities of the charmed quarks and of charmed hadrons in the medium are negligible. This is the situation expected for the rather low-energy CBM experiment. For the discussion of charmonium production at RHIC and at LHC the inclusion of these terms can be invoked.

At the 2nd Born order, we distinguish two classes of collisions with light clusters (hadrons)
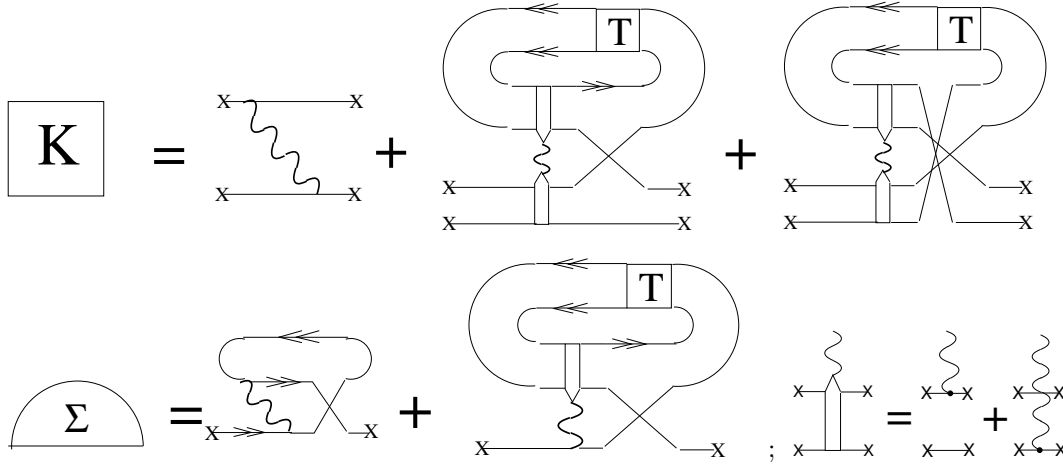
Figure 2: Cluster expansion for interaction kernel for the two-particle problem in a strongly correlated medium (upper equation) and the corresponding self-energy (lower left equation) with a dipole ansatz for the vertex (lower right equation).
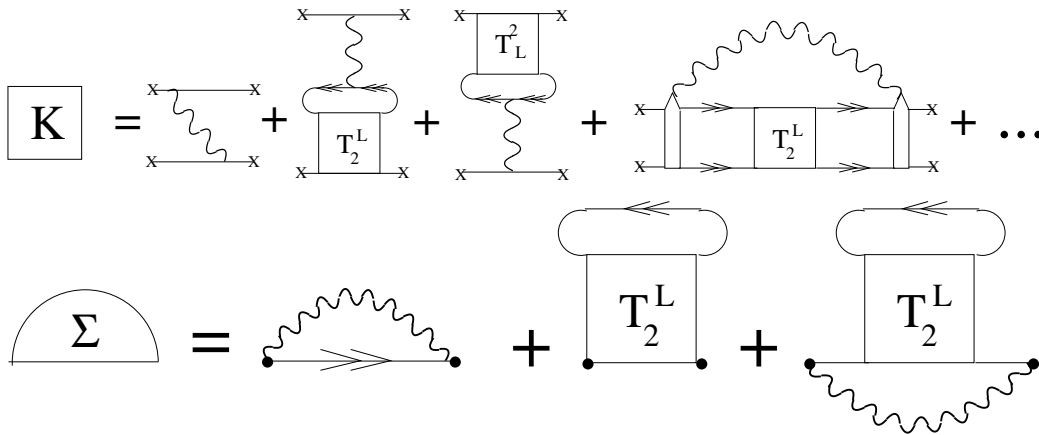

Figure 3: Alternative way of drawing the diagrams for the cluster expansion of the interaction kernel and the corresponding self-energy of Fig. 2 in a form familiar in plasma physics and nuclear physics.

that can give rise to spectral broadening of the charmonia. The first class concerns hadron impact without quark rearrangement inducing transitions to excited states, shown in the left panel of Fig. 5. These processes have been considered for charmonium-hadron interactions within the operator product expansion techniques following Peskin and Bhanot [21, 22], see [23, 24]. The result is a deformation of the charmonium spectrum under conservation of the spectral weight integrated over all charmonia states. In the second class are quark rearrangement (string-flip) processes, as indicated in the right panel of Fig. 5. They induce transitions to open charm hadrons responsible for charmonium dissociation in hadronic matter, cf. Sect. 4.
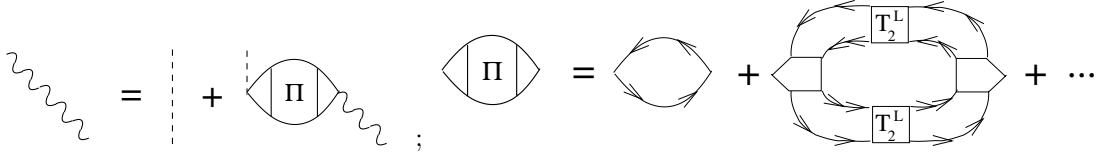
Figure 4: Left panel: The dynamically screened interaction potential $V_{ab}^S(\omega, q)$ (wavy line), determined by the bare potential (dashed line) and the polarization function $\Pi_{ab}(\omega, q)$. Right panel: Cluster expansion for the generalized RPA, when besides free particles (RPA) also two-particle states (cluster-RPA) contribute to the polarizability of the medium, see Ref. [19].
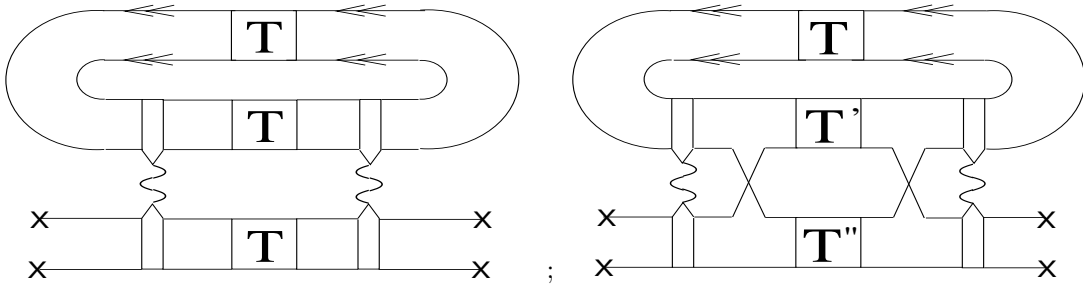

Figure 5: Contributions to the dynamical self-energy of a two-particle system in a correlated medium at 2nd Born order. Left panel: impact by two-particle states without constituent exchange (van-der-Waals or dipole-dipole interaction). Right panel: constituent-rearrangement collisions (string-flip process), from Ref. [25], see also [26].

Example 2: String-flip model of charmonium dissociation. Here we give a second example for the use of insights from plasma physics by discussing charmonium dissociation within the string-flip model of quark matter [7, 8, 27, 28]. In this model the string-type color interactions between quarks get saturated within the sphere of nearest neighbors so that in a dense system of overlapping quark-antiquark pairs frequent string-flip processes take place in order to assure the system is at any time in its minimal energy configuration, see the left panel of Fig. 6.

When considering a heavy quark-antiquark pair in dense matter with negligible heavy-flavor fraction, the Pauli blocking and exchange self-energy contributions are negligible, but the strong correlations with light quarks of complementary color within the nearest neighbor sphere will result in a meanfield selfenergy shift (Hartree shift Δ^H) for all quarks [29]. This determines the shift of the continuum edge, see the graph (b) in the right panel of Fig. 6. Because of the compensation in the Bethe-Salpeter kernel between the effects of the screening of the interaction and the self energy shifts calculated with it (see discussion above), it is suggested that to lowest order the bound state energies remain unshifted when increasing the temperature and/or density of the medium. In contrast to the first example of Debye screening of long-range Coulombic interactions, the screening mechanism in the string flip model is color saturation within nearest neighbors, applicable for strong, short-range interactions as appropriate for the case of the sQGP at RHIC or dense systems at FAIR CBM. The resulting two-particle energy spectrum for charmonium and bottomonium states is shown in the right panel of Fig. 6, where the static screening picture (graph (a) as a function of the screening parameter $\mu = \mu_D(T)$ in the
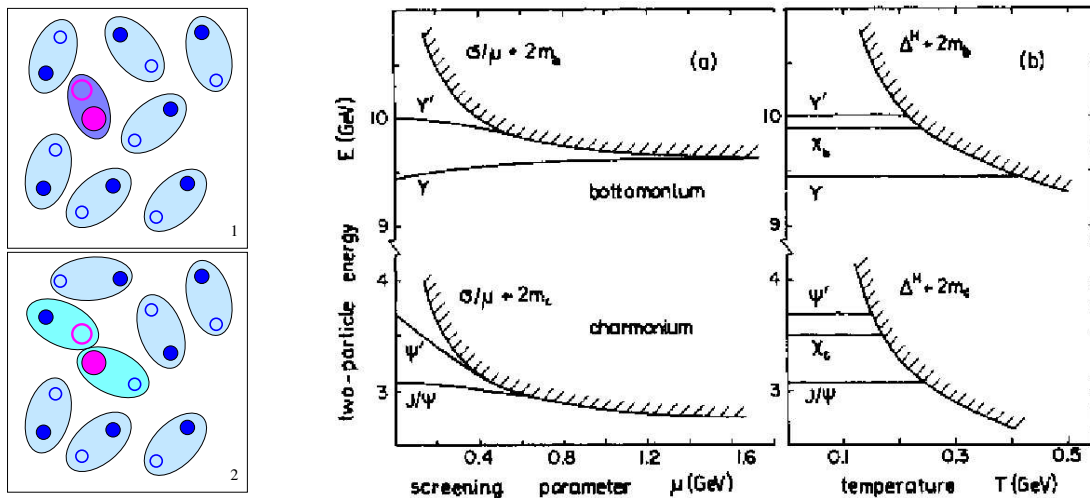
Figure 6: Left panel: String-flip process in a dense quark-antiquark system, see also [8, 26]. Right panel: Two-particle energies of charmonia and bottomonia states in a statically screened potential (a) and in the string-flip model (b), from Ref. [31].

screened Cornell potential [30] is compared to the string-flip picture (graph (b) as a function of the temperature T), from Ref. [29, 31]. From this Figure one can read-off the in-medium lowering of the dissociation threshold k_0^{diss}, which is the energy difference between the considered bound state level and the continuum edge shown as the border of the hatched region. This lowering of k_0^{diss} with increasing density and/or temperature leads to a strong increase in the quarkonium breakup cross sections by thermal impact [31] and to the bound state dissociation, even before the binding energies vanish at the critical Mott densities and temperatures for the corresponding states.

4 Charmonium dissociation in a resonance gas

An interesting phenomenological guideline for the present discussion is provided by Ref. [32] where the authors show that universal J/ψ-hadron breakup cross sections with correct kinematic thresholds but otherwise constant at 3 mb for meson and 5 mb for baryon impact are sufficient to explain the observed anomalous J/ψ suppression pattern of the NA50 experiment within a multi-component hadron gas. For a recent update, see [33]. The question arises: How do these assumptions relate to microscopic calculations of charmonium dissociation reactions in hadronic matter? Those can generally be divided into two categories, based on hadronic or quark degrees of freedom. We will primarily review and compare the studies of processes in a mesonic medium (predominantly composed of pions and rho mesons) within both approaches, including a discussion of in-medium effects.

Historically, a first calculation of the quark-exchange reaction, $J/\psi + \pi \rightarrow D + \bar{D}^* + c.c.$, was performed in a nonrelativistic quark model [34] based on applications of the diagrammatic technique developed by Barnes and Swanson [35] for meson-meson scattering, see also Ref. [36]. This calculation showed a strong energy dependence of the cross section with a peak value
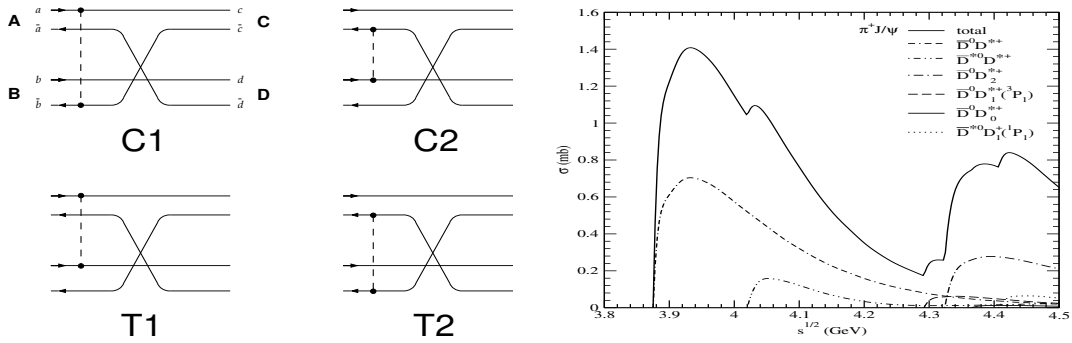
Figure 7: Born diagrams for quark-exchange processes (denoted as C1, C2 for "capture" and T1, T2 for "transfer" diagrams) contributing to heavy quarkonium dissociation by meson impact (left panels) and the corresponding cross section for J/ψ breakup by pion impact (right panel); from Refs. [37, 38]. Note that in the total cross section also the processes with charge conjugated final states are accounted for.

of about 6 mb at threshold and a fast decrease due to a momentum mismatch in the overlap integrals between the meson wave functions. The thermally averaged cross section, which is the relevant quantity for estimating the J/ψ dissociation rate, was below 1 mb, roughly in accordance with phenomenological expectations based on the observed suppression in heavy-ion reactions at the SPS. These calculations were extended to other light mesons and excited charmonia in Refs. [37, 38], where also more realistic quark-interaction potentials have been used. In Fig. 7 we show the diagrams for quark-exchange processes at first Born order, which are classified as "capture" (C) and "transfer" (T) diagrams depending on whether the quark interaction can be absorbed into the external meson lines; the latter are to be understood as a resummation of ladder-type quark-antiquark interactions. There are cancellations among the contributions of the different diagrams due to the small color dipole of the charmonium state. These cancellations reduce the peak value of the cross section to about 1 mb, as also illustrated in Fig. 7. An open question in this approach is whether the double nature of the pion – a Goldstone boson of the broken chiral symmetry and a strongly bound quark-antiquark – has a strong influence on these results. In the nonrelativistic approach the pion emerges due to a large hyperfine splitting in the Fermi-Breit Hamiltonian (as opposed to, e.g., instanton-induced interactions), which is not a robust interpretation. Another question concerns the applicability of the truncation of the transfer diagram contributions at the first Born order. Ladder-type resummations would lead to s- and t-channel D-meson exchange processes, which are disregarded in the nonrelativistic quark exchange. Finally, these models are beset with the "post-prior" problem due to the ambiguity in the ordering of quark exchange and interaction lines.

These problems can be resolved within relativistic quark models developed on the basis of Dyson-Schwinger equations [39] for applications to the charmonium dissociation problem [40, 41, 42]. In this approach, the meson-meson interactions are represented by quark-loop diagrams with three (triangle) and four (box) meson legs. The appearance of meson-exchange processes can be understood as a ladder resummation of quark interaction diagrams in s- and t-channels, see Fig. 8. The results for the J/ψ dissociation cross section by pion impact within the relativistic quark model [41], shown in Fig. 8, basically confirm those of the nonrelativistic
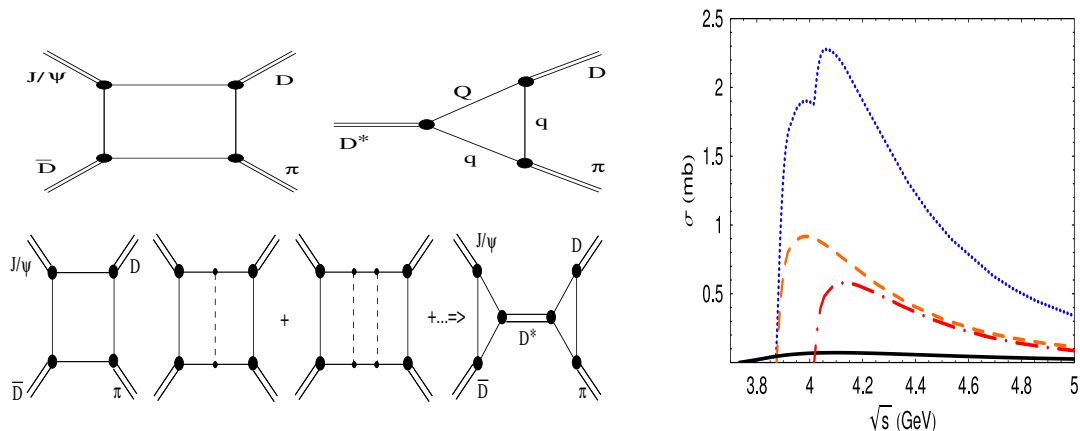
Figure 8: Left panel: box and triangle diagrams for meson-meson interaction vertices contributing to J/ψ breakup by meson impact in the relativistic quark model [40] (upper part), and the origin of D-meson exchange from ladder-type resummation (lower part). Right panel: cross section for pion induced J/ψ dissociation into open-charm mesons (dotted line) composed of subprocesses with different final-state D-meson pairs: $D + \bar{D}$ (solid), $D + \bar{D}^*$ (dashed), $D^* + \bar{D}^*$ (dash-dotted); from Ref. [41]. The total cross section includes also the subprocess with $\bar{D} + D^*$ final state for which the cross section is identical to the charge conjugated one (dashed).

approaches [34, 37, 38] shown in Fig. 7; residual differences may be traced back to the treatment of the transfer-type diagrams. In the relativistic treatment these diagrams are resummed beyond the first Born approximation and result in D-meson exchange diagrams which are absent in the nonrelativistic models. This difference may explain small differences in cross section results from both approaches.

Already in 1998, Matinyan and Müller [43] pioneered an alternative approach to charmonium absorption by light mesons on the basis of an effective meson Lagrangian, with a local $U(4)$ flavor symmetry strongly broken by the pseudoscalar and vector meson mass matrices. This initial version of the chiral Lagrangian approach gave rather small cross sections, $\sigma_{\pi\psi} \approx 0.3$ mb at threshold. It turned out [44, 45] that triple vector-meson couplings and contact terms, not included in Ref. [43], result in an increase of the breakup cross section by up two orders of magnitude, with a rising energy dependence. A problem for the chiral Lagrangian approaches is the treatment of hadrons as pointlike objects, which, as usual for an effective theory, becomes unreliable at high momentum transfers (due to quark-exchange substructure effects). The composite nature of hadrons can be accounted for in an approximate way by vertex form factors [45, 46], which reduce the magnitude, and affect the energy dependence, of the cross sections, see Fig. 9. The choice of the cutoff parameters in the form factors has a large effect on the charmonium breakup cross sections and remains a matter of debate [48, 49, 50, 51]. Progress may be made by calibrating the form factors with microscopic approaches as, e.g., the nonrelativistic or the relativistic quark models [52]. While the calculations with the relativistic quark model are very cumbersome, the chiral Lagrangian models offer a very effective tool to assess many other dissociation processes required for phenomenology, once the formfactor question is settled. In particular, these applications include dissociation processes by nucleon
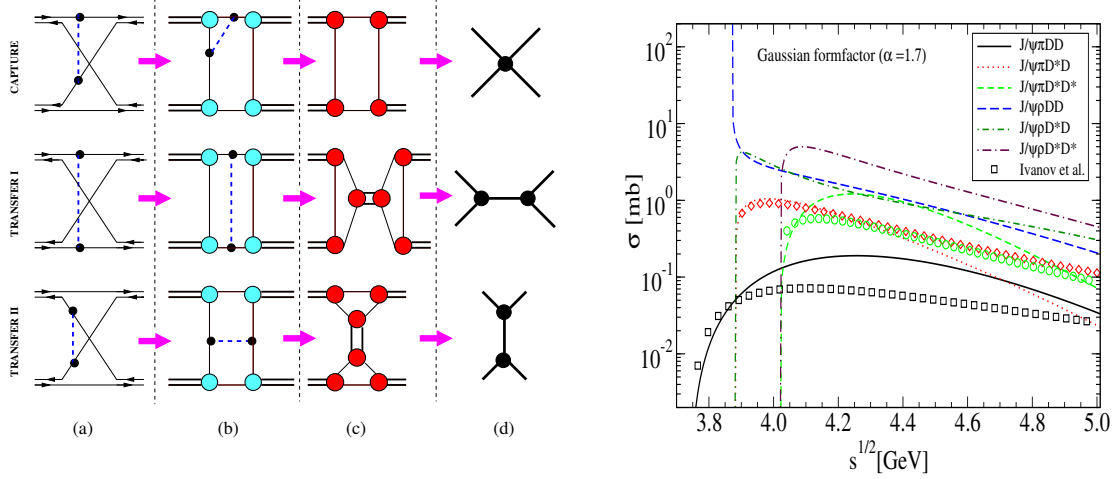
Figure 9: Feynman diagrams for J/ψ breakup by meson impact in the chiral Lagrangian approach (left) and the resulting cross sections for pion- and rho-meson induced processes (right), from Ref. [52]. The left panel illustrates the interrelation of the different approaches to charmonium breakup cross sections: The nonrelativistic potential model diagrams (a) can be redrawn as quark loop diagrams with Born order insertions (b). The latter can be either absorbed into the nonperturbative meson-quark-antiquark vertices (c, upper line) or after partial resummation of all ladder-type diagrams of the Born series redrawn as t-channel and s-channel meson exchanges (c, lower lines). The locan limit of the relativistic quark model diagrams (c) leads to the chiral Lagrangian diagrams (d) with formfactors originating from the quark loop diagrams for the meson vertices in (c).

impact [53, 54] and bottomonium dissociation [55].

The energy dependent cross sections for heavy quarkonia dissociation by hadron impact enable to evaluate the temperature- (and density-) dependent dissociation rates in hadronic matter. Assuming the (short-distance) vertex functions not to be altered by the surrounding medium, there remains the issue of mass and widths changes of open-charm hadrons with temperature and density. These, in particular, imply modifications of the thresholds for the breakup processes [58, 59, 60, 61, 62, 63]. In Fig. 10 we show the diagrammatic representation of the quark-exchange contribution to the J/ψ self-energy which develops an imaginary part (determining its width or inverse lifetime) due to the coupling to open-charm mesons. For the interaction vertex U_{ex} three different approaches have been discussed above and the corresponding vacuum cross sections are shown in Figs. 7-9. The theoretical basis for the discussion of quark exchange effects to the self-energy of heavy quarkonia in strongly correlated quark matter comes from systematic cluster expansion techniques developed in the context of plasma physics. For details, see the next subsection and Figs. 2, 3 and 5. Fig. 11 illustrates the effect of the spectral broadening of D-mesons at the chiral phase transition due to the opening of the decay channel into their quark constituents (Mott effect) for temperatures exceeding the D-meson Mott temperature $T^{\mathrm{Mott}} \approx 172$ MeV. Due to an effective lowering of the J/ψ breakup
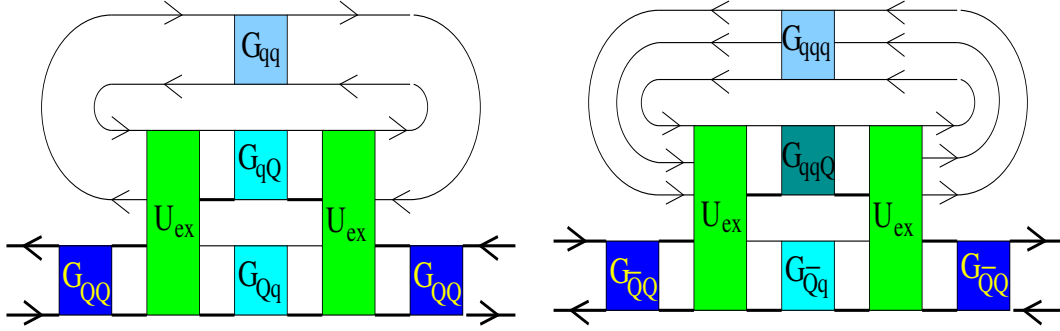
Figure 10: Left panel: Diagrammatic representation of the quark exchange process contribution to the heavy quarkonium self-energy in a mesonic medium [64]; right panel: same as left panel but for quark exchange with baryons in the medium [57]. Three different approaches to the interaction vertex U_{ex} are discussed in the text and shown in Figs. 7-9. Diagrams of this type appear in the cluster expansion for two-particle properties, see Fig. 5.
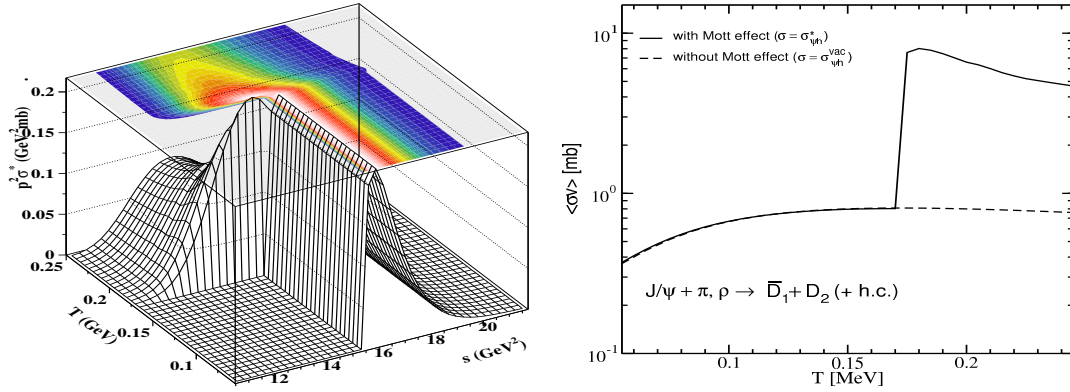
Figure 11: Left panel: energy (s) and temperature (T) dependence of the effective cross section (σ^*) for J/ψ breakup by ρ-meson impact. We display $p^2\sigma^*(s;T)$ for better visibility of the effective lowering of the breakup threshold when temperatures exceed the D-meson Mott temperature $T^{\mathrm{Mott}} \approx 172$ MeV; right panel: temperature dependence of the thermally averaged J/ψ breakup cross section in a π-ρ meson gas; the calculation with vacuum D-mesons (dashed line) is compared to one with an in-medium broadening of the D-meson spectral function (due to the Mott effect at the chiral phase transition) which exhibits a steplike enhancement (solid line) caused by the effective lowering of the breakup threshold; from Ref. [56].

threshold the temperature dependence of the thermally averaged J/ψ breakup cross section in a π-ρ meson gas exhibits a steplike enhancement [56]. This effect has been discussed as a possible mechanism underlying the threshold-like anomalous suppression pattern of J/ψ's observed by the CERN NA50 experiment [61, 64] and should also play a role in explaining the final state interactions of heavy quarkonia produced in the RHIC experiments.

5 Perspectives

In this lecture we have adapted a general thermodynamic Green function formalism developed in the context of nonrelativistic plasma physics for the case of heavy quarkonia states in strongly correlated quark matter. Besides the traditional folklore explanation of charmonium suppresion by (Debye-) screening of the strong interaction, we discuss further effects of relevance when heavy quarkonia states propagate in a medium where strong correlations persist in the form of hadronic resonances. These effects may be absorbed in the definition of a plasma Hamiltonian, which was the main result of this contribution. This plasma Hamiltonian governs the in-medium modification of the bound state energy levels as well as the lowering of the continuum edge which leads not only to the traditional Mott effect for the dissociation of bound states in a plasma, but can also be applied to calculate the in-medium modification of quarkonium dissociation rates in a consistent way. A detailed recent review [65] summarizes the phenomenological applications to heavy quarkonia production heavy-ion collision experiments at CERN and RHIC. Further developments of the presented approach shall include in particular applications to quarkonia production in dense baryonic matter such as envisaged for the PANDA and CBM experiments at FAIR Darmstadt and possibly also for NICA at JINR Dubna.

Acknowledgments

References

[1] R. Redmer, Phys. Rep. **282** (1997) 35.

[2] W. Ebeling, W.-D. Kraeft, D. Kremp, G. Röpke, *Quantum Statistics of Charged Many-Particle Systems*, Plenum, New York (1986).

[3] M. Schlanges, Th. Bornath and D. Kremp, Phys. Rev. A **38** (1988) 2174.

[4] R. Zimmermann, K. Kilimann, W. D. Kraeft, D. Kremp and G. Röpke, Phys. Stat. Sol. (b) **90** (1978) 175.

[5] G. Röpke, et al., Nucl. Phys. A **379** (1982) 536.

[6] G. Röpke, et al., Nucl. Phys. A **399** (1983) 587.

[7] C. J. Horowitz, E. J. Moniz and J. W. Negele, Phys. Rev. D **31** (1985) 1689.

[8] G. Röpke, D. Blaschke and H. Schulz, Phys. Rev. D **34** (1986) 3499.

[9] N. F. Mott, Rev. Mod. Phys. **40**, 677 (1968).

[10] G. Baym, Phys. Rev. **127** (1962) 1391.

[11] N. Brambilla, J. Ghiglieri, A. Vairo and P. Petreczky, Phys. Rev. D **78** (2008) 014017.

[12] A. Beraudo, J. P. Blaizot and C. Ratti, Nucl. Phys. A **806** (2008) 312.

[13] W. Ebeling and K. Kilimann, Z. Naturforsch. **44a** (1989) 519.

[14] F. J. Rogers, H. C. Garboske Jr., and D. J. Harwood, Phys. Rev. A **1** (1970) 1577.

[15] W. D. Kraeft, D. Kremp, K. Kilimann, and H. E. DeWitt, Phys. Rev. A **42** (1990) 2340.

[16] G. W. Fehrenbach, W. Schäfer, J. Treusch, and R. G. Ulbrich, Phys. Rev. Lett. **49** (1981) 1281.

[17] G. Ecker and W. Weitzel, Ann. Phys. (Lpz.) **17** (1956) 126.

[18] V. V. Dixit, Mod. Phys. Lett. A **5** (1990) 227.

[19] G. Röpke and R. Der, Phys. stat. sol. (b) **92** (1979) 501.

[20] G. Röpke, et al., Nucl. Phys. A **424** (1984) 594.

[21] G. Bhanot and M. E. Peskin, Nucl. Phys. B **156** (1979) 391.

[22] M. E. Peskin, Nucl. Phys. B **156** (1979) 365.

[23] D. Kharzeev and H. Satz, Phys. Lett. B **334** (1994) 155.

[24] F. Arleo, P.B. Gossiaux, T. Gousset and J. Aichelin, Phys. Rev. D **65** (2002) 014005.

[25] D. Blaschke and V. L. Yudichev, AIP Conf. Proc. **842** (2006) 38.

[26] H. Satz, arXiv:hep-ph/0602245.

[27] H. Miyazawa, Phys. Rev. D **20** (1979) 2953.

[28] D. Blaschke, F. Reinholz, G. Röpke and D. Kremp, Phys. Lett. B **151** (1985) 439.

[29] G. Röpke, D. Blaschke and H. Schulz, Phys. Lett. B **202** (1988) 479.

[30] F. Karsch, M. T. Mehr and H. Satz, Z. Phys. C **37** (1988) 617.

[31] G. Röpke, D. Blaschke and H. Schulz, Phys. Rev. D **38** (1988) 3589.

[32] D. Prorok and L. Turko, Phys. Rev. C **64** (2001) 044903.

[33] D. Prorok, L. Turko and D. Blaschke, AIP Conf. Proc. **1038** (2008) 73.

[34] K. Martins, D. Blaschke and E. Quack, Phys. Rev. C **51** (1995) 2723.

[35] T. Barnes and E. S. Swanson, Phys. Rev. D **46** (1992) 131.

[36] D. Blaschke and G. Röpke, Phys. Lett. B **299** (1993) 332.

[37] C. Y. Wong, E. S. Swanson and T. Barnes, Phys. Rev. C **62** (2000) 045201.

[38] T. Barnes, E. S. Swanson, C. Y. Wong and X. M. Xu, Phys. Rev. C **68** (2003) 014903.

[39] C. D. Roberts and A. G. Williams, Prog. Part. Nucl. Phys. **33** (1994) 477.

[40] D. B. Blaschke, G. R. G. Burau, M. A. Ivanov, Yu. L. Kalinovsky and P. C. Tandy, arXiv:hep-ph/0002047.

[41] M. A. Ivanov, J. G. Körner and P. Santorelli, Phys. Rev. D **70** (2004) 014005.

[42] A. Bourque and C. Gale, Phys. Rev. C **80** (2009) 015204.

[43] S. G. Matinyan and B. Müller, Phys. Rev. C **58** (1998) 2994.

[44] K. L. Haglin, Phys. Rev. C **61** (2000) 031902.

[45] Z. W. Lin and C. M. Ko, Phys. Rev. C **62** (2000) 034903.

[46] K. L. Haglin and C. Gale, Phys. Rev. C **63** (2001) 065201.

[47] Z. W. Lin and C. M. Ko, Nucl. Phys. A **715** (2003) 533.

[48] Y. S. Oh, T. Song and S. H. Lee, Phys. Rev. C **63** (2001) 034901.

[49] V. V. Ivanov, Yu. L. Kalinovsky, D. Blaschke and G. R. G. Burau, arXiv:hep-ph/0112354.

[50] Y. S. Oh, T. S. Song, S. H. Lee and C. Y. Wong, J. Korean Phys. Soc. **43** (2003) 1003.

[51] A. Bourque, C. Gale and K. L. Haglin, Phys. Rev. C **70** (2004) 055203.

[52] D. B. Blaschke, H. Grigorian and Yu. L. Kalinovsky, arXiv:0808.1705 [hep-ph].

[53] A. Sibirtsev, K. Tsushima and A. W. Thomas, Phys. Rev. C **63** (2001) 044906.

[54] W. Liu, C. M. Ko and Z. W. Lin, Phys. Rev. C **65** (2002) 015203.

[55] Z. W. Lin and C. M. Ko, Phys. Lett. B **503** (2001) 104.

[56] D. Blaschke, G. Burau, Yu. Kalinovsky and T. Barnes, Eur. Phys. J. A **18** (2003) 547.

[57] D. Blaschke, Y. Kalinovsky and V. Yudichev, Lect. Notes Phys. **647** (2004) 366.

[58] L. Grandchamp, R. Rapp and G. E. Brown, Phys. Rev. Lett. **92** (2004) 212301.

[59] A. Sibirtsev, K. Tsushima, K. Saito and A. W. Thomas, Phys. Lett. B **484** (2000) 23.

[60] K. Tsushima, A. Sibirtsev, K. Saito, A. W. Thomas and D. H. Lu, Nucl. Phys. A **680** (2001) 280.

[61] G. R. G. Burau, D. B. Blaschke and Y. L. Kalinovsky, Phys. Lett. B **506** (2001) 297.

[62] D. Blaschke, G. Burau, Yu. Kalinovsky, V. Yudichev, Prog. Theor. Phys. Suppl. **149** (2003) 182.

[63] C. Fuchs, B. V. Martemyanov, A. Faessler and M. I. Krivoruchenko, Phys. Rev. C **73** (2006) 035204.

[64] D. Blaschke, G. Burau and Yu. L. Kalinovsky, arXiv:nucl-th/0006071.

[65] R. Rapp, D. Blaschke and P. Crochet, arXiv:0807.2470 [hep-ph].

Model-independent analysis indications on nature of the scalar mesons

Yurii Surovtsev[1], *Tanja Branz*[2], *Thomas Gutsche*[2], *Valery E. Lyubovitskij*[2*]

[1]Bogoliubov Laboratory of Theoretical Physics, JINR, Dubna 141 980, Russia
[2]Institut für Theoretische Physik, Universität Tübingen, Auf der Morgenstelle 14,
D-72076 Tübingen, Germany

The experimental data on processes $\pi\pi \to \pi\pi, K\overline{K}, \eta\eta, \eta\eta'$ in the $I^G J^{PC} = 0^+ 0^{++}$ channel and on the $K\pi$ scattering in the $I(J^P) = \frac{1}{2}(0^+)$ channel have been analyzed jointly for studying the status and QCD nature of the f_0- and the K_0^*-mesons. The analysis method is based on analyticity and unitarity and uses an uniformization procedure. An evidence for existence of the $K_0^*(900)$ is obtained. Some spectroscopic implications from the analysis results are discussed.

1 Introduction

We present results of the coupled-channel analysis of data on processes $\pi\pi \to \pi\pi, K\overline{K}, \eta\eta, \eta\eta'$ in the the channel with $I^G J^{PC} = 0^+ 0^{++}$ and on the $K\pi$ scattering in the channel with $I(J^P) = \frac{1}{2}(0^+)$. Generally, scalar mesons are very intriguing objects constituting the Higgs sector of strong interactions and being the most direct bearers of information on the QCD vacuum structure. An exceptional interest to this sector is supported by the fact that there, possibly indeed, we deal with a glueball $f_0(1500)$ (see, e.g., [1, 2]). However, as to parameters of the scalar mesons and even the status of some of them, there is a considerable disagreement [2]. Especially this concerns the $f_0(600)/\sigma$-meson and $K_0^*(900)/\kappa(800)$. In view of these circumstances, there are the known problems as to determining a QCD nature of the observed mesonic states and their assignment to the quark-model configurations in spite of a big amount of work devoted these problems (see, e.g., [3] and references therein).

Here we have applied to analysis of data a model-independent method based only on analyticity and unitarity and developed in work [4]. That approach permits us to omit theoretical prejudice in extracting resonance parameters. Considering the obtained disposition of resonance poles on the Riemann surface, obtained coupling constants with channels and resonance masses, we draw definite conclusions about nature of the investigated states.

2 The coupled-channel formalism

Our model-independent method which essentially utilizes an uniformizing variable can be used only for the 2- and 3-channel cases where we obtain a simple (easily interpreted) picture of the resonance poles and zeros of the S-matrix on the uniformization plane. The S-matrix is determined on the 4- and 8-sheeted Riemann surfaces for the 2- and 3-channel cases, respectively. The matrix elements $S_{\alpha\beta}$, where $\alpha, \beta = 1, 2, 3$ denote channels, have the right-hand cuts along

---

*On leave of absence from the Department of Physics, Tomsk State University, 634050 Tomsk, Russia

the real axis of the s complex plane (s is the invariant total energy squared), starting with the channel thresholds s_i ($i = 1, 2, 3$), and the left-hand cuts. The Riemann-surface sheets are numbered according to the signs of analytic continuations of the channel momenta $k_i = \sqrt{s - s_i}/2$ ($i = 1, 2, 3$) as follows: signs $(\text{Im}k_1, \text{Im}k_2, \text{Im}k_3) = + + +, - + +, - - +, + - +, + - -, - - -, - + -, + + -$ correspond to sheets I, II,···, VIII, respectively.

The resonance representations on the Riemann surfaces are obtained with using formulas from Ref.[4], expressing analytic continuations of the S-matrix elements to unphysical sheets in terms of those on sheet I that have only the resonance zeros (beyond the real axis), at least, around the physical region. Then, starting from the resonance zeros on sheet I, one can obtain an arrangement of poles and zeros of resonance on the whole Riemann surface. In the 2-channel case, we obtain *3 types* of resonances described by a pair of conjugate zeros on sheet I only in S_{11} – the type (**a**), only in S_{22} – (**b**), and in each of S_{11} and S_{22} – (**c**). In the 3-channel case, we obtain *7 types* of resonances corresponding to 7 possible situations when there are resonance zeros on sheet I only in S_{11} – (**a**); S_{22} – (**b**); S_{33} – (**c**); S_{11} and S_{22} – (**d**); S_{22} and S_{33} – (**e**); S_{11} and S_{33} – (**f**); S_{11}, S_{22}, and S_{33} – (**g**).

The resonance of every type is represented by the pair of complex-conjugate clusters (of poles and zeros on the Riemann surface). The cluster type is related to the nature of state. E.g., a flavor singlet (glueball) must be represented by the type-(**g**) cluster (of type (**c**) in the 2-channel consideration) as a necessary condition. Note that whereas cases (**a**), (**b**) and (**c**) can be simply related to the representation of resonances by Breit-Wigner (BW) forms, cases (**d**), (**e**), (**f**) and (**g**) practically are lost at the BW description. We can distinguish, in a model-independent way, a bound state of the channel particles (e.g., $K\overline{K}$ molecule) and a $q\bar{q}$ bound state [4, 5]. In analysis, we use the Le Couteur-Newton relations [6]. They express the S-matrix elements of all coupled processes in terms of the Jost matrix determinant $d(k_1, \cdots, k_n)$ that is a real analytic function with the only square-root branch-points at the channel momenta $k_i = 0$. The important branch points, related to the thresholds of the coupled channels and to the crossing ones, are taken into account in the proper uniformizing variable.

3   Analysis of the isoscalar-scalar sector

Considering the S-waves of processes $\pi\pi \to \pi\pi, K\overline{K}, \eta\eta, \eta\eta'$ in the model-independent approach, we have performed two variants of the 3-channel analysis: variant I – the combined analysis of $\pi\pi \to \pi\pi, K\overline{K}, \eta\eta$; variant II – analysis of $\pi\pi \to \pi\pi, K\overline{K}, \eta\eta'$. Influence of the $\eta\eta'$-channel in the I case and of the $\eta\eta$ in the II one are taken into account in the background.

In the new uniformizing variable used, we neglect the $\pi\pi$-threshold branch point (however, unitarity on the $\pi\pi$-cut is considered) and consider the threshold branch-points related to two remaining channels and the left-hand branch-point at $s = 0$ concerned the crossed channels. It is (all, related to variant II, are primed)

$$w = 2\frac{m_\eta k_2 + m_K k_3}{\sqrt{s(m_\eta^2 - m_K^2)}} \quad \text{for variant I}, \quad w' = \frac{(m_\eta + m_{\eta'})k_2' + 2m_K k_3'}{\sqrt{s[\frac{1}{4}(m_\eta + m_{\eta'})^2 - m_K^2]}} \quad \text{for variant II}.$$

On the w-plane, the Le Couteur-Newton relations are

$$S_{11} = d^*(-w^*)/d(w), \quad S_{22} = d(-w^{-1})/d(w), \quad S_{33} = d(w^{-1})/d(w),$$
$$S_{11}S_{22} - S_{12}^2 = d^*(w^{*-1})/d(w), \quad S_{11}S_{33} - S_{13}^2 = d^*(-w^{*-1})/d(w).$$

$d = d_B d_{res}$ is the product of the resonance part $d_{res}(w) = w^{-\frac{M}{2}} \prod_{r=1}^{M}(w + w_r^*)$ with M being the number of resonance zeros and the background $d_B = \exp[-i(a + \sum_{n=1}^{3}(k_n/m_n)(\alpha_n + i\beta_n))]$ with $\alpha(\beta)_n = a(b)_{n1} + \sum_{j=\sigma,v} a(b)_{nj} (s - s_j)/s_j \, \theta(s - s_j)$ where s_σ is the $\sigma\sigma$ threshold, s_v is the combined threshold of the $\eta\eta'$, $\rho\rho$, $\omega\omega$ ones. In variant II, the terms $a'_{n\eta} (s - 4m_\eta^2)/4m_\eta^2 \, \theta(s - 4m_\eta^2)$ and $b'_{n\eta} (s - 4m_\eta^2)/4m_\eta^2 \, \theta(s - 4m_\eta^2)$ should be added to α'_n and β'_n.

For the $\pi\pi$ scattering, the data from the threshold to 1.89 GeV are taken from [7]; references to other sources of the data below the $K\overline{K}$ threshold can be find in [8]. For $\pi\pi \to K\overline{K}$, practically all the accessible data are used (see the references also in [8]). For $\pi\pi \to \eta\eta$, we used data for $|S_{13}|^2$ from the threshold to 1.72 GeV, for $\pi\pi \to \eta\eta'$ the data for $|S_{13}|^2$ from the threshold to 1.813 GeV [9]. A satisfactory description is obtained in both variants. In variant I, the $f_0(600)$ is described by the cluster of type (**a**); $f_0(1370)$, type (**c**); $f_0(1500)$, type (**g**); $f_0(1710)$, type (**b**); the $f_0(980)$ is represented only by the pole on sheet II and shifted pole on sheet III in both variants. The total χ^2/NDF is $314.452/(301 - 41) \approx 1.21$ in variant I. The background parameters are: $a = 0.1199$, $a_{11} = 0.2813$, $a_{1\sigma} = -0.008$, $a_{1v} = 0$, $b_{11} = 0$, $b_{1\sigma} = 0$, $b_{1v} = 0.0462$, $a_{21} = -1.3267$, $a_{2\sigma} = -0.5829$, $a_{2v} = -7.544$, $b_{21} = 0.0344$, $b_{2\sigma} = 0$, $b_{2v} = 6.862$, $b_{31} = 0.6386$, $b_{3\sigma} = 0.4384$, $b_{2v} = 0$; $s_\sigma = 1.638$ GeV^2, $s_v = 2.085$ GeV^2. In variant II, the $f_0(600)$ is described by the cluster of type (**a'**); $f_0(1370)$, type (**b'**); $f_0(1500)$, type (**d'**); $f_0(1710)$, type (**c'**). The total χ^2/NDF is $283.151/(293 - 38) \approx 1.11$. The background parameters are: $a' = 0.2315$, $a'_{11} = 0$, $a'_{1\eta} = -0.0616$, $a'_{1\sigma} = 0.0298$, $a'_{1v} = 0.0622$, $b'_{11} = b'_{1\eta} = b'_{1\sigma} = 0$, $b'_{1v} = 0.0449$, $a'_{21} = -3.1359$, $a'_{2\eta} = 0$, $a'_{2\sigma} = 0.4866$, $a'_{2v} = -4.532$, $b'_{21} = 0$, $b'_{2\eta} = -0.7478$, $b'_{2\sigma} = 2.5545$, $b'_{2v} = 1.948$, $b'_{31} = 0.4489$, $s'_\sigma = s_\sigma$, $s'_v = 2.126$ GeV^2. In Table 1, the obtained pole clusters for resonances on the complex $\sqrt{s}$-plane are shown.

The $f_0(1370)$ and $f_0(1710)$ are represented by the pole clusters corresponding to states with the dominant $s\bar{s}$ component; $f_0(1500)$, with the dominant glueball component. This confirms conclusions based on the coupling constants with channels, which were obtained in our previous analysis of processes $\pi\pi \to \pi\pi, K\overline{K}$ [8]. Note a surprising result obtained for the $f_0(980)$. It turns out that this state lies slightly above the $K\overline{K}$ threshold and is described by the pole on sheet II and by the shifted pole on sheet III under the $\eta\eta$ threshold without the corresponding poles on sheets VI and VII, as it was expected for standard clusters. This corresponds to describing the $\eta\eta$ bound state. Masses and widths of states should be calculated from the pole positions. If the resonance part of amplitude is taken in the form $T^{res} = \sqrt{s}\Gamma_{el}/(m_{res}^2 - s - i\sqrt{s}\Gamma_{tot})$, we obtain values of masses and total widths of the f_0-resonances respectively (in MeV): in variant I – 784.6 and 1118 for $f_0(600)$, 1012.6 and 72.8 for $f_0(980)$, 1406.7 and 344.6 for $f_0(1370)$, 1542.9 and 712.8 for $f_0(1500)$, 1724.5 and 299 for $f_0(1710)$; in variant II – 769.4 and 1058 for $f_0(600)$, 1009.5 and 63.6 for $f_0(980)$, 1431 and 470 for $f_0(1370)$, 1510 and 397 for $f_0(1500)$, 1746.8 and 229.4 for $f_0(1710)$.

4   Analysis of the $K\pi$ scattering

When analyzing data [10] for the module of the $K^-\pi^+$-scattering amplitude $T = (S - 1)/2i$ and its phase shift δ in the $I(J^P) = \frac{1}{2}(0^+)$ channel, we applied the model-independent method taking into account in the uniformizing variable the branch-points related to the thresholds of the $K\pi$ and $K\eta$ channels assuming that the influence of remaining channels and the left-hand cuts can be accounted via the background. The proper uniformizing variable has the form: $v = (\sqrt{s - s_0} + \sqrt{s - s_1})/\sqrt{s_1 - s_0}$, where s_0 and s_1 are the thresholds of the $K^-\pi^+$ and $K^0\eta$ channels, respectively. The $K\pi$-scattering S-matrix element is taken as $S = S_{res} \exp 2i\delta_{bg}$ where

Table 1: Pole clusters for the f_0-resonance (in MeV; $\sqrt{s_r} = E_r - i\Gamma_r$).

Sheet		II	III	IV	V	VI	VII	VIII
Variant I								
$f_0(600)$	E_r	550.05±13	624±14			628.9±16	555.4±15	
	Γ_r	559±17	559±19			559±18	559±20	
$f_0(980)$	E_r	1011.9±4	978.2±9					
	Γ_r	36.4±6	56.3±10					
$f_0(1370)$	E_r				1396.1±16	1396.1±18	1396.1±18	1396.1±13
	Γ_r				287.1±17	270.5±15	155.7±9	172.3±7
$f_0(1500)$	E_r	1501.2±11	1495.8±13	1501.2±12	1497.7±12.5	1510.4±16	1502±12	1501.2±10
	Γ_r	357.4±15	140.7±12	238±13	140.5±14	186.9±17	90.9±11	356.4±14
$f_0(1710)$	E_r		1718±12	1718±10	1718±13	1718±15		
	Γ_r		149.5±9	166.3±8	321.9±14	305.1±13		
Variant II								
$f_0(600)$	E_r	558.7±8	564.3±10			541.3±12	535.7±12.5	
	Γ_r	529±11	529±12			529±14	529±13	
$f_0(980)$	E_r	1009±3	986±6					
	Γ_r	31.8±4	57.4±5.5					
$f_0(1370)$	E_r		1411.6±9	1411.6±11	1428.4±13	1428.4±14		
	Γ_r		215.6±10	235±12	235±12	215.6±19		
$f_0(1500)$	E_r	1496.9±12	1503±10	1496.9±13	1496.9±14	1494.6±12	1496.9±15	
	Γ_r	198.5±15	236±10	193.1±9	198.5±11	193.7±8.5	193.1±10	
$f_0(1710)$	E_r				1743±12	1743±13	1743±12	1743±10
	Γ_r				144.1±9	111.5±8	82.1±8	114.7±7

the resonance part of the form $S_{res} = d(-v^{-1})/d(v)$ has no cuts on the v-plane. The $d(v)$-function is $d(v) = v^{-M} \prod_{n=1}^{M}(1 - v_n^* v)(1 + v_n v)$ with M the number of pairs of the conjugate zeros corresponding to resonances. The phase shift $\delta_{bg} = \sqrt{(s - s_0)/s}\,(a + ib)$ describes the background: a relates to its elastic part, b to the inelastic one.

Since the question stands about the status of the $K_0^*(900)$, first we carried out the analysis considering only one resonance $K_0^*(1450)$ of type (**a**). It is possible to obtain a satisfactory description with the total $\chi^2/\text{NDF} = 92.09/(68 - 6) \approx 1.48$. The calculated mass and total width were 1428 and 282 MeV, respectively, and the background parameters $a = 0.6951$ and $b = -0.0614$. A negative sign of the quantity b means the increasing inelastic part of the background. Note an important point: *The increasing inelastic background part implies a necessity to consider explicitly some physical phenomenon.* In the previous analysis of scalar sector, the analogous situation in variant II implied necessity of the explicit consideration of the $\eta\eta$-threshold branch-point. In the given case, the increasing inelastic background part implies necessity to consider explicitly one more resonance of the expected type (**b**). Indeed, it turned out that for the reasonable description two resonances, $K_0^*(900)$ of type (**b**) and $K_0^*(1450)$ of type (**a**), should be considered. The total χ^2/NDF is $75.707/(68 - 9) \approx 1.28$, i.e., the description is better than without the $K_0^*(900)$, and, furthermore and this is principal, *the background parameter b equals zero in this case*. The fact, that δ_{bg} turned out to be elastic with the only parameter $a = 0.6503$, means that the influence of other channels such as $K\pi\pi\pi$ and $K\pi\sigma$ is negligible, except for the $K^0\eta'$ channel, at opening of which there is a small deviation of our curve for the module of amplitude from the data.

The obtained pole-clusters of resonances consist of the following poles on the lower $\sqrt{s}$-half-

plane (in MeV) of the 4-sheeted Riemann surface (the conjugate poles on the upper half-plane are not shown): for the $K_0^*(900)$ – the poles $859.9 - i221.6$ on sheet III and $885.6 - i280.8$ on sheet IV; for the $K_0^*(1450)$ – the poles $1441.7 - i172.3$ on sheet II and $1430 - i144$ on sheet III. These pole-clusters mean that the $K_0^*(1450)$ is coupled mainly with the $K\pi$ channel, whereas the $K_0^*(900)$ is coupled weaker with this channel than with other ones such as the $K\eta$ and $K\eta'$ channels. Masses and total widths can be calculated from the pole positions on sheet II for resonance of type (**a**) and on sheet IV for resonance of type (**b**). The obtained values are respectively (in MeV): 929 and 561.6 for the $K_0^*(900)$ and 1452 and 344.6 for the $K_0^*(1450)$.

5   Discussion and conclusions

In the combined model-independent analysis of data on the $\pi\pi \to \pi\pi, K\overline{K}, \eta\eta, \eta\eta'$ processes in the $I^G J^{PC} = 0^+0^{++}$ channel, an additional confirmation of the σ-meson with mass 785 MeV is obtained. This mass value remarkably accords with prediction ($m_\sigma \approx m_\rho$) on the basis of mended symmetry by S. Weinberg [11].

Some indication for $f_0(980)$ ($m_{res} = 1012.6$ GeV, $\Gamma_{tot} = 72.8$ GeV) is obtained to be the $\eta\eta$ bound state. However, one can see from a consideration of the $f_0(980)$ listing in the PDG issue [2] that the mass of this state is obtained above the $K\overline{K}$ threshold in analyses of the $\pi\pi$ scattering, of the multi-channel $\pi\pi$ scattering ($\pi\pi \to \pi\pi, K\overline{K}, \eta\eta, \eta\eta'$) and of processes $\bar{p}p(n) \to M_1M_2M_3$, whereas below the $K\overline{K}$ threshold in analyses of the decays of D^+-, B^+-, J/ψ-, and Z-bosons, of processes $e^+e^- \to M_1M_2\gamma, \phi M_1M_2\gamma, e^+e^- M_1M_2, M_1M_2X$ and $pp \to ppM_1M_2$. Since the mass value below the $K\overline{K}$ threshold is important for a dynamical interpretation of the $f_0(980)$ as the $K\overline{K}$ molecule [12], it seems that the nature of this state is more complicated than the simply $\eta\eta$ bound state or $K\overline{K}$ molecule. From the point of view of quark structure, this two possibilities are the 4-quark states. Maybe, this is consistent somehow with arguments in favour of the 4-quark nature of $f_0(980)$ in works [13].

The $f_0(1370)$ and $f_0(1710)$ have the dominant $s\bar{s}$ component. Conclusion about the $f_0(1370)$ quite well agrees with the one of work of Crystal Barrel Collaboration [14] where the $f_0(1370)$ is identified as $\eta\eta$ resonance in the $\pi^0\eta\eta$ final state of the $\bar{p}p$ annihilation at rest. Conclusion about the $f_0(1710)$ is quite consistent with the experimental facts that this state is observed in $\gamma\gamma \to K_S K_S$ and not observed in $\gamma\gamma \to \pi^+\pi^-$ [15].

As to the $f_0(1500)$, we suppose that it is practically the eighth component of octet mixed with a glueball being dominant in this state. Its biggest width among enclosing states tells also in behalf of its glueball nature [16]. So, we suppose that in this energy region, indeed, there are two states: a narrow one, seen in the decay processes [2], and a large one (glueball) dominating in the scattering processes. This supposition is supported by results of the combined K-matrix analysis of many processes [16].

In the model-independent analysis of the $K\pi$ scattering data [10] in the $I(J^P) = \frac{1}{2}(0^+)$ channel, the evidence for existence of the $K_0^*(900)$ with the mass 929 MeV and total width 564 MeV is obtained. Our mass value differs from the average one (672 ± 40 MeV) cited in the PDG tables [2], whereas the width practically coincides. Our values of the mass and width correspond most near to the ones (909^{+65}_{-30} and 545^{+235}_{-110} MeV, respectively) from work [17], obtained in the analysis of the $K\pi$ scattering using an so-called interfering BW amplitudes. However, unlike the indicated work, *we did not need the repulsive background*, not very clear in the $K\pi$ scattering. The second K_0^* resonance in the $K\pi$ scattering has the mass 1452 MeV and total width 346 MeV in some accordance with the values cited in the PDG tables.

We propose a following assignment of scalar mesons below 1.9 GeV to lower nonets, when excluding the $f_0(980)$ as the possible $\eta\eta$ bound state or other something of the non-$q\bar{q}$ nature. The lowest nonet: the isovector $a_0(980)$, the isodoublet $K_0^*(900)$, and $f_0(600)$ and $f_0(1370)$ as mixtures of the 8th component of octet and the SU(3) singlet. Then the Gell-Mann–Okubo (GM-O) formula $3m_{f_8}^2 = 4m_{K_0^*}^2 - m_{a_0}^2$ gives $m_{f_8} = 910$ MeV. In relation for masses of nonet $m_\sigma + m_{f_0(1370)} = 2m_{K_0^*}$, the left-hand side is by about 18 % bigger than the right-hand one.

For the next nonet of the radial excitations we find: $a_0(1450)$, $K_0^*(1450)$, and $f_0(1500)$ and $f_0(1710)$, the $f_0(1500)$ being mixed with a glueball which is dominant in this state. From the GM-O formula, $m_{f_8} \approx 1453$ MeV. In formula $m_{f_0(1500)} + m_{f_0(1710)} = 2m_{K_0^*(1450)}$ the left-hand side is by about 12.5 % bigger than the right-hand one.

This assignment moves a number of questions, stood earlier, and does not put the new ones. The mass formulas indicate to non-simple mixing scheme, a search of which is complicated by the circumstance that here there is also a remainder chiral symmetry, though, on the other hand, this permits one to predict correctly, e.g., the σ-meson mass.

Acknowledgements

References

[1] C.Amsler and F.E.Close, Phys. Rev. **D53**, 295 (1996).

[2] C. Amsler *et al.* (PDG), Phys. Lett. **B667** (2008) 1.

[3] V.V. Anisovich, Int. J. Mod. Phys. **A21**, 3615 (2006).

[4] D. Krupa, V.A. Meshcheryakov and Yu.S. Surovtsev, Nuovo Cim. **A109**, 281 (1996).

[5] D. Morgan and M.R. Pennington, Phys. Rev. **D48**, 1185 (1993).

[6] K.J. LeCouteur, Proc. Roy. Soc. **A256**, 115 (1960); R.G. Newton, J. Math. Phys. **2**, 188 (1961); M. Kato, Ann. Phys. **31**, 130 (1965).

[7] B. Hyams *et al.*, Nucl. Phys. **B64**, 134 (1973); ibid. **100**, 205 (1975).

[8] Yu.S. Surovtsev, D. Krupa and M. Nagy, Eur. Phys. J. **A15**, 409 (2002).

[9] F. Binon *et al.*, Nuovo Cim. **A78**, 313 (1983); ibid. **80**, 363 (1984).

[10] D. Aston *et al.*, Nucl. Phys. **B296**, 493 (1988).

[11] S. Weinberg, Phys. Rev. Lett. **65**, 1177 (1990).

[12] T. Branz, T. Gutsche and V. E. Lyubovitskij, Eur. Phys. J. **A37**, 303 (2008); Phys. Rev. **D78**, 114004 (2008).

[13] N.N. Achasov, Nucl. Phys. **A675**, 279c (2000); M.N. Achasov *et al.*, Phys. Lett. **B438**, 441 (1998); ibid. **440**, 442 (1998).

[14] C. Amsler *et al.*, Phys. Lett. **B355**, 425 (1995).

[15] S. Braccini, Frascati Phys. Series **XV**, 53 (1999); R. Barate *et al.*, Phys. Lett. **B472**, 189 (2000).

[16] V.V. Anisovich *et al.*, Nucl. Phys. Proc. Suppl. **A56**, 270 (1997).

[17] S.Ishida *et al.*, Progr. Theor. Phys. **98**, 621 (1997).

Pair correlations of neutral K, D, B and B_s mesons with close momenta generated in inclusive multiparticle processes

V.L.Lyuboshitz, V.V.Lyuboshitz [†]

Joint Institute for Nuclear Research, 141980, Dubna, Moscow Region, Russia
[†] E-mail: Valery.Lyuboshitz@jinr.ru

The phenomenological structure of inclusive cross-sections of the production of two neutral K mesons in collisions of hadrons and nuclei is investigated taking into account the strangeness conservation in strong and electromagnetic interactions. Relations describing the dependence of the correlations of two short-lived and two long-lived neutral kaons $K_S^0 K_S^0$, $K_L^0 K_L^0$ and the correlations of "mixed" pairs $K_S^0 K_L^0$ at small relative momenta upon the space-time parameters of the generation region of K^0 and $\bar{K}^0$ mesons have been obtained. It is shown that under the strangeness conservation the correlation functions of the pairs $K_S^0 K_S^0$ and $K_L^0 K_L^0$, produced in the same inclusive process, coincide, and the difference between the correlation functions of the pairs $K_S^0 K_S^0$ and $K_S^0 K_L^0$ is conditioned by the production of the pairs of non-identical neutral kaons $K^0 \bar{K}^0$. Analogous correlations for the pairs of neutral heavy mesons D^0, B^0 and B_s^0, generated in multiple processes with the charm (beauty) conservation, are analyzed, and differences from the case of neutral K mesons are discussed .

1 Consequences of the strangeness conservation for neutral kaons

In the work [1] the properties of the density matrix of two neutral K mesons, following from the strangeness conservation in strong and electromagnetic interactions, have been investigated. By definition, the diagonal elements of the non-normalized two-particle density matrix coincide with the two-particle structure functions, which are proportional to the double inclusive cross-sections.

Strangeness is the additive quantum number. Taking into account the strangeness conservation, the pairs of neutral kaons $K^0 K^0$ (strangeness $S = +2$), $\bar{K}^0 \bar{K}^0$ (strangeness $S = -2$) and $K^0 \bar{K}^0$ (strangeness $S = 0$) are produced incoherently. This means that in the K^0-$\bar{K}^0$- representation the non-diagonal elements of the density matrix between the states $K^0 K^0$ and $\bar{K}^0 \bar{K}^0$, $K^0 K^0$ and $K^0 \bar{K}^0$, $\bar{K}^0 \bar{K}^0$ and $K^0 \bar{K}^0$ are equal to zero. However, the non-diagonal elements of the two-kaon density matrix between the two states $|K^0\rangle^{(\mathbf{p}_1)}|\bar{K}^0\rangle^{(\mathbf{p}_2)}$ and $|\bar{K}^0\rangle^{(\mathbf{p}_1)}|K^0\rangle^{(\mathbf{p}_2)}$ with the zero strangeness are not equal to zero, in general. Here $\mathbf{p}_1$ and $\mathbf{p}_2$ are the momenta of the first and second kaons.

The internal states of K^0 meson ($S = 1$) and $\bar{K}^0$ meson ($S = -1$) are the superpositions of the states $|K_S^0\rangle$ and $|K_L^0\rangle$, where K_S^0 is the short-lived neutral kaon and K_L^0 is the long-lived one. Neglecting the small effect of CP non-invariance, the CP-parity of the state K_S^0 is equal

to $(+1)$, and the CP-parity of the state K_L^0 is equal to (-1); in doing so,

$$|K^0\rangle = \frac{1}{\sqrt{2}}(|K_S^0\rangle + |K_L^0\rangle), \quad |\bar{K}^0\rangle = \frac{1}{\sqrt{2}}(|K_S^0\rangle - |K_L^0\rangle).$$

It is clear that both the quasistationary states of the neutral kaon have no definite strangeness.

It follows from the Bose-symmetry of the wave function of two neutral kaons with respect to the total permutation of internal states and momenta that the CP-parity of the system $K^0\bar{K}^0$ is always positive [2] (the C-parity is $(-1)^L$, the space parity is $P = (-1)^L$, where L is the orbital momentum).

The system of two non-identical neutral kaons $K^0\bar{K}^0$ in the symmetric internal state, corresponding to even orbital momenta, is decomposed into the schemes $|K_S^0\rangle|K_S^0\rangle$ and $|K_L^0\rangle|K_L^0\rangle$ [2]:

$$|\psi^+\rangle = \frac{1}{\sqrt{2}}(|K^0\rangle^{(\mathbf{p}_1)} \otimes |\bar{K}^0\rangle^{(\mathbf{p}_2)} + |\bar{K}^0\rangle^{(\mathbf{p}_1)} \otimes |K^0\rangle^{(\mathbf{p}_2)}) =$$

$$= \frac{1}{\sqrt{2}}(|K_S^0\rangle^{(\mathbf{p}_1)} \otimes |K_S^0\rangle^{(\mathbf{p}_2)} - |K_L^0\rangle^{(\mathbf{p}_1)} \otimes |K_L^0\rangle^{(\mathbf{p}_2)}); \tag{1}$$

meantime, the system $K^0\bar{K}^0$ in the antisymmetric internal state, corresponding to odd orbital momenta, is decomposed into the scheme $|K_S^0\rangle|K_L^0\rangle$ [2]:

$$|\psi^-\rangle = \frac{1}{\sqrt{2}}(|K^0\rangle^{(\mathbf{p}_1)} \otimes |\bar{K}^0\rangle^{(\mathbf{p}_2)} - |\bar{K}^0\rangle^{(\mathbf{p}_1)} \otimes |K^0\rangle^{(\mathbf{p}_2)}) =$$

$$= \frac{1}{\sqrt{2}}(|K_S^0\rangle^{(\mathbf{p}_1)} \otimes |K_L^0\rangle^{(\mathbf{p}_2)} - |K_L^0\rangle^{(\mathbf{p}_1)} \otimes |K_S^0\rangle^{(\mathbf{p}_2)}). \tag{2}$$

The strangeness conservation leads to the fact that all the double inclusive cross-sections of production of pairs $K_S^0 K_S^0$, $K_L^0 K_L^0$ and $K_S^0 K_L^0$ (two-particle structure functions) prove to be symmetric with respect to the permutation of momenta $\mathbf{p}_1$ and $\mathbf{p}_2$.

Besides, due to the strangeness conservation, the structure functions of neutral K mesons produced in inclusive processes are invariant with respect to the replacement of the short-lived state K_S^0 by the long-lived state K_L^0, and *vice versa* [1]:

$$f_{SS}(\mathbf{p}_1, \mathbf{p}_2) = f_{LL}(\mathbf{p}_1, \mathbf{p}_2) = \frac{1}{4}\left[f_{K^0 K^0}(\mathbf{p}_1, \mathbf{p}_2) + f_{\bar{K}^0 \bar{K}^0}(\mathbf{p}_1, \mathbf{p}_2) + \right.$$

$$\left. + f_{K^0 \bar{K}^0}(\mathbf{p}_1, \mathbf{p}_2) + f_{\bar{K}^0 K^0}(\mathbf{p}_1, \mathbf{p}_2)\right] + \frac{1}{2}\operatorname{Re}\rho_{K^0\bar{K}^0 \to \bar{K}^0 K^0}(\mathbf{p}_1, \mathbf{p}_2), \tag{3}$$

$$f_{SL}(\mathbf{p}_1, \mathbf{p}_2) = f_{LS}(\mathbf{p}_1, \mathbf{p}_2) = \frac{1}{4}\left[f_{K^0 K^0}(\mathbf{p}_1, \mathbf{p}_2) + f_{\bar{K}^0 \bar{K}^0}(\mathbf{p}_1, \mathbf{p}_2) + \right.$$

$$\left. + f_{K^0 \bar{K}^0}(\mathbf{p}_1, \mathbf{p}_2) + f_{\bar{K}^0 K^0}(\mathbf{p}_1, \mathbf{p}_2)\right] - \frac{1}{2}\operatorname{Re}\rho_{K^0\bar{K}^0 \to \bar{K}^0 K^0}(\mathbf{p}_1, \mathbf{p}_2), \tag{4}$$

where $\rho_{K^0\bar{K}^0 \to \bar{K}^0 K^0}(\mathbf{p}_1, \mathbf{p}_2) = (\rho_{\bar{K}^0 K^0 \to K^0 \bar{K}^0}(\mathbf{p}_1, \mathbf{p}_2))^*$ are the non-diagonal elements of the two-kaon density matrix. The difference between the two-particle structure functions f_{SS} and f_{SL} is connected just with the contribution of these non-diagonal elements.

2 Structure of pair correlations of identical and non-identical neutral kaons with close momenta

Now let us consider, within the model of one-particle sources [2-7], the correlations of pairs of neutral K mesons with close momenta (see also [8-10]). In the case of the identical states $K_S^0 K_S^0$ and $K_L^0 K_L^0$ we obtain the following expressions for the correlation functions R_{SS}, R_{LL} (proportional to the structure functions), normalized to unity at large relative momenta:

$$R_{SS}(\mathbf{k}) = R_{LL}(\mathbf{k}) = \lambda_{K^0 K^0} \left[1 + F_{K^0}(2\mathbf{k}) + 2\, b_{\text{int}}(\mathbf{k})\right] +$$

$$+\lambda_{\bar{K}^0 \bar{K}^0} \left[1 + F_{\bar{K}^0}(2\mathbf{k}) + 2\, \tilde{b}_{\text{int}}(\mathbf{k})\right] + \lambda_{K^0 \bar{K}^0} \left[1 + F_{K^0 \bar{K}^0}(2\mathbf{k}) + 2\, B_{\text{int}}(\mathbf{k})\right]. \tag{5}$$

Here $\mathbf{k}$ is the momentum of one of the kaons in the c.m. frame of the pair, and the quantities $\lambda_{K^0 K^0}$, $\lambda_{\bar{K}^0 \bar{K}^0}$ and $\lambda_{K^0 \bar{K}^0}$ are the relative fractions of the average numbers of produced pairs $K^0 K^0$, $\bar{K}^0 \bar{K}^0$ and $K^0 \bar{K}^0$, respectively ($\lambda_{K^0 K^0} + \lambda_{\bar{K}^0 \bar{K}^0} + \lambda_{K^0 \bar{K}^0} = 1$) . The "formfactors" $F_{K^0}(2\mathbf{k})$, $F_{\bar{K}^0}(2\mathbf{k})$ and $F_{K^0 \bar{K}^0}(2\mathbf{k})$ appear due to the contribution of Bose-statistics:

$$F_{K^0}(2\mathbf{k}) = \int W_{K^0}(\mathbf{r}) \cos(2\mathbf{k}\mathbf{r})\, d^3\mathbf{r}, \qquad F_{\bar{K}^0}(2\mathbf{k}) = \int W_{\bar{K}^0}(\mathbf{r}) \cos(2\mathbf{k}\mathbf{r})\, d^3\mathbf{r},$$

$$F_{K^0 \bar{K}^0}(2\mathbf{k}) = \int W_{K^0 \bar{K}^0}(\mathbf{r}) \cos(2\mathbf{k}\mathbf{r})\, d^3\mathbf{r}. \tag{6}$$

where $W_{K^0}(\mathbf{r})$, $W_{\bar{K}^0}(\mathbf{r})$ and $W_{K^0 \bar{K}^0}(\mathbf{r})$ are the probability distributions of distances between the sources of emission of two K^0 mesons, between the sources of emission of two $\bar{K}^0$ mesons and between the sources of emission of the K^0 meson and $\bar{K}^0$ meson, respectively, in the c.m. frame of the kaon pair. Meantime, the quantity $b_{\text{int}}(\mathbf{k})$ describes the contribution of the S-wave interaction of two K^0 mesons, the quantity $\tilde{b}_{\text{int}}(\mathbf{k})$ describes the contribution of the S-wave interaction of two $\bar{K}^0$ mesons and the quantity $B_{\text{int}}(\mathbf{k})$ describes the contribution of the S-wave interaction of the K^0 meson with the $\bar{K}^0$ meson. Due to the CP invariance, the quantities $b_{\text{int}}(\mathbf{k})$ and $\tilde{b}_{\text{int}}(\mathbf{k})$ can be expressed by means of averaging the same function $b(\mathbf{k}, \mathbf{r})$ over the different distributions:

$$b_{\text{int}}(\mathbf{k}) = \int W_{K^0}(\mathbf{r}) b(\mathbf{k}, \mathbf{r}) d^3\mathbf{r}, \quad \tilde{b}_{\text{int}}(\mathbf{k}) = \int W_{\bar{K}^0}(\mathbf{r}) b(\mathbf{k}, \mathbf{r}) d^3\mathbf{r}.$$

The quantity $B_{\text{int}}(\mathbf{k})$ has the structure : $B_{\text{int}}(\mathbf{k}) = \int W_{K^0 \bar{K}^0}(\mathbf{r}) B(\mathbf{k}, \mathbf{r}) d^3\mathbf{r}$, where $B(\mathbf{k}, \mathbf{r}) \neq b(\mathbf{k}, \mathbf{r})$.

Let us emphasize that when the pair of non-identical neutral kaons $K^0 \bar{K}^0$ is produced but the pair of identical quasistationary states $K_S^0 K_S^0$ (or $K_L^0 K_L^0$) is registered over decays, the two-particle correlations at small relative momenta have the same character as in the case of usual identical bosons with zero spin [2].

For the pairs of non-identical kaon states $K_S^0 K_L^0$ the correlation functions at small relative momenta have the form:

$$R_{SL}(\mathbf{k}) = R_{LS}(\mathbf{k}) = \lambda_{K^0 K^0} \left[1 + F_{K^0}(2\mathbf{k}) + 2\, b_{\text{int}}(\mathbf{k})\right] +$$

$$+\lambda_{\bar{K}^0 \bar{K}^0} \left[1 + F_{\bar{K}^0}(2\mathbf{k}) + 2\, \tilde{b}_{\text{int}}(\mathbf{k})\right] + \lambda_{K^0 \bar{K}^0} \left[1 - F_{K^0 \bar{K}^0}(2\mathbf{k})\right]. \tag{7}$$

It follows from Eqs.(5) and (7) that the correlation functions of pairs of neutral K mesons with close momenta, which are created in inclusive processes, satisfy the relation

$$R_{SS}(\mathbf{k}) + R_{LL}(\mathbf{k}) - R_{SL}(\mathbf{k}) - R_{LS}(\mathbf{k}) = 2\left[R_{SS}(\mathbf{k}) - R_{SL}(\mathbf{k})\right] =$$

$$= 4\lambda_{K^0 \bar{K}^0}\left[F_{K^0 \bar{K}^0}(2\mathbf{k}) + B_{\text{int}}(\mathbf{k})\right]. \tag{8}$$

We see that the difference between the correlation functions of the pairs of identical neutral kaons $K_S^0 K_S^0$ and pairs of non-identical neutral kaons $K_S^0 K_L^0$ is conditioned exclusively by the generation of $K^0 \bar{K}^0$-pairs.

The relations connecting the contribution of the S-wave strong interaction into the pair correlations of particles at small relative momenta with the parameters of low-energy scattering were obtained earlier in the papers [4-7]. It is essential that the "formfactors" (6) and the functions $b_{\text{int}}(\mathbf{k})$, $\tilde{b}_{\text{int}}(\mathbf{k})$ and $B_{\text{int}}(\mathbf{k})$ depend on the space-time parameters of the generation region of neutral kaons and tend to zero at high values of the relative momentum $q = 2|\mathbf{k}|$ of two neutral kaons. Concretely, the expression for the function $B(\mathbf{k}, \mathbf{r})$ in the case of the $K^0 \bar{K}^0$ system has been obtained in the paper [10]. In the same paper, the estimate of contribution of the transition $K^+ K^- \to K^0 \bar{K}^0$ has also been presented .

3   Correlations of neutral heavy mesons

Formally, analogous relations are valid also for the neutral heavy mesons D^0, B^0 and B_s^0 . In doing so, the role of strangeness conservation is played, respectively, by the conservation of charm and beauty in inclusive multiple processes with production of these mesons . In these cases the quasistationary states are also states with definite CP parity, neglecting the effects of CP nonconservation .

For example,

$$|B_S^0\rangle = \frac{1}{\sqrt{2}}(|B^0\rangle + |\bar{B}^0\rangle), \ CP \text{ parity } (+1); \quad |B_L^0\rangle = \frac{1}{\sqrt{2}}(|B^0\rangle - |\bar{B}^0\rangle), \ CP \text{ parity } (-1).$$

The difference of masses between the respective CP-odd and CP-even states is very insignificant in all the cases, ranging from 10^{-12} MeV for K^0 mesons up to 10^{-8} MeV for B_s^0 mesons . Concerning the lifetimes of these states, in the case of K^0 mesons they differ by 600 times, but for D^0, B^0 and B_s^0 mesons the respective lifetimes are almost the same. In connection with this, it is practically impossible to distinguish the states of D^0, B^0 and B_s^0 mesons with definite CP parity by the difference in their lifetimes. These states, in principle, can be identified through the purely CP-even and purely CP-odd decay channels ; however, in fact the branching ratio for such decays is very small . For example,

$$Br\left(D^0 \to \pi^+ \pi^-\right) = 1.62 \cdot 10^{-3} \ (\ CP = +1); \quad Br\left(D^0 \to K^+ K^-\right) = 4.25 \cdot 10^{-3} \ (\ CP = +1\ );$$

$$Br\left(B_s^0 \to J/\Psi \ \pi^0\right) < 1.2 \cdot 10^{-3} \ (\ CP = +1); \quad Br\left(B^0 \to J/\Psi \ K_S^0\right) = 9 \cdot 10^{-4} \ (\ CP = -1\ ) .$$

Just as in the case of neutral K mesons, the correlation functions for the pairs of states of neutral D, B and B_s mesons with the same CP parity ($R_{SS} = R_{LL}$) and for the pairs of states with different CP parity (R_{SL}) do not coincide, and the difference between them

is conditioned exclusively by the production of pairs $D^0 \bar{D}^0$, $B^0 \bar{B}^0$ and $B_s^0 \bar{B}_s^0$, respectively. In particular, for B_s^0 mesons the following relation holds:

$$R_{SS}(\mathbf{k}) - R_{SL}(\mathbf{k}) = 2\lambda_{B_s^0 \bar{B}_s^0} \left[F_{B_s^0 \bar{B}_s^0}(2\mathbf{k}) + B_{\text{int}}(\mathbf{k}) \right] ; \qquad (9)$$

here $\lambda_{B_s^0 \bar{B}_s^0}$ is the relative fraction of generated pairs $B_s^0 \bar{B}_s^0$,

$$F_{B_s^0 \bar{B}_s^0}(2\mathbf{k}) = \int W_{B_s^0 \bar{B}_s^0}(\mathbf{r}) \, \cos(2\mathbf{kr}) \, d^3\mathbf{r}, \qquad B_{\text{int}}(\mathbf{k}) = \int W_{B_s^0 \bar{B}_s^0}(\mathbf{r}) \, B(\mathbf{k}, \mathbf{r}) \, d^3\mathbf{r},$$

$$B(\mathbf{k}, \mathbf{r}) = |A_{B_s^0 \bar{B}_s^0}(k)|^2 \frac{1}{r^2} + 2\,\text{Re}\left(A_{B_s^0 \bar{B}_s^0}(k) \frac{\exp(ikr) \cos \mathbf{kr}}{r} \right),$$

where $A_{B_s^0 \bar{B}_s^0}(k) \equiv A_{B_s^0 \bar{B}_s^0 \to B_s^0 \bar{B}_s^0}(k)$ is the amplitude of S-wave $B_s^0 \bar{B}_s^0$ - scattering, $k = |\mathbf{k}|$, $r = |\mathbf{r}|$.

4 Summary

1. It is shown that, taking into account the strangeness conservation, the correlation functions for two short-lived neutral K mesons (R_{SS}) and two long-lived neutral K mesons (R_{LL}) are equal to each other. This result is the direct consequence of the strangeness conservation.

2. It is shown that the production of $K^0 \bar{K}^0$-pairs with the zero strangeness leads to the difference between the correlation functions R_{SS} and R_{SL} of two neutral kaons.

3. The character of analogous correlations for neutral heavy mesons D^0 , B^0, B_s^0 with nonzero charm and beauty is discussed . Contrary to the case of K^0 mesons, here the distinction of respective CP-even and CP-odd states encounters difficulties, which are connected with the insignificant difference of their lifetimes and the relatively small probability of purely CP -even and purely CP-odd decay channels .

References

[1] V.L. Lyuboshitz, Yad. Fiz. **23** 1266 (1976) [Sov. J. Nucl. Phys. **23** 673 (1976)].

[2] V.L. Lyuboshitz and M.I. Podgoretsky, Yad. Fiz. **30** 789 (1979) [Sov. J. Nucl. Phys. **30** 407 (1979)].

[3] M.I. Podgoretsky, Fiz. Elem. Chast. At. Yadra **20** 628 (1989) [Sov. J. Part. Nucl. **20** 266 (1989)].

[4] R. Lednicky and V.L. Lyuboshitz, Yad. Fiz. **35** 1316 (1982) [Sov. J. Nucl. Phys. **35** 770 (1982)].

[5] V.L. Lyuboshitz, Yad. Fiz. **41** 820 (1985) [Sov. J. Nucl. Phys. **41** 523 (1985)].

[6] V.L. Lyuboshitz, Yad. Fiz. **48** 1501 (1988) [Sov. J. Nucl. Phys. **48** 956 (1988)].

[7] R. Lednicky, V.V. Lyuboshitz and V.L. Lyuboshitz, Yad. Fiz. **61** 2161 (1998) [Phys. At. Nucl. **61** 2050 (1998)].

[8] V.L. Lyuboshitz and V.V. Lyuboshitz, Nukleonika, v.**51**, Suppl. 3, p. S69 (2006) - in Proceedings of Quark Matter 2005 Conference (Budapest, Hungary, August 4 - 9, 2005).

[9] V.L. Lyuboshitz and V.V. Lyuboshitz, in Proceedings of the IV International Conference on Quarks and Nuclear Physics – QNP-06 (Madrid, Spain, June 5 - 10, 2006), Berlin - Heidelberg, 2007, p.109 .

[10] V.L. Lyuboshitz and V.V. Lyuboshitz, Pis'ma v EchaYa, v.**4**, No.5 (141), p.654 (2007) [Particles and Nuclei. Letters. v.**4**, No.5, p.388 (2007)] .

Lecturers

1. Ali, Ahmed (DESY)

2. Bevan, Adrian John (London, PPRC)

3. Blaschke, David B. (Wroclaw U.)

4. Borisov, Anatoly V.(MSU)

5. Faustov, Rudolf N. (Dorodnicyn Computing Centre RAS, Moscow)

6. Galkin, Vladimir O. (Dorodnicyn Computing Centre RAS ,Moscow)

7. Gerasimov, Sergo B. (JINR)

8. Golob, Bostjan (Ljubljana U.):

9. Grozin, Andrey G. (INP, Novosibirsk)

10. Haisch, Ulrich (Mainz U.)

11. Ivanov, Mikhail A.(JINR)

12. Koerner, Juergen G. (Mainz U.)

13. Kotikov, Anatoly V. (JINR)

14. Likhoded, Anatolii (IHEP, Protvino)

15. Lunghi, Enrico (Fermilab)

16. Lyubovitskij, Valery E. (Tuebingen U.)

17. Nierste, Ulrich (Karlsruhe):

18. Parkhomenko, Alexander Ya. (Yaroslavl U.)

19. Pecjak, Ben (DESY)

20. Pivovarov, Alexei A. (INR, Moscow)

21. Saleev, Vladimir A. (Samara U.)

22. Stewart, Iain (MIT)

23. Teryaev, Oleg V. (JINR)

24. Vysotsky, Mikhail I. (ITEP)

25. Wittig, Hartmut (Mainz U.)

26. Zotov Nikolai P. (SINP, Moscow)

Participants

1. Abrahamyan, Alisa Ashot (Yerevan State University, Armenia)

2. Andreev, Mikhail Sergeevich (Yaroslavl State Univ., Russia)

3. Avakyan, Elena Zinovievna (P.Sukhoi Gomel State Technical University, Belarus)

4. Avakyan, Sergey Levonovich (P.Sukhoi Gomel State Technical University, Belarus)

5. Ayvazyan, Narine Semyon (Yerevan State University, Armenia)

6. Braguta, Victor (IHEP, Protvino, Russia)

7. Charnukha, Aliaksei Sergeevich (University of Stuttgart, Germany)

8. Cherednikov, Igor Olegovich (JINR, Russia)

9. Davidkov, Momchil Miltanov (University of Karlsruhe, Germany)

10. Degtiareva, Anna Pavlovna (Moscow State University, Russia)

11. Dorokhov, Alexander Evgenyevich (JINR, Russia)

12. El-Bennich, Bruno (Argonne National Lab, USA)

13. Gorbunova, Olesya Gennadevna (Tomsk State Pedagogical University, Russia)

14. Jankowski, Jakub Marek (University of Wroclaw, Poland)

15. Juettner, Andreas (Johannes-Gutenberg Universitt, Germany)

16. Kiselev, Alexey Vladimirovich (Sobolev Institute for Mathematics, Novosibirsk, Russia)

17. Klopot, Yaroslav Nikolayevich (JINR, Russia)

18. Kochelev, Nikolai Innokentievich (JINR, Russia)

19. Kopnin, Petr Nikolaevich (MIPT, Russia)

20. Krutov, AndreiAlexandrovich (Samara State University, Russia)

21. Kudinov, Maxim Yurievich (Samara State University, Russia)

22. Kurbanov, Serdar Geldimuratovich (Moscow State University, Russia)

23. Lyuboshitz, Valery Vladimirovich (JINR, Russia)

24. Makhaldiani, Nugzar Vladimirovich(JINR, Russia)

25. Martynov, Mikhail Victorovich (Yaroslavl State Univ., Russia)

26. Nikitin, Nikolai Viktorovich (Moscow State University, Russia)

27. Novoselov, Alexey Anatolevich (IHEP, Russia)

28. Orlovsky, Vsevolod Dmitrievich (ITEP, Russia)

29. Parsi Sreenivas, VijayVittal (University of Stuttgart, Germany)

30. Pasechnik, Roman (JINR, Russia)

31. Poghosyan, Sergey Suren (JINR, Russia)

32. Radchenko, Olga Vasilevna (Tomsk State Pedagogical University, Russia)

33. Radovskaya, Anna (JINR, Russia)

34. Reznichenko, Alexey Victorovich (Budker Institute of Nuclear Physics, Russia)

35. Scherer, Dominik (Karlsruhe University, Germany)

36. Sharma, Manoj Kumar (Aligarh Muslim University, India)

37. Shipilova, Alexandera Victorovna (Samara State University, Russia)

38. Shtol, Dmitry Aleksandrovich (Sobolev Institute for Mathematics, Novosibirsk, Russia)

39. Surovtsev, Yury Stepanovich (JINR, Russia)

40. Zaytsev, YuriySergeevich (Yaroslavl State University, Russia)